KTB REPORT 93-1

Basic Research and Borehole Geophysics (Report 14)

Borehole logging in the KTB-Oberpfalz HB
- Interval 4512.0 - 6018.0 m -

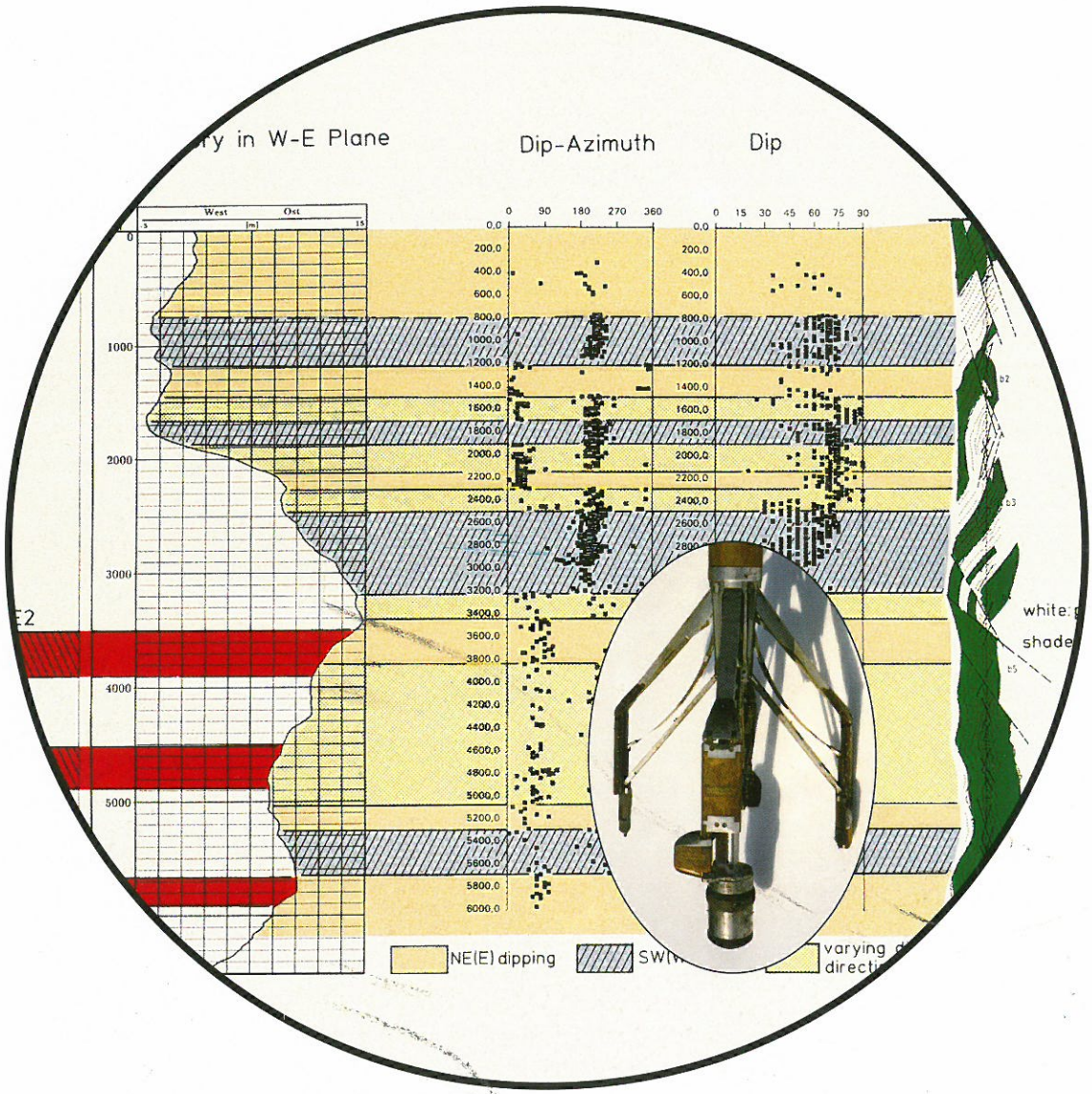

Edited by
the Project Management of the Continental Deep Drilling
Programme of the Federal Republic of Germany
in the Geological Survey of Lower Saxony

K. Bram, J. K. Draxler

KTB REPORT 93-I

Basic Research and Borehole Geophysics (Report 14)

Borehole logging in the KTB-Oberpfalz HB
- Interval 4512.0 - 6018.0 m -

Edited by
the Project Management of the Continental Deep Drilling
Programme of the Federal Republic of Germany
in the Geological Survey of Lower Saxony

K. Bram, J. K. Draxler

Editors: Dr. K. Bram
Dipl. Ing. J. K. Draxler

Printed by: Wittmann & Wäsch, D-30989 Gehrden

Distribution: E. Schweitzerbart'sche Verlagsbuchhandlung

Orders: E. Schweitzerbart'sche Verlagsbuchhandlung
Johannesstr. 3A
D-70176 Stuttgart

Front cover: Analysis of formation dip and strike direction with the help of Formation MicroImager logs. Inferred structural model and comparison with major seismic reflectors drilled in the KTB-Oberpfalz HB.
(Interpretation by Hirschmann and photo by Draxler)

All projects reported hereafter are entirely funded by the Federal Ministry of Research and Technology. The editors cannot be held responsible for the opinions given and statements made in the articles published, the responsibility resting with the authors.

Editors' address:
Niedersächsisches Landesamt für Bodenforschung, POB 51 01 53,
D-30631 Hannover
Phone: 0511/643-2675

ISSN 0939-8732
ISBN 3-928559-09-5

Foreword

Borehole logging provides insight into the drilled section of the Earth's crust and allows, therefore, the acquisition of important geoscientific data under almost in situ conditions. In the very beginning of the KTB project a working group headed by R. Hänel was established with the aim to prepare an appropriate logging programme and to study the most economic way for its realization. As a result when the drilling activity started in 1987 KTB owned a permanently installed logging unit at the drill site as well as a basic logging tool set. Once the comprehensive logging of the pilot borehole ended, the logging programme was thoroughly revised and adapted to the needs of the main geoscientific goals defined for the superdeep borehole KTB-Oberpfalz HB:

- geophysical phenomena, structures and heterogeneities
- stress field
- temperature field
- crustal structure, evolution and composition
- transport mechanisms and fluids.

Borehole logging contributes further to quick operational decisions and provides support to drilling operations in case of needs.

A staff of seven engineers, technicians and scientists is assigned to the Logging Department of the KTB Project Management responsible for the downhole measurements. It is assisted by three Schlumberger employees, an engineer, an electronician and an operator, one software engineer (Geco-Prakla) and one log analyst (Gatto).

On March 10, 1992 the KTB superdeep borehole, the Hauptbohrung, reached after 522 days drilling a depth of 6018 m. Having crossed the important landmark of 6000 m of the currently planned 10,000 m deep borehole, this offers an excellent opportunity to summarize the various logging campaigns performed so far in the superdeep borehole.

The "6000 m" campaign which followed immediately after March 10, 1992 is presented and explained in a well proven manner by means of exemplary log sections. Prototype or other tools for the first time run in the KTB borehole are described. Preliminary results deduced from logging data or testing experiments are given. For detailed information concerning the logging campaigns carried out at the depths of 305 m, 762.5 m, 1720 m, 3003 m and 4512 m refer to KTB Reports 91-2 and 92-1.

With this issue an additional set of depth and borehole corrected data are at the disposal of interested scientists for

further evaluation and interpretation. Data can be requested with the attached data sheets from the Project Management*. Scientists must then report regularily on the progress of their studies either to the Project Management or to the Chief-Coordinator of the DFG priority programme KTB. Results should first be published in the "KTB Report" series in order to quickly disseminate important information to other working groups. This does not replace an independently reviewed publication in an international scientific journal. In that case the origin of the data must be stated and a copy of an off-print should be sent to the Project Management.

*Niedersächsisches Landesamt für Bodenforschung
Projektleitung KTB
Referat Bohrlochmessungen
P.O.Box 510153 Phone: 49/511/643-2673
D-30631 Hannover Fax: 49/511/643-2686

or:
Niedersächsisches Landesamt für Bodenforschung
KTB Außenstelle Windischeschenbach
Referat Bohrlochmessungen
P.O.Box 67 Phone: 49/9681/400-62
D-92667 Windischeschenbach Fax: 49/9681/400-67

CONTENTS

1. Logging and Testing in the Superdeep Borehole KTB-Oberpfalz HB:

Concept and First Results of the Depth Interval 0 – 6018 m

K. Bram

LOGGING AND TESTING IN THE SUPERDEEP BOREHOLE KTB-OBERPFALZ HB: CONCEPT AND FIRST RESULTS OF THE DEPTH INTERVAL 0 - 6018 M

K. Bram

Summary

Borehole measurements and tests are an integral part of the geoscientific investigations within the framework of the German Continental Deep Drilling Program. Because logging superdeep boreholes is a challenging task, an appropriate concept has been developed. The strategy and the infrastructure set up by the KTB Project Management's Logging Department is described. Major contributions to the geoscientific objectives from the hitherto carried out five bigger logging and testing campaigns down to 6018 m are briefly summarized.

Introduction

On October 6, 1990, the superdeep borehole KTB-Oberpfalz HB, in the following called Hauptbohrung, was spudded. The Continental Deep Drilling Program of the Federal Republic of Germany entered at this moment into its decisive, scientifically and technically most challenging phase. Guided by a very tight financial framework the target depth of 10 000 m shall be reached by September 1994. At this depth pressures of 100 to around 150 MPa are expected, and following an improved prognosis based on the results obtained to date from the pilot borehole as well as the Hauptbohrung temperatures will be about 300 °C. With respect to downhole data acquisition either by logging or coring, the experience gained in the pilot borehole helps to cope with the new tasks and furthers appropriate instrumental development.

The coring concept (Engeser, 1990) of the Hauptbohrung provides for discontinuous coring beyond 4000 m depth, the total depth of the pilot borehole, situated 200 m to the west, with a core recovery of 89 %. Logging the Hauptbohrung is, therefore, of particular importance: it will give not only an almost continuous in situ information on physical rock parameters and structural data, but will allow also for depth correlation and post-orientation of cores.

Author's address:
Niedersächsisches Landesamt für Bodenforschung, Projektgruppe KTB, Stilleweg 2, D-3655 Hannover

This contribution is aimed at describing the concept for logging the Hauptbohrung. A brief introduction follows for those chapters in this KTB-Report dealing in detail with infrastructure, logging data archives and presentation, and summarizes the most important results of the five bigger logging campaigns performed to date.

Logging Concept

As early as in 1986 Devay et al. conceived a logging program for the KTB Hauptbohrung taking into account the current knowledge at that time on logging in crystalline rocks, available logging tools and planned drilling scheme. Results obtained from the pilot borehole, from geophysical, geological and geochemical investigations in the surroundings of the drilling location and new geoscientific information lead to a modification of the previously established priority list of the scientific targets (Emmermann, 1991):

- Origin and in situ conditions of geophysical phenomena, structures and heterogeneities.
- Stress field of the Earth's crust: orientation and magnitude of stress and its variation with depth.
- Temperature distribution in the Earth's crust: heat sources, heat production and heat transport.
- Structure, composition and evolution of a repeatedly renewed crustal type.
- Fluids and transport mechanisms.

The logging concept had to be adjusted to these nowadays valid targets. From intensive discussions amongst scientists and the project management a modified, well balanced logging program for the Hauptbohrung emerged (Bram, 1991; Draxler, chapter 4 of this report). Therefore, it is aiming mainly at the determination of geophysical parameters such as e.g. the behaviour of seismic wave propagation, temperature and stress field distribution with depth, on structural information such as orientation and inclination of faults, fissures and foliation as well as on hydraulic parameters including fluid sampling. The program was adopted by the expert commission of the German Federal Ministry of Research and Technology on April 25, 1990.

Due to the tight financial and timing framework of the main project phase numerous additional experiments and tests have had to be discarded. Those like e.g. time dependent measurements of the variation of the Earth's magnetic field or intensive hydraulic testing should be postponed to a long term logging and testing program similar to that performed in the pilot borehole (Bram et al., 1990).

Logging strategy

In order to realize the logging program the well proven strategy during the drilling of the pilot borehole was revised. Developed around a permanent readiness for carrying out down-hole measurements, the logging strategy has been guided by cost minimization in setting up operational procedures for saving rig time (Zoth, chapter 2 of this report) and by utilizing as much as possible commercially available logging equipment. With temperatures below 175 °C standard equipment will be used.

Cable and data telemetry

A severe problem for logging superdeep boreholes remains with the logging cable serving not only as a mechanical link to the measuring device but also as an electrical link for power supply, tool steering signals and data transmission. Taking into account all the available information on borehole measurements in comparable superdeep boreholes (Berta Rogers: 9583 m, Zistersdorf ÜT-2: 8553 m, Kola SG-3: 12066 m (today: 12 260 m)) this problem was considered to be more or less solved in the early planning stage (Hänel, 1986).

The density of the drilling mud used for the KTB Hauptbohrung ranges between 1.0 and 1.5 g cm^{-3} maximum (Ellins and Tran Viet, 1990). This means for a single 7-conductor cable, even with high strength steel armor, that due to an almost missing buoyancy effect the cable will mechanically break by its own weight before reaching 10 000 m. Further increasing the mechanical breaking strength by increasing the armor's wires diameter and/or using other steel qualities is, however, limited. This would again result in an increase of the cable weight. Recent calculations including various parameters do show the limitations of single logging cables (Kessels, 1990b, 1991). Not considered here is the long term behaviour of high temperature insulation materials like Teflon when exposed to temperatures around 300 °C. Experiences from the Salton Sea State 2-14 borehole showed a complete desintegration of TFE insulation after several hours exposure to temperatures above 300 °C (J. Sass, personal communication).

Assisted by logging cable manufacturers, the KTB Logging Department completely reconsidered the cable concept. The essential element of the concept is a dual or even multi cable system (Zoth, chapter 2 of this report) with an active telemetry link in order to improve the electrical transfer characteristics. The latest information on logging techniques applied at the Kola SG-3 borehole (3-conductor dual cable system composed of a Russian and a Japanese cable with diameters of 14.0 mm and 10.2 mm, respectively) has been integrated as well as the experience gained with the geothermal Salton Sea State 2-14 borehole (J. Sass, personal communication). In the lowermost depth range commercially available and extreme conditions

resisting mineral insulated cables may be used. The development of the corresponding cable heads and connectors, commissioned by the KTB Logging Department, is underway.

Logging tools

During the past years hydrocarbon exploration became more interested in greater target depths. In parallel the service industry, challenged by the higher temperature and pressure conditions undertook considerable efforts to provide for the neccessary downhole measurement equipment. Devay et al. (1983) performed a market study on high temperature, high pressure logging tools. For the Hostile Environment Logging (HEL) range (temperature up to 260 °C and pressure up to 150 MPa), today there is a series of tools definitively available. Table 1 shows commercial tools offered by one or several companies for specific purposes. KTB owned standard tools (Zoth, chapter 2 of this report) are subject for getting upgraded to higher temperatur conditions. In order to improve other standard tools which are of essential interest to KTB like e.g. a Formation Micro-Imager, an unrealistic effort in cost and time would be needed to push them beyond the 175 °C range. The HEL-temperature limit of 260 °C will be expected in the Hauptbohrung at a depth of 8.5 to 9.3 km (Burkhardt et al., 1989; 1991).

Table 1
Available HEL-tools

Tool	T_{max} (°C)	p_{max} (MPa)	window (h)
4-arm caliper (without inclination/orientation)	260	170	5
gyro systems	260	140	6
Dual Laterolog	260	170	8
Induction Log	260	170	6
Induced Polarization	260	130	?
Gamma Ray	260	170	5
Natural Gamma Spectroscopy	260	170	5
Litho Density	260	170	5.5
Compensated Neutron	260	170	4
Sonic/Full Wave Form	260	170	6
Triaxial Geophone	250	160	15
Borehole Televiewer	260	140	6
Fluid Sampler	260	140	2

The Very Hostile Environmental Logging (V-HEL) range is defined by temperatures up to 300 °C and pressures up to 170 MPa. For this range there are only few geothermal tools available (Table 2). In many cases their pressure limitation must be improved before using them down to 10 000 m. Further instrumental improvement is also needed for fluid samplers as experiences showed (e.g. Sass and Elders, 1986; Zoth, 1990).

The development of specific tools which are of less interest to the hydrocarbon exploration industry has been funded by KTB. A borehole televiewer (Schepers, 1991), a fluxgate magnetometer (Kuhnke and Musmann, 1991) and a magnetic susceptibility probe (Krammer and Pohl, 1991) have been proven operational partly up to 230 °C. Work is in progress to achieve their 300 °C version.

Table 2
Available V-HEL tools

Tool	T_{max} (°C)	p_{max} (MPa)	window (h)
4-arm caliper (without orientation/inclination)	315	170	1
Gyro	300	140	4.5
Temperature	315	130	?
Flowmeter	315	100	10
Pressure	315	100	?
Fluid Sampler	350	140	?

A recently completed feasibility study defined the steps for improving those digital or analog tools deemed absolutly necessary to realize the technical and scientific goals. This holds particularly for tools measuring the borehole geometry including orientation and inclination as well as fishing operations emphasizing explosives and detonator development.

Borehole geometry reflects the stress field of the Earth's crust, too. Therefore, such a tool is also of topmost interest for geoscientists. Further emphasis has to be led on the measurements of natural gamma radiation, formation density, electrical resistivity and seismic wave velocities.

Tough logging conditions and the use of memory tools have been discussed in length and eventually discarded. To get an effective and sufficient cooling, too long mud circulation times would be needed as model calculations showed (e.g. Kessels, 1990a) or there is a complete lack of operational control.

Data archives, processing and presentation

Rapid access to logging data is of primordial importance for many purposes. This is guaranteed by assigning each logging run a job number and a tape number (Sowa, 1992; Draxler, chapter 5 of this report) under which the appropriate data can be retrieved from the LOGDV-database. This database is linked to KTBase, the master database containing a full record of the contents of the LOGDV-database. In addition data are stored on films and paper copies.

Users outside the KTB Project Management and the field laboratory request logging data by means of a particular form attached at the end of this report. Standard data format on tapes is LIS (Log Interchange Standard).

Before data are stored on any data storage medium a severe quality control has been performed.

In order to ease the data handling of the different borehole measurements for future interpretation, a particular and user friendly interactive software package **SEL** has been developed within the KTB Logging Department (Sturmeit, chapter 9 of this report). This package fullfills the following functions:

- **SEL**ecting the data from the database,
- processing the data e.g. filtering, editing, resampling,
- performing arithmetical and logical operations as well as
- their numerical or graphical presentation.

Structered around a separate binary storage database SEL uses the VAX/VMS command language, thus avoiding tedious data conversion, and on the other hand enabling quick acquaintance by the user.

This flexible package serves also to display rapidly the most important data from drilling and logging operations and from field laboratory analyses. 44 parameters have been selected (Table 3) and are routinely presented as **QUICKLOOK logs** (Kück, chapter 9 of this report). The KTB Project Management uses these logs for rapid data correlation in order to decide on necessary actions of technical or geoscientific importance. Besides the standard plots any combination of the parameters or other parameters not mentioned here is possible depending on specific questions. Recently this presentation has been extended to purely mud logging data.

Table 3
KTB-Oberpfalz HB: QUICKLOOK parameter

Lithology	Logging	Drilling	Mud I	
main units	gamma ray	tool	density	i/o
alteration	caliper	rate of penetr.	temperature	i/o
cataclases	inclination	weight on bit	el. conduct	i/o
sulfides	azimuth	rotation p.min.	pH	i/o
graphites	ellipticity	torque	Redox	
	dogleg sev.	pumping rate i/a	total gas	i/o
	mud resist.	pumping pressure		
	temperature			

Table 3 cont.

RDA	Gas anlysis	Geophysics	Mud II
quartz	helium	rock density	Cl^-
plagioclas	methane	magn. suscept.	$SO4^{--}$
amphibolite		gamma ray	Ca^{++}
biotite			D-HT (weight%)
chlorite			
epidote			
garnet			
pyrite			

Summary of results

Borehole trajectory

The vertical drilling strategy specially developed for the KTB Hauptbohrung (Chur et al., 1990) proved to be very effective and successful. With respect to its wellhead location the maximum horizontal distance amounts to about 20 m at a depth of 3200 m to 3400 m ; at 6000 m this distance is less than 7 m (see also chapter 3 of this report). The overall inclination down to 6000 m is less than 0.2°.

Borehole azimuth and inclination have been determined by means of gyroscope tools (down to 3000 m) and the KTB owned Borehole Geometry Tool (BGT). Due to tool specifications the azimuth values obtained by the BGT are relatively uncertain in almost vertical sections (Kessels, 1988). Compared to the orientation system of the highly sensitive borehole Fluxgate Magnetometer (FML) of the University of Brunswick (Kuhnke and Musmann, 1991) the data agree quite well, and are confirmed, too, by the azimuth values of the Formation MicroImager (FMI).

Temperature

The determination of the undisturbed formation temperature plays an important role within the geoscientific objectives. Since the temperature distribution in the upper 4000 m is fairly well known from measurements in the KTB pilot borehole (e.g. Burkhardt et al., 1991; Jobmann and Schulz, 1992), only bottom hole temperatures were measured in the Hauptbohrung at 762 m, 1720 m and 3003 m (Zoth, 1992). The data are close to the temperatures observed in the pilot borehole at comparable depths. During both the 4500 m and the 6000 m logging campaign several temperature logs were run at logarithmic time intervals as recommended by the KTB geothermal working group. The temperatures obtained by extrapolation amount to 132 °C and 173 °C respectively, with an average temperature gradient of 27.3 K/km (Zoth, chapter 9 of this report).

From the Natural Gamma Spectroscopy log performed from surface to 3000 m the heat production has been calculated (Gatto, 1992). The mean values of about 0.5 $\mu W/m^{-3}$ and 1.6 $\mu W/m^{-3}$ for metabasites and gneisses, respectively, are similar to those used by Clauser (1992) for conductive-advective thermal modelling.

Stress field

The KTB boreholes offer a rare opportunity to study the state of stress from the surface to the depth of the middle crust. Breakout analyses of caliper and borehole televiewer (BHTV) data yield mean values for the orientation of the maximum principal stress (S_H) of N140°E $\pm$ 26° for the depth range 800 m to 4000 m (Apel et al., 1991) and N149°E $\pm$ 18° for the depth range 3000 m to 6000 m (e.g. Brudy et al., chapter 9 of this report). This is in acceptable agreement with the results obtained from the pilot borehole (Mastin et al., 1991). An almost perpendicular orientation of drilling-induced vertical tensile fractures observed in BHTV and FMI images confirm these values (e.g. Bram et al., 1992).

Within the framework of the integrated stress measurement strategy in the Hauptbohrung two hydrofrac experiments were made to get stress magnitude data complementing those already obtained in the pilot borehole down to 3011 m (Baumgärtner et al., 1990). The experiment at a depth of 4138 m failed due to technical reasons: the attempt to drill a 96 mm pilothole using a 1 3/4" coiled tubing system failed. Therefore, the preparation for a wireline hydraulic frac test was cancelled. The second experiment, however, performed in the depth interval from 6013 m to 6031 m was very successful (Engeser et al., chapter 9 of this report): for the first time a magnitude of the minimum principal stress (S_{hmin}) was measured in situ at a depth below 6000 m. At a constant flow rate of about 30 l/min

pressure dropped suddenly after having reached a peak value of 114 MPa. A BHTV was run immediately after the experiment. Due to insufficient data quality the frac and its orientation could not be detected.

Geological structures and lithology

The geological and tectonical interpretation of the rocks intersected by the boreholes depends on the availability of structural information. The high quality core material of the almost completely cored KTB pilot borehole showed excellent structural features described and interpreted in e.g. Emmermann et al., 1990. Their spatial orientation as a fact of the coring strategy was possible by comparison with borehole wall images depicted from appropriate logging tools such as the Formation MicroScanner (FMST) or the BHTV (e.g. Schmitz, 1988; Kohl et al., 1991; Kessels and Kück, 1992).

These tools in particular the FMST and its highly sophisticated derivative, the Formation MicroImager (FMI) are of topmost importance for structural analysis of the Hauptbohrung. Only few, not oriented cores were recovered showing intermediate to steeply dipping foliation planes (Lich et al., 1992). Integrated into the oriented images of the FMST, run from 1720 m to surface, and the FMI, run from 6023 m to 1720 m, a very complicated structural pattern appeared (Hirschmann, 1992a). Obviously there is a close link between structural elements, some of them may be correlated with seismic reflectors (Hirschmann, 1992b) and the course of the Hauptbohrung (Hirschmann and Kück, chapter 9 of this report).

Further structural information has been deduced from wireline core slices and side wall cores taken from selected depths (Draxler, 1992; Dietrich et al., 1992).

Cuttings are the principal material to establish the lithological profile of the KTB Hauptbohrung. With increasing depth cutting samples get smeared over increasing depth intervals, thus correct depth correlation becomes more and more difficult. In addition, samples may be contaminated by cavings. Therefore, samples are checked and thickness and depth of lithological boundaries are corrected using borehole logging data, especially Caliper, Gamma Ray, Electrical Resistivity and Magnetic Susceptibility (Lich et al., 1992). In this respect, the logged Gamma Ray plays a particular role for it serves as depth reference.

Another approach to reconstruct the lithological profile is based on pure logging data. Due to the 17 1/2" borehole diameter only the logs of NGS, DLL and SDT have thoroughly been analysed for the interpretation of the first 3000 m of the KTB Hauptbohrung (Pechnig and Wohlenberg, chapter 9 of this

report). Despite the reduced number of log data 16 electrofacies have been determined allowing a reliable differentiation not only of the different gneisses and amphibolite varieties but also of metagabbros and faulted or cataclastic zones. Eberle (1992) works on the interpretation of multi-method geophysical data, too, applying multivariate statistical analyses successfully tested on data sets of the KTB pilot borehole.

Mineral analysis using a number of particular logs like density, photoelectric absorption, neutron, potassium and data from the Geochemical Logging Tool (GLT) contribute significantly to the interpretation of the encountered crystalline rocks (Gatto and Lauterjung, 1990). As mentioned above in the Hauptbohrung cavings are a serious concern for correct cutting analysis and depth correlation. A quantitative mineral analysis for the first 3000 m of the superdeep borehole clearly distinguishes between the principal rock types: gneisses and amphibolites (Gatto, chapter 9 of this report).

Hydraulics

The investigation into fluids and hydraulic parameters is of great importance to elucidate questions raised in connection with "fluids and transport mechanisms", one of the main scientific objectives.

Testing large diameter boreholes by e.g. drillstem tests is rather problematic, and furthermore tedious and very costy. In the Hauptbohrung similar effects could be achieved performing draw down tests by simply lowering the drilling mud level, thus reducing the hydrostatic pressure. At 3000 m, 4500 m, 5000 m and 6000 m depths mud levels were lowered by 235 m, 201 m, 230 m and 513 m provoking an inflow of formation fluids of 5.3 m^3, 0.7 m^3, 1.7 m^3 and 30 m^3, respectively. An evaluation of the data yield mean permeabilites varying between about 1 μD and 60 μD for the various test depth intervals (Kessels et al., 1992; Kessels & Kück, chapter 9 of this report). Kessels et al. (1992) pointed out that fresh water prevails the depth range from surface to about 1500 m. Below that depth highly saline waters have been observed.

Fluid inflow was always accompagnied by temperature and mud electrical resistivity anomalies. Analysing the appropriate logs depth intervals were determined and in situ fluid samples were taken (Draxler and Kück, 1992; Draxler, chapter 5 of this report). Results of the chemical fluid and gas analysis show significant Ca, Sr and Cl^- enrichments as well as N_2/Ar, He and CH_4 contents (Figgemeier et al., 1992).

Geophysical phenomena

Geophysical borehole measurements in the Hauptbohrung are to be seen in the light of results of numerous surface geophysical surveys conducted prior and during drilling the KTB boreholes reported e.g. by Emmermann and Wohlenberg (1989) and Bram (1988).

Anomalies of the induced polarization and the electrical resistivity often closely correlate with graphite or pyrite bearing fissure or fracture zones. Mostly positive, short wavelength SP amplitudes observed in the same depth intervals suggest a current flow along these electron conductors. The large surface SP anomaly together with this observation supports the existence of a huge geoelectrochemical cell (Stoll et al., 1992). To find out the lateral extent of such an electron conductor, Stoll (chapter 9 of this report) describes a mise-à-la masse experiment using the casings of both boreholes as electrodes. The observed SP anomalies indicate that the steeply inclined prominent Nottersdorf fault zone intersected by the boreholes very likely acts as such an electron conductor.

First results of the borehole gravity measurements performed during the 6000 m logging program yield Bouguer anomalies of 3 to 6 m Gal with decreasing magnitude beyond 4000 m. Forward modelling indicates that the previously established structural model (Wolfgram et al., 1992) has to be revised (Gobashy, Casten and Neubauer, personal communication).

Very interesting magnetic features were revealed when measuring the magnetic field using triaxial fluxgate magnetometers (Bosum et al., 1992a; Fieberg and Kuhnke, personal communication). The intersected matabasites are characterized by broad anomalies and partly by distinguished narrow anomaly bands indicating a higher magnetization than the gneisses. Some gneiss varieties, however, do show also a high magnetization. The anomaly bands observed between 1000 m and 1500 m depth are obviously linked to faults. This may shed new lights on the interpretation of rock magnetic results. Suggesting that chemical processes in connection with hydrothermal circulation are responsible for the magnetization, NRM could be explained in this case by chemoremanent effects (Bosum et al., 1992b).

Unfortunately the measurement of the magnetic susceptibility in the Hauptbohrung failed. From the almost identical magnetic pattern observed in the upper 4000 m of both boreholes and investigations of rock magnetic properties including magnetic susceptibility on cuttings and cores pyrrhotite still prevails over magnetite as carrier of the magnetization (Lich et al., 1992; Pribnow et al., 1992).

An interesting effect is the large scale anomalous increase of the magnetic field with depth below 1500 m. This gradient observed in both KTB boreholes is slightly more than twice the normal one which amounts to 22 nT/km (Fieberg and Kuhnke, personal communication). For the time being there is no other explanation than seeking its origin in deeper parts of the Earth's crust.

The nature and the origin of seismic reflectors in crystalline rocks of the crust is one of the most intriguing questions asked by scientists. From 2D seismic reflection profiles (Schmoll et al., 1989) and the comprehensive Integrated Seismic Oberpfalz experiment (ISO 89) (DEKORP 1990) two groups of reflectors have been identified. The first group consists of more or less steeply dipping (after migration) reflectors which can be partly traced from the upper to the middle crust. Reflectors of the second group are flat and mainly found in the middle crust at about 4 s TWT.

Evaluating the first breaks of the direct P-wave of several VSPs run in the KTB boreholes average and interval velocities have been derived representing a very reliable velocity-depth curve at the KTB site for migration and time-depth conversion problems (Rühl and Hanitzsch, 1992). Söllner et al. (1992) extent the velocity-depth curve by analysing the data from the VSP6000 of the Hauptbohrung. They show that the average velocity, starting with 5.4 km/s at the surface, increases to 6.15 km/s at 6000 m depth. A similar result has been obtained from sonic logs (Bram and Gatto, chapter 9 of this report) despite the different frequency contents of the source signals. VSP data reveal different S-wavelengths and frequencies. Shear wave splitting can clearly be recognized: the polarization direction of the faster S-wave is nearly NW (Rabbel, 1992).

Sonic wave propagation, and hence velocities obviously correlate with foliation dip: the steeper the foliation the higher the velocities (Bram and Gatto, chapter 9 of this report). This holds particular for the gneiss sections, and clearly indicates the strong seismic anisotropy reported elsewhere (e.g. Lüschen et al., 1990; Soffel et al., 1992). The v_p/v_s-ratio must, therefore, be interpreted rather in terms of structural effects than in terms of lithology or porosity effects.

Prominent seismic reflectors were already drilled through by the Hauptbohrung, their depths of intersection have been carefully determined (DEKORP Research Group, 1993). Most likely the SE2 is related to a bundle of faults between 3530 m and 3580 m. Others, however, are more difficult to interpret (Hirschmann, 1992b). The most prominent reflector SE1 dipping about 55° to the NE may be represented by a cataclastic fault system which was met now by the Hauptbohrung in the depth interval from 6800 m to 7100 m.

Conclusions

The logging concept for the KTB Hauptbohrung has been adjusted to the modified and nowadays valid geoscientific objectives. The KTB Logging Department set up an appropriate infrastructure in order to realise the logging programme taking into account the tight financial and timing framework. However, logging beyond temperatures of 260 °C, expected at a depth of 8.5 to 9.3 km, will be limited due to restrictions in tool development.

Borehole data complement laboratory data and contribute significantly to the geoscientific key questions. The results summarized above reflect just a condensed spectrum of current geoscientific investigations within the KTB project. A full evaluation and interpretation of all the data obtained down to 6018 m will still take some time.

References

Apel, R., Barton, C., Brudy, M. & Huber, K.: 1991. Sofort-interpretation von ausgewählten Bohrlochmeßdaten als operative Entscheidungshilfe zur Bohrlochstabilität. Final Report (unpublished), Karlsruhe.

Baumgärtner, J.; Rummel, F. & Zoback, M. D.: 1990. Hydraulic Fracturing in situ Stress Measurements to 3 km Depth in the KTB Pilot Hole VB (eds). KTB Report 90-6a, 353-399.

Bosum, W., Eberle, D., Worm, H.-U., Böhm, V. & Geipel, H. : 1992a. Magnetische Gesteinsparameter und Felder bei hohen Temperaturen und Drücken - kombinierte in situ- und Labormessungen. BGR Archivbericht Nr. 110009, Hannover (unpublished).

Bosum, W., Eberle, D., Fieberg, F., Pohl, J. & Worm, H.U.: 1992b. Magnetische Anomalien und gesteinsphysikalische Effekte in der KTB Vor- und Hauptbohrung. In: Protokolle und Kurzbeiträge. 5 DFG-Schwerpunktkolloquium KTB, Gießen.

Bram, K. (ed): 1988. Ergebnisse geowissenschaftlicher Umfelduntersuchungen - Geophysikalische Erkundung. KTB Report 88-12, Hannover.

Bram, K., Draxler, J.K., Kessels, W. & Zoth, G.: 1990. Grundlagenforschung und Bohrlochgeophysik (Bericht 10), KTB Report 90-6a, pp 458, Hannover.

Bram, K.: 1991. Bohrlochmessungen in der übertiefen Bohrung KTB-Oberpfalz HB: Konzept und Aufgaben. Bram, K. & Draxler, J.K. (eds): KTB Report 91-2, 3-11, Hannover.

Bram, K., Draxler, J.K., Gatto, H., Kessels, W., Kück, J. & Zoth, G.: 1992. Bohrlochmessungen in der KTB-Oberpfalz HB bis 6000 m: Eine Übersicht. 5. KTB Kolloquium, Gießen.

Bram, K. & Gatto, H.: 1993. Determination of seismic velocities from KTB borehole sonic logs. KTB-Report 93-1, Hannover.

Brudy, M., Fuchs, K. & Zoback, M.D.: 1993. Stress Orientation Profile to 6 km Depth in the KTB Main Borehole (eds). KTB Report 93-1, Hannover.

Burkhardt, H., Erbas, K., Giese, P. Haack, U., Hornamand, H., Huenges, E., Stiefel, A., Wilhelm, H., Zoth, G., Buntebarth, G. & Schulz, R.: 1989. Das vorhergesagte und das gemessene Temperaturprofil (eds). KTB Report 89-3, 216-242, Hannover.

Burkhardt, H., Erbas, K., Giese, P., Haack, U., Honarmand, H., Huenges, E., Stiefel, A., Wilhelm, H., Zoth, G., Buntebarth, G. & Schulz, R.: 1991. The measured and the predicted temperature profile in the KTB pilot-hole. Scientific Drilling, Vol. 2, 244-257.

Chur, C., Engeser, B. & Oppelt, J.: 1990. Vertical Drilling Concept for the Main Well. Oil Gas 16, 4, 26-29.

Clauser, Ch.: 1992. Temperatur- und Wärmetransport an der KTB - derzeitiger Wissensstand. Mitteilungen der DGG, 1-2, 36-46.

DEKORP 1990: Integrated Seismics Oberpfalz 1989. KTB Report 90-9b, Hannover.

DEKORP Research Group: 1992. Depth Determination of Prominent Seismic Structures beneath the KTB Main Drillhole KTB-HB. KTB Report 92-5, 149-160, Hannover.

Devay, L., Fries, A.P. & Hänel, R.: 1983. Tätigkeitsbe- richt der Arbeitsgemeinschaft Bohrlochmessungen (ARGE 2). BGR/NLfB, Archiv-Nr. 95 173, 174 S., Hannover (unpublished).

Devay, L., Draxler, J.K. & Hänel, R.: 1986. Konzept eines Meß- und Untersuchungsprogrammes für die Vor- und Hauptbohrung des Kontinentalen Tiefbohrprogramms. BGR/NLfB, Archiv-Nr. 99550, 149 S., Hannover (unpublished).

Dietrich, H.-G.; Lauterjung, J. & Wöhrl, Th.: 1992. Introduction. Results of Geoscientific Investigation in the KTB Field Laboratory - 0-6000 m. KTB Report 92-2, A1-A26, Hannover.

Draxler, J.K.: 1992. Meßprogramm - Planung und Durchführung. Bram, K. & Draxler, J.K. (eds). KTB-Report 92-1, 9-13.

Draxler, J.K. & Kück, J.: 1992. Übersicht über bohrlochgeophysikalische Aktivitäten (eds). KTB Report 92-1, 61-66, Hannover.

Draxler, J.K.: 1993. Logging Programme. KTB Report 93-1, Hannover.

Draxler, J.K.: 1993. Summary of Logging Activities. KTB Report 93-1, Hannover.

Eberle, D.: 1992. Interpretation of multi-method geophysical borehole logging data from KTB Oberpfalz VB using multivariate statistical analyses. Scientific Drilling, Vol. 3, 16-26.

Ellins, M. & Tran Viet, T.: 1990. Spülungskonzept und Mud Logging-System für die KTB-Hauptbohrung. Erdöl Erdgas Kohle, 106, 12, 491-495.

Emmermann, R. & Wohlenberg, J. (eds): 1989. The German Continental Deep Drilling Programm (KTB). Springer, Heidelberg.

Emmermann, R.; Dietrich, H.-G.; Lauterjung, J. & Wöhrl, Th.: 1990. Results of Geoscientific Investigation in the KTB Field Laboratory - 0-4000,1 m. KTB-Report 90-8, A1-A23, Hannover.

Emmermann, R.: 1991. KTB 10000. Vortrag, 4. KTB-Kolloquium 25. - 27.04.1991, Gießen.

Engeser, B.: 1990. The Coring Strategy for the Main Well. Oil Gas 16, 4, 36-41.

Engeser, B., Huenges, E., Kessels, W., Jück, J. & Wohlgemuth, L.: 1993. The 6000 m hydrofrac test in the KTB main borehole design, implementation and preliminary results. KTB Report 93-1, Hannover.

Figgemeier, Ch.; Machon, L.; Kamm, H., Hansmann, J., Gleiß, N., Umsonst, T. & Zimmer, M.: 1992 (eds). Results of Geoscientific Investigation in the KTB Field Laboratory - 0-6000 m, KTB Report 92-2, C1-C45, Hannover.

Gatto, H. & Lauterjung, J.: 1990. Quantitative and Qualitative Determination of Minerals in Crystalline Rocks. Transactions, 13th European Formation Evaluation Symposium, N1-N19, Budapest.

Gatto, H.: 1992. Relationen zwischen Konzentration, Aktivität und Wärmeproduktion von natürlichen Radioaktiven Isotopen (eds). KTB Report 92-1, 215-217, Hannover.

Gatto, H.: 1993. Determination of Elements through Geochemical Logging in Crystalline Rocks. KTB Report 93-1, Hannover.

Hänel, R.: 1986. Logging strategy for the KTB. Paper presented at the 2nd KTB-Kolloquium, Sept. 19-21, 1986, Seeheim.

Hirschmann, G.: 1992a. The Geological Section of the KTB Hauptbohrung - Correlation with the KTB Vorbohrung and Preliminary Structural Interpretation (eds). KTB-Report 92-2, B47-B52, Hannover.

Hirschmann, G.: 1992b. On the Geological Interpretation of the 3-D-Seismic Data with Special Regard to the Information from the KTB Boreholes. KTB Report 92-5, 351-373, Hannover.

Hirschmann, G. & Kück, J.: 1993. KTB Hauptbohrung - relations between the borehole deviation and the geological sructure. KTB Report 93-1, Hannover.

Jobmann, M. & Schulz, R.: 1992. Temperatures, fractures and heat flow density in the pilot-hole of the Continental Deep Drilling Project (Oberpfalz, Germany). Scientific Drilling, Vol. 3, 83-88.

Kessels, W.: 1988. Fehlerbetrachtung zur Bestimmung von Bohrlochorientierung und Orientierung der Kalibermeßsonde mit einer Pendelanordnung. KTB Report 88-11, 475-503, Hannover.

Kessels, W.: 1990a. Tough Logging in der KTB-Hauptbohrung. Interner Bericht der KTB-Projektleitung (unpublished).

Kessels, W.: 1990b. Auslegungsrechnungen zum Einsatz eines Bohrlochmeßkabels in der KTB-Hauptbohrung. BGR/NLfB, Archiv-Nr. 106 817, 28 S., Hannover (unpublished).

Kessels, W.: 1991. Design calculations for the application of a well logging cable in the main KTB borehole. Scientific Drilling, Vol. 2, No. 4, 215-229.

Kessels, W. & Kück, J.: 1992. Computer-aided matching of plane core structures with borehole measurements for core orientation. Scientific Drilling, Vol. 3, 225-238.

Kessels, W., Kück, J. & Zoth, G.: 1992. Hydraulische Untersuchungen in der Bohrung KTB-Oberpfalz HB bis 5000 m (eds). KTB Report 92-1, 169-197, Hannover.

Kessels, W. & Kück, J: 1993. Hydraulic communication of the crystalline rocks between the KTB boreholes. KTB Report 93-1, Hannover.

Kohl, R., Kück, J., Sigmund, J. & Wöhrl, Th.: Bohrkernorientierung und Teufenkorrelation der KTB Vorbohrung. KTB Report 91-3, F1-F22, Hannover.

Krammer, K. & Pohl, J.: 1990. Das Suszeptibilitätslog der Bohrung KTB-Oberpfalz VB von 27 bis 3980 m (eds). KTB Report 90-6a, 119-134, Hannover.

Krammer, K. & Pohl, J.: 1991. New tools for measuring the magnetic susceptibility in deep drill holes. Scientific Drilling, Vol. 2, No. 4, 188-196.

Kück, J.: 1993. The rapid data presentations BGLQUICK and MUDQUICK. KTB Report 93-1, Hannover.

Kuhnke, F. & Musmann, G.: 1991. KTB high temperature triaxial magnetometer. Scientific Drilling, Vol. 2, No. 4, 166-179.

Lich, S., Duyster, J., Godizart, G., Keyssner, S. & de Wall, H.: 1992. German Continental Deep Drilling Programm (KTB) - Geological Survey of the Hauptbohrung 0 - 6000 m (eds). KTB Report 92-2, B1-B42, Hannover.

Lüschen, E.L., Söllner, W., Hohrath, A. & Rabbel, W.: 1990. Integrated P- and S-Wave Borehole Experiments at the KTB-Deep Drilling Site (eds). KTB Report 90-6b, 85-134, Hannover.

Mastin, L.G., Heinemann, B., Krammer, A., Fuchs, K. & Zoback, M.D.: 1991. Stress orientation in the KTB pilot hole determined from wellbore breakouts. Scientific Drilling, Vol 2, 1-12.

Pechnig, R. & Wohlenberg, J.: 1993. EFA-LOG - The upper 3 km of the KTB-Hauptbohrung. KTB Report 93-1, Hannover.

Pribnow, D., Bücker, Ch., Rauen, A., Spangenberg, E., Wienand, J. & Soffel, H.C.: 1992. KTB Hauptbohrung, Geoscientific Investigations in the KTB-Field-Labo-ratory, Depth Interval 0-6000 m (eds). KTB Report 92-2, D1-D42, Hannover.

Rabbel, W.: 1992. Seismic Anisotropy at the KTB Deep Drilling Site. 275-289, KTB Report 92-5, Hannover.

Rühl, T. & Hanitzsch, C.: 1992. Average and Interval Velocities Derived from First Breaks of Vertical Seismic Profiles at the KTB Pilot Hole. KTB Report 92-5, 201-219, Hannover.

Sass, J.H. & Elders, W.A.: 1986. Salton Sea Scientific Drilling Project: Scientific Program. Geoth. Res. Council, Transactions, 10, 473-478.

Schepers, R.: 1991. Development of a new acoustic borehole imaging tool. Scientific Drilling, Vol. 2, No.4, 203-214.

Schmitz, D.: 1988. Zur Methodik der Kernorientierung. KTB Report 88-7, 153-155, NLfB, Hannover.

Schmoll, J., Bittner, R., Dürbaum, H.-J., Heinrichs, T., Meißner, R., Reichert, C., Rühl, T. & Wiederhold, H.: 1989. Oberpfalz Deep Seismic Reflection Survey and Velocity Studies. In: Emmermann, R. & Wohlenberg, J. (eds): The German Continental Deep Drilling Program (KTB), 99-150, Springer, Heidelberg.

Söllner, W., Lüschen, E., Li, X.-P., Hubral, P., Gut, T.W. & Widmaier, M.: 1992. VSP - A Link between Reflection Seismic Profiling and Lithology. KTB Report 92-5, 169-199, Hannover.

Soffel, H.C., Bücker, Ch., Gebrande, H., Huenges, E., Lippmann, E., Pohl, J., Rauen, A., Schult, A., Streit, K.M. & Wienand, F.: 1992. Physical Parameters Measured on Cores and Cuttings from the Pilot Well (0 m - 4000,1 m) of the German Continental Deep Drilling Program (KTB) in the Oberpfalz Area, Bavaria, Federal Republic of Germany. Surveys in Geophysics 13, 1-34.

Sowa, M.: 1992. Archivierung von Bohrlochmeßdaten der KTB-Oberpfalz HB (eds). KTB Report 92-1, 21-26, Hannover.

Stoll, J., Aulbach, E., Bigalke, J. & Winter, H.: 1992. Die Eigenpotentialmessungen in der KTB-Oberpflaz VB und HB im Vergleich mit Messungen der induzierten Polarisation, des elektrischen spezifischen Widerstandes und Graphit- und Pyritmineralisationen. KTB Report 92-1, 253-286, Hannover.

Stoll, J.: 1993. A Mise-á-la Masse experiment for detecting an electric network in cataclastic zones around the KTB-site. KTB Report 93-1, Hannover.

Sturmeit, K.D.: 1993. SEL - A computer program to manage and present data of downhole measurements. KTB Report 93-1, Hannover.

Wolfgram, P.A., Casten, U., Gatto, H., Neubauer, F.M, Richter, J.E.T. & Strack, K.-M.: 1992. Interpretation of borehole gravity data from the German Continental Deep Drilling Project. Scientific Drilling, Vol. 3, 70-75.

Zoth, G.: 1990. Test des LASL-Fluidprobennehmers im Hinblick auf den Einsatz in der Hauptbohrung (eds). KTB Report 90-6a, 343-350, Hannover.

Zoth, G.: 1992. Bohrlochmeßprogramm Geothermie: Ergebnisse, Erfahrungen und Folgerungen für die nächste Meßkampagne (eds). KTB Report 92-1, 227-235, Hannover.

Zoth, G.: 1993. The Logging Center. KTB Report 93-1, Hannover.

Zoth, G.: 1993. Temperature measurements during the 6000 m logging campaign. KTB Report 93-1, Hannover.

2. Logging Center

G. Zoth

2 LOGGING CENTER

G. Zoth

2.1 Introduction

The Logging Center (LC) contributes significantly to the overall objectives of the Continental Deep Drilling Programme of the Federal Republic of Germany (KTB). The ambitious nature of these objectives makes it a very cost intensive research project. Therefore, planning for its technical implementation particular attention has to be paid to cost minimization of time-intensive repetitive tasks such as:

- drilling: automatic pipe handling system to minimise the round trip costs

- sampling: automatic sampling system to save personnel costs

- borehole logging: cable guide system to save derrick time.

In the early planning stage an economy study turned out already, that purchase and operation of an own logging unit, including technical assistance by the appropriate service industry, is the most economic solution.

This concept proved to be very efficient while drilling the KTB pilot hole, the Vorbohrung. When the KTB superdeep drillhole, the Hauptbohrung, was spudded on October 6, 1990, this concept was extended to a Logging Center comprising a technical and an office unit. It is located 60 m north to the Hauptbohrung outside the drill site's EX area and consists exclusively of containers. The logging unit itself and the working area are covered by a tent (Fig. 2.1 and 2.2).

Log quality control, evaluation and presentation of logging data, operation, testing and maintaining all of the necessary equipment are the key responsibilities of the Logging Center.

In the following a description of the LC is given:

Author's address:
Niedersächsisches Landesamt für Bodenforschung, KTB-Projekt,
P.O. Box 510153, 30631 Hannover, Germany

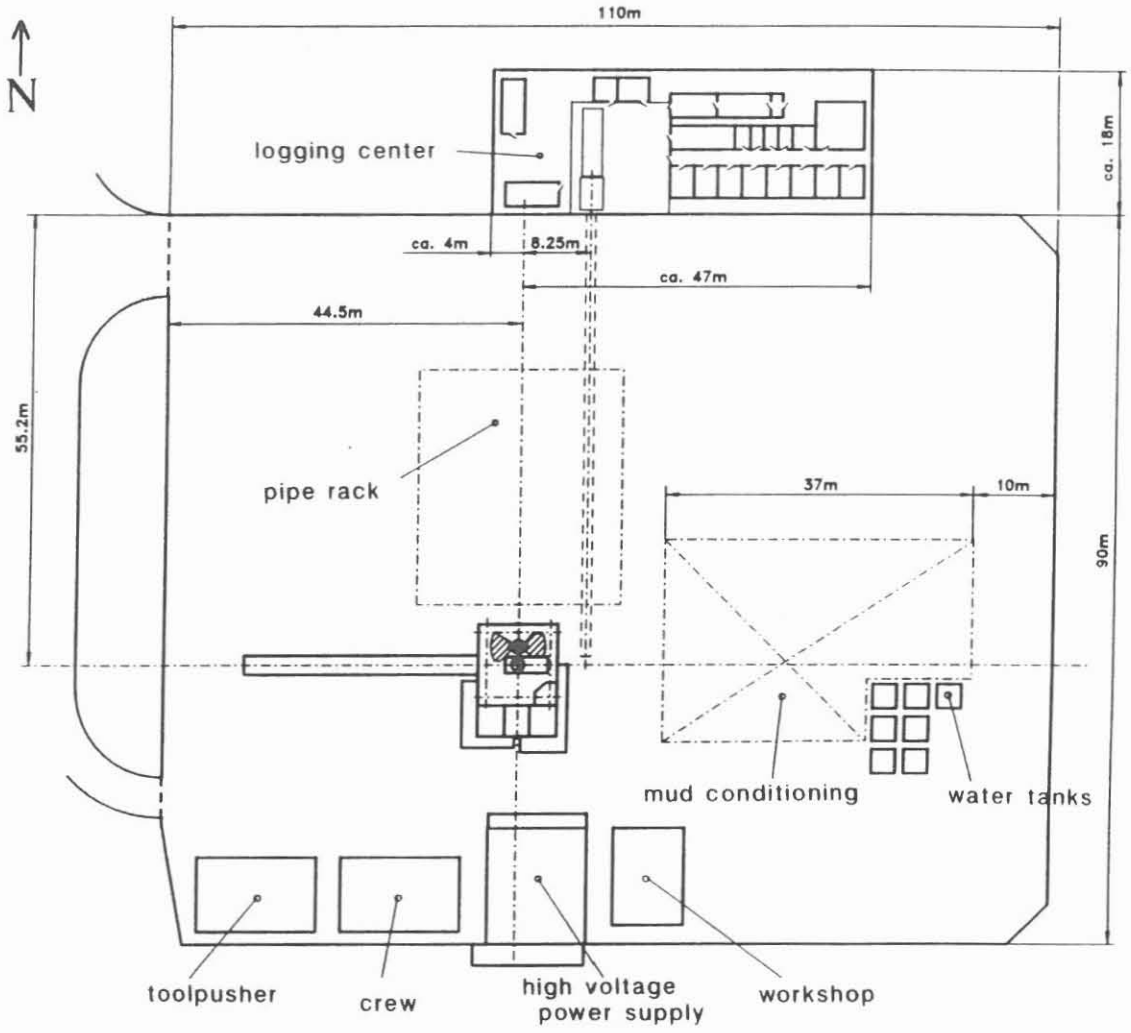

Fig.2.1: Overview, installation of drilling location

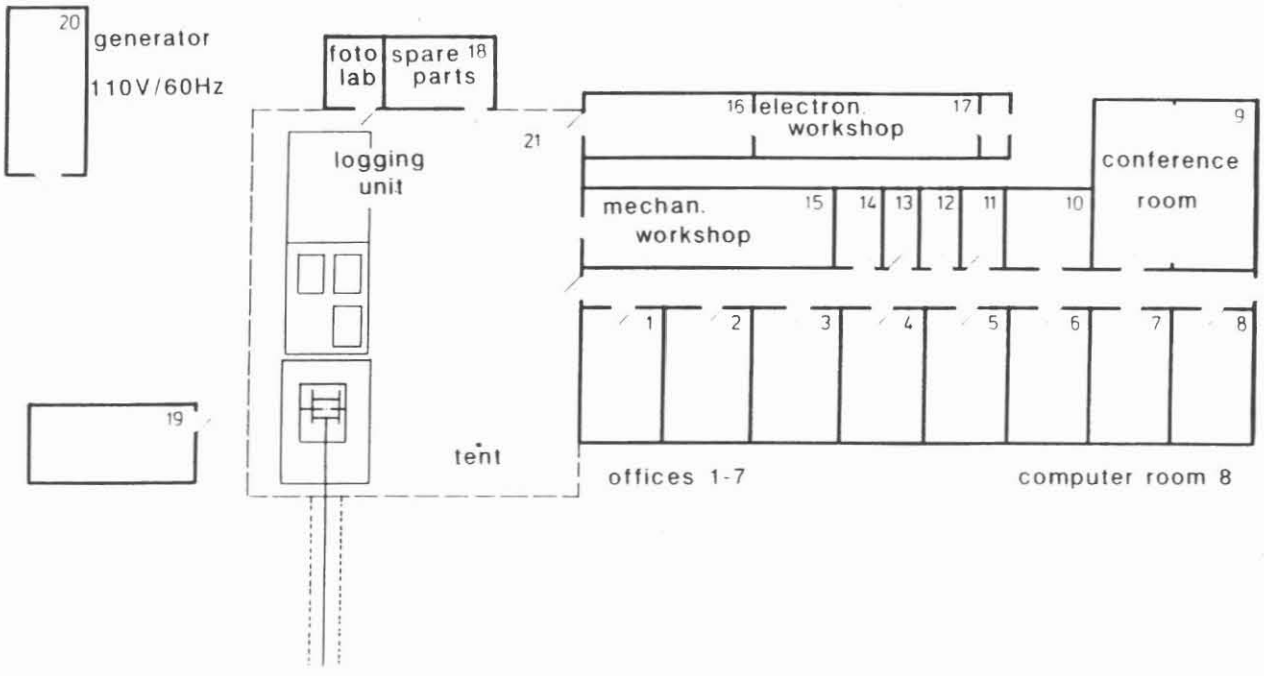

Fig.2.2: Overview, logging center

2.2 Technical unit

The technical unit consists of the logging unit, the logging equipment and various workshops. Logging down to 10,000 m and the expected extreme temperature and pressure conditions at this depth needs a carefully planned and thoroughly designed logging installation. Its various components and technical details are described below.

2.2.1 Cable guidance to the derrick

The conventional cable guidance system for borehole logging is shown schematically in Fig. 2.3. The rigging up and down of the cable, the guide blocks and the logging tools conventionally takes a total of approximately two hours derrick time. Additional time is often required for testing the tools prior to running them into the hole.

In order to optimize rigging up and down times for the KTB-Hauptbohrung a particular system was designed allowing for:

1. - keeping the cable in the derrick

2. - being able to rig up the logging tools in the derrick while drilling continues

3. - being able to test the tools without interfering with the work in the derrick

4. - being able to run the tools into the borehole with minimum technical effort as soon as the rig is cleared for logging.

Leaving the cable permanently in the derrick, the cable must be laid out in such a way that its part between the cable winch and the derrick neither hinders the operation in the drilling area nor itself becomes damaged as a result of ongoing non-logging activity. A solution was finally adapted which places cable and cable winch underground (Fig. 2.4) (Zoth, 1991).

The following special equipment and work was required to put the above into practice.

- Winch cellar

The cable winch had to be installed in a cellar deep enough to allow the cable to run to the derrick underneath the drilling area in a cable tunnel.

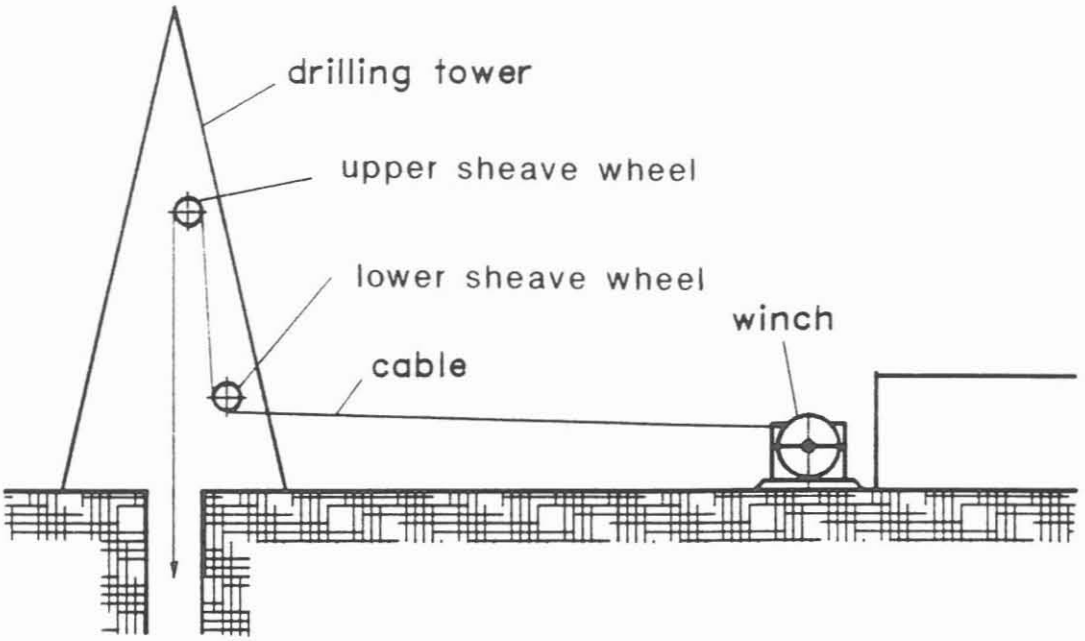

Fig. 2.3: Conventional Cable Installation

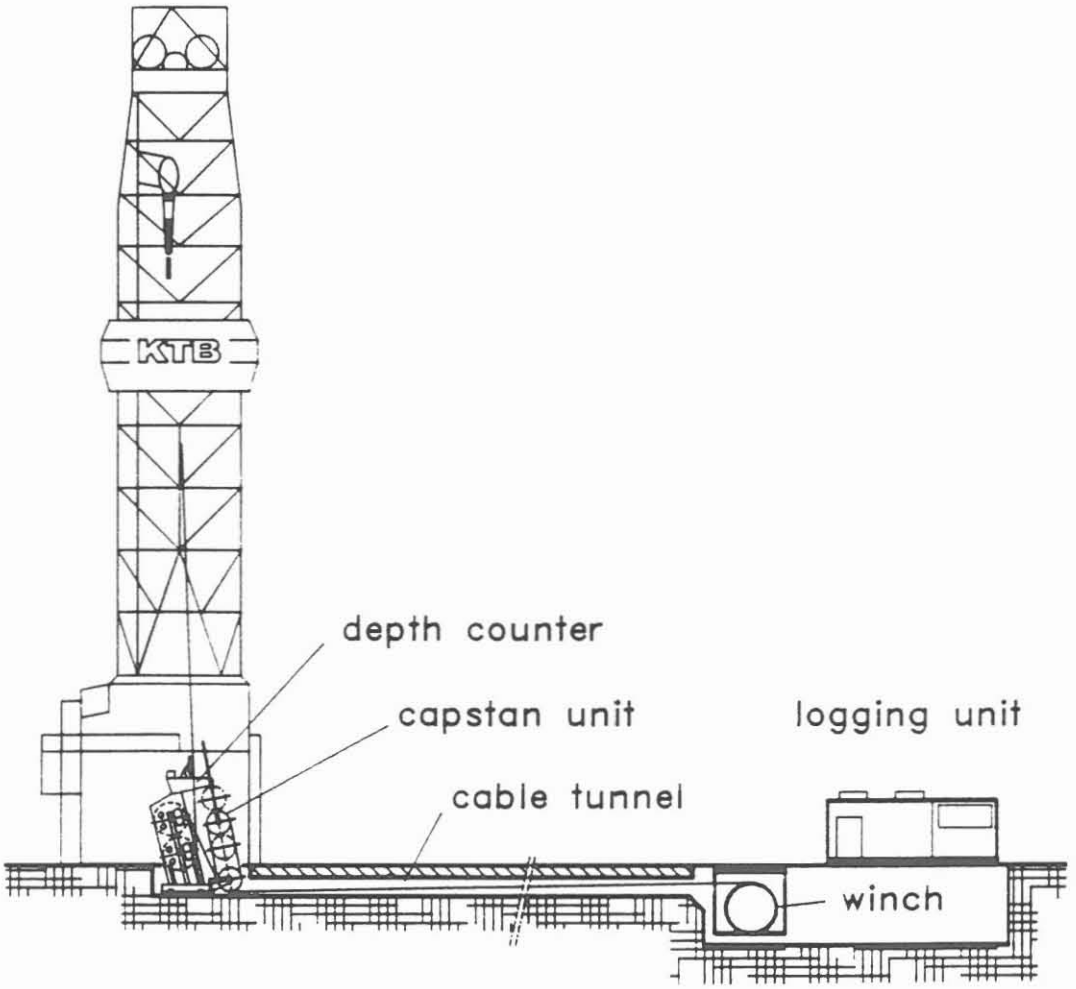

Fig. 2.4: KTB–Logging System, Installation for Cable Guidance

- Cable tunnel

The cable tunnel running from the winch cellar to the eastern side of the derrick has a length of 55 m, a height of 0.6 m and a width of 1.1 m. The height is determined by the maximum winding height of the winch drum and the width is determined by the maximum drum winding width. This guarantees that the cable can be wound in and out freely and without any additional guidance.

Two plastic pipes with diameters of 200 mm run parallel to the tunnel. They contain the supply cables for telecommunications, for visual monitor control, a tensiometer cable, a borehole logging cable for tool testing in the derrick and finally the power and control cables for the operation of the capstan unit.

At end of the cable tunnel a capstan unit (see section 2.4) is located within the approximately 3 m x 1 m opening. From the capstan unit the logging cable goes up to the top guide block located outside of the derrick, 31 m above the capstan unit. From here the logging cable goes into the derrick to the upper sheave wheel, located on a retractable arm.

- Retractable arm

The retractable arm (Fig. 2.5) swings the upper sheave wheel out over the drill floor during logging (Pos. 1), and after logging swings back into its resting position (Pos. 2) where it does not hinder drilling activity. In the resting position, the upper sheave wheel can be loaded up to a maximum of 1500 daN. In its extended position, the retractable arm can be loaded up to 15000 daN. The upper sheave wheel lies approximately 27 m above the drill floor being high enough to maneuver long logging tools into the borehole.

Up to 3 tools with an individual length of approx. 8 m can be stored in the "tool magazine" above the drill floor. This allows logging tools to be pulled up to the drill floor, tested and prepared ready for logging even during drilling activity. As soon as the borehole has been cleared for logging the tool is swung out over the borehole and run in without any delay.

- Cost savings calculations

Fig. 2.6 shows the cost savings that are possible by removing the log run rigging up and down times. The abscissa in the diagram represents the savings in hours and days while the ordinate represents the savings in DM. Straight lines show the rig costs at day rates of 80,000 DM/day, 100,000 DM/day and 150,000 DM/day. With a calculated saving of only one hour per log run at a day rate of 150,000 DM,

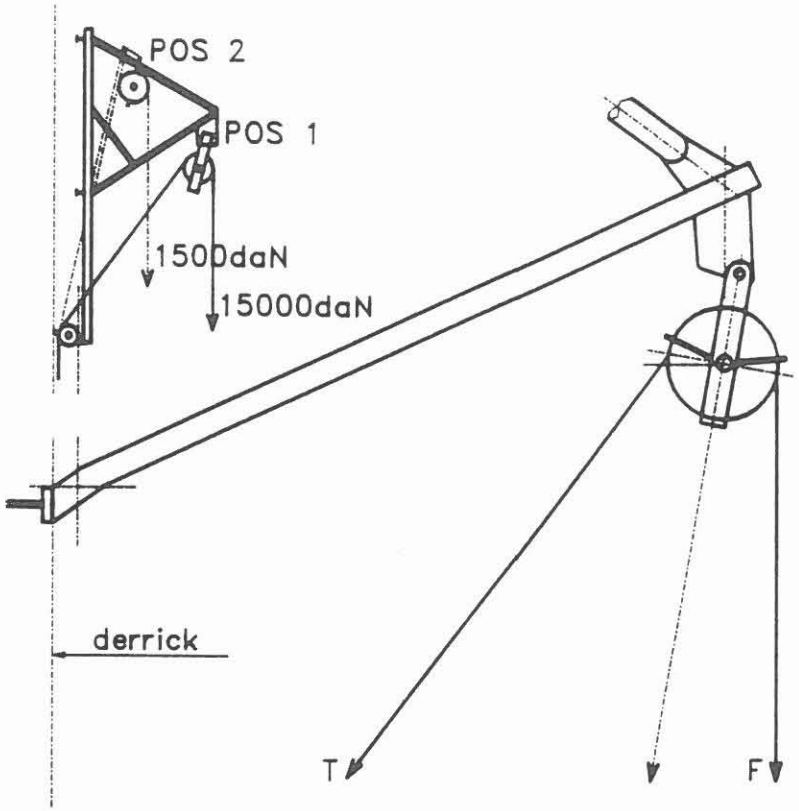

Fig. 2.5: Retractable arm,

Pos.1 - logging position

Pos.2 - resting position

T - max. pulling load

F - effective load

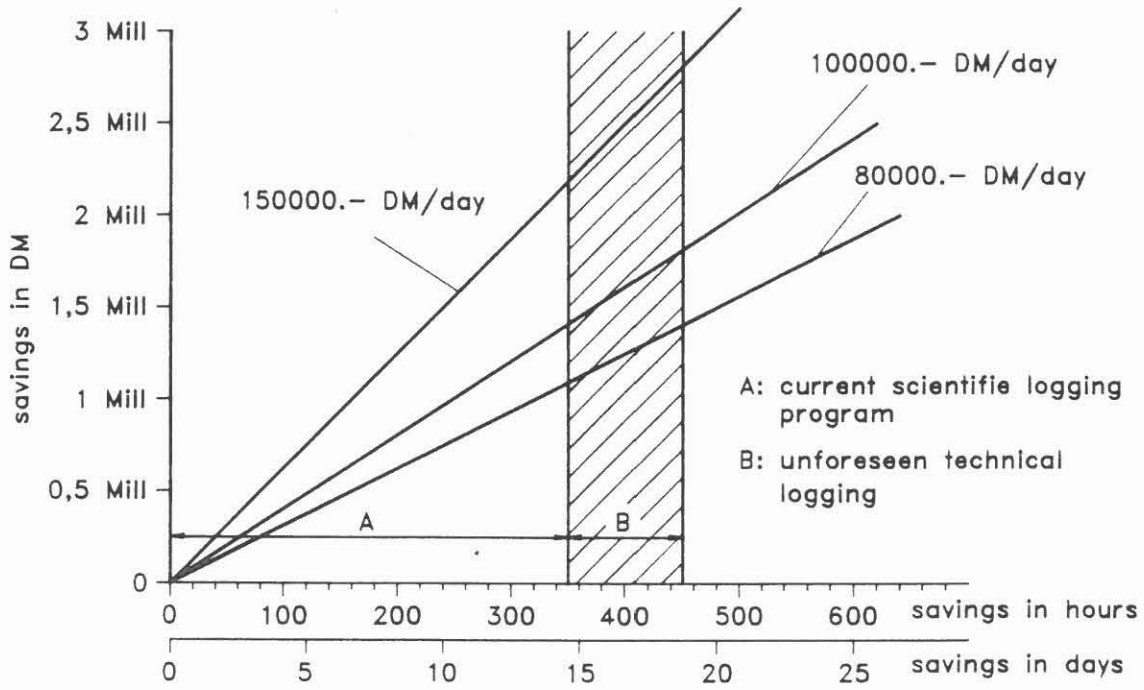

Fig. 2.6: Cost savings calculations

the complete set of logs of the current logging program down to total depth gives a saving of approx. DM 2.2 million.

2.3 Cable winch

Down to a depth of 6000 m, a conventional cable winch was used.

The hydraulic motor drive of the cable winch is transferred via a chain and appropriate gearing to the drum axle giving infinately variable logging speeds between 0.5 - 250 m/min.

The capacity of the cable drum was 7500 m when used together with the 7-46V type cable. With regard to the needs for logging deeper than 6000 m, modifications of the cable winch and drum were necessary. The drum had to be replaced in order to carry a special cable (see section 2.6 - Logging cable) with a total length of 9100 m. In addition, the winch had to be modified accordingly to take account of the increased bulk of the cable and the dimensions of the new drum.

2.4 Capstan unit

In order to cope with the increased loads associated with a longer and heavier borehole logging cable, it was necessary to install a capstan unit.

The capstan unit is intended - at logging depths deeper than 6500 m - to take up the tensile forces handled at shallower depths by the winch. The capstan unit consists of two drums in series each containing five inset running grooves, that act as the cable seat and must be customised exactly to the size of the logging cable. The five-fold winding of the cable over the two drive wheels transfers the frictional force onto a cable length of approx. 34 m thus spreading the load. This protects the logging cable and avoids the development of kinks and other damage that may occur with a conventional cable drum. With the capstan unit the cable winch is in effect transformed into a cable storage drum.

Each of the capstan unit drums is driven by two hydraulic motors. The hydraulic power is generated by the power unit situated directly adjacent to the capstan unit.

The capstan unit is anchored to supports concreted-in to the cable tunnel (Fig. 2.7). Each of the supports is designed to bear a tensile force of 25,000 daN.

Capstan Unit

(KTB - Logging System)

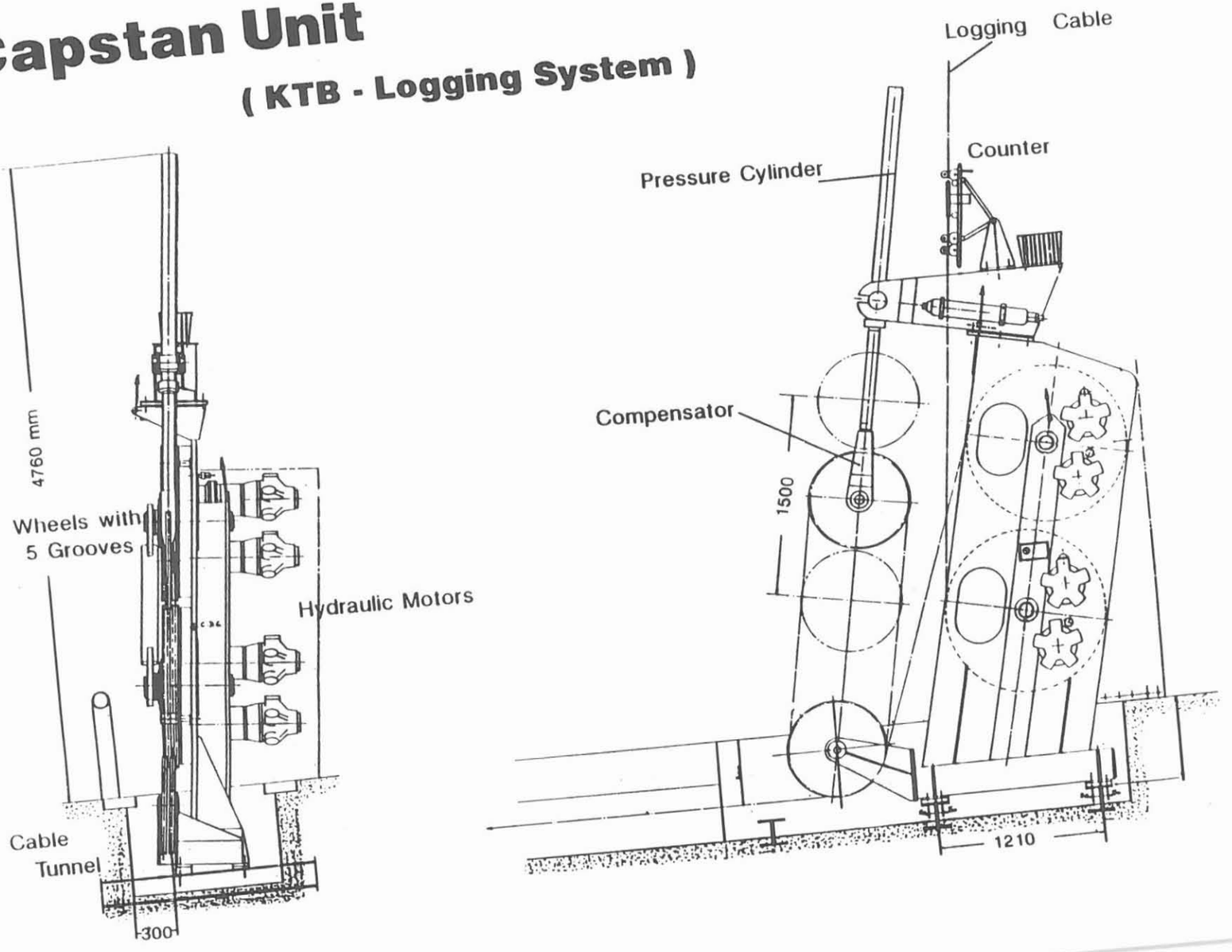

Fig. 2.7

Table 2.1: Capstan unit specifications

Max. tensile force	: max. dynamic 9000 daN : max. static (braking) 10,000 daN
Running speed	: max. 100 m/min : min. 1 m/min
Capstan drums	: 2 drums, OD = 1180 mm each 5 cable grooves per drum
Drive	: 2 hydraulic motors per drum Vickers Staffa HMB.-030 Q = 442 cm^3/rev.
Gears	: 4 x transmittal Bonfiglioli 306L1-3H planet gears with integral brakes ratio 1 : 3.6

- Compensator

The capstan unit is fitted with a hydraulic compensator. The purpose of this system is to ensure that the mass acceleration force of the running cable winch does not damage the logging cable between the winch and the capstan unit in the event of a sudden stop.

Fig. 2.8 shows schematically the compensator's working. Two pressure vessels are connected directly to the compensator cylinder in a closed system. The nitrogen reserve in the pressure vessels keeps the piston in its upper resting position. Before logging operations, a tension of approx. 700 daN - 1000 daN is manually set between the capstan unit and the cable drum and kept constant during the operation. This results in a piston stroke of approx. 750 mm. With a maximum available stroke of 1500 mm, this means that ~ 750 mm is available to compensate for sudden tensional loading.

- Tension control

The tension between the capstan unit and the cable winch is controlled dependent on the diameter of the cable wound onto the cable drum. Fig. 2.9 shows the monitoring and control principle. The measured value of the wound cable diameter is transferred directly to a potentiometer via a measuring arm resting on the outside of the wound cable. The changes in resistivity of the potentiometer controls the hydraulic drive system and thus the tension. The control signal for the electronic control of the tension is generated via a load sensor fitted to the axle of the lower capstan wheel.

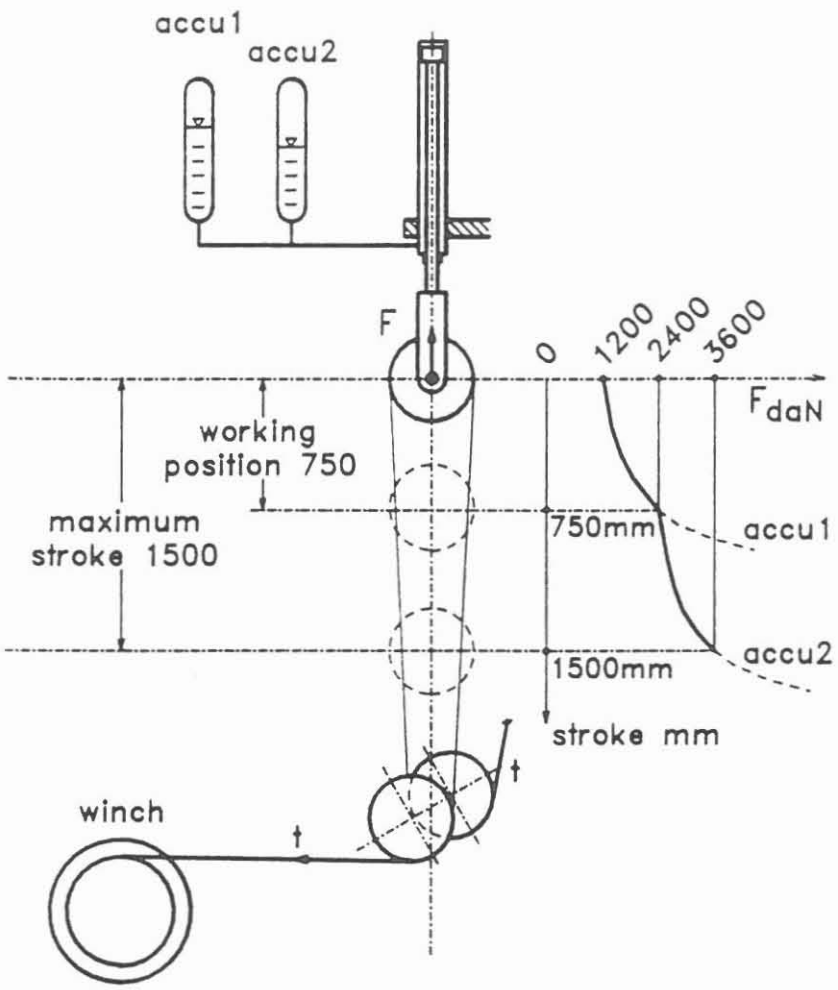

Fig. 2.8: Tension compensator on capstan

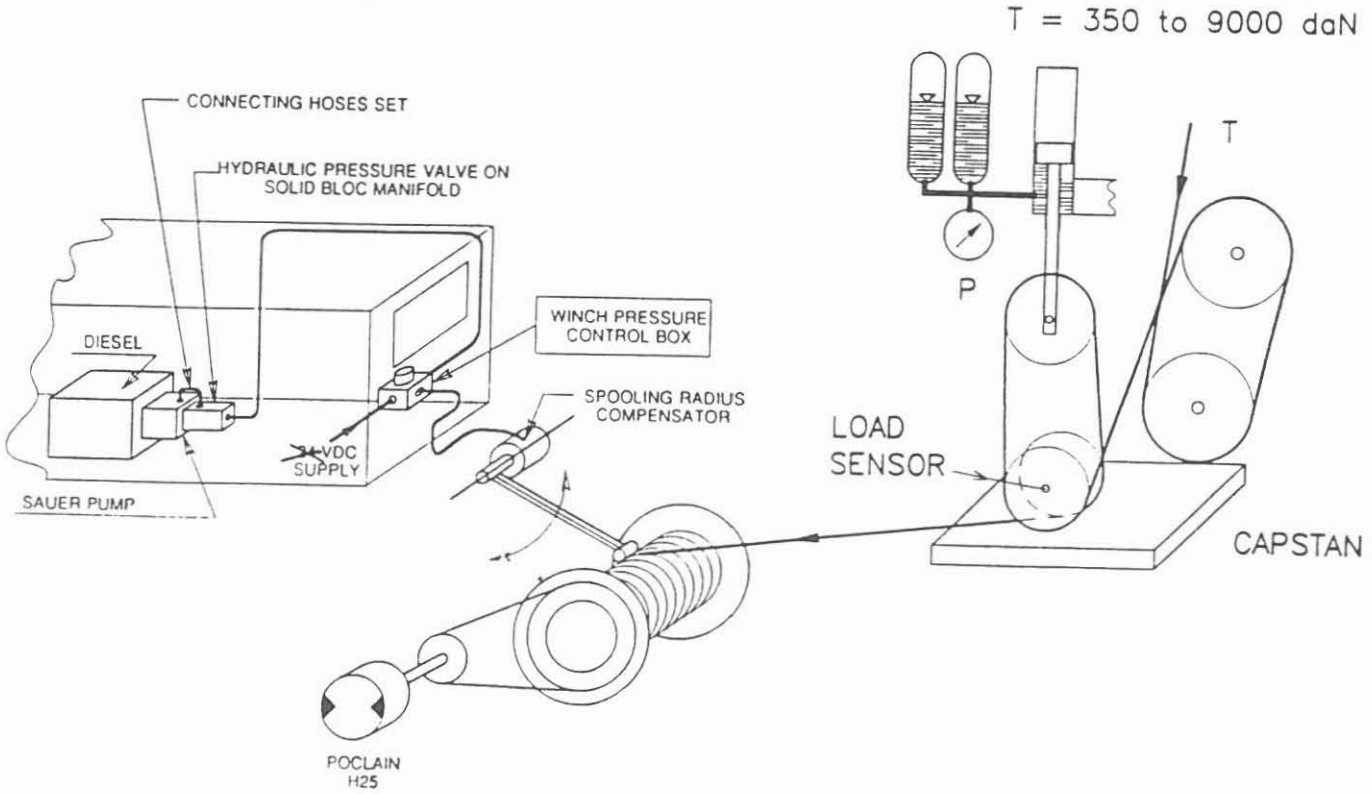

Fig. 2.9: Tension regulation system

- Hydraulic power unit

The hydraulic power unit for the capstan has built-in redundancy provided by an electric motor (ME1) with a through axle (Fig. 2.10). Each end of the axle is connected to a hydraulic pump (P1 and P4). Both pumps provide power in parallel to the capstan unit hydraulic drive system. Should one of the pumps fail, then approximately half of the power is still available for an emergency run. The power specification of the electric motor is 220 kW. The electric motor meets the EX regulations: protection category EExdIICT4. The power supply is designed to be compatible with the 660 V/50 Hz drilling rig power supply. All other electric cables are also connected to the rig's electric power supply.

Table 2.2: Hydraulic power specifications

Electric motor	:	CEN, model HAQ315LZ4 power: 220 kW voltage: 660 V, 50 Hz
Hydraulic pumps	:	2 x Mannesmann-Rexroth, type A3VSG (axial reciprocating pumps) Q = 310 l/min P = 250 bar
Charge pumps	:	2 gearwheel pumps Mannesmann-Rexroth, model 1PF2G3 Q = 53 l/min
Tank capacity	:	600 l
Oil coolers	:	2 cooling capacity 2 x 40 kW (136 l/min) 2 cooling fans 0.75 kW.

- Upper sheave wheel and tensiometer

The upper sheave wheel had to be designed to withstand the increased tensile forces associated with the unusually high cable loads. The maximum loading capacity on the hangers is 24,000 daN. This means that a cable tension of approx. 14,000 daN is possible. This is approx. 5000 daN higher than the maximum tensile force of the capstan unit (Table 2.1).

In contrast to conventional logging systems where the sensor measuring the logging cable tension is located in a special housing above the upper sheave wheel, the sensor here is located within the upper sheave wheel - on its axle. The data is transmitted via a shielded cable to the data acquisition unit (Fig. 2.11).

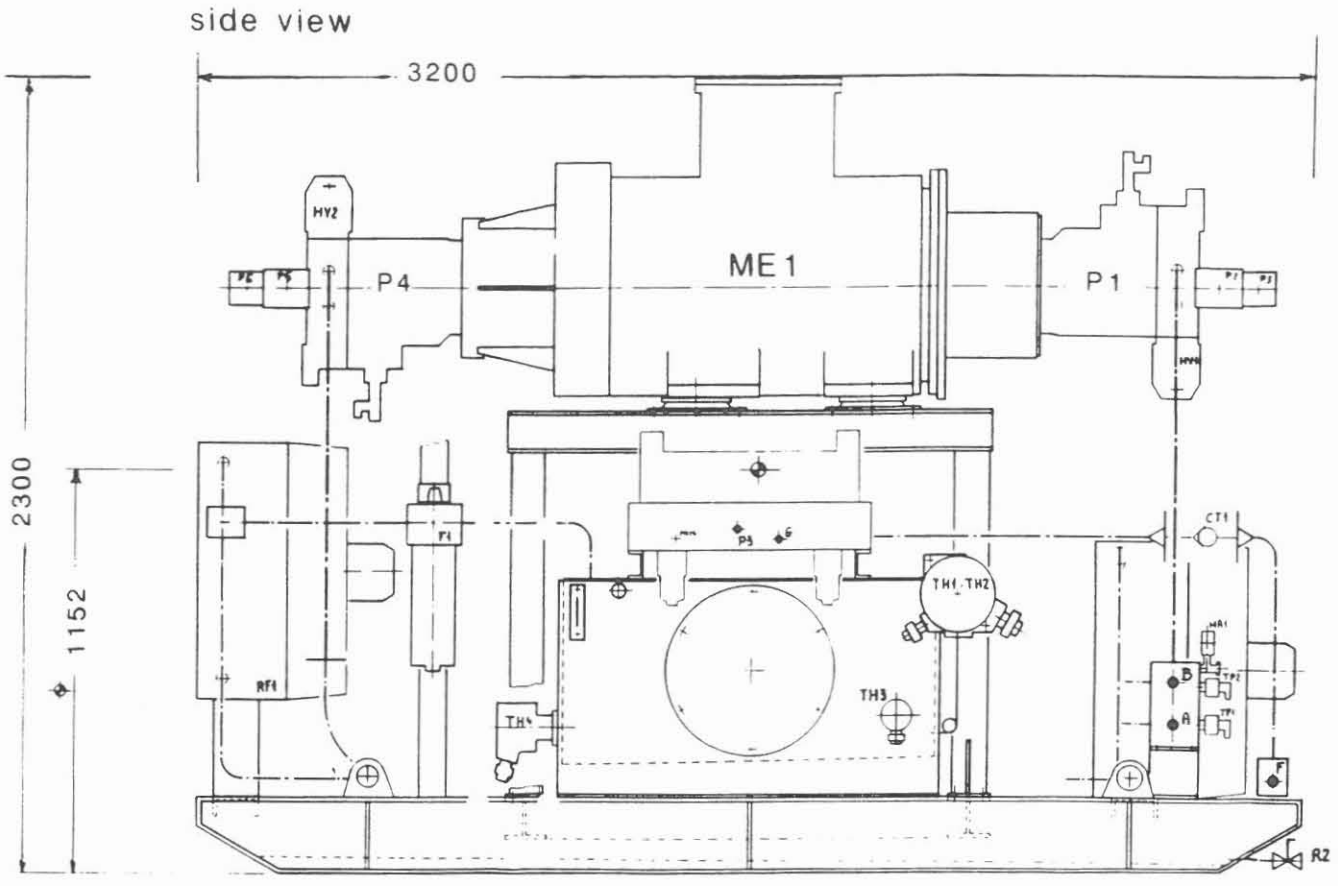

Fig. 2.10: Hydraulic power station

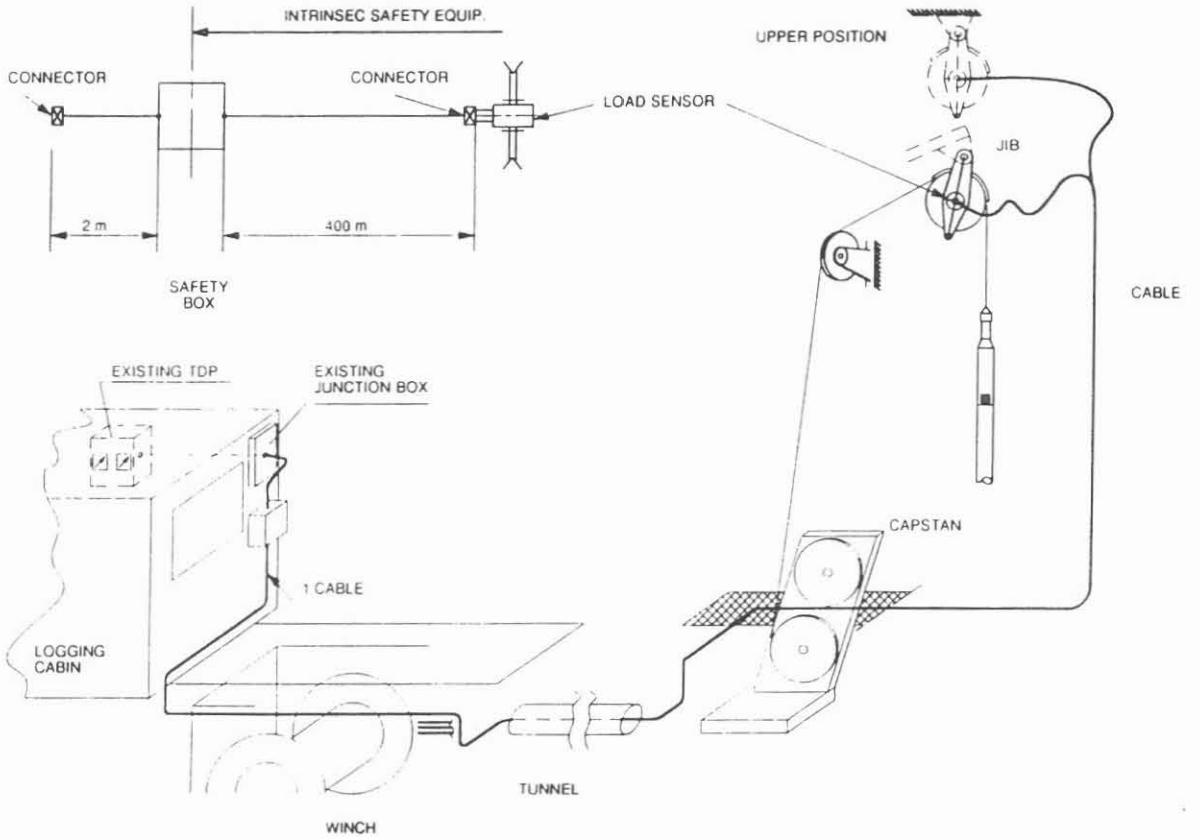

Fig. 2.11: Tension "T" masurement set up

Table 2.3: Upper sheave wheel specifications

total height	:	1680 mm
max. width	:	310 mm
wheel diameter	:	1135 mm
groove width	:	13.22 mm
maximum pull	:	28,000 daN
weight	:	200 daN

- Depth counter

The depth counter consists of two springloaded measuring wheels running on the cable. The axles of the measuring wheels are connected directly with revolution encoders. The encoder log impulses are transmitted to the data acquisition unit. The logging cable runs through the measuring wheels in such a way that guiding is exclusively tangential (Fig. 2.12). The measuring accuracy is given as ~ 0.3 m/1500 m log depth. The depth counter is located above the capstan unit because this is where the cable is under greatest tension thus guaranteeing optimal depth measurement. Fig. 2.13 shows schematically the position of the depth counter (IDW-E) and the cable path to the data acquisation unit.

2.5 Logging unit

The KTB's own logging unit comprises all the equipment required for carrying out borehole logging. The main parts, consisting of the logging cabin, power supply unit and cable winch are covered by a protective tent.

2.5.1 Logging cabin

The logging cabin contains the control panel operating the winch, the data acquisition unit (Cyber Service Unit - CSU) and all other operating and monitoring equipment required for logging. The cabin contains work places for the operator controlling the cable winch, and for the logging engineer who is responsible for logging and operation of the CSU.

The operator cannot look onto the disguised drill floor situated 60 m away and 11.8 m above ground. In order to guarantee the smooth running of the logging operation it was therefore necessary to fit monitoring cameras in the derrick and at the capstan unit and link them to two monitors in the logging cabin. A conventional two-way intercom system and a radio link via headphones are available for communication between the logging cabin and the drill floor. For redundancy two telephone lines are available too. From the operator's control panel cable winch and capstan unit can be monitored and safely operated as well as the motors and the generator located in the power cabin.

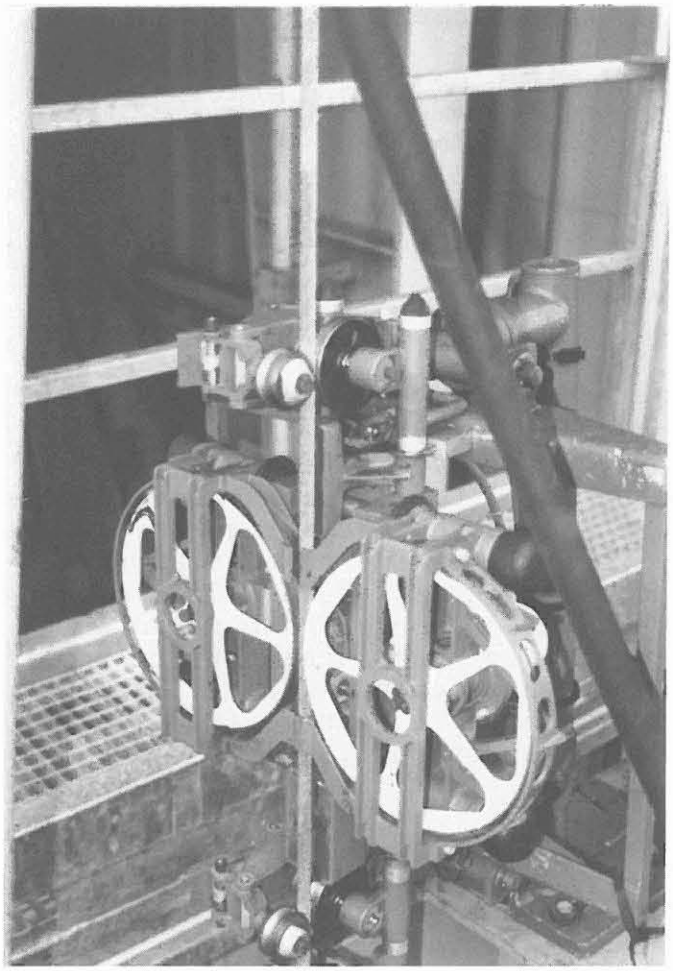

Fig. 2.12: Depth counter "IDW-E", - explosion proof equipment.

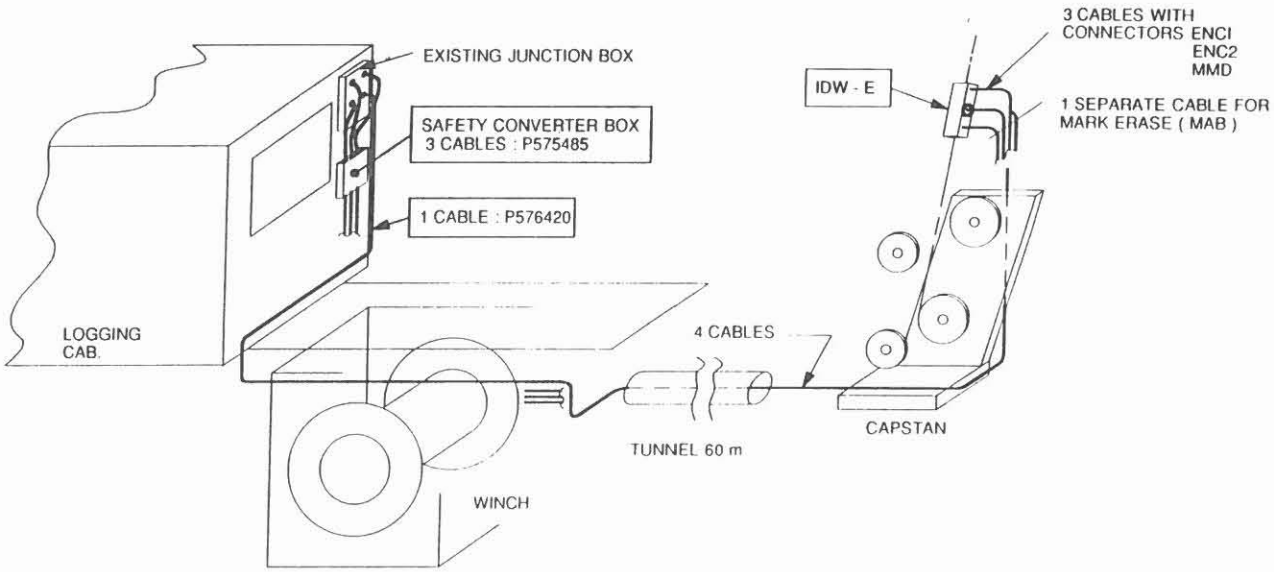

Fig. 2.13: Depth counter "IDW-E", - cable set up -

In contrast to the logging unit, which was purchased, the CSU is rented from Schlumberger. The kernel of the unit comprises two PDP 11/84 computers - one for normal operation and the second available as back-up.

The unit also comprises:

- a high density tape drive (1600 BPI) for digital log data recording in LIS format (log information standard format),
- three cassette tape drives to load the programs and record data
- two disks for recording logging data,
- a monitor for visual display of the logging results,
- an oscilloscope module for monitoring the electrical signals transmitted via the cable,
- two optical recording devices for recording the log data on films,
- a cable interface module,
- several panel-interface modules,
- a printer for paper and film printouts of the logging results,
- other plug-in units and operating equipment for running the unit and controlling the logging tools (e.g. voltage and power regulators, depth counter monitor etc.).

The logging engineer's workplace is also fitted out with a Compaq computer for communicating with the logging computer. The unit is only operated by Schlumberger personnel.

The digital log signals can be transmitted immediately out of the unit to any fax equipment via a telephone line.

2.5.2 Power supply

Power for safe logging operations is supplied by independently working Diesel engines and, if needed, via a frequency converter by the public main power network. The Diesel engines are installed in a sound insulated container - the power cabin - reducing the noise level to less than 40 dBA at 100 m distance. The frequency converter is placed in an extra container. Tables 2.4 and 2.5 give technical specifications of that equipment and Table 2.6 lists its operating times.

Table 2.4: Equipment in the power cab

- driving unit for hydraulic pressure generation
  - 6 cylinder in-line motor, diesel OM 353 A turbo compressor, water cooled
  - power: 106 kW at 2800 rpm

- hydraulic pump
  - max. 2900 rpm
  - max. working pressure: 420 bar (42 MPa)

- electricity generator
  - 2 cylinder diesel motor, air cooled
  - power: 14.6 kW, for short periods 16.2 kW
  - generator I: 110 V/60Hz, 16 kVA
  - generator II: 28 V, 55 A

- air compressor

Table 2.5: Frequency converter specifications

Threephase AC-synchron motor and generator (both located on one frame)

- input : 380 V - 50 Hz
- output : 110 V - 60 Hz, without neutral point
  - voltage : ± 2%
  - frequency : ± 1%
  - power : 34 - 36 kVA, cos phi = 0.8

All maintenance work and minor repairs to the equipment and machines are carried out by own staff.

Table 2.6: Equipment operating times from 01.08.1987 to 31.12.1992

Equipment	time in hours
hydraulic drive	3952 h
converter	4509 h
generator	4443 h
CSU	8591 h

2.6 Logging cable

Logging cable for depths to 6000 m

Logging down to 6000 m should have been performed using a standard 7-conductor logging cable of type 7-46V. The original length of the cable of 7500 m had been reduced since the beginning of the logging operations in the Vorbohrung in September 1987 to 5800 m as a result of wear,

renewal of cable connections etc. The accumulated logged length of logs recorded up to the laying down of the cable amounts to 1,940,000 m. This required a total running length of approximately double the amount.

In order to close the gap emerging for logging operations in the Hauptbohrung from 5800 m to 6000 m and to economise a new special cable described below, a 7-46PNT cable was leased for a transitional period of five months.

Logging cable for depths to 8000 m

As early as 1984 first analysis and calculations on the use of a logging cable at extreme depths have been carried out by Fries & Hänel assuming different values for mud density, target depth and temperature. For example, a mud density of approximately 1.03 g/cm^3, actually the KTB mud's density, reduces the cable loading capacity because of its minor buoyancy. Lowering the mud density by about 0.5 g/cm^3 a cable stretching effect of about 13% would result.

Besides the mechanical stability criteria, defined by the cable's own weight, steel strength and safety coefficient another important factor concerns the electrical insulation material that must withstand the ambient temperature and pressure conditions. Fig. 2.14 shows the mesured and extrapolated temperature-depth relation. The shaded area represents the temperature range assuming temperature gradients varying between 29 K/km (upper bound) and 27 K/km (lower bound). The expected temperature at 8000 m depth will be about 230 °C. The external pressure on the cable, assuming a mud density of 1.03 to 1.06 g/cm^3, will be about 83 to 85 MPa.

Current insulation materials for these conditions offered today by the industry are known under names like e.g. VECTOREN and NEOPRENE etc. resisting temperatures up to 190 °C and 230 °C, respectively.

With regard to the borehole measurements down to 8000 m, the cable selected by KTB possesses the following specifications:

- 7-conductor cable of continuous double opposed steel armoring with a total length of 9100 m. An extra length of 800 m is required to take into account cable cuts due to wear and another 500 m safety length is needed on the winch drum.

- Steel quality: extra high strength.

- Insulation: in order to meet the predicted temperature conditions the cable was manufactured in one piece but of two different insulation materials:

Cable Configuration and Spooling System for KTB–Deep Hole Logging

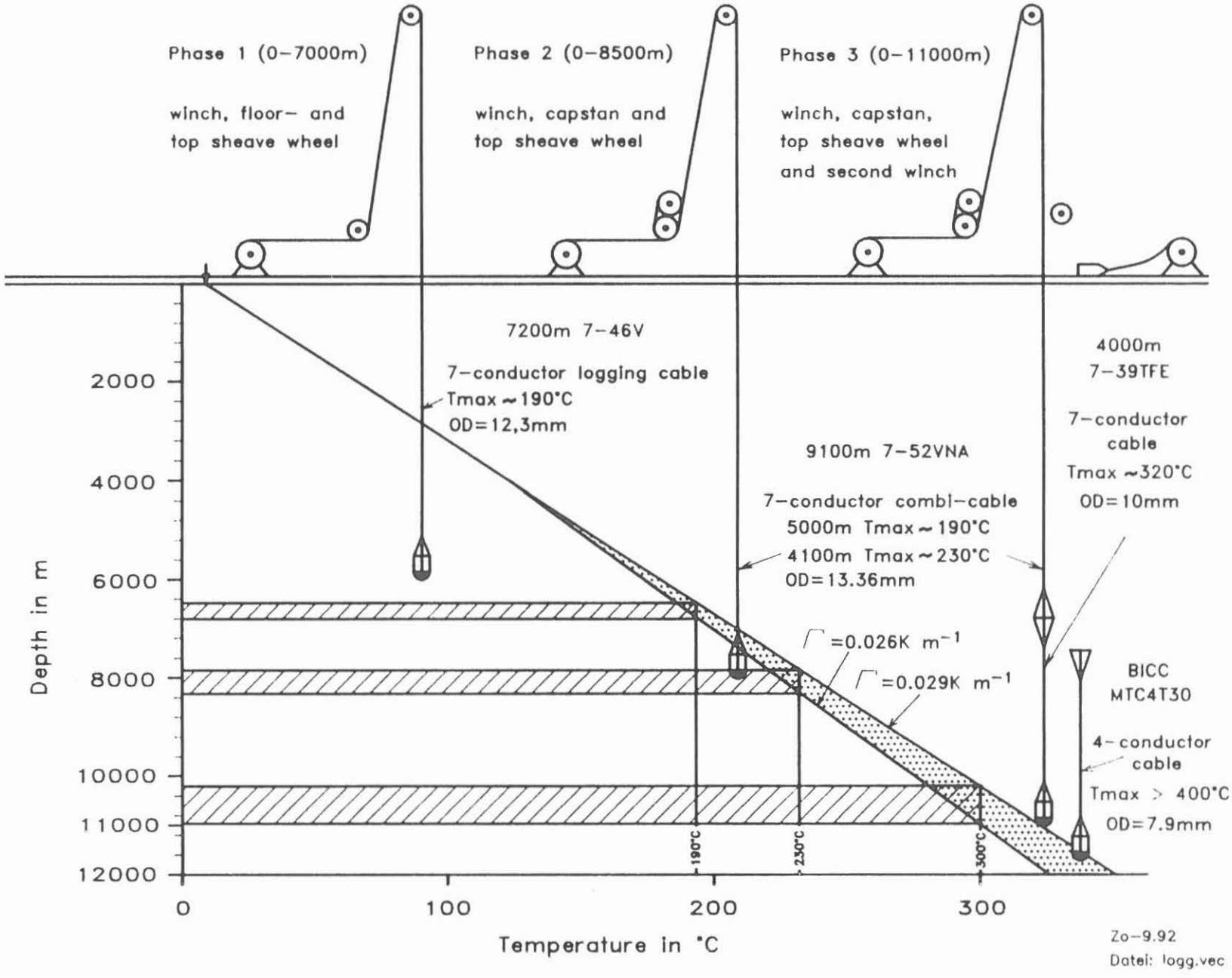

Fig. 2.14

VECTOREN (V, max. 190 °C) for the upper 5000 m length and NEOPRENE (NA, max. 230 °C) for the lower 4100 m length.

- Logging cable for depths greater than 8000 m

In order to decide on which cable should be used at the maximum depth of the Hauptbohrung, at the expected ambient conditions of 300 °C and approximately 120 to 140 MPa, an assessment was made of the products of all the leading cable manufacturers. Based on cable layout calculations (Kessels, 1991) it was concluded that logging to 10 km depth or even more with a single cable is not possible maintaining the standard safety coefficient of 0.5 (50% of the breaking strength). Taking into considerations the conditions set out in Table 2.7 and assuming a mud density of 1.03 g/cm^3 only a depth of roughly 8400 m can be reached (Fig. 2.15) with a 7-conductor, high strength steel armored cable.

Table 2.7: Assumptions for cable layout calculations.

cable weight in water	500 daN/km
frictional force	100 daN/km
overpull	800 daN
tool weight	300/500 daN
breaking load	13,100 daN

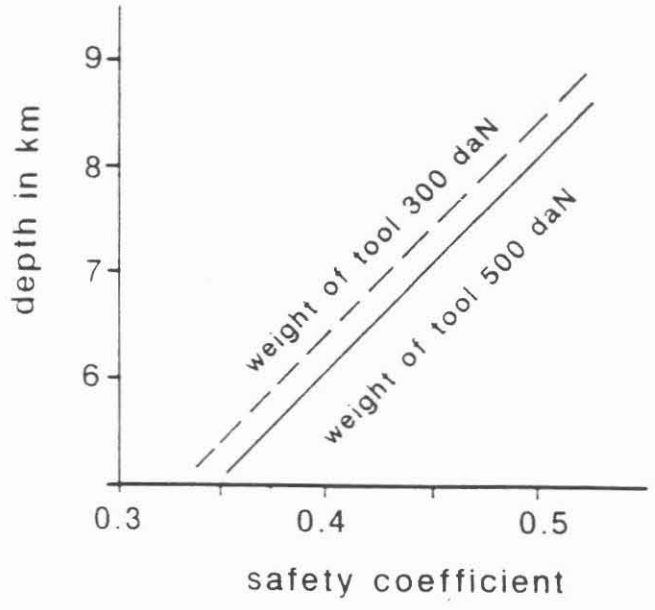

Fig. 2.15: Logging depth of a 7-conductor, high strength steel armored cable versus safetey coefficient.

Therefore, a solution was adopted to deploy a dual or even multiple cable system with the upper cable carrying the weight of the lower cable too. In other words, the lower cable must be a very lightweight one in order to take the weight off the upper cable. In addition, it must respond to more severe temperature conditions.

Based on cable specifications provided by cable manufacturers Figs. 2.16 and 2.17 show results calculated for two different dual cable systems (Kessels, 1991). The calculations also take into account other physical characteristics such as the reduction in breaking strength of steel with increasing temperature and the influence of the mud density. Deduced from observations in the Vorbohrung a value of 100 daN/km is used for the friction of the cable on the borehole wall. The overpull is set at 800 daN.

The upper part in Figs. 2.16 and 2.17 represents the depth range of each individual cable limited by its temperature rating and/or safety coefficient of 0.6. In the lower part of the figures is shown again the carrier cable assuming its full mechanical and thermal load together with the accumulated length of the dual cable systems.

Maximum cable lengths at safety coefficients of 0.4 and 0.5 are given in Tables 2.8 and 2.9. KTB adopted the standard safety coefficient of 0.5. This decision led to a dual cable system consisting of a 7-52 VNA cable in combination with a 7-39 PFA cable (Fig. 2.18). With the parameters listed in Table 2.10 a depth of 9979 m can theoretically be reached.

Table 2.10:

weight (7-52 VNA in water)	:	550 daN/km
weight (7-39 PFA in water)	:	300 daN/km
frictional force	:	100 daN/km
overpull	:	800 daN
tool weight	:	300 daN
breaking strength (7-52 VNA)	:	13,100 daN

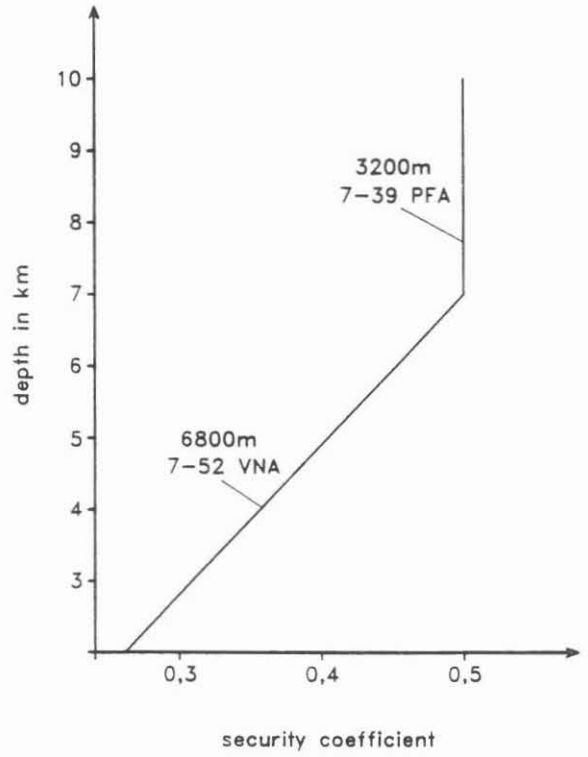

Fig. 2.18:
cable calculations
for: typ 7-52VNA
with a length of
3200 m typ 7-39PFA.

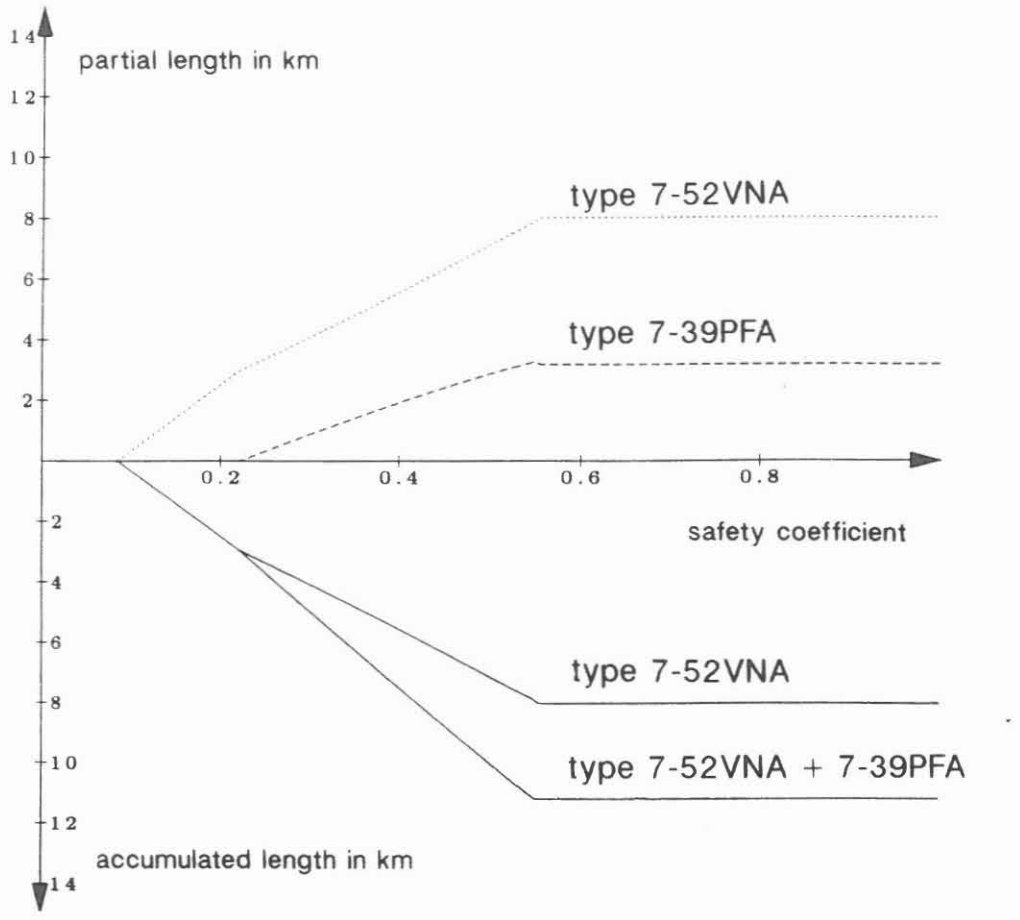

Fig. 2.16: Result of cable calculation

Table 2.8: Cable calculations (KESSELS,1991)

mud weight : 1.03 g/cm³
friction coefficient :100 daN/km
tool weight :294 daN
taking into account the temperature-dependent breaking stength

length at safety coeficient 0.4
7.491 km
length at safety coeficient 0.5
9.977 km
length at safety coeficient 0.6
11.214 km

	Properties of cable 1 type 7-52VNA	Properties of cable 2 type 7-39PFA
breaking strength fixed end :	13 100 daN	5 300 daN
assumed overpull :	800 daN	800 daN
weight in air :	664 daN/km	371 daN/km
buoyant weight :	150 daN/km	78 daN/km
assumed temperature rating :	-10 - 235°C	0 - 302°C
length at safety coeff. 0.4 :	5.571 km	1.901 km
length at safety coeff. 0.5 :	7.121 km	2.856 km
length at safety coeff. 0.6 :	8.036 km	3.178 km
breaking strength at cable top :	13 100 daN	4 419 daN
max. allowable weight at cable end :	1 410 daN	294 daN

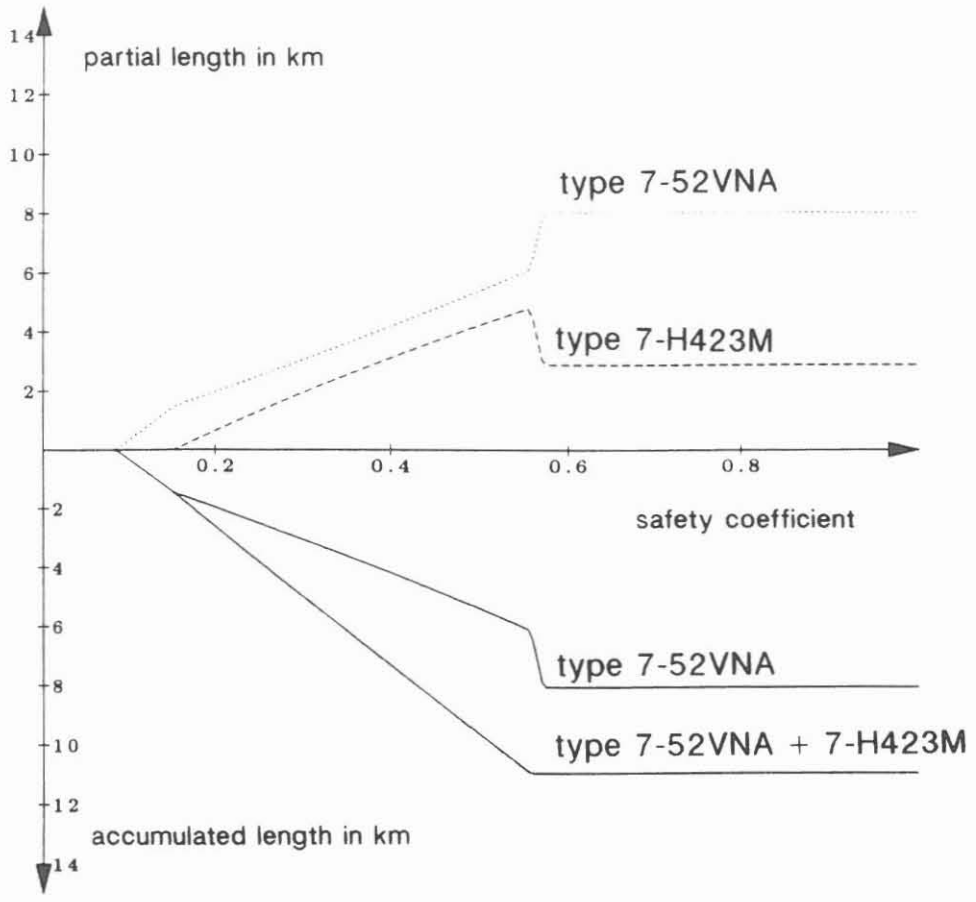

Fig. 2.17: Result of cable calculation

Table 2.9: Cable calculations (KESSELS,1991)

mud weight : 1.03 g/cm³
friction coefficient :100 daN/km
tool weight :294 daN
taking into account the
temperature-dependent breaking
stength

length at safety coeficient 0.4
7.287 km
length at safety coeficient 0.5
9.609 km
length at safety coeficient 0.6
10.929 km

	Properties of cable 1 type 7-52VNA	Properties of cable 2 type 7-H423M
breaking strength fixed end :	13 100 daN	7 470 daN
assumed overpull :	800 daN	800 daN
weight in air :	664 daN/km	498 daN/km
buoyant weight :	150 daN/km	81 daN/km
assumed temperature rating :	-10 - 235°C	0 - 316°C
length at safety coeff. 0.4 :	4.172 km	3.115 km
length at safety coeff. 0.5 :	5.389 km	4.219 km
length at safety coeff. 0.6 :	8.036 km	2.892 km
breaking strength at cable top :	13 100 daN	6 530 daN
max. allowable weight at cable end :	2 465 daN	294 daN

- **Cable connection and handling**

The mechanical and electrical connection of the load bearing cable with the second, high temperature cable is achieved with a specially constructed torpedo. The torpedo has appropriate rope sockets at either end to match the different cable diameters. In the middle of the torpedo is the box for the high temperature resistant connectors of the electrical conductors. Kalrez is used for all sealing elements in the torpedo.

Because this torpedo cannot be pulled over the sheaves nor through the capstan unit, handling of the second cable requires an additional winch as already shown in fig. 2.14 phase 3. This winch will be permanently positioned on the west side of the drilling rig in front of the V-door. A service cable and the 7-39 PFA high temperature cable are wound on the drum of the second winch. The service cable is just needed to bring the end of the high temperature cable up to the drill floor. The service cable and the high temperature cable are connected using the above mentioned torpedo, which in normal position is stored in the modified drum flange.

The actual method for running in and out the two logging cables is described as follows and illustrated in Figs. 2.19 through 2.22:

A. Running in

Basic setup

Capstan and winch 1 with approximately 8000 m 7-52 VNA-cable

Winch 2 with 3200 m high temperature cable and a service cable running from the winch to the floor sheave in the 'V-door'.

Phase 1 (Fig. 2.19):
The high temperature cable is run via the floor sheave at the V-door and through the upper sheave at the travelling block down to the drill floor where the logging tool can be connected. The cable of winch 1 hangs ready for use on the retractable arm with one half of the torpedo.

Phase 2 (Fig. 2.20):
The logging tool is run in with winch 2 until the torpedo between the service cable and the high temperature cable reaches the floor sheave.

Phase 3 (Fig. 2.21):
The travelling block with the upper sheave is run down to its lowest position, the cable clamp fixed into position, and the cable unhooked on the rotary table.

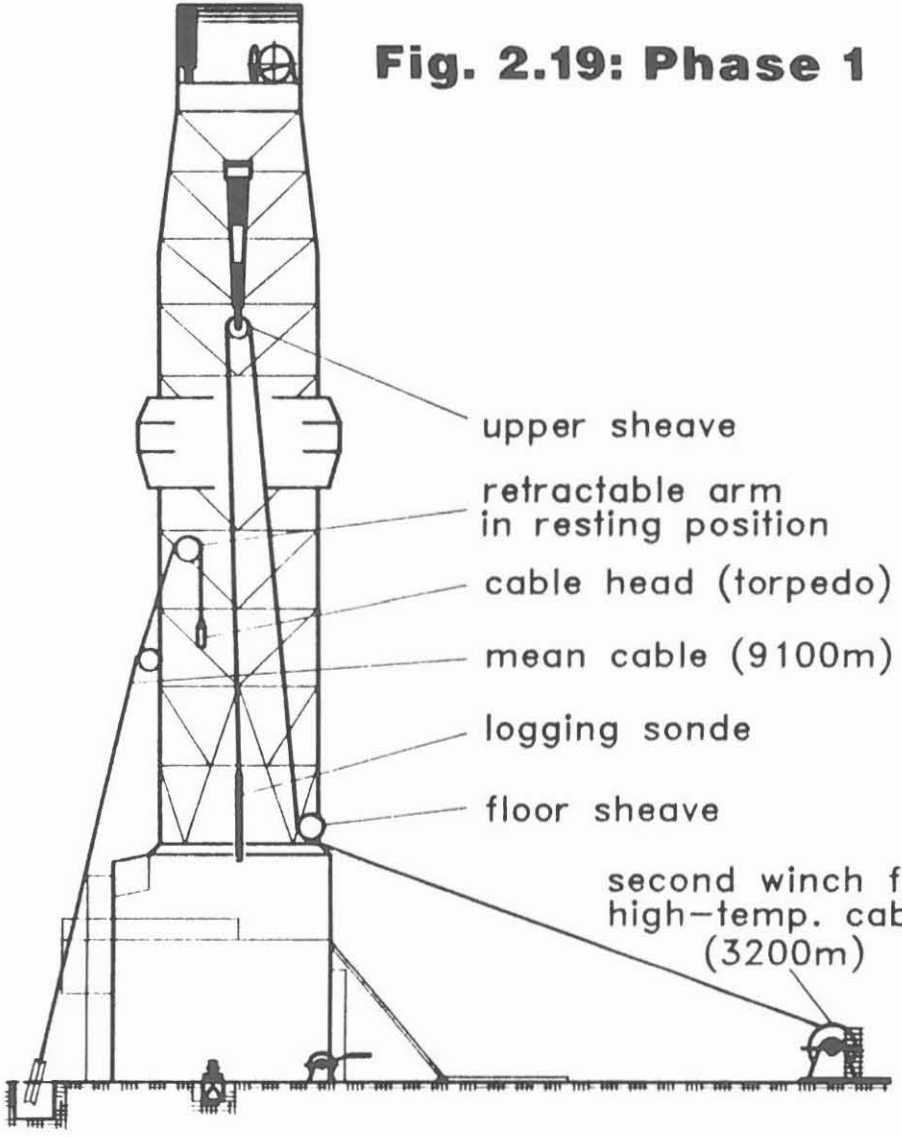

Fig. 2.19: Phase 1

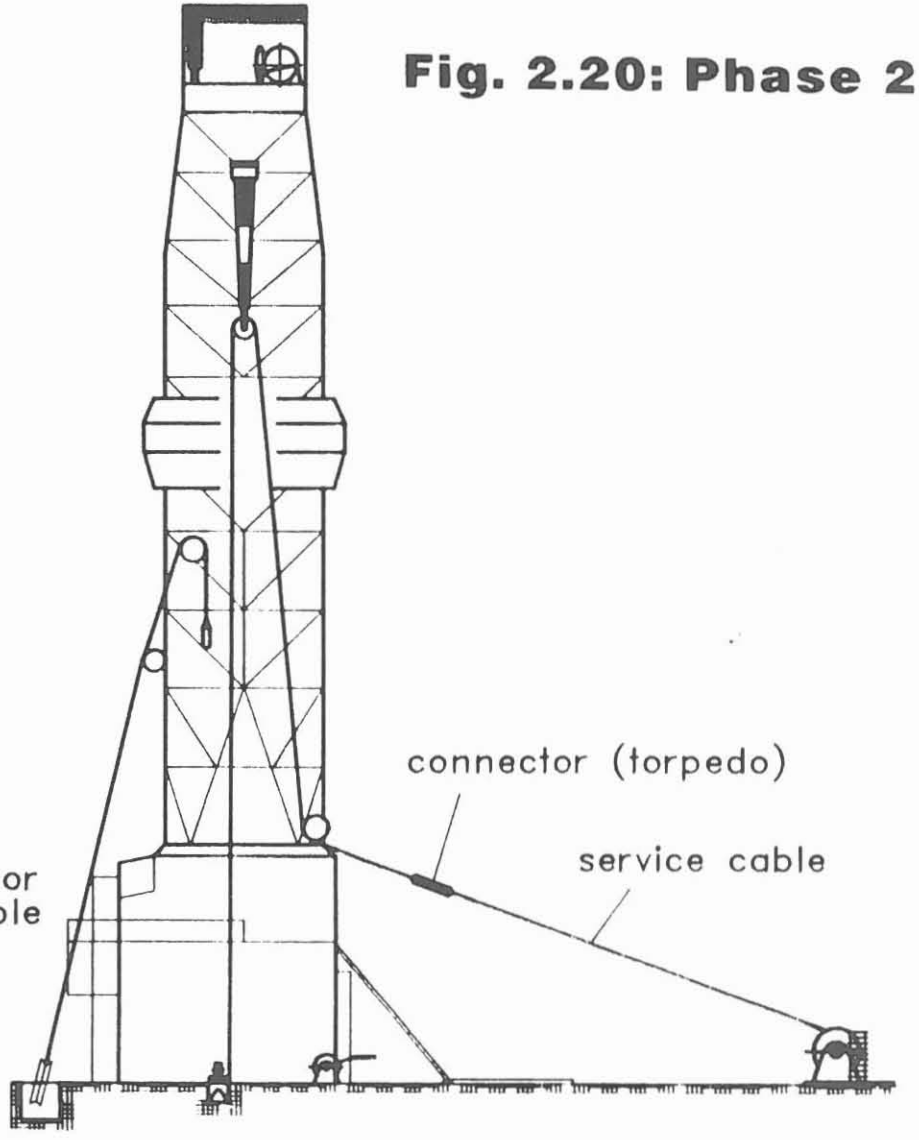

Fig. 2.20: Phase 2

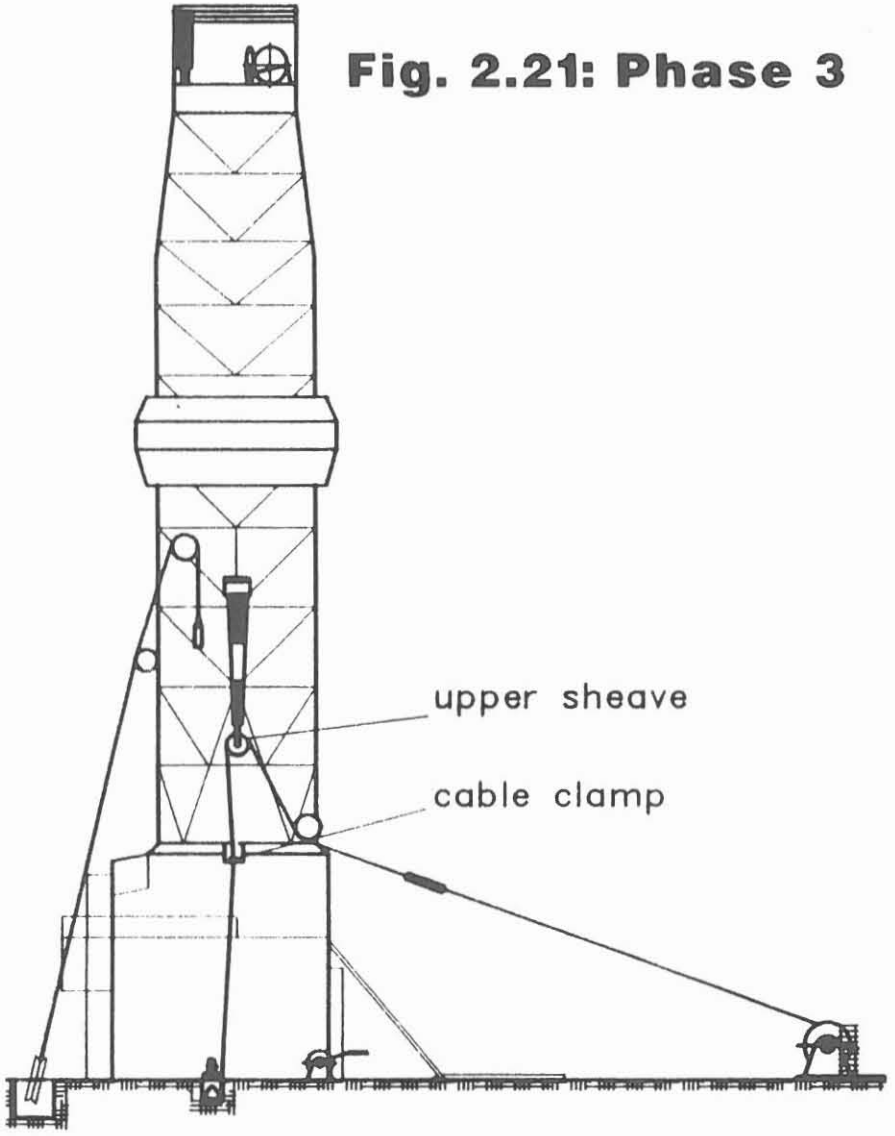

Fig. 2.21: Phase 3

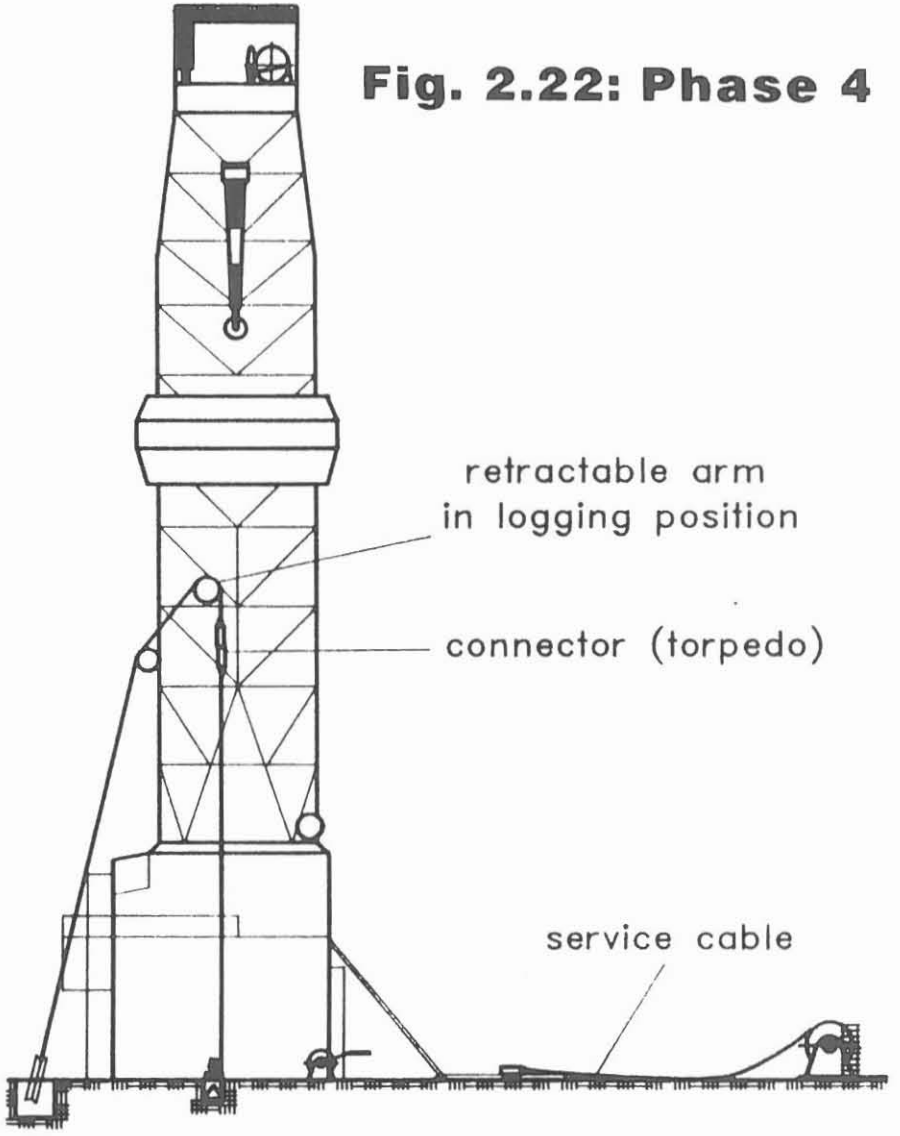

Fig. 2.22: Phase 4

Phase 4 (Fig. 2.22):
The travelling block is run back up, the retractable arm with the cable from winch 1 is swung out over the borehole, the service cable on winch 2 is uncoupled, and the two cables are connected using the torpedo. The cable clamp on the rotary table can be released and the whole combination run in with the capstan.

B. Running out

Running out takes place in reverse order.

2.7 Workshops

The LC has a mechanics and an electronics workshop including calibration and test facilities. These workshops helps to save considerably repair and maintenance costs of logging tools and other equipment of the LC, as well as to carry out own tool development. The mechanics and electronics workshops are permanently staffed. In this way, the necessary repairs, calibrations, testing and development work can be done when no logging is taking place.

2.7.1 Mechanics workshop

The mechanics workshop is equipped with the usual tools and the special tools required for handling the KTB's own borehole probes. The workshop is also used by the Field Laboratory Group. A detailed description of the mechanics as well as the electronics workshop is given in ZOTH (1991).

The most important spare parts for the logging unit and the logging tools are available on site in a small spare parts store.

The workshop (Fig. 2.23) is easily reached from the tented area thus keeping distances to a minimum.

2.7.2 Electronics workshop

The electronics workshop is also equipped with all the special tools required for repairing the KTB's own logging tools as well as the usual equipment found in a conventional electronics workshop. The workshop has a calibration room containing the following equipment:

- An oil filled bath for calibrating the temperature tools. A reference thermometer with highly accurate quartz sensors. The calibration bath, containing a special liquid (Ultratherm 250 W), can be heated up to a temperature of 250 °C. The dimensions of the bath are such that the whole temperature probe including electronics can be submerged

Fig. 2.23: Mechanics workshop, logging tool repairs

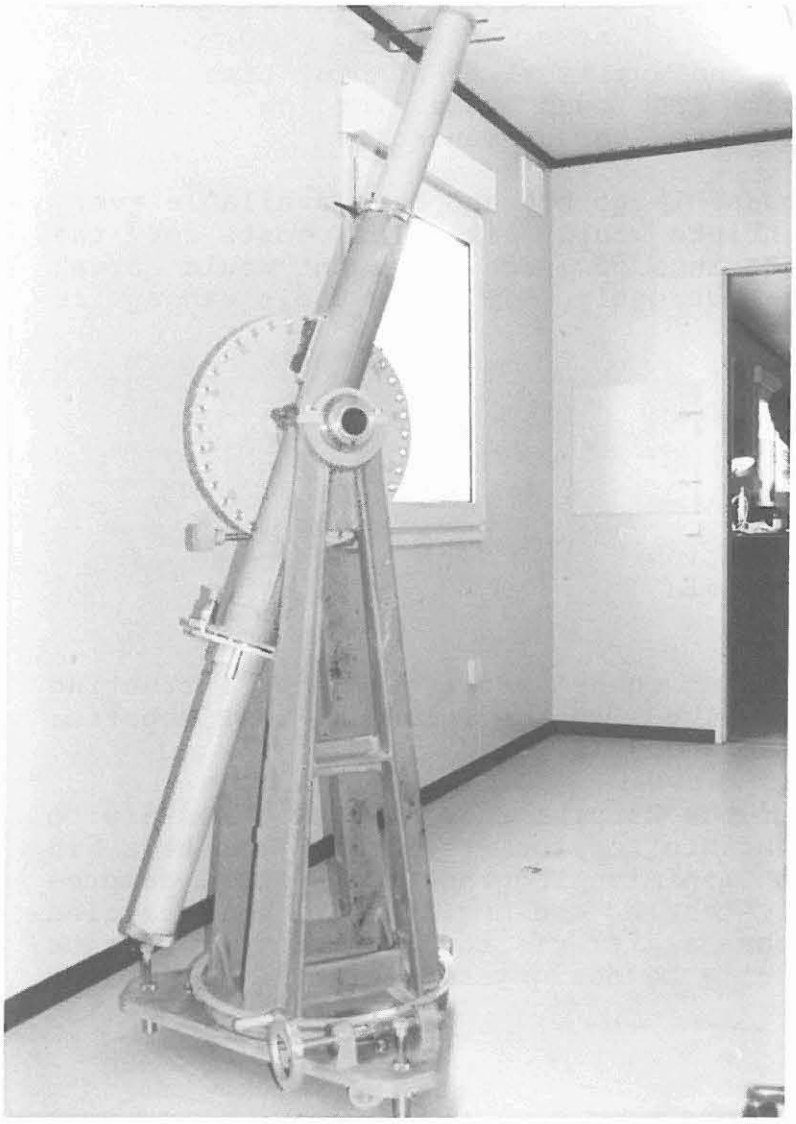

Fig. 2.24: Calibration equipment for azimuth and declination

in the bath bringing them up to the same temperature as the temperature sensor to be calibrated.

- An air heated oven is available for testing and checking electronic components. The oven is designed to hold logging tool parts up to three meters long in the heated area. Three Pt 100 sensors measure the temperature at different positions on the tool. Twelve additional Pt 100 sensors between the heating plates ensure that the set value for the temperature remains constant. Maximum oven temperature is 300 °C.

- The readjustment of azimuth and inclination tools is carried out in a special test apparatus (Fig. 2.24). This apparatus consists of non magnetic materials (bronze, aluminium, and titanium threads) and is designed so that the different tools can be fitted to the carrying tube by using different sized bushings. The inclination can be measured with a vertical arc 40 cm in diameter and the azimuth can be controlled with a horizontal arc with a diameter of 45 cm - both have engraved divisions. The test apparatus is set up using an axial adjuster with fine adjustment.

2.8 Logging tools

With respect to cost and availability at any time it was deemed necessary that KTB owns some logging tools for certain frequently requested measurements.

However, it is not possible to buy and have available every tool that the scientists would like. The costs for the acquisition and maintenance of some equipment would break the project's budget. Currently, KTB's own tools can aquire the following logs:

- borehole caliper
- azimuth
- inclination
- mud resistivity
- temperature
- natural gamma radiation
- spontaneous potential
- fluid sampling.

The tools for measuring these parameters and extracting fluid samples are described in the following KTB Reports: 87-3, 87-4, 90-5, 90-6a and 91-2.

The high rig costs of the Hauptbohrung made it necessary to log as many as possible of the required parameters in parallel in order to minimize logging time. Thus, comprehensive calculations, testing and modification were carried out - mainly by the staff of the LC and the on-site Schlumberger personnel - to design a practical combination

logging tool. This tool can log all of the above mentioned borehole parameters - with the exception of fluid sampling - in one logging run. Enlargement of the scope to include an extra pressure sensor is still planned. Fig. 2.25 is a schematic representation of the tool. On the right hand side are the descriptions of the components and on the left hand side abbreviations of the logged parameters. The distance between the lower tool end and the sensors is given in meters. The total tool length including cable head is 12.73 m and it has a weight of about 340 daN. Temperature rating is standard 175 °C. Modifications to the tool involved an additional temperature sensor (TMP1) and spontaneous potential (SP). In order to place the temperature sensor at the tip of the tool it was necessary to run a pressure resistant cable through the hydraulic and mechanical parts of the caliper tool (BGT), and to construct an adapter for screwing on the temperature sensor. The standard BGT has neither mechanical nor electrical connection possibilities for adding on tools underneath. The temperature sensor is protected from mechanical damage in the borehole by five lateral steel ribs. The ribs are arranged in such a way that there is good mud circulation around the sensor during the logging run to prevent drill cuttings from sticking to the tool. The half-life value of the sensor in the mud is less than 5 sec. (ZOTH, 1992). Thus, the difference between the temperature measured by the sensor and the actual temperature of the mud at a logging speed of 10 m/min is less than 0.03 K.

With the temperature sensor located at the tip of the combination tool, the temperature is only measured during the run in. Temperature is measured analog via a four conductor circuit. This is only possible when the conductors are not required for other measurements. When running in, the only other parallel measurements possible with the three remaining conductors are the SP and GR. For the run out, the AMS/MTEM temperature sensor is used.

Previously, spontaneous potential logging required a separate run incurring extra costs. The combination tool is designed in such a way that the spontaneous potential can be measured during the run in as well as during the run out. This is based on suggestions made by KESSELS. When running in, an insulated part of the tool housing is used for the SP electrode as with conventional logging. However, when running out, the spontaneous potential contact is taken over by the caliper arm running up the borehole wall. The first measurements showed amazing results with new information content. A detailed description including the first results is currently in preparation (KESSELS, personal communication).

Fig. 2.25

KTB - Combi-Sonde

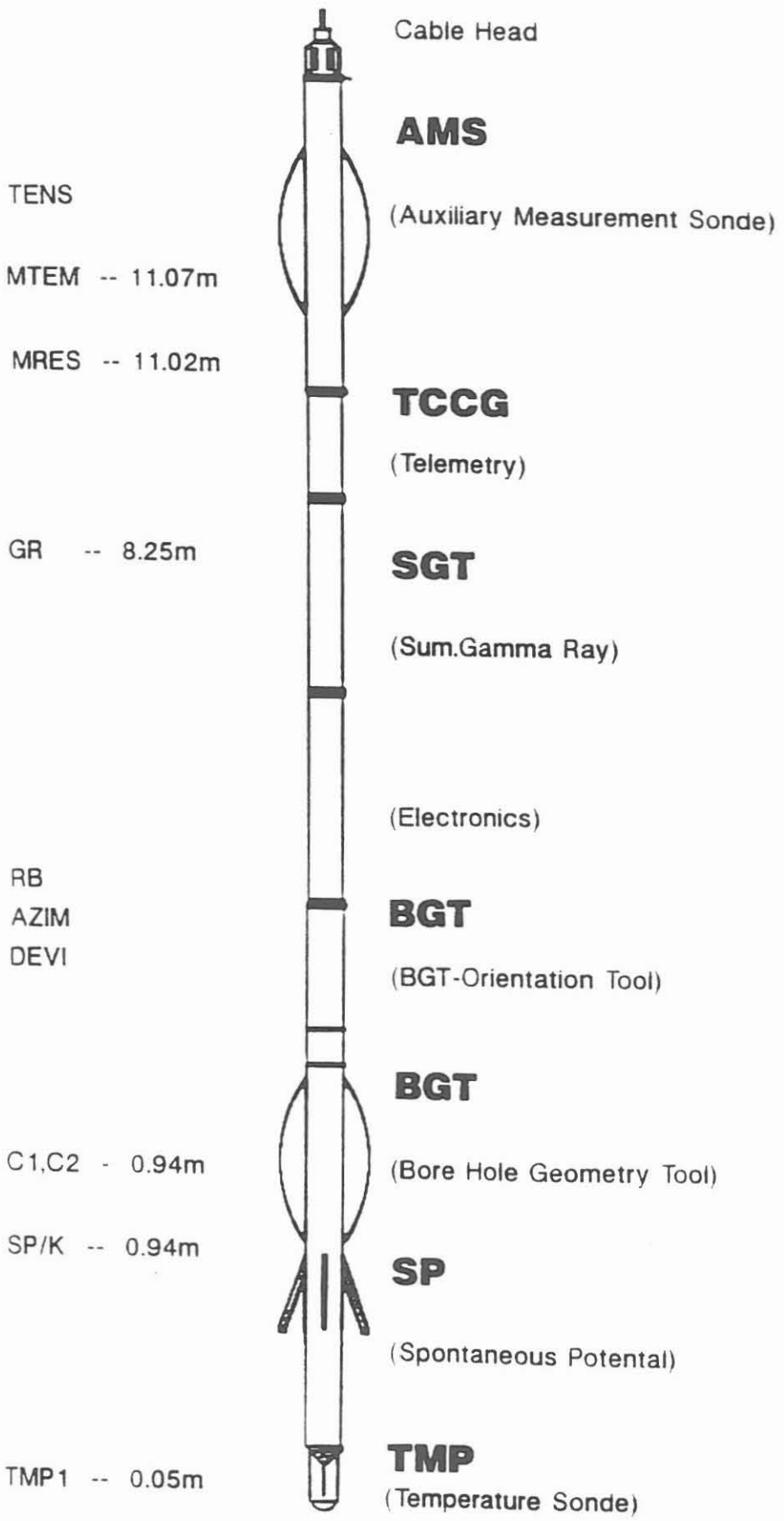

- **High temperature BGT**

The standard KTB combination tool was originally only suitable for temperatures up to 175 °C. Because of the expected higher temperatures at greater depths, the present tool is currently being improved by replacing the old housing with a Dewar pressure housing. A problem still remains with the mud resistivity sensor and the mechanical part of the caliper tool, solutions are currently being sought. A HEL version of the AMS will soon be available from the manufacturer. The caliper part of the KTB combination tool has already been replaced with a 200 °C version. Other modifications are going on to extend the temperature rating of the combination tool to 230 °C.

- **High temperature fluid sampler**

A high temperature version is currently being worked on in collaboration with industry.

2.9 Office unit

An important task of the Logging Center is the rapid and comprehensive presentation of the log data. This is particularly important when they are required for drilling operational decision making. This means that an evaluation team must be on site with the appropriate hard- and software. For this reason an office unit was installed.

Fig. 2.2 shows seven offices, a computer room equipped with Micro VAX III, Versatec plotter, terminal server, printer etc. and a meeting room adjacent to the LC's technical area. The whole unit is made up of separate containers. All of the office rooms are fitted with terminals for the Borehole Logging Group staff. In addition, the meeting room contains three workplaces for temporarily present scientists from universities.

2.10 Logging center statistics

The LC statistics are reproduced separately for the Vorbohrung and for the Hauptbohrung. Table 2.11 lists the data as of December, 31st, 1992.

Tabelle 2.11:

Statistical data on logging activities in the KTB-pilot borehole (Vorbohrung) and the KTB-superdeep borehole (Hauptbohrung) as of December 31, 1992

	KTB-Vorbohrung	KTB-Hauptbohrung				
cable type	7-46 V	7-46V	7-46PNT	7-52NA	total HB	total
number of logging runs:						
- for geosciences	375				101	476
- for technical support	18				107	125
- total	393				206	601
number of different tools	65	21	5			
comulated logging length in m	1 670 000	270 000	363 000	142 300	775 300	2 445 300 m
operating time of logging equipment: (in h)						
- data aquisition	5 571				3 020	8 591 h
- hydraulic equipment (Diesel engine)	2 588				1 364	3 952
- generator (Diesel engine)	3 759				684	4 443 h
- generator (electr. driven)	1 325				3 184	4 509
fishing operations						
- for logging tools	-				-	-
- for cables	-				-	-

2.11: References

Fries, A.P. & Hänel, R.: 1984. Untersuchungen zu einer Dauermeßstation (Well Logging Unit) für das deutsche Kontinentale Tiefbohrprogramm (Bericht 1). BGR/NLfB, Hannover, Archiv-Nr. 96 396, 50 S, unpublished.

Fries, A.P. & Hänel, R.: 1985. Untersuchungen zu einer Dauermeßstation (Well Logging Unit) für das deutsche Kontinentale Tiefbohrprogramm (Bericht 2). BGR/NLfB, Hannover, Archiv-Nr. 97 746, 24 S, unpublished.

Hänel, R.: 1987. Grundlagenforschung und Bohrlochgeophysik (Bericht 2). KTB-Report 87-3, 79-90, Hannover.

Kessels, W.: 1991. Design calculations for the application of a well logging cable in the main KTB borehole. Scientific Drilling, Vol. 2, No. 4, 215-229.

Zoth, G.: 1991. Logging Center, KTB Report 91-2, 21-57, Hannover.

Zoth, G.: 1993. Betrachtungen zum Temperaturverhalten der KTB-Temperaturmeßsonde. KTB Report 93-1, Hannover.

Acknowledgement

Such a project can never be the work of a single person. I would like, therefore, to express my sincere gratitude to my collegues Dr. K. Bram, J. Draxler, Prof. Dr. R. Hänel, Dr. P. Kehrer and Dr. W. Kessels for assisting me in the planning and realization of the Logging Center.

In particular, I wish to thank the "Schlumberger Team", M. Kühr, I. De Grefte and K. Bohn, who is actively involved in the Logging Center since July 1987. Their personal interest and everlasting cooperation made the LC to an institution of safe and high technological standard.

Last not least the help and assistance of the companies "Etudes et Prospection Schlumberger, Clamart, and Schlumberger Geophysikalische Service GmbH, Diepholz, is greatly acknowledged. They provided not only valuable advise but also technical and material assistance.

3. Information on the Borehole
KTB-Oberpfalz HB

K. Bram
J. Kück

3 Information on the borehole KTB-Oberpfalz HB

The information given in the first part of this chapter is of importance for carrying out the logging operations and the subsequent data evaluation and interpretation.

The second part deals with the borehole's geometry. Depth differences between driller and logger are explained in part three.

3.1 General information

Location

Coordinates: Latitude : 49° 48′ 58.8" N
Longitude : 12° 7′ 19.2" E

Gauß-Krüger coordinates: H : 5519 864.4
R : 4508 775.3

Height above s.l. : 513.8 m (ground level)
Seismic reference level: 500 m a.s.l.
Topographic map : TK 25, Nr. 6138 Erbendorf
· Community : Windischeschenbach
· District : Neustadt an der Waldnaab
· Land : Bavaria
. State : Germany

Drilling Rig

· Type : UTB-1 GH 3000 EG
· Height of rotary table above ground : 11.75 m
· Depth reference : ground level

Casing

· Casing depths : 32" down to 5,7 m (cemented)
24" down to 290,0 m (cemented)
16" down to 3000.5 m (cemented)
13 3/8"/13 5/8" down to 6013.5 m (cemented)*
(13 3/8" from 6013.5 m to 2806.7 m)
(13 5/8" from 2806.7 m to 0.0 m)

* top of cement according to temperature log: 4350 m

Mud conditions

The mud conditions encountered at the beginning of the logging series at 762.5 m and 1720.0 m as well as 3003 m and 4512 m are documented in the KTB-Report 91-2 and KTB-Report 92-1, respectively.

Mud condition at the beginning of the logging campaign 6018 m on March 13, 1992

Fresh water with 0.69 % Dehydril HT and 0.82 % Hostadrill (HOE 3118) (calculated concentration)

- Density : 1.04 g/cm^3
- Viskosity : 60/59 s
- Conductivity : 1.05 Ohm m at 18 °C
- pH : 11.5

3.2 Borehole geometry

The geometry of the borehole is described by its spatial trajectory and cross section. The horizontal projection of the borehole course is shown in Fig. 1. For comparison this figure shows also the projection of the pilot borehole, total depth 4000.1 m, at equal scale, assuming a common surface location.

The horizontal deviation with a maximum value of about 20 m at a depth of 3200 m to 3400 m is extremely small. The overall inclination yields a value of less than 0.2°. The vertical projection onto the WE and SN planes are given in Fig. 2.

Maximum and minimum caliper, reduced by bit size, are given in Fig. 3 together with the lithological profile and the reference gamma ray log. With a minimum caliper rarely exceeding 30 mm the borehole's cross section is strongly ovalized. The long axis corresponds with the direction of the minimum horizontal stress.

3.3 Depth difference driller : logger

As already observed and reported when drilling the pilot hole, a depth difference of approximately 1.0 m/1000 m between driller and logger exists. The depth measured by the logger being deeper.

The same difference has been recorded in the borehole KTB-Oberpfalz HB. At 6000 m the difference amounts to 6.3 m.

The reason for the difference is the uncorrected pipe tally. Drill pipe is measured at surface and not corrected for temperature and weight elongation.

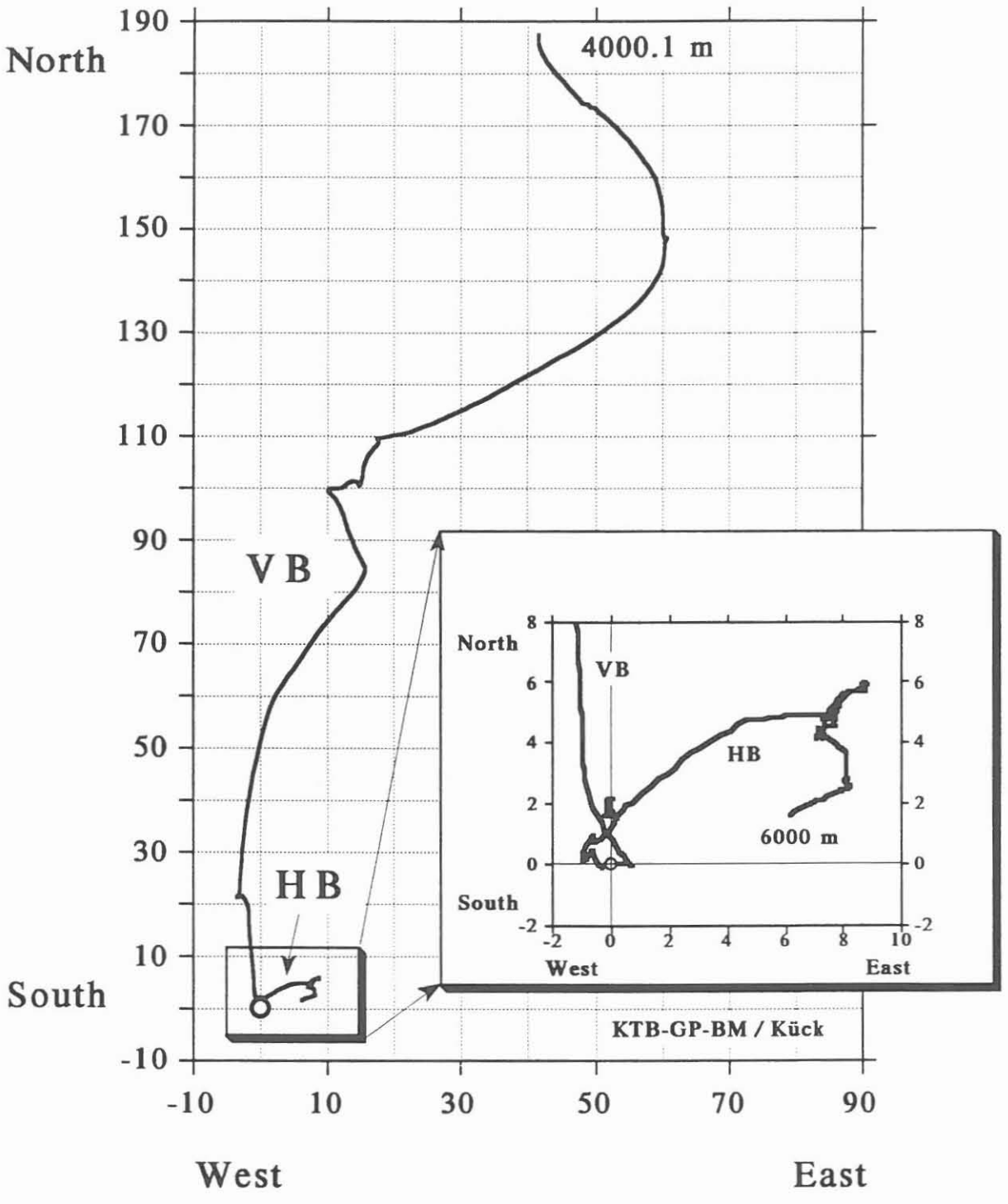

Fig. 1: Horizontal projection of the KTB pilot hole (VB) and superdeep borehole (HB) assuming a common surface location.

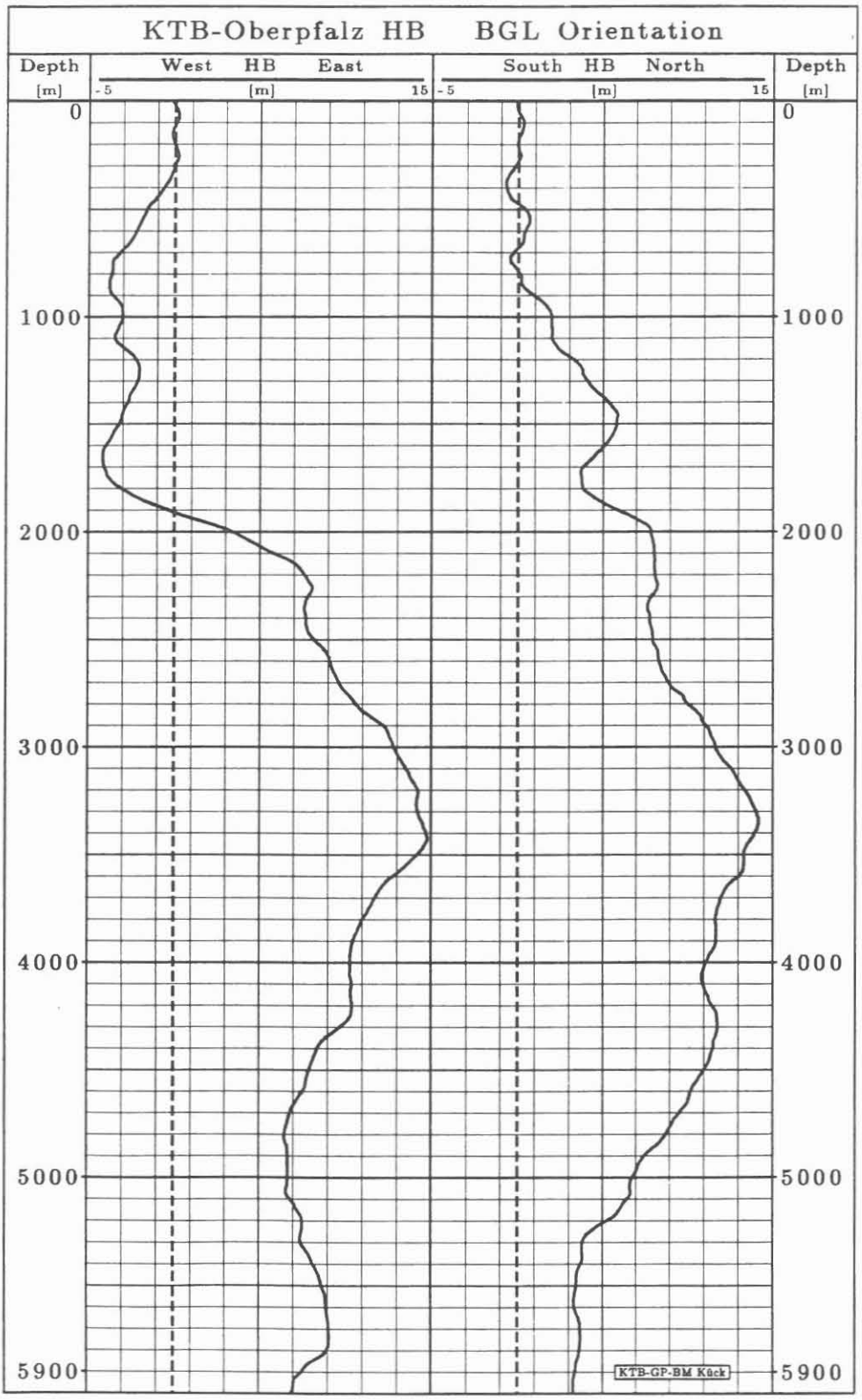

Fig. 2: Vertical projection of the KTB superdeep borehole.

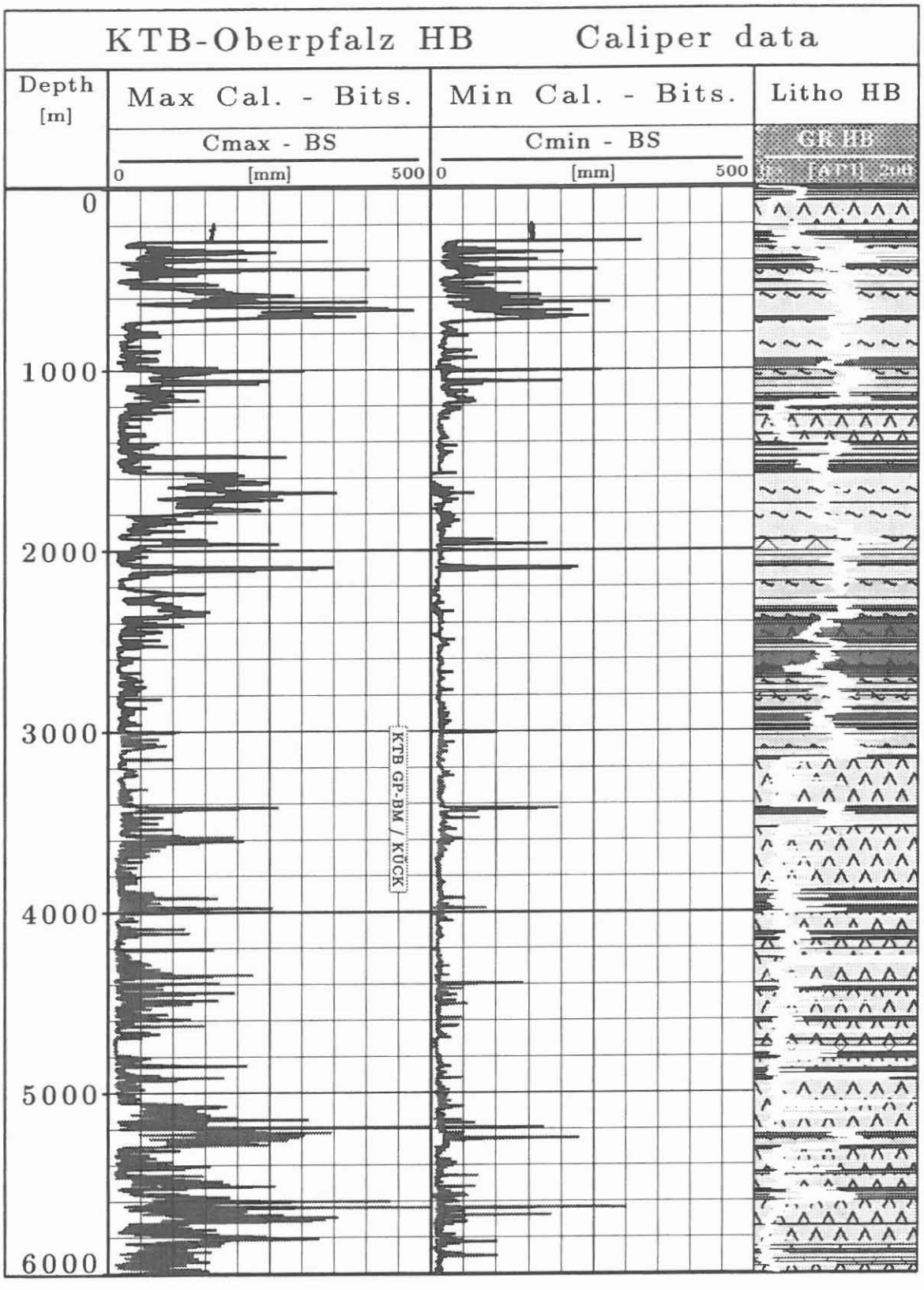

Fig. 3: Maximum and minimum caliper reduced by bit size of the KTB superdeep borehole.

4. Logging. Programme

J. K. Draxler

4. Logging Programme

The plan for the logging and testing programme for the well KTB-Oberpfalz HB has last been revised on May 12th, 1992.

The programme calls for logging services from three major groups:

KTB-logging: frequent services with KTB tools.

Service Companies: commercial logging services requested for logging campaigns.

Institutes, Universities: speciality tools requested for logging campaigns.

KTB-logging:
The plan was set up in such a way, that down to a depth of 4000 m every 500 m a Borehole Geometry Log with Gamma Ray (BGL/GR) should be run to control the caliper and trajectory of the borehole. From 4000 m downwards the frequency of this logging service was increased, as every 250 m newly drilled borehole a caliper log was planned.

The KTB-tool was modified to include a temperature (TEMP) and self potential (SP) measurement and is combineable with the Auxiliary Measurement Sonde (AMS), which records mud resistivity, temperature and head tension. The combination tool run is therefore: BGL/GRL/AMS/TEMP/SP. With this combination the control of the borehole, requested by the drilling department, the first information about lithology for the geologists and data about the temperature development are recorded. In addition, by measuring the mud resistivity continuously zones of inflow can be detected and selected for fluid sampling.

From surface down to a depth of 6018.0 m (driller's depth) 64 runs in the borehole have been made with the combination tool. This represents a strong deviation from the plan, which calls for 27 individual runs only (BGT/GR; TEMP/AMS/GR; SP/GR) and demonstrates the usefulness of the combination tool. The additional logs served as control for the vertical drilling technique. The fluid sampler (FS/GR) was run 15 times and recovered samples successfully.

On request from the working group "geothermics" 5 temperature logs (TEMP/GR) were run during the 6000 m logging campaign to record the recuperation of the formation temperature.

Service Companies:
The logging plan was followed with only slight deviations. Down to a depth of 3000.5 m the Formation MicroScanner and the newly developed Formation MicroImager (prototype) were

added for obtaining structural information. As the new Formation MicroImager produced good results, the Formation MicroScanner was phased out.

For the logging campaign at 6018.0 m another prototype tool became operational: the Azimuthal Resistivity Imager (ARI) as replacement for the Dual Laterolog (see section 8 "New Tools" - of this KTB Report). The interval from 6018.0 to 3000.5 m was logged, overlapping the previously recorded Dual Laterolog from 4512.0 to 3000.5 m.

Due to a tool failure and constrains on logging time only one core could be drilled with the Mechanical Sidewall Coring Tool (MSCT/GR). The Vertical Seismic Profile (VSP) was run only over the open hole section from 6018.0 to 3000.5 m, and not to surface as planed.

Down to a depth of 6000 m provisions for Free Point Indicator (FPI) and Back-Off (BO) operations have been made in the plan. Fortunately, these services were not needed due to the trouble free drilling operation.

Institutes and Universities.
According to the revised logging and testing plan the Magnetic Susceptibility (MS) was to be logged over the total open hole interval from 6000 - 3000 m. The tool from the University of Munich failed at 4278 m due to temperature. The modification to house the tool in a dewar has not yet been realized.

The same comment must be made about the Fluxgate Magnetometer Tool (FML) from the University of Braunschweig. In difference, this tool lasted for the whole logging operation, when deployed at the 6018.0 m campaign.

In addition, the 3-D Magnetometer Tool from the "Bundesanstalt für Geowissenschaften und Rohstoffe", was run. The tool has been modified for high temperature operations. The logging job with this tool was successful and was, in consequence to the cooperation agreement with the international Ocean Drilling Programm (ODP), rated as a test for classification as "Certified Third-Party Tool".

Testing:
While drilling the interval from casing shoe at 3000.5 m to 6018.0 m two drawdown tests and during the logging campaign at 6018.0 one more test has been made. All three tests indicated fluid production from several fracture zones within this interval. After running casing at 6018.0 m the planned hydro-frac was made.

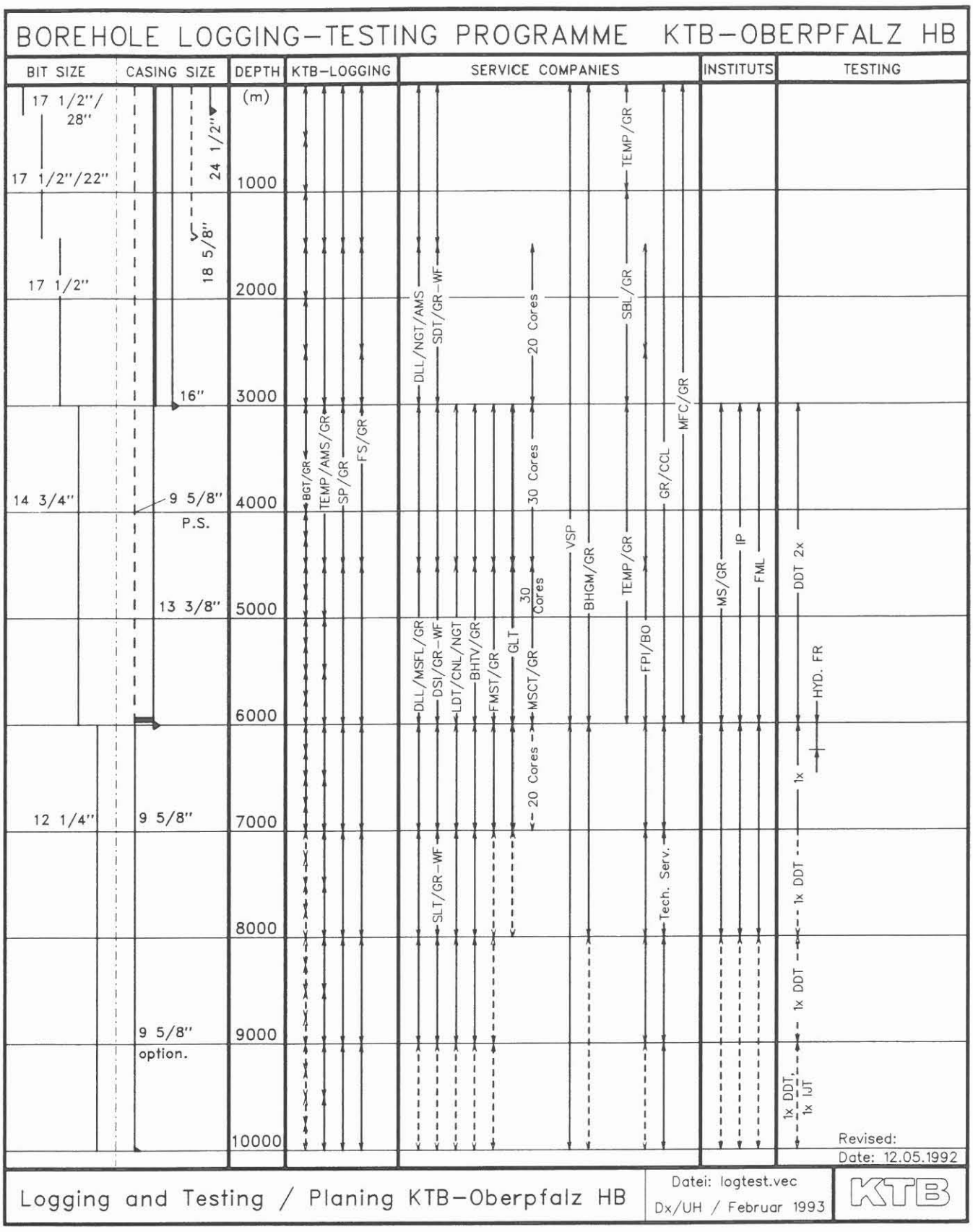
BOREHOLE LOGGING–TESTING PROGRAMME KTB–OBERPFALZ HB
BIT SIZE
CASING SIZE
DEPTH
KTB–LOGGING
SERVICE COMPANIES
INSTITUTS
TESTING
(m)
17 1/2"/ 28"
17 1/2"/22"
17 1/2"
14 3/4"
12 1/4"
24 1/2"
18 5/8"
16"
9 5/8" P.S.
13 3/8"
9 5/8"
9 5/8" option.
1000
2000
3000
4000
5000
6000
7000
8000
9000
10000
BGT/GR
TEMP/AMS/GR
SP/GR
FS/GR
DLL/NGT/AMS
SDT/GR–WF
20 Cores
30 Cores
TEMP/GR
SBL/GR
GR/CCL
MFC/GR
VSP
BHGM/GR
FPI/BO
DLL/MSFL/GR
DSI/GR–WF
LDT/CNL/NGT
BHTV/GR
FMST/GR
GLT
MSCT/GR
SLT/GR–WF
Tech. Serv.
MS/GR
IP
FML
DDT 2x
HYD. FR
1x
1x DDT
1x DDT
1x DDT
1x IJT
Revised:
Date: 12.05.1992
Logging and Testing / Planing KTB–Oberpfalz HB
Datei: logtest.vec
Dx/UH / Februar 1993
KTB

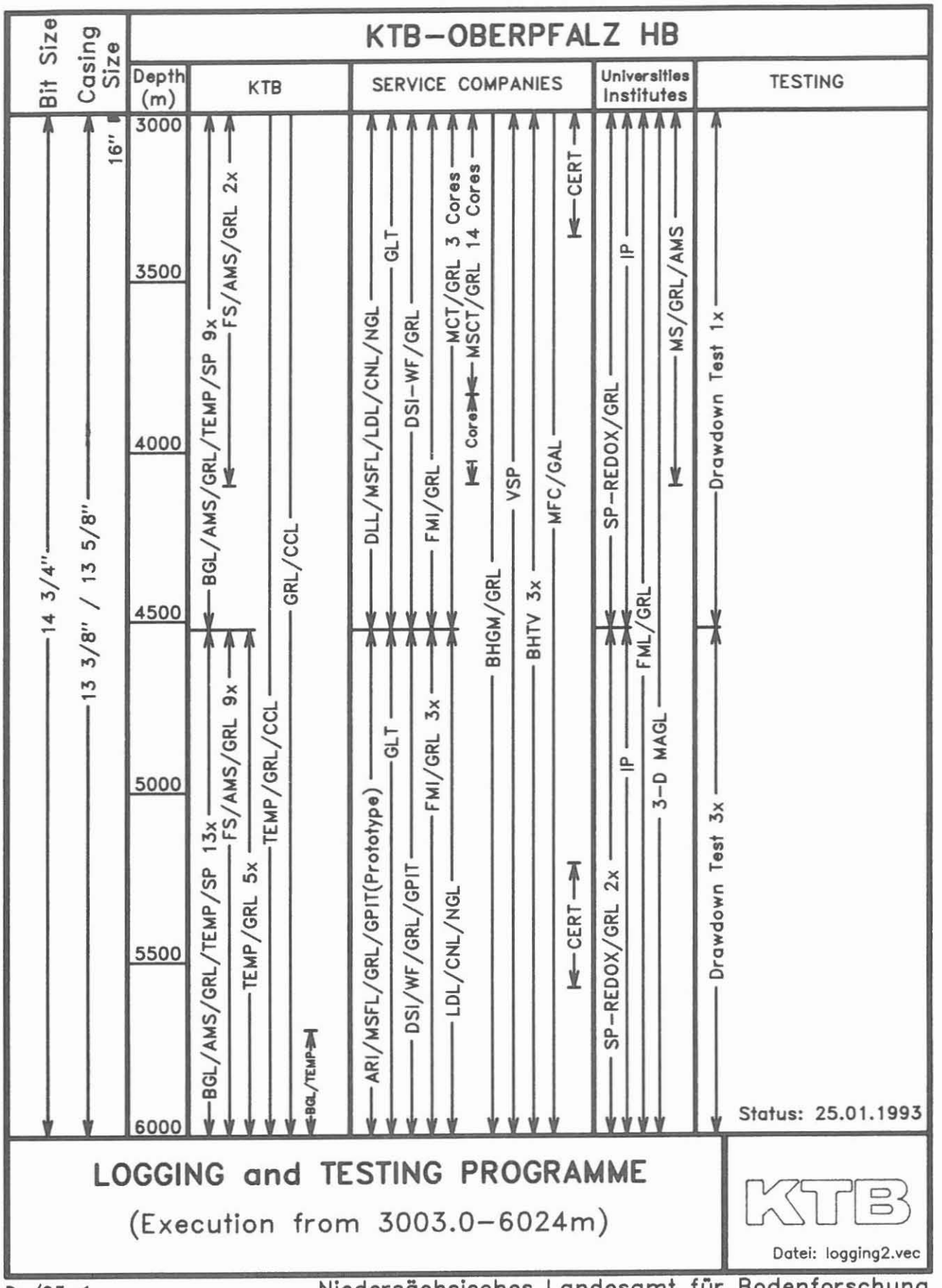

Dx/93-1

Niedersächsisches Landesamt für Bodenforschung

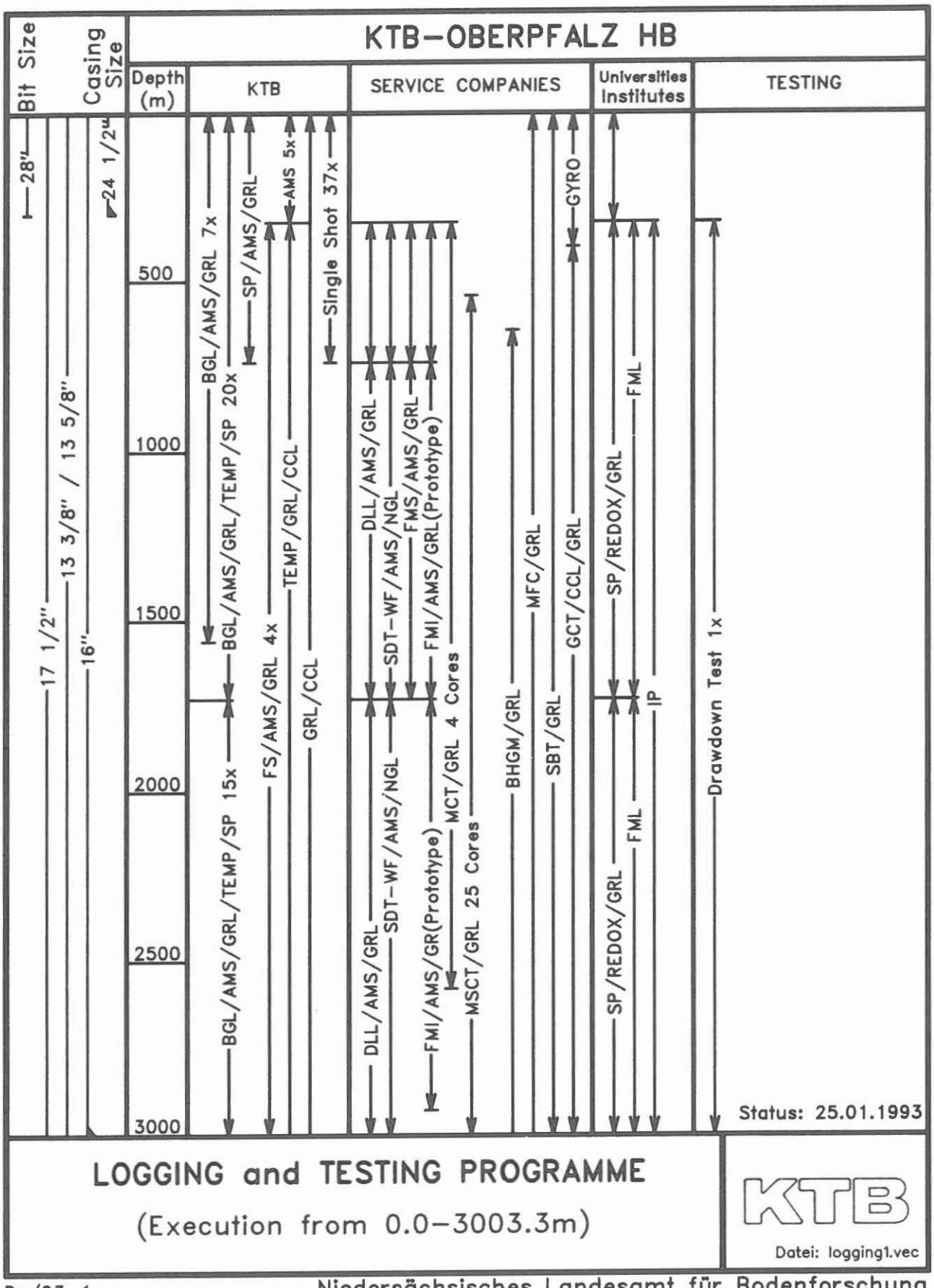

Dx/93-1

Niedersächsisches Landesamt für Bodenforschung

5. Logging Activity in the Borehole
KTB-Oberpfalz HB

J. K. Draxler
J. Kück

5. Logging Activity in the Borehole KTB-Oberpfalz HB

Table 5.1 gives a complete list of all logging and other wireline operations performed in the KT-HB borehole down to a driller's depth of 6018.0 m. The list provides the following information:

Header: List of operators (Service Industry, University Institutes, Scientific Laboratories)
List of codes for data outputs
List of codes for scales
Logs/Operation requested by: Geoscience (G) or Drilling Department (T)
Job No. and type of log, interval

List: Job No., date, starting time of logging operation, total operating time, logging time, interval: top - bottom (basis), operator, type of log (operation), data output, scale, remarks, tape number, operation requested by, file number on tape of reference log.

This list covers the operational side only.

In section 8 on table 8.1 evaluations and reports are listed.

Both lists serve as guides for easy reference when requesting data and are important sources for information of statistical nature (operating times, types of logs, intervals etc.)

Since spudding the KTB-HB the computer log evaluation facilities have been transfered from Hannover to the drilling site in Windischeschenbach. This change resulted in providing direct acces to logging data, shortly after completion of logging operations, by entering the data into the KTB LOGDV data base "KTBase".

In addition "Ouick-Look"-Plots are available already during, or only hours after logging operations or series of operations.

All logging data are scrutinized, corrected for environment, evaluated and archived on location.

In addition, software development, data integration (drilling data and measurements from the field laboratories) and data distribution is handled by the staff of the Logging Center.

File: HBLIST.DAT;

Stand: 27.10.1992 / Kück

Liste der Ausführenden

Nr.	Name
1	KTB
2	NLfB
3	BGR
4	Schlumberger
5	Western Atlas
6	DMT (WBK)
7	ELGI (Ungarn)
8	Prakla-Seismos
9	Petrodata
10	UNI München
11	Preussag
13	Lynes
16	Halliburton
17	Edcon
19	UNI Braunschweig
20	UNI Frankfurt
21	MeSy GmbH
24	Los Alamos Sc.Lab.
25	BLM Gommern
26	Scientific Drilling
27	GSF Potsdam
28	UNI Aachen

Liste der Datenträger

Kürzel	Bedeutung
A	Plot
B	Western-Atlas-Tape (BIT)
D	Datenliste
F	Film
L	Schlumberger-Tape (LIS)
O	Floppy
P	Pause
R	Report/Bericht
S	Seismic-Tape (SEGY)
T	Transparent
W	DMT(WBK)-Format Tape
N	Neigung, Single Shot Photos

Liste der Maßstäbe

Kürzel	Bedeutung
0	2000
1	1000
2	200
4	40
5	50
8	80
A	25
B	10
C	5
D	400
E	20
S	stationär

Liste der auftraggebenden Referate (AR)

Kürzel	Bedeutung
G	Geowissenschaften
T	Technik

Bezeichnung der Messungen

Lfd.Nr.	Bedeutung	gemessene Strecken
HB-0000x	für Bohrung HB1	von 0.0 - m

Lfd.Nr.	Datum	Uhr-zeit	Ges. zeit	Mess zeit	Tiefe Top	Tiefe Basis	Ausf.	Messungen	Daten-träger	Maß-stab	Bemerkungen	HBT-Nr.	AR	
HB-00001	121090	1240	150	077	0.0	72.2	1	BGL-AMS-GR	F/L	1,2		1	T	3
HB-00002	131090	1130	725		37.0	75.0	1	Single-Shot	F		drei Einfahrten (70m)		T	
HB-00003	201090	2230	200	070	0.0	305.0	1	BGL-AMS-GR	F/L	1,2		1	G	7
HB-00004	211090	030	175	095	0.0	305.0	1/20	SP-EP-Redox	F/L	1,2	Uni Frankfurt	1	G	10
HB-00005	271090	2130	200	148	0.0	249.8	1	BGL-TEMP-SP-AMS-GR	F/L	1,2	1. Run Kombinat.-Sonde	1	G	13
HB-00006	311090	200	450			250.0	1	Single-Shot	F				T	
HB-00007	311090	1315	100			262.0	1	Single-Shot	F				T	
HB-00008	311090	2135	047			269.4	1	Single-Shot	F				T	
HB-00009	011190	1645	050			279.4	1	Single-Shot	F				T	
HB-00010	021190	015	100			285.0	1	Single-Shot	F				T	
HB-00011	021190	900	083			290.0	1	Single-Shot	F				T	
HB-00012	021190	1415	083			292.0	1	Single-Shot	F				T	
HB-00013	031190	230	200	077	0.0	294.0	1	BGL-TEMP-SP-AMS-GR	F/L	1,2	aufgebohrt. Bohrl., 28"	1	T	15
HB-00014	061190	2115	075			290.1	1	Single-Shot	F				T	
HB-00015	071190	1020	100			292.2	1	Single-Shot	F				T	
HB-00016	071190	1730	100			294.0	1	Single-Shot	F				T	
HB-00017	071190	2215	067			295.8	1	Single-Shot	F				T	
HB-00018	081190	930	050			298.0	1	Single-Shot	F				T	
HB-00019	081190	1500	075			300.0	1	Single-Shot	F				T	
HB-00020	091190	015	100			303.3	1	Single-Shot	F				T	
HB-00021	091190	445	125	075	0.0	305.6	1	BGL-TEMP-SP-AMS-GR	F/L	1,2	Nach Durchbohren Zement.	1	T	16
HB-00022	091190	2200	050			306.0	1	Single-Shot	F				T	
HB-00023	141190	2300	050			314.9	1	Single-Shot	F				T	
HB-00024	151190	730	075			329.0	1	Single-Shot	F				T	
HB-00025	151190	1930	075			344.9	1	Single-Shot	F				T	
HB-00026	161190	100	050			354.0	1	Single-Shot	F				T	
HB-00027	161190	900	083			369.0	1	Single-Shot	F				T	
HB-00028	161190	1925	058			369.0	1	Single-Shot	F				T	
HB-00029	161190	2035	092			382.1	1	Single-Shot	F				T	
HB-00030	171190	330	175			395.5	1	Single-Shot	F		3 Einfahrten/Messungen		T	
HB-00031	171190	1215	200	123	0.0	397.0	1	BGL-TEMP-SP-AMS-GR	F/L	1,2	3 BGL-Meßfahrten Aufw.	2	T	4
HB-00032	201190	1800	250			404.0	1	Single-Shot	F		3 Einfahrten/Messungen		T	
HB-00033	211190	900	060			413.5	1	Single-Shot	F				T	
HB-00034	211190	2030	225			424.0	1	Single-Shot	F		3 Einfahrten/Messungen		T	
HB-00035	221190	1125	058			435.8	1	Single-Shot	F				T	
HB-00036	231190	615	425			449.3	1	Single-Shot	F		3 Einfahrten/Messungen		T	
HB-00037	231190	1915	200	138	0.0	462.5	1	BGL-TEMP-SP-AMS-GR	F/L	1,2	3 BGL-Meßfahrten Aufw.	3	T	4
HB-00038	241190	1600	850	383	0.0	450.0	1/26	Bohrl.Orient. mit Gyro			Messung Hängen/Aufwärts		T	
HB-00039	251190	2245	142			462.5	1	Single-Shot	F		2 Einfahrten/Messungen		T	
HB-00040	291190	1435	342	157	0.0	563.8	1	BGL-TEMP-SP-AMS-GR	F/L	1,2	2 Hängen, 2 Aufwärts	4	G	4

Lfd.Nr.	Datum	Uhr-zeit	Ges. zeit	Mess zeit	Tiefe Top	Tiefe Basis	Ausf.	Messungen	Daten-träger	Mass-stab	Bemerkungen	HBT-Nr.	AR	
HB-00041	051290	0955	208	103	0.0	633.8	1	BGL-TEMP-SP-AMS-GR	F/L	1,2,S	stationär über Sohle	5	T	4
HB-00042	071290	0200	200	058	247.0	653.0	1	BGL-AMS-GR	F/L	1,2		6	T	2
HB-00043	071290	1630	175	092	630.0	653.0	1	BGL-AMS-GR	F/L	1,2,S	stationär über Sohle		T	
HB-00044	091290	1045	100			661.0	1	Single-Shot	F				T	
HB-00045	091290	2230	150			637.5	1	Single-Shot	F				T	
HB-00046	111290	2030	200			683.6	1	Single-Shot	F				T	
HB-00047	121290	0830	100			701.0	1	Single-Shot	F				T	
HB-00048	121290	0945	100			701.0	1	Single-Shot	F				T	
HB-00049	131290	0145	150			714.0	1	Single-Shot	F				T	
HB-00050	151290	1145	183	048	258.0	735.0	1	BGL-SP-AMS-GR	F/L	1,2,S	stationär über Sohle	7	T	5
HB-00051	171290	1200	125			746.5	1	Single-Shot	F				T	
HB-00052	201290	0300	350	178	260.8	764.9	1	BGL-TEMP-SP-AMS-GR	F/L	1,2,S	stationär über Sohle	8	G	4
HB-00053	201290	0630	300	128	269.0	762.5	1	SP-AMS-GR	F/L	2,S	Stillstand auf Sohle	9	G	10
HB-00054	201290	0930	475	238	262.0	759.1	1/4	DLL-AMS-GR	F/L	2		12	G	1
HB-00055	201290	1635	633	475	290.0	763.0	1/4	FMS-AMS-GR					G	
HB-00056	201290	2315	250	120	259.0	765.0	1	BGL-TEMP-SP-AMS-GR	F/L	1,2,S	1 stat. Messung	9	G	15
HB-00057	211290	0145	625	288	284.0	763.0	1/4	SDT/WF-NGS-AMS	F/L	2		12	G	4,6
HB-00058	211290	0800	1300	975	290.0	763.0	1/4	FMI-GR			(Prototyp)		G	
HB-00059	211290	2100	300	220	258.0	763.0	1	BGL-TEMP-SP-AMS-GR	F/L	1,2,S	5 stationäre Messungen	9	G	18
HB-00060	291290	0130	275	132	23.7	854.8	1	BGL-TEMP-SP-AMS-GR	F/L	1,2,S	6 stationäre Messungen	10	T	9
HB-00061	030191	0030	825	668	266.0	896.0	1	BGL-TEMP-SP-AMS-GR	F/L	1,2,S	53 stat. Messungen	11	T	2
HB-00062	070191	0930	325	178	249.0	935.4	1	BGL-TEMP-SP-AMS-GR	F/L	1,2,S	9 stat. Messungen	13	T	2
HB-00063	130191	1000	350	182	261.8	1008.6	1	BGL-AMS-GR	F/L	1,2,S	1 stat. Messung	14	T	2
HB-00064	190191	1300	350	208	0.0	1070.0	1	BGL-TEMP-SP-AMS-GR	F/L	1,2,S	6 stat. Messungen	15	T	10
HB-00065	220191	1915	300	233	0.0	1090.0	1	BGL-TEMP-SP-AMS-GR	F/L	1,2,S	5 stat. Messungen	16	T	7
HB-00066	260191	0915	825	697	0.0	1131.6	1	BGL-TEMP-SP-AMS-GR	F/L	1,2,S	4 stat. Messungen	17	G	7
HB-00067	300191	0630	600	413	266.6	1141.7	1	BGL-TEMP-SP-AMS-GR	F/L	1,2,S	3 stat. Messungen	18	T	5
HB-00068	120291	0615	400	278	258.0	1243.0	1	BGL-TEMP-SP-AMS-GR	F/L	1,2,S	4 stat. Messungen	19	T	6
HB-00069	240291	1900	300	068	1150.0	1535.0	1	BGL-AMS-GR	F/L	1,2,S	1 stat. Messung	20	T	2
HB-00070	020391	2200	567	385	0.0	1721.0	1	BGL-TEMP-SP-AMS-GR	F/L	1,2,S	5 stat.M. Neue DEVI/AZIM	21	G	7
HB-00071	030391	0345	375	143	284.0	1716.5	1/4	DLL-AMS-GR (GPIT)	F/L	1,2	Orientierung durch GPIT	22	G	2
HB-00072	030391	0730	1000	750	720.0	1718.0	1/4	FMI-GR			(Prototyp)		G	
HB-00073	030391	1730	850	637	713.0	1718.0	1/4	FMS-AMS-GR					G	
HB-00074	040391	0200	800	575	278.0	1718.0	1/4	SDT/WF-NGS-AMS	F/L	1,2	exzentr. &25	24	G	1
HB-00075	040391	1000	600	438	0.0	1720.0	1/20	SP-EP-REDOX			Uni Frankfurt	27	G	
HB-00076	040391	1600	850	590	262.0	1719.0	1/19	FML-GR			Uni Braunschweig	26	G	
HB-00077	040391	0300	500	395	270.0	1720.0	1	BGL-TEMP-SP-AMS-GR	F/L	1,2,S	5 stat. Messungen	23	G	7
HB-00078	100391	1230	200	075	1498.0	1776.0	1	BGL-TEMP-SP-AMS-GR	F/L	1,2,S	9 stat. Messungen	28	T	12
HB-00079	130391	0245	183	050	1693.0	1794.0	1	BGL-TEMP-SP-AMS-GR	F/L	1,2,S	5 stat. Messungen	28	T	19
HB-00080	160391	2055	167	055	1697.0	1822.0	1	BGL-TEMP-SP-AMS-GR	F/L	1,2,S	8 stat. Messungen	28	T	28

Lfd.Nr.	Datum	Uhr-zeit	Ges. zeit	Mess zeit	Tiefe Top	Tiefe Basis	Ausf.	Messungen	Daten-träger	Mass-stab	Bemerkungen	HBT-Nr.	AR	
HB-00081	200391	0700	175	043	1696.0	1861.0	1	BGL-SP-AMS-GR	F/L	1,2,S	6 stat. Messungen	29	T	9
HB-00082	240391	1445	200	087	1672.0	2025.7	1	BGL-TEMP-SP-AMS-GR	F/L	1,2,S	3 stat. Messungen	30	T	1
HB-00083	020491	2130	483	422	249.3	2244.1	1	BGL-TEMP-SP-AMS-GR	F/L	1,2,S	3 stat. Messungen	31	G	1
HB-00084	060491	1500	150	112	2062.1	2296.4	1	BGL-TEMP-SP-AMS-GR	F/L	1,2,S	3 stat. Messungen	32	T	4
HB-00085	120491	1230	200	067	2030.0	2403.0	1	BGL-TEMP-SP-AMS-GR	F/L	1,2,S	3 stat. Messungen	33	T	4
HB-00086	280491	0045	350	237	1950.0	2720.0	1	BGL-TEMP-SP-AMS-GR	F/L	1,2,S	2 stat. Messungen	33	T	11
HB-00087	040591	1930	150	112	2650.0	2770.0	1	BGL-TEMP-SP-AMS-GR	F/L	1,2,S	5 stat. Messungen	34	T	6
HB-00088	150591	2230	225	065	2647.0	2896.0	1	BGL-TEMP-SP-AMS-GR	F/L	1,2,S	5 stat. Messungen	35	T	5
HB-00089	250591	1015	675	285	306.0	2658.0	1	MCT-GR	F/L	1,2	1. Einsatz, 4 Tiefen		G	
HB-00090	250591	1700	875	707	1650.0	2957.2	4/1	FMI-GR	F	1,2	kont. & 4 MCT-Tiefen		G	
HB-00091	310591	0520	642	562	48.3	3003.0	1	BGL-TEMP-SP-AMS-GR	F/L	1,2,S		36	G	3
HB-00092	310591	1330	1025	767		1000.0	4/1	Druckregistrierung (HP)		S	Sensor stationär	39	G	3
HB-00093	310591	2345	825	733	0.0	3003.0	1	BGL-TEMP-SP-AMS-GR	F/L	1,2,S		37	G	6
HB-00094	010691	0800	600	450	701.5	1530.0	1	FS-AMS-GR	F/L			42	G	
HB-00095	020691	1700	2150	1245	700.0	3003.0	4/1	SDT/WF-NGS-AMS	F/L	1,2,S	1.Run SDT defekt,	40	G	6,7
HB-00096	010691	2200	200	150		1960.0	1	FS-AMS-GR	F/L			42	G	
HB-00097	020691	0000	1250	935	280.0	3003.0	1/2	IP	F/L		NLfB	113	G	
HB-00098	020691	1230	450	230	1548.0	3001.0	4/1	DLL-AMS-GR	F/L	1,2,S		39	G	2
HB-00099	030691	0630	300	140		2975.0	1	FS-AMS-GR	F/L			43	G	
HB-00100	030691	0930	600	383	208.0	3003.0	1/20	SP-EP-Redox	F/L			41	G	
HB-00101	030691	1530	1050	900	0.0	3003.0	1/19	FML-GR	F/L			44	G	
HB-00102	040691	0200	250	085		2999.6	1	FS-AMS-GR	F/L			43	G	
HB-00103	040691	0430	1225	918	510.0	2507.5	4/1	MSCT	F/L		1.Run=7 Samp,2.Run=18 S.		G	
HB-00104	040691	0945	725	540	185.0	3005.9	1	BGL-TEMP-SP-AMS-GR	F/L	1,2,S		38	G	3
HB-00105	130691	0900	1300	975	0.0	2932.0	4/1	GCT-CCL-GR	F/L	D	Gyro-Kompass	45	T	1
HB-00106	040791	0600	400	205	2851.0	3299.0	4/1	BGL-TEMP-SP-AMS-GR	F/L	1,2,S	stat. Temp.messung	46	T	3
HB-00107	040791	1000	1250	935	0.0	3000.0	5/4/1	SBL-CCL-GR	F/L	2	Zementbondlog		T	
HB-00108	040791	2230	275	205		3299.0	4/1	CERT-CCL-GR	F/L		Elektromagnet		T	
HB-00109	170791	2030	400	332	112.6	3499.8	4/1	BGL-TEMP-SP-AMS-GR	F/L	1,2,S	stat. Temp.messung	47	T	1
HB-00110	070891	1415	425	332	3394.7	3799.9	4/1	BGL-TEMP-SP-AMS-GR	F/L	1,2,S	4 stat. Messungen	48	T	6
HB-00111	140891	2230	225	047	3700.0	3875.0	4/1	BGL-TEMP-SP-AMS-GR	F/L	1,2,S	4 stat. Messungen	49	T	6
HB-00112	230891	0715	300	090	3811.0	3982.0	4/1	BGL-TEMP-SP-AMS-GR	F/L	1,2,S	4 stat. Messungen	50	T	6
HB-00113	230891	1015	200	025		3950.5	4/1	FS-AMS-GR	F/L	2			G	
HB-00114	010991	1445	333	273	3867.0	4134.0	4/1	BGL-TEMP-SP-AMS-GR	F/L	1,2,S	4 stat. Messungen	51	T	7
HB-00115	121091	2230	1050	948	0.0	4516.6	4/1	BGL-TEMP-SP-AMS-GR	F/L	1,2,S	1 stat. Messung	52	T	3
HB-00116	121091	0900	1200	605	2979.0	4520.0	4	DLL-MSFL-LDL-CNL-NGS	F/L	1,2		53	G	2
HB-00117	131091	2130	950	807	0.0	4518.0	4/1	BGL-TEMP-SP-AMS-GR	F/L	1,2	1 stat. Messung	54	G	1
HB-00118	131091	0700	2600	1950	2994.0	4455.0	4	GLT-GR	F/L			59	G	1
HB-00119	141091	0900	1300	975	3000.0	4500.0	4	DSI-GR/WF	F/L				G	
HB-00120	141091	2200	950	903	0.0	4521.5	4/1	BGL-TEMP-SP-AMS-GR	F/L	1,2	1 stat. Messung	55	G	1

Lfd.Nr.	Datum	Uhr-zeit	Ges. zeit	Mess zeit	Tiefe Top	Tiefe Basis	Ausf.	Messungen	Daten-träger	Mass-stab	Bemerkungen	HBT-Nr.	AR	
HB-00121	151091	0730	350	262		4115.0	4/1	FS-GR	F/L				G	
HB-00122	151091	1130	1150	862	3209.0	4521.5	4/1	MCT-GR	F/L		3 Schlitzkerne		G	
HB-00123	151091	2300	1050	787	3925.0	4513.0	4	FMI-GR	F/L		Gerät defekt ab 3925 m		G	
HB-00124	161091	0930	1000	750	3030.0	3961.5	4/1	MSCT-GR	F/L	1,2	14 Kerne		G	
HB-00125	171091	0400	1200	888	0.0	4517.7	4/1	BGL-TEMP-SP-AMS-GR	F/L	1,2	1 stat. Messung	57	T	2
HB-00126	171091	1600	900	820	0.0	4504.5	1/20	SP-EP-Redox				56	G	
HB-00127	181091	0100	1350	1010	3000.0	4500.0	1/19	IP				60	G	1
HB-00128	231191	0445	837	427	2880.0	5007.0	4/1	BGL-TEMP-SP-AMS-GR	F/L	1,2	1 stat. Messung	61	G	4
HB-00129	231191	1315	350	262		3184.0	4/1	FS-GR	F/L				G	
HB-00130	041291	0115	875	556	2994.0	4470.0	4/1	FMI-GR			3 Meßstrecken		G	
HB-00131	030192	0745	900	617	2800.0	5519.0	4/1	BGL-TEMP-SP-AMS-GR	F/L	1,2	Neues Kabel, 1. Einfahrt	64	G	4
HB-00132	030192	1645	1700	1275	3000.0	5505.0	4/1	FMI-GR			3000-3651m, 4269-5504m		G	
HB-00133	040192	1330	400	300		5388.0	4/1	FS-GR			FS-II	65	G	
HB-00134	040192	0400	375	281	-	-	1/6	BHTV Facsimile			DMT, ohne Datengewinnung		G	
HB-00135	100192	2015	500	218		5570.0	4/1	CERT			Elektromagnet			
HB-00136	150192	1415	325	072	5372.4	5595.8	4/1	BGL-TEMP-SP-AMS-GR	F/L	1,2		66	T	2
HB-00137	180192	1400	550	292	2950.0	5531.0	4/1	BGL-TEMP-SP-AMS-GR	F/L	1,2	Neue BGL/HDS-Sonde 1.Run	67	T	4
HB-00138	230192	1905	325	117	5400.0	5585.5	4/1	BGL-TEMP-SP-AMS-GR	F/L	1,2		68	T	4
HB-00139	040292	1310	508	318	2950.0	5699.0	4/1	BGL-TEMP-SP-AMS-GR	F/L	1,2	Azimut & P1AZ fehlerhaft	69	T	2
HB-00140	170292	2225	692	412	2948.0	5816.0	4/1	BGL-TEMP-SP-AMS-GR	F/L	1,2	Test TMP3	99	T	5
HB-00141	250292	1530	275	030	5728.0	5895.0	4/1	BGL-TEMP-SP-AMS-GR	F/L	1,2	HDS-Sonde	100	T	2
HB-00142	250292	1815	1150	227	4566.0	5875.0	1/6	BHTV Facsimile	F				G	
HB-00143	130392	0945	650	418	2400.0	6023.0	4/1	BGL-TEMP-SP-AMS-GR	F/L	1,2	HDS-Sonde, BGL > 5500 m	102	G	4
HB-00144	130392	1615	1600	917	2942.0	6023.0	19/1	FML-GR	F/L				G	
HB-00145	140392	0815	2175	1708	4397.0	6023.0	4/1	GLT	F/L	1,2			G	
HB-00146	150392	0600	700	430	2365.0	6023.0	4/1	TEMP-GR	F/L	1,2		106	G	
HB-00147	150392	1300	1700	782	4427.0	6024.0	4/1	LDL-CNL-NGS	F/L	1,2		107	G	
HB-00148	160392	0600	700	380	2387.0	6025.0	4/1	TEMP-GR	F/L	1,2		105	G	
HB-00149	160392	1300	1600	1400	4450.0	6020.0	4/1	DSI-GR/WF-GPIT	F/L	1,2			G	
HB-00150	170392	0500	600	500	5450.0	6023.0	4/1	FMI-GR	F/L	1,2			G	
HB-00151	170392	1100	1175	1000	3000.0	6020.0	4/1	ALAT-MSFL-GR-GPIT	F/L	1,2	Azimuthal LATerolog	111	G	
HB-00152	170392	2245	700	432	2345.0	6023.0	4/1	TEMP-GR	F/L	1,2		108	G	
HB-00153	180392	0545	1445	1250	2990.0	6023.0	6/1	BHTV	F	E			G	
HB-00154	180392	2030	1300	1100	3000.0	6020.0	3/1	3D-MAGL			Bosum		G	
HB-00155	190392	0930	500	370	2400.0	6024.0	4/1	TEMP-GR	F/L	1,2		109	G	
HB-00156	190392	1430	1230	942	3000.0	6024.0	7/1	IP			Elgi	123	G	
HB-00157	200392	0300	945	303	3000.0	6024.0	20/1	SP-Redox				112	G	
HB-00158	200392	1245	1125	640	2891.0	6024.0	4/1	BGL-TEMP-SP-AMS-GR	F/L	1,2	el. X-hole Experiment	114	G	4
HB-00159	220392	2100	225	063	394.0	484.0	4/1	AMS-TEMP	F/L		7 Pegelmessungen		G	
HB-00160	220392	2315	425	225	2982.0	4278.0	10/1	MS-AMS-GR					G	

Lfd.Nr.	Datum	Uhr-zeit	Ges. zeit	Mess zeit	Tiefe Top	Tiefe Basis	Ausf.	Messungen	Daten-träger	Mass-stab	Bemerkungen	HBT-Nr.	AR	
HB-00161	230392	0330	1275	747	2949.0	6022.0	4/1	BGL-TEMP-SP-AMS-GR	F/L			115	G	4
HB-00162	230392	1615	645	263	2969.0	6000.0	20/1	SP-Redox				118	G	
HB-00163	230392	2300	650	197	4852.0	5272.0	4/1	FS-SP-AMS-GR	F/L		1. Leutert, 2 Proben	116	G	
HB-00164	240392	1530	700	388		3162.5	4/1	FS-AMS-GR	F/L		GEOCOM	119	G	
HB-00165	240392	2230	900	382	3817.0	4822.5	4/1	FS-AMS-GR	F/L		Leutert Sampler	117	G	
HB-00166	250392	0730	10425	9000	3000.0	6000.0	4/8/1	VSP			Stat. alle 12.5 m		G	
HB-00167	260392	1700	1275	817	2381.0	6026.0	4/1	BGL-TEMP-SP-AMS-GR	F/L		BGL > 5480 m defekt	120	G	5
HB-00168	270392	0900	900	150	3243.0	4077.4	4/1	FS-AMS-GR	F/L		Leutert Sampler		G	
HB-00169	270392	1800	4500	3800	3480.0	6010.0	4/17	BHGM-GR			EDCON, 120 Stationen		G	
HB-00170	300392	0130	750		3062.8	3648.0	4/1	FS-AMS-GR	F/L		Leutert Sampler		G	
HB-00171	010492	2030	1200	745	2686.0	6026.0	4/1	BGL-TEMP-SP-AMS-GR	F/L		>5065m: C2 defekt	122	G	4
HB-00172	020492	2215	1525	650		4294.9	4/1	MSCT-GR	F/L		1 Kern, dann defekt		G	
HB-00173	140492	1645	625	487	21.0	5979.8	4/1	TEMP-GR-CCL			Zem.kopf ca. 4350 m	147	T	
HB-00174	230492	0600	1050	982	0.0	6015.0	4/1	GR-CCL				149	T	
HB-00175	240492	0130	1675	1080	0.0	6018.0	4/1	MFC-GR					T	
HB-00176	260492	1045	375	080	5988.0	6034.0	4/1	BGL-TEMP	F/L		12 stat. Deviation	185	T	
HB-00177	280492	1000	650	350	-	-	6/1	BHTV			Tool defekt, keine Mess.		G	
HB-00178	020592	0045	250	087	660.0	666.0	4/1	AMS			Beobachtung Pegel		G	
HB-00179	020592	0315	575	300	6000.0	6035.0	6/1	BHTV			Frac Kontrolle		G	
HB-00180	020592	0900	250	033	644.0	680.0	4/1	AMS			Beobachtung Pegel		G	
HB-00181	020592	1130	575	060	642.0	6038.0	4/1	FS-AMS			Beobachtung Pegel		G	
HB-00182	020592	1715	275	013	645.0	681.0	4/1	AMS			Beobachtung Pegel		G	

6. Intermediate Logs

J. K. Draxler

6. Intermediate Logs: Interval 4512.0 - 6018.0 m

Time: 18.10.1991 - 13.03.1992

During this period 15 wireline operations were run either with KTB-logging tools or with tools from the service industry:

BGL/GR/AMS/TEMP/SP	: 8 logs
FMI/GR/AMS	: 2 logs
FS/GR	: 2 runs
BHTV-Facsimile	: 2 logs (1 test)
CERT/AMS/GR	: 1 run

The caliper logs (BGL/GR/AMS/TEMP/SP) were run mainly on request of the drilling department. The run with the electro-magnet (CERT/AMS/GR) was required to fish for junk in the borehole.

The other logs (FMI/GR and BHTV) were run to obtain geoscientific information. Two runs with the fluid sampler (FS/GR) recovered samples from zones of inflow.

The drilling department is interested in close control of the deviation and orientation of the borehole and about the break-out situation. The "Quick-Look"-presentations, developed by the Logging Center provide fast answers (see section 8).

These plots are available within hours after completion of the logging operations. Logging, drilling and lithology data are integrated.

Newly logged intervals are merged to provide a continuous profile of the borehole. Overlapping logs are plotted together to record - for example - hole diameter enlargements with time (break-out development).

The information obtained with the scientific logs was required by the field laboratory for the analysis of the lithology, structure, texture and tectonic features of the newly drilled interval. Fracture detection is another key issue, where these logs give an answer for.

As all these logs are run with the Auxiliary Measurement Sonde (AMS), the mud resistivity is measured in situ. Any change in resistivity indicate zones of inflow. Fluid samples were taken from these intervals confirming inflow of saline formation waters.

The information gained by runnig these intermediate logs was essential for planning the logging series at casing depth 6000 m. Examples of intermediate logs are presented in Fig. 6.1 - 6.4.

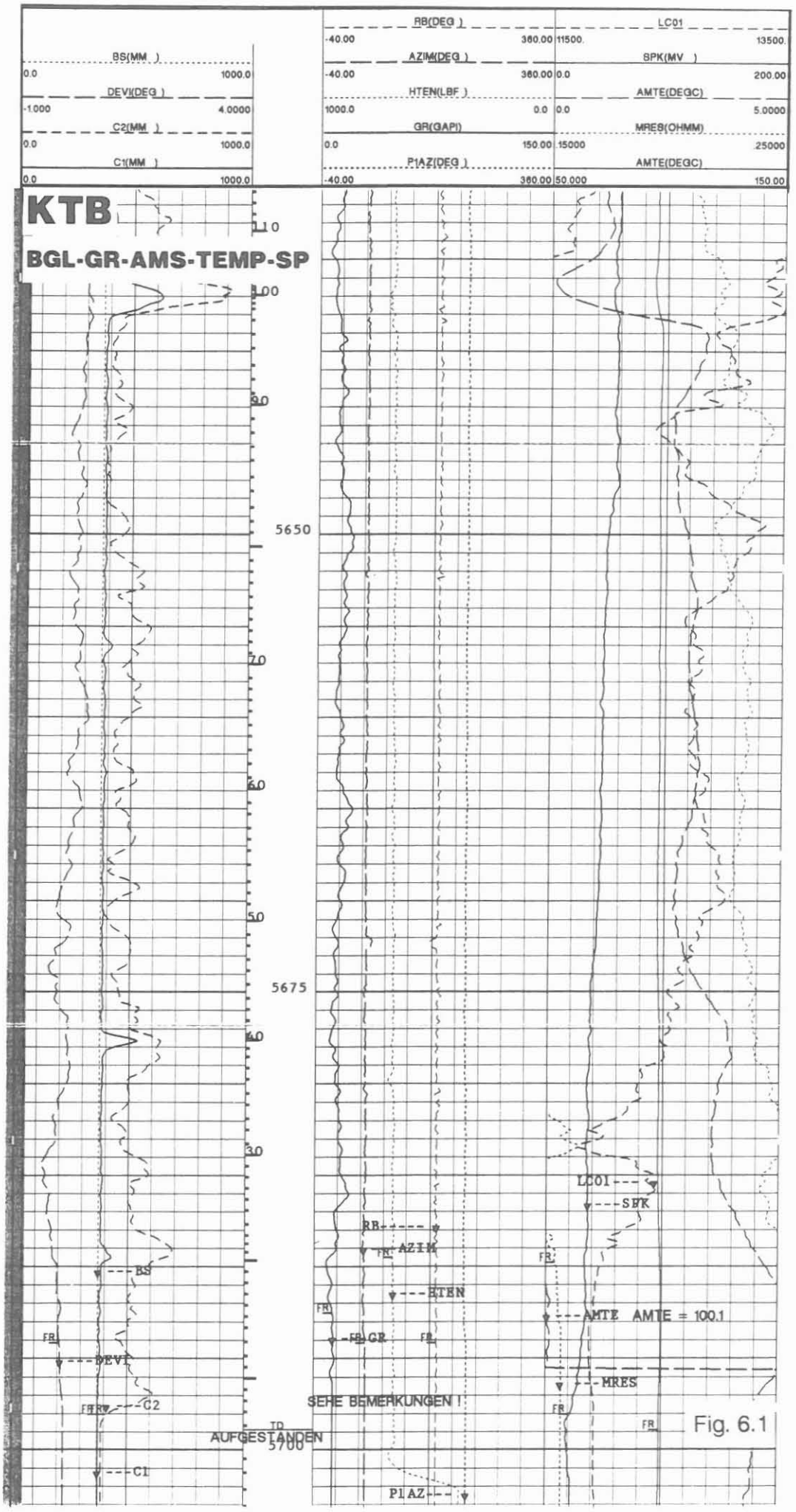
BS(MM)
0.0
1000.0
DEVI(DEG)
-1.000
4.0000
C2(MM)
0.0
1000.0
C1(MM)
0.0
1000.0
RB(DEG)
-40.00
360.00
AZIM(DEG)
-40.00
360.00
HTEN(LBF)
1000.0
0.0
GR(GAPI)
0.0
150.00
P1AZ(DEG)
-40.00
360.00
LC01
11500.
13500.
SPK(MV)
0.0
200.00
AMTE(DEGC)
0.0
5.0000
MRES(OHMM)
.15000
.25000
AMTE(DEGC)
50.000
150.00
KTB
BGL-GR-AMS-TEMP-SP
5650
5675
TD
AUFGESTANDEN
5700
BS
DEVI
C2
C1
RB
AZIM
HTEN
GR
P1AZ
LC01
SPK
AMTE
AMTE = 100.1
MRES
SEHE BEMERKUNGEN !
FR

Fig. 6.1

FMI/GR (Formation MicroImager/Gamma Ray)

Operator: Schlumberger Diepholz/KTB

Job No.	Date	Interval
HB-0001-0076	KTB-Report 91-2	0.0 - 1720.0 m
HB-0077-0127	KTB-Report 92-1	1720.0 - 4512.0 m
HB-0132	03.01.1992	3000.0 - 5505.0 m

Example:
Sections of logs: Resistivity Curves Control Plot: 4975.0 - 5039.0 m, **Fig. 6.2**

Images Field Plot: 5018.0 - 5075.0 m, **Fig. 6.3**

Caliper, Deviation and Orientation Plot: 5100.0 - 5168.0 m, **Fig. 6.4**

Purpose of log:
To obtain information about structure, texture, foliation and tectonic features, like slickensides, shear planes, folds and for the detection of fractures and fracture systems.

Operation:
This new logging tool requires as surface instrumentation the MAXIS 500 logging unit. Making a temporary connection from this mobile unit to the stationary logging unit on location, the logs are recorded. In 14 3/4" borehole the measurement covers 43 % of the circumference of the borehole.

As real-time record the Resistivity Curve Control Plot Fig. 6.2 ist registered. This plot gives information about the tool performance quality. Via play-back the other plots are made on location, like Image Field Plot Fig. 6.3 and Caliper, Deviation and Orientation Plot Fig. 6.4.

Depth scales: 1/200, 1/40 (in the field); logging speed: 6 m/min.

Technical information:
This new logging tool from Schlumberger makes a resistivity scan of sections of the borehole circumference by applying electrode arrays, mounted on four caliper arms, against the wall. Every caliper arm carries a pad and flap with 24 electrodes each. Magnetometer and inclinometer measurements record not only the trajectory of the borehole but allow in combination with the resistivity records the evaluation of dip and strike direction of the formation.

The data rate from the 192 resistivity electrodes is enormous and requires the computer system of the MAXIS 500. From these "fast channels" a complete set of data are recorded at increments of 0.1" (2,5 mm). The "slow channels" (accelerometer, inclinometer, magnetometer data) are recorded at the standard rate of 6".

Mnemonics and Units:

Mnemonic	Description	Unit
BS	Bit Size	(MM)
C1	Caliper 1 - 3	(MM)
C2	Caliper 2 - 4	(MM)
DEVI	Deviation	(DEG)
EI	Emex Intensity	(AMPS)
EV	Emex Voltage	(V)
FBCR	FMI Correlation Resistance	(KOHMS)
GR	Gamma Ray	(GAPI)
HAZI	Hole Azimuth	(DEG)
P1AZ	Pad 1 Azimuth	(DEG)
TENS	Tension	(LBF)

Description of Plots:

Resistivity Curves Control Plot (Fig. 6.2): This real-time plot serves as quality control during the logging operation. The response of 16 resistivity electrodes, the four-arm caliper, the deviation and orientation, pad 1 azimuth, EMEX current and voltage, gamma ray, bit size, tension and a correlation resistance are recorded. During the logging operation it is possible to step-through the arrays of resistivity electrodes to control the response.

Images Field Plot (Fig. 6.3): Fast optical presentation of resistivity images are given by this plot. This plot is made from uncorrected raw data and is unscaled horizontally. Detailed feature detection (fractures, foliation etc.) is therefore limited, but a first approximation is possible (quality control).

Caliper, Deviation and Orientation Plot (Fig. 6.4): This plot gives the borehole trajectory and caliper data presented in profile simulating the short and long axis of an ovalized borehole. The gamma ray is plotted as depth correlation log.

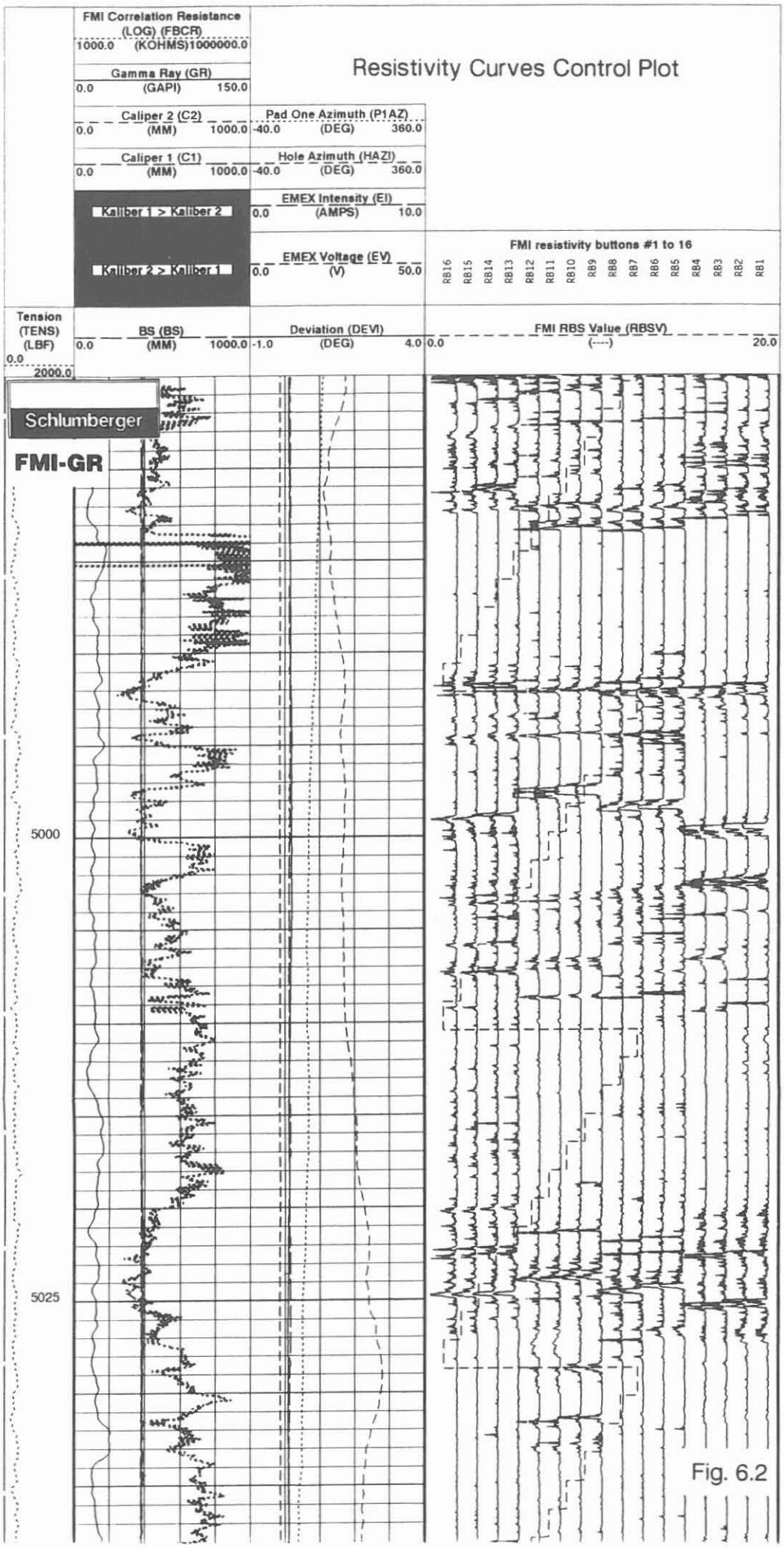
Resistivity Curves Control Plot
FMI Correlation Resistance (LOG) (FBCR)
1000.0 (KOHMS) 1000000.0
Gamma Ray (GR)
0.0 (GAPI) 150.0
Caliper 2 (C2)
0.0 (MM) 1000.0
Caliper 1 (C1)
0.0 (MM) 1000.0
Kaliber 1 > Kaliber 2
Kaliber 2 > Kaliber 1
Pad One Azimuth (P1AZ)
-40.0 (DEG) 360.0
Hole Azimuth (HAZI)
-40.0 (DEG) 360.0
EMEX Intensity (EI)
0.0 (AMPS) 10.0
EMEX Voltage (EV)
0.0 (V) 50.0
FMI resistivity buttons #1 to 16
RB16 RB15 RB14 RB13 RB12 RB11 RB10 RB9 RB8 RB7 RB6 RB5 RB4 RB3 RB2 RB1
Tension (TENS) (LBF)
0.0
2000.0
BS (BS)
0.0 (MM) 1000.0
Deviation (DEVI)
-1.0 (DEG) 4.0
FMI RBS Value (RBSV)
0.0 (----) 20.0
Schlumberger
FMI-GR
5000
5025

Fig. 6.2

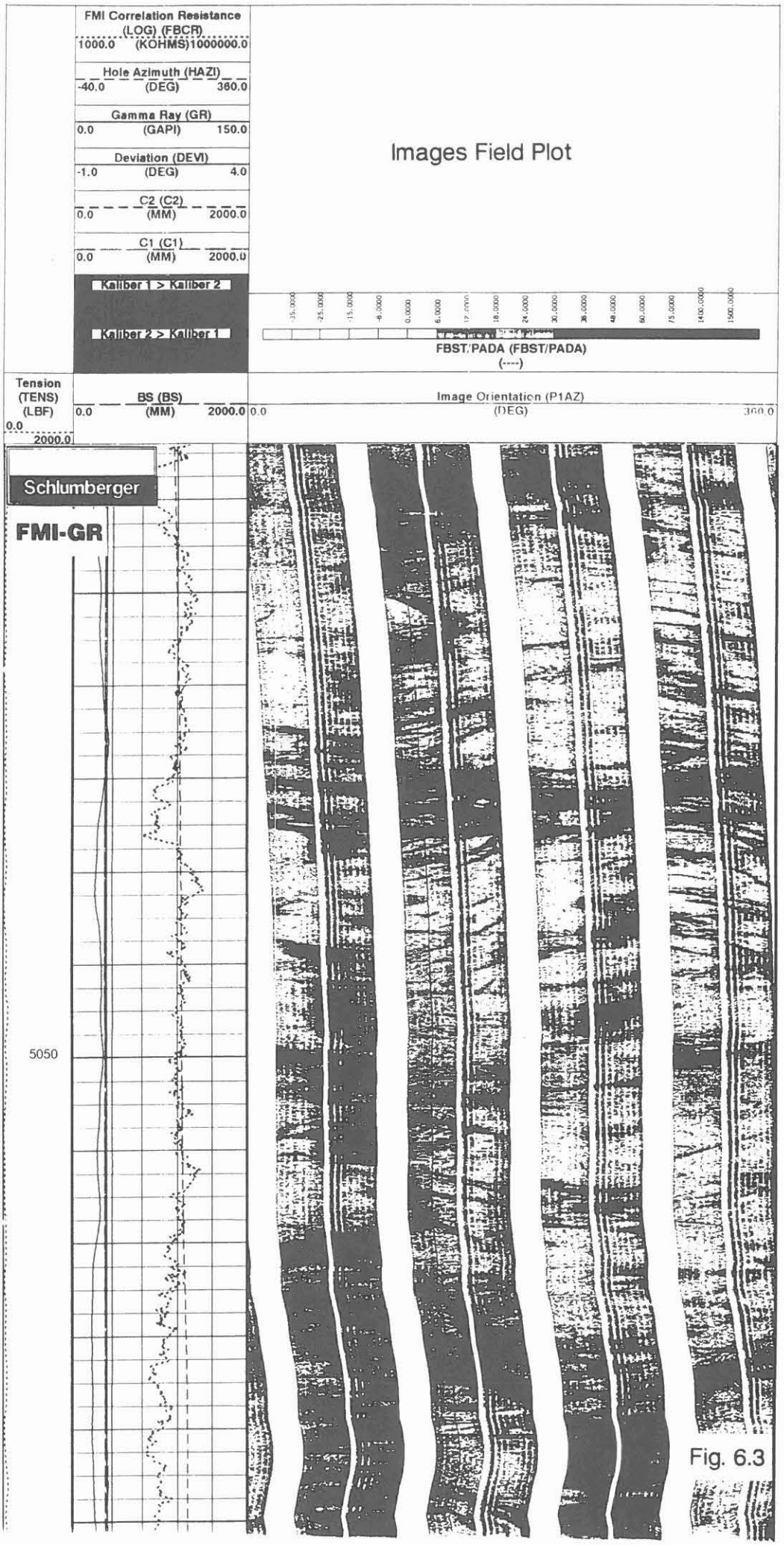
FMI Correlation Resistance (LOG) (FBCR)
1000.0 (KOHMS) 1000000.0
Hole Azimuth (HAZI)
-40.0 (DEG) 360.0
Gamma Ray (GR)
0.0 (GAPI) 150.0
Deviation (DEVI)
-1.0 (DEG) 4.0
C2 (C2)
0.0 (MM) 2000.0
C1 (C1)
0.0 (MM) 2000.0
Kaliber 1 > Kaliber 2
Kaliber 2 > Kaliber 1
Images Field Plot
FBST/PADA (FBST/PADA)
(----)
Tension (TENS) (LBF)
0.0
2000.0
BS (BS)
0.0 (MM) 2000.0
Image Orientation (P1AZ)
0.0 (DEG) 360.0
Schlumberger
FMI-GR
5050

Fig. 6.3

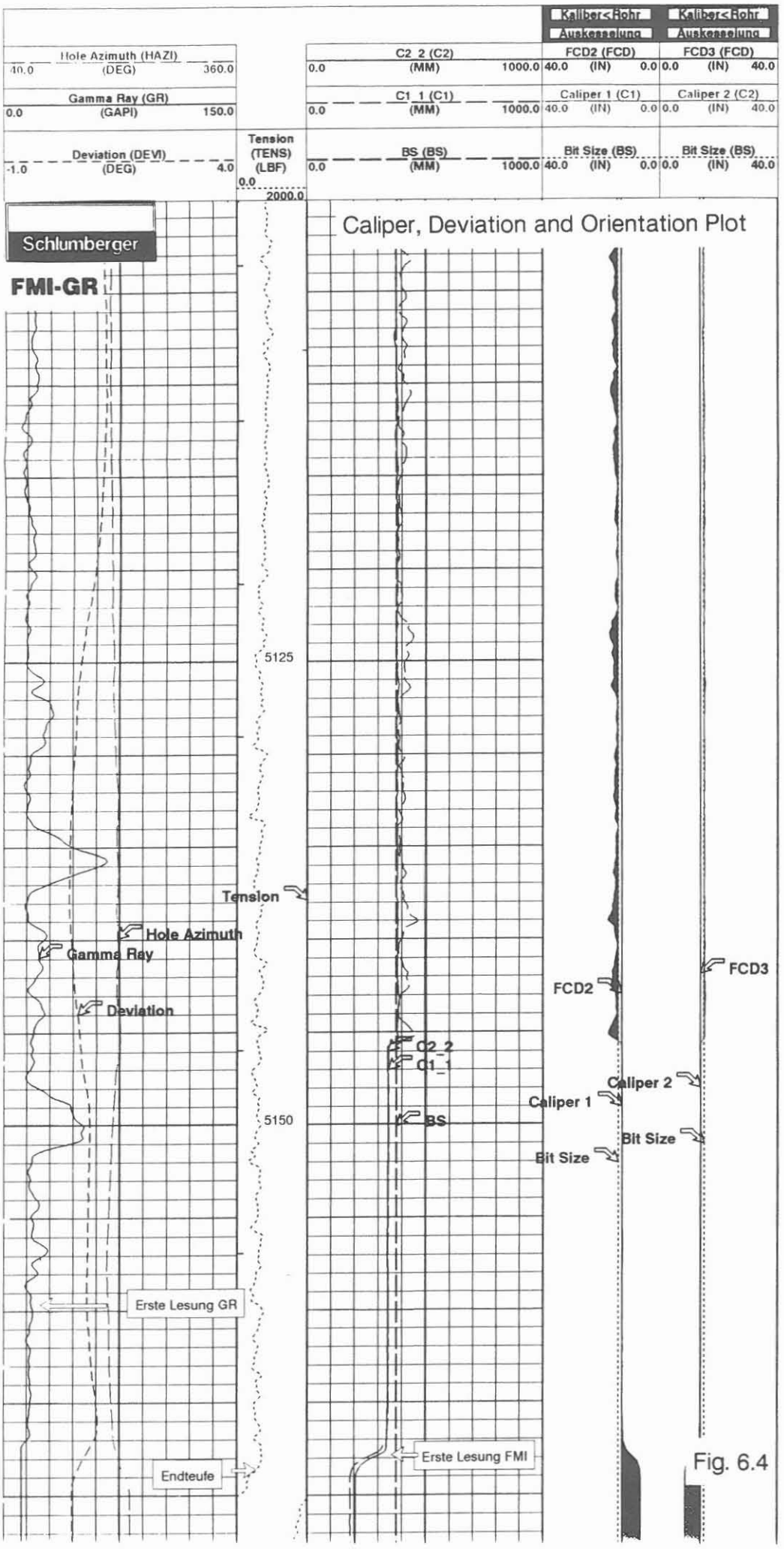
Kaliber<Rohr
Auskesselung
Kaliber<Rohr
Auskesselung
Hole Azimuth (HAZI)
40.0 (DEG) 360.0
Gamma Ray (GR)
0.0 (GAPI) 150.0
Deviation (DEVI)
-1.0 (DEG) 4.0
Tension (TENS) (LBF)
0.0
2000.0
C2_2 (C2)
0.0 (MM) 1000.0
C1_1 (C1)
0.0 (MM) 1000.0
BS (BS)
0.0 (MM) 1000.0
FCD2 (FCD)
40.0 (IN) 0.0
Caliper 1 (C1)
40.0 (IN) 0.0
Bit Size (BS)
40.0 (IN) 0.0
FCD3 (FCD)
0.0 (IN) 40.0
Caliper 2 (C2)
0.0 (IN) 40.0
Bit Size (BS)
0.0 (IN) 40.0
Caliper, Deviation and Orientation Plot
Schlumberger
FMI-GR
5125
5150
Tension
Hole Azimuth
Gamma Ray
Deviation
C2_2
C1_1
BS
FCD2
FCD3
Caliper 2
Caliper 1
Bit Size
Bit Size
Erste Lesung GR
Erste Lesung FMI
Endteufe

Fig. 6.4

7. Logging Operations at Casing Depth
6018.0 m (driller's depth)

J. K. Draxler

7. Logging Operations at Casing Depth 6018.0 m (driller's depth)

According to the operational plan for the KTB-HB borehole drilling with 14 3/4" bit continued to the depth of 6018.0 m. At this depth 13 3/8"/13 5/8" casings were set and cemented.

Before setting casings, the open section of the borehole was logged extensively.

A detailed plan was developed for this logging operation as the estimated formation temperature at this depth reached 175 °C, the temperature rating of standard logging tools. Tools from university institutes had a rating of 125 °C only and deployment was considered.

In addition, the geothermic working group requested a series of temperature records, over a period of pregiven time, for predicting the undisturbed formation temperature.

After setting casings, production tests can only be performed by perforating the casings. To avoid this and not take the risk of drill stem tests (DST) in open hole, a test was performed by lowering the mud level in the borehole and observe the inflow from the formation volumetric-, temperature- and salinity-wise.

To satisfy all requests from the scientific community and take into account the limits given by the rating of the logging tools and not to risk the borehole, the logging operation was split into two phases:

Phase 1:

Start of the logging operation after cooling the borehole by circulation while drilling and/or additional circulation.

The mud level in the borehole is to be kept constant and should be at surface. After running the first temperature log of the six temperature logs within this phase, the Fluxgate-Magnetometer (FML) from the University of Braunschweig (temperature rating 125 °C) was deployed. The tool performed satisfactory and the total interval was logged.

The Geochemical Logging Tool (150 °C rating) was next. Here again, the total interval was logged.

All logging tools requiring the MAXIS 500 logging unit were pooled together for operational and costs reason (DSI, FMI). The new prototype "Azimuthal Laterolog", - a MAXIS-tool, was run successful over the total open hole section.

The Borehole Televiewer (BHTV) from Deutsche Montan Technologie, Bochum, and the 3-D Magnetometer from the Bundesanstalt für Geowissenschaften und Rohstoffe (BGR), Hannover, did perform at already elevated temperatures.

During this phase a good record of temperature built-up with time was logged allowing an extrapolation to the undisturbed formation temperature of 173° ± 2 °C. When starting the logging operation of phase 1 a bottom hole temperature of 111 °C was recorded. After 180 hours the temperature had reached 164 °.

Phase 2:

After reconditioning and cooling the borehole again by circulation, the drill pipes were pulled without filling the borehole with mud. By this procedure the mud level in the borehole was lowered to a calculated depth of 540 m. After observing the rise of the mud level for several hours, the logging operation continued. The Magnetic Susceptibility Tool (MS) from the University of Munich was run first (125 °C temperature rating). The interval from 2982.0 - 4278.0 m could be logged going "in" the hole, before the tool failed.

After running caliper, temperature, mud resistivity and self potential logs, several producing zones were detected and fluid samples were taken from these zones. The VSP was attempted with the new Combinable Seismic Imager (CSI) in combination with the General Purpose Inclination Tool (GPIT) from Schlumberger. After few stations the tool failed. The replacement tools of the same type failed too. The VSP was completed using the Seismic Acquisition Tool (SAT) without orientation system. This certainly degraded the results of the VSP.

With the Borehole Gravity Meter (BHGM) from EDCON, Denver, 120 stations were surveyed and brought good results.

The Mechanical Sidewall Coring Tool (MSCT) developed a problem in the hydraulic system after cutting the first core. Due to time constraints the continuation after repair was cancelled.

When running the Self Potential (SP) log at the end of phase 1 and at the beginning of phase 2, a cross-hole experiment between the pilot hole and the main hole was conducted. Electrical current was applied to both wells using the casing strings as electrodes. The change of potential was recorded in the open hole section of the main hole.

During phase 2 the logging operation was interrupted three times for work on the drilling rig. The standard travelling block (700 t) was exchanged for the heavy duty block (1000 t) required for running the 13 3/8"/13 5/8" casing string.

Table 7.1 is a detailed summary of the logging series phases 1 and 2. The time change from "Middle European Time" to "Middle European Summer Time" was made on Sunday, March 29th, 1992 (advance 1.00 hour).

After running the 13 3/8"/13 5/8" casing string to a depth of 6013.5 m (driller) the string was cemented. Due to the unfavourable conditions (very small clearance 14 3/4" borehole - 13 3/8" casing, no centralizer, tight crystalline formation) the decision was made not to run a Cement Bond Log - but record a temperature log for cement top detection. The cement top was found at 4350.0 m (lower than calculated - indicating loss of cement into fractures).

To control the possible wear of the 13 3/8"/13 5/8" casing string the "zero-reference" Multi-Finger Caliper log (MFC) was run from casing shoe to surface.

In addition, a Gamma Ray - Casing Collar Log (GR/CCL) was recorded inside the drill string to cross-correlate driller to logger depth. A difference of 6.3 m at 6000 m was observed, the logger being deeper than the driller. This difference represents the elongation of the 5"/5 1/2" drill string at 6000 m in mud of 1.04 g/cm^3 density.

After drilling the casing shoe the hole was drilled deeper with 12 1/4" bit size to 6031.0 m in preparation of a hydraulic frac-experiment. A four-arm caliper log (BGL) was recorded showing hole enlargements below the casing shoe. To obtain information about possible frac-orientation a Borehole Televiewer was attempted before the frac, but the tool failed. After the frac a second log was attempted, but the results produced were not conclusive. After the frac, flow from the formation was observed. The fluid sample collected from the interval showed higher salinity, confirming production from the fractured formation.

Drilling continued with 12 1/4" bit size after this frac-experiment.

The log heading from the first log (BGL-GR-AMS-TEMP-SP) of this series, gives the information of the conditions in the borehole at the beginning of the logging operation phase 1 (Fig. 7.1).

Tool sketches of most of the tools run during this series are presented on Fig. 7.2 - 7.12.

Sketches for third-party-tools are not available.

Examples and descriptions of the logs deployed during this series are given on Fig. 7.13 - 7.51 The sequence follows the operation outlined on table 7.1 The logs run after setting the casing follow the normal time sequence of operation.

Logging programme at casing depth 6000 m (phases 1 and 2)

(X) electrical cross-hole experiment
* completed operations

Starting time: Fr 13.03.92 09:45

Tool	Total [d-hh:mm]	Start	End
Phase 1			
* TEMP-GR-AMS-SP-BGL	6:30	Fr 13.03. 09:45	Fr 13.03. 16:15
* FML	16:00	Fr 13.03. 16:15	Sa 14.03. 08:15
* GLT	21:45	Sa 14.03. 08:15	Su 15.03. 06:00
* TEMP-GR	7:00	Su 15.03. 06:00	Su 15.03. 13:00
* LDL-CNL-NGS	17:00	Su 15.03. 13:00	Mo 16.03. 06:00
* TEMP-GR	7:00	Mo 16.03. 06:00	Mo 16.03. 13:00
* DSI-GR WF + GPIT	16:00	Mo 16.03. 13:00	Tu 17.03. 05:00
* FMI-GR	6:00	Tu 17.03. 05:00	Tu 17.03. 11:00
* ALAT-MSFL-GR + GPIT	11:45	Tu 17.03. 11:00	Tu 17.03. 22:45
* TEMP-GR	7:00	Tu 17.03. 22:45	We 18.03. 05:45
* BHTV	14:45	We 18.03. 05:45	We 18.03. 20:30
* 3D-MAGL (FML)	13:00	We 18.03. 20:30	Th 19.03. 09:30
* TEMP-GR	5:00	Th 19.03. 09:30	Th 19.03. 14:30
* IP	12:30	Th 19.03. 14:30	Fr 20.03. 03:00
* SP-Redox	9:45	Fr 20.03. 03:00	Fr 20.03. 12:45
* TEMP-GR-AMS-SP-BGL (X)	11:15	Fr 20.03. 12:45	Sa 21.03. 00:00
* Round trip/add.circulat.	1-21:00	Sa 21.03. 00:00	Su 22.03. 21:00
Phase 2			
* AMS-TEMP	2:15	Su 22.03. 21:00	Su 22.03. 23:15
* MS	4:15	Su 22.03. 23:15	Mo 23.03. 03:30
* BGL-GR-AMS-SP-TEMP	12:45	Mo 23.03. 03:30	Mo 23.03. 16:15
* SP-Redox	6:45	Mo 23.03. 16:15	Mo 23.03. 23:00
* FS-SP-AMS-GR (X)	6:30	Mo 23.03. 23:00	Tu 24.03. 05:30
* Travell. block demounting	10:00	Tu 24.03. 05:30	Tu 24.03. 15:30
* FS-SP-AMS-GR	7:00	Tu 24.03. 15:30	Tu 24.03. 22:30
* FS-SP-AMS-GR	9:00	Tu 24.03. 22:30	We 25.03. 07:30
* VSP	1-09:30	We 25.03. 07:30	Th 26.03. 17:00
* BGL-GR-AMS-SP-TEMP	12:40	Th 26.03. 17:00	Fr 27.03. 05:40
* Preparation of FS-tool	3:20	Fr 27.03. 05:40	Fr 27.03. 09:00
* FS-SP-AMS-GR	9:00	Fr 27.03. 09:00	Fr 27.03. 18:00
* BHGM	1-21:00	Fr 27.03. 18:00	Su 29.03. 15:00
* CET --->> CE summer time	1:00	Su 29.03. 15:00	Su 29.03. 16:00
* VSP	9:30	Su 29.03. 16:00	Mo 30.03. 01:30
* FS-SP-AMS-GR	7:30	Mo 30.03. 01:30	Mo 30.03. 09:00
* VSP	2-11:15	Mo 30.03. 09:00	We 1.04. 20:15
* Waiting time during VSP,	2:00	We 1.04. 20:15	We 1.04. 22:15
* Unloading of rig equipment	:00	We 1.04. 22:15	We 1.04. 22:15
* BGL-GR-AMS-SP-TEMP	9:30	We 1.04. 22:15	Th 2.04. 07:45
* Mounting of travell. block	14:30	Th 2.04. 07:45	Th 2.04. 22:15
* MSCT-GR	15:15	Th 2.04. 22:15	Fr 3.04. 13:30
Total time	21-03:45		

End of operation: Fr 3.04.92 13:30

Schlumberger

HB144 *GR-AMS MIT FML (UNI-BS)*13/3/92

CSU Field Log

COMPANY: NIEDERSAECHSISCHES LANDESAMT F. BODENFORSCHUNG

WELL: KTB-OPF-HB

FIELD: OBERPFALZ
KREIS : NEUSTADT/WN
LAND: BAYERN
NATION: BRD
LOCATION: NAABDEMENREUTH
WINDISCHESCHENBACH

LATITUDE: H 55 19 864,35
LONGITUDE: R 45 08 775,24

PERMANENT DATUM: ACKERSOHLE ELEVATIONS-
ELEV. OF PERM. DATUM: 513.8 M KB:
LOG MEASURED FROM: ACKERSOHLE DF: 11.8 M
0.0 M ABOVE PERM. DATUM GL: 513.8 M
DRLG. MEASURED FROM: ACKERSOHLE

DATE: 13 MAR 92
RUN NO: HB144

OTHER SERVICES-
BGL, FML, GLT,
LDL-CNL-NGS,
FMI, ALAI-MSF
-GPIT, DSI,
FACSIM. BHTV
IP, SP-REDOX

PROGRAM
TAPE NO:
33.243A
SERVICE
ORDER NO:
HB144

DEPTH-DRILLER:	6018.0 M		
DEPTH-LOGGER:	6024.7 M		
BTM. LOG INTERVAL:	5815.5 M		
TOP LOG INTERVAL:	2950.0 M		
CASING-DRILLER:	290.0 M	3000.5 M	
CASING-LOGGER:	290.0 M	3000.0 M	
CASING:	24-1/2"K55	16" K55	OPEN HOLE
BIT SIZE:	28"	17-1/2"	14-3/4"

TYPE FLUID IN HOLE: DEHYDRIL
DENSITY: 1.04 G/C3
VISCOSITY: 6469 S
PH: 11.5
FLUID LOSS: 14.0 C3
SOURCE OF SAMPLE: UMLAUF
RM: 1.050 OHMM AT 18.0 DEGC
RMF: .920 OHMM AT 19.0 DEGC
RMC: 1.100 OHMM AT 19.0 DEGC
SOURCE RMF/RMC: PRESSE/PRESSE
RM AT BHT: .314 OHMM AT 111. DEGC
RMF AT BHT: .282 OHMM AT 111. DEGC
RMC AT BHT: .337 OHMM AT 111. DEGC

TIME CIRC. STOPPED: 00:00 13/3
TIME LOGGER ON BTM.: 21:37 13/3

MAX. REC. TEMP: 111.0 DEGC

LOGGING UNIT NO: 701
LOGGING UNIT LOC: KTB
RECORDED BY: KUEHR/DEGREFTE
WITNESSED BY: DRAXLER/ZOTH

REMARKS:

MAX TEMP VON VORHERGEMESSENE *BGL-GR-AMS-TEMP-SP* UEBERNOMME
GEBOHRT BIS 11:45 10/3/92 (2 METER GEKERNT)
DIESE MESSUNG WURDE FUER TEUFENKORRELATION GEFAHREN
ES WURDEN NUR GR UND MRES REGISTRIERT.
MESSGESCHWINDIGKEIT 12 M/MIN
SONDE MIT SWIVELADAPTERHEAD GEFAHREN.
MAGNETOMETER : .8 M UEBER UNTERKANTE SONDE.

Fig. 7.1

EQUIPMENT NUMBERS-

TCM-AB 449	TCC-B 190	SGC-SA 1247	AME-1720
-	-	-	-
SAH-E 796	-		

KTB

Tool Sketch: BGL-GR-AMS-TEMP-SP

LOGGING TOOL STRING SKETCH

	PEH HEAD	
EQF1, 3 3/8" OD	SWIVEL	11.23 M
AMS, 3 5/8" OD		10.34 M
	HTEN	9.45 M
	MRES	9.19 M
	CENTRALISER	
TCCB, 3 3/8" OD		7.62 M
SGTL, 3 3/8" OD		6.71 M
	GR	6.43 M
BGTX, 3 5/8" OD		5.03 M
	CENTRALISER	DEVI RB AZIM 4.83 M
	ISOL. ADAPTER	
	4-ARM KALIB.	
		C2 C1 0.91 M
	TEMP. FUEHLER	AMTE 0.05 M
		TOOL ZERO

TOTAL TOOL STRING LENGTH IS 11.79 M.
TOTAL TOOL STRING WEIGHT IS 325.2 KG IN AIR.

Fig. 7.2

KTB/University Braunschweig

Tool Sketch: FML-GR-AMS

LOGGING TOOL STRING SKETCH

	PEH HEAD	
EQF1, 3 3/8" OD	SWIVEL	10.03 M
AMS, 3 5/8" OD		9.14 M
	MRES	8.00 M
	CENTRALISER	
TCCB, 3 3/8" OD		6.43 M
SGTL, 3 3/8" OD		5.51 M
	GR	5.23 M
		TOOL ZERO

TOTAL TOOL STRING LENGTH IS 10.59 M.
TOTAL TOOL STRING WEIGHT IS 200.5 KG IN AIR.

Fig. 7.3

LOGGING TOOL STRING SKETCH

Schlumberger

Tool Sketch: GLT

AMS, 3 5/8" OD		20.78 M
	HTEN	18.59 M
TCCB		18.57 M
NGTD, 3 5/8" OD		17.65 M
	SGR	17.14 M
CNTG, 3 3/8" OD		14.83 M
EXZENTRIERER		
ACTD, 3 5/8" OD		11.15 M
GSTA, 3 3/8" OD		8.33 M
	ADCG ADCZ	2.84 M
		TOOL ZERO

Fig. 7.4

TOTAL TOOL STRING LENGTH IS 20.78 M.
TOTAL TOOL STRING WEIGHT IS 589.7 KG IN AIR.

LOGGING TOOL STRING SKETCH

Schlumberger

Tool Sketch: LDL-CNL-NGL

	KABELKOPF/ AH64	
AMS		21.26 M
	HTEN	19.08 M
TCCB		19.05 M
NGTD		18.14 M
	SGR	17.63 M
CNTG		15.32 M
	CNT-EXZENTRIERER	
LDTD		11.63 M
	CALI	5.94 M
FLEX2		5.13 M
FLEX1		4.52 M
BGTX, 3 5/8" OD		3.91 M
	CME-MB 2 ARM EXZENT.	
	2-ARM BGT	
		TOOL ZERO

Fig. 7.5

TOTAL TOOL STRING LENGTH IS 22.33 M.
TOTAL TOOL STRING WEIGHT IS 559.3 KG IN AIR.

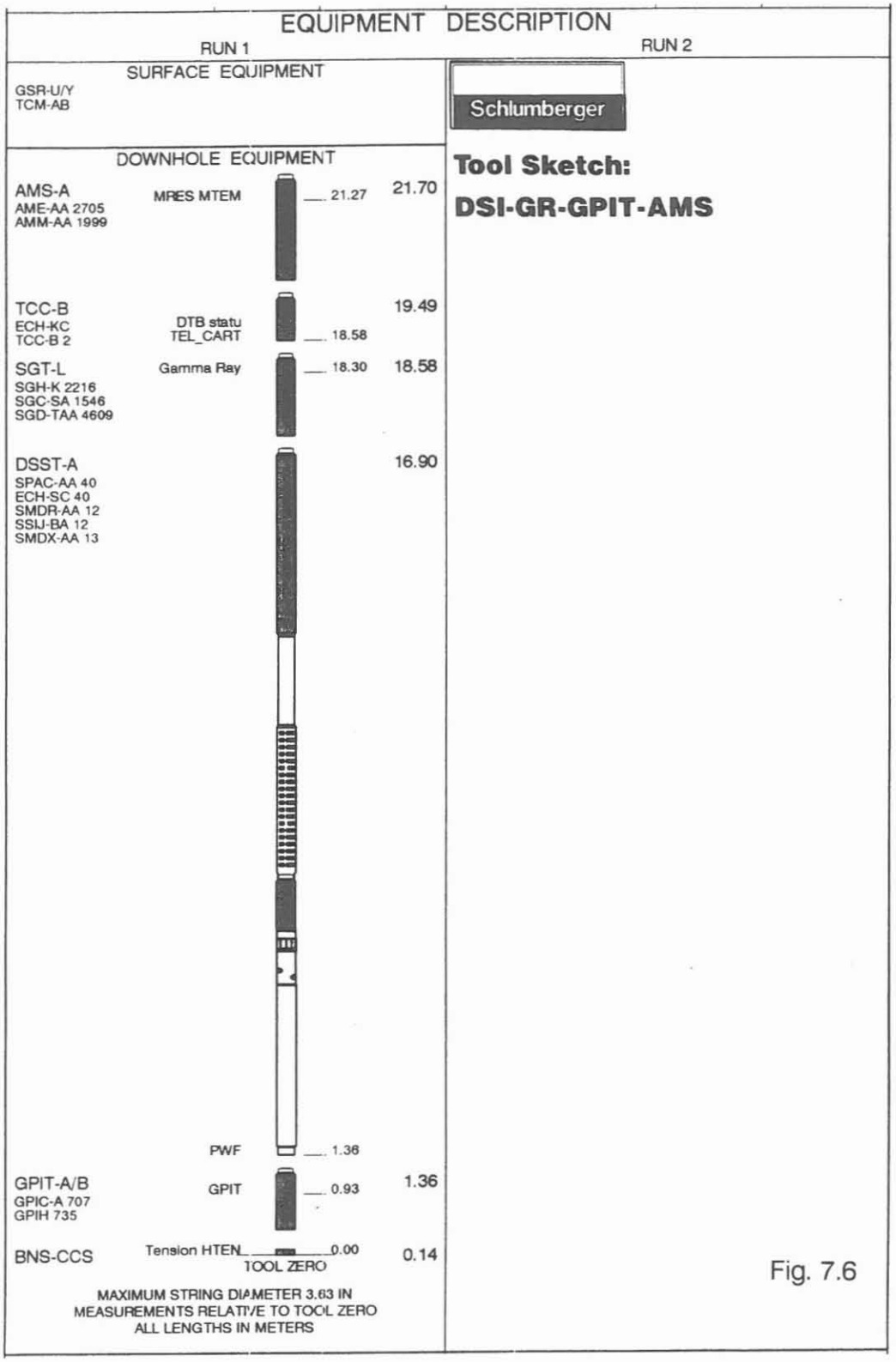
EQUIPMENT DESCRIPTION
RUN 1
RUN 2
SURFACE EQUIPMENT
GSR-U/Y
TCM-AB
Schlumberger
Tool Sketch:
DSI-GR-GPIT-AMS
DOWNHOLE EQUIPMENT
AMS-A
AME-AA 2705
AMM-AA 1999
MRES MTEM
21.27
21.70
TCC-B
ECH-KC
TCC-B 2
DTB statu
TEL_CART
18.58
19.49
SGT-L
SGH-K 2216
SGC-SA 1546
SGD-TAA 4609
Gamma Ray
18.30
18.58
DSST-A
SPAC-AA 40
ECH-SC 40
SMDR-AA 12
SSIJ-BA 12
SMDX-AA 13
16.90
PWF
1.36
GPIT-A/B
GPIC-A 707
GPIH 735
GPIT
0.93
1.36
BNS-CCS
Tension HTEN
0.00
0.14
TOOL ZERO
MAXIMUM STRING DIAMETER 3.63 IN
MEASUREMENTS RELATIVE TO TOOL ZERO
ALL LENGTHS IN METERS

Fig. 7.6

EQUIPMENT DESCRIPTION

RUN 1 | RUN 2

SURFACE EQUIPMENT

GSR-U/Y
DTM-A

DOWNHOLE EQUIPMENT

DTC-A
ECH-KN
DTC-A

TEL_CART — 12.70

13.00

FTB statu — 10.57

DTA-A
ECH-KE
DTA-A

10.57

ADAPTER — 9.35

SGT-L
SGH-K
SGC-SA
SGD-TAA

Gamma Ray — 9.07

9.35

FBST-A
FBCC-A
AH-185
GPIC-A
FBSC-A
FBSS-A

7.67

GPIT FBCC
PADS FBSC — 0.58

Tension — 0.00

TOOL ZERO

MAXIMUM STRING DIAMETER 5.00 IN
MEASUREMENTS RELATIVE TO TOOL ZERO
ALL LENGTHS IN METERS

Schlumberger

Tool Sketch: FMI-GR

Fig. 7.7

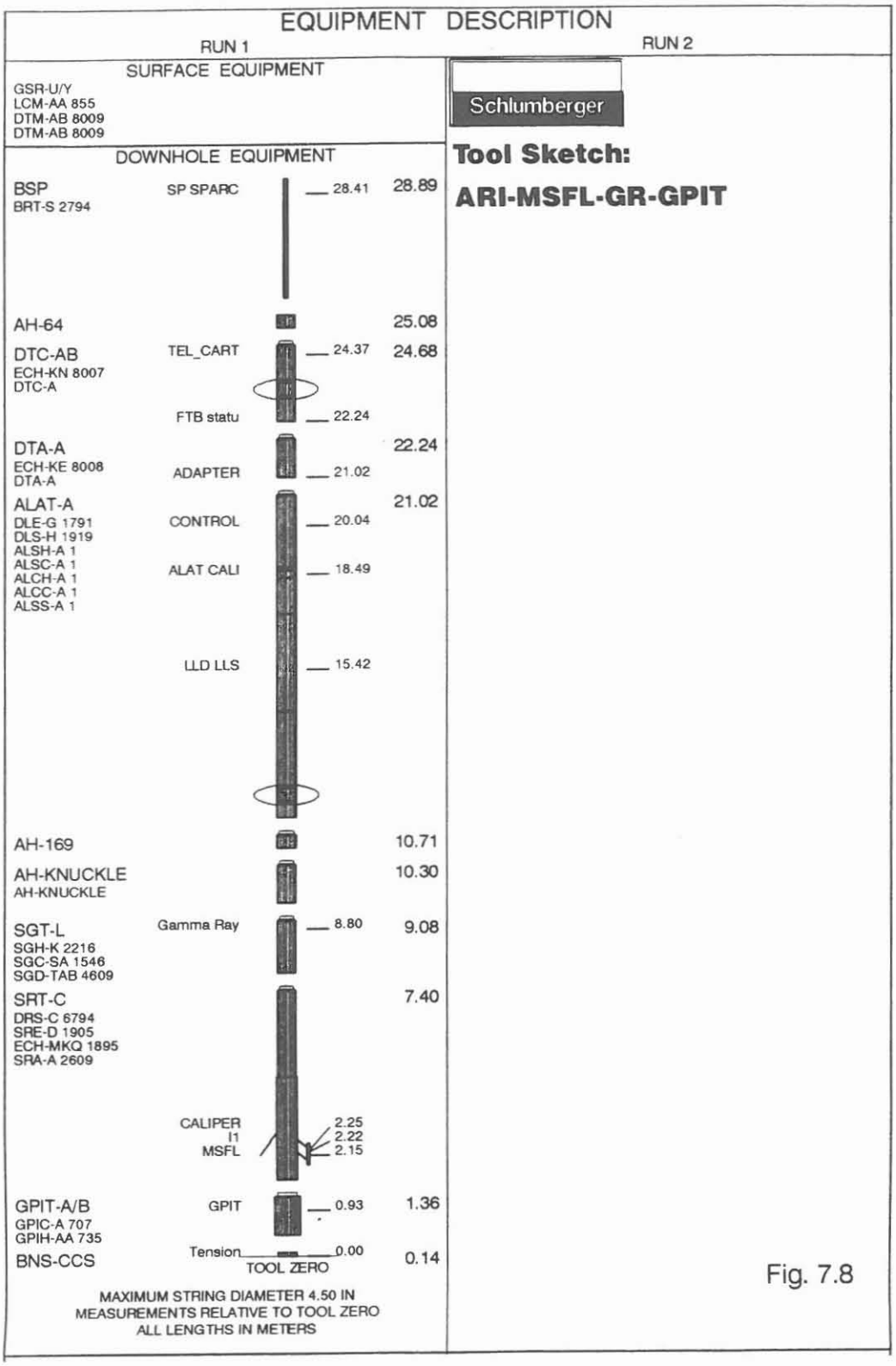
EQUIPMENT DESCRIPTION
RUN 1
RUN 2
SURFACE EQUIPMENT
GSR-U/Y
LCM-AA 855
DTM-AB 8009
DTM-AB 8009
DOWNHOLE EQUIPMENT
Schlumberger
Tool Sketch:
ARI-MSFL-GR-GPIT
BSP
BRT-S 2794
SP SPARC
28.41
28.89
AH-64
25.08
DTC-AB
ECH-KN 8007
DTC-A
TEL_CART
24.37
24.68
FTB statu
22.24
DTA-A
ECH-KE 8008
DTA-A
22.24
ADAPTER
21.02
ALAT-A
DLE-G 1791
DLS-H 1919
ALSH-A 1
ALSC-A 1
ALCH-A 1
ALCC-A 1
ALSS-A 1
21.02
CONTROL
20.04
ALAT CALI
18.49
LLD LLS
15.42
AH-169
10.71
AH-KNUCKLE
AH-KNUCKLE
10.30
SGT-L
SGH-K 2216
SGC-SA 1546
SGD-TAB 4609
Gamma Ray
8.80
9.08
SRT-C
DRS-C 6794
SRE-D 1905
ECH-MKQ 1895
SRA-A 2609
7.40
CALIPER
2.25
I1
2.22
MSFL
2.15
GPIT-A/B
GPIC-A 707
GPIH-AA 735
GPIT
0.93
1.36
BNS-CCS
Tension
0.00
0.14
TOOL ZERO
MAXIMUM STRING DIAMETER 4.50 IN
MEASUREMENTS RELATIVE TO TOOL ZERO
ALL LENGTHS IN METERS

Fig. 7.8

LOGGING TOOL STRING SKETCH

KTB

Tool Sketch: GR-TEMP

Fig. 7.9

TOTAL TOOL STRING LENGTH IS 5.84 M.
TOTAL TOOL STRING WEIGHT IS 56.7 KG IN AIR.

LOGGING TOOL STRING SKETCH

KTB/UNI-Frankfurt

Tool Sketch: SP-REDOX

Fig. 7.10

TOTAL TOOL STRING LENGTH IS 5.03 M.

KTB/Leutert

Tool Sketch: FS-GR-AMS

LOGGING TOOL STRING SKETCH

KABELKOPF

AMS, 3 5/8" OD — 8.94 M
HTEN — 8.56 M
AMTE — 8.36 M
MRES — 8.31 M

TCCB, 3 3/8" OD — 6.73 M

SGTL, 3 3/8" OD — 5.82 M
GR — 5.54 M

4 1/2" OD — 4.14 M

GEHAEUSE FUER MAX.
3 FLUIDSAMPLER

EINLASS FLUIDSAMPLER

TOOL ZERO

Fig. 7.11

TOTAL TOOL STRING LENGTH IS 10.06 M.

Schlumberger

Tool Sketch: MSCT-GR

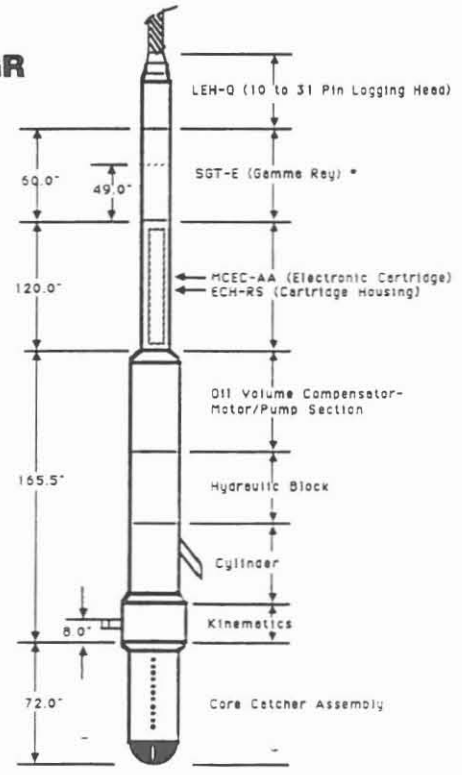

Fig. 7.12

BGL/GR/AMS/TEMP/SP (Borehole Geometry Log/Gamma Ray/Auxiliary Measurement Sonde/Temperature/Self Potential)

Operator: KTB

Job No.	Date	Interval
HB-0001-0076	KTB-Report 91-2	0.0 - 1720.0 m
HB-0077-0127	KTB-Report 92-1	1720.0 - 4512.0 m
HB-0143	13.03.1992	2400.0 - 6024.6 m

Example:
Section of log: 5964.0 - 6024.6 m, **Fig. 7.13**

Purpose for log:
Deviation, orientation and caliper control of the borehole. Measurements of borehole temperature, mud resistivity and self potential for inflow zone detection.

Operation:
The temperature, mud resistivity (salinity) and self potential are recorded going "in" the borehole. After reaching bottom the caliper arms are opened and the reading of the caliper-, deviation- and orientation sensors are recorded in addition to the other parameters coming "out" the borehole.
Depth scales: 1/1000 and 1/200; logging speed: 15 m/min.

Technical information:
This combination tool consists of a Schlumberger four-arm caliper with pendulum deviation and compass orientation systems (BGL), gamma ray (GR), mud resistivity, temperature and head tension sensors (AMS) and two additional measurement systems - temperature and self potential - integrated by a modification made by KTB. With this tool modification it is possible to measure the temperature at the lowest depth reached as the sensor is at the bottom of the tool.
Data rate: set of data in increments of 6".

Mnemonics and Units:

Mnemonics	Description	Unit
AMTE	Temperature AMS-Sensor	(DEGC)
AZIM	Azimuth	(DEG)
BS	Bit size	(MM)
C1	Caliper 1-3	(MM)
C2	Caliper 2-4	(MM)
DEVI	Deviation	(DEG)
GR	Gamma Ray	(GAPI)
HTEN	Head Tension	(LBF)
LC01	Mud Salinity (equivalent)	(PPM)
MRES	Mud Resistivity	(OHMM)
P1AZ	Pad 1 Azimuth	(DEG)
RB	Relative Bearing	(DEG)
SPK	Self Potential (contact)	(MV)

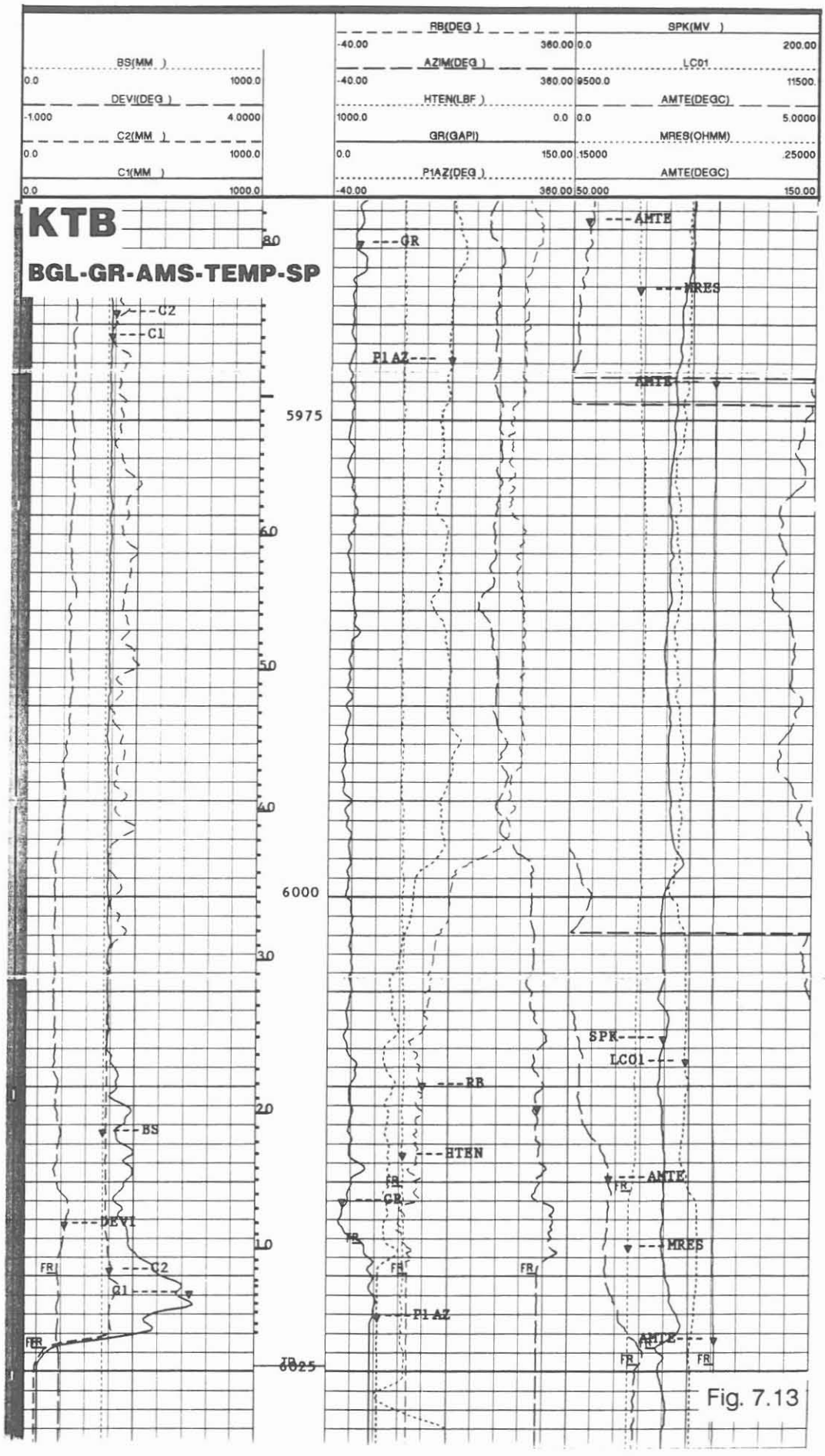
BS(MM)
0.0
1000.0
DEVI(DEG)
-1.000
4.0000
C2(MM)
0.0
1000.0
C1(MM)
0.0
1000.0
RB(DEG)
-40.00
360.00
AZIM(DEG)
-40.00
360.00
HTEN(LBF)
1000.0
0.0
GR(GAPI)
0.0
150.00
P1AZ(DEG)
-40.00
360.00
SPK(MV)
0.0
200.00
LC01
9500.0
11500.
AMTE(DEGC)
0.0
5.0000
MRES(OHMM)
.15000
.25000
AMTE(DEGC)
50.000
150.00
KTB
BGL-GR-AMS-TEMP-SP
5975
6000
6025
C2
C1
BS
DEVI
GR
P1AZ
RB
HTEN
AMTE
MRES
SPK
LC01
FR

Fig. 7.13

FML/GR/MRES (Fluxgate Magnetometer/Gamma Ray/Mud Resistivity)

Operator: University of Braunschweig/KTB

Job No.	Date	Interval
HB-0144	13.03.1992	2942.0 - 6023,0 m

Example:
Section of depth reference log only: 5600.0 - 5965.0 m, **Fig. 7.14**

Purpose of Log:
With this instrument three-dimensional measurements of the magnetic field are made. With the logs recorded in a borehole information can be obtained about the total magnetisation of the surrounding rocks. This will allow the detection of magnetic anomalies indicating also magnetic bodies not penetrated by the borehole.

Operation:
This newly developed magnetometer from the University of Braunschweig is run in combination with the GR and AMS (for MRES) from KTB. The responses of the magnetisation in the X, Y and Z-axis are measured. The sum represents the total magnetic field.
Depth scale: 1/1000; logging speed: 9 m/min.

Technical information:
The magnetometer is a digital tool and was designed and manufactured in such a way, that it can be connected to standard Schlumberger cable heads or tools (GR). Presently the tool has a temperature rating of 125 °C.

Mnemonics and Units:

Mnemonic	Description	Unit
GR	Gamma Ray	(GAPI)
MRES	Mud Resistivity	(OHMM)
TENS	Tension	(LBF)

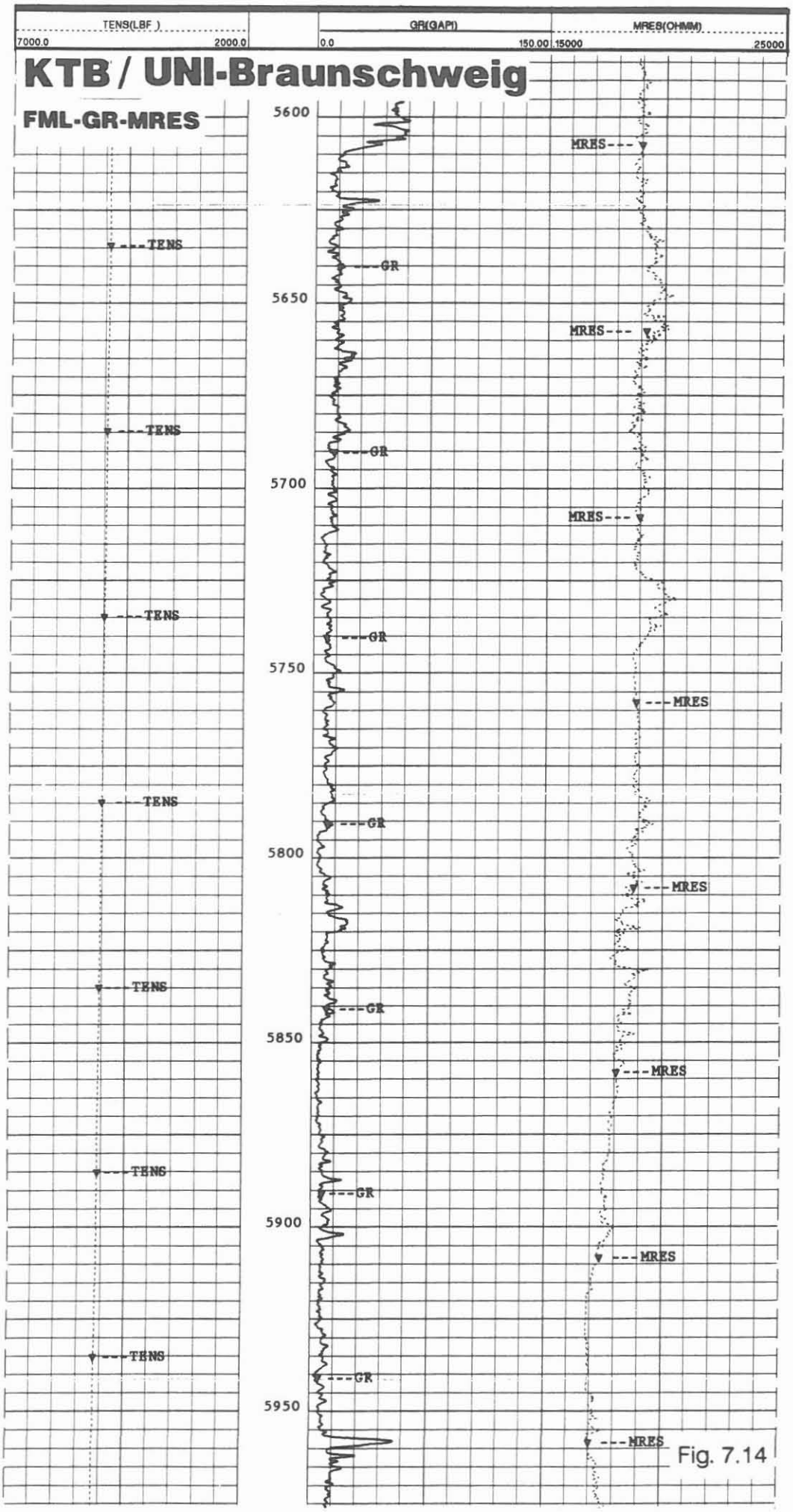
TENS(LBF)
7000.0
2000.0
GR(GAPI)
0.0
150.00
MRES(OHMM)
15000
25000
KTB / UNI-Braunschweig
FML-GR-MRES
5600
5650
5700
5750
5800
5850
5900
5950
TENS
GR
MRES

Fig. 7.14

GLT (Geochemical Logging Tool)

Operator: Schlumberger Diepholz/KTB

Job No.	Date	Interval
HB-0118	KTB-Report 92-1	2994.0 - 4455.0 m
HB-0145	14.03.1992	4397.0 - 6023.0 m

Example:
Section of log: 5721.0 - 5789.0 m, **Fig. 7.15**

Purpose of log:
In situ elemental analysis by spectroscopic measurements will provide information about concentrations of 10 elements in the rock. Transfering elemental yields into oxide concentrations a continuous estimation of mineral composition of the rocks can be made.

Operation:
All relevant data is recorded digitally on magnetic tape. The analog data record presented on Fig. 7.15 is considered as quality record only and gives computed ratios from certain elements. The analysis of the recorded spectra in respect of the yields, in weight percent, of the elements Si, Ca, Fe, S, Al, Ti, Gd, Th, U, K is either done at the KTB logging centre on location, or the Schlumberger computing centre in Hannover. Further processing is done at KTB.
Depth scales: 1/100, 1/200; logging speed: 2 m/min.

Technical information:
This combination consists of the Gamma Ray Spectrometer (GST), Aluminum Activation Clay Tool (AACT), Natural Gamma Spectrometer (NGS) and a Compensated Neutron Tool (CNT) to carry a 252 Californium-source. This source and a neutron generator provide the energie for activating the formation. The log was recorded in "Capture Mode".
Data rate: 6".

Mnemonics and Units:

Mnemonics	Description	Unit
ALUM	Aluminum Indicator	
CSIG	Corrected Sigma	(CU)
HTEN	HEAD Tension	(LBF)
IIR	Iron Indicator Ratio	
LIR	Lithology Indicator Ratio	
PIR	Porosity Indicator Ratio	
SIR	Salinity Indicator Ratio	
SGR	Sum Gamma Ray	(GAPI)

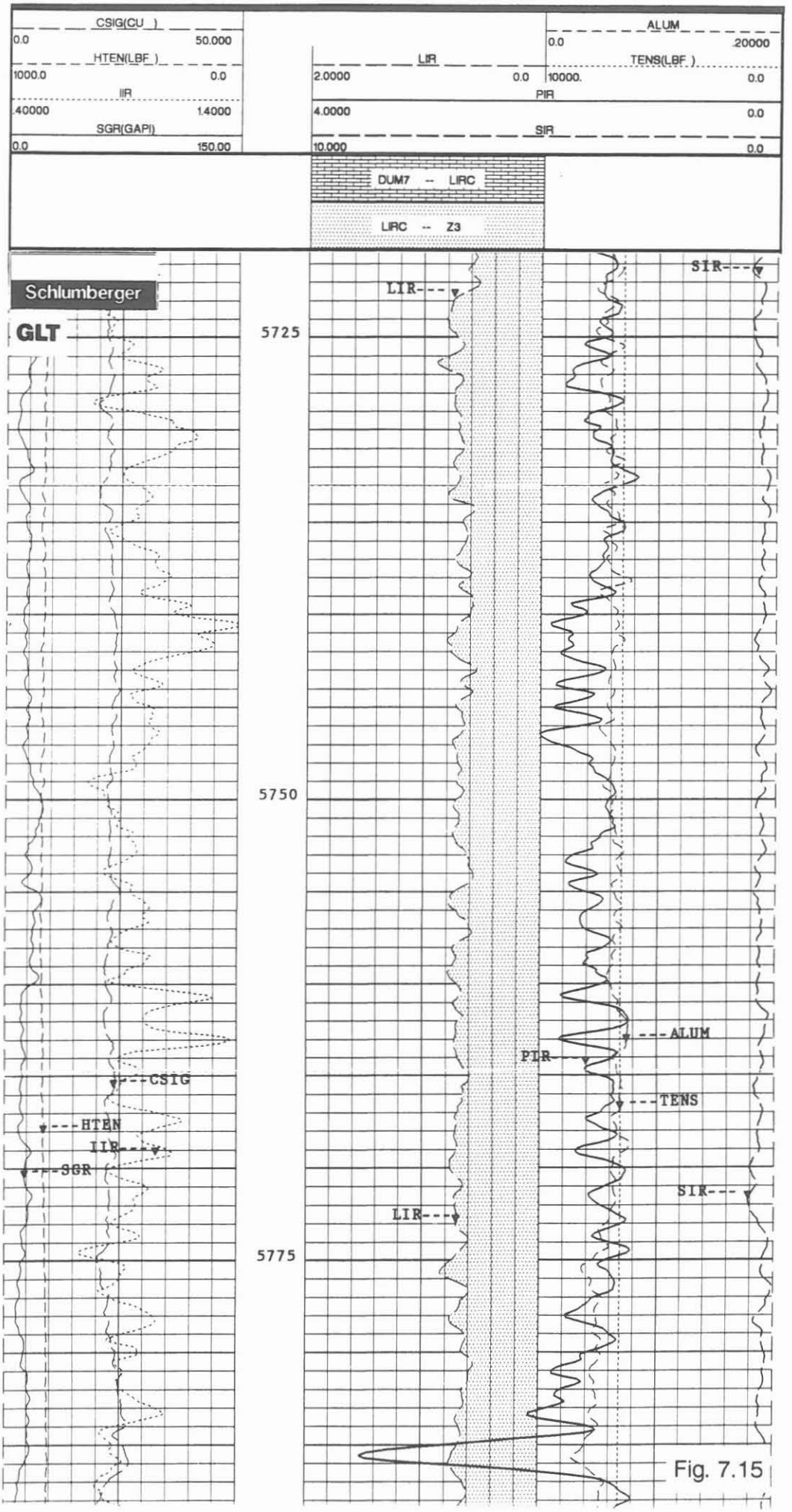
CSIG(CU)
0.0
50.000
HTEN(LBF)
1000.0
0.0
IIR
.40000
1.4000
SGR(GAPI)
0.0
150.00
LIR
2.0000
0.0
PIR
4.0000
0.0
SIR
10.000
0.0
ALUM
0.0
.20000
TENS(LBF)
10000.
0.0
DUM7 -- LIRC
LIRC -- Z3
Schlumberger
GLT
5725
5750
5775
LIR---
SIR---
---ALUM
PLR---
---TENS
---CSIG
---HTEN
IIR---
---SGR

Fig. 7.15

GR/TEMP (Gamma Ray/Temperature Log)

Operator: KTB

Job No.	Date	Interval
HB-0001-0076	KTB-Report 91-2	0.0 - 1720,0 m
HB-0077-0127	KTB-Report 92-1	1720.0 - 4512.0 m
HB-0146	15.03.1992	2365.0 - 6023.0 m

Example:
Section of log: 5635.0 - 6015.0 m, **Fig. 7.16**

Purpose of log:
During a logging series several temperature logs are recorded at pregiven time intervals. With the help of this sequence of temperature logs an estimation of the true formation temperature is possible by extrapolation.

Operation:
The temperature log is recorded going "in" the borehole. By this method "undisturbed" conditions are present. At the bottom of the hole stationary readings are recorded for a minimum of time, lasting for 30 - 45 minutes.

Technical information:
This tool is a simple combination of two KTB tools - a gamma ray and temperature section. This simple configuration is used for time sequence temperature logging operations.
Data rate: 6"; logging speed: 18 m/min.

Mnemonics and Units:

Mnemonics	Description	Unit
GR	Gamma Ray	(GAPI)
TEMP3	Temperature	(DEGC)
TENS	Tension	(LBF)

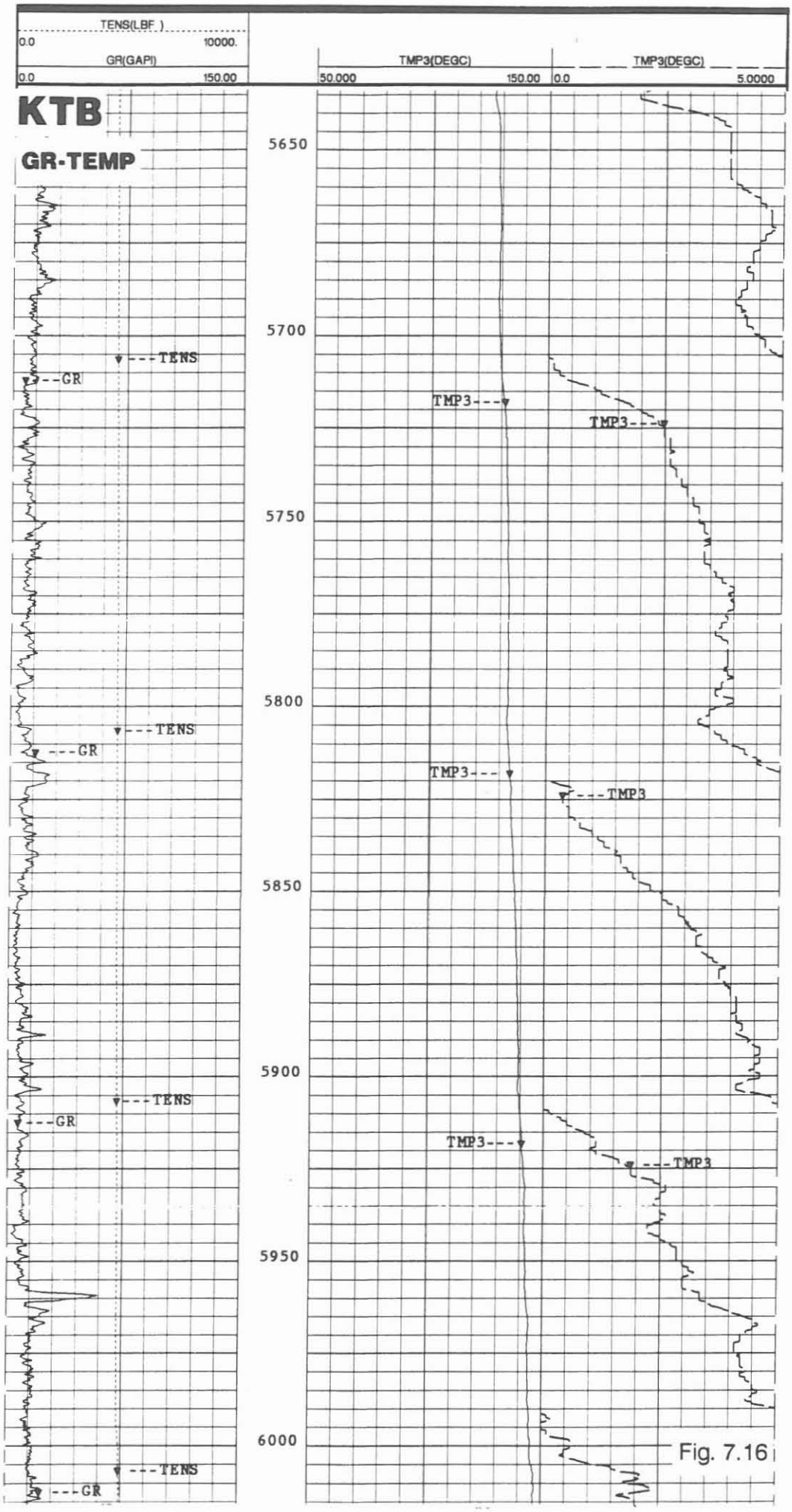
TENS(LBF)
0.0
10000.
GR(GAPI)
0.0
150.00
TMP3(DEGC)
50.000
150.00
TMP3(DEGC)
0.0
5.0000
KTB
GR-TEMP
5650
5700
5750
5800
5850
5900
5950
6000
---TENS
---GR
TMP3---
---TMP3

Fig. 7.16

LDL/CNL/NGL (Litho-Density-/Compensated Neutron-/Natural Gamma Spectrometer Log)

Operator: Schlumberger Diepholz/KTB

Job No.	Date	Interval
HB-0116	KTB-Report 92-1	2995.0 - 4520.0 m
HB-0147	15.03.1992	4427.0 - 6024.0 m

Example:
Section of log: 5705.0 - 5770.0 m, **Fig. 7.17**

Purpose of log:
This combination logging tool is deployed to obtain information on porosity and lithology. Two methods are used to measure porosity indirectly: bulk density and hydrogen index measured by neutron activation. Density, Neutron and Gamma Spectrometer respond to lithology. In addition, these measurements can be used to calculate the heat production rate due to radioactive decay.

Operation:
This combination tool has to be run excentralized. The caliper arm of the density and an excentralizer for the neutron is normally used. For this operation the "short axis logging technique" was applied. With this technique the sensors from the density and neutron tools are forced to travel along the short axis of the ovalized borehole. Data quality is increased significantly this way.
Depth scale: 1/200, 1/1000; logging speed: 6 m/min.

Technical information:
This is a nuclear logging string, it means mechanical nuclear sources are used to activate the formation. For the density measurement a cesium-source is needed for gamma activation, while an americium-beryllium-source is used for neutron activation. The scale of the density and neutron record is different from sediments. The density is scaled from 2.20 to 3.20 g/cm^3 and the neutron from 0.0 to 30 % (3000 V/V). The high neutron response is not due to porosity but is a clear indication of neutron absorbing minerals in the formation. Sampling rate: 6".

Mnemonics:

Mnemonics	Description	Unit
BS	Bit Size	(mm)
CALI	Caliper	(mm)
DRHO	Density Correction	(G/C3)
HTEN	Head Tension	(LBF)
NPHI	Neutron Porosity	(V/V)
PEF	Photoelectric Factor	(B/E)
RHOB	Bulk Density	(G/C3)

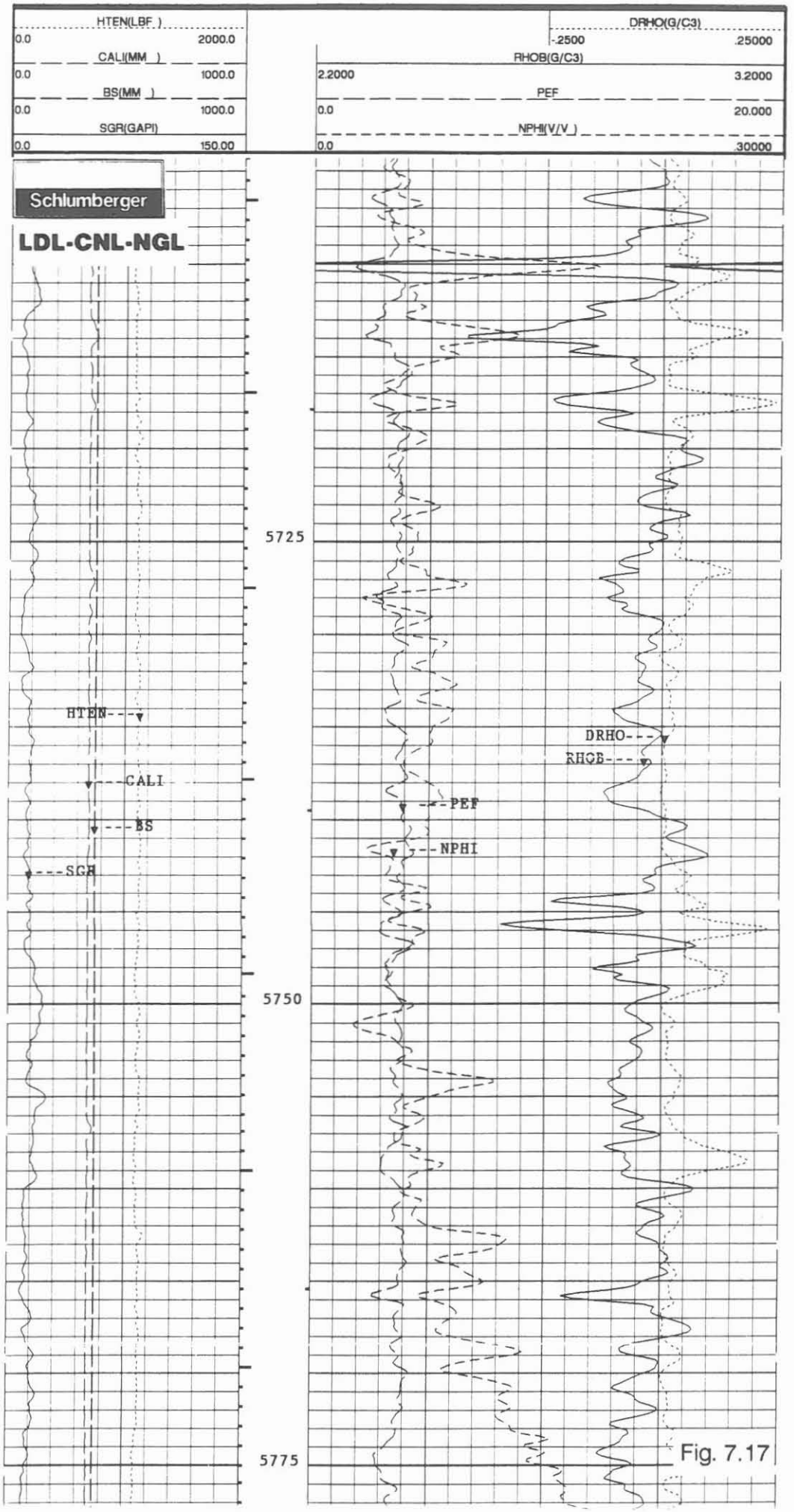
HTEN(LBF)
0.0
2000.0
CALI(MM)
0.0
1000.0
BS(MM)
0.0
1000.0
SGR(GAPI)
0.0
150.00
DRHO(G/C3)
-.2500
.25000
RHOB(G/C3)
2.2000
3.2000
PEF
0.0
20.000
NPHI(V/V)
0.0
.30000
Schlumberger
LDL-CNL-NGL
5725
5750
5775
HTEN
CALI
BS
SGR
DRHO
RHOB
PEF
NPHI

Fig. 7.17

CNL (Compensated Neutron Log - Epithermal Neutron)

Operator: Schlumberger Diepholz/KTB

Job No.	Date	Interval
HB-0116	KTB-Report 92-1	2979.0 - 4520.0 m
HB-0147	15.03.1992	4427.0 - 6024.0 m

Example:
Section of log: 5712.0 - 5784.0 m, **Fig. 7.18**

Purpose of log:
Neutron logs are used for lithology determination and porosity evaluation. In crystalline rocks the porosity evaluation is difficult, as these types of rocks contain neutron absorbing minerals masking the primarily response to hydrogen content.

Operation:
The Compensated Neutron Log is recorded in combination with the Litho-Density (LDL) and Natural Gamma Spectrometer Log (NGL). The log itself presents two neutron curves: the epithermal neutron (ENPH) and the neutron porosity (NPHI). In addition, the total gamma rays (SGR), caliper (CALI), bit size (BS) and head tension (HTEN) are recorded.
Depth scales: 1/1000, 1/200; logging speed: 6 m/min.

Technical information:
The neutron measurement system requires a neutron source which bombards the formation with fast neutrons. The neutrons are slowed down mainly by hydrogen atoms in the formation. The slowed neutrons are counted by detectors - epithermal (intermediate) and thermal (slow) neutrons. Using two detectors for each system, borehole compensation is provided. Sampling rate: 6".

Mnemonics and Units:

Mnemonics	Description	Unit
BS	Bite Size	(MM)
CALI	Caliper	(MM)
ENPH	Epithermal Neutron	(V/V)
HTEN	Head Tension	(LBF)
NPHI	Neutron Porosity	(V/V)
SGR	Total Gamma Ray	(GAPI)

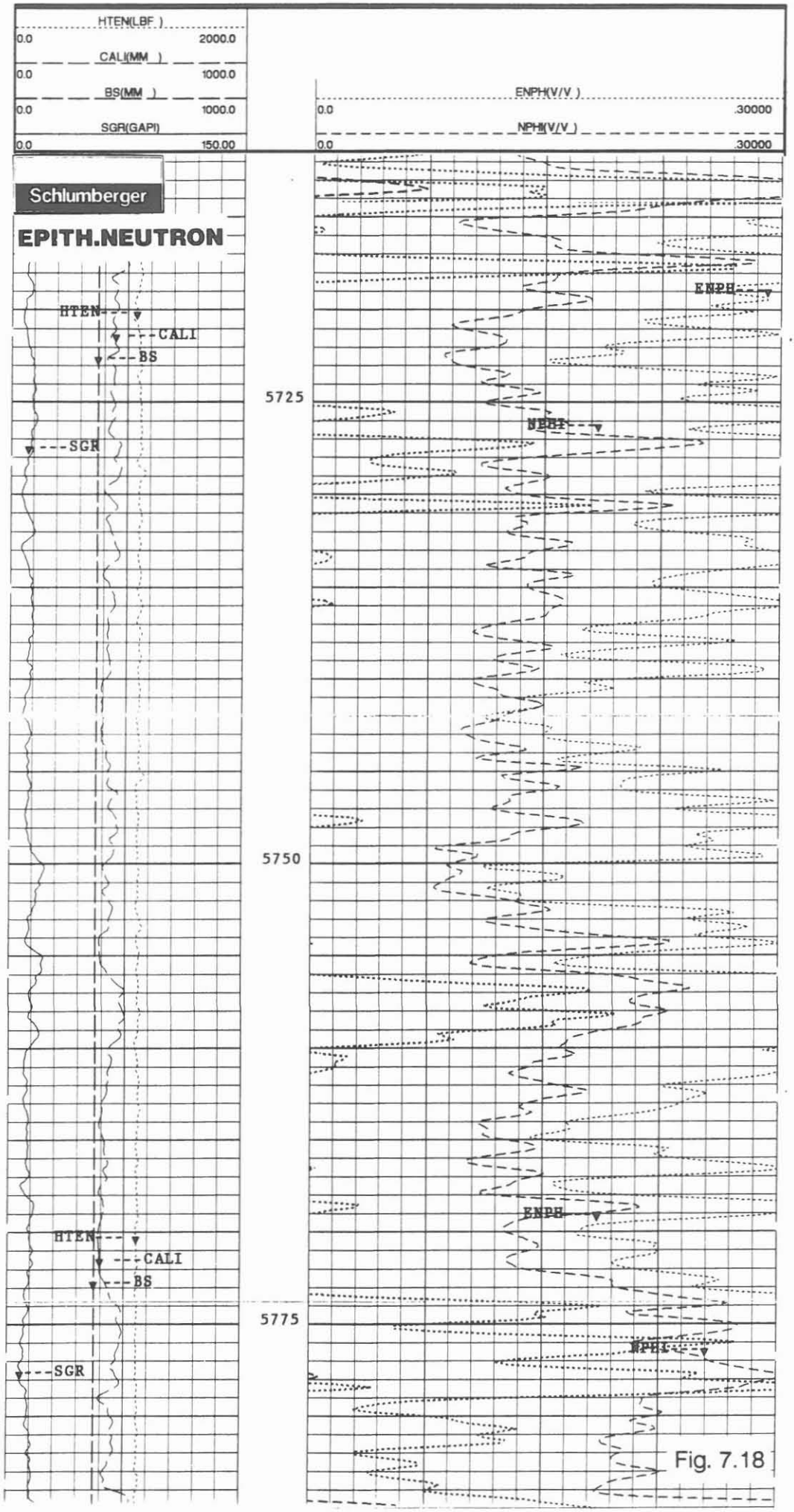
HTEN(LBF)
0.0
2000.0
CALI(MM)
0.0
1000.0
BS(MM)
0.0
1000.0
SGR(GAPI)
0.0
150.00
ENPH(V/V)
0.0
.30000
NPH(V/V)
0.0
.30000
Schlumberger
EPITH.NEUTRON
HTEN
CALI
BS
SGR
5725
5750
5775
ENPH
NPHI

Fig. 7.18

NGL-Ratio (Natural Gamma Spectrometer - Ratio Presentation)

Operator: Schlumberger Diepholz/KTB

Job No.	Date	Interval
HB-0076	KTB Report 91-2	262.0 - 1719.0 m
HB-0095	KTB Report 92-1	700.0 - 3003.0 m
HB-0116	KTB Report 92-1	2979.0 - 4520.0 m
HB-0147	15.03.1992	4427.0 - 6024.0 m

Example:
Section of log: 5725.0 - 5795.0 m, **Fig. 7.19**

Purpose of log:
The registration of the natural gamma ray spectra is to resolve the total spectra into the three most common components of naturally occuring radiation: uranium, thorium and potassium. With the measurement of these three elements information about the mineral content of the formation can be obtained. Additional application of the log is in lithology evaluation, fracture detection and special radioactive mineral detection.

Operation:
The log was recorded in combination with the Litho-Density and Compensated Neutron Logs. It was run excentralized for better response in the rather large borehole of 14 3/4". The log records in track I the total gamma ray spectra (SGR) and the gamma ray minus the uranium component (CGR), a caliper curve (CALI) and the head tension (HTEN). In track II are the ratios and in track III the single component curves presented.
Depth scale: 1/1000, 1/200; logging speed: 7 m/min.

Technical information:
A five-window spectroscopy analysing system is used to resolve for uranium, thorium and potassium content. As the results have large statistical variations Kalmann - filtering is applied. The single components are than used to compute the ratios uranium:thorium, uranium:potassium and potassium: thorium and the difference total gamma ray minus uranium.
Data rate: 6".

Mnemonics and Units:

Mnemonics	Description	Unit
CALI	Caliper	(MM)
CGR	Computed Gamma Ray	(GAPI)
HTEN	Head Tension	(LBF)
POTA	Potassium Content	(%)
SGR	Spectroscopy Gamma Ray	(GAPI)
THOR	Thorium Content	(PPM)
TPRA	Thorium:Potessium Ratio	
TURA	Thorium:Uranium Ratio	
UPRA	Uranium:Potessium Ratio	
URAN	Uranium Content	(PPM)

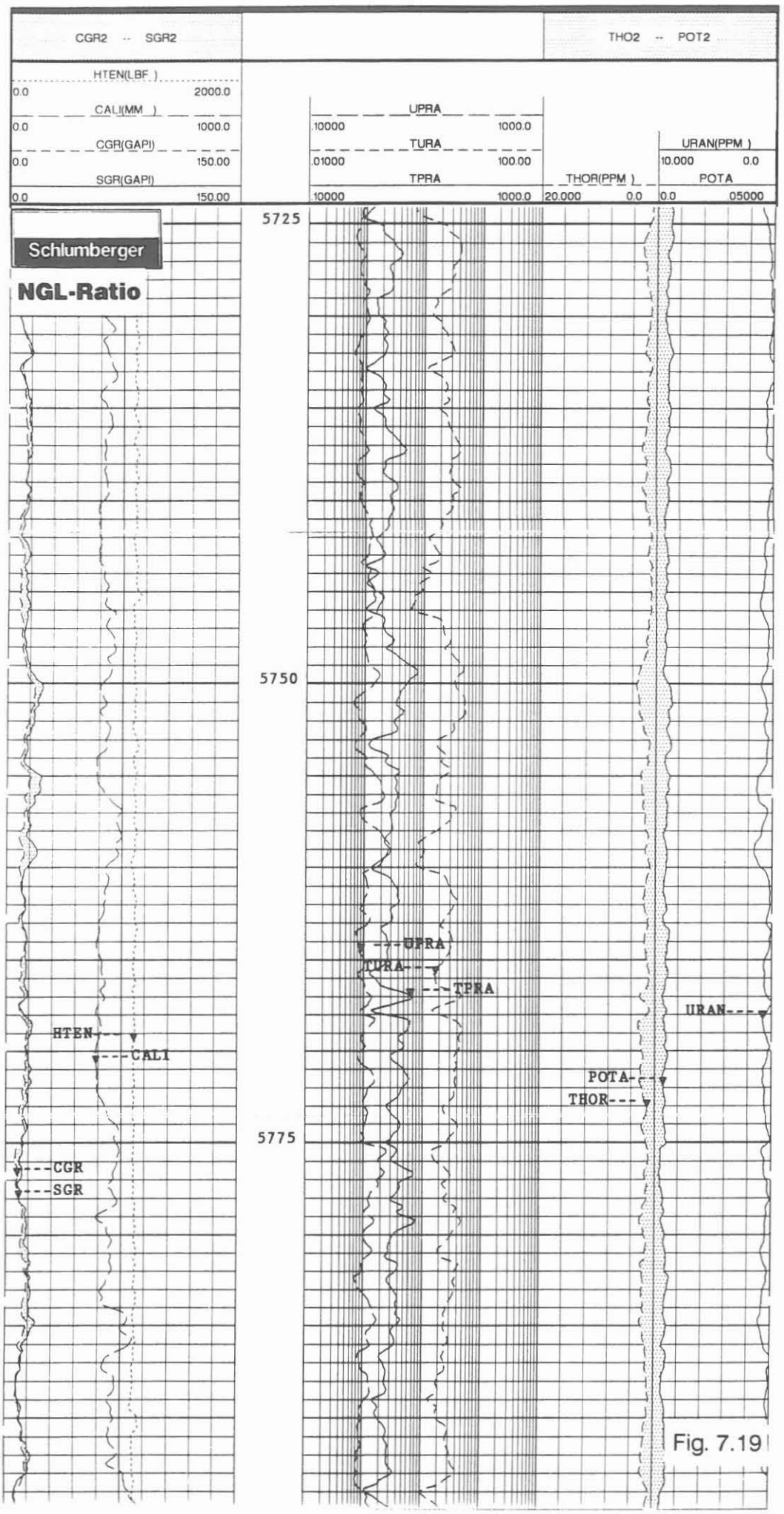
CGR2 -- SGR2
HTEN(LBF)
0.0
2000.0
CALI(MM)
0.0
1000.0
CGR(GAPI)
0.0
150.00
SGR(GAPI)
0.0
150.00
UPRA
10000
1000.0
TURA
01000
100.00
TPRA
10000
1000.0
THO2 -- POT2
THOR(PPM)
20.000
0.0
URAN(PPM)
10.000
0.0
POTA
0.0
05000
Schlumberger
NGL-Ratio
5725
5750
5775
---UPRA
TURA---
---TPRA
URAN---
HTEN---
---CALI
POTA---
THOR---
---CGR
---SGR

Fig. 7.19

NGL-Spec. (Natural Gamma Spectrometer - Special Presentation)

Operator: Schlumberger Diepholz/KTB

Job No.	Date	Interval
HB-0076	KTB Report 91-2	262.0 - 1719.0 m
HB-0095	KTB Report 92-1	700.0 - 3003.0 m
HB-0116	KTB Report 92-1	2979.0 - 4520.0 m
HB-0147	15.03.1992	4427.0 - 6024.0 m

Example:
Section of log: 5721.0 - 5798.0 m, **Fig. 7.20**

Purpose of log:
The registration of the natural gamma ray spectra is to resolve the total spectra into the three most common components of naturally occuring radiation: uranium, thorium and potassium. With the measurement of these three elements information about the mineral content of the formation can be obtained. Additional application of the log is in lithology evaluation, fracture detection and special radioactive mineral detection.

Operation:
The log was recorded in combination with the Litho-Density and Compensated Neutron Logs. It was run excentralized for better response in the rather large borehole of 14 3/4". The log records in track I the total gamma ray spectra (SGR) and the gamma ray minus the uranium component (CGR), a caliper curve (CALI) and the head tension (HTEN). In track II and track III are the single component curves presented.
Depth scale: 1/1000, 1/200; logging speed: 7 m/min.

Technical information:
A five-window spectroscopy analysing system is used to resolve for uranium, thorium and potassium content. As the results have large statistical variations Kalmann - filtering is applied. The single components are recordet. In addition the total spectra minus uranium is computed.
Data rate: 6".

Mnemonics and Units:

Mnemonics	Description	Unit
CALI	Caliper	(MM)
CGR	Computed Gamma Ray	(GAPI)
HTEN	Head Tension	(LBF)
POTA	Potassium Content	(%)
SGR	Spectroscopy Gamma Ray	(GAPI)
THOR	Thorium Content	(PPM)
URAN	Uranium Content	(PPM)

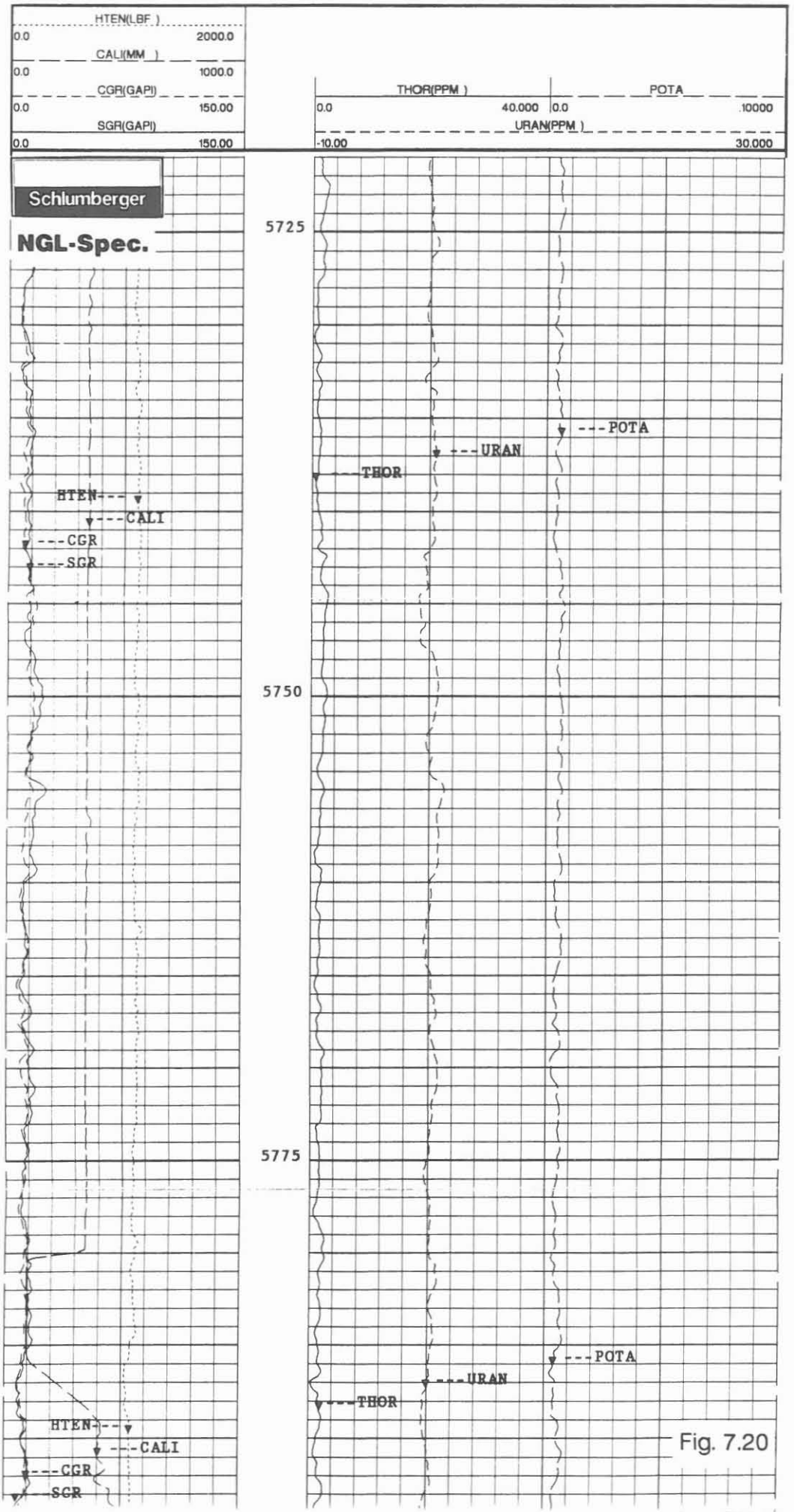
HTEN(LBF)
0.0
2000.0
CALI(MM)
0.0
1000.0
CGR(GAPI)
0.0
150.00
SGR(GAPI)
0.0
150.00
THOR(PPM)
0.0
40.000
POTA
0.0
.10000
URAN(PPM)
-10.00
30.000
Schlumberger
NGL-Spec.
5725
5750
5775
HTEN
CALI
CGR
SGR
THOR
URAN
POTA

Fig. 7.20

DSI/GR/AMS/GPIT (Dipole Shear Sonic Imager/Gamma Ray/Auxiliary Measurement Sonde/General Purpose Inclinometer Tool)

Operator: Schlumberger Diepholz/KTB

Job No.	Date	Interval
HB-0119	KTB-Report 92-1	3000.0 - 4500.0 m
HB-0149	16.03.1992	4450.0 - 6020.0 m

Examples:

List of Mnemonics and Units,		**Fig. 7.21**
Sections of logs:	BHC Sonic Plot 5968.0-6012.0 m,	**Fig. 7.22**
	DT-P-S-Stoneley 5970.0-6014.0 m,	**Fig. 7.23**
	P-FMD 5948.0-6006.0 m,	**Fig. 7.24**
	P&S Mode-STC 5975.0-6014.0 m,	**Fig. 7.25**
	P&S Mode-VDL 5958.0-6014.0 m,	**Fig. 7.26**
	Stoneley-STC 5890.0-5948.0 m,	**Fig. 7.27**
	Stoneley-VDL 5880.0-5947.0 m,	**Fig. 7.28**
	Lower Dipole-STC 5964.0-6014.0 m,	**Fig. 7.29**
	Lower Dipole-VDL 5960.0-6016.0 m,	**Fig. 7.30**
	Upper Dipole-STC 5965.0-6014.0 m,	**Fig. 7.31**
	Upper Dipole-VDL 5960.0-6016.0 m,	**Fig. 7.32**

Purpose of log:
With this tool the acoustic properties of formations are measured. Velocity correlation with seismic profiles in compressional and shear mode are possible. The velocities are determined using acoustic waveform measurements and slowness-time-coherence computations. The slownesses (inverse velocities) have geophysical, petrophysical and rock mechanical application like porosity estimation, fracture detection and wellbore stability calculations.

Operation:
The tool combination requires the MAXIS 500 surface recording unit. For this operation the following recording modes have been logged in one single run in the borehole: First motion detection, P&S mode, upper and lower dipole and Stoneley mode. The GPIT was run in combination to orient the dipole measurements. This could provide information about anisotropy and breakout orientation.
Depth scale: 1/200; logging speed: 1,5 m/min.

Technical information:
The Dipole Shear Sonic Imager (DSI) combines Mono- and Dipole measurement systems. It enhances the measurements of compressional, shear and Stoneley waveforms in all types of formations. The tool itself consists of a transmitter section housing one monopole and two dipole transducers. The dipole transducers are mounted perpendicular to each other. The monopole transducer operates at high frequency for

compressional and shear wave propagation and at low frequency for Stoneley waves. Low frequency is used for the dipole transducers to create shear waves.

The receiver section consists of 8 receiver stations. Each receiver station contains two hydrophone pairs, which are mounted in line with the dipole transducers.

The signals received are separated for dipole detection and summed for monopole reception.

The waveform processing is done using the slowness-time-coherence technique (STC). A fixed window of pregiven time length is advanced across the array of waveforms. A coherence function is computed for each step and the similarity of the waveforms is measured. If the waveforms are similar the coherence will be very high. This will mean, that the detection of a specific component of the waveform (compressionel, shear, Stoneley) has been possible and the respective slowness has been determined.

The digital first motion detection processing (DFMD) applies a treshold system for analysing waveforms. The time crossings of the first arrivals are selected and the given travel times are used for slowness computations.

The dipole waveform processing is used for true shear slowness detection. Depending on type of formation the detection might be influenced by distortion. Band pass filtering will than be required.

Borehole compensation is achieved by processing receiver array and pseudo-transmitter array waveforms and the average out of these waveforms. This will produce borehole compensated P and S results.

Acoustic frequencies: 80 Hz - 5 KHz for Stoneley and dipole; 8 KHz - 30 KHz for high frequency monopole.
Sampling rate: 6".

Description of logs:
1. BHC Sonic Plot (Fig. 7.22). This plot is equivalent to the standard Sonic Log. It provides travel time data in borehole compensated registration. The log includes gamma ray data and the travel time integration.

2. DT-P-S & Stoneley (Fig. 7.23). This log gives the following data: DT (compressional) from first motion detection (DFMD); and from P&S computations; DT shear from P&S, upper and lower dipole computations; and DT-Stoneley. In addition the integration of DT comp., the gamma ray and pad one azimuth is presented.

3. P-FMD (Fig. 7.24). DT-Comp. for transmitter and receiver mode and average is given. All measurements are coming from first motion detection. The coherence for transmitter and receiver modes are presented like gamma ray and integrated travel time.

4. P&S Mode-STC (Fig. 7.25). With the software available in the MAXIS 500 surface unit, the first Slowness-Time-Coherence (STC) computations are made. P- and S-travel times for transmitter and receiver modes are computed and presented as colour plot. Gamma Ray, Peak Coherences, Waveform Depth and Waveform Gain are given in track I of the log.

5. P&S Mode-VDL (Fig. 7.26). This log is a presentation as Variable Density Log (VDL). The waveforms are presented over 5000 μsec in a grey-scale log. Gamma Ray, Waveform Depth and Waveform Gain are given in track I.

6. Stoneley-STC (Fig. 7.27). This plot gives the Stoneley travel time computed by the Slowness-Time-Coherence (STC) function in a colour presentation. Information in track I is same as in Fig. 7.25 - but for Stoneley-wave only.

7. Stoneley-VDL/Fig. 7.28). The Variable Density Log (VDL) of the Stoneley-Waveforms over 10 000 μsec shows characteristic "Chevron Pattern". These pattern are typical indications for irregularities of the borehole wall, like for example fractures. Presentation is made in a grey-scale log. Gamma Ray and Waveform Depth/Waveform Gain are given in track I.

8. Lower Dipole-STC (Fig. 7.29). The shear wave created by the Lower Dipole is recorded and via the Slowness-Time-Coherence (STC) the shear travel time is computed and presented as colour plot. In track I the information is given as on Fig. 7.25 - but for Lower Dipole.

9. Lower Dipole - VDL (Fig. 7.30). Variable Density Log of Lower Dipole waveform presentation in grey-scale.

10. Upper Dipole - STC (Fig. 7.31). Same as Fig. 7.29 - but for Upper Dipole.

11. Upper Dipole - VDL (Fig. 7.32). Same as Fig. 7.30 - but for Upper Dipole.

Mnemonics and Units:

Mnemonics	Description	Units
See Fig. 7.21		

DSI Mnemonics & Units

Parameters

DLIS Name	Description	Value	
ACPP	Accelerometer PROM Presence	ABSENT	
AFMO	Accelerometer Filtering Mode	HAMMING	
ART	Accelerometer Reference Temperature	0	DEGC
BHS	Bore Hole Status	OPEN	
BHT	Bottom Hole Temperature (used in calculations)	140	DEGC
BILI	Bond Index Level for Zone Isolation	0.8	
BS	Bit Size	14.750	IN
BSAL	Borehole Salinity	-50000.0	PPM
CDTS	C-Delta-T Shale	100	US/F
COLL	Label Slowness Lower Limit - P & S Comp	40	US/F
COUL	Label Slowness Upper Limit - P & S Comp	160	US/F
CSTR	Compressive Strength of Cement	0	KPA
DO	Depth Offset	1.1	M
DPPM	Density Porosity Processing Mode	STAN	
DSHL	Label Slowness Lower Limit - Dipole Shear	60	US/F
DSHU	Label Slowness Upper Limit - Dipole Shear	775	US/F
DTCS	Comp Delta-T Source	PS_COMP	
DTF	Delta-T Fluid	189	US/F
DTM	Delta-T Matrix	56	US/F
DTSS	Shear Delta-T Source	LOWER_DIPOLE	
FCF	CBL Fluid Compensation Factor	1	
FMLL	Slowness Lower Limit - FMD	40	US/F
FMUL	Slowness Upper Limit - FMD	180	US/F
GCSE	Generalized Caliper Selection	BIT_SIZE	
GDT4	Gain Delta-T 4	160	US/F
GLM	GPIT Logging Mode	STAN	
GOBO	Good Bond	2	MV
GRSE	Generalized Mud Resistivity Selection	AMS_RESIST	
GTSE	Generalized Temperature Selection	AMS_AVG_TEMP	
ICMO	Inclinometry Computation MOde	OPEN_HOLE	
ITTS	Integrated Transit Time Source	DTCO	
MAI5	Slowness Averaging Interval - FMD	42	IN
MAPP	Magnetometer PROM Presence	ABSENT	
MATR	Rock Matrix Type	LIMESTONE	
MCI	Minimum Cemented Interval	3.048	M
MDEC	Magnetic Field Declination	0.72734	DEG
MRTE	Magneto Reference Temperature	0	DEGC
MSA	Minimum Sonic Amplitude	0	MV
RSMN	Label Shear/Comp Minimum Ratio - P & S	1.2	
RSMX	Label Shear/Comp Maximum Ratio - P & S	2.12	
RW	Resistivity of Connate Water	1.0000	OHMM
SAM1	Sonic Acquisition Mode 1 (lower dipole)	EVEN	
SAM2	Sonic Acquisition Mode 2 (upper dipole)	ODD	
SAM3	Sonic Acquisition Mode 3 (Stoneley)	EVEN	
SAM4	Sonic Acquisition Mode 4 (p & s)	ODD	
SAM5	Sonic Acquisition Mode 5 (FMD)	ODD	
SAMX	Sonic Acquisition Mode X (expert)	OFF	
SAS5	Sonic Array Status - FMD	255	
SFC1	Sonic Formation Character - Lower Dipole	SELECTABLE	
SFC2	Sonic formation Character - Upper Dipole	SELECTABLE	
SFC3	Sonic formation Character - Stoneley	SELECTABLE	
SFC4	Sonic formation Character - P & S	SELECTABLE	
SHLL	Label SLowness Lower Limit - P & S Shear	75	US/F
SHT	Surface Hole Temperature	10	DEGC
SHUL	Label Slowness Upper Limit - P & S Shear	160	US/F
SLL1	STC Slowness Lower Limit - Lower Dipole	75	US/F
SLL2	STC Slowness Lower Limit - Upper Dipole	75	US/F
SLL3	STC Slowness Lower Limit - Stoneley	180	US/F
SLL4	STC Slowness Lower Limit - P & S	40	US/F
SPFS	Sonic Porosity Formula	RAYMER_HUNT	
SPSO	Sonic Porosity Source	DTCO	
STKT	STI Stuck Threshold	1.524	M
STLL	Label Slowness Lower Limit - Stoneley	120	US/F
STUL	Label Slowness Upper Limit - Stoneley	780	US/F
SUL1	STC Slowness Upper Limit - Lower Dipole	775	US/F
SUL2	STC Slowness Upper Limit - Upper Dipole	775	US/F
SUL3	STC Slowness Upper Limit - Stoneley	780	US/F
SUL4	STC Slowness Upper Limit - P & S	160	US/F
TD	Total Depth	6025	M
TLCK	TLC Kit	OFF	
TWS	Temperature of Connate Water Sample	37.8	DEGC
WFM1	Waveform Mode 1	W1	
WFM2	Waveform Mode 2	W1	
WFM3	Waveform Mode 3	W1	
WFM4	Waveform Mode 4	W1	
WFMX	Waveform Mode X	W1	

Fig. 7.21

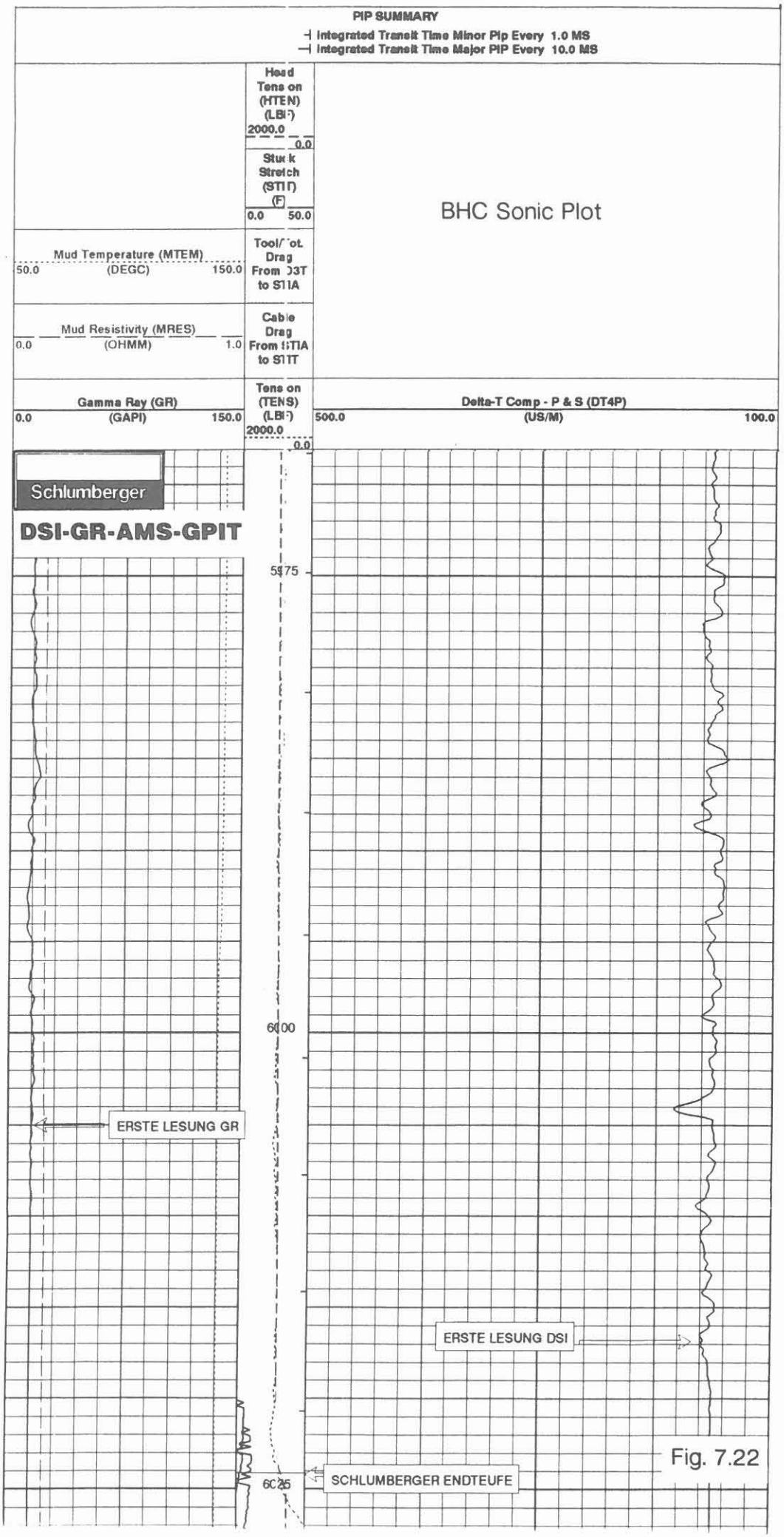
PIP SUMMARY
Integrated Transit Time Minor Pip Every 1.0 MS
Integrated Transit Time Major PIP Every 10.0 MS
Head Tension (HTEN) (LBF) 2000.0 0.0
Stuck Stretch (STIT) (F) 0.0 50.0
BHC Sonic Plot
Mud Temperature (MTEM) 50.0 (DEGC) 150.0
Tool Rot. Drag From DT to ST1A
Mud Resistivity (MRES) 0.0 (OHMM) 1.0
Cable Drag From ST1A to STIT
Gamma Ray (GR) 0.0 (GAPI) 150.0
Tension (TENS) (LBF) 2000.0 0.0
Delta-T Comp - P & S (DT4P) 500.0 (US/M) 100.0
Schlumberger
DSI-GR-AMS-GPIT
5975
6000
ERSTE LESUNG GR
ERSTE LESUNG DSI
6025
SCHLUMBERGER ENDTEUFE

Fig. 7.22

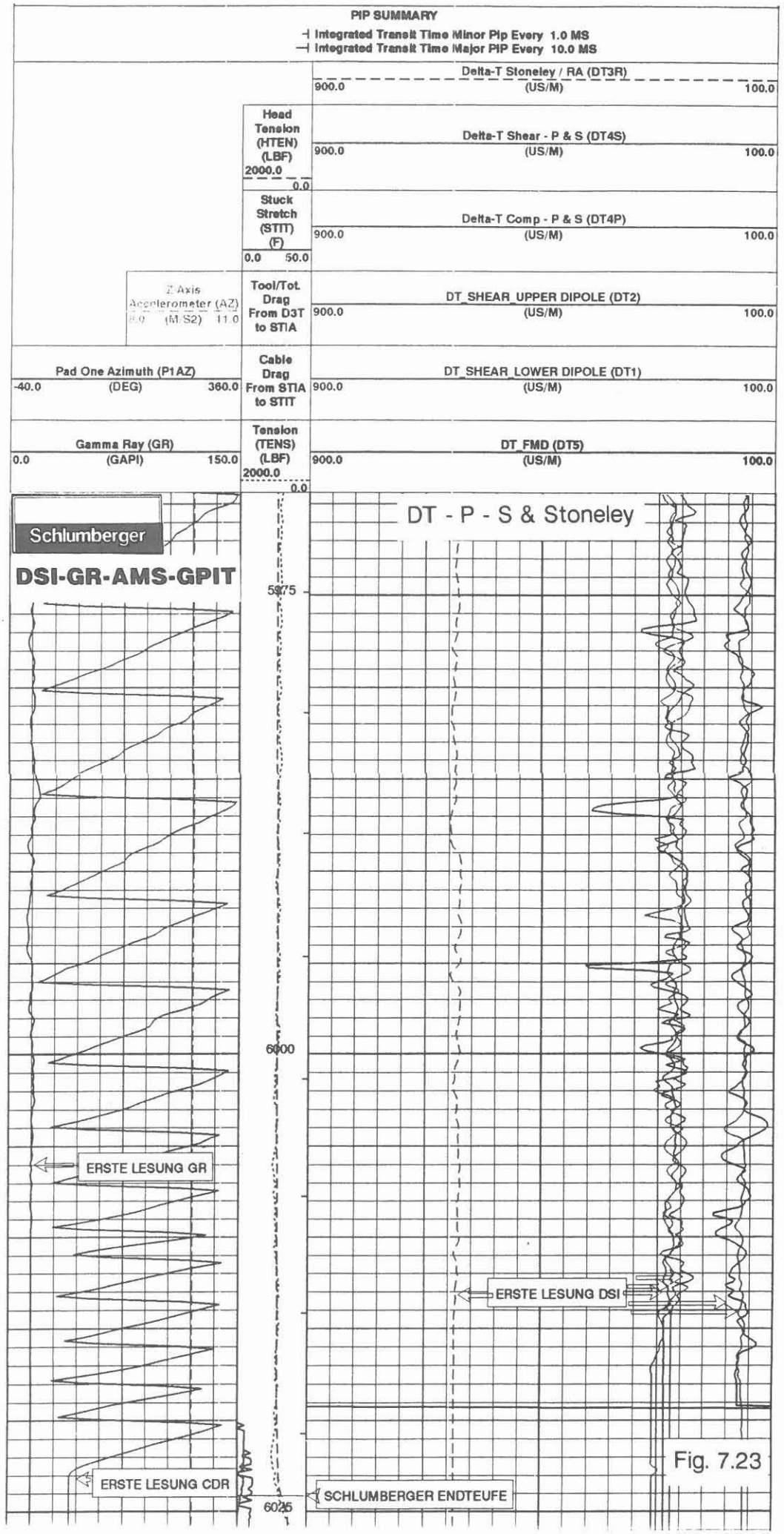
PIP SUMMARY
Integrated Transit Time Minor Pip Every 1.0 MS
Integrated Transit Time Major PIP Every 10.0 MS
Delta-T Stoneley / RA (DT3R)
900.0 (US/M) 100.0
Head Tension (HTEN) (LBF)
2000.0 0.0
Delta-T Shear - P & S (DT4S)
900.0 (US/M) 100.0
Stuck Stretch (STIT) (F)
0.0 50.0
Delta-T Comp - P & S (DT4P)
900.0 (US/M) 100.0
Z Axis Accelerometer (AZ)
8.0 (M/S2) 11.0
Tool/Tot. Drag From D3T to STIA
DT_SHEAR_UPPER DIPOLE (DT2)
900.0 (US/M) 100.0
Pad One Azimuth (P1AZ)
-40.0 (DEG) 360.0
Cable Drag From STIA to STIT
DT_SHEAR_LOWER DIPOLE (DT1)
900.0 (US/M) 100.0
Gamma Ray (GR)
0.0 (GAPI) 150.0
Tension (TENS) (LBF)
2000.0 0.0
DT_FMD (DT5)
900.0 (US/M) 100.0
Schlumberger
DSI-GR-AMS-GPIT
DT - P - S & Stoneley
5975
6000
6025
ERSTE LESUNG GR
ERSTE LESUNG CDR
ERSTE LESUNG DSI
SCHLUMBERGER ENDTEUFE

Fig. 7.23

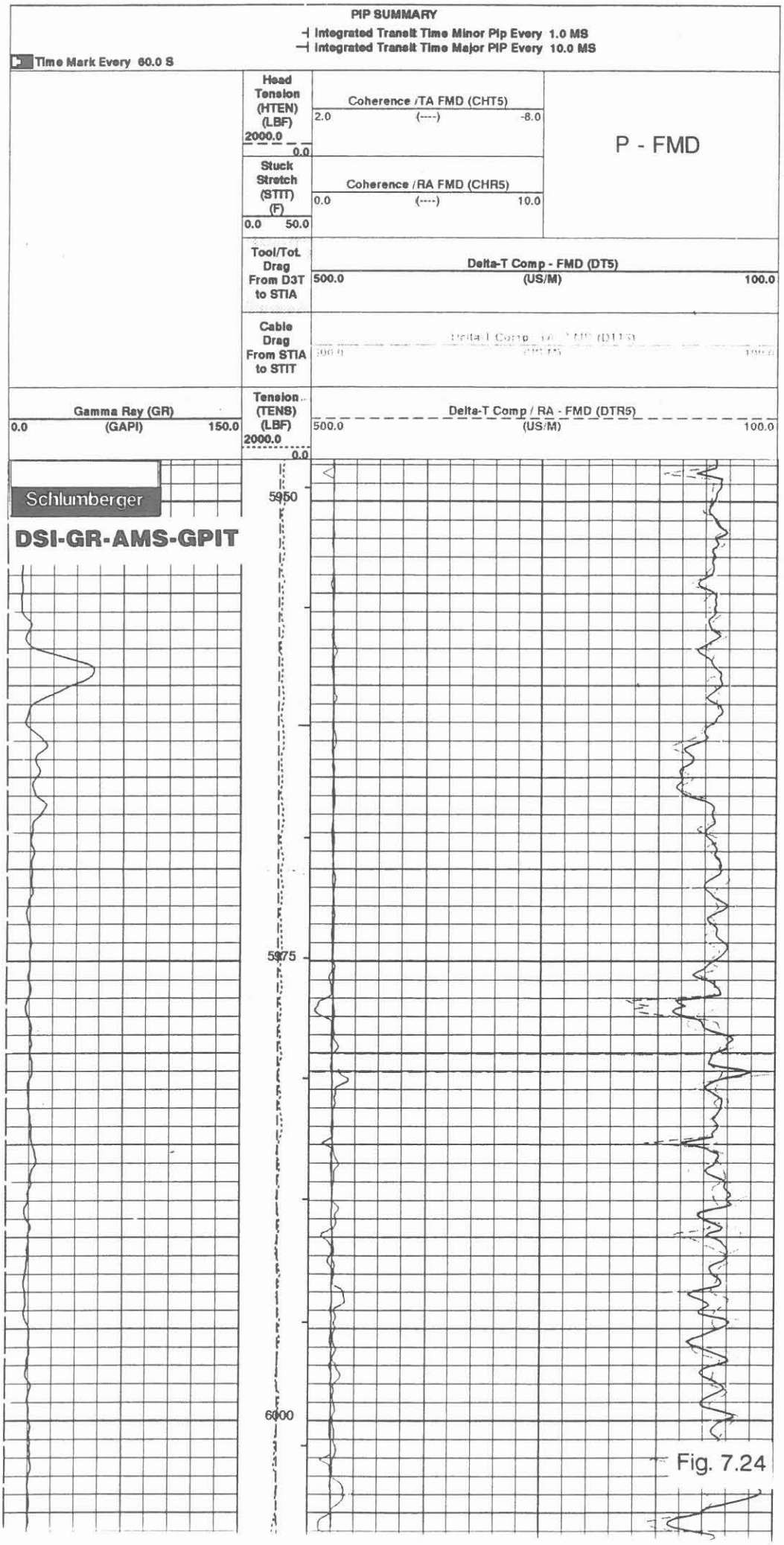
PIP SUMMARY
Integrated Transit Time Minor Pip Every 1.0 MS
Integrated Transit Time Major PIP Every 10.0 MS
Time Mark Every 60.0 S
Head Tension (HTEN) (LBF)
2000.0
0.0
Coherence /TA FMD (CHT5)
2.0 (----) -8.0
P - FMD
Stuck Stretch (STIT) (F)
0.0 50.0
Coherence /RA FMD (CHR5)
0.0 (----) 10.0
Tool/Tot. Drag From D3T to STIA
Delta-T Comp - FMD (DT5)
500.0 (US/M) 100.0
Cable Drag From STIA to STIT
Gamma Ray (GR)
0.0 (GAPI) 150.0
Tension (TENS) (LBF)
2000.0
0.0
Delta-T Comp / RA - FMD (DTR5)
500.0 (US/M) 100.0
Schlumberger
DSI-GR-AMS-GPIT
5950
5975
6000

Fig. 7.24

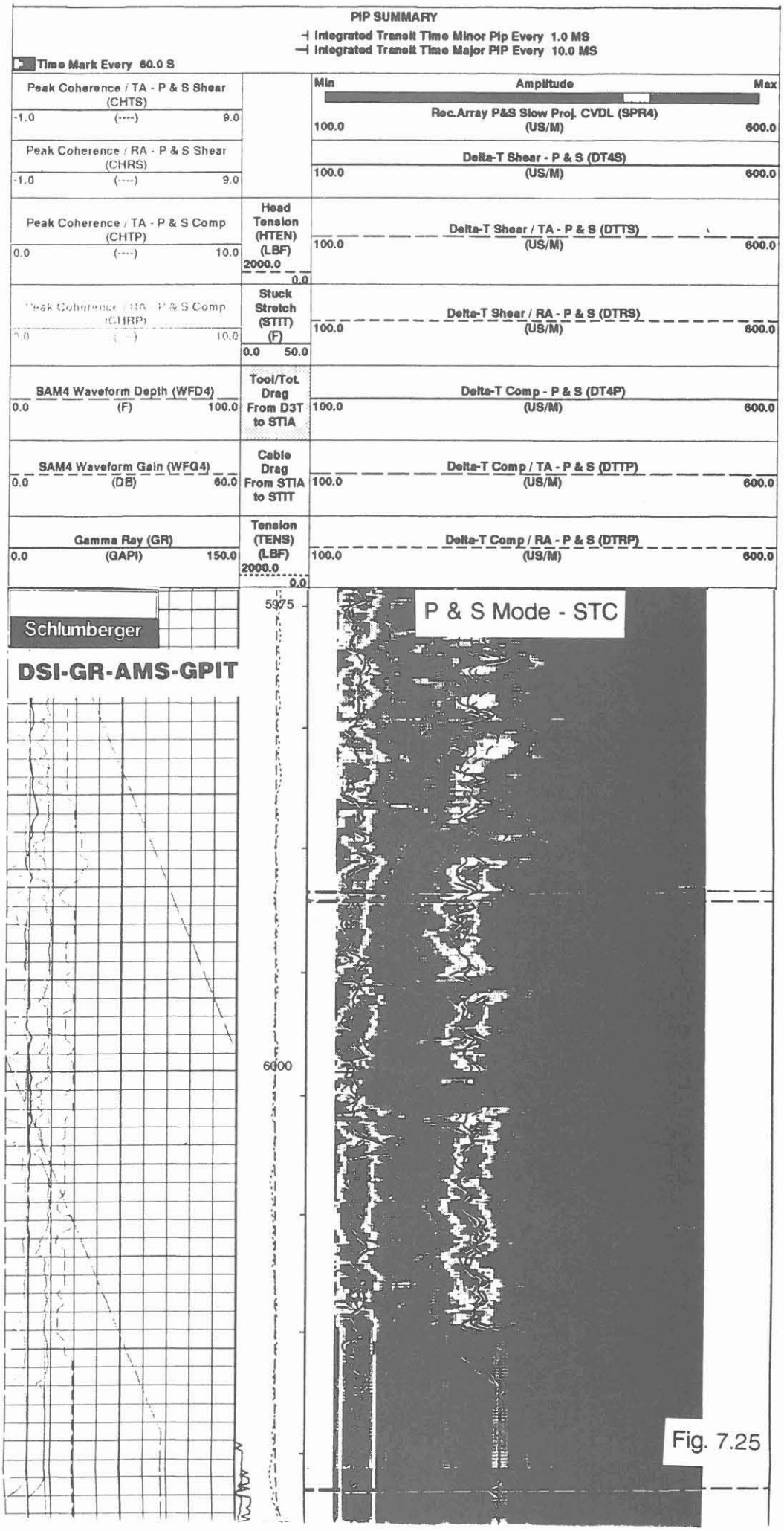
PIP SUMMARY
Integrated Transit Time Minor Pip Every 1.0 MS
Integrated Transit Time Major PIP Every 10.0 MS
Time Mark Every 60.0 S
Peak Coherence / TA - P & S Shear (CHTS)
-1.0 (----) 9.0
Peak Coherence / RA - P & S Shear (CHRS)
-1.0 (----) 9.0
Peak Coherence / TA - P & S Comp (CHTP)
0.0 (----) 10.0
Peak Coherence / RA - P & S Comp (CHRP)
0.0 (----) 10.0
SAM4 Waveform Depth (WFD4)
0.0 (F) 100.0
SAM4 Waveform Gain (WFG4)
0.0 (DB) 60.0
Gamma Ray (GR)
0.0 (GAPI) 150.0
Head Tension (HTEN) (LBF)
2000.0 0.0
Stuck Stretch (STIT) (F)
0.0 50.0
Tool/Tot. Drag From D3T to STIA
Cable Drag From STIA to STIT
Tension (TENS) (LBF)
2000.0 0.0
Min Amplitude Max
Rec.Array P&S Slow Proj. CVDL (SPR4)
100.0 (US/M) 600.0
Delta-T Shear - P & S (DT4S)
100.0 (US/M) 600.0
Delta-T Shear / TA - P & S (DTTS)
100.0 (US/M) 600.0
Delta-T Shear / RA - P & S (DTRS)
100.0 (US/M) 600.0
Delta-T Comp - P & S (DT4P)
100.0 (US/M) 600.0
Delta-T Comp / TA - P & S (DTTP)
100.0 (US/M) 600.0
Delta-T Comp / RA - P & S (DTRP)
100.0 (US/M) 600.0
Schlumberger
DSI-GR-AMS-GPIT
5975
6000
P & S Mode - STC

Fig. 7.25

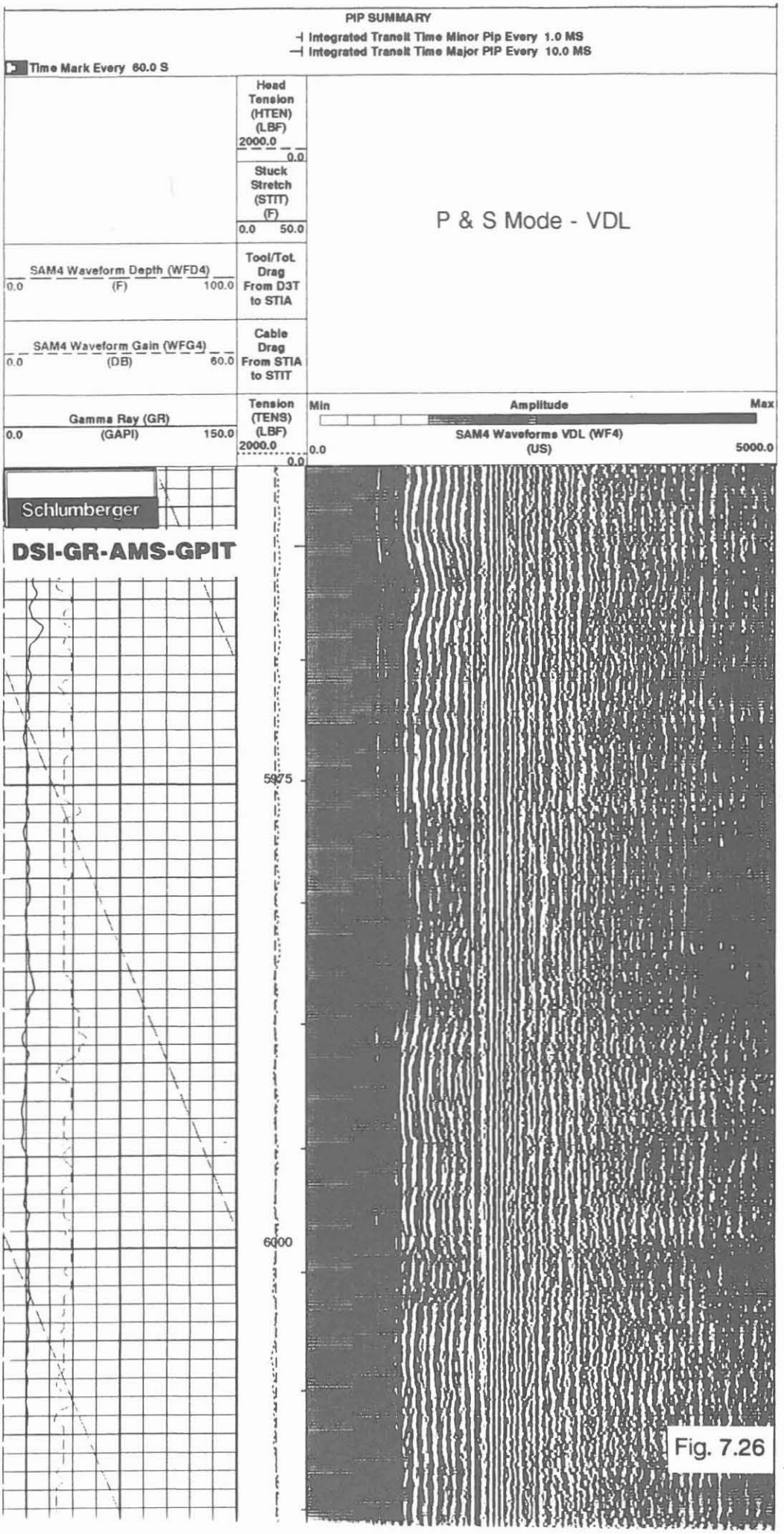
PIP SUMMARY
Integrated Transit Time Minor Pip Every 1.0 MS
Integrated Transit Time Major PIP Every 10.0 MS
Time Mark Every 60.0 S
Head Tension (HTEN) (LBF)
2000.0
0.0
Stuck Stretch (STIT) (F)
0.0 50.0
P & S Mode - VDL
SAM4 Waveform Depth (WFD4)
0.0 (F) 100.0
Tool/Tot. Drag From D3T to STIA
SAM4 Waveform Gain (WFG4)
0.0 (DB) 60.0
Cable Drag From STIA to STIT
Gamma Ray (GR)
0.0 (GAPI) 150.0
Tension (TENS) (LBF)
2000.0
0.0
Min
Amplitude
Max
SAM4 Waveforms VDL (WF4)
0.0 (US) 5000.0
Schlumberger
DSI-GR-AMS-GPIT
5975
6000

Fig. 7.26

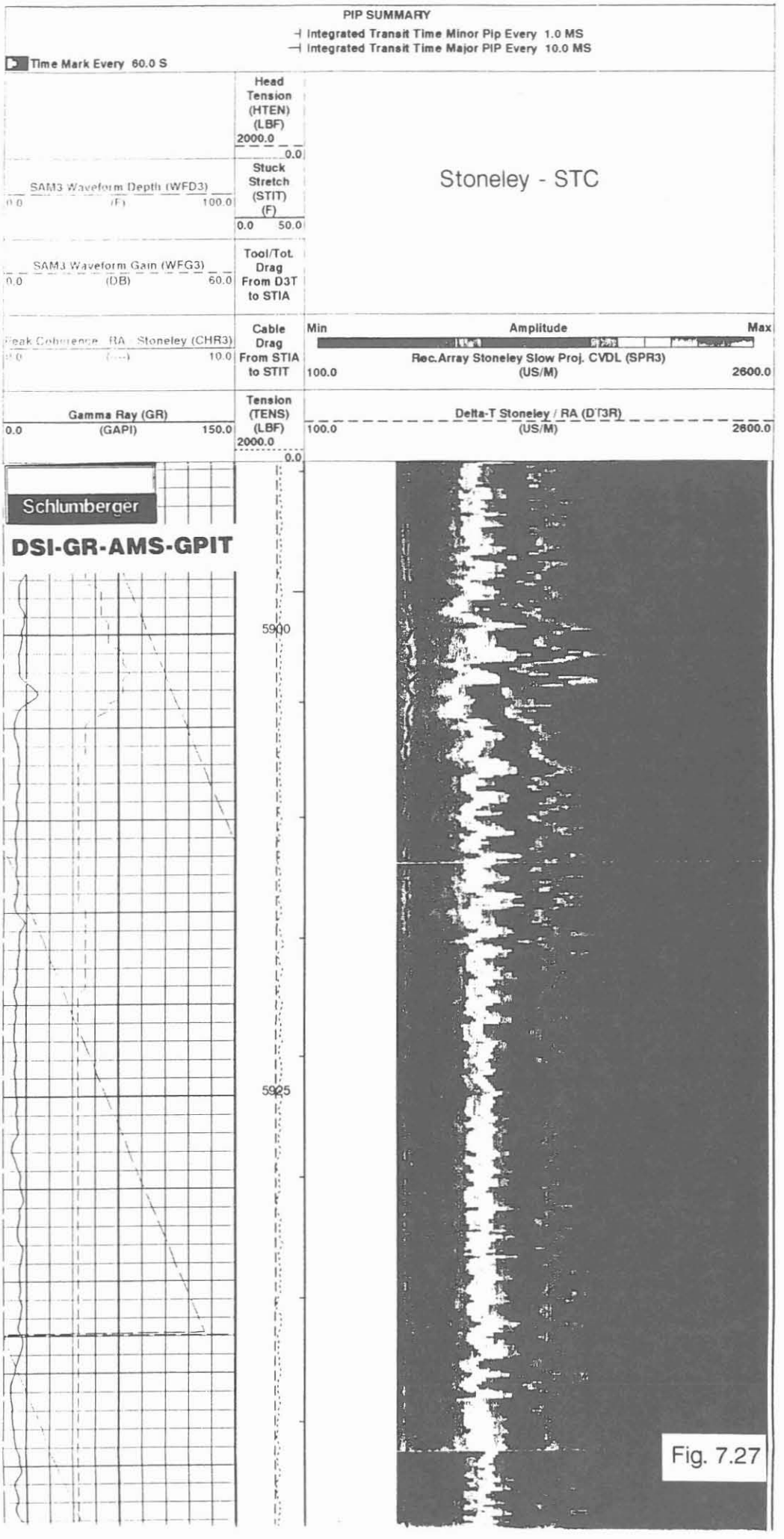
PIP SUMMARY
Integrated Transit Time Minor Pip Every 1.0 MS
Integrated Transit Time Major PIP Every 10.0 MS
Time Mark Every 60.0 S
Head Tension (HTEN) (LBF) 2000.0 0.0
Stuck Stretch (STIT) (F) 0.0 50.0
Stoneley - STC
SAM3 Waveform Depth (WFD3) 0.0 (F) 100.0
SAM3 Waveform Gain (WFG3) 0.0 (DB) 60.0
Tool/Tot. Drag From D3T to STIA
Peak Coherence RA Stoneley (CHR3) 0.0 (---) 10.0
Cable Drag From STIA to STIT
Min Amplitude Max
Rec.Array Stoneley Slow Proj. CVDL (SPR3)
100.0 (US/M) 2600.0
Gamma Ray (GR) 0.0 (GAPI) 150.0
Tension (TENS) (LBF) 2000.0 0.0
Delta-T Stoneley / RA (DT3R) 100.0 (US/M) 2600.0
Schlumberger
DSI-GR-AMS-GPIT
5900
5925
Fig. 7.27

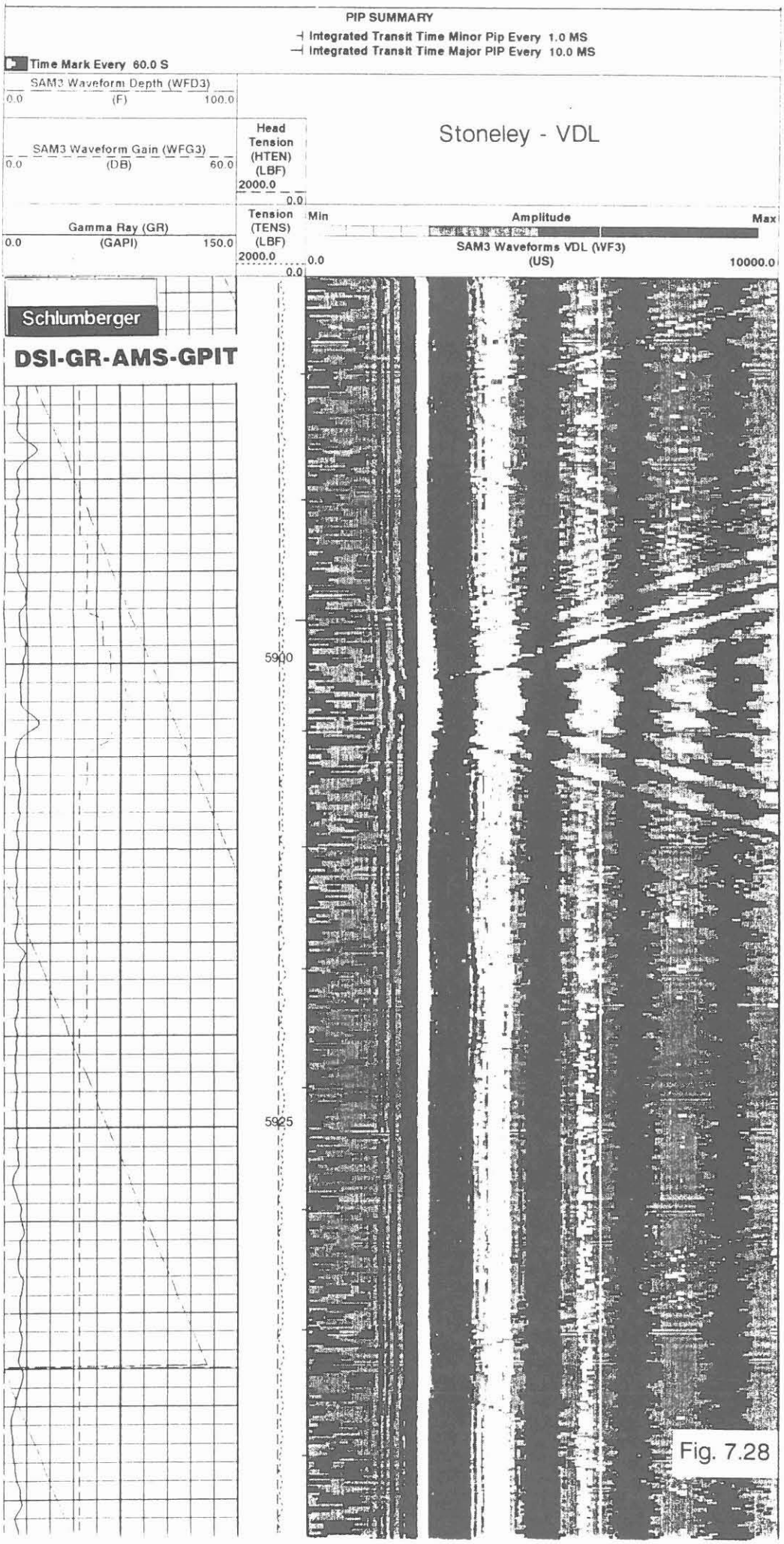
PIP SUMMARY
Integrated Transit Time Minor Pip Every 1.0 MS
Integrated Transit Time Major PIP Every 10.0 MS
Time Mark Every 60.0 S
SAM3 Waveform Depth (WFD3)
0.0 (F) 100.0
SAM3 Waveform Gain (WFG3)
0.0 (DB) 60.0
Gamma Ray (GR)
0.0 (GAPI) 150.0
Head Tension (HTEN) (LBF)
2000.0 0.0
Tension (TENS) (LBF)
2000.0 0.0
Stoneley - VDL
Min Amplitude Max
SAM3 Waveforms VDL (WF3) (US)
0.0 10000.0
Schlumberger
DSI-GR-AMS-GPIT
5900
5925

Fig. 7.28

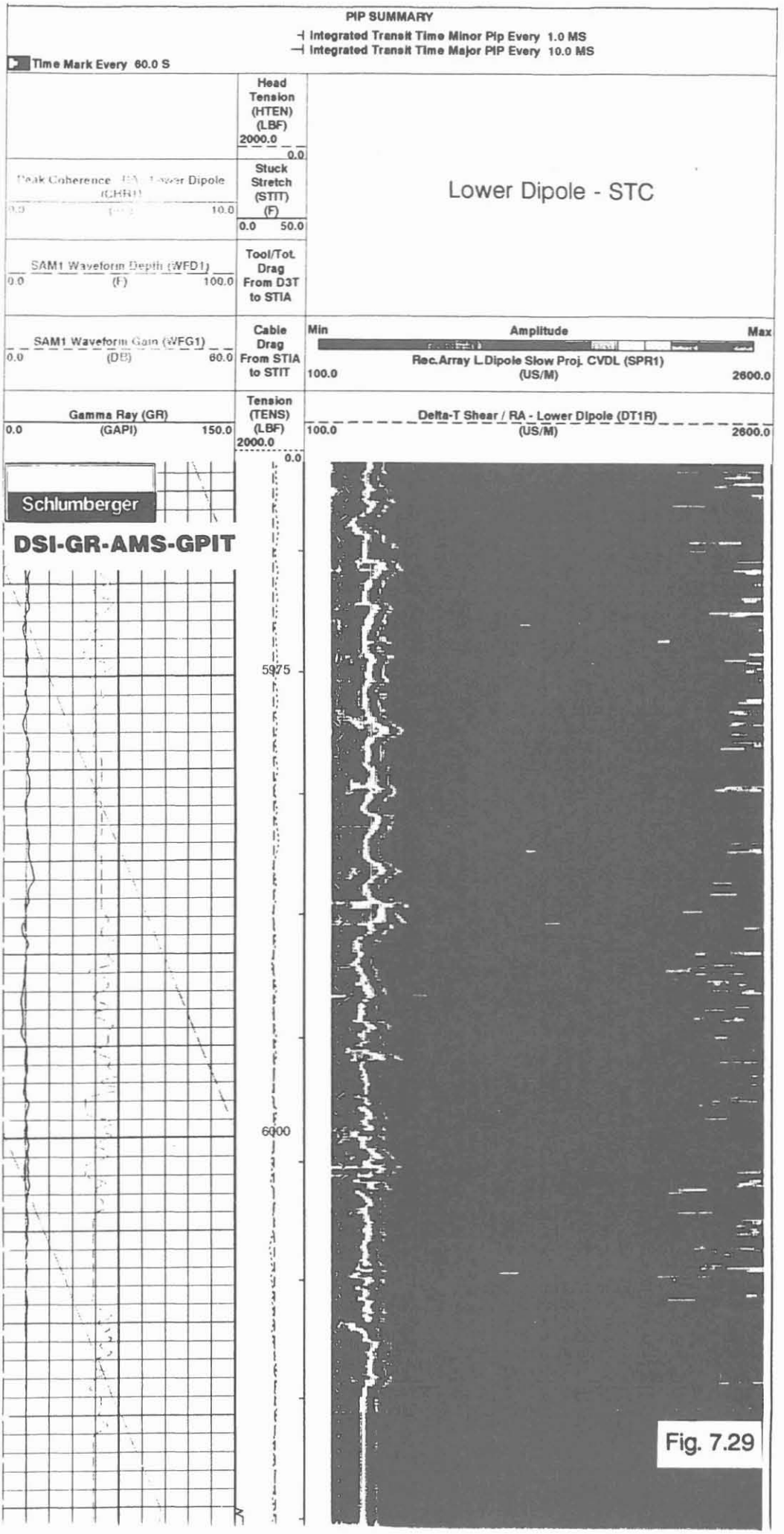
PIP SUMMARY
Integrated Transit Time Minor Pip Every 1.0 MS
Integrated Transit Time Major PIP Every 10.0 MS
Time Mark Every 60.0 S
Head Tension (HTEN) (LBF)
2000.0
0.0
Stuck Stretch (STIT) (F)
0.0 50.0
Lower Dipole - STC
Tool/Tot. Drag From D3T to STIA
SAM1 Waveform Depth (WFD1)
0.0 (F) 100.0
Cable Drag From STIA to STIT
Min Amplitude Max
SAM1 Waveform Gain (WFG1)
0.0 (DB) 60.0
Rec.Array L.Dipole Slow Proj. CVDL (SPR1)
100.0 (US/M) 2600.0
Gamma Ray (GR)
0.0 (GAPI) 150.0
Tension (TENS) (LBF)
2000.0
Delta-T Shear / RA - Lower Dipole (DT1R)
100.0 (US/M) 2600.0
Schlumberger
DSI-GR-AMS-GPIT
0.0
5975
6000

Fig. 7.29

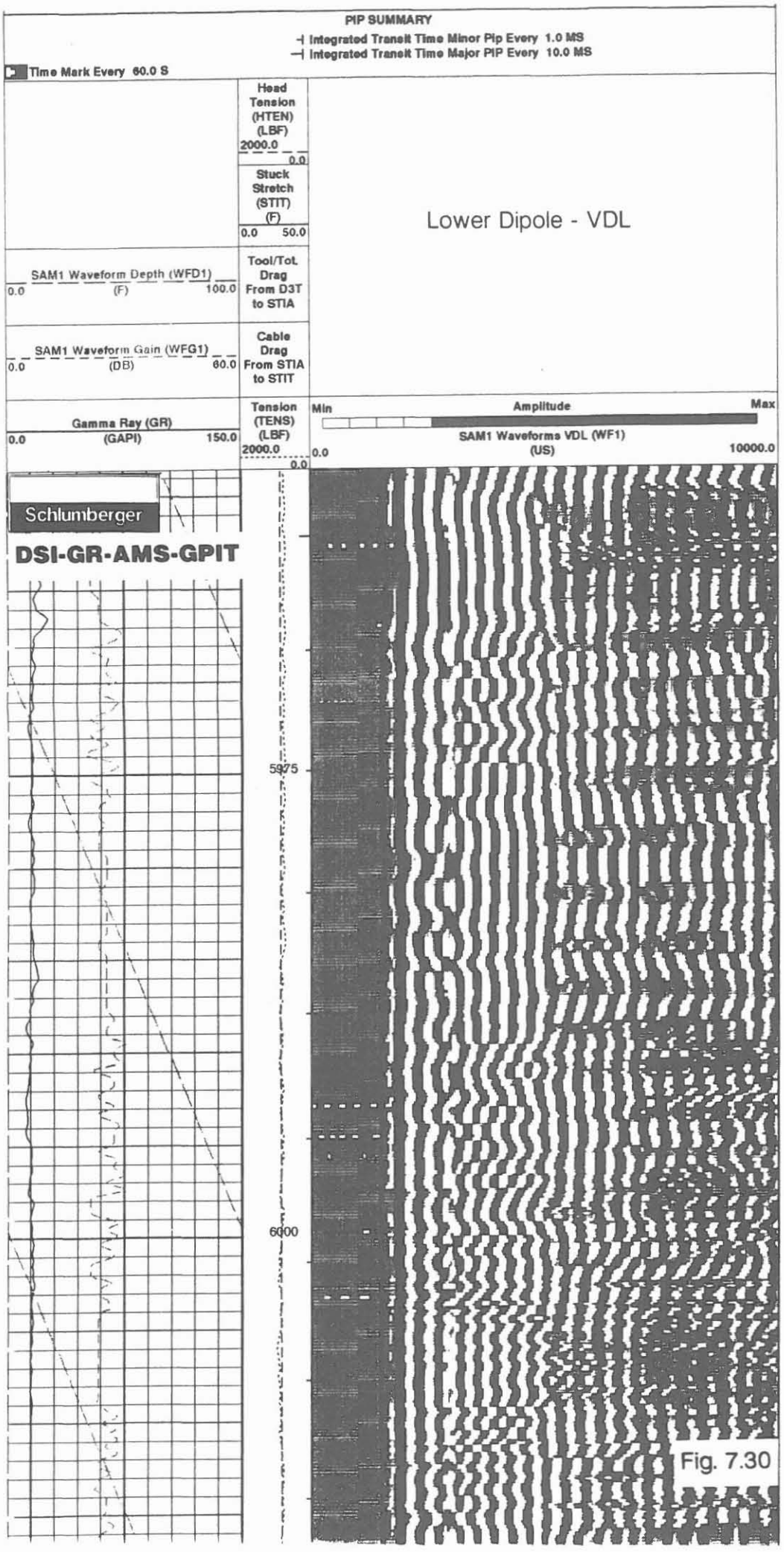
PIP SUMMARY
Integrated Transit Time Minor Pip Every 1.0 MS
Integrated Transit Time Major PIP Every 10.0 MS
Time Mark Every 60.0 S
Head Tension (HTEN) (LBF)
2000.0
0.0
Stuck Stretch (STIT) (F)
0.0 50.0
Lower Dipole - VDL
SAM1 Waveform Depth (WFD1)
0.0 (F) 100.0
Tool/Tot. Drag From D3T to STIA
SAM1 Waveform Gain (WFG1)
0.0 (DB) 60.0
Cable Drag From STIA to STIT
Gamma Ray (GR)
0.0 (GAPI) 150.0
Tension (TENS) (LBF)
2000.0
0.0
Min
Amplitude
Max
SAM1 Waveforms VDL (WF1)
0.0 (US) 10000.0
Schlumberger
DSI-GR-AMS-GPIT
5975
6000

Fig. 7.30

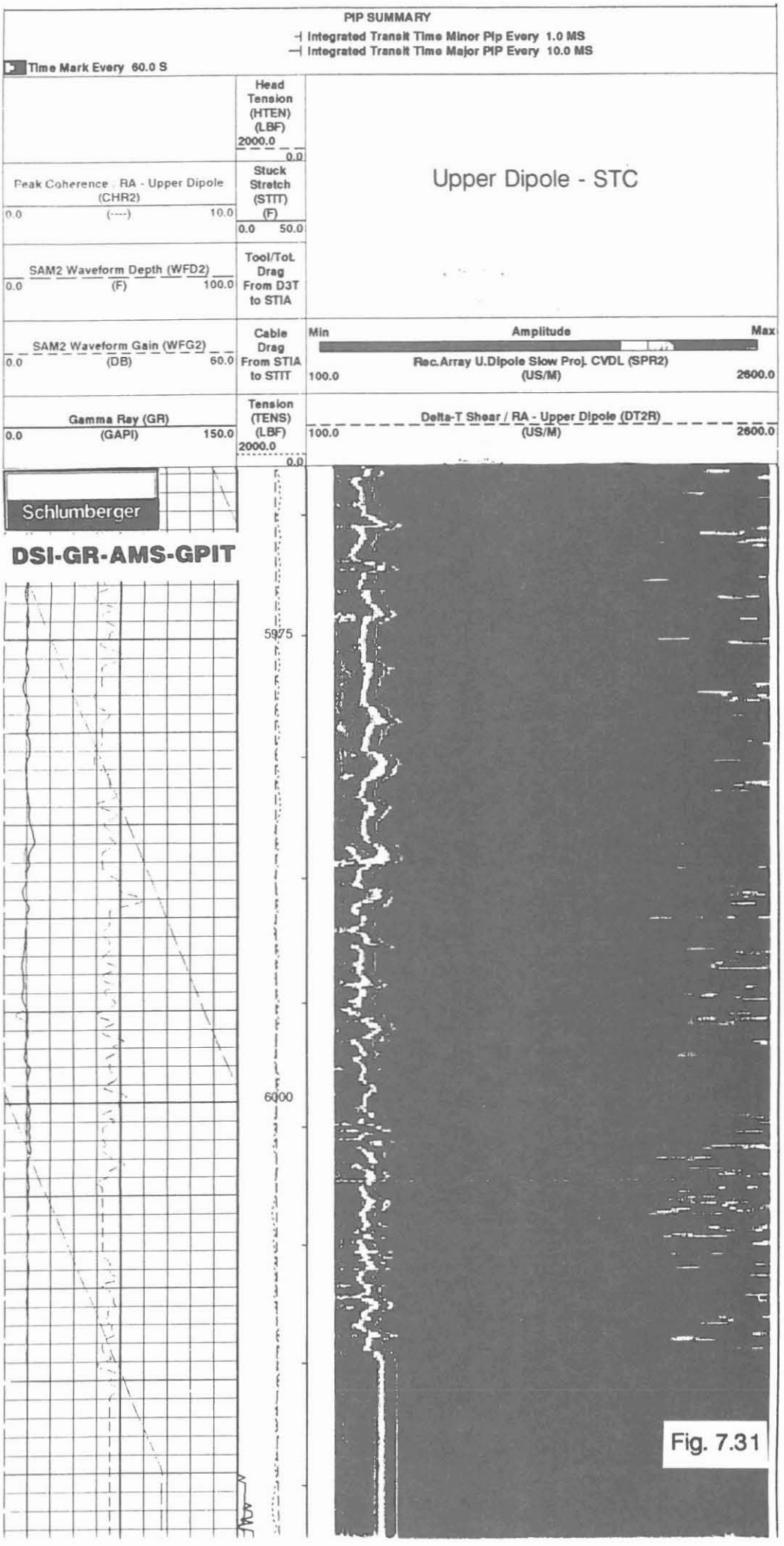
PIP SUMMARY
Integrated Transit Time Minor Pip Every 1.0 MS
Integrated Transit Time Major PIP Every 10.0 MS
Time Mark Every 60.0 S
Head Tension (HTEN) (LBF)
2000.0
0.0
Upper Dipole - STC
Peak Coherence : RA - Upper Dipole (CHR2)
0.0 (----) 10.0
Stuck Stretch (STIT) (F)
0.0 50.0
SAM2 Waveform Depth (WFD2)
0.0 (F) 100.0
Tool/Tot. Drag From D3T to STIA
SAM2 Waveform Gain (WFG2)
0.0 (DB) 60.0
Cable Drag From STIA to STIT
Min Amplitude Max
Rec.Array U.Dipole Slow Proj. CVDL (SPR2)
100.0 (US/M) 2600.0
Gamma Ray (GR)
0.0 (GAPI) 150.0
Tension (TENS) (LBF)
2000.0
0.0
Delta-T Shear / RA - Upper Dipole (DT2R)
100.0 (US/M) 2600.0
Schlumberger
DSI-GR-AMS-GPIT
5975
6000

Fig. 7.31

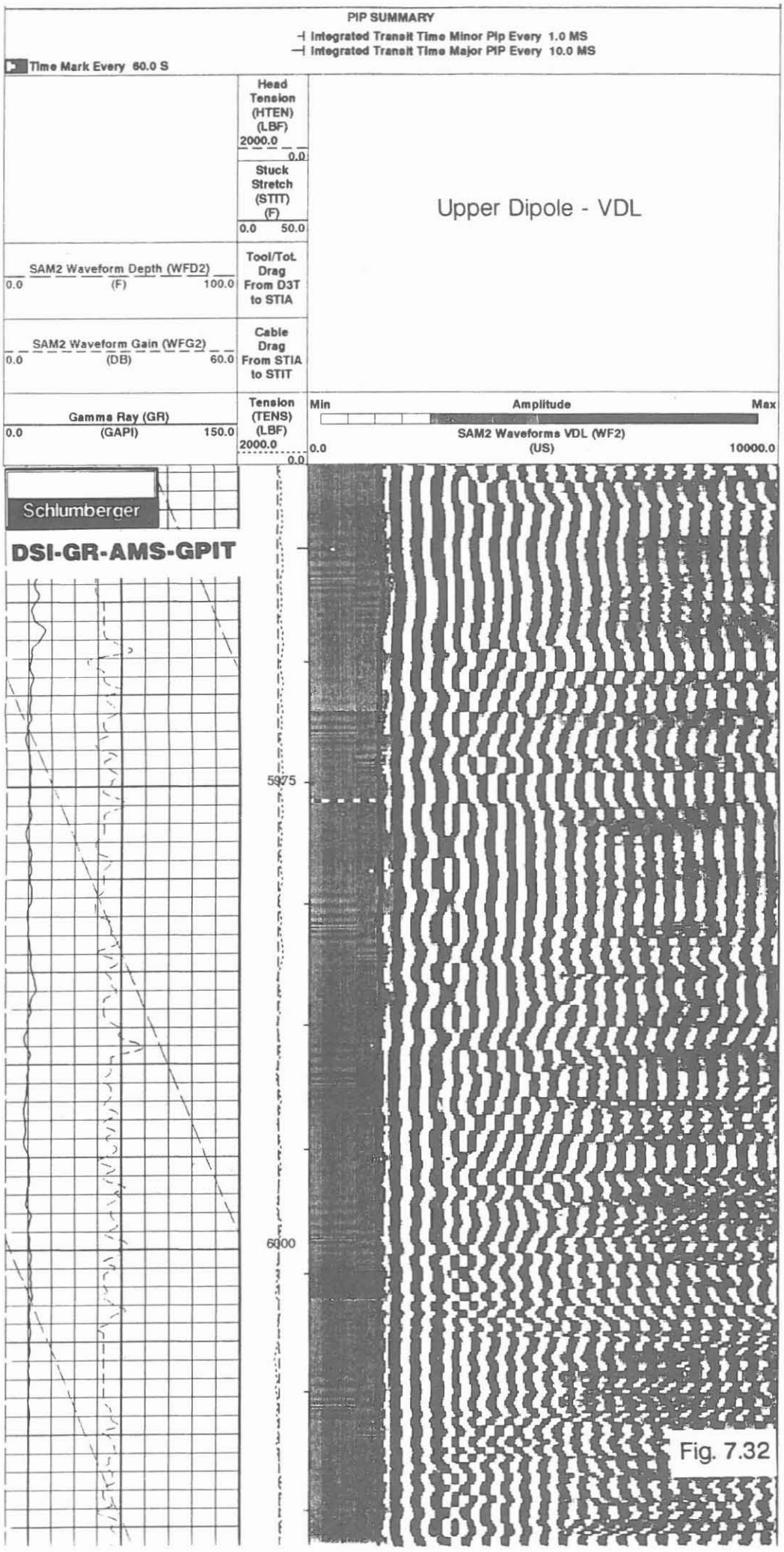
PIP SUMMARY
Integrated Transit Time Minor Pip Every 1.0 MS
Integrated Transit Time Major PIP Every 10.0 MS
Time Mark Every 60.0 S
Head Tension (HTEN) (LBF)
2000.0
0.0
Stuck Stretch (STIT) (F)
0.0 50.0
Upper Dipole - VDL
SAM2 Waveform Depth (WFD2)
0.0 (F) 100.0
Tool/Tot. Drag From D3T to STIA
SAM2 Waveform Gain (WFG2)
0.0 (DB) 60.0
Cable Drag From STIA to STIT
Gamma Ray (GR)
0.0 (GAPI) 150.0
Tension (TENS) (LBF)
2000.0
0.0
Min
Amplitude
Max
SAM2 Waveforms VDL (WF2)
0.0 (US) 10000.0
Schlumberger
DSI-GR-AMS-GPIT
5975
6000

Fig. 7.32

FMI/GR (Formation MicroImager/Gamma Ray)

Operator: Schlumberger Diepholz/KTB

Job No.	Date	Interval
HB-0001-0076	KTB-Report 91-2	0.0 - 1720.0 m
HB-0077-0127	KTB-Report 92-1	1720.0 - 4512.0 m
HB-0132	03.01.1992	3000.0 - 5505.0 m
HB-0150	17.03.1992	5450.0 - 6023.0 m

Example:
Sections of logs: Resistivity Curves Control Plot: 5700.0 - 5975.0 m, **Fig. 7.33**

Images Field Plot: 6002.4 - 6016.5 m, **Fig. 7.34**

Caliper, Deviation and Orientation Plot: 5959.0 - 6023.0 m, **Fig. 7.35**

Cyber Dip Plot: 5945.0 - 6012.0 m, **Fig. 7.36**

Accelerometer-Magnetometer Plot: 5962.0 - 6023.0 m, **Fig. 7.37**

Purpose of log:
To obtain information about structure, texture, foliation and tectonic features, like slickensides, shear planes, folds and for the detection of fractures and fracture systems.

Operation:
This new logging tool requires as surface instrumentation the MAXIS 500 logging unit. Making a temporary connection from this mobile unit to the stationary logging unit on location, the logs are recorded. In 14 3/4" borehole the measurement covers 43 % of the circumference of the borehole.

As real-time record the Resistivity Curve Control Plot Fig. 7.33 ist registered. This plot gives information about the tool performance quality. Via play-back the other plots are made on location, like Image Field Plot Fig. 7.34 and Caliper, Deviation and Orientation Plot Fig. 7.35.

Depth scales: 1/200, 1/40 (in the field); logging speed: 6 m/min.

Technical information:
This new logging tool from Schlumberger makes a resistivity scan of sections of the borehole circumference by applying electrode arrays, mounted on four caliper arms, against the wall. Every caliper arm carries a pad and flap with 24

electrodes each. Magnetometer and inclinometer measurements record not only the trajectory of the borehole but allow in combination with the resistivity records the evaluation of dip and strike direction of the formation.

The data rate from the 192 resistivity electrodes is enormous and requires the computer system of the MAXIS 500. From these "fast channels" a complete set of data are recorded at increments of 0.1" (2,5 mm). The "slow channels" (accelerometer, inclinometer, magnetometer data) are recorded at the standard rate of 6".

Mnemonics and Units:

Mnemonic	Description	Unit
BS	Bit Size	(MM)
C1	Caliper 1 - 3	(MM)
C2	Caliper 2 - 4	(MM)
DEVI	Deviation	(DEG)
EI	Emex Intensity	(AMPS)
EV	Emex Voltage	(V)
FBCR	FMI Correlation Resistance	(KOHMS)
GR	Gamma Ray	(GAPI)
HAZI	Hole Azimuth	(DEG)
P1AZ	Pad 1 Azimuth	(DEG)
TENS	Tension	(LBF)

Description of Plots:

Resistivity Curves Control Plot (Fig. 7.33): This real-time plot serves as quality control during the logging operation. The response of 16 resistivity electrodes, the four-arm caliper, the deviation and orientation, pad 1 azimuth, EMEX current and voltage, gamma ray, bit size, tension and a correlation resistance are recorded. During the logging operation it is possible to step-through the arrays of resistivity electrodes to control the response.

Images Field Plot (Fig. 7.34): Fast optical presentation of resistivity images are given by this plot. This plot is made from uncorrected raw data and is unscaled horizontally. Detailed feature detection (fractures, foliation etc.) is therefore limited, but a first approximation is possible (quality control).

Caliper, Deviation and Orientation Plot (Fig. 7.35): This plot gives the borehole trajectory and caliper data presented in profile simulating the short and long axis of an ovalized borehole. The gamma ray is plotted as depth correlation log.

Cyber Dip Plot (Fig. 7.36): Field evaluation of Dipmeter results. Evaluation gives first information of dip and strike of formations.

Accelerometer-Magnetometer Plot (Fig. 7.37): Control of Orientation and speed correction system. Release of stuck tool (like at 5996.0 - 5993.0 m, 5986.0 - 5983,0 m) clearly indicated by larger signals on X, Y and Z components.

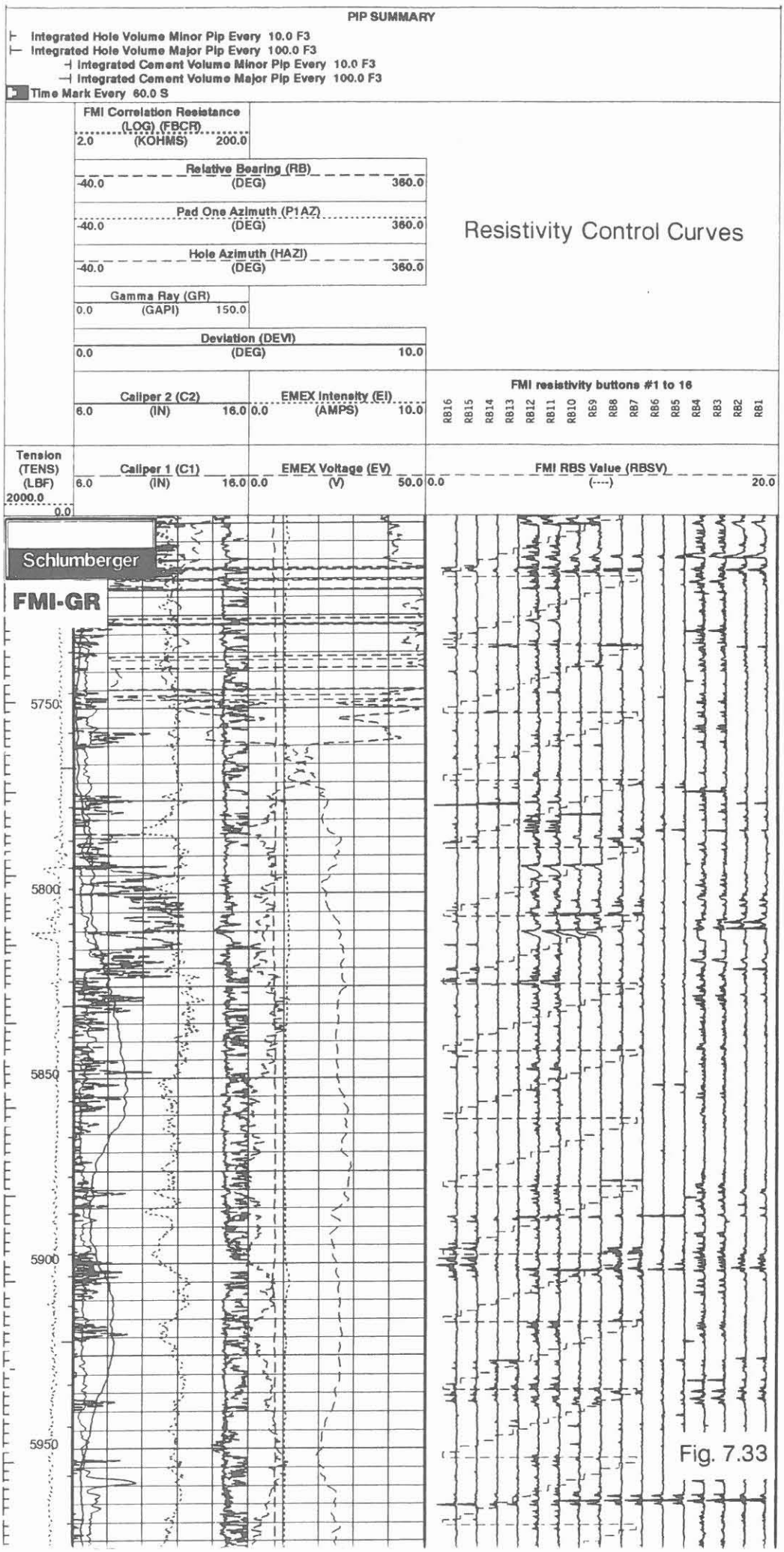
PIP SUMMARY
Integrated Hole Volume Minor Pip Every 10.0 F3
Integrated Hole Volume Major Pip Every 100.0 F3
Integrated Cement Volume Minor Pip Every 10.0 F3
Integrated Cement Volume Major Pip Every 100.0 F3
Time Mark Every 60.0 S
FMI Correlation Resistance (LOG) (FBCR)
2.0 (KOHMS) 200.0
Relative Bearing (RB)
-40.0 (DEG) 360.0
Pad One Azimuth (P1AZ)
-40.0 (DEG) 360.0
Hole Azimuth (HAZI)
-40.0 (DEG) 360.0
Gamma Ray (GR)
0.0 (GAPI) 150.0
Deviation (DEVI)
0.0 (DEG) 10.0
Caliper 2 (C2)
6.0 (IN) 16.0
EMEX Intensity (EI)
0.0 (AMPS) 10.0
FMI resistivity buttons #1 to 16
RB16 RB15 RB14 RB13 RB12 RB11 RB10 RB9 RB8 RB7 RB6 RB5 RB4 RB3 RB2 RB1
Tension (TENS) (LBF)
2000.0
0.0
Caliper 1 (C1)
6.0 (IN) 16.0
EMEX Voltage (EV)
0.0 (V) 50.0
FMI RBS Value (RBSV)
0.0 (----) 20.0
Resistivity Control Curves
Schlumberger
FMI-GR
5750
5800
5850
5900
5950

Fig. 7.33

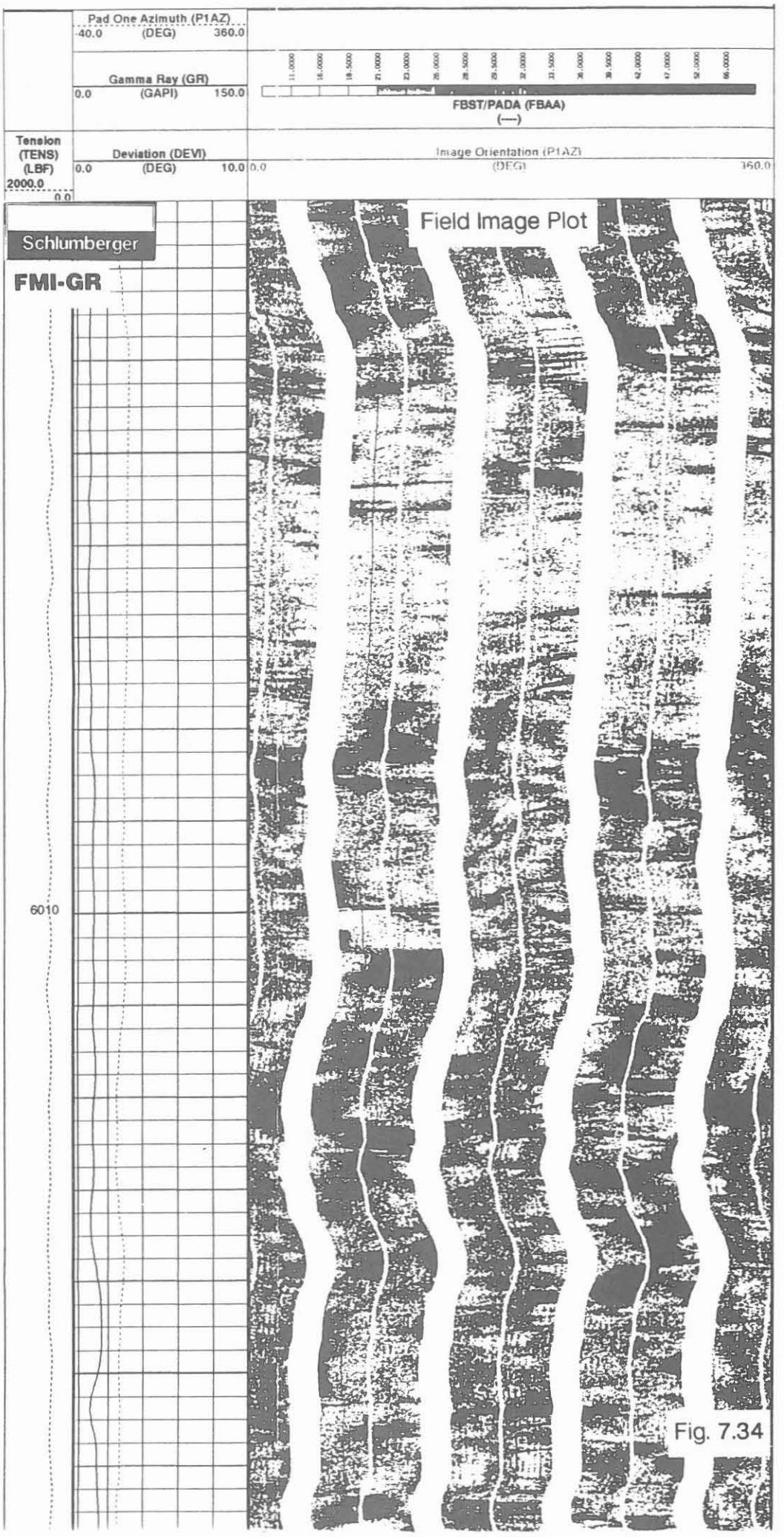
Pad One Azimuth (P1AZ)
40.0 (DEG) 360.0
Gamma Ray (GR)
0.0 (GAPI) 150.0
FBST/PADA (FBAA)
(---)
Tension (TENS) (LBF)
2000.0
0.0
Deviation (DEVI)
0.0 (DEG) 10.0
Image Orientation (P1AZ)
0.0 (DEG) 360.0
Schlumberger
FMI-GR
Field Image Plot
6010

Fig. 7.34

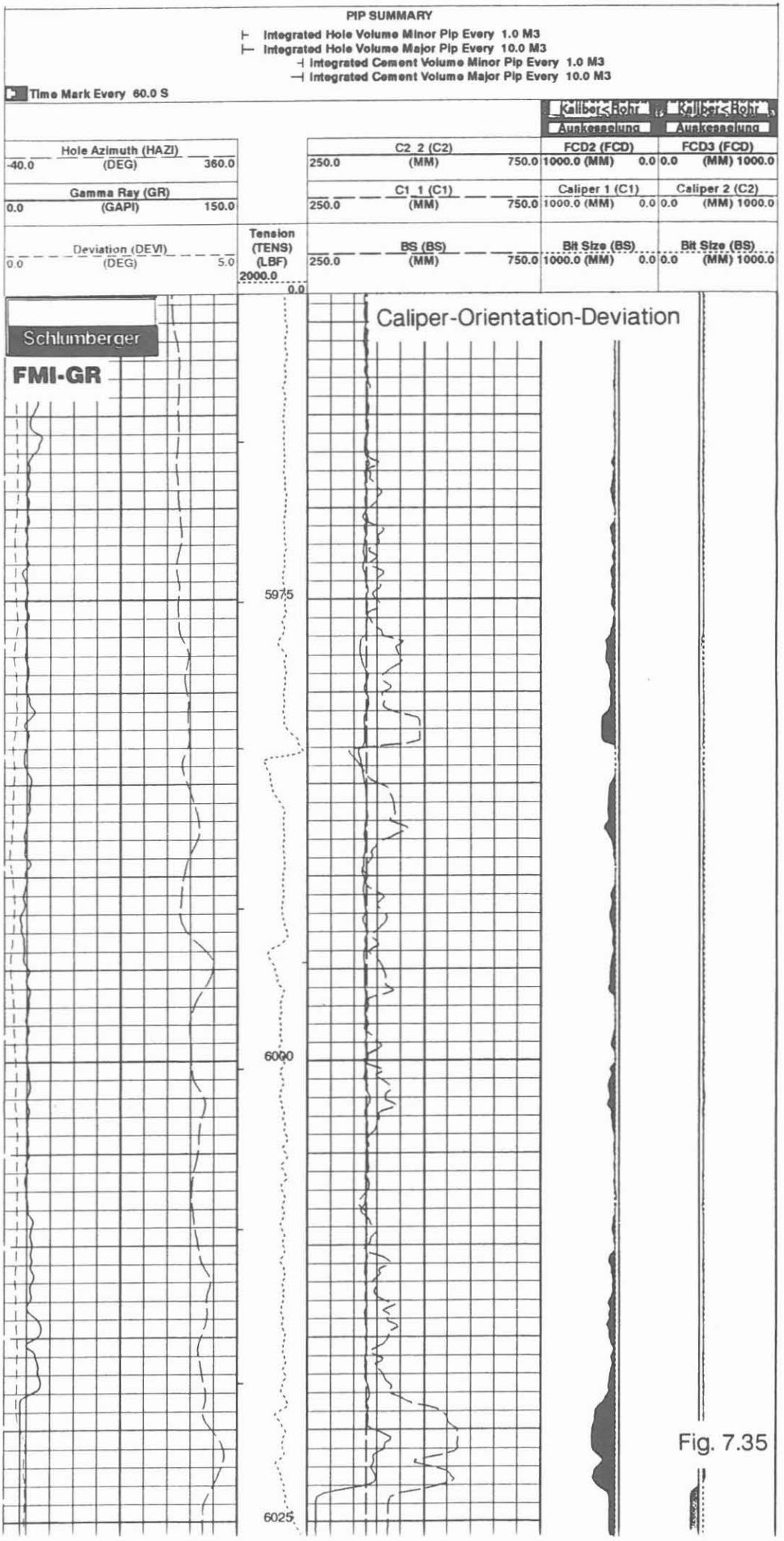
PIP SUMMARY
Integrated Hole Volume Minor Pip Every 1.0 M3
Integrated Hole Volume Major Pip Every 10.0 M3
Integrated Cement Volume Minor Pip Every 1.0 M3
Integrated Cement Volume Major Pip Every 10.0 M3
Time Mark Every 60.0 S
Kaliber<Rohr
Auskesselung
Hole Azimuth (HAZI)
-40.0 (DEG) 360.0
C2_2 (C2)
250.0 (MM) 750.0
FCD2 (FCD)
1000.0 (MM) 0.0
FCD3 (FCD)
0.0 (MM) 1000.0
Gamma Ray (GR)
0.0 (GAPI) 150.0
C1_1 (C1)
250.0 (MM) 750.0
Caliper 1 (C1)
1000.0 (MM) 0.0
Caliper 2 (C2)
0.0 (MM) 1000.0
Deviation (DEVI)
0.0 (DEG) 5.0
Tension (TENS) (LBF)
2000.0
0.0
BS (BS)
250.0 (MM) 750.0
Bit Size (BS)
1000.0 (MM) 0.0
Bit Size (BS)
0.0 (MM) 1000.0
Schlumberger
FMI-GR
Caliper-Orientation-Deviation
5975
6000
6025

Fig. 7.35

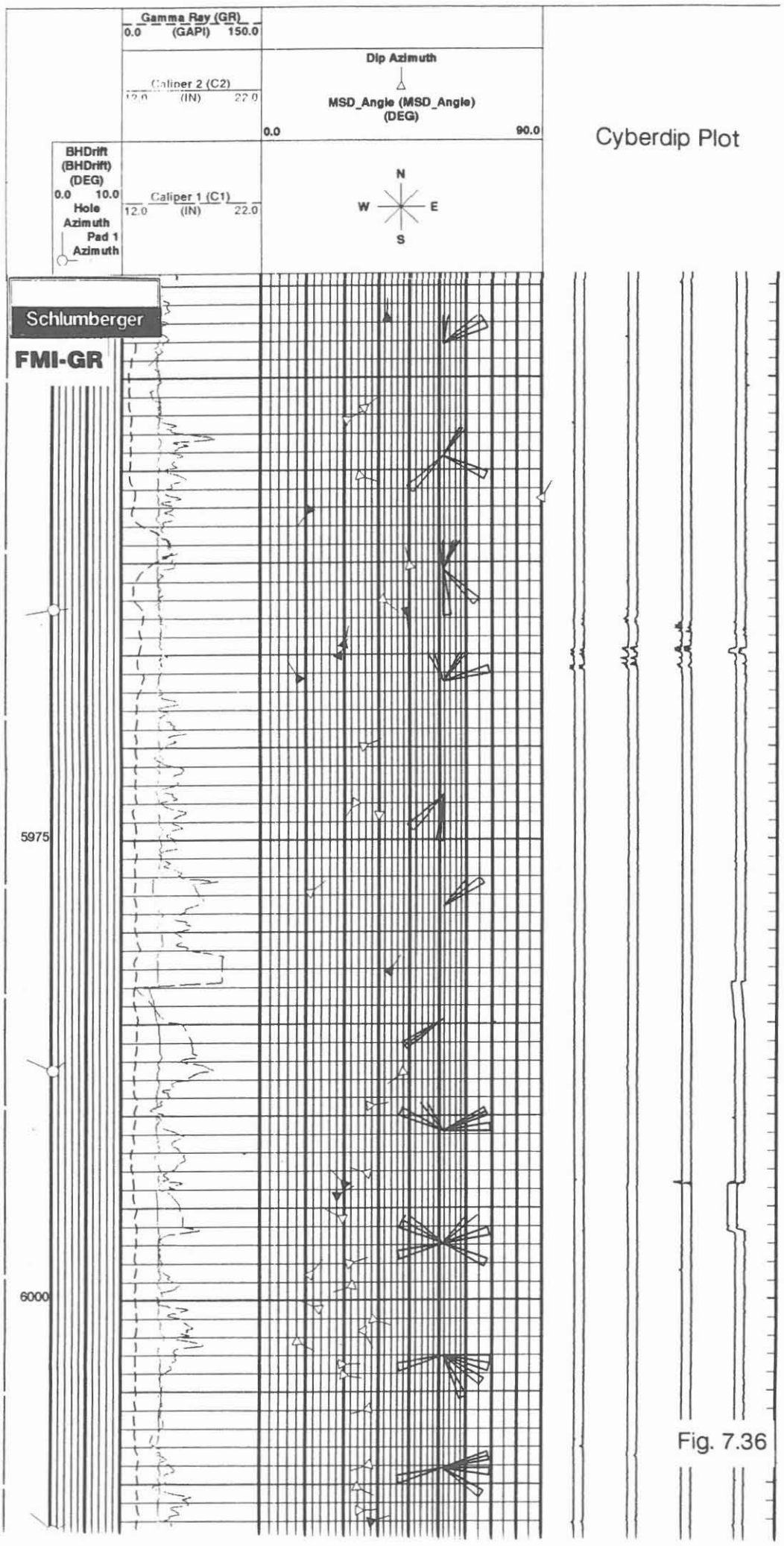
Gamma Ray (GR)
0.0 (GAPI) 150.0
Caliper 2 (C2)
12.0 (IN) 22.0
Dip Azimuth
MSD_Angle (MSD_Angle)
(DEG)
0.0 90.0
BHDrift
(BHDrift)
(DEG)
0.0 10.0
Hole
Azimuth
Pad 1
Azimuth
Caliper 1 (C1)
12.0 (IN) 22.0
N
W E
S
Cyberdip Plot
Schlumberger
FMI-GR
5975
6000

Fig. 7.36

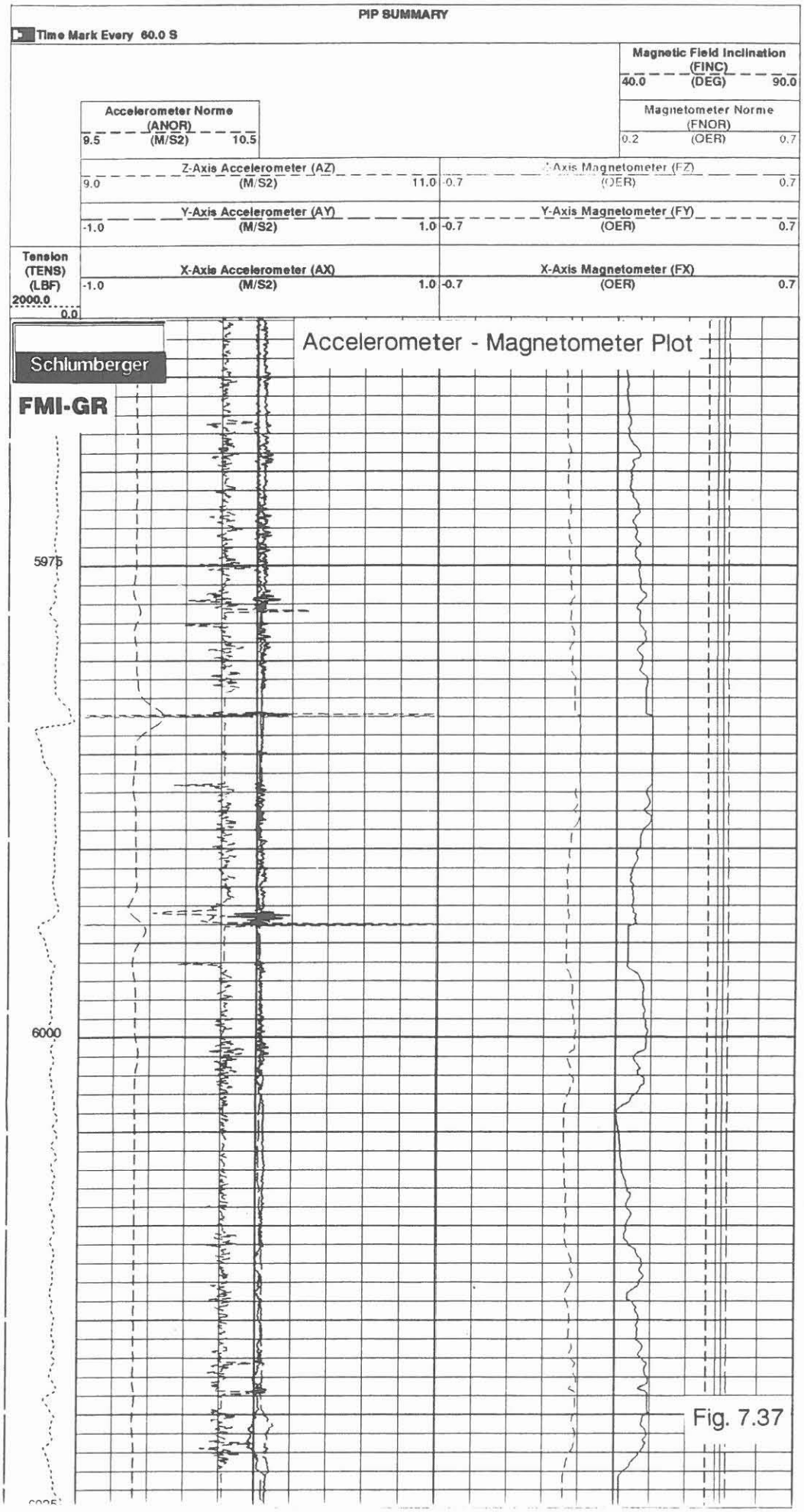
PIP SUMMARY
Time Mark Every 60.0 S
Magnetic Field Inclination (FINC)
40.0 (DEG) 90.0
Accelerometer Norme (ANOR)
9.5 (M/S2) 10.5
Magnetometer Norme (FNOR)
0.2 (OER) 0.7
Z-Axis Accelerometer (AZ)
9.0 (M/S2) 11.0
Z-Axis Magnetometer (FZ)
-0.7 (OER) 0.7
Y-Axis Accelerometer (AY)
-1.0 (M/S2) 1.0
Y-Axis Magnetometer (FY)
-0.7 (OER) 0.7
Tension (TENS) (LBF)
2000.0
0.0
X-Axis Accelerometer (AX)
-1.0 (M/S2) 1.0
X-Axis Magnetometer (FX)
-0.7 (OER) 0.7
Schlumberger
FMI-GR
Accelerometer - Magnetometer Plot
5975
6000

Fig. 7.37

ARI/MSFL/GR/GPIT (Azimuthal Resistivity Imager/Microspherical Focused Log/Gamma Ray/General Purpose Inclinometer Tool)

Operator: Schlumberger Paris - Diepholz/KTB

Job No.	Date	Interval
HB-0151	17.03.1992	3000.0 - 6022.0 m

Examples:
Sections of logs: DLL-MSFL Plot 5958.0-6022.0 m, **Fig. 7.38**
Azimuthal Resistivity Plot 5977.0-6005.0 m **Fig. 7.39**
Field Image Plot 5963.0-6000.0 m, **Fig. 7.40**

Purpose of log:
With this newly developed tool the standard resistivity measurement according to the Dual Laterolog principle is made. In addition, 12 focused and oriented Laterolog curves are recorded. These additional Laterolog curves will measure the resistivity of 30° sectors of the borehole circumference. From the data information about the structure, texture and anisotropy will be obtained. Due to the deeper investigation of the Laterolog the detection of open fractures, mineralised fault planes and slickensides will be possible.

Operation:
The standard Dual Laterolog (DLL) Microspherical Focused Log (MSFL) is combined with the new tool section carrying the array of the 12 sectoral focused resistivity sensing devices. For obtaining oriented resistivity measurements the General Purpose Inclinometer Tool (GPIT) is run in combination. For depth correlation the Gamma Ray recording is used.

The tool requires the MAXIS 500 surface unit. After recording the raw data in real time the different plots are made in playback mode. Data equalisation and normalisation is necessary for image presentations. These computations are done in the field with the MAXIS 500 unit.
Depth scale: 1/1000, 1/200; logging speed: 10 m/min.

Technical information:
A detailed description of the tool is given in chapter 8: "New Tools" of this report.

Description of logs:
DLL/MSFL Plot (Fig. 7.38). This plot was created in playback mode. It corresponds to an improved standard DLL/MSFL presentation giving four Laterolog resistivities: Laterolog Shallow (LLS), Laterolog Deep (LLD), Laterolog Groningen (LLG). High Resolution Laterolog (LLHR) and the Microspherical Focused Log (MSFL), in track I the Gamma Ray (GR) and the Accelerometer reading (AZ).

Azimuthal Resistivity Plot (Fig. 7.39). This record was registered in real time mode. The data recorded represents the resistivities recorded by the electrode array for the 12 sectors (RR01-RR12) and the High Resolution Laterolog (LLHR). In track I the Gamma Ray (GR) and the 12 caliper conductivities (CC01 - CC12) and pad 1 azimuth (P1AZ) are recorded.

Field Image Plot (Fig. 7.40). This record is made after data normalisation and equalisation in playback mode. Three Laterolog curves Laterolog Shallow (LLS), Laterolog Deep (LLD) and High Resolution Laterolog (LLHR) are presented with a resistivity scale shifted by one decade. In addition the processed data of the resistivity array is presented in form of the 12 resistivity curves.

The image transforms are given on the left side of the plot. First column "raw data" (ARI Raw Sta), middle column "normalized data" (ALAT Raw. Norm) and right column "equalized and normalized data" (ALAT Eq Norm).

Betweeen the image columns the Gamma Ray (GR), the Standard Caliper (CALS), the Back-up Caliper (CALB), the Deviation (DEVI), Hole (Hole AZ) and Pad 1 Azimuth (Pad 1 AZ) are given.

Mnemonics and Units:

Mnemonics	Description	Unit
ALAT	Azimuthal Laterolog	
ARI	Azimuthal Resistivity Image	
AZ	Accelerometer	(M/S2)
CCO1-CC12	Caliper Conductivity 1-12	(MMHO)
CALB	Caliper Back-up	(INCH)
CALS	Caliper Standard	(INCH)
CDR	Continuous Directional Recording	(DEG)
DEVI	Deviation	(DEG)
GR	Gamma Ray	(GAPI)
LLD	Laterolog Deep	(OHMM)
LLG	Laterolog Groningen	(OHMM)
LLHR	Laterolog High Resolution	(OHMM)
LLS	Laterolog Shallow	(OHMM)
MSFL	Micropherical Focused Log	(OHMM)
RR01-RR12	Azimuthal Resistivities 1-12	(OHMM)
P1AZ	Pad 1 Azimuth	(DEG)
TENS	Tension	(LBF)

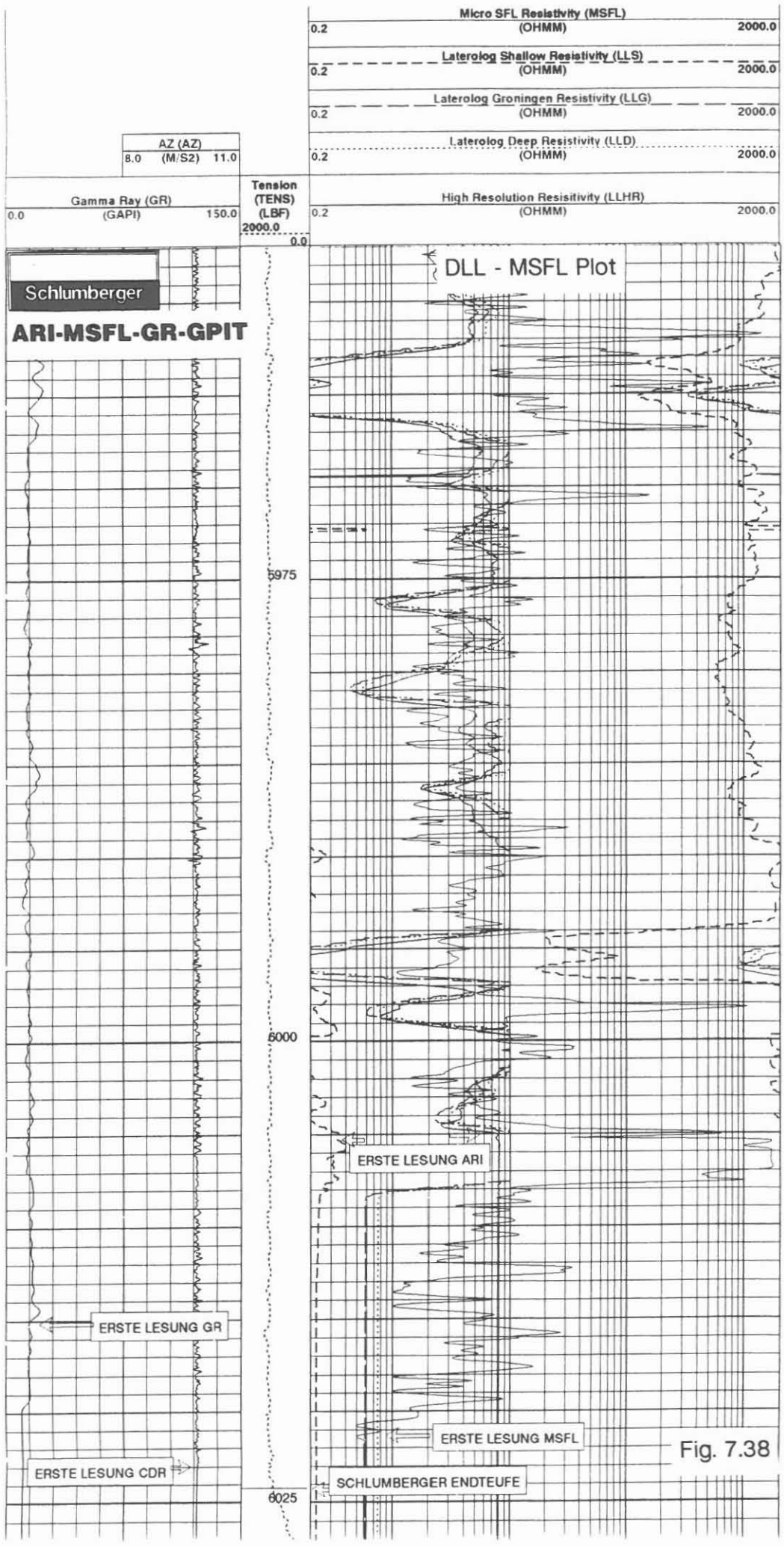
Micro SFL Resistivity (MSFL)
0.2 (OHMM) 2000.0
Laterolog Shallow Resistivity (LLS)
0.2 (OHMM) 2000.0
Laterolog Groningen Resistivity (LLG)
0.2 (OHMM) 2000.0
Laterolog Deep Resistivity (LLD)
0.2 (OHMM) 2000.0
AZ (AZ)
8.0 (M/S2) 11.0
Gamma Ray (GR)
0.0 (GAPI) 150.0
Tension (TENS) (LBF)
2000.0
0.0
High Resolution Resisitivity (LLHR)
0.2 (OHMM) 2000.0
Schlumberger
ARI-MSFL-GR-GPIT
DLL - MSFL Plot
5975
6000
6025
ERSTE LESUNG ARI
ERSTE LESUNG GR
ERSTE LESUNG CDR
ERSTE LESUNG MSFL
SCHLUMBERGER ENDTEUFE

Fig. 7.38

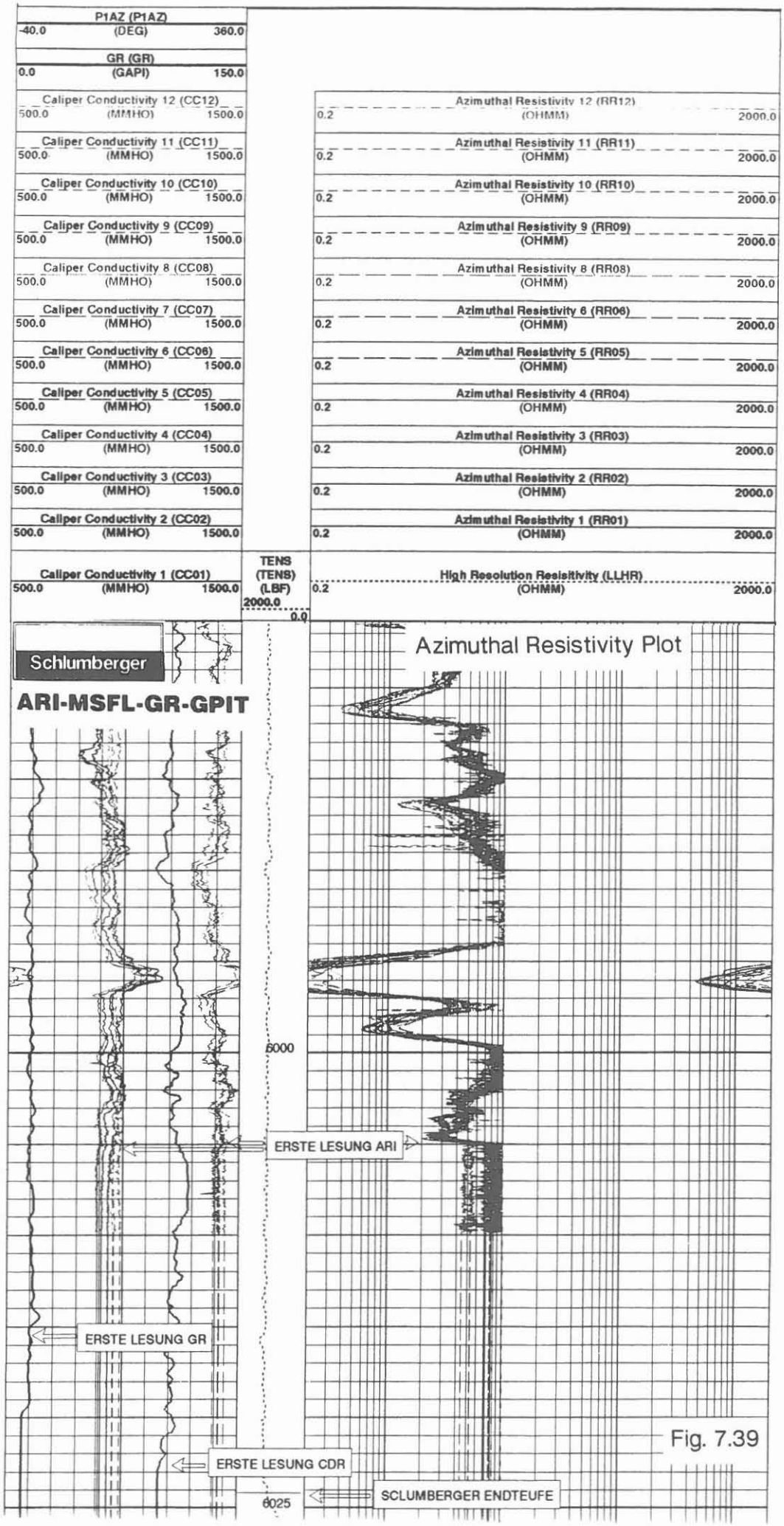
P1AZ (P1AZ)
-40.0 (DEG) 360.0
GR (GR)
0.0 (GAPI) 150.0
Caliper Conductivity 12 (CC12)
500.0 (MMHO) 1500.0
Caliper Conductivity 11 (CC11)
500.0 (MMHO) 1500.0
Caliper Conductivity 10 (CC10)
500.0 (MMHO) 1500.0
Caliper Conductivity 9 (CC09)
500.0 (MMHO) 1500.0
Caliper Conductivity 8 (CC08)
500.0 (MMHO) 1500.0
Caliper Conductivity 7 (CC07)
500.0 (MMHO) 1500.0
Caliper Conductivity 6 (CC06)
500.0 (MMHO) 1500.0
Caliper Conductivity 5 (CC05)
500.0 (MMHO) 1500.0
Caliper Conductivity 4 (CC04)
500.0 (MMHO) 1500.0
Caliper Conductivity 3 (CC03)
500.0 (MMHO) 1500.0
Caliper Conductivity 2 (CC02)
500.0 (MMHO) 1500.0
Caliper Conductivity 1 (CC01)
500.0 (MMHO) 1500.0
TENS (TENS) (LBF)
2000.0
0.0
Azimuthal Resistivity 12 (RR12)
0.2 (OHMM) 2000.0
Azimuthal Resistivity 11 (RR11)
0.2 (OHMM) 2000.0
Azimuthal Resistivity 10 (RR10)
0.2 (OHMM) 2000.0
Azimuthal Resistivity 9 (RR09)
0.2 (OHMM) 2000.0
Azimuthal Resistivity 8 (RR08)
0.2 (OHMM) 2000.0
Azimuthal Resistivity 6 (RR06)
0.2 (OHMM) 2000.0
Azimuthal Resistivity 5 (RR05)
0.2 (OHMM) 2000.0
Azimuthal Resistivity 4 (RR04)
0.2 (OHMM) 2000.0
Azimuthal Resistivity 3 (RR03)
0.2 (OHMM) 2000.0
Azimuthal Resistivity 2 (RR02)
0.2 (OHMM) 2000.0
Azimuthal Resistivity 1 (RR01)
0.2 (OHMM) 2000.0
High Resolution Resistivity (LLHR)
0.2 (OHMM) 2000.0
Schlumberger
ARI-MSFL-GR-GPIT
Azimuthal Resistivity Plot
6000
ERSTE LESUNG ARI
ERSTE LESUNG GR
ERSTE LESUNG CDR
6025
SCLUMBERGER ENDTEUFE

Fig. 7.39

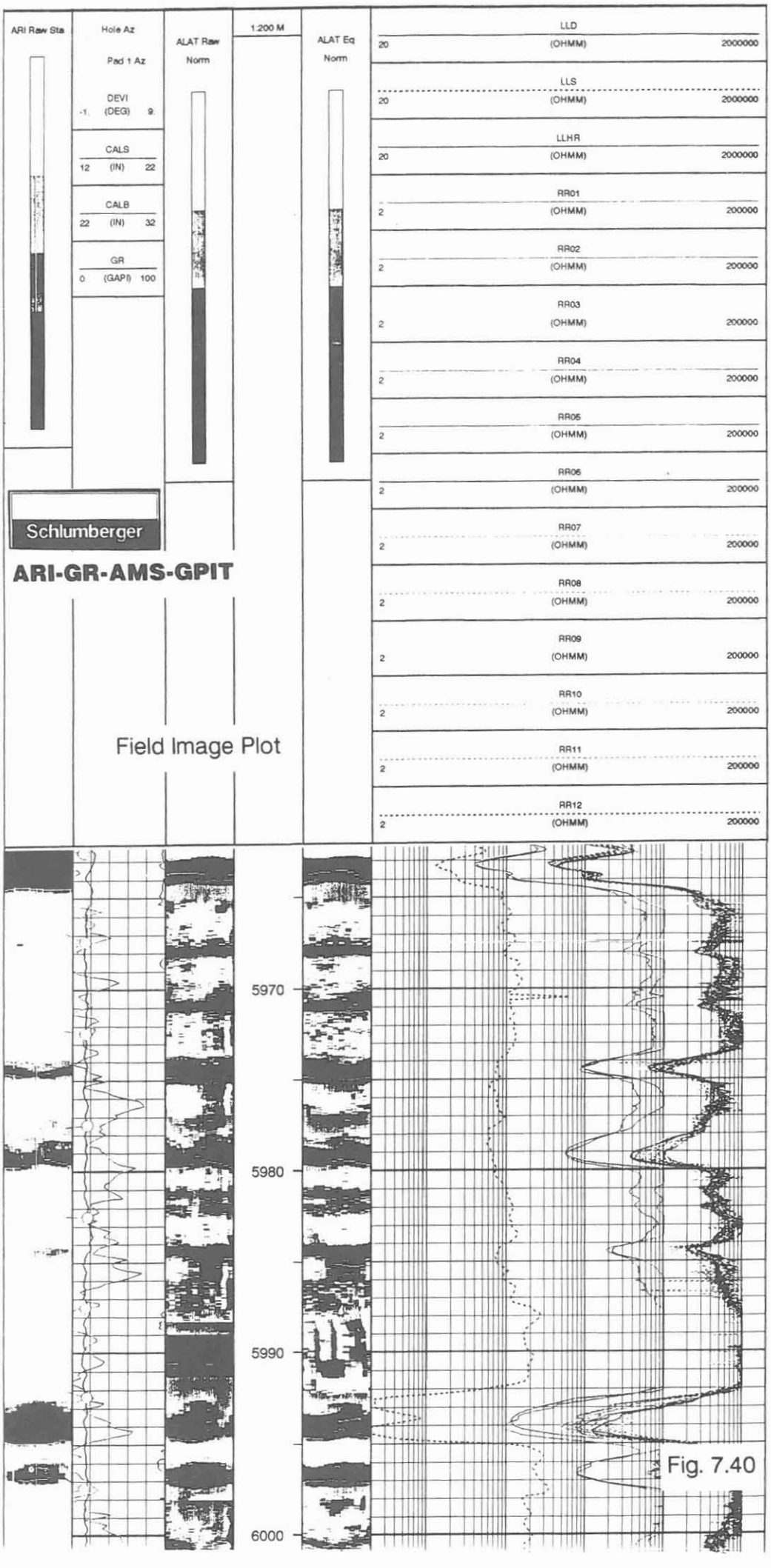
ARI Raw Sta
Hole Az
Pad 1 Az
DEVI
-1. (DEG) 9.
CALS
12 (IN) 22
CALB
22 (IN) 32
GR
0 (GAPI) 100
ALAT Raw
Norm
1:200 M
ALAT Eq
Norm
LLD
20 (OHMM) 2000000
LLS
20 (OHMM) 2000000
LLHR
20 (OHMM) 2000000
RR01
2 (OHMM) 200000
RR02
2 (OHMM) 200000
RR03
2 (OHMM) 200000
RR04
2 (OHMM) 200000
RR05
2 (OHMM) 200000
RR06
2 (OHMM) 200000
RR07
2 (OHMM) 200000
RR08
2 (OHMM) 200000
RR09
2 (OHMM) 200000
RR10
2 (OHMM) 200000
RR11
2 (OHMM) 200000
RR12
2 (OHMM) 200000
Schlumberger
ARI-GR-AMS-GPIT
Field Image Plot
5970
5980
5990
6000

Fig. 7.40

GR/IP (Gamma Ray/Induced Polarisation)

Operator: Hungarian Geophysical Institute Roland Eötvös, Budapest (ELGI)/KTB.

Job No.	Date	Interval
HB-0156	19.03.1992	3000.0 - 6024.0 m

Example:
Section of log: 5500.0 - 5885.00 m, **Fig. 7.41**

Purpose of log:
This type of log is used for special mineral detection like graphite and sulfides, which are normally associated with fault zones or slickensides. In addition, due to the sensitivity to saline fluids the response of the measurement could provide information about porosity and permeability.

Operation:
The tool was run in combination with the KTB-Gamma Ray sonde on the KTB cable.
Depth scale: 1/200, 1/1000; logging speed: 5 m/min.

Technical information:
The principle of the Induced Polarisation measurement is explained in detail in KTB-Report 87-3, pages 96-99. Interpretation reports are given in KTB-Reports 88-4 and 90-6a.
Data rate: 6".

Mnemonics and Units:

Mnemonics	Description	Unit
GR	Gamma Ray	(GAPI)
KAPA	Calculated chargeability at "zero time"	(%)
TAU	General time constant	(MS)
TENS	Tension	(LBF)

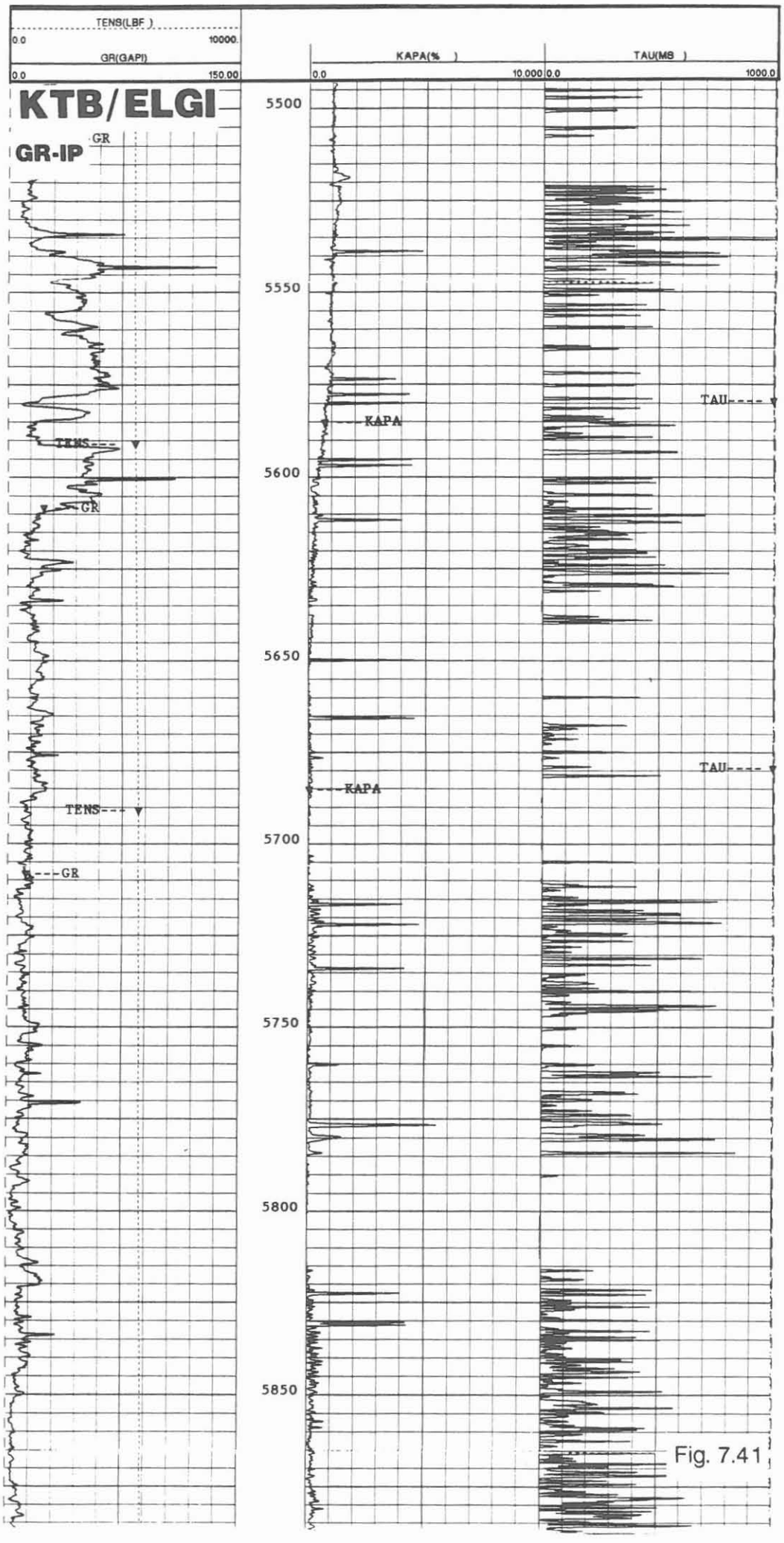
TENS(LBF)
0.0
10000.
GR(GAPI)
0.0
150.00
KTB/ELGI
GR-IP
GR
TENS
GR
TENS
GR
KAPA(%)
0.0
10.000
TAU(MS)
0.0
1000.0
5500
5550
5600
5650
5700
5750
5800
5850
KAPA
KAPA
TAU
TAU

Fig. 7.41

SP/REDOX/SAL/TEMP (Self Potential/REDOX Potential/Mud Salinity/Temperature)

Operator: University Frankfurt/KTB

Job No.	Date	Interval
HB-0100	KTB-Report 92-1	208.0 - 3003.0 m
HB-0157	20.03.1993	3000.0 - 6024.0 m

Example:
Section of log: 5200.0 - 5570.0 m, **Fig. 7.42**

Purpose of log:
With the record of the Self Potential, Redox Potential, Mud Salinity and Temperature indications are obtained for the detection of permeable zones, inflow of fluids to the borehole, mineralisation (graphite, pyrite) and an estimation of the formation water salinity can be made.

Operation:
The tool was developed by the University of Frankfurt and run on the KTB logging unit. As the tool is fully compatible with the logging unit, the data registration is made via the CSU. Depth scale: 1/200, 1/1000; logging speed: 25 m/min.

Technical information:
The Electrical Potential (EP) is recorded as the voltage difference (in mV) between a moving Ag-AgCl electrode in the borehole and a stationary electrode of the same material at surface.

The Spontaneous Potential (SP) measures the voltage difference (in mV) between a steel electrode in the borehole and a lead electrode on surface.

The voltage difference (PSP), measured in mV between a platinum electrode in the borehole and an Ag-AgCl electrode on the surface, is used for the computation of the REDOX potential. It represents the difference between PSP and EP. The salinity of the mud is computed from mud resistivity measurements using the standard conversion chart for NaCl equivalence.

Mnemonics and Units:

Mnemonics	Description	Unit
EP	Electrial Potential	(MU)
LCO1	Mud Salinity	(PPM)
REDOX	Redox Potential	(MV)
SP	Self Potential	(MV)
STMP	Temperature	(DEGC)
TENS	Tension	(LBF)

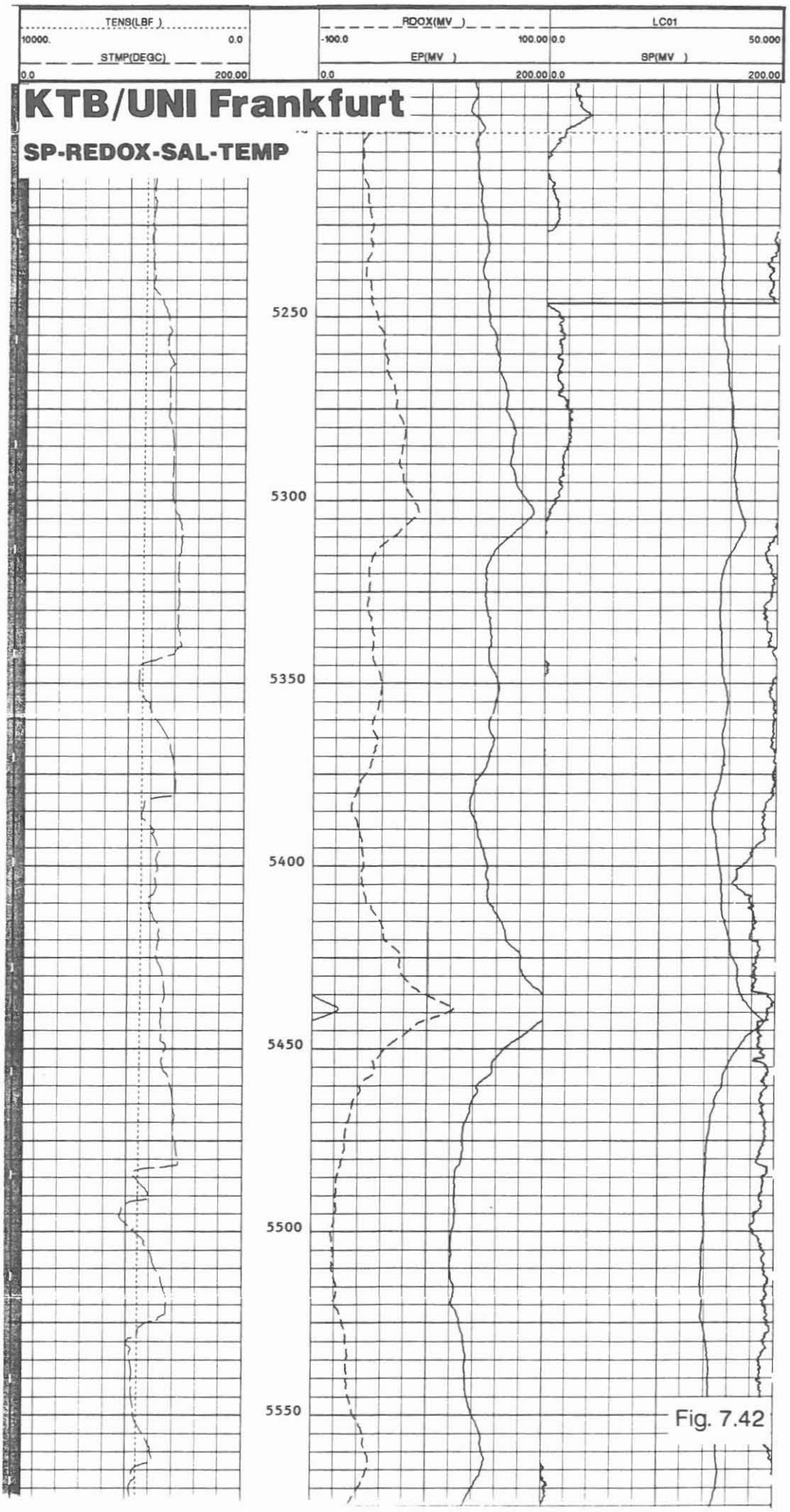
TENS(LBF)
10000.
0.0
STMP(DEGC)
0.0
200.00
REDOX(MV)
-100.0
100.00
EP(MV)
0.0
200.00
LC01
0.0
50.000
SP(MV)
0.0
200.00
KTB/UNI Frankfurt
SP-REDOX-SAL-TEMP
5250
5300
5350
5400
5450
5500
5550

Fig. 7.42

GR/AMS (Gamma Ray/Auxiliary Measurement Sonde)

Operator: KTB

Job No.	Date	Interval
HB-0159	22.03.1992	394.0 - 484.0 m

Example:
Section of logs: 455.0 - 482.0 m, **Fig. 7.43**

Purpose of log:
Record of the rise of the mud level during a production test.

Operation:
Decreasing the hydraulic pressure on the formation by lowering the mud level in the borehole will provoke production of formation fluids. The inflow volume is measured by the observation of the rise of the mud level in the borehole. An estimation of "productivity" can be made by measuring the volume versus time.
Depth scale: 1/200; logging speed: 10 m/min.

Technical information:
The measurements are made using the Auxiliary Measurement Sonde (AMS) recording temperature and mud resistivity. For depth control the Gamma Ray is recorded in combination.
Data rate: 6".

Mnemonics and Units:

Mnemonics	Description	Unit
AMTE	Temperature	(DEGC)
GR	Gamma Ray	(GAPI)
HTEN	Head Tension	(LBF)
MRES	Mud Resistivity	(OHMM)
TENS	Tension	(LBF)

KTB

GR-AMS (Mud Level Observation)

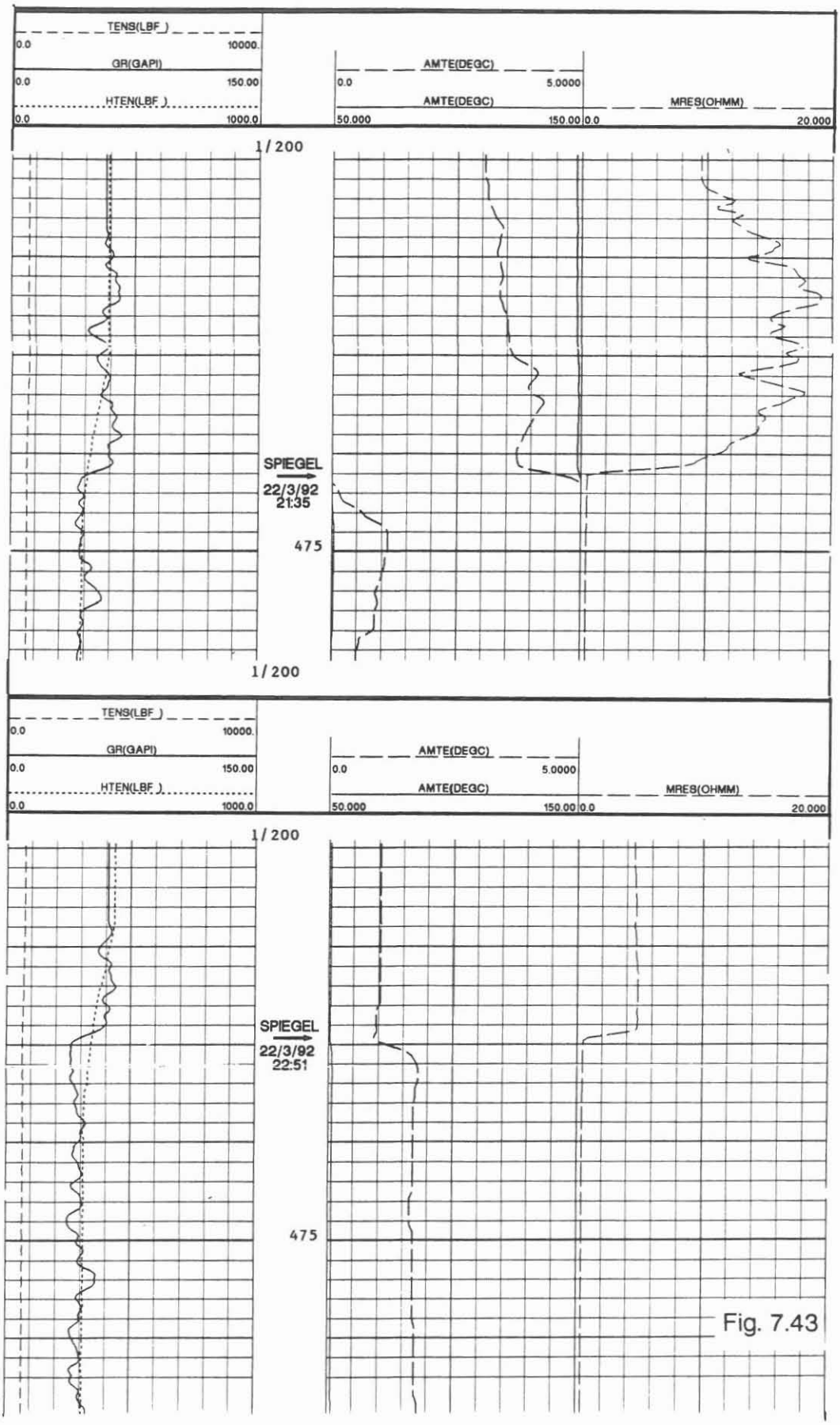

Fig. 7.43

SP/REDOX/SAL/TEMP (Self Potential/Redox Potential/Mud Salinity and Temperature)

Operator: University of Frankfurt/KTB

Job No.	Date	Interval
HB-0162	23.03.1992	2969.0 - 6000.0 m

Example:
Section of log 5265.0 - 5625.0 m, **Fig. 7.44**

Purpose of log:
This log had been recorded after a produktion test. By lowering the hydrostatic head inflow of formation fluid was provoked. With this log producing zones could be located.

Operation:
Log was recorded after the test going in the borehole. In comparison to log run on 19.03.1992 (Fig. 7.42), several producing intervals can be separated.

Technical information:
See explanation provided with log dated 19.03.1992 (Fig. 7.42).

Mnemonics and Units:

Mnemonics	Description	Unit
EP	Electrical Potential	(MV)
LCO1	Mud Salinity	(PPM)
REDOX	Redox Potential	(MV)
SP	Self Potential	(MV)
STMP	Temperature	(DEGC)
TENS	Tension	(LBF)

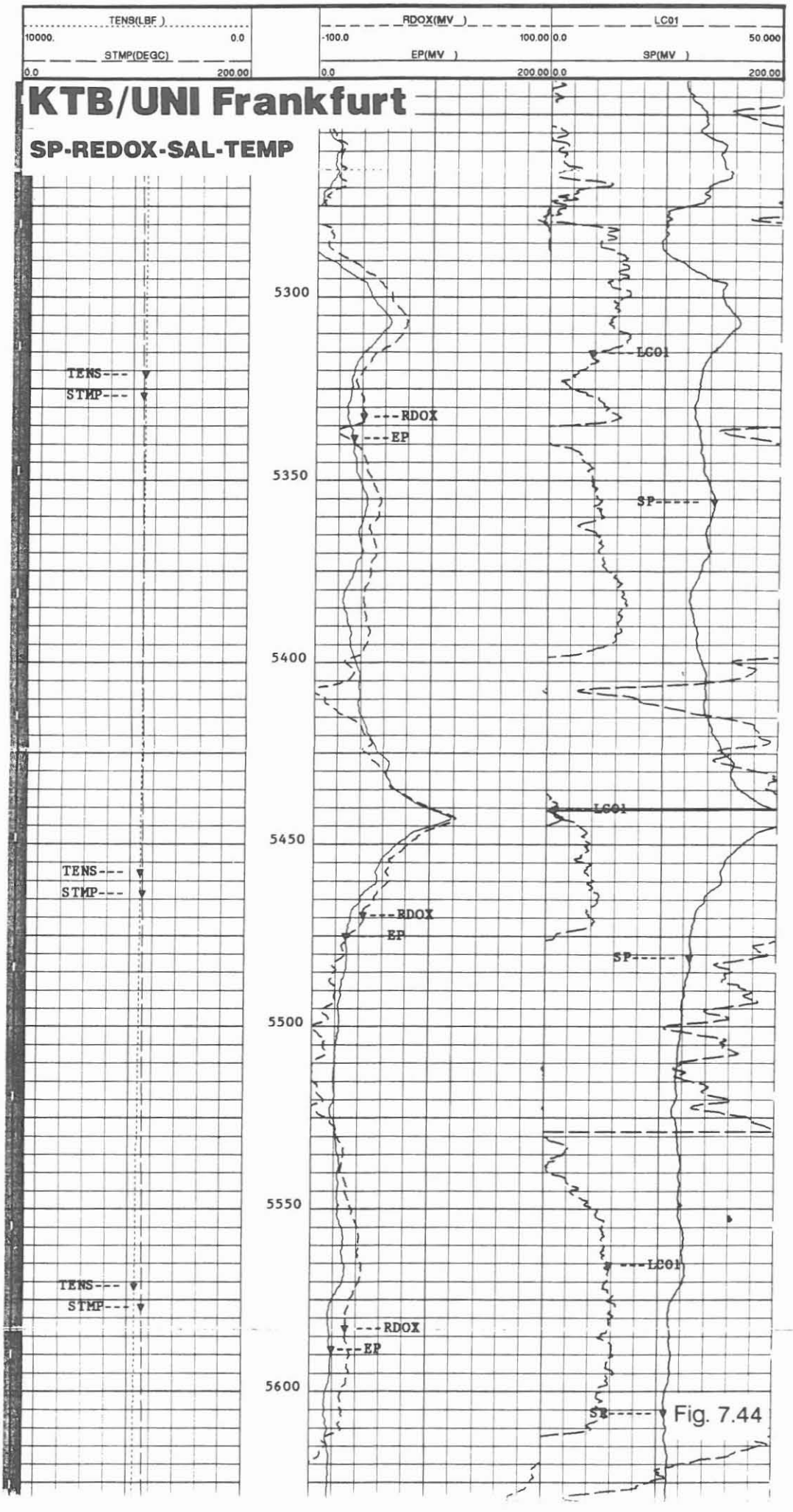
TENS(LBF)
10000.
0.0
STMP(DEGC)
0.0
200.00
RDOX(MV)
-100.0
100.00
EP(MV)
0.0
200.00
LC01
0.0
50.000
SP(MV)
0.0
200.00
KTB/UNI Frankfurt
SP-REDOX-SAL-TEMP
5300
5350
5400
5450
5500
5550
5600
TENS---
STMP---
---RDOX
---EP
LC01
SP-----

Fig. 7.44

FS/GR/MRES/TEMP (Fluid Sampler/Gamma Ray/Mud Resistivity/ Temperature

Operator: Leutert/KTB

Job No.	Date	Interval
HB-0094-0129	KTB-Report 92-1	701.3 - 4115.0 m
HB-0163-0165	23./24.03.1992	3162.5 - 5275.0 m

Example:
Section of log 5100.0 - 5450.0 m, **Fig. 7.45**

Purpose of log:
The log was run in combination with the fluid sampler to verify the best position for collecting the sample.

Operation:
During the production test formation water has entered the borehole. From mud resistivity and temperature logs the intervals of inflow can be detected. These zones are selected and fluid samples are collected at these depths. The log example clearly indicates a producing interval from 5270.0 - 5295.0 m. Two samples were taken from depth 5272.0 - 5275.0 m.
Depth scale: 1/1000; logging speed: 20 m/min.

Technical information:
The fluid sampler consists of a closed-in chamber which is run in the borehole either under internal vacuum or athmospheric pressure. At sampling depth valves are electrically operated to allow borehole fluid enter and being sealed in the chamber for retrieval. The sample, collected at in-situ conditions, is brought to surface for analysis.
Data rate: 6"

Mnemonics and Units:

Mnemonics	Description	Unit
ATEM	Temperature	(DEGC)
GR	Gamma Ray	(GAPI)
HTEN	Head Tension	(LBF)
LCO1	Mud Salinity	(PPM)
MRES	Mud Resistivity	(OHMM)

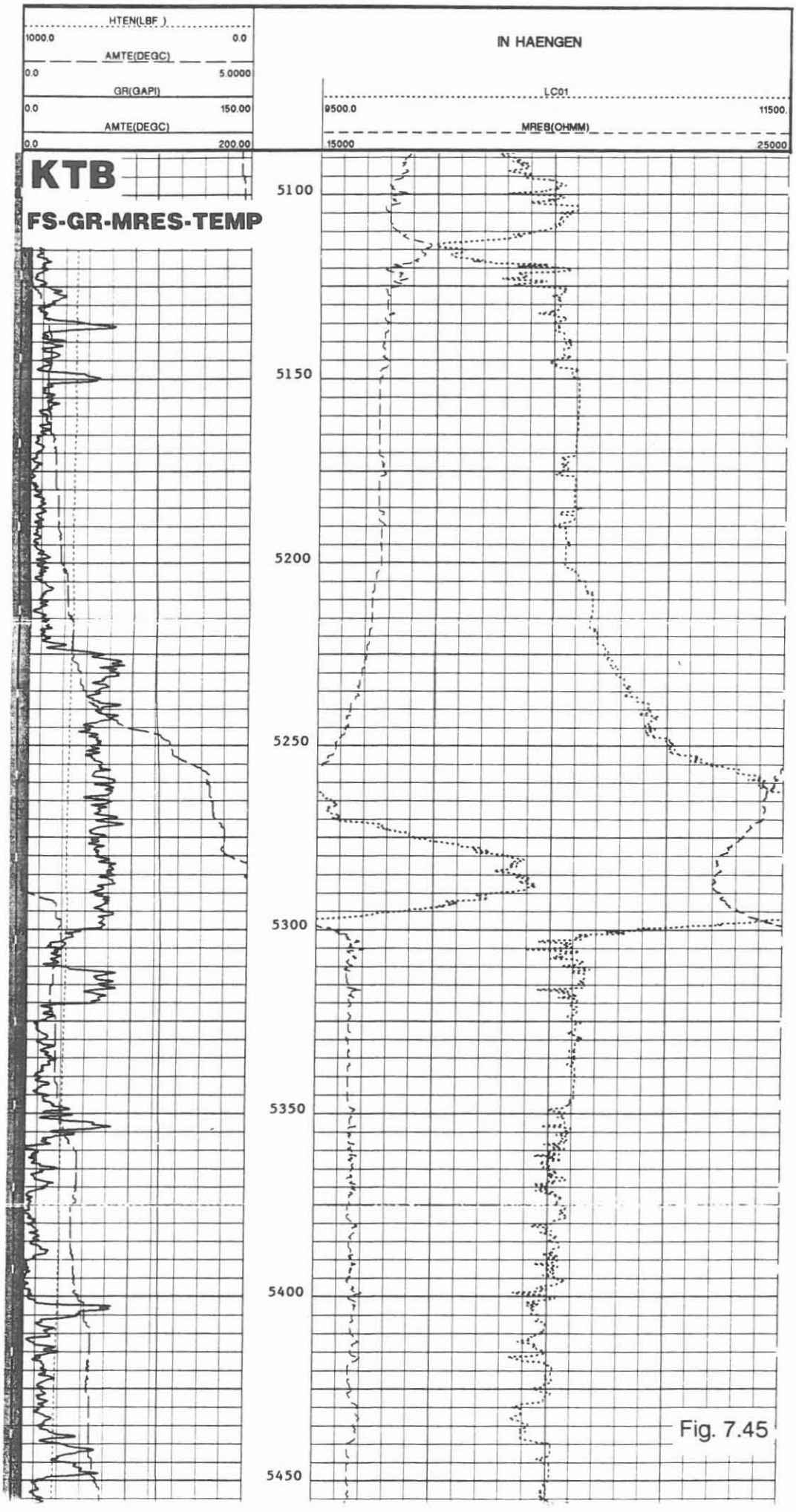
HTEN(LBF)
1000.0
0.0
AMTE(DEGC)
0.0
5.0000
GR(GAPI)
0.0
150.00
AMTE(DEGC)
0.0
200.00
IN HAENGEN
LC01
9500.0
11500.
MRES(OHMM)
15000
25000
KTB
FS-GR-MRES-TEMP
5100
5150
5200
5250
5300
5350
5400
5450

Fig. 7.45

VSP (Vertical Seismic Profile)

Operator: GECO-Prakla, Schlumberger Biberach/KTB

Job No.	Date	Interval
HB-0166	25.03.1992	3000.0 - 6000.0 m

Example:
Example of Stacked Field Records at 5887.5 m, 5900.0 m, 5912.5 m, **Fig. 7.46**

Purpose of log:
Vertical Seismic Profiles (VSP) are made to obtain detailed information about the structure being drilled. In addition, the link between surface seismic exploration and reality, verified by the borehole, can be established. This will improve the knowledge of the regional geology.

Operation:
A 3-component geophone is stationed at pregiven depth positions in the borehole to record the acoustic signals created by vibrators on surface. At each geophone position 5 - 10 vibrator sweeps are generated and the recorded signals are stacked and registered for further processing. For this operation 3 vibrators were used simultaneously. They were stationed about 200 m west of the drilling location.
Depth scale: stationary readings; logging speed: stationary readings.

Technical information:
The operation was started with the Combinable Seismic Imager (CSI) as downhole tool. The tool failed after only a few records. The tool was replaced by the Seismic Acquisition Tool (SAT). Unfortunately, this replacement caused the loss of the information of the tool orientation in space, as the SAT can not be combined with the General Purpose Inclinometer Tool (GPIT).
The surface reference 3-D geophones were located in a shallow borehole at 70 and 40 m depth, west of the main borehole and near the vibrator positions.
The reference borehole is called VSP 2, with coordinates:

H : 55 19 809.4
R : 45 08 590.4

The first vibrator station has the coordinates:

H : 55 19 852.1
R : 45 08 550.6

From this station the vibrators were moved in steps of 1.0 - 1.1 m seven times in the direction of 164°.

Mnemonics and Units:

Mnemonics	Description	Unit
TTIM	Transit time	(MS)
DX1	Z-Axis	
DY1	Y-Axis	
DZ1	Z-Axis	

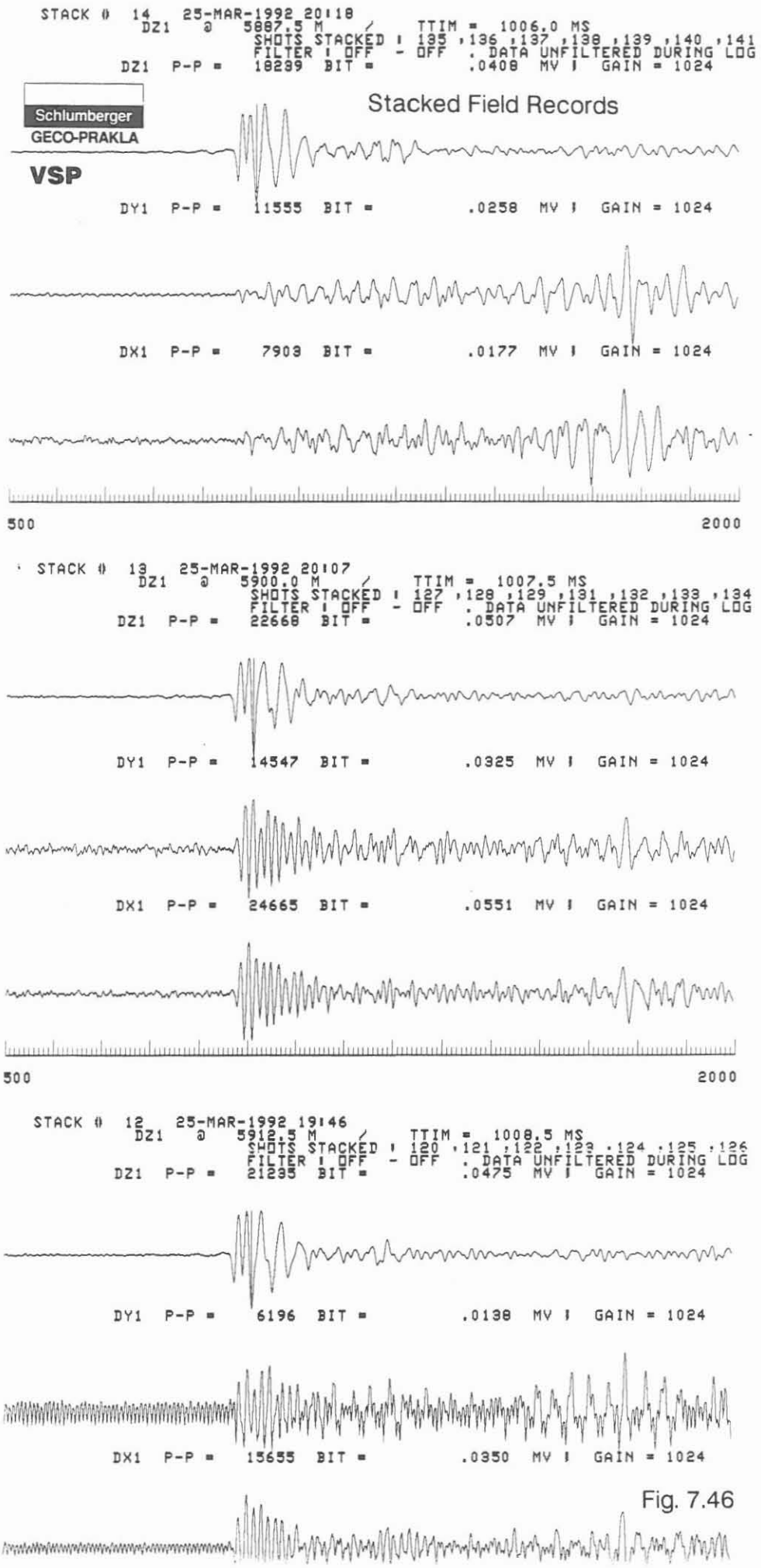
STACK # 14 25-MAR-1992 20:18
DZ1 @ 5887.5 M TTIM = 1006.0 MS
SHOTS STACKED : 135 ,136 ,137 ,138 ,139 ,140 ,141
FILTER : OFF - OFF . DATA UNFILTERED DURING LOG
DZ1 P-P = 18239 BIT = .0408 MV : GAIN = 1024
Schlumberger
GECO-PRAKLA
Stacked Field Records
VSP
DY1 P-P = 11555 BIT = .0258 MV : GAIN = 1024
DX1 P-P = 7903 BIT = .0177 MV : GAIN = 1024
500
2000
STACK # 13 25-MAR-1992 20:07
DZ1 @ 5900.0 M TTIM = 1007.5 MS
SHOTS STACKED : 127 ,128 ,129 ,131 ,132 ,133 ,134
FILTER : OFF - OFF . DATA UNFILTERED DURING LOG
DZ1 P-P = 22668 BIT = .0507 MV : GAIN = 1024
DY1 P-P = 14547 BIT = .0325 MV : GAIN = 1024
DX1 P-P = 24665 BIT = .0551 MV : GAIN = 1024
500
2000
STACK # 12 25-MAR-1992 19:46
DZ1 @ 5912.5 M TTIM = 1008.5 MS
SHOTS STACKED : 120 ,121 ,122 ,123 ,124 ,125 ,126
FILTER : OFF - OFF . DATA UNFILTERED DURING LOG
DZ1 P-P = 21235 BIT = .0475 MV : GAIN = 1024
DY1 P-P = 6196 BIT = .0138 MV : GAIN = 1024
DX1 P-P = 15655 BIT = .0350 MV : GAIN = 1024

Fig. 7.46

MSCT/GR (Mechanical Sidewall Coring Tool/Gamma Ray)

Operator: Schlumberger Diepholz/KTB

Job No.	Date	Interval
HB-0103-0124	KTB-Report 92-1	510.0 - 4521.0 m
HB-0172	02.04.1992	4294.9 m

Example:
Record of coring operation at 4294.9 m depth, **Fig. 7.47**

Purpose of log:
Due to limited cores drilled, the possibility of drilling sidewall cores with the wireline tool provides the requested rock samples for the geologists.

Operation:
The MSCT was run to the depth of 4294.9 m and anchored to the formation. The drilling of the first sidewall core progressed very slow. After completion of the coring operation and releasing the tool, hydraulic problems developed and the tool could not be reset. Coring operation was interrupted after this first core.
Depth scale: stationary reading - record versus time.
Logging speed: time record (11 minutes for coring).

Technical information:
Technical details and a tool description is given in KTB-Report 90-1, pages 210-215.

Mnemonics and Units:

Mnemonics	Description	Unit
CMDV	Coring Motor Downhole Voltage	(V)
CMLP	Coring Motor Linear Position	(IN)
HMCU	Hydraulic Motor Current	(AMPS)
HMDV	Hydraulic Motor Downhole Voltage	(V)
HPPR	Hydraulic Pump Pressure	(PSTG)
LMVL	Lower Motor Voltage Limit	(V)
RPPR	Rotating Plate Pressure	(PSIG)
SST	Solenoid Status	
UMVL	Upper Motor Voltage Limit	(V)

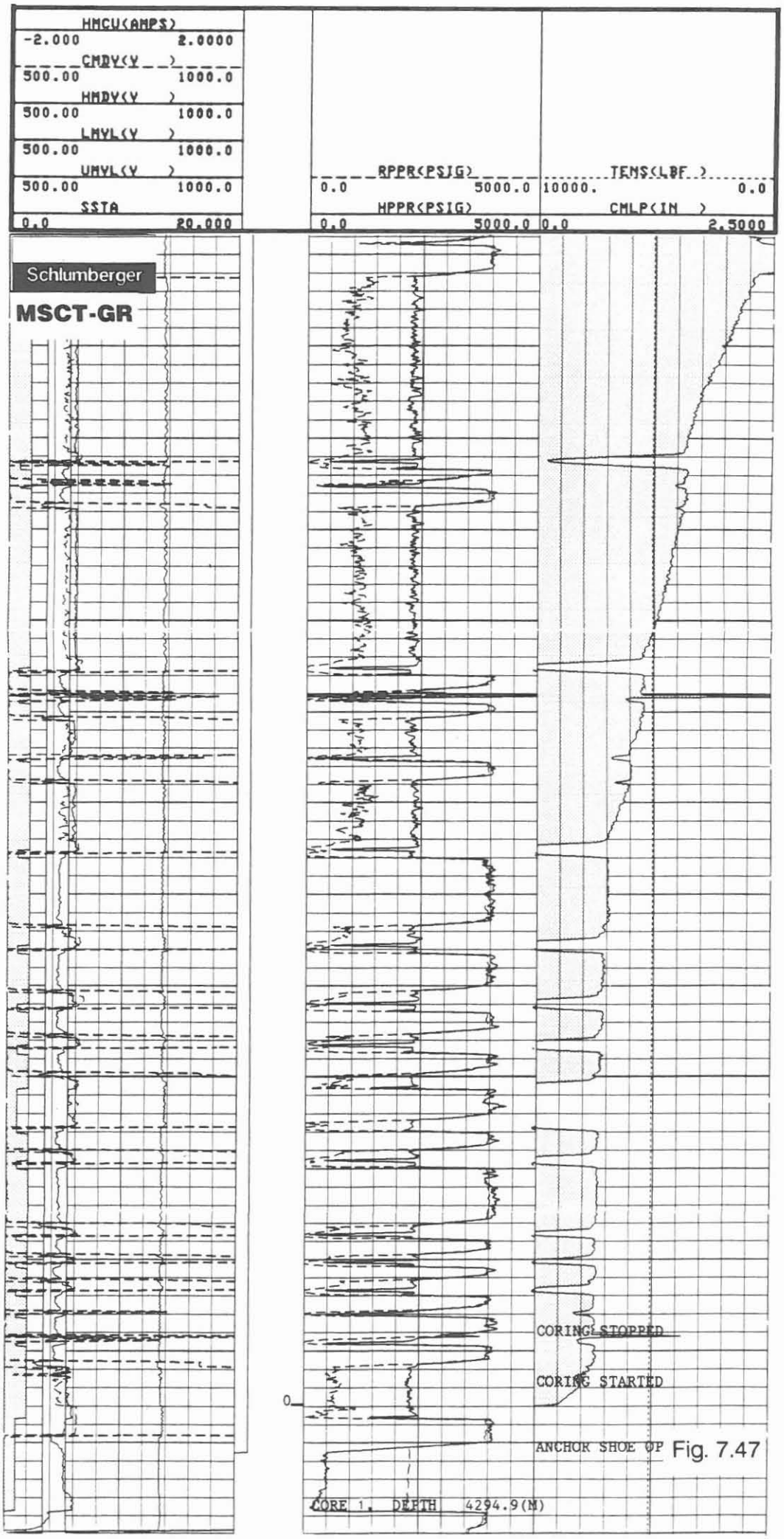
HMCU(AMPS)
-2.000
2.0000
CMDV(V)
500.00
1000.0
HMDV(V)
500.00
1000.0
LMVL(V)
500.00
1000.0
UMVL(V)
500.00
1000.0
SSTA
0.0
20.000
RPPR(PSIG)
0.0
5000.0
HPPR(PSIG)
0.0
5000.0
TEMS(LBF)
10000.
0.0
CMLP(IN)
0.0
2.5000
Schlumberger
MSCT-GR
CORING STOPPED
CORING STARTED
ANCHOR SHOE UP
CORE 1, DEPTH 4294.9(M)

Fig. 7.47

TEMP/GR/CCL (Temperature/Gamma Ray/Casing Collar Locator)

Operator: Schlumberger Diepholz/KTB

Job No.	Date	Interval
HB-0173	14.04.1992	21.0 - 5979.8 m

Example:
Section of log: 4175.0 - 4550.0 m, **Fig. 7.48**

Purpose of log:
The temperature log was run after the cementation of the 13 3/8"/13 5/8" casing string to find the top of the cement.

Operation:
The log was recorded downwards. This procedure guarantees that the undisturbed temperature in the borehole is measured. During the hardening of cement, heat is generated. The temperature gradient will change over intervals with uncemented and cemented casings. In zones with caliper enlargements greater cement volumes will create temperature anomalies like shown on this log section.
Depth scale: 1/1000; logging speed: 5 m/min.

Technical information:
The tool combination included, in addition to the temperature sensor, the Gamma Ray for depth correlation and the Casing Collar Locator for recording the casing joints.
Data rate: 6"

Mnemonics and Units:

Mnemonics	Description	Unit
CCL	Casing Collar Locator	
GR	Gamma Ray	(GAPI)
TENS	Tension	(LBF)
TMP3	Temperature	(DEGC)

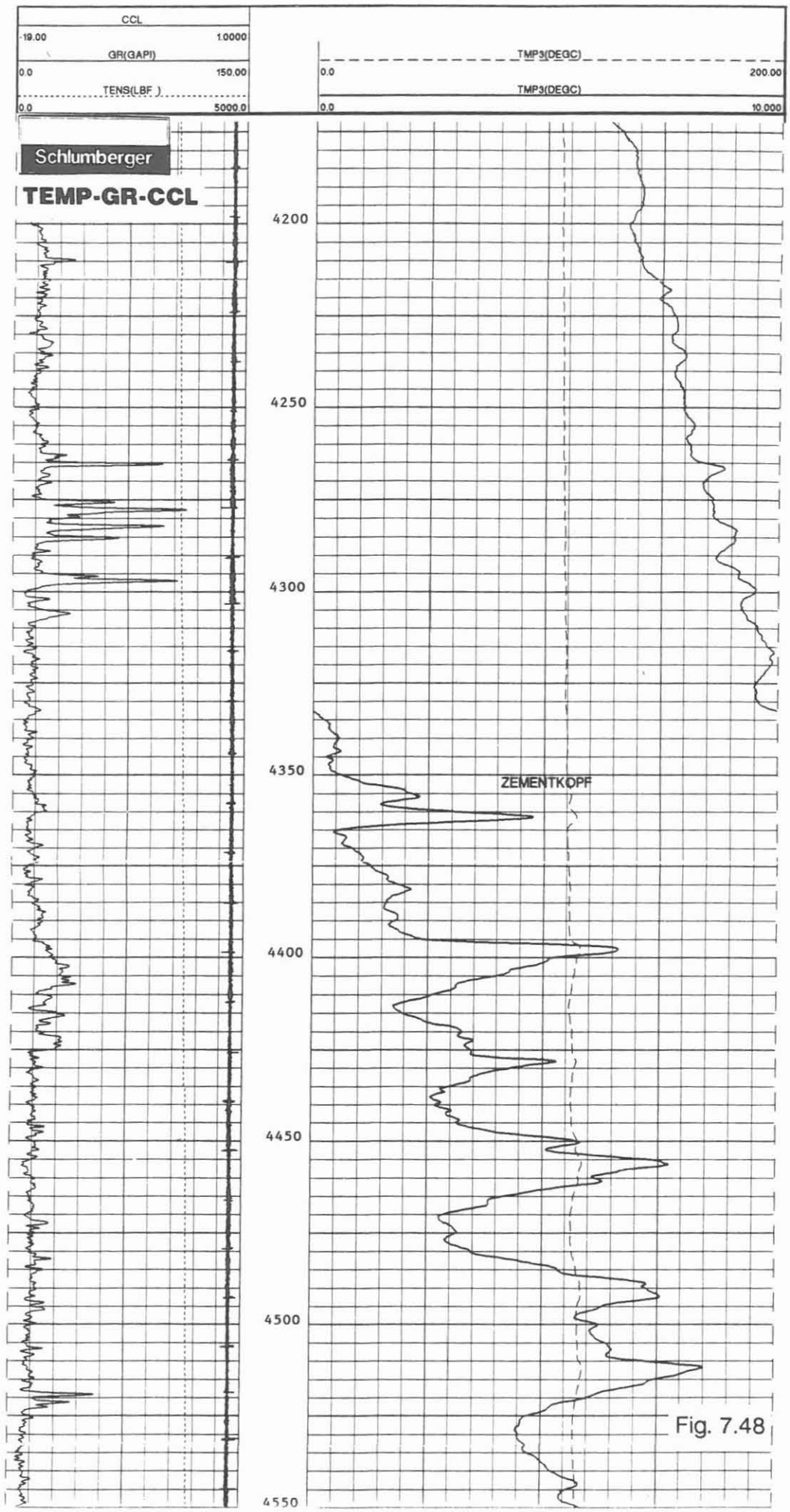
CCL
-19.00
1.0000
GR(GAPI)
0.0
150.00
TENS(LBF)
0.0
5000.0
TMP3(DEGC)
0.0
200.00
TMP3(DEGC)
0.0
10.000
Schlumberger
TEMP-GR-CCL
4200
4250
4300
4350
4400
4450
4500
4550
ZEMENTKOPF

Fig. 7.48

GR/CCL (Gamma Ray/Casing Collar Locator)

Operator: Schlumberger Diepholz/KTB

Job No.	Date	Interval
HB-0174	23.04.1992	0.0 - 6015.0 m

Example:
Section of log: 5605.0 - 5990.0 m, **Fig. 7.49**

Purpose of log:
This log was recorded to establish the depth correlation between "driller's depth" and "logger's depth".

Operation:
The log was recorded with a slimhole Gamma Ray/Casing Collar Locator Tool inside the drill pipes. This way, the depth correlation between the open hole reference: Gamma Ray and the drill pipes: Casing Collar Locator can be recorded. The difference in depth between driller and logger at 6000 m is 6.30 m, logger being deeper.
Depth scale: 1/1000; logging speed: 5 m/min.

Technical information:
For this through-drill pipe-operation the GR/CCL-tool with 1 11/16" outer diameter had to be deployed due to the small inner diameter in the drill collars.

Data rate: 6"

Mnemonics and Units:

Mnemonics	Description	Unit
CCL	Casing Collar Locator	
GR	Gamma Ray	(GAPI)
RCCL	Depth corrected CCL	
TENS	Tension	(LBF)

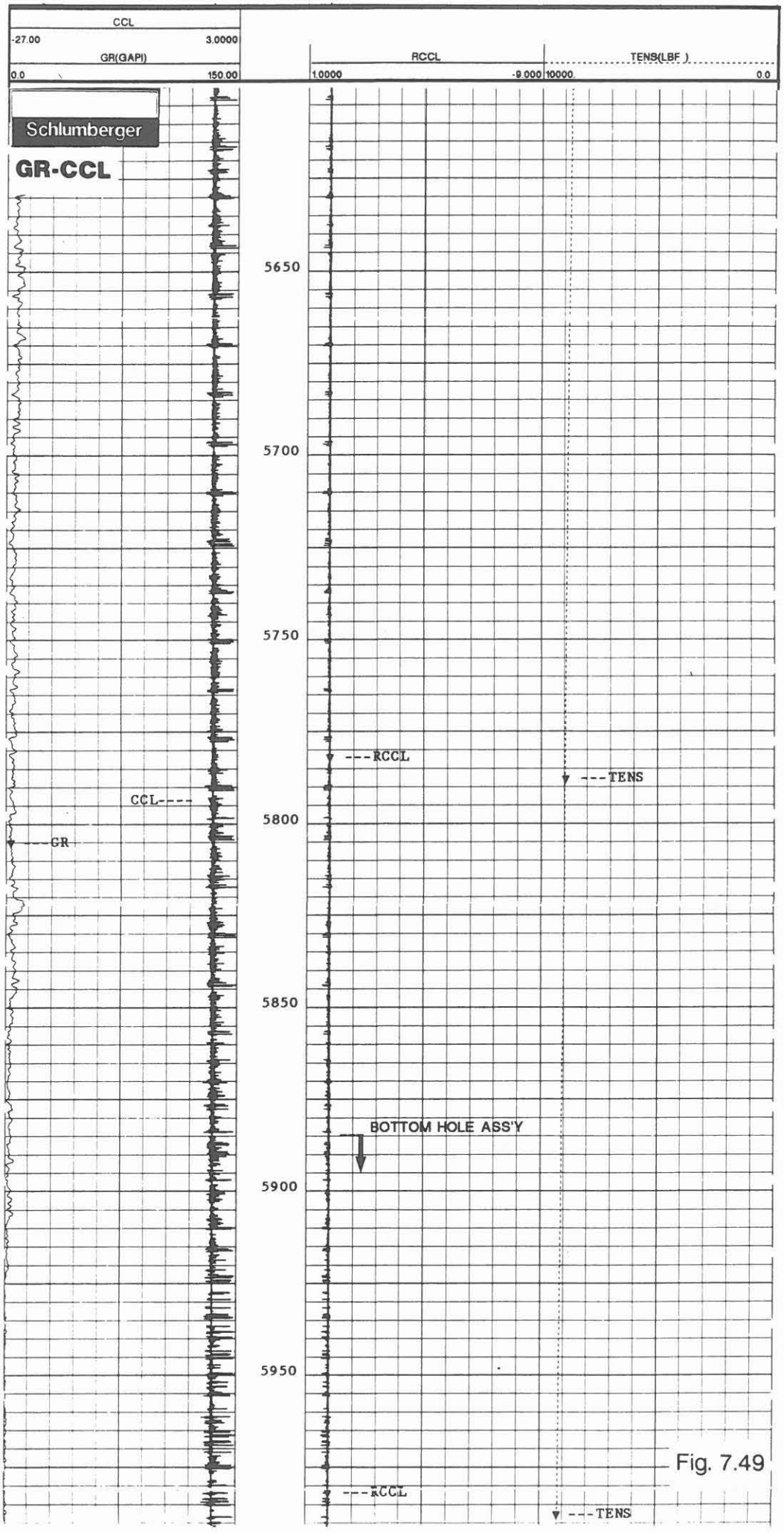
CCL
-27.00
3.0000
GR(GAPI)
0.0
150.00
RCCL
1.0000
-9.000
TENS(LBF)
10000.
0.0
Schlumberger
GR-CCL
5650
5700
5750
---RCCL
---TENS
CCL----
5800
---GR
5850
BOTTOM HOLE ASS'Y
5900
5950
---RCCL
---TENS

Fig. 7.49

GR/MFC (Gamma Ray/Multi-Finger Caliper)

Operator: Schlumberger Diepholz/KTB

Job No.	Date	Interval
HB-0175	24.04.1992	0.0 - 6018.0 m

Example:
Section of log: 5830.0 - 5895.0 m, **Fig. 7.50**

Purpose of log:
With this log corrosion and/or mechanical wear of the 13 3/8"/13 5/8" casing string will be determined using the time lapse technique with repeat surveys.

Operation:
The log was recorded as the "reference survey" in new casings. To detect corrosion or mechanical damage repeat surveys will be recorded and correlation to the "reference" will highlight these problems.

During the operation, the caliper tool had to be closed several times due to debris (cement) collected while logging. Depth scale: 1/1000, 1/200; logging speed: 9 m/min.

Technical informaton:
An array of 72 independent movable fingers, mounted around the circumference of the tool, ride at the inner surface of the casing and record any anomalies. For three sectors of 120° each the minimum and maximum caliper signals will be recorded. In addition, the minimum and maximum readings of the total circumference are recorded separately.

An interpretation of the logging results is presented in chapter 9 of this KTB Report.
Date rate: 6"

Mmemonics and Units:

Mmemonics	Description	Unit
DRIF	Drift radius	(MM)
GR	Gamma Ray	(GAPI)
MNRD	Minimum radius	(MM)
MXRD	Maximum radius	(MM)
OCR	Outer Casing radius	(MM)
RAD1-6	Radii 1-6	(MM)

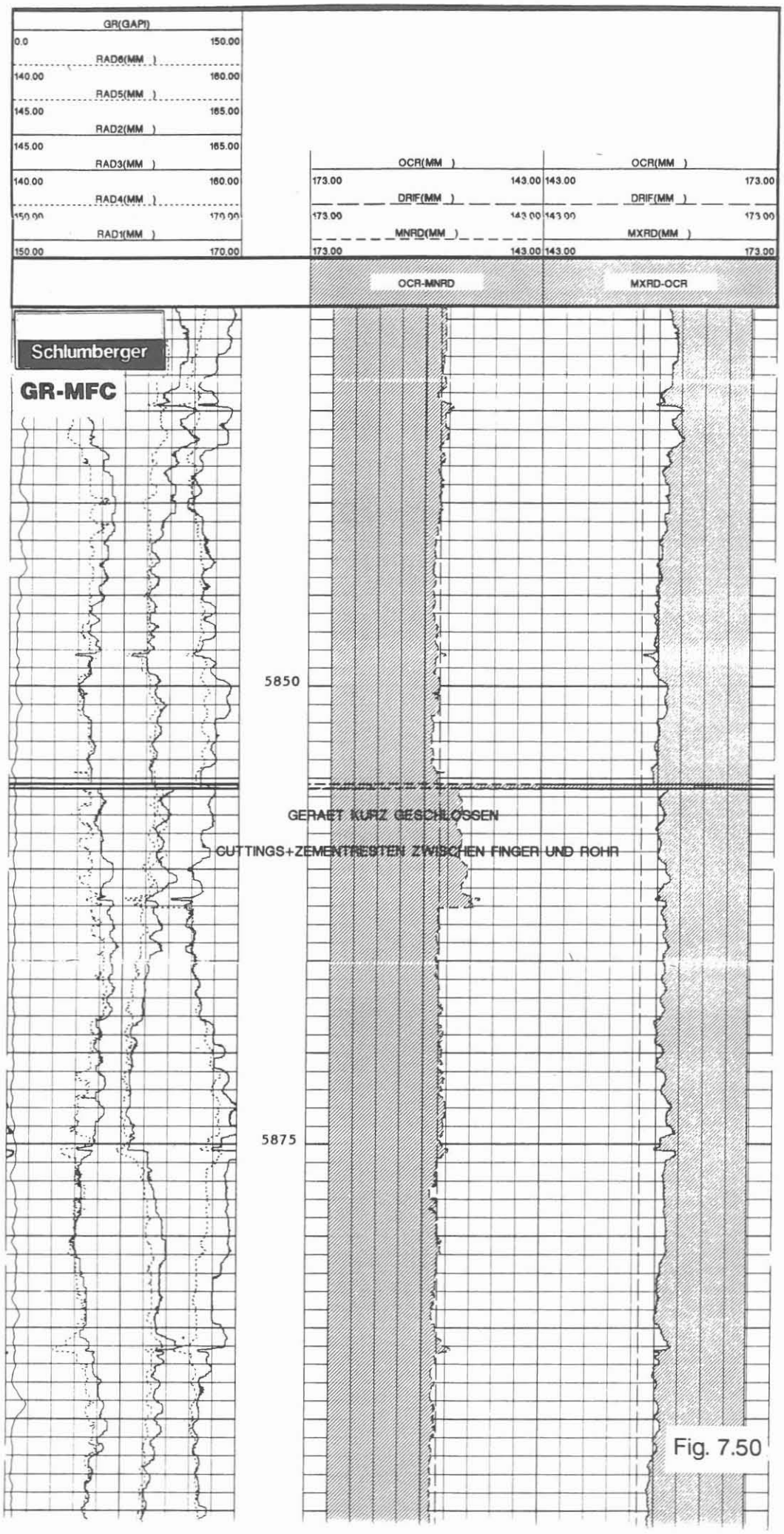
GR(GAPI)
0.0
150.00
RAD6(MM)
140.00
160.00
RAD5(MM)
145.00
165.00
RAD2(MM)
145.00
165.00
RAD3(MM)
140.00
160.00
RAD4(MM)
150.00
170.00
RAD1(MM)
150.00
170.00
OCR(MM)
173.00
143.00
DRIF(MM)
173.00
143.00
MNRD(MM)
173.00
143.00
OCR(MM)
143.00
173.00
DRIF(MM)
143.00
173.00
MXRD(MM)
143.00
173.00
OCR-MNRD
MXRD-OCR
Schlumberger
GR-MFC
5850
GERAET KURZ GESCHLOSSEN
CUTTINGS+ZEMENTRESTEN ZWISCHEN FINGER UND ROHR
5875

Fig. 7.50

BGL/TEMP/SP (Borehole Geometry Log/Temperature/Self Potential)

Job No.	Date	Interval
HB-0176	26.04.1992	5988.0 - 6033.0 m

Example:
Section of log: 6008.0 - 6033.0 m, **Fig. 7.51**

Purpose of log:
The reason for this log was to record the borehole condition below the casing shoe in preparation for the hydrofrac experiment.

Operation:
The Four-arm Caliper was run to record the borehole conditions below the casing shoe in the newly drilled section. This section was drilled in preparation for the hydro-frac experiment.
Depth scale: 1/200; logging speed: 10 m/min.

Technical information:
For the hydro-frac experiment correct depth and information about the borehole conditions were required.
Data rate: 6"

Mnemonics	Description	Units
AZIM	Azimuth	(DEG)
BS	Bite size	(MM)
C1,2	Caliper 1,2	(MM)
DEVI	Deviation	(DEG)
P1AZ	Pad 1 azimuth	(DEG)
RB	Relative bearing	(DEG)
SPK	Self Potential	(MV)
TENS	Tension	(LBF)

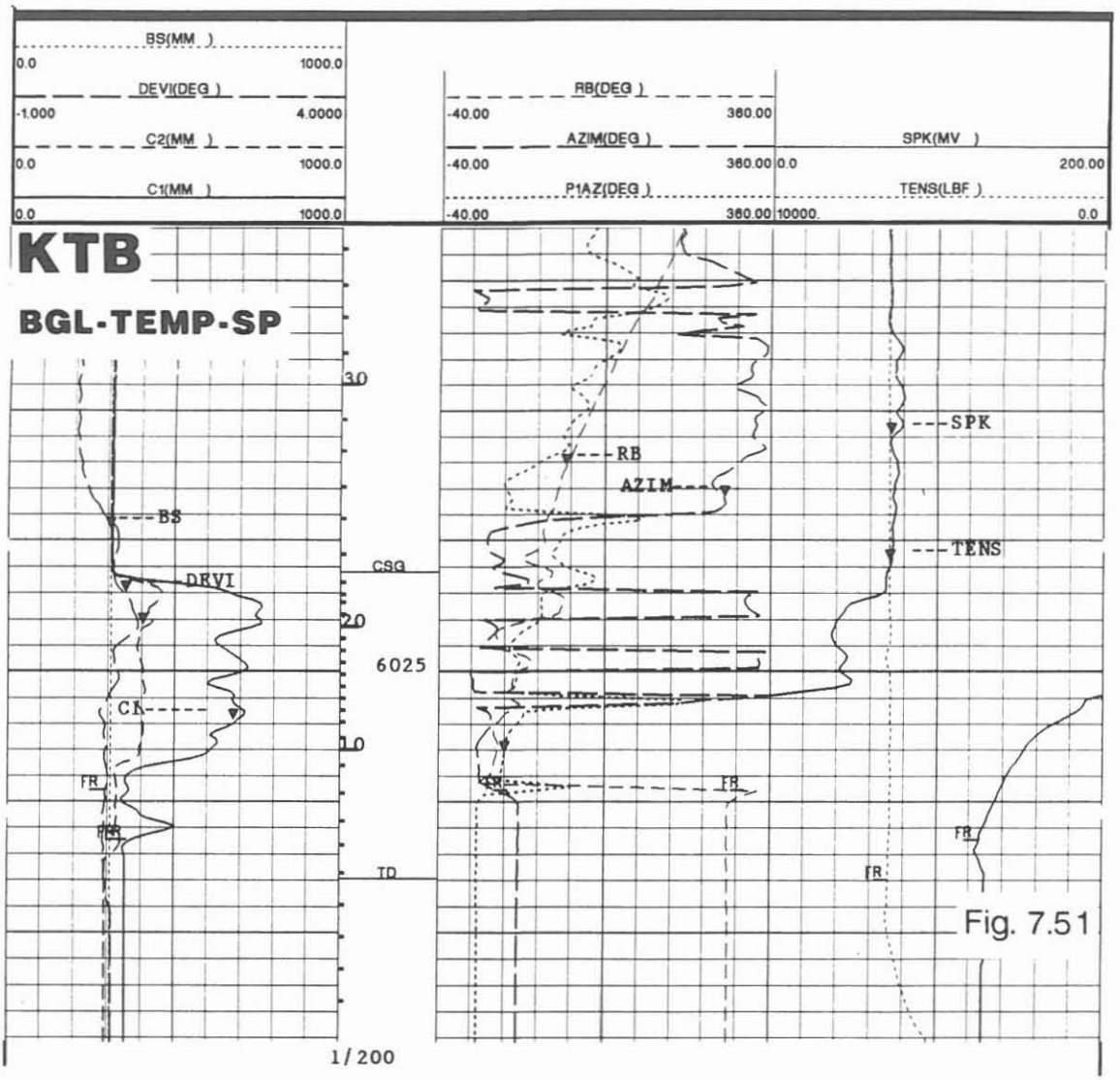
BS(MM)
0.0
1000.0
DEVI(DEG)
-1.000
4.0000
C2(MM)
0.0
1000.0
C1(MM)
0.0
1000.0
RB(DEG)
-40.00
360.00
AZIM(DEG)
-40.00
360.00
P1AZ(DEG)
-40.00
360.00
SPK(MV)
0.0
200.00
TENS(LBF)
10000.
0.0
KTB
BGL-TEMP-SP
3.0
2.0
1.0
BS
DEVI
C1
FR
CSG
6025
TD
SPK
RB
AZIM
TENS
FR
FR
FR
1/200

Fig. 7.51

8. New Tools

J. K. Draxler

8. New Tools
8.1 Tool descriptions - references

Borehole measurements represent a significant and important source of data acquisitions within the scientific program of KTB. Therefore, KTB is very interested - and has supported - the development of new borehole logging systems or to test improvements to existing logging tools.

Since drilling operations started with the pilot hole KTB-Oberpfalz VB in September 87, a great number of prototype or modified logging tools have been deployed and the results of the measurements evaluated.

To introduce these new or modified tools to the scientific community, short tool descriptions have been issued in the following KTB Reports:

KTB Report 88-4	Formation MicroScanner Tool (FMST) Correlated Electromagnetic Retrieval Tool (CERT)
KTB Report 88-7	Temperature and Salinity Tool
KTB Report 90-1	Mechanical Sidewall Coring Tool (MSCT) Guidance Continuous Tool (GCT) Slimhole Formation MicroScanner Tool (SFMST) Borehole Gravity Meter (BHGM)
KTB Report 90-6a	Fluxgate Magnetometer - BGR 3D-Magnetometer - University Braunschweig Magnetic Susceptibility Sonde - University Munich Gradient Magnetometer - University Göttingen Induced Polarisation (IP) - NLfB and ELGI FACSIMILE - Borehole Televiewer (BHTV) Multi-Fluid Sampler - Schlumberger Fluid Sampler - Los Alamos Six-Arm Caliper Sonde Germanium Spectrometer Tool
KTB Report 91-2	Tool Combination: BGL/AMS/GRL/TEMP/SP Single shot MAXIS 500 (Multi-Task Acquisition and Imaging System) Formation MicroImager (Prototype-FMI) Redox - and Self Potential Sonde - University Frankfurt
KTB Report 92-1	Dipole Shear Sonic Imager (DSI) Segmented Bond Tool (SBT) Formation MicroImager (FMI) Mechanical Coring Tool (MCT)

8.2 Azimuthal Resistivity Imager (ARI)

The Azimuthal Resistivity Imager Tool is a new development from Schlumberger. A prototype tool was deployed during the logging series in March 1992 at 6020.0 m. The interval from 6020.0 to 3000.5 m was logged.

Azimuthal Array Imager Principle Fig. 1:
The tool consists of the well known and proven Dual Laterolog Tool (DLL) and a new array of electrodes mounted on an additional tool section.

12 individual electrodes, distributed over the circumferance of the tool body form the array. Focused current, following the Laterolog 3 principle is sent from these electrodes into the formation.

The current from an electrode will be measured and the potential difference close to the electrode relative to the remote reference will be taken and measured too. The potential difference divided by the current and multiplied by a geometrical factor will give the resistivity of the formation. This will be done for all 12 electrodes of the array.

The tool must operate under the condition that monitor electrodes, placed in the center of each current electrode, have the same potential, eliminating the effects of series impedance on the current electrodes. A feedback loop controlls the current from each electrode in such a way that the potential of the monitor electrodes is equal to the mean potential from the annular monitor electrodes situated inside the guard electrodes.

Vertical focusing of the current beams is achieved by the current beams from the guard electrodes, and in azimuth by currents from the neighboring azimuthal electrodes, because the mud immediately in front of the array is at equipotential.

12 additional focused resistivity measurements are recorded representing resistivities of 30° segments of the circumference of the borehole.

This system operates at a frequency of 35 Hz, the Laterolog Deep measurement frequency. The return is at surface.

From the azimuthal currents and the mean potential of the annular monitor electrodes related to cable armor an "average resistivity" is computed. This "average resistivity" is referred to as "high resolution resistivity" since its vertical resolution is superior to the standard LLd measurement.

With a frequency of 64 KHz a second measurement is made, using the same array. This high frequency measurement has limited horizontal resolution and is used as an electrical caliper. With this measurement environmental corrections are made to the azimuthal formation resistivites. The tool specifications are given in Fig. 2.

Field recording:
This tool requires the MAXIS 500 surface unit. All the resistivity measurements are made simultaneously and recorded digitally. Normal practice is, to register the standard Dual Laterolog as analog record in real time, and produce all other logs in playback mode. Especially the image processing from the array measurements is very time intensive and should only be made after the logging operation in the borehole is completed.

AZIMUTHAL ARRAY IMAGER

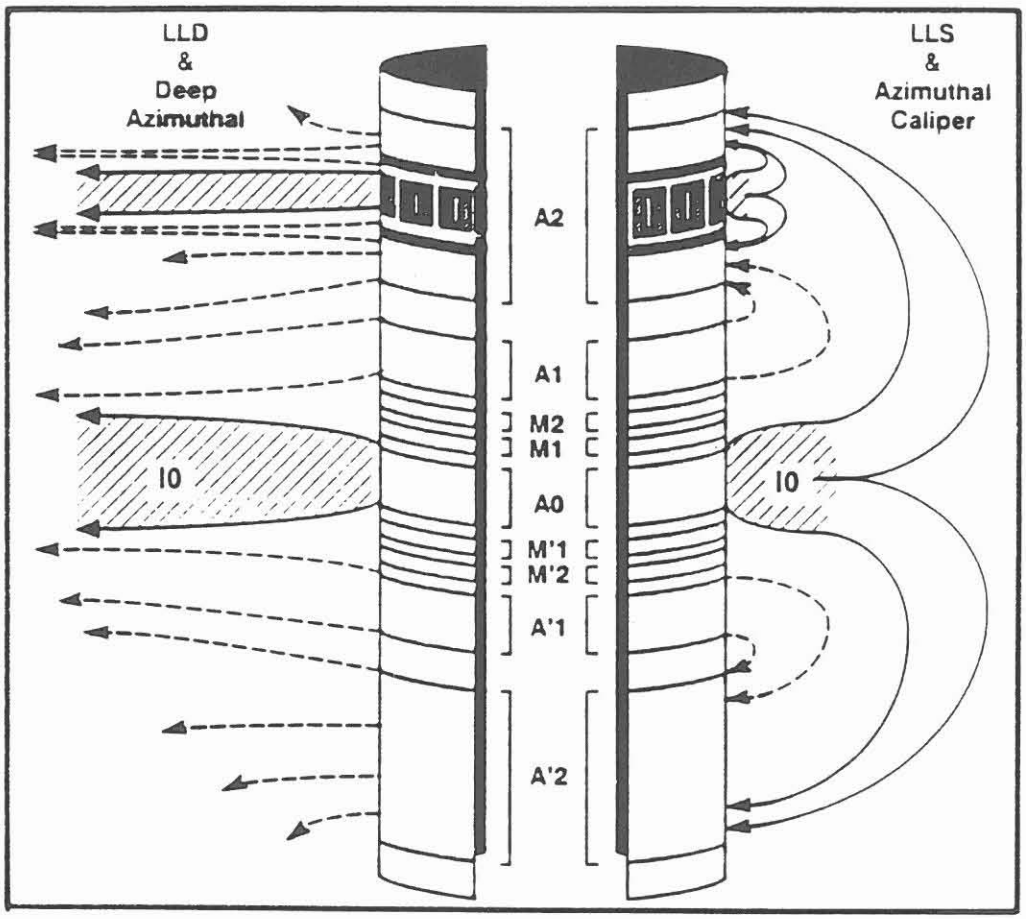

- 12 Electrode array located on two identical half shells
- Measures current from an electrode and takes potential difference between monitor electrodes and a remote reference
- Azimuthal and high resolution function in deep mode only (35 hz)
- 12 shallow resistivity measurements at 64khz

Fig. 1

TOOL SPECIFICATIONS

Logging Speed:	3600 fph for 1" Az/h.r. sampling 7200 fph for DLL only operation
Operating Temperature:	-25º C to 175º C
Operating pressure:	20,000 psi
Minimum Borehole Diameter:	4 1/2 "
Maximum Borehole Diameter:	12 1/4" optimal performance 21" operation
Operating Limitations	Conductive muds only, up to 1.5 ohm.m 5 ohm.m for passive mode
Total Tool Length:	~ 33 ft.
Tool Diameter: normal sonde medium subs	3 5/8" 6", (7-1/4" with standoffs)
Total Tool Weight:	~ 240 Kg.
Fishing Strength:	40,000 lbs.
Telemetry Compatibility:	DTS (with DTB thro' wiring)
Combinability:	Anywhere in DTS tool string GPIT needed for orientation with FBST, the FBCC acts as A'2
Combinability Limitations	Bridle (BRT) mandatory AH169 needed below Incompatible with MEST, SHDT, HDT (tools with housing shorted to # 10)
Resistivity Range:	0.2 - 40.000 Ω-m
Instrument Accuracy:	5 % (1 ≤ Ra ≤ 2000) 10% (.2 ≤ Ra ≤ 5000) 20% (5000 ≤ Ra ≤ 40.000)
Vertical Resolution:	~ 6 - 8"
Azimuthal resolution:	~ 60 deg fractures for 1" standoff

Fig. 2

9. Data Evaluation and Reports

KTB Hauptbohrung - relations between the borehole deviation and the geological structure

Gottfried Hirschmann[1] & Jochem Kück[2]

In spite of corrections by three directional drilling phases, the borehole trajectory of the KTB Vorbohrung is characterized by a total deviation of 190 m to the NNE at the final depth of 4000,1 m. The deviation is mainly caused by the rock anisotropy, i.e. the metamorphic foliation which dips predominantly to the SSW down to a depth of 3000 m.

In the KTB Hauptbohrung, the deviation has been successfully reduced by using vertical drilling systems (VDS), so that down to a depth of 7000 m the distance from the starting point did not exceed 20 m. Nevertheless, even the small deviations shows remarkable characteristics which can be compared with the geological structure. Fig.1 shows the correlation of the borehole trajectory with the foliation data, the resulting structural model and the depth position of seismic reflections.

The trajectory displays repeated bending from W to E. The most remarkable turning points are near 1700 m, between 3200 and 3400 m and near 5700 m. With respect to the dip azimuth, the structural profile may be subdivided into NE (or E) dipping sections, SW (or W) dipping sections and sections of strongly varying dip direction. These variations are the expression of a large-scale semiductile folding of the paragneiss-metabasite succession (Hirschmann 1992). In the paragneiss units, the azimuth of foliation is rather regular. On the other hand, the foliation of the larger metabasic units is often less distinct and shows a broad azimuthal scatter.

Similar to the Vorbohrung, the upper part of the drilled section is dominated by sections of SW(W) dipping foliation. This corresponds well to the general borehole deviation to the E(NE). Repeated changes of the dip azimuth correspond more or less exactly to minor turning points of the borehole trajectory. In the depth intervall of the most prominent fold hinge between 3200 und 3400 m the borehole reaches its maximum distance from the starting point and turns back to the W(SW). This corresponds to the prevailing dip of the foliation to the E in the lower part of the drilled section. Due to the less distinct foliation and the scatter of azimuthal values in the metabasites of this part of the borehole, the correlation between structural data and the borehole trajectory is more difficult. The best example of correlation is the turning point which coincides with the change from W dipping to E dipping foliation at approximately 5700 m.

---

[1] Niedersächsisches Landesamt für Bodenforschung, Stilleweg 2, D-30655 Hannover

[2] Niedersächsisches Landesamt für Bodenforschung, Außenstelle Windischeschenbach, Postfach 67, D-92667 Windischeschenbach

In the upper parts of the profile, the dip of the foliation is steep to very steep. It flattens below 2400 m and attains the lowest values in some intervals between 2800 and 3500 m. In the lower part of the profile, it varies from intermediate to steep. In contrast to some expectations, a distinct correlation between the dip of foliation and the borehole deviation is not obvious.

Repeatedly, correlations between the borehole trajectory and the position of seismic reflections have been discussed. Fig.1 illustrates the calculated depth of intersection of some major 3-D-seismic reflections with the borehole (after Wiederhold 1993, velocity model 1005). The best fit can be observed in the case of the SE3 reflection which correlates rather well with the turning point of the borehole trajectory near 5700 m. It can be assumed that this turning point as well as the reflection are caused by the structural change (fold hinge) in this part of the section. On the other hand, there are no clear correlations between the borehole deviations and the reflections SE2 and SE12.

References

HIRSCHMANN,G. (1992): Vorläufige strukturelle Interpretation von KTB-Vor- und Hauptbohrung. - KTB Report 92-4: 3-6, Hannover

WIEDERHOLD,H. (1993): Interpretation of Envelope-Stacked 3D-Seismic Data and its Migration - Another Approach. - KTB Report 92-5 (DEKORP Report), Hannover (in preparation)

Fig.1. KTB Hauptbohrung - correlation of the borehole trajectory (E-W plane) with the foliation data (FMS/FMI interpretation; plot: ktb field laboratory, working group geology), The structural model and the depth position of 3-D-seismic reflections (after Wiederhold 1993; velocity model 1005)

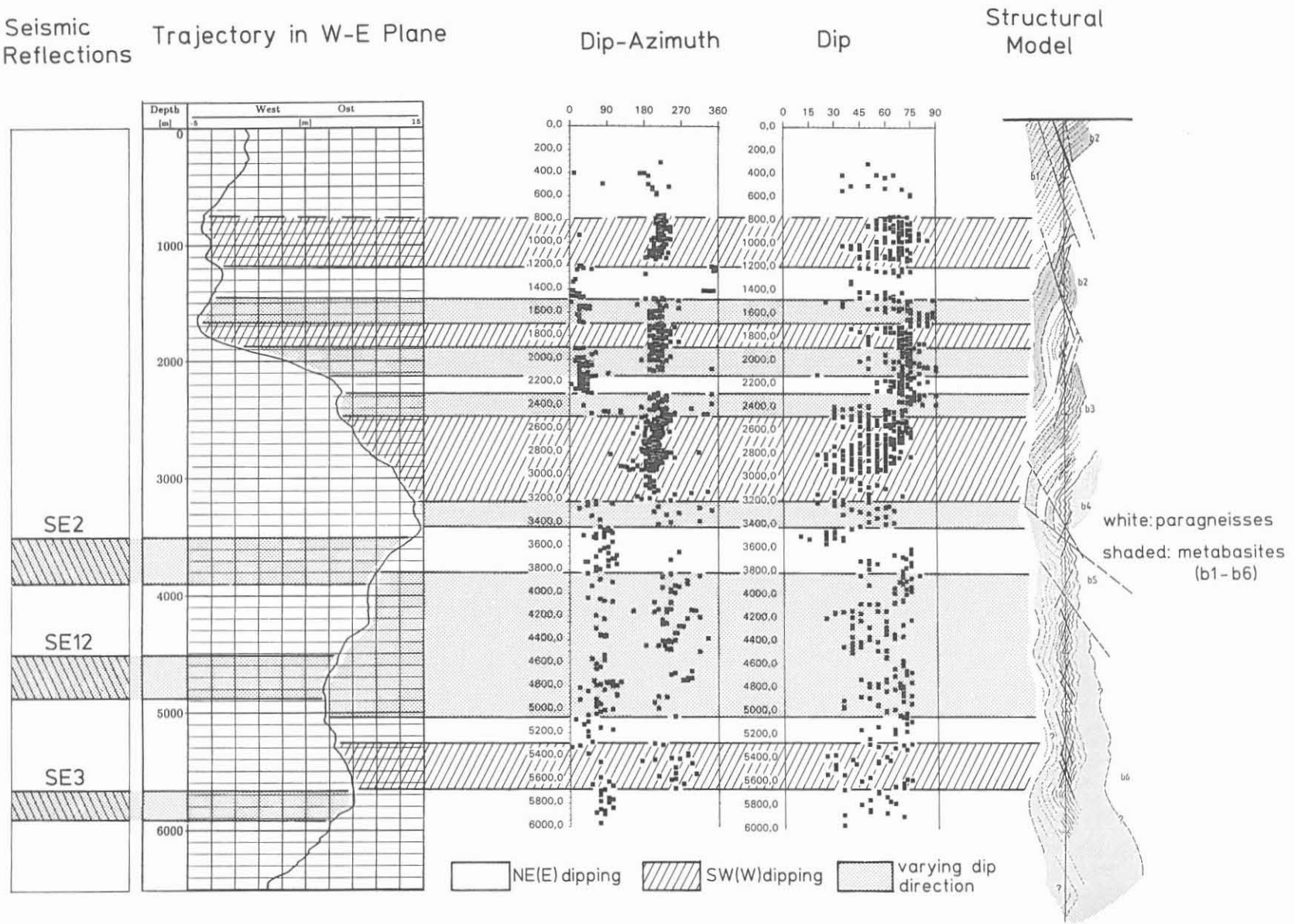
Seismic Reflections
Trajectory in W-E Plane
Dip-Azimuth
Dip
Structural Model
Depth [m]
West
Ost
SE2
SE12
SE3
NE(E) dipping
SW(W)dipping
varying dip direction
white: paragneisses
shaded: metabasites (b1-b6)

BGLQUICK and MUDQUICK quicklook data plots

J. Kück

1. Introduction

The KTB every day produces numerous measured values covering drilling, mud logging, field laboratory and borehole logs. In order to rapidly evaluate the drilling situation and correlate the appropriate geoscientific data, it proved to be a matter of urgency to develop a method for presenting selected data rapidly and clearly. The BGLQUICK data plot concept makes it possible to produce graphics from the borehole logging, borehole engineering and field laboratory areas as soon as the data becomes available. Moreover, the method also allows the interactive integration of other depth related data. The standard plots consist of four quicklook plots, as briefly described below.

2. BGLQUICK

The BGLQUICK plot is a composite log giving a clear representation of the continually recorded data from borehole logs, the field laboratory and the drilling operation. The individual characteristics of each measured parameter require manual preparation (scale setting, corrections etc.) to create the plot. The selection of the optimal scale allows high resolution plots of selected important parameters to be presented.

Fig. 1 shows an example of a BGLQUICK plot covering the depth section 3320 m to 3520 m. The plot presents the following measured values from left to right: borehole caliper and bit size, the grey shaded area shows the ovalisation of the borehole, current bottom hole assembly (BHA), hole deviation, azimuth and breakout orientation, dog leg severity, the cuttings derived lithology together with the reference gamma ray, ellipticity and roughness, mud resistivity together with the corresponding NaCl-equivalent and mud temperature as well as the horizontal distances from the vertical projected on the WE and SN planes respectively.

The derived parameters such as breakout orientation is the azimuth of the borehole cross section's long axis averaged over 25 m. The dog-leg severity is calculated over a 5 m depth segment and the ellipticity is defined as $1-C_{min}/C_{max}$.

Author's address:
Niedersächsisches Landesamt für Bodenforschung, Außenstelle Windischeschenbach, P.O. Box 67, D-92667 Windischeschenbach, Germany

It should be born in mind that bottom hole assembly and lithology depths are not correlated with the logging depths, there may be obvious differences between these plots. However, this must be accepted because the quicklook only represents the current data situation.

3. BGL_X

The horizontal projection of the course of the borehole is calculated from the BGL log orientation measurements. Fig. 2 shows the course of the main borehole from ground level to 6024 m. The data sets have been spliced together from several BGL logs. The borehole course curve is marked at 500 m depth intervals in the standard plot.

4. BGLVOLUMES

The change of the borehole wall with time can be derived from several borehole geometry logs recorded at different times over the same depth section. The plot (fig. 3) shows minimum (C_{min}) and maximum (C_{max}) caliper from up to five log runs, as well as the caliper differences calculated from the mean calipers and the caliper derived borehole volumes versus nominal volume (bit size), their differences and total volumes. This plot also includes information on the bottom hole assembly, the lithology column and the reference gamma ray.

The changes over time in the borehole caliper reveal the areas which generate the most cavings. This is an important piece of information for the depth classification of cuttings.

However, when evaluating the results from the caliper it must not be forgotten that the caliper arm in sequential logs will most probably be running down a different side of the borehole, thus producing spurious changes in the caliper log, e.g. even apparent reductions in diameter.

5. MUDQUICK

After the difficulties that led to the fishing operations at the beginning of August 1992, the engineering department and the field laboratory developed a plot of mud relevant parameters against time (fig. 4). This involves, integration of 18 time dependent parameters provided by both departments into a uniform MUDQUICK plot. The plot data management is carried out by the borehole logging department. The MUDQUICK plot is generated every four weeks. Currently, proposals are being discussed for enlarging the MUDQUICK plot.

Evaluation parameters for the mud condition plot are: rheological parameters, e.g. plastic viscosity; flow limit; water release; filtration behaviour; concentration of mud constituents; ion concentrations, e.g. calcium content, chloride content; borehole engineering parameters and shaker analyses.

6. Summary

The four quicklook plots produce easy readable standardised plots showing the borehole situation shortly after measurements are recorded. In addition to the standard plots, it is also easy to produce special plots. The plots are frequently used in all KTB management areas a well as in the field laboratory.

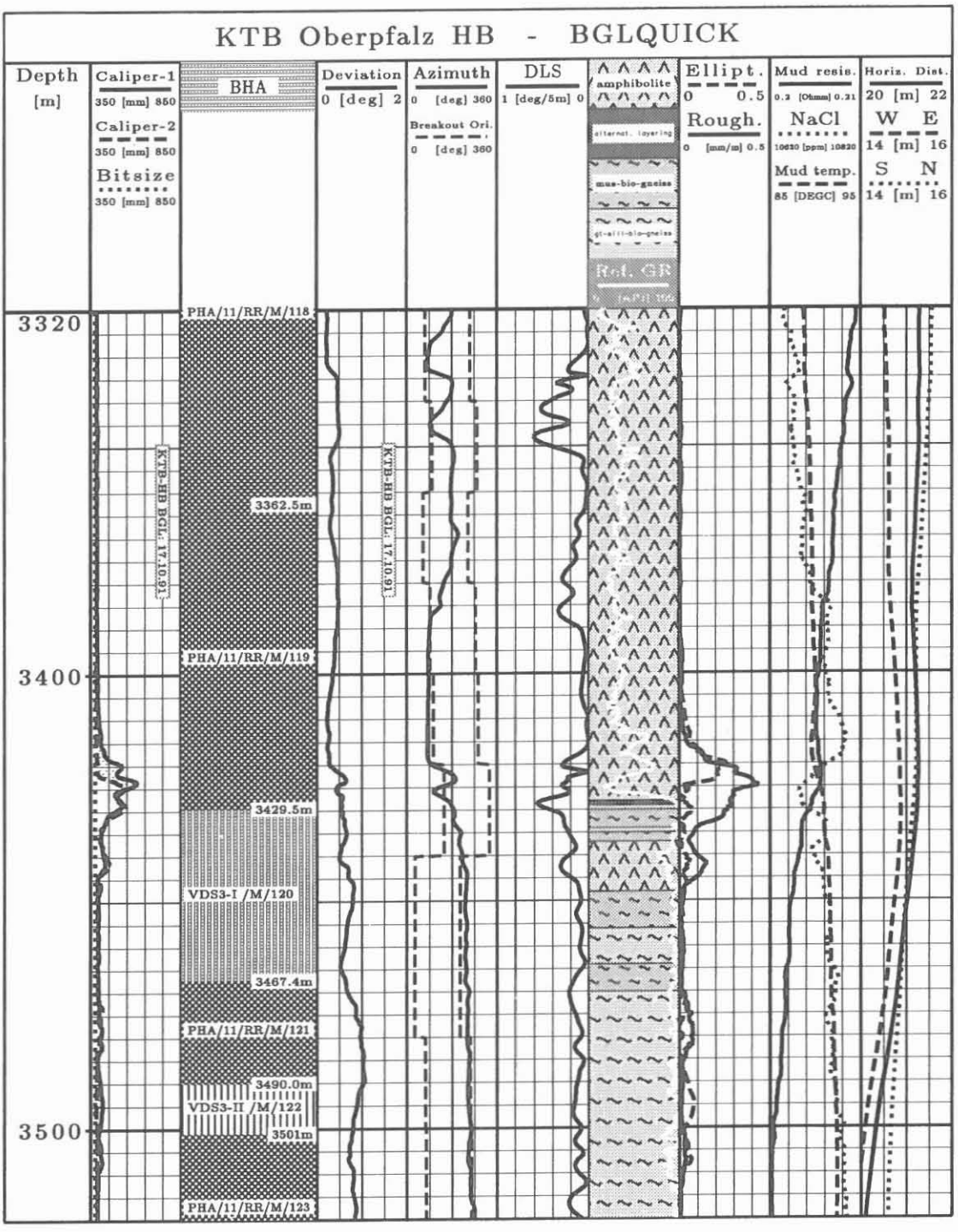

Fig. 1: Example of 'BGLQUICK' presentation of depth section 3320 m to 3520 m in the borehole KTB-Oberpfalz HB. The standard format is in a scale of 1 : 1000. BHA is the bootom hole assembly, 'DLS' is the dog leg severity, 'rough' is the roughness of the borehole wall, 'NaCl' is the NaCl-equivalent salinity.

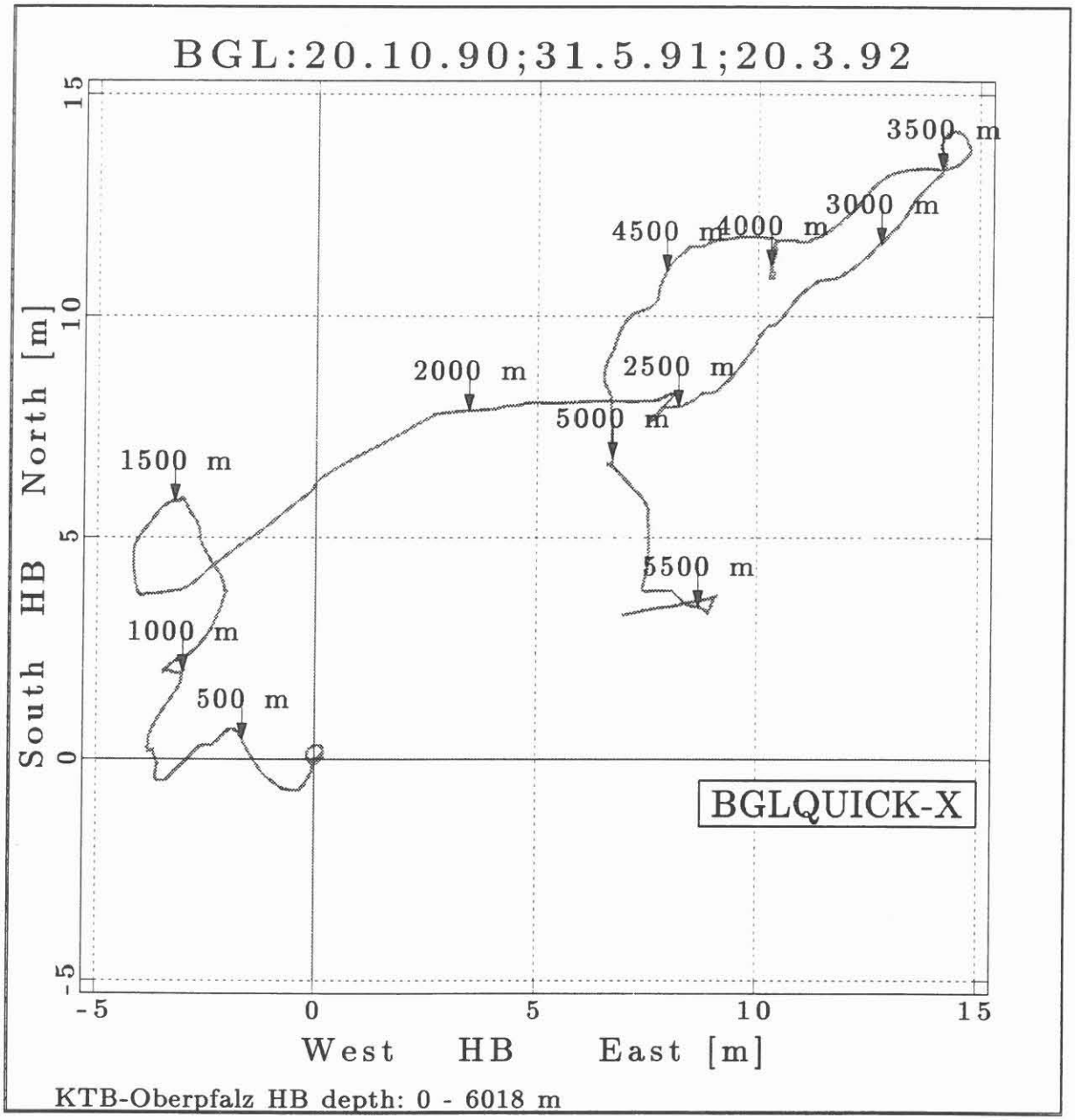

Fig. 2: Example of the 'BGL-X' surface projection of the borehole KTB-Oberpfalz HB of the depth interval 0 - 6018 m. The trajectory has been assembled from three BGL measurements.

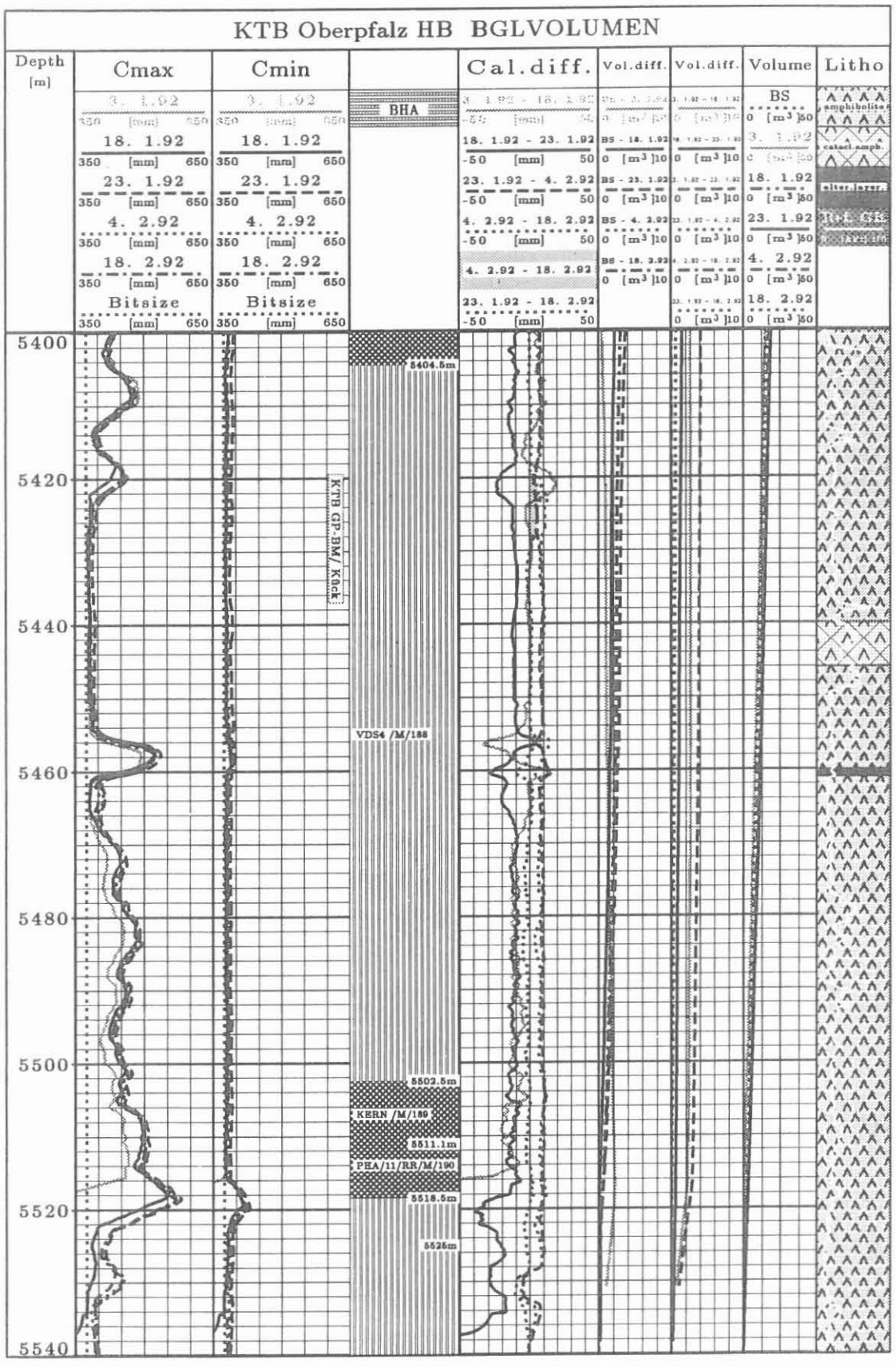

Fig. 3: Example of 'BGLVOLUMEN' data presentation of the depth interval 5400 - 5540 m of the borehole KTB-Oberpfalz HB. Standard presentation is coloured and at a scale of 1:1000. Dates shown are times of data acquisition.

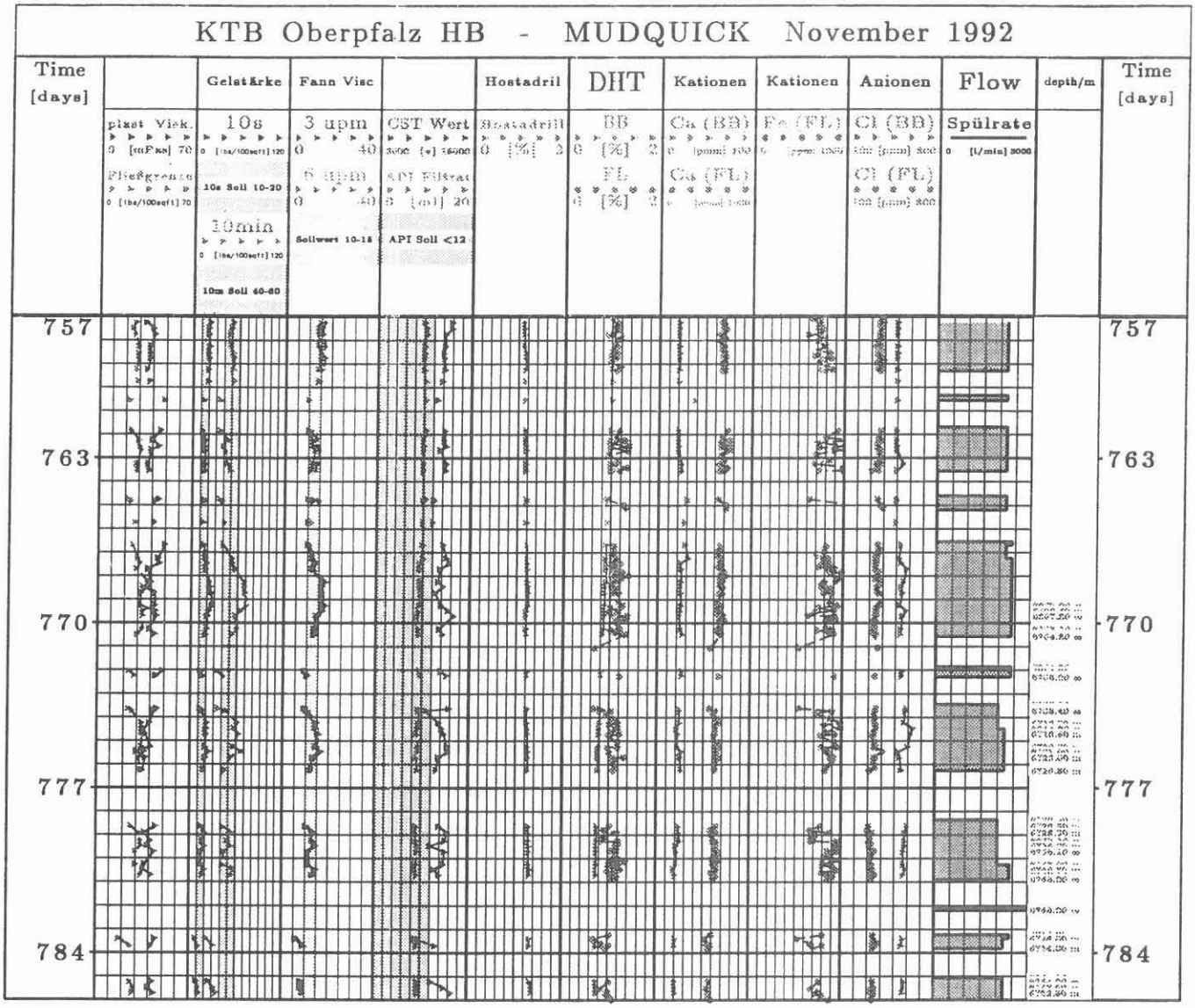

3-FEB-1993 20:00 / KTB-HB Referat Bohrlochmessungen / Kück / Sturmeit

Fig 4: Monthly mud data presentation 'MUDQUICK'. Presentation of 18 parameters describing the mud condition in the KTB main well in November 92. Shaded areas are the nominal values.

SEL*

A computer program to manage and present data of downhole measurements

K.–D. Sturmeit **

Abstract

SEL is a computer program for the management, analysis and presentation of most of the data from downhole measurements. In addition, it is able to handle data measured in the field laboratory.
The user controls the program by commands, read either interactively from the keyboard or from command procedures. Graphic outputs are sent by SEL via GKS to the terminal or plotter. SEL provides complete online HELP.
The SEL program was developed for the KTB–project. It was written in "FORTRAN" on a VAX/VMS System.

The SEL program structure

The SEL program is structured hierarchical:

- the *main program*
  manage all resources (memory, files, ...), controls the command interpreter, save all commands into a journal file, generate error messages, ...
- the *command interpreter*
  read subsequent commands, parse them and start the appropriate process if the command is syntactically correct.
- the *processes*
  For each command there is at least one process in the SEL. The process gets the parameter and options from the command line via command interpreter. If required, the main program manages all input and output data.

  There are no dependencies between the processes.

To add a new process only the command table will have to be modified and SEL will then link with the new process.
At this time there are about 50 'simple' processes in the SEL. With these tools it is easy to create powerful procedures.

---

*SEL is a proprietary product of KTB.
**under NLfB–KTB contract from GECO–PRAKLA, 30635 Hannover, Germany

The SEL database

Most of the datasets in the SEL database are logging data. For an estimation of disk space needed for one dataset of a standard borehole measurement see the following table:

logging length	1 000 m		
Sample distance	6 inch	$\Rightarrow$	$>$ 6 500 Samples
average Number of Channels	40	$\Rightarrow$	$>$ 260 000 Data
for each Data	4 byte	$\Rightarrow$	$>$ 1.4 Mbyte

Today, the SEL database contains about 210 Mbyte pilot hole and 300 Mbyte main borehole data.
For data distribution on the KTB–project the standard format should be the LIS† format. So the LIS tape structure is converted directly to the SEL database structure on the VAX/VMS†† operating system.

external description	realized on VAX/VMS
name of tape	**main directory**
number of file on tape	**sub directory**
channel number and name on file	**file**

On disk, all data are stored in binary format to increase the I/O speed. There are two programs to import any external data format into the SEL database:

- The ASCDB program convert files from ASCII, MUDLOG and GEOCOM format to the VAX/VMS format.
- The DECODE program convert tapes and files from the very special LIS format to the VAX/VMS format.

In the SEL database, the name of a tape is composed from a 2 character abbreviation of the hole ("VB" Vor-Bohrung (pilot hole) or "HB" Haupt-Bohrung (main hole)), the character "T" (for Tape) and a number (e.g. HBT00201). The relation between the measurements and the tapes is stored in the LOGDV database.
In addition, every user can create his private database also used by the SEL.

The SEL data objects

The most important objects in the SEL are:

1. *Curves*
   A curve contains samples with their depth. Each curve is referenced by a name entered by the user. A new curve will be created either by read measured samples from database, modify an existing curve (e.g. FILTER) or evaluate algebraic or logical new samples (e.g. COMPUTE).

   Curve attributes are stored in the curve header. Internal attributes evaluated by SEL describes the samples (depth, sample distance, absent value, value range, statistical values, ...). External attributes describes the representation of the samples (plot limits, line color, line width, line pattern, title, unit, ...). The SEL pre-sets all external attributes with default or propagated values, but the user can modify all.

†LIS is trademark of Schlumberger.
††VAX, VMS are trademarks of Digital Equipment Corporation.

2. *Tables*
   A table is a dataset with several columns. Each column can be referenced by a mnemonic.

   SEL use tables to

   - store segments. Often segments simplify the instruction for the COMPUTE process.
   - define areas. The AREA process checks samples inside or outside of the area and the CROSS and XY_PLOT processes are able to plot the areas.
   - store strings which illustrate all kinds of plots.
   - describe the lithology for plotting.

To avoid disk operations the SEL stores all objects (curves and tables) into dynamical memory. At this time, the memory is limited by a system parameter (Page File Quota) to 50 Mbyte, so a number of 100 curves in one SEL session is a typical value.

The SEL command language

The VAX/VMS command language is also used for the SEL.
Parts of a command are:

- *Command verb*
  The verb has to be the first in a command. It determines the process to start. For example, the verb "GET" starts a process which reads curves from the SEL database.
- *Parameter* (optional)
  A parameter supplies the process with information about existing curves to read or new curves to create. Parameters are separated by a blank. The command interpreter prompts the user for missing but required parameters. For example, the command

  "GET HBT00201.1.SGR GR"

  starts a process which read the channel SGR from file 1 on tape HBT00201 into the curve GR.
- *Qualifier* (optional)
  A qualifier modifies the running off a process. It starts always with a slash-character ("/"). For example, with the qualifier "/LOG" some processes displays, what they have done.

  Some qualifiers need values. See the following example.

  Most of the qualifiers have their default. So the user has to specify only qualifiers when values deviate from the default.

For example, FILTER processes the curve "A":

```
FILTER  A  B1
FILTER/length=20  A  B2
FILTER/type=6/len=124  A B3
```

In the FILTER process, the default values for filter type is 1 (average) and filter operator length is 3 samples. The first FILTER processes curve A using the defaults and stores the result in curve B1. The second application for filter type 1 has a filter length of 20 samples. The third FILTER processes curve A with the filter type 6 (median) and a operator length of 124 samples.
The most important command is **HELP**. This online help is available not only during an interactive SEL session but also for the text editor while creating SEL procedures.

Graphic output

In the interactive part, SEL is able to display the following graphics on any screen supported by GKS.

process	function
DISPLAY	curves against depth
XY_PLOT	many curves against each other
CROSS	two curves against each other
HISTO	histogram
WAVE	"Waveforms" of SONIC†

In addition, hardcopies of all screen graphics are possible on electrostatic, laser or pen plotter. There is only one process in the SEL, called PLOT, which is designed only for plotter output. This process is able to create any kind of log plots inclusive lithology and image plots of SONIC and BHTV measurements. See the contribution BGLQUICK in this report for plots created by the SEL.
For all graphic outputs SEL uses GKS (Graphic Kernel System). With one exception all screens and plotters are supported by GKS. Only the driver for the electrostatic plotter is an own development.

Numerical output

There are three processes in the SEL for numerical output of curves.

process	function
PUT	write into private database
ASCII	creates ASCII formatted files
BINARY	creates binary file as preliminary stage to LIS

Conclusions

Since the SEL database is extended with field laboratory and technical data all departments of the KTB-project use this program to display their measurements for correlation.

Examples

The first example shows the ability of the SEL process COMPUTE.

Comments	**SEL commands**
read caliber C1 and C2	`GET BGT.2.C1 C1_MM`
from database	`GET BGT.2.C2 C2_MM`
	`!`
convert Millimeter to Meter	`COMPUTE "C1_MM/1000" C1`
	`COMPUTE "C2_MM/1000" C2`
	`!`
evaluate average caliber $C_{\text{avg}} = \frac{C_1+C_2}{2}$	`COMPUTE "(C1+C2)/2"  CAVG`
	`!`
evaluate maximum caliber $C_{\text{max}} = \max(C_1, C_2)$	`COMPUTE "LMAX(C1,C2)" CMAX`
	`!`
numerical eccentricity of ellipse $E = \sqrt{1 - \left(\frac{\min(C_1,C_2)}{\max(C_1,C_2)}\right)^2}$	`COMPUTE "SQRT(1-(LMIN(C1,C2)/CMAX)^2)" E`
	`!`
mark for $E > 0.3$ with value 1, all other with absent -999.25	`COMPUTE "LGT(E,0.3,1,-999.25)" MARK`
	`!`
evaluate volume with ellipse C1, C2 and sample distance $\Delta z = 0.1524$ m $V_{\text{e}} = \sum(\pi C_1 C_2 \Delta z)$	`COMPUTE "SUM(PI*C1*C2*0.1524)" V_E`
	`!`
evaluate volume with circle CAVG and sample distance $\Delta z = 0.1524$ m $V_{M} = \sum\left(\pi {C_{\text{avg}}}^2 \Delta z\right)$	`COMPUTE "SUM(PI*CAVG^2*0.1524)" V_M`

The second example produces a CROSS–Plot:

Comments	**SEL commands**
read data from database	`GET COMP_GLT.1.WFE FE`
	`GET COMP_GLT.1.WSI SI`
	`!`
set plot limits	`SET CURVE FE /LEDG=0 /REDG=10`
	`SET CURVE SI /LEDG=15 /REDG=40`
	`!`
display cross plot	`CROSS FE SI -`
	`/CODED/CTYPE=SIZE/PTYPE=19/HIST/HEADER=UR`

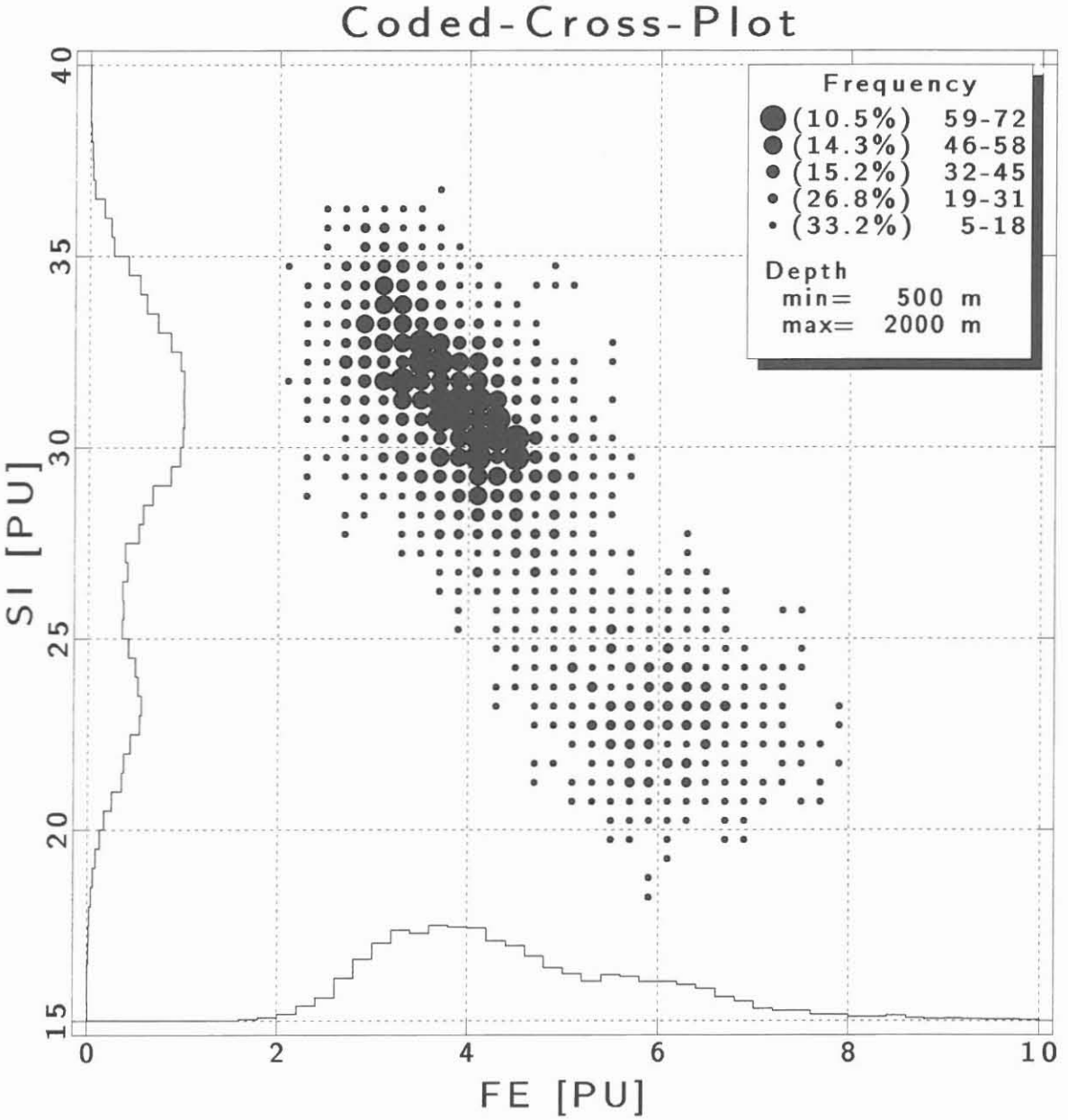

Evaluation of Multi-Finger Caliper Survey in 13 3/8"/13 5/8" Casing String-"Reference Log"

J. K. Draxler

The combined 13 3/8"/13 5/8" casing string was run into the borehole KTB-Oberpfalz HB to a depth of 6013.5 m (driller) from April 4th - 10th 1992. A Multi-Finger Caliper (MFC) survey was made on April 23rd/24th 1992 after cementation and cleaning of the casing by a scraper run. The Multi-Finger Caliper Log was run in combination with a Gamma Ray as depth correlation reference for further repeat logs. Corrosion and/or damage of the casings will be evaluated using the time lapse technique.

Casing tally:
According to the casing tally the following number of different casing sizes were run in the 14 3/4" borehole:

Size	Material	from	to	Length (m)	Number
13 3/8"	MW 125 HC	5386.64	6013.54	626.86	50
13 3/8"	MW 125	2806.65	5386.64	2579.99	197
13 5/8"	MW 125 (XO)	2805.55	2806.65	1.10	1
13 5/8"	P 110	1062.04	2805.55	1743.51	136
13 5/8"	MW 125	551.26	1062.04	510.78	43
13 5/8"	V 150	0.00	551.26	551.26	43

Inner diameter : 13 3/8" = 313.58 mm
13 5/8" = 314.34 mm

Outer diameter : 13 3/8" = 339.70 mm
13 5/8" = 346.10 mm

Outer diameter
of casing joints: 13 3/8" = 344.50 mm
13 5/8" = 352.40 mm

Drift diameter both casing sizes: 312.0 mm

Bit size, open borehole (3005.5-6018.0 m):14 3/4"= 374.6 mm

Checking the casing tally versus the caliper log the following disagreement was noticed: the casing shoe and the float collar were counted as "pipes", while the X-over 13 3/8" : 13 5/8" was counted separately. Therefore, only 245 joints of 13 3/8" casing (full length) were run in the hole and not 247.

Author's address:
Niedersächsisches Landesamt für Bodenforschung, KTB-Projekt, P.O. Box 510153, 30631 Hannover, Germany

A second difference was recognized within the 13 5/8" tally. The caliper log recorded 221 joints versus 222 joints of the tally. The difference must be at the P-110 pipes. The pipe list records a total length of 1743.51 m for 136 joints, while the caliper log gives a length of 1746.0 m for 135 joints (depth from 2810.0 - 1046.0 m).

The casing joints are measured horizontally on the pipe rack and the different lengths are added for the tally. This "calculated" length will be different after the casings have been run in the hole. Due to the weigth of the string and the temperature in the borehole elongation will occure, which is compensated by buoyancy to a certain degree (true depth).

In reference to the Gamma Ray (open hole) the depth positions for "marker joints" are:

X-over 13 3/8"/13 5/8"(XO):	calculated depth:	2805.55-2806.65	m
	true depth :	2810.00-2811.10	m
Float collar (FC) :	calculated depth:	5986.56-5987.70	m
	true depth :	5994.20-5995.35	m
Casing shoe (CS) :	calculated depth:	6012.75-6013.50	m
	true depth :	6020.40-6021.15	m*

*) This depth was not recorded by the caliper log. For safety reasons the caliper tool was not run outside the casing shoe. The log was started within the first casing joint at 6016.0 m and the true depth of the casing shoe was calculated from the first measured joint at 6008.70 m.

Logging Operation:
The log was run in two sections. The first record covered the interval from 3047.0 m to surface.

After this log worn fingers were replaced and the tool was recalibrated before logging the second section from 6016.0 - 2983.0 m. Due to debris left in the mud and scale not cleaned by the scraper run, the fingers of the caliper tool became blocked several times. Therefore, the following intervals were repeated: 4376.0 - 4235.0 m and 5898.0 - 5426.0 m. In addition, when signs of restricted mobility of the fingers was recognized, the tool was intermittently closed, shaking-off the "dirt" (cement, cuttings, scale). Over certain intervals the log quality is degraded by remaining debris.

Data recording:
Analog record - film:
Track I: Gamma Ray (GR) - depth reference
Scale 0 - 150 GAPI

Radii 1 - 6: (RAD1-6; MM) Radii for segments of 120° (24 fingers). Maximum and minimum value with each segment.
Scale 150 - 170 mm (RAD1,4)
Offset for RAD2,5 and RAD3,6 5 mm each.

Track II and III: Minimum (MNRD) and Maximum (MXRD) Radii in mm (MM), from 72 fingers measurement.
Scale 143.0 - 173.0 mm (profile)
Drift (DRIF) in mm (MM), manually set at 156 mm.
Scale 143.0 - 173.0 mm (profile).
Outside calculated radius (OCR), manually set for 13 3/8" at 169.85 mm and for 13 5/8" at 173.05 mm.
Scale 143.0 - 173.0 mm (profile)
Shading between MNRD/MXRD and OCR is casing wall thickness.

Data was recorded analog on film and digital on tape in LIS-format.

Fig. 1 gives a sketch of the tool combination. The sensor section of the Multi-Finger Caliper is guided by two strong in-line centralizers while the electronic cartridge, gamma ray sonde and telemetry are supported by two additional bow-spring centralizers. To suppress possible excentralization of the sensor section universal joints are mounted between this section and the other components of the tool combination.
The logging speed was 10 m/min.

Interpretation:

The in situ calibration of the Multi-Finger Caliper Tool was done at the depth of 6018.0 m. Adding up all 6 radii (RAD1-RAD6), the measured average is 156.8 mm, which corresponds to an inside diameter of the 13 3/8" casing = 313.06 mm. In all casing connections a decrease of the inside diameter is recorded which is due to the special MID OMEGA-XSC-casing threads.

As already mentioned, over several intervals the quality of the log suffers from debris collected between the fingers hindering proper function. Correlating the readings with repeat logs differences still exist, confirming a "dirty" logging environment.

Over several casing joints all six radii run parallel and

show diameter variations in the millimeter-range. These are wall thickness variations created by the pipe rolling (milling) process (Fig. 2).

Slight oval deformation is recognized in a few casing sections. But these deformations are within the accepted tolerances (Fig. 3).

In detail interpretaion:

To achieve coherance, the pipe numbers of the casing tally are used for easy correlation.

Pipe No.	Comments
2nd run:	**6016.0 - 2983.0 m including repeats.**
1	casing shoe (not logged)
2	7 m logged, milling traces
3	milling traces
4	float collar
5	milling traces, dirty pipe
6	RAD3 - 8.5 m blocked
7 - 8	readings influenced by dirt
9 - 11	milling traces
12 - 48	readings influenced by debris, repeat log brings only slight improvement, milling traces still visible
49	milling traces
50 - 75	pipes dirty, readings influenced milling traces
76 - 79	milling traces
80 - 88	readings influenced, milling traces
89 - 92	milling traces
93 - 105	readings influenced, milling traces
106 - 108	milling traces, slight oval deformation (1.2 mm)
109	dirty casing, reading influenced
110 - 112	milling traces
113	dirty casing

114 - 115	milling traces, slight oval deformation (1.6 mm)
116 - 120	milling traces, RAD4 slightly blocked
121 - 122	milling traces, slight oval deformation (1.5 mm)
123 - 126	milling traces, readings influenced
127 - 137	readings influenced, repeat run shows improvement, slight oval deformation (1.2 mm), milling traces, tool intermittently closed within pipe 130
138 - 141	readings influenced, RAD4 slightly blocked
142 - 144	readings influenced, milling traces
145 - 157	readings strongly influenced
158 - 161	milling traces, RAD4 slightly blocked
162 - 165	milling traces, oval deformation (1.6 mm)
166 - 170	readings influenced, RAD4 slightly blocked, milling traces, oval deformation (1.4 mm)
171 - 173	milling traces
174 - 178	fingers partly blocked
179 - 193	milling traces, fingers partly blocked
194 - 202	milling traces
203 - 204	fingers partly blocked
205 - 215	milling traces, slight oval deformation (1.6 mm)
216 - 221	fingers partly blocked
222 - 234	milling traces, slight oval deformation (1.6 mm)

1st run 3047.0 - 5.0 m, casing cleaner than in bottom section

230 - 234	overlap with run 2., better record, milling traces
235 - 244	milling traces
245 - 247	slight oval deformation (1.6 mm)
248	X-over 13 3/8"/13 5/8"
249 - 383	no milling traces visible within the P-110 13 5/8" casings, small diameter variations

	within tolerances, slight oval deformation of pipes 306 - 308 (1.6 mm)
384	change of steel quality (V-150), milling traces are again visible
383 - 428	milling traces, fingers slightly blocked
429 - 431	slight oval deformation (1.8 mm) RAD3 blocked
432 - 447	milling traces
448 - 449	strong oval deformation (3.6 mm)
450 - 454	milling traces
455 - 465	slight milling traces
466 - 468	milling traces
469	last casing joint, only 5.0 m measured.

Conclusions:
The log recorded during the first run from 3047.0 - 5.0 m is of far better quality than the second run from 6016.0 - 2983.0 m, confirming the decision to split the recording of the 6000 m casing string and running the top section first. Less debris was encountered during this log, than while logging the bottom interval.

Several short casing joints (between 9.99 and 11.95 m length) could be used as correlation points between tally and logs. These pipes are: 13, 24, 25, 37, 48, 67, 144, 152, 157, 189, 216, 242, 285, 353, 366, 386, 392, 393, 397, 404, 426.

Outside the slight oval deformation of a few casing joints, no damage was recorded (new pipe - "zero reference log").

To improve log quality the mud must be cleaned by circulating longer while making the scraper run. Running a junk basket on wireline prior to the caliper run should be considered.

As all data is available in digital form, correlation with repeat logs, run at certain time intervals, should highlight any damage immediately.

Multi-Finger Caliper Tool (MFC)

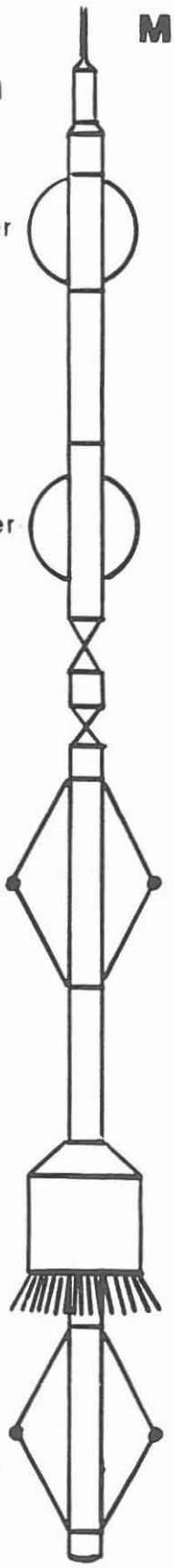

Cable

Cablehead

Centralizer

Telemetry

Gamma Ray

Centralizer

Multi-Finger Caliper Electronic

Universal Joint

Universal Joint

In-line Centralizer

Multi-Finger Caliper Sonde

Finger Section(72 Fingers)

In-line Centralizer

Schlumberger

Fig.: 1

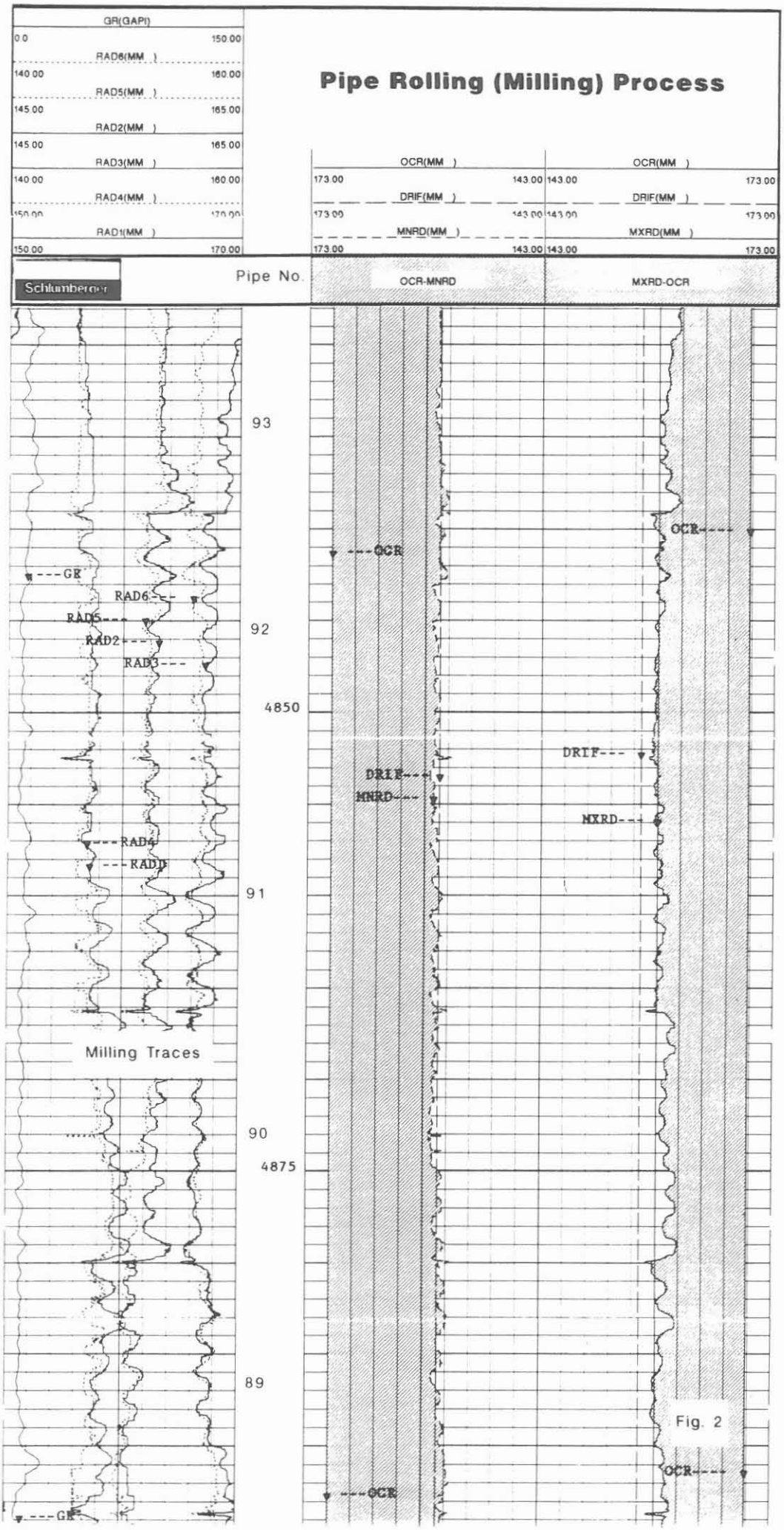
GR(GAPI)
0.0
150.00
RAD6(MM)
140.00
160.00
RAD5(MM)
145.00
165.00
RAD2(MM)
145.00
165.00
RAD3(MM)
140.00
160.00
RAD4(MM)
150.00
170.00
RAD1(MM)
150.00
170.00
Pipe Rolling (Milling) Process
OCR(MM)
173.00
143.00
DRIF(MM)
173.00
143.00
MNRD(MM)
173.00
143.00
OCR(MM)
143.00
173.00
DRIF(MM)
143.00
173.00
MXRD(MM)
143.00
173.00
Schlumberger
Pipe No.
OCR-MNRD
MXRD-OCR
93
92
4850
91
90
4875
89
Milling Traces
---GR
RAD6---
RAD5---
RAD2---
RAD3---
---RAD4
---RAD1
---OCR
DRIF---
MNRD---
OCR----
DRIF---
MXRD---
OCR----
---GR
---OCR

Fig. 2

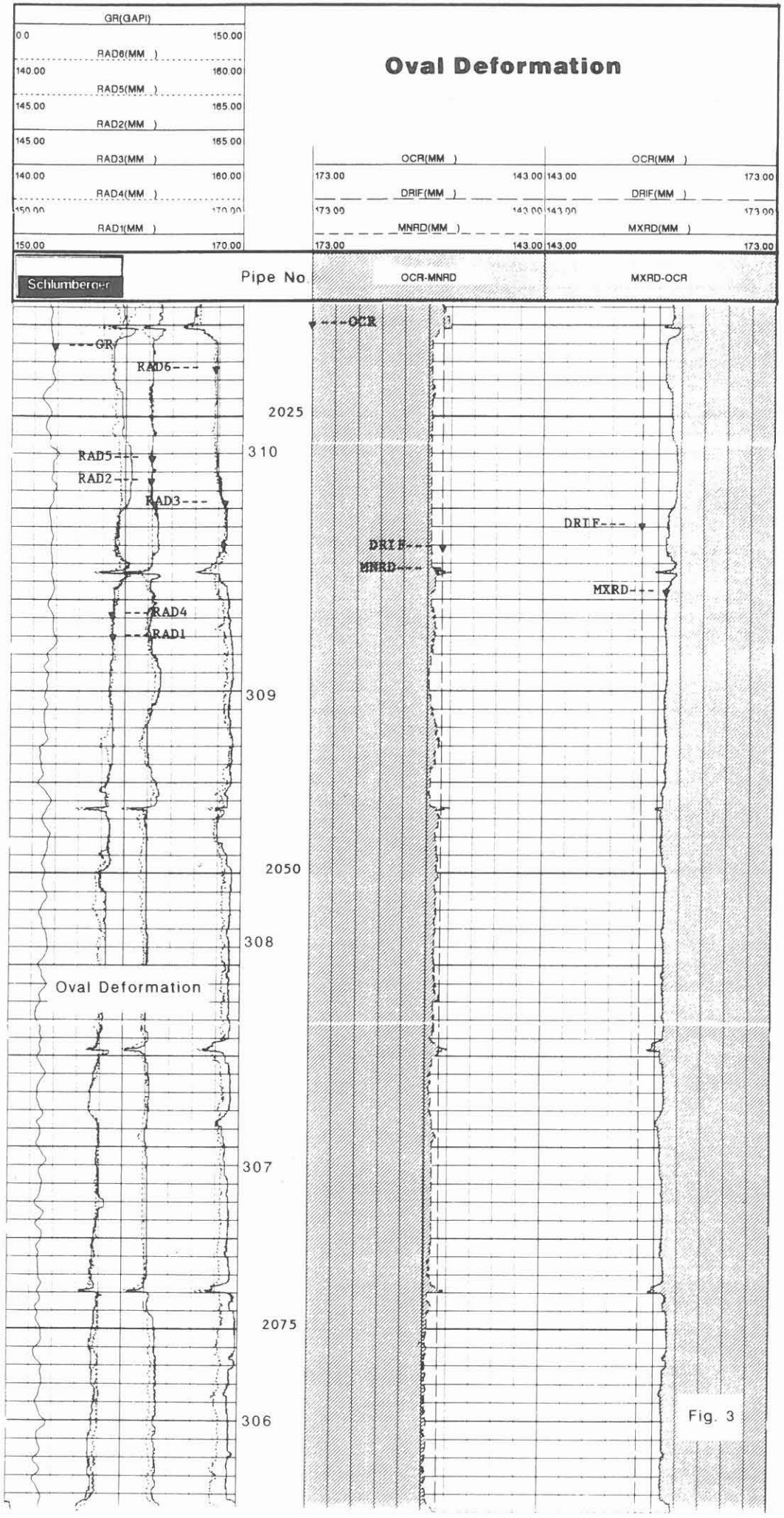
GR(GAPI)
0.0
150.00
RAD6(MM)
140.00
160.00
RAD5(MM)
145.00
165.00
RAD2(MM)
145.00
165.00
RAD3(MM)
140.00
160.00
RAD4(MM)
150.00
170.00
RAD1(MM)
150.00
170.00
Oval Deformation
OCR(MM)
173.00
143.00
DRIF(MM)
173.00
143.00
MNRD(MM)
173.00
143.00
OCR(MM)
143.00
173.00
DRIF(MM)
143.00
173.00
MXRD(MM)
143.00
173.00
Schlumberger
Pipe No
OCR-MNRD
MXRD-OCR
GR
RAD6
RAD5
RAD2
RAD3
RAD4
RAD1
OCR
DRIF
MNRD
DRIF
MXRD
2025
310
309
2050
308
307
2075
306
Oval Deformation

Fig. 3

Temperature measurements during the 6000 m logging campaign in the KTB-Oberpfalz HB

G. Zoth

During the 6000 m logging campaign six temperature logs were run at irregular time intervals taking into account recommendations of the task group on geothermics. First measurements started when temperature readings were taken at the depth of 2400 m, well above the neutral or cross over point between warming and cooling, which has been estimated to be at about 2875 m depth. Logging speed was 15 m per minute down to the bottom of the well. The thermal load due to drilling operations is given in table 1:

Table 1:

circulation	interval:	51 hours	(drilling)
round trip	interval:	21 hours	
circulation	interval:	19 hours	(reaming and circulating off bottom)
circulation	interval:	2 hours	(drilling)
roundtrip	interval:	46 hours	
circulation	interval:	2 hours	(coring)
roundtrip	interval:	19 hours	
circulation	interval:	41 hours	(circulating without drilling, Z = 6018 m)
round trip	interval:	10 hours	

In fig. 1 all six temperature logs are presented as well as bit size, maximum and minimum caliper and gamma ray (left column). The curve drawn from 0 m to 4000 m shows the temperature measured 19 months after circulation stop in the KTB pilot borehole, which is situated 200 m to the west of the KTB superdeep borehole, briefly called the "Hauptbohrung". This temperature curve represents almost the equilibrium formation temperature. The dots at 760 m, 1720 m, 3000 m and 4500 m correspond to the temperatures extrapolated from bottom hole measurements during the previous logging campaigns in the Hauptbohrung.

The first of the six temperature runs, as indicated in Table 2, was made already 14 hours after circulation stop. Obviously, the last circulation block without drilling caused a stronger cooling than expected.

Author's address:
Niedersächsisches Landesamt für Bodenforschung, KTB-Projekt, P.O. Box 510153, 30631 Hannover, Germany

Table 2:

date	time	time since end of the circulation	temperature (°C)
15.03.	14:10	14 h 10′	113.5
15.03.	11:50	59 h 50′	141.5
16.03.	11:31	83 h 31′	148
18.03.	04:18	124 h 18′	153.5
19.03.	13:00	157 h	159
20.03.	20:38	188 h 30′	162

Using a numerical simulation model (Kessels, 1987, unpublished)) the temperature readings given in table 2 yield a value of 172 ± 2 °C for the equilibrium temperature. This value agrees well with the result obtained by applying the Horner Plot technique (Dowdle & Cobb, 1975).

Alltogether there are now five reliable bottom hole temperature values available for the Hauptbohrung. Out of these BHT-values temperature gradients have been calculated starting with an average annual surface temperature T_o = (7.7 ± 0.5) °C at the location. Results are summarized in Table 3.

Table 3:

depth (m)	temperature T (°C)	temperature gradient Γ (Km^{-1})			
0	7,7				
		> 0.0279			
762	29 ± 0,5				
		> 0.0251			
1720	53 ± 1		0.0263		
		> 0.0281			
3003	89 ± 1			0.0271	
		> 0.0285			
4512	132 ± 1				0.0276
		> 0.0265			
6024	172 ± 2				0.0273

Apparently, the temperature gradient tends to decrease slightly below 4512 m. It is reminded, however, that the depth intervals are very large and further temperature measurements beyond 6024 m have to be made in order to confirm this observation.

Reference:

DOWDLE, W.L. & COBB, W.M. (1975): Static formation temperature from well logs - An empirical method. - J. of Petr. Techn., 27: 1326-1330.

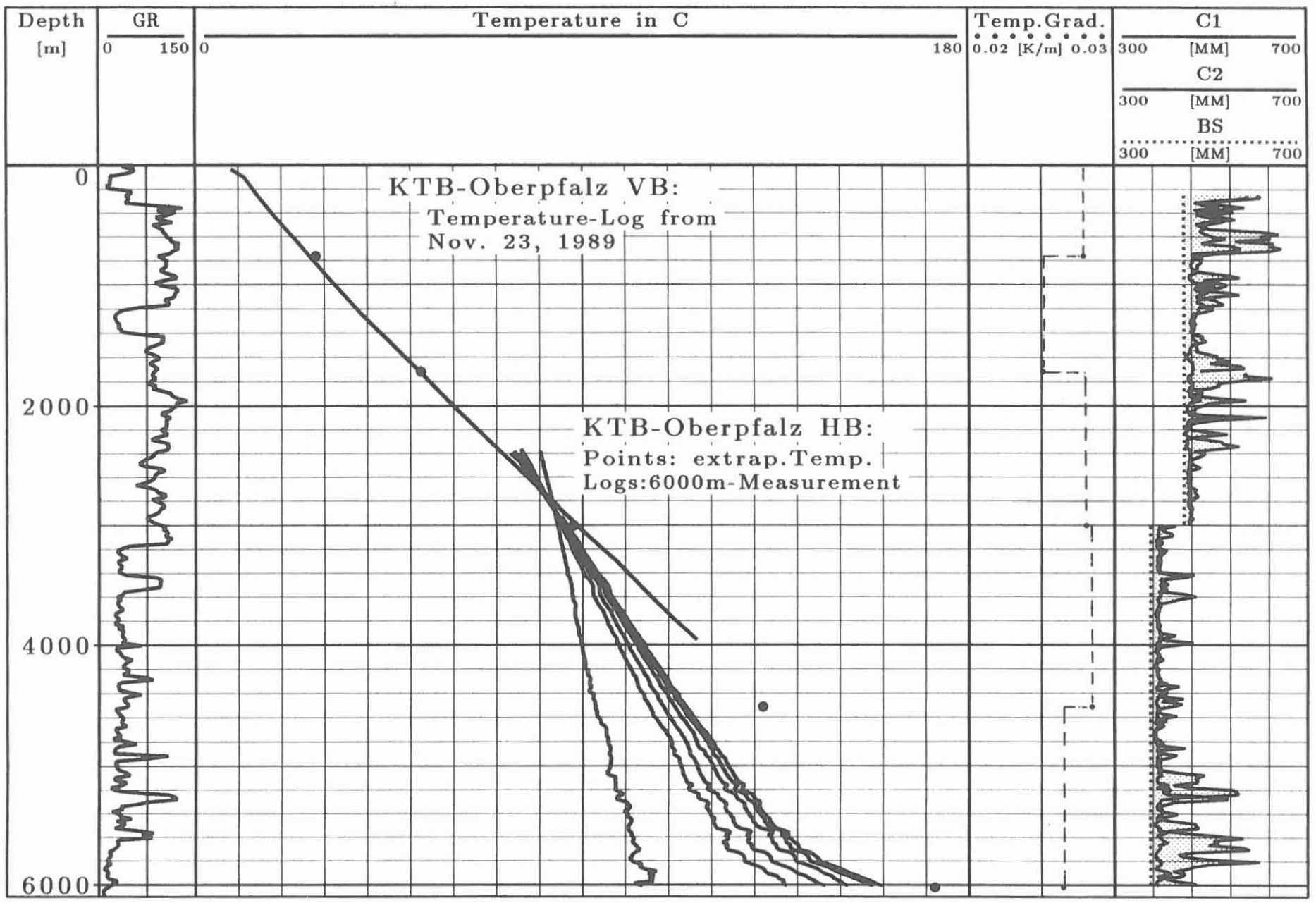
Depth
[m]
GR
0 150
Temperature in C
0 180
Temp.Grad.
0.02 [K/m] 0.03
C1
300 [MM] 700
C2
300 [MM] 700
BS
300 [MM] 700
0
2000
4000
6000
KTB-Oberpfalz VB:
Temperature-Log from
Nov. 23, 1989
KTB-Oberpfalz HB:
Points: extrap.Temp.
Logs:6000m-Measurement
5-MAR-1993 12:46 / ZOTH

Fig. 1

Determination of sonic velocities from KTB borehole acoustic logs.

K. Bram[1] and H. Gatto[2]

Abstract

Sonic logs provide a very detailed information on velocities of seismic waves propagating along the borehole wall. Acoustic measurements were performed in the KTB pilot borehole down to the total depth of 4000 m and in the KTB superdeep borehole so far down to 6000 m. Interval compressional and shear wave velocities in the metabasite units yield average values of 6360 m/s and 3560 m/s. Interval P-wave velocities in the gneiss complexes vary between 5510 m/s and 6150 m/s and the S-wave velocities between 3130 m/s and 3760 m/s. Foliation dipping up to 90° particularly in the gneiss complexes is responsible for seismic anisotropies of 8% and 13% for P- and S-wave velocities, respectively. In consequence, the Vp/Vs - ratio in crystalline rocks appears to be rather a function of structural effects.

Introduction

Sonic measurements in a borehole are a well established link of high resolution information with surface seismics of lower resolution, but much larger lateral extent. In connection with check shot surveys acoustic logging provides a reliable velocity information for correct depth correlation in hydrocarbon exploration.

With regard to the interpretation of the seismic surveys conducted around the KTB drill site (e.g. Schmoll et al., 1989; Dürbaum et al., 1990) where steeply dipping reflector elements prevail, correct depth determination turned out to be a particular difficult problem (e.g. Wiederhold, 1992; Hanitzsch et al., 1992).

In the KTB pilot borehole and in the KTB superdeep borehole, in the following called the "Vorbohrung" and the "Hauptbohrung", respectively, sonic measurements as well as vertical seismic profiles (VSP) were performed. This paper intends to evaluate the time-depth relation of seismic wave

Authors' address:
1) Nieders. Landesamt für Bodenforschung, Projektgruppe KTB, P.O.Box 510153, D-30631 Hannover
2) Consultant, KTB Logging Center, P.O.Box 67 D-92667 Windischeschenbach

propagation observed by acoustic logging, which in turn yields a precise velocity-depth function valid at least in the vicinity of the boreholes. If not otherwise stated all depth figures given throughout this paper correspond to logger's depths.

Data acquisition and tools

Acoustic logging:
Conventional sonic logging aims at detecting the arrival of a compressional wave. The inverse of wave velocity, referred to as interval transit time Delta-T (DT) or slowness, is then computed from the difference in transit times for various transmitter-receiver spacings. As a standard four Delta-Ts are recorded analog in real time in a borehole compensated mode which by tradition are spaced: 3'-5' (DT), 5'-7' (DTL), 8'-10' (DTLN) and 10'-12' (DTLF).

To extract more information, the full acoustic sonic waveform is digitized downhole so as to be free of cable induced distortions. The usual recording time is 10 to 20 ms with a sampling rate of 10 μs. The linear array of eight receivers permits the acquisition of more spatial samples of the propagating wavefield than the standard two-receiver tool. This allows to extract more accurately estimates of the slowness for various wave types such as compressional, shear and Stoneley waves by using modern signal processing techniques, like e.g. Slowness Time Coherence (STC) which is based on a digital semblance method (Kimball and Marzetta, 1984). The processing is usually done in receiver and transmitter mode and averaged for borehole compensation.

In this study interval transit times or velocities discussed below have been deduced by the STC method from monopole data for better fitting the prevailing KTB borehole conditions.

Vorbohrung: According to the logging and testing programme for the Vorbohrung, sonic data were obtained during six campaigns covering the depth interval from 27.4 m to 3994 m. The full waveform generated by a monopole source was recorded circumferentially by the Sonic Digital Tool (SDT) with an operating frequency of 18 kHz.

Hauptbohrung: In the Hauptbohrung sonic data are for the time being available from 278 m to 6020 m. The interval from 278 m to 3003 m was logged eccentered with the SDT in combination with the Natural Gamma Spectroscopy Tool to save an extra run. In the following reduced diameter borehole section, the newly developed Dipole Shear Sonic Imager (DSI) acquired the data down to 6020 m. This tool is equipped with one omnidirectional monopole and two unidirectional dipole transducers, as well as 8 receiver stations containing each two in-line

mounted hydrophone pairs. The operating frequencies are adjustable between 8 - 30 kHz for monopole and between 80 Hz - 5 kHz for dipole modes.

A more detailed description of both tools can be found in e.g. Serra (1984), Williams et al. (1991) Draxler (1992) or in technical brochures published by the Service Industry.

Vertical Seismic Profiles:
Vertical seismic profiles are commonly used to infer interval and average velocities for surface seismic data interpretation, to elucidate structural information due to their high resolution capacity and to calibrate sonic measurements (check shots). In the Vorbohrung a check shot like survey was conducted down to 478 m, and according to drilling progress was followed by a zero-offset VSP down to a depth of 2200 m (Bram, 1988). Using a dynamite source the level spacing of 25 m turned out to implicate spatial aliasing due to an unexpected high frequency spectrum. Within the ISO 89 experiment a second zero-offset VSP was performed with a level spacing of 12.5 m and the lowermost level at 3622.5 m. In addition to dynamite a vibrator source was used. Shots were recorded with a 5-level three component downhole seismic array (Mylius et al. 1990). For technical details of the surveys and first results refer to Lüschen et al. (1990, 1991). Interpretations of the VSP data are published by Kästner et al. (1989), Hohrath et al. (1992) and Söllner et al. (1992).

As part of the 6000 m logging campaign in the Hauptbohrung a zero-offset VSP was performed in the interval from 6000 m to the casing shoe at 3000 m followed by check-shots every 500 m from the casing shoe up to 500 m depth. The vibrator source was situated 240 m west of the wellhead, and the sweep was set from 8 to 123 Hz. A non-oriented three component digital sonic acquisition tool measured the source signals again every 12.5 m. Technical details and first results are given by e.g. Draxler (1993) and Söllner et al. (1992).

Discussion of acoustic parameters

Fig. 1 shows a comparison of STC processed and analog computed compressional data of the depth interval from 2000 m to 2200 m of the Hauptbohrung. The differences between the various Delta-Ts, either digital or analog are usually very small, except in large breakouts. STC determined slowness values (DTCO), are the lowest throughout this section, hence represent the highest velocity. They are on the average 4μs/m lower than the ones computed analog, whereas DT and DTL are quasi identical with only 1μs/m offset on average. Improved

data of DTCO have been obtained in the breakout section around 2100 m where an enlargement can be observed on both calipers.

In the entire Vorbohrung and Hauptbohrung shear waves were excited through a monopole source. In the deeper part of the Hauptbohrung starting at 3000 m, additional shear waves were made available through the excitation of two dipole sources phased 90°. The resulting slownesses are displayed in Fig. 2. As can be seen, only the values from the lower dipole match the ones from the monopole, whereas those from the upper dipole aré constantly lower. Anisotropy is not likely the case, for the tool rotated through 360° and the borehole is almost circular. The histograms in Fig. 3a and Fig. 3b highlight these differences. Over the interval, the respective slowness is on average 293 μs/m for the monopole, 290 μs/m for the lower dipole and 276 μs/m for the upper dipole. The reason for these discrepancies is being investigated.

Results and discussion

The composite log in the annex (Plots #2a and #2b) shows the two wells side by side in an identical arrangement, with the Vorbohrung being on the left. The first column contains the maximum caliper, bit size and gamma ray. Compressional and shear wave velocities as well as pips for integrated compressional transit times corresponding to 10 ms are displayed in column 2. For the topmost depth intervals not accessible to logging, constant values of 5700 m/s for Vp and 3000 m/s for Vs have been assumed in order to make the necessary computations from the surface. Both values are average velocities deduced from the upper alternating sequence. Continuous integrated compressional and shear wave transit times as well as the rock density is depicted in column 3. Column 4 represents the simplified lithological profiles of the boreholes.

Influence of well conditions:
Among the various processing modes, data from the borehole compensated mode was chosen and no other borehole corrections applied. When interpreting sonic data care has to be taken to account for large borehole breakouts (Fig. 1). In this interval from 2090 m to 2120 m of the Hauptbohrung breakouts reach almost twice the amount of the borehole diameter. This is immediately reflected by an increase of the DT and the DTL slownesses whereas STC slowness (DTCO) is less affected.
In the Vorbohrung the sonic interval transit times, and hence the velocities, are only occasionally influenced by breakouts. This holds in particular for the upper 600 m. Breakouts, alteration and high fracture density (Röhr et al., 1989), indicated also by a drop of the log derived formation density, account for abnormal velocity decreases e.g. at the depth of about 1630 m and 2160 m to 2180 m. The velocity and

density decrease at 3202 m correlates with a drilling break and a core loss (Müller et al., 1989). Results of an injection test (Jobmann, 1990) do show the existence of a permeable, less dense fracture zone at that depth.

The Hauptbohrung has a much larger borehole diameter and the breakout situation is quite similar but much more enhanced. Beyond the total depths of the Vorbohrung, larger breakouts indicated by the caliper in the Hauptbohrung occur from about 5100 m down to 6000 m (Plot #2b). The minimum caliper, not displayed in this plot, rarely exceeds 30 mm above nominal bit size. The frequently observed abnormally low density values are easily explained by a tool rotation back into the long caliper axis despite the application of a short axis logging technique. This long axis corresponds with the direction of the minimum horizontal stress field (e.g. Brudy et al. 1993, this report). Due to the large borehole diameter of 17 1/2" no density log was run down to 3000 m.

Due to the more spatial sampling of the wavefield, waves travelling in general along the minimum caliper ray path are first recorded. Taking the fastest wave, STC derived velocities are considered to actually reflect formation velocities even in borehole sections with rather strong ellipticity.

Lithological and structural control:
The lithological profiles consist of a sequence of paragneisses and metabasites with intercalated alternating units. These units again are composed of different gneiss varieties and metabasites of variable thicknesses. Below about 3500 m metabasites prevail.

Sonic velocities clearly reflect the lithological changes. As expected, velocities in metabasites are generally higher than in paragneisses. This is well demonstrated e.g. for the metabasite complexes intersected in the Vorbohrung from 1160 m to 1610 m and from 3580 m on. Alternating units show up by a sonic log with strong velocity variations (Plot #2a). The average and interval velocity-depth relations of the compressional and shear waves are shown in Fig. 4 (VB) and Fig. 5 (HB). Interval P-wave velocities, averaged over 50 m in the metabasite complexes, increase sharply to values above 6000 m/s with peak values up to 6600 m/s. The increase of the S-wave interval velocities with maximum values of 3730 m/s is less pronounced. Taking a gross mean the metabasite complex below 3500 m can be characterized by compressional and shear velocities of 6420 m/s and 3560 m/s, respectively. Comparable mean axial P-wave velocities measured on cores (Rauen et al., 1990; Pribnow et al., 1992) are lower. Reasons may be changes in structural features like frequency, distribution and incident angle of fractures and microcracks (influence of pressure-temperature relaxation) or simply fabric loosening

while coring with roller cone bits.

Velocities in the paragneisses are particularly influenced by the amount of dip of the foliation (Figs. 4 and 5). Interval P-wave velocities vary between 5510 m/s and 6150 m/s and S-wave velocities between 3130 m/s and 3760 m/s. Not surprising, the highest velocities can be observed in the section with the steepest dip and the lowest in zones of low dip. Based on the data of the Vorbohrung slowness versus foliation dip has been analysed for the three main paragneiss sections (Figs. 6a-c). The points are grouped in six frequency classes with their respective amounts in brackets. For each interval an ellipse with its origin in the center of gravity is positioned in such a way that it encompasses the majority of the points. Also shown is the regression line and the histogram of each variable. This helps in better locating the different sections in the composite plot in Fig. 6d. Velocities are more affected by dip than by overburden pressure - the lowest velocities occurring in the deepest interval (Fig. 6c). The composite plot in Fig. 6d indicates a hardly noticeable difference between the top and bottom interval whereas the middle section can be clearly distinguished.

Bremer (1993) showed that as a first approach slowness linearly depends on the cosine of the foliation dip. Correcting the above mentioned velocities (values taken at dips of about 20° and 80°) paragneisses reveal a P-wave anisotropy (A = (Vmax - Vmin)/Vmean) of about 8% and an S-wave anisotropy of about 13%. This is in good agreement with anisotropy values reported and discussed e.g. by Lippmann et al. (1989), Kern et al. (1991), Bopp (1992) and Rabbel (1992). The inclination of the Vorbohrung which exceeds only in few and relatively short depth intervals five degrees has been neglected for foliation dip correction, and hence, for anisotropy determination.

A low velocity zone indicated both by sonic and VSP (Söllner et al., 1992) average velocities in the depth range 2800 m to 3600 m is indeed an effect of anisotropy due to a net change of foliation dip from about 50 to less than 20 degrees.

The metabasites are generally more massive and only occasionally well foliated (Lich et al., 1992). Therefore, sonic velocities scatter less, and no anisotropy values have been deduced using the sonic log data. From core analysis a much lower anisotropy has been reported (Rauen et al., 1990).

Lippmann et al. (1989) and Wiederhold (1992) discussed in detail seismic velocities obtained from KTB core measurements and sonic logs. Velocity differences between VSP and sonic measurements in the KTB Vorbohrung are discussed by Hohrath et al. (1992) and Rühl and Hanitzsch (1992). Attention is drawn by these authors that sonic velocities are generally lower than velocities measured on cores or from VSP. On a

first glance P-wave sonic velocities appear indeed to be lower in certain depth intervals than the velocities measured on cores or from the VSP surveys. Wiederhold explains these apparent discrepancies by the effects of anisotropy and dispersion stressing the different geometry of the velocity measurements and their different frequency ranges: core measurements are performed in the MHz-range, sonic measurements in the kHz-range and VSP surveys in the order of 100 Hz or less. Rühl and Hanitzsch suggest geometric ray path effects, and thus possible wrong traveltime corrections. Interpreting the VSP run from 6000 m to 3000 m (16" casing shoe) in the Hauptbohrung, Söllner et al. (1992) reports a mean interval velocity of 6490 m/s for the more massive metabasites in the depth range 3625 m to 5325 m. This is in good agreement with the corresponding sonic velocity. Nevertheless, even in these metabasites anisotropy cannot be excluded too, taking into account the observed structural dips of about 55° on average. With this in mind, the reported negative drift between sonic and VSP velocities turns out to be an apparent one.

Sonic velocity cross-multiplied with the density is normally used to produce an acoustic impedance log. The inferred synthetic seismogramme is an important step for tying a borehole in a seismic cross section. Despite the many seismic reflectors observed in the surface reflection data mentioned above, no attempt has been made here to calculate an acoustic impedance log, and hence a synthetic seismogramme. Reasons are simply the strong anisotropic behaviour of the wave propagation and in the majority steeply dipping foliation and structures such as fractures and lithological changes, not accounted for in the routinely used formula.

The Vp/Vs-ratio, easily calculated from sonic log data, is in general a key figure for determining elastic characteristics of rocks allowing for statements on lithology and facies changes as well as for indications of pore filling and porosity variations. In crystalline rocks the ratio appears to be rather a function of structural effects like e.g. foliation dip. This is particularly well demonstrated in Fig. 4: in the paragneiss sections with a foliation dipping more than about 50° the Vp/Vs-ratio, calculated from the sonic interval velocities, drops below 1.7. With decreasing dip, for example in the depth interval from 2700 m to 3600 m, the Vp/Vs-ratio is 1.71 in average. Otherwise stated, the ratio reflects the velocity anisotropy. Care has to be taken, however, when interpreting abnormal high values such as observed e.g. at a depth of 1900 m with relatively good caliper conditions in the Hauptbohrung (Fig. 5). In this case the S-wave velocity obviously decreases much stronger than the P-wave velocity due to a severely altered garnet-sillimanit-biotite gneiss of high fracture density.

In the metabasites the Vp/Vs-ratio lies above 1.75 with an average value of about 1.8. As mentioned above, metabasites may show also structural features like foliation. An increase in the S-wave velocity in the depth interval 3800 m to 3950 m correlates with an increase of the foliation dip whereas the P-wave remains less affected thus reducing considerably the Vp/Vs-ratio.

The Vp/Vs-ratios in the topmost alternating sequence are essentially characterized by borehole breakouts and velocity variations due to surface effects.

Conclusions

In order to assess correctly the information contained in the sonic log data hitherto obtained in the KTB boreholes, the used logging tools are briefly described and the measured acoustic parameters are discussed. STC derived slowness values are considered to actually reflect formation velocities despite severe elliptical breakouts observed particularly in the Hauptbohrung over large depth intervals. Sonic velocities clearly reflect the drilled lithological units: metabasites having generally higher velocities than the paragneisses. The velocities in the paragneisses do show a strong anisotropic behaviour as a result of the foliation dip. Anisotropy amounts up to 8% and 13% for P- and S-wave velocities, respectively.

In the crystalline rocks investigated here, the Vp/Vs-ratio is strongly dominated by structural effects like dipping foliation. This holds especially in the gneiss sections and to a limited extent in some metabasic units. The more massive metabasites have a ratio of about 1.8 and higher, gneisses have ratios less than 1.7 on average depending on the degree of foliation dip.

References

Bopp, M.: 1992. Shear-wave splitting observed by wide-angle measurement. KTB Report 92-5, 297-308, Hannover.

Bram, K.: 1988. VSP Messungen in der Bohrung KTB-Oberpfalz VB. KTB Report 88-7, 165-178, Hannover.

Bremer, M.: 1993. Untersuchungen und Entwicklung eines Auswerteverfahrens zur Analyse und Interpretation von geophysikalischen Bohrlochmessungen in komplexen Lithologien. PhD-Thesis, TH Clausthal, pp 105.

Brudy, M., Fuchs, K. and Zoback, M.: 1993. Stress orientation profile to 6 km depth in the KTB Main Borehole. KTB Report 93-1, Hannover.

Pribnow, D., Bücker, Ch., Rauen, A., Spangenberg, E., Wienand, J. and Soffel, H.C.: 1992. KTB Hauptbohrung, geoscientific investigations in the KTB-field-laboratory, depth interval 0-6000 m. KTB Report 92-2, D1-D42, Hannover.

Draxler, J.: 1992. Neue Meßgeräte. KTB Report 92-1, 289-299, Hannover.

Draxler, J.: 1993. New tools. KTB Report 93-1, Hannover.

Dürbaum, H.-J., Reichert, Ch. and Bram, K.: 1990. DEKORP Report: Integrated Seismics Oberpfalz 1989. KTB Report 90-6b, pp 211, Hannover.

Hanitzsch, Ch., Hubral, P., Rühl, T. and Söllner, W.: 1992. Migration of steeply dipping reflectors at the KTB site: Depth errors caused by inaccurate velocity models. KTB Report 92-5, 333-341, Hannover.

Hohrath, A., Bram, K., Hanitzsch, C., Hubral, P., Kästner, U. Lüschen, E., Rühl, Th., Schruth, P.K. and Söllner, W.: 1992. Evaluation and interpretation of VSP-measurements in the KTB-Oberpfalz pilot borehole. Scientific Drilling, 3, 89-99.

Jobmann, M.: 1990. Thermischer Injektionstest und Temperaturmessung nach sechmonatiger Standzeit in der KTB-Oberpfalz VB. KTB Report 90-6a, 229-243, Hannover.

Kästner, U., Bram, K., Hubral, P., Kiefer, W., Köninger, C., MacDonald, C., Merz, J., Rühl, Th. and Sandmeier, K.-J.: 1989. Seimische Untersuchungen an der KTB-Lokation. KTB Report 89-3, 169-210, Hannover.

Kern, H., Schmidt, R. and Popp, T.: 1991. The velocity and density structure of the 4000 m crustal segment at the KTB drilling site and their relationship to lithological and microstructural characteristics of the rocks: an experimental approach. Scientific Drilling Vol. 2, 130-145.

Kimball, C.V. and Marzetta, T.M.: 1984. Semblance processing of borehole acoustic array data. Geophys., 49, 264-281.

Lich, S., Duyster, J., Godizart, G., Keyssner, S. and de Wall, H.: 1992. German Continental Deep Drilling Program (KTB) - Geological Survey of the Hauptbohrung 0-6000 m. KTB Report 92-2, B1-B42, Hannover.

Lippmann, E., Bücker, Ch., Huenges, E., Rauen, A., Wienand,J. and Wolter, K.E.: 1989. Gesteinsphysik im KTB-Feldlabor: Messungen und Ergebnisse. KTB Report 89-3, 120-129, Hannover.

Lüschen, E., Söllner, W., Hohrath, A. and Rabbel, W.: 1990. Integrated P- and S-wave borehole experiments at the KTB-deep drilling site. KTB Report 90-6b, 85-134, Hannover.

Lüschen, E., Söllner, W., Hohrath, A. and Rabbel, W.: 1991. Integrated P- and S-wave borehole experiments at the KTB-deep drilling site in the Oberpfalz area (SE Germany). In R. Meissner, L. Brown, H.-J. Dürbaum, W. Franke, K. Fuchs and F. Seifert (eds): Continental Lithosphere: Deep Seismic Reflections. AGU, Washington D.C., 121-133.

Müller, H., Hacker, W., Keyssner, S., Röhr, C., Sigmund, J., Kohl, J., Stroh, A. and Tapfer, M.: 1989. Tiefbohrung KTB-Oberpfalz VB 1a, Ergebnisse der geowissenschaftlichen Bohrungsbearbeitung im KTB-Feldlabor (Windischeschenbach), Teufenbereich von 3009.7 bis 3500 m. KTB Report 89-5, B1-B94, Hannover.

Mylius, J., Nolte, E. and Scharf, U.: 1990. Use of the seismic receiver chain SEKAN 5 within the framework of Integrated Seismics in the Oberpfalz. KTB Report 90-6b, 159-179, Hannover.

Rabbel, W.: 1992. Seismic anisotropy at the KTB deep drilling site. KTB Report 92-5, 275-289, Hannover.

Rauen, A., Huenges, E., Bücker, Ch., Wolter, K.E. and Wienand, J.: 1990. Tiefbohrung KTB-Oberpfalz VB, Ergebnisse der geowissenschaftlichen Bohrungsbearbeitung im KTB-Feldlabor (Windischeschenbach), Teufenbereich von 3500 bis 4000.1 m. KTB Report 90-2, D1-D64, Hannover.

Röhr, C., Hacker, W., Keyssner, S., Johl, J. and Müller, H.: 1989. Tiefbohrung KTB-Oberplfaz VB, Ergebnisse der geowissenschaftlichen Bohrungsbearbeitung im KTB-Feldlabor, Teufenbereich von 1709 bis 2500 m. KTB Report 89-2, B1-B114, Hannover.

Rühl, T. and Hanitzsch, Ch.: 1992. Average and interval velocities derived from first breaks of vertical seismic profiles at the KTB Pilot Hole. KTB Report 92-5, 201-219, Hannover.

Schmoll, J., Bittner, R., Dürbaum, H.-J., Heinrichs, T., Meißner, R., Reichert, C., Rühl, T. and Wiederhold, H.: 1989. Oberpfalz deep seismic reflection survey and velocity studies. In Emmermann, R. and Wohlenberg, J. (eds): The German Continental Deep Drilling Program (KTB). Springer, Heidelberg, 99-149.

Serra, O.: 1984. Fundamentals of well-log interpretation. Elsevier, Amsterdam.

Söllner, W., Lüschen, E., Li, X.-P., Hubral, P., Gut, T.W. and Widmaier, M.: 1992. VSP - A link between reflection seismic profiling and lithology. KTB Report 92-5, 169-199, Hannover.

Wiederhold, H.: 1992. Interpretation of envelope-stacked 3D seismic data and its migration. KTB Report 92-5, 67-114, Hannover.

Williams, D.M., Cowper,D.R. Nieto, J.A., Hurley, M.T. and Schmitt, D.P.: 1991. Shear wave acoustic logging in slow formations - examples and problems. Paper D, in Transactions 14th European Formation Evaluation Symposium, London.

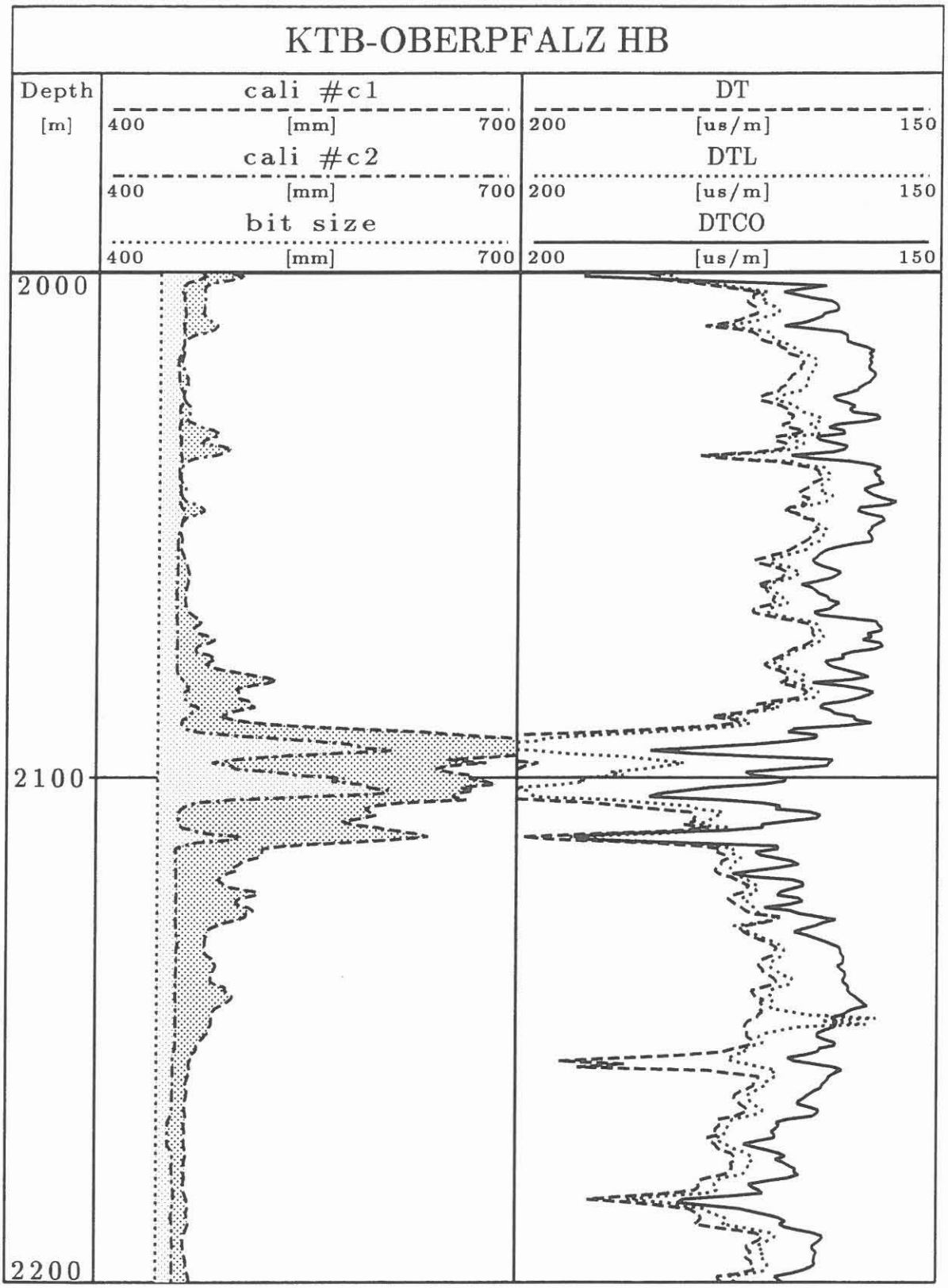

Fig. 1: Comparison of different slowness computations
dt,dtl ... analog first motion detection
dtco ... slowness time coherence

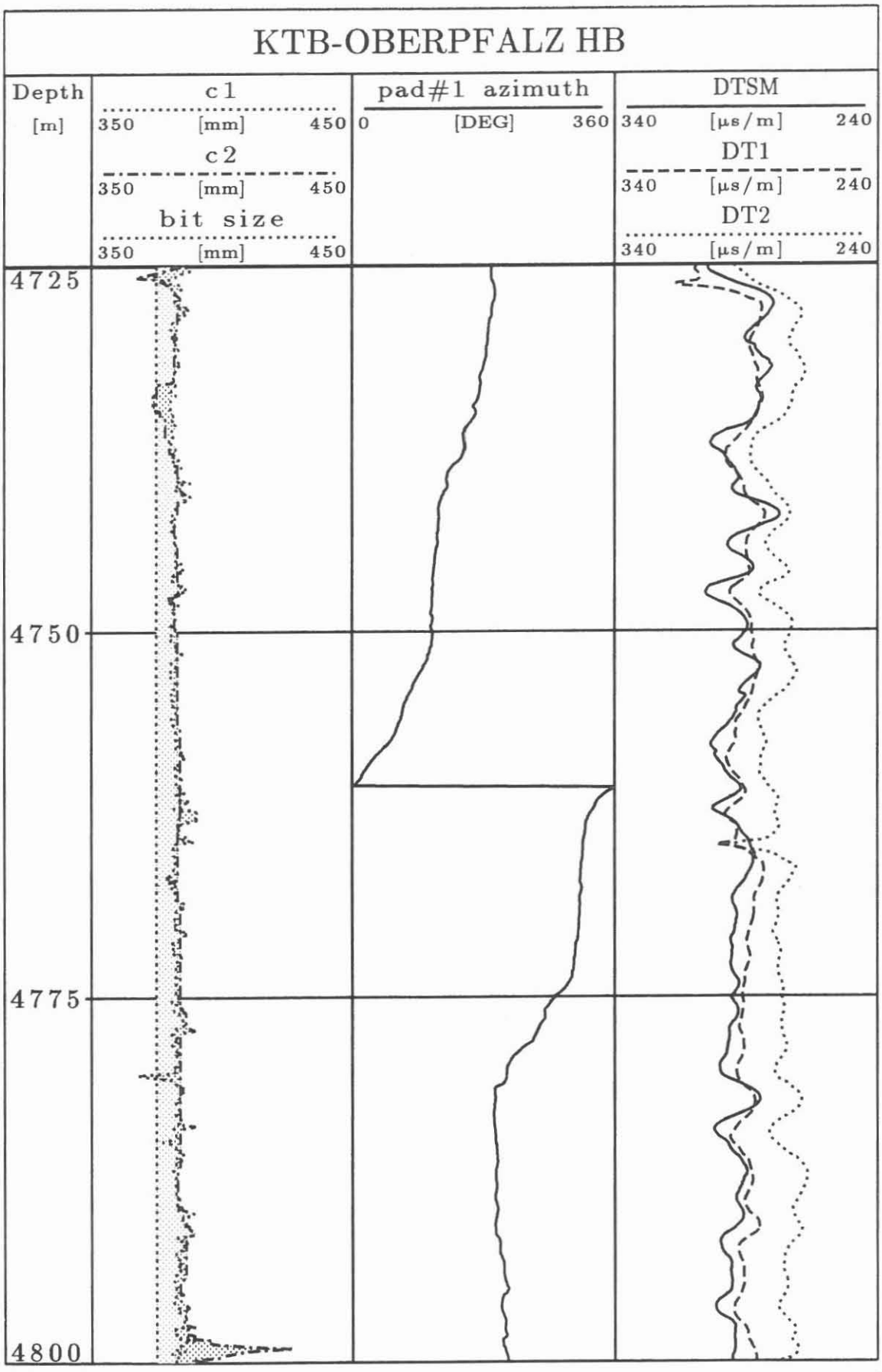

Fig. 2: Comparison of different shear computations
dtsm ... monopole
dt1,dt2 ... lower and upper dipole

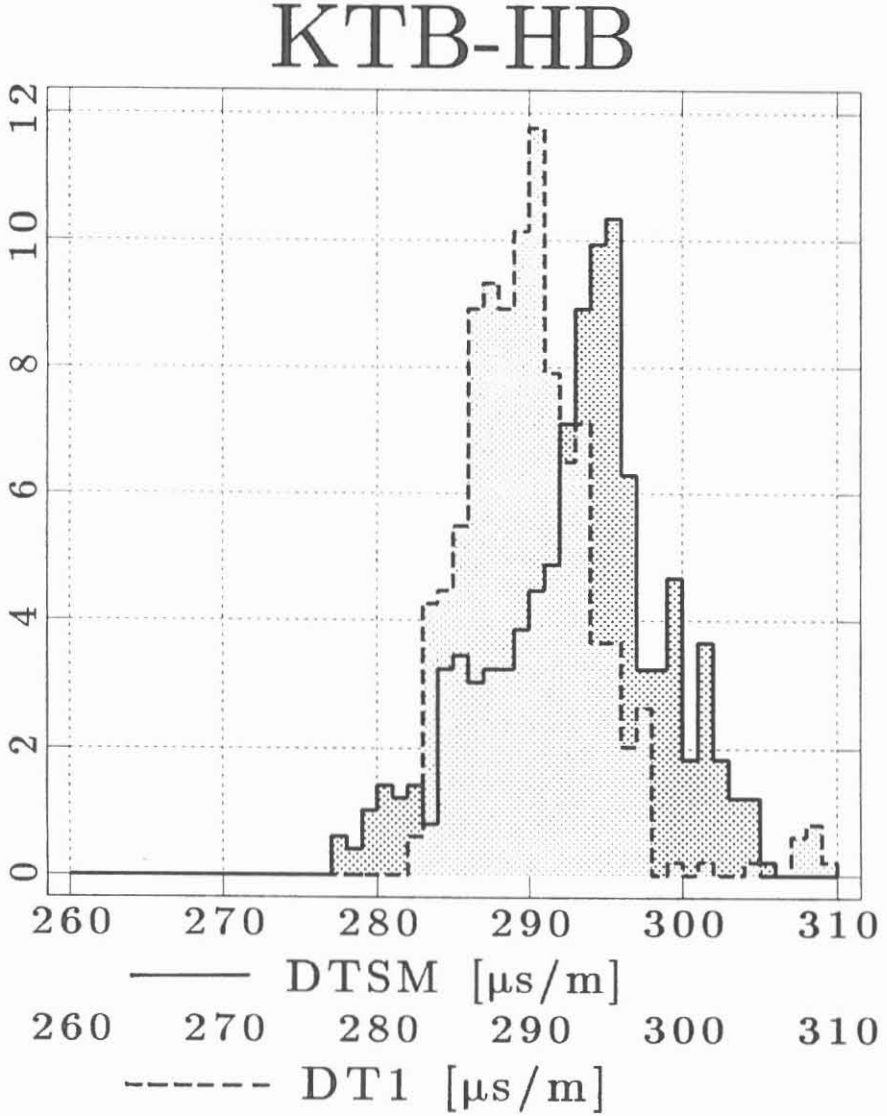

Fig. 3a: Slowness of monopole and lower dipole shear from 4725m to 4800m

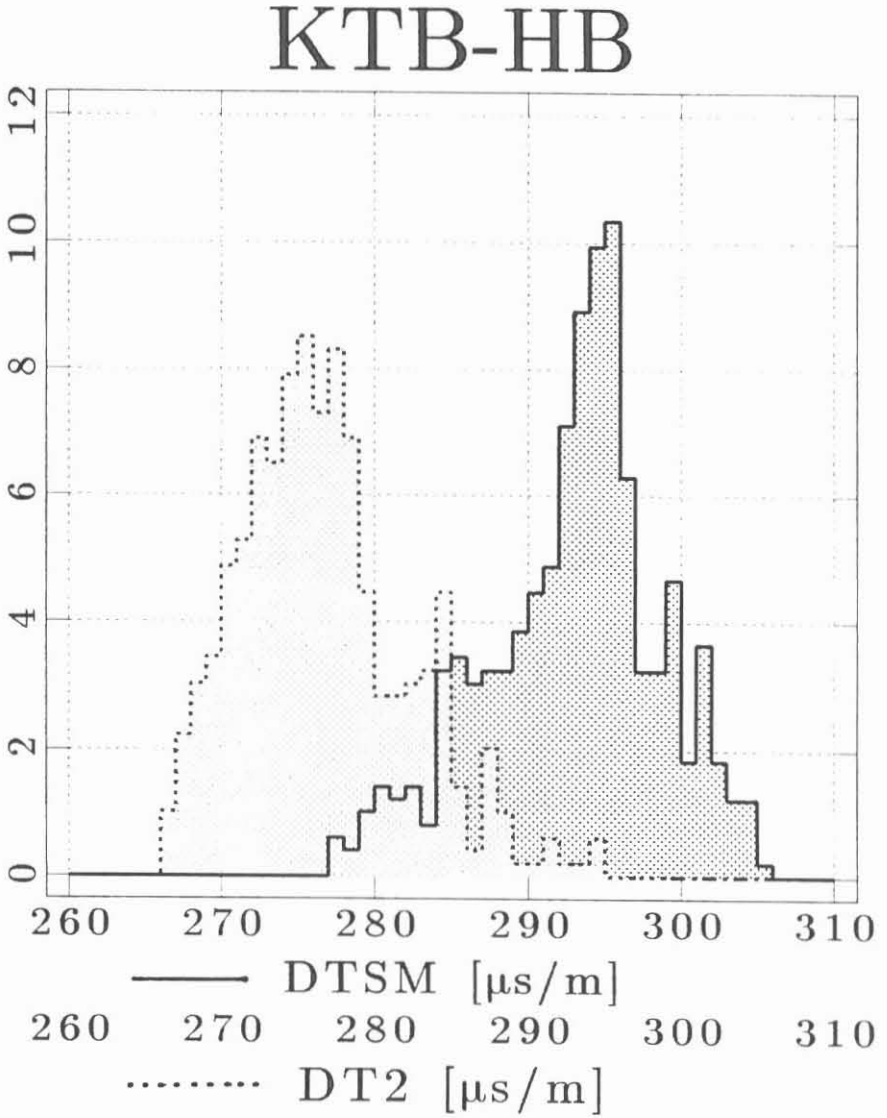

Fig. 3b: Slowness of monopole and upper dipole shear from 4725m to 4800m

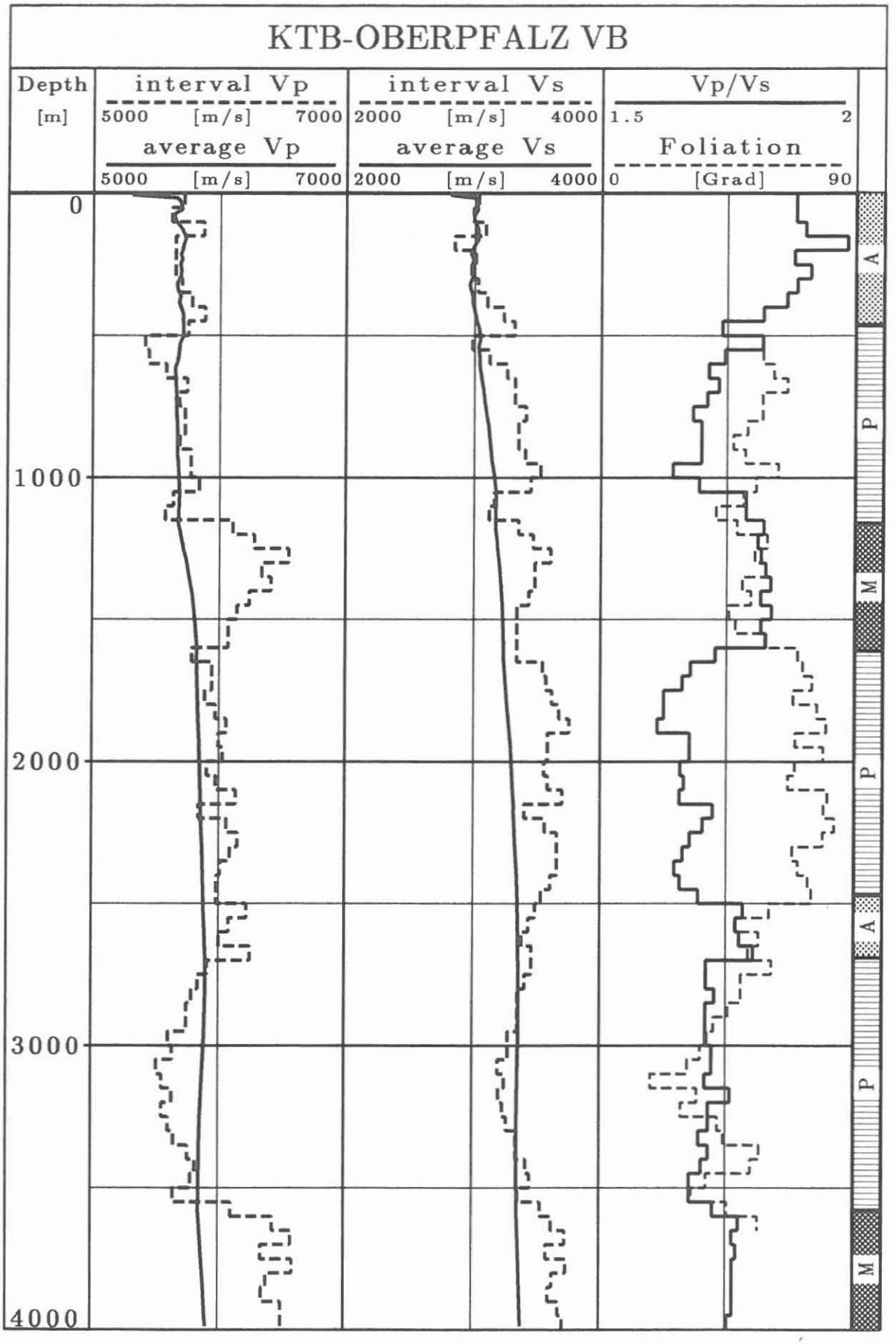

Fig. 4: Velocity profiles of KTB-VB

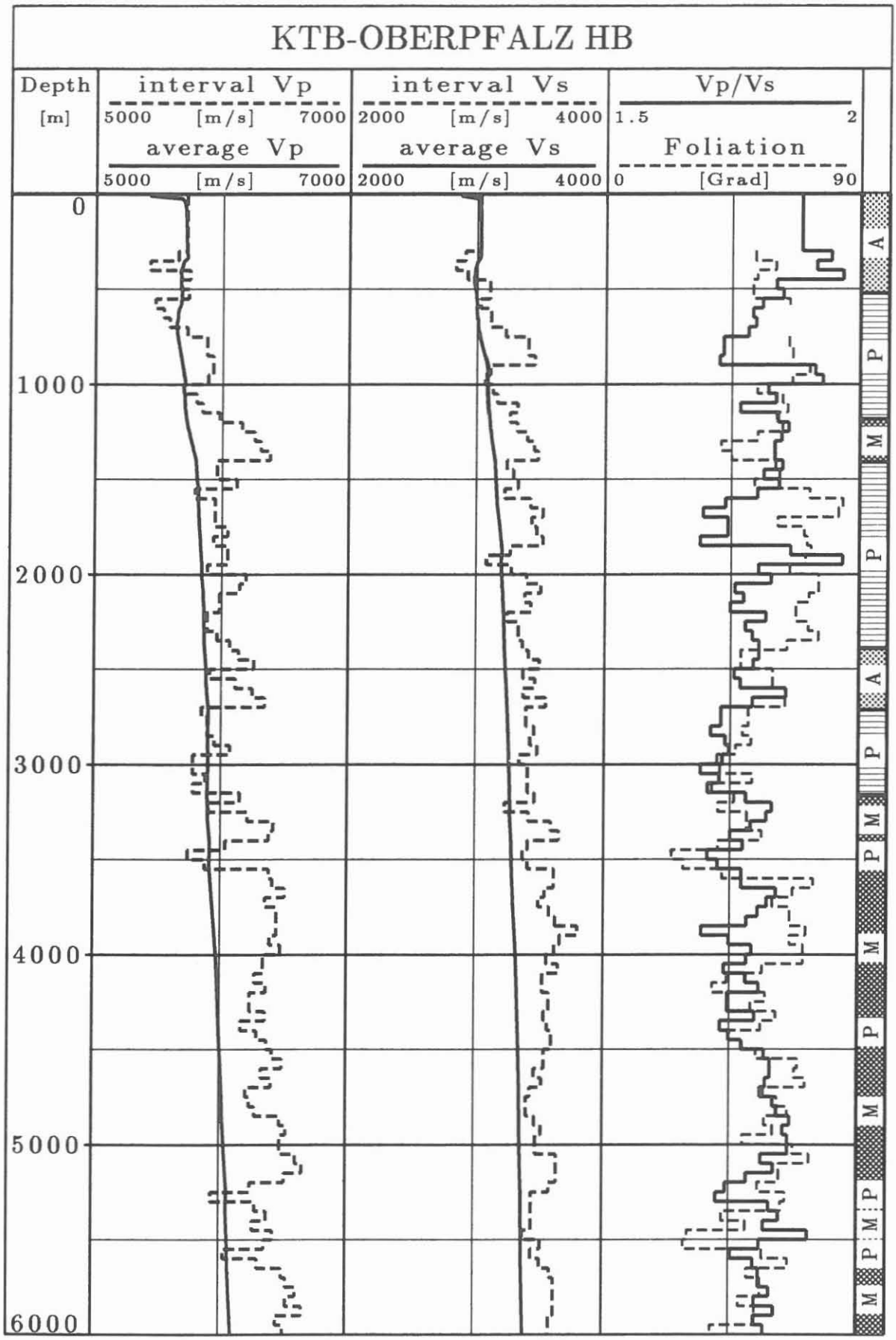

Fig. 5: Velocity profiles of KTB-HB

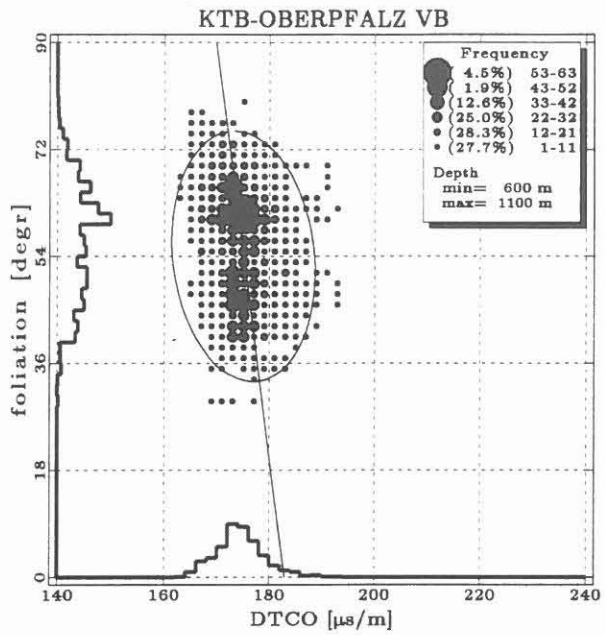

Fig. 6a Slowness versus dip in gneiss (600 - 1100m)

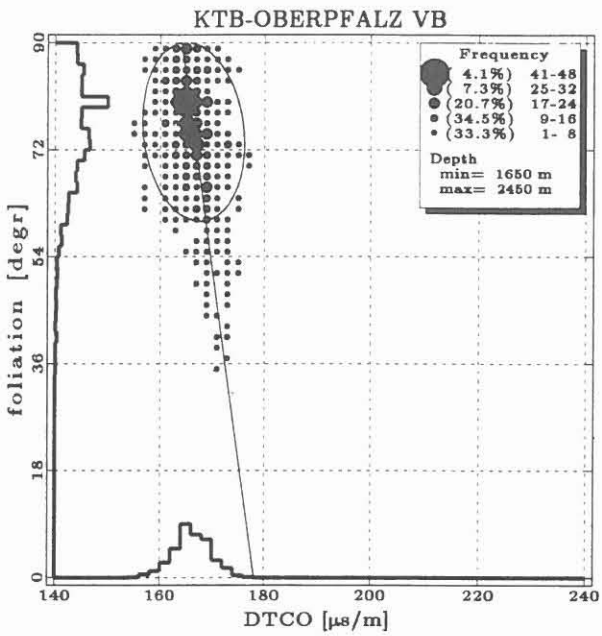

Fig. 6b Slowness versus dip in gneiss (1650 - 2450m)

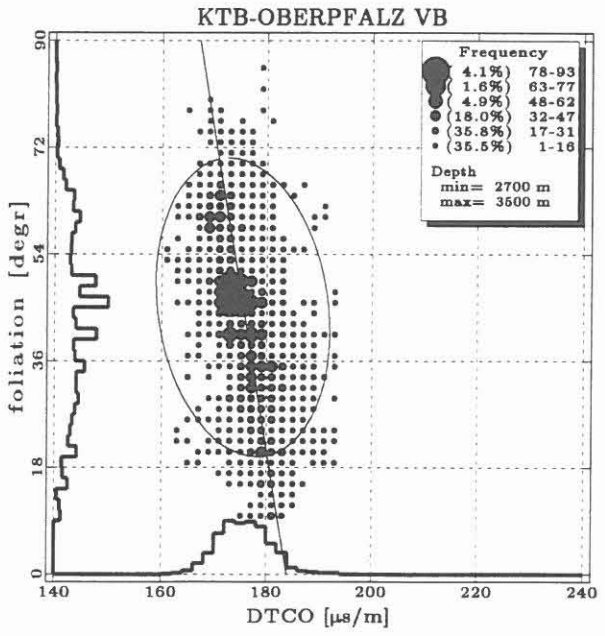

Fig. 6c Slowness versus dip in gneiss (2700 - 3500m)

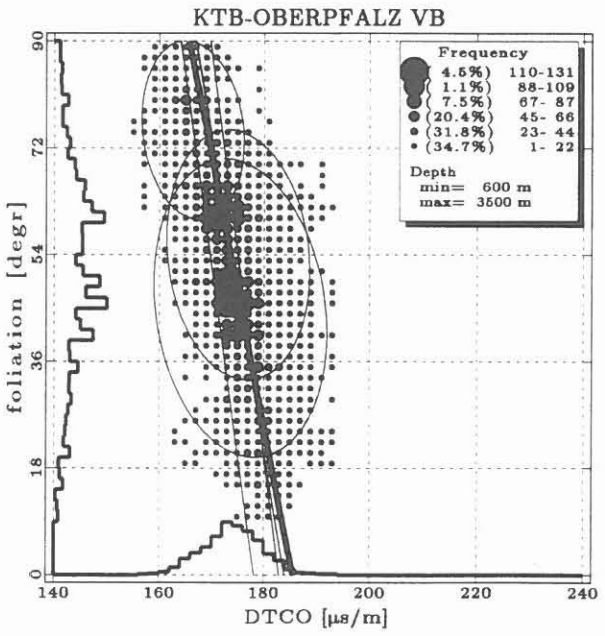

Fig. 6d Slowness versus dip in gneiss (600 - 3500m)

A Mise-à-la-Masse experiment for detecting an electric network in cataclastic zones around the KTB-site

Johannes Stoll*

Contents

1. Summary

The casings of the KTB pilot- and main boreholes were used to inject an electrical current into the formation. The artificial potential field of this current was measured along a small profile close to the KTB drilling sites to detect changes in the potential. The observed changes indicate a connection of an electric conductor with one of the casings and support the assumption of a general conducting layer extending over distances of several hundred meters. From the tectonic map it is assumed that the detected conductive layer belongs to the prominent Nottersdorf fault zone, which is steeply inclined and crosses the main borehole between 250 and 1500 m.

---

* Johann-Wolfgang-Goethe-Universität Frankfurt, Institut für Meteorologie und Geophysik, 60054 Frankfurt/Main, Germany

2. Introduction

Results from several geoelectric soundings (direct current-, very low frequency resistivity-, audiomagnetotelluric measurements) around the KTB drilling sites suggest that the pilot (KTB-VB) and main (KTB-HB) boreholes are drilled into a several hundred meter wide NNW-SSE striking zone with an extremely low electrical resistivity (Haak et al., 1991). Whereas in the surrounding crystalline rocks resistivities of 10^3-10^4 Ωm were measured, this zone exhibits less than 10 Ωm locally. In comparison to crystalline rocks these very low values doubtless are based on graphitic and sulfuric (especially pyrite) accumulations on many cataclastic shearzones observed in both boreholes, which lower the resistivity by several orders of magnitude. Even graphite is exposed on the surface in some places. This increase of the conductivity inside crystalline rocks could be caused by graphite only if it forms an interconnected network. Such interconnections along shearzones of several hundred meters in vertical extent represent one of a few most important constituents to establish self-potential anomalies. An anomaly of about -600 mV has been detected close to the KTB site (Stoll, 1990). Following the theory of Sato & Mooney (1960), the graphitic shearzones serve as a bridging conductor, in which electrons are transferred from electrochemical reducing agents at depth to oxidizing agents near the surface. However, according to the graphite-bearing rocks around the KTB site this interconnection is still a basic question.

The Mise-à-la-Masse method is an appropriate possibility to use to verify this hypothesis. Since the casings of the boreholes are used as electrodes to inject the current into the formation, the penetrated shearzones will be electrically connected. It is assumed that the electrical current flows along these zones to the surface and changes the electrical potential field there. This change is measured.

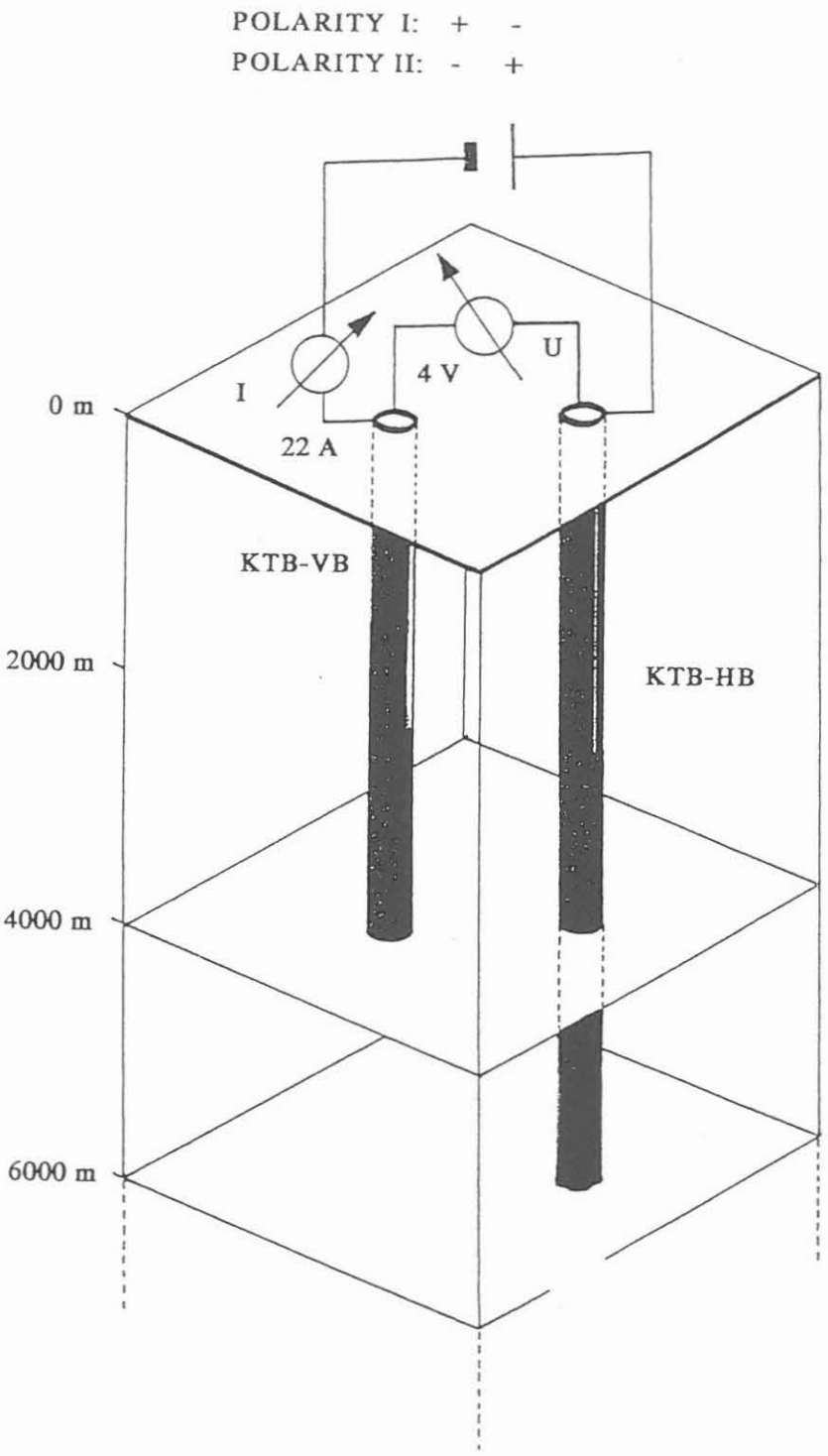

Fig.1

Circuit diagram of the Mise-à-la-Masse experiment in the KTB boreholes
U1: Injection voltage (10V)
U2: Voltage between the casings (4V)
I : Injection current (22V)

current source

3. Mise-à-la -Masse in the KTB boreholes

3.1 The experiment

The two casings of the pilot and main drilling holes will be used as electrodes to inject an electrical current into the formation. At the time of the experiment (24.3.1992) the casings had a vertical extension of 3850 m (KTB pilot hole) and 3000 m (KTB main hole). Because of the high conductivity of the drilling fluid (0.2 Ωm) the complete extension of the boreholes (KTB-VB 4000 m and KTB-HB 6000 m) can be considered as electrodes. The electrical current is taken from the public net and is transformed in a direct current. Two cables which are fixed on the top of the casings conduct the current from the source into the formation (Fig. 1). The interstitial water between the casing and the formation supports the impedance matching, so the measured transition resistance of the casings amounts to 0.212 Ω, which allows to inject strong electrical currents with moderate voltages. The terminal voltage amounts to 10.23 V and decreases because of the cable resistor to 3.46V (U2 in Fig.1) with 22 A between the casings. Electrical polarisations of the casings increased this voltage to 4.2 V, while the current decreased to 18.18 A.
The potential measurements at the surface were carried out close to the drilling area along a profile in radial distance of 100 m to the pilot hole (Fig. 2). Four copper-coppersulphate electrodes (E1..E4) were installed at a spacing of 50 m. The potential is measured with respect to a reference electrode (BE) before and during injecting the current into the formation by reversing the polarity once. In the following the registered values are:

(A): without current; i.e. self-potential EP

BE -> E1 : - 61 mV
" -> E2 : -238 mV
" -> E3 : -306 mV
" -> E4 : -223 mV

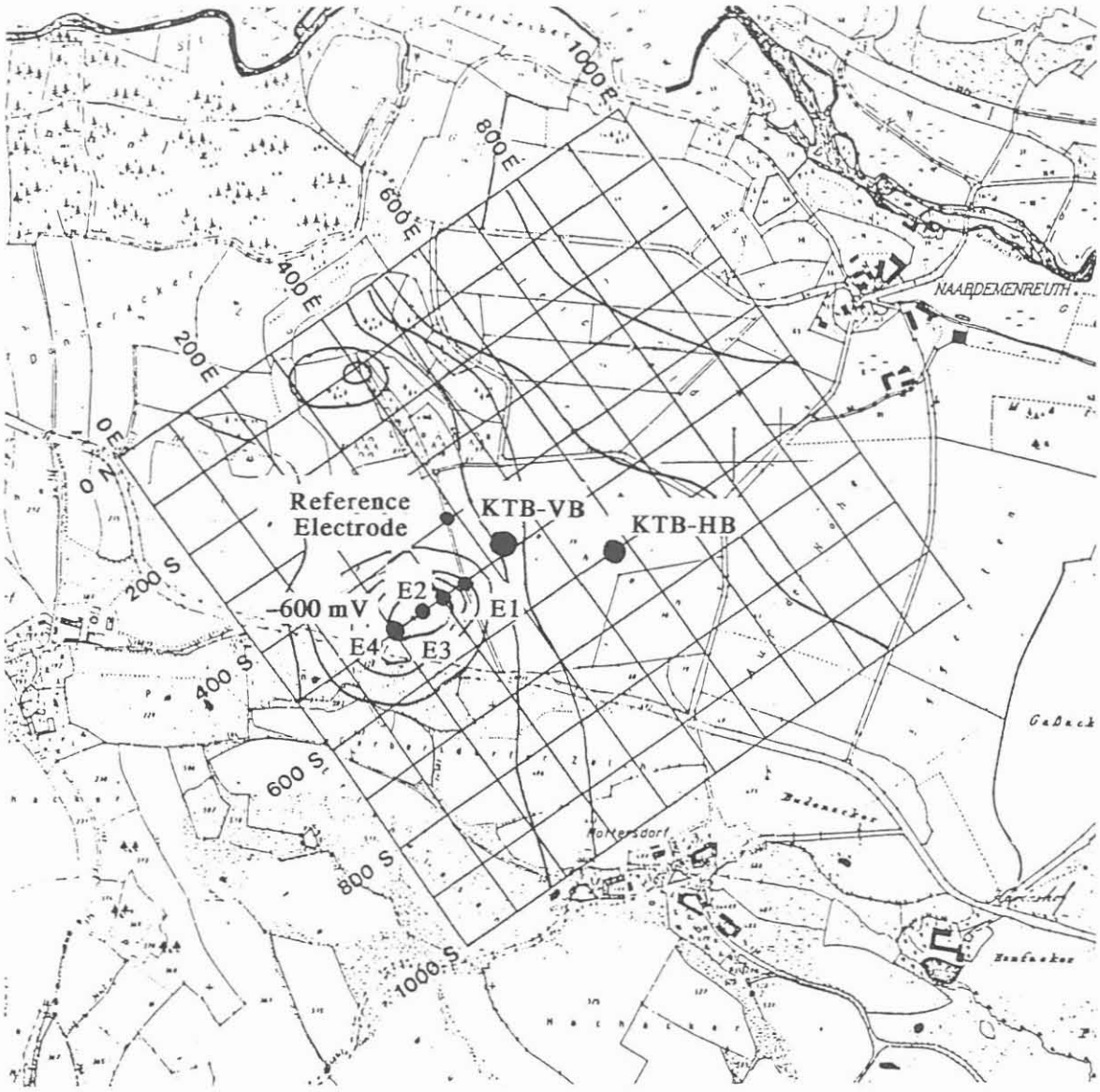

Fig.2

Location map of the KTB drilling site and of the potential electrodes (E1, E2, E3, E4) on the 1 km^2 net. The isolines represent the self-potential anomaly which extends close to the KTB boreholes. The distance between two isolines amounts 50 mV. The potential difference of the electrodes E1.. E4 is measured to the reference electrode.

(B): polarity I
with injecting current (KTB-VB positive, KTB-HB negative)

BE -> E1 : -538 mV
" -> E2 : -870 mV
" -> E3 : -953 mV
" -> E4 : -878 mV

(C): polarity II
with injecting current (KTB-VB negative, KTB-HB positive)

BE -> E1 : +465 mV
" -> E2 : +436 mV
" -> E3 : +383 mV
" -> E4 : +480 mV

3.2 Results

Before injecting the current into the formation the measured potential V_{meas} at the points E1, E2, E3, E4 represents the static electrical potential field. During the experiment this is superimposed upon by the potential field DP of the injected current.

$$V_{meas} = EP + DP$$

Subtracting V_{meas} for one polarisation from the other reveals DP.

$$V_{meas}(positive) = EP + DP$$
$$V_{meas}(negative) = EP - DP$$
$$DP = (V_{meas}(pos.) - V_{meas}(neg.)) / 2$$

Where it occurs, the potential DP is influenced by electric conductors, especially if these conductors are close to the electrodes E1..E4 and are connected with one or both of the boreholes. In order to obtain this influence, the potential DP is compared with a calculated potential CP in a homogenous halfspace considering line electrodes which represent the casings under voltage. The equipotential surface of such line

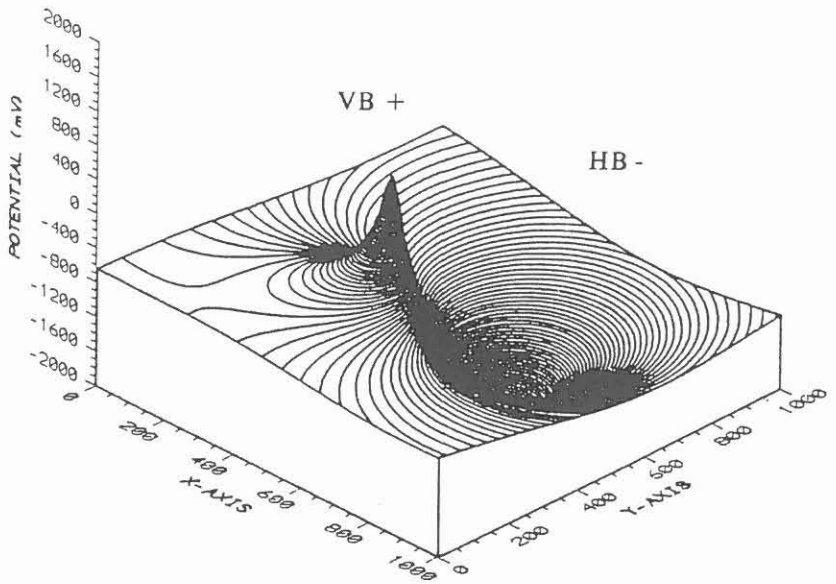

Fig. 3a

Calculated potential CP on the 1 km^2 net of Fig.2 considering electrodes with a length:
L (KTB-VB) = 4000 m
L (KTB-HB) = 6000 m

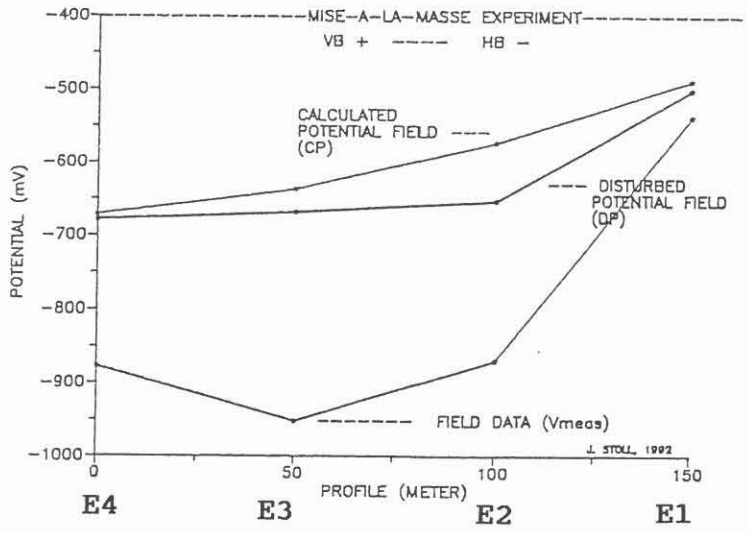

Fig.3b

Representation of the measured field data (V_{meas}) of polarity I. The disturbed potential DP is yielded by removing the self-potential (EP) from the field data Vmeas. These are compared with the calculated potential CP.

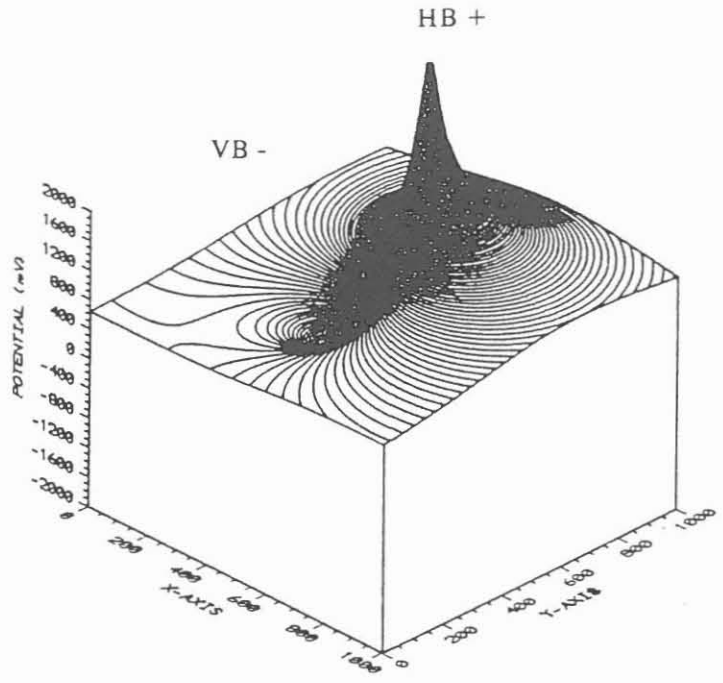

Fig. 4a

Calculated potential CP on the 1 km^2 net of Fig.2 considering electrodes with a length:
L (KTB-VB) = 4000 m
L (KTB-HB) = 6000 m

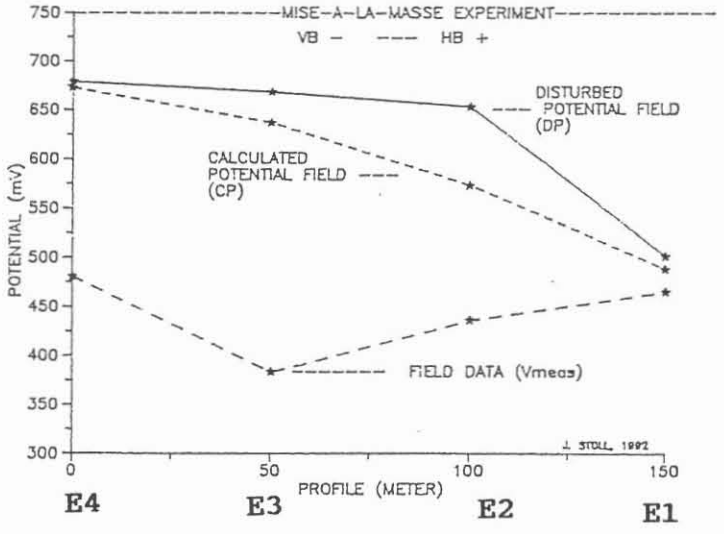

Fig.4b

Representation of the measured field data (V_{meas}) of polarity II. The disturbed potential DP is yielded by removing the self-potential (EP) from the field data Vmeas. These are compared with a calculated potential CP.

electrodes correspond to the shape of a hyperboloid of revolution. They are calculated by the following equation (Keller and Frischknecht, 1982):

$$CP = CP^{+} + CP^{-} \quad , \text{ where } CP = -CP^{+}$$

where

$$CP^{+}(Z,r) = \frac{\rho * I}{4 * \pi} \; LN \; \frac{Z + L + [r^2 + (Z + L)]^{\frac{1}{2}}}{Z - L + [r^2 + (Z - L)]^{\frac{1}{2}}}$$

Z and r are cylindrical coordinates measured from the midpoint of the electrode; L is the electrode half-length, also measured from the midpoint to one end of the electrode; ρ is the resistivity (Ωm) and I (A) is the injected current. For the boreholes in question, L = 2000 m (KTB-VB), L = 3000 m (KTB-HB)

For this arrangement the potential field was calculated inside a 1 km^2 area referring to both polarities and using an injection current of 22 A (Fig. 3a and 4a). The larger depth extension of the main borehole causes a greater width of the potential field. The figures 3b and 4b show the field data (V_{meas}) referring to both polarities, the potential DP, which is disturbed by the electronic conductor, and the calculated potential CP of a homogeneous halfspace. So far as possible the potential CP was matched to the DP by varying the resistivity of the halfspace using 310 Ωm at least. This value corresponds rather well to the resistivities which were observed at AMT stations close to the KTB site (Leonhardt, 1987). Nevertheless an absolute difference of about 75 mV of opposite sign for each polarities can be detected at electrode E2 (Fig. 5).

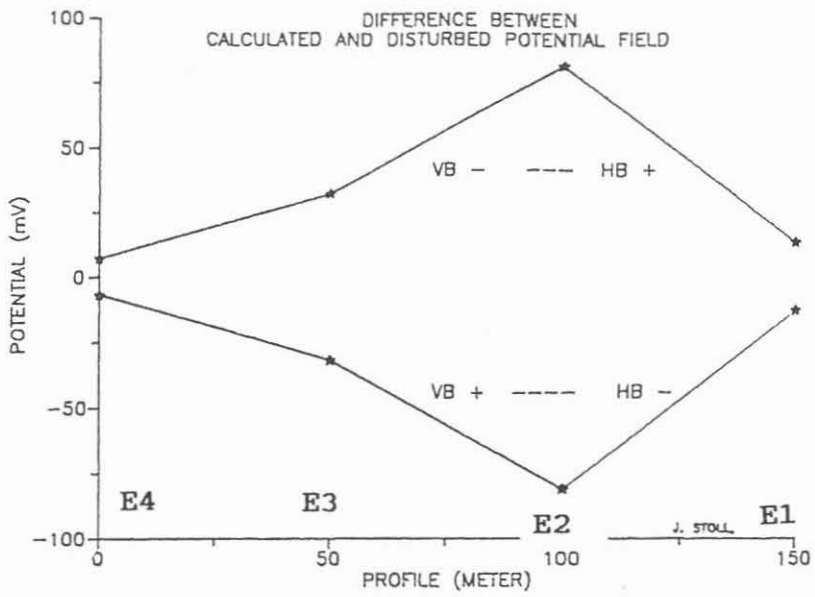

Fig.5

Differences between the CP, which contains the influence of an electric conductor (e.g. graphitic layers) close to the ground electrodes onto the injected potential field, and the calculated potential CP.

4. Discussion

The Mise-à-la-Masse experiment is designed to detect differences between the disturbed potential field (DP), which is influenced by electric conductors in contact with the boreholes, and an undisturbed potential field. This undisturbed potential is obtained by using the above formula. The essential observation consists in the simultaneous change in sign of this potential difference with a change in polarity. This indicates that there is a conducting zone in contact with one of the boreholes. This concept is further illustrated by the following three possibilities:

A: A steeply inclined layer has contact with the pilot borehole and outcrops in the vicinity of the potential electrodes (Fig. 6a). In consequence of the low resistivity of this layer the current is conducted close to the surface and causes a local maximum in the potential field when the KTB-VB has positive polarity.

B: A conductive layer has contact with the main borehole, and outcrops just in the vicinity of the electrodes (6b). This produces a minimum in the potential field in the case of a negative polarity at the KTB-HB.

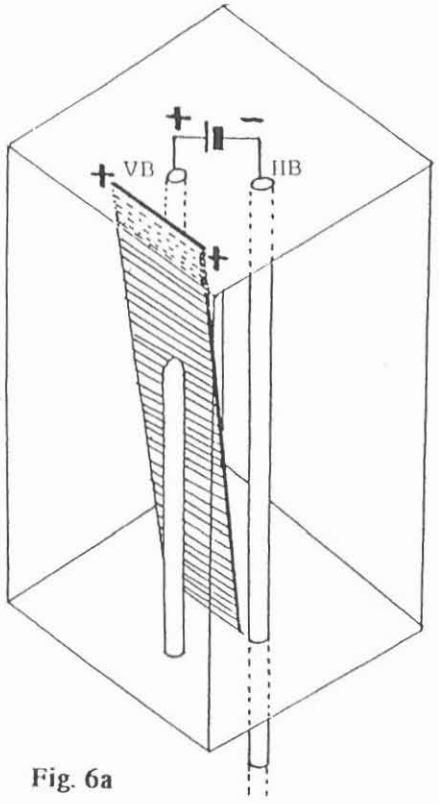

Fig. 6a

conductive layer with contact to the KTB-VB

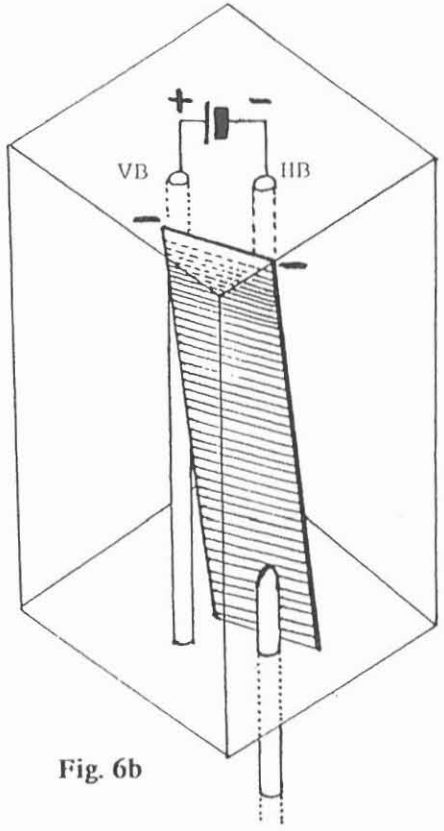

Fig. 6b

conductive layer with contact to the KTB-HB

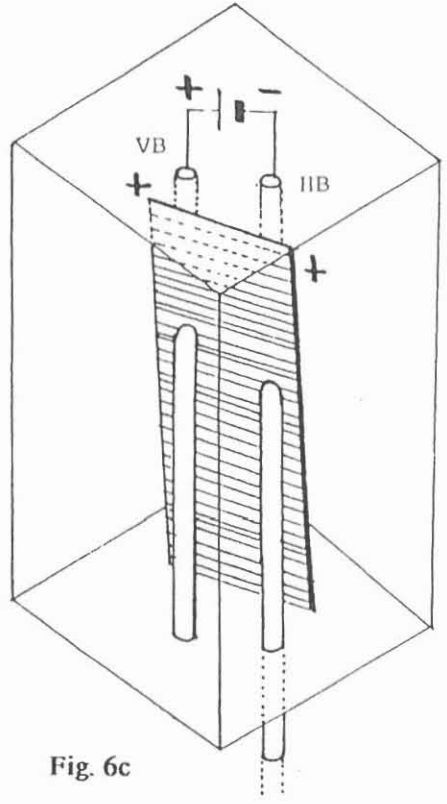

Fig. 6c

conductive layer with contact to both boreholes

C: At least a conductive layer has contact with both boreholes. In this case the potentials reveal a superposition of both contacts but the difference depends from the distance between the contact and the potential electrodes.

During the experiments the potential differences at the potential electrodes show a local minimum at polarity I and a local maximum at polarity II (Fig 5). With reference to the above three cases this implies an electrical contact of a conducting zone with the main borehole. From the KTB boreholes it becomes evident that graphite is bounded to a number of steeply inclined shear planes corresponding to cataclastic zones within the gneisses. It accumulates as fine dispersed grains within the rock matrix but abundantly occurs on polished slickensides with a thickness of up to some centimeters (Zulauf, 1990). There is some evidence from the surface tectonic map of the KTB site (Hirschmann, 1992) for the existence of faults in the vicinity of the potential electrodes (Fig. 7b). Referring to the geological results these faults belong to the prominent bundle of the Nottersdorf fault zone (NSZ), which have an inclination of about 60^0 to the NE, cross the main borehole in the upper section between 250 to 1570 m depth (Hirschmann, 1992) and show strong graphitic and sulphuric mineralizations in some extent. Likewise some of them cross the pilot hole in the uppermost part between 0 and 515 m.

These oberservations lead to following conclusions:

a) Close to the KTB drilling sites there exist general conducting layers, which obviously extend over distances of several hundred meters.

b) Obviously these layers belong to the Nottersdorf fault zone which crosses the KTB boreholes.

c) These layers are enriched by strong, graphitic accumulations of up to several centimeters in thickness and seem to be responsible for the high conductivity zone over a large depth extent.

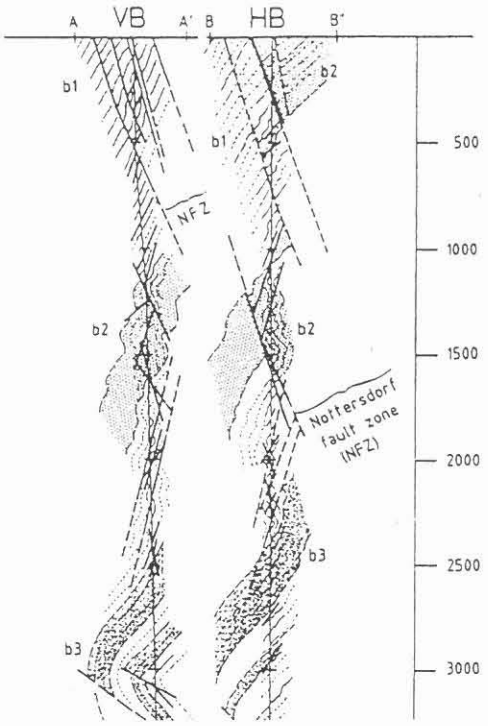

Fig. 7a

Structural interpretation of the pilot- and main borehole (Hirschmann, 1992)

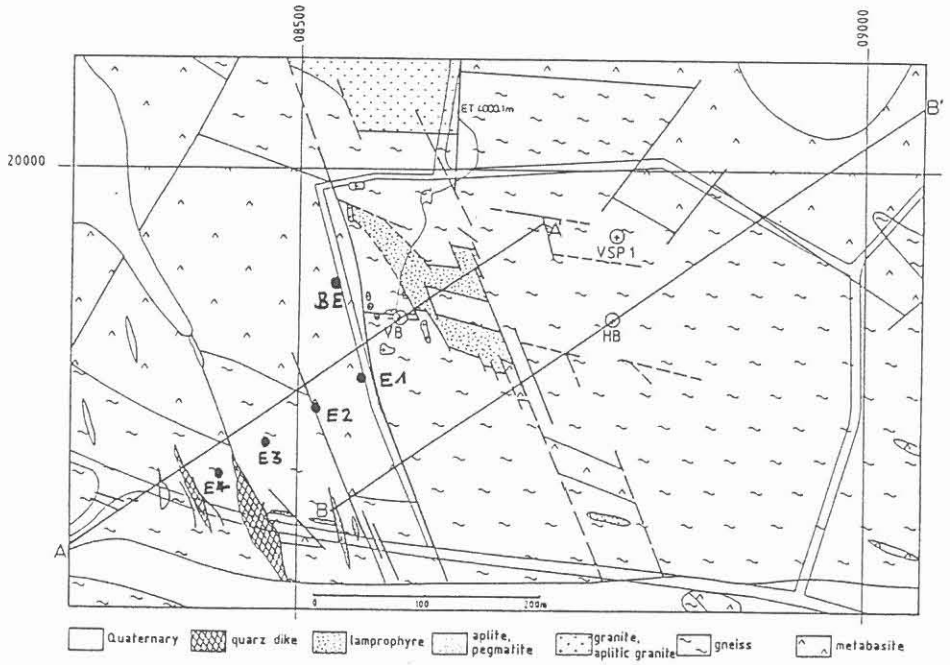

Fig. 7b

Geological map of the drilling site and its immediate surroundings. The lines A-A' and B-B' correspond to the lines in Fig. 7a (Hirschmann, 1992). The maximum and minimum of the difference curves in Fig.5 is located at electrode E2 and coincides with one fault of the Nottersdorf zone.

Acknowledgements

I would like to thank Dr. W. Kessels (Project Management of the KTB in the Geological Survey of Lower Saxony) for his initiative to carry out this experiment in the KTB and M. Sowa (KTB), who mounted the system and performed the injection of the current.

References

HAAK, V., STOLL, J. and WINTER, H., 1991. Why is the electrical resistivity around the KTB hole so low? Phys. Earth Planet. Int., 66, pp. 12-23

HIRSCHMANN, G., 1992. The geological section of the KTB-Hauptbohrung - Correlation with the KTB Vorbohrung and preliminary structural interpretation. in: R. Emmermann, H.-G. Dietrich, J. Lauterjung and Th. Wöhrl (eds.) KTB-Report 92-2 KTB Hauptbohrung, Results of the Geoscientific Investigation in the KTB field laboratory 0 - 6000 m, pp. B47 - B52

KELLER, G.V. and FRISCHKNECHT, F.C., 1982. Electrical methods in geophysical prospecting. International series in electromagnetic waves, Vol. 10. Pergamon Press

LEONHARDT, F.,1987. Audiomagnetotellurische Untersuchungen in der Oberpfalz. Diplomarbeit, Technische Universität Berlin, 91 pp.

SATO, M., MOONEY, H.M., 1960. The electrochemical mechanism of sulfide self-potentials, Geophysics, 25, 1, pp. 226-249

STOLL, J., 1990. Messung der Eigenpotentialanomalie im KTB-Umfeld und deren Interpretation. in: K. Bram (Hrsg.), KTB Report 90-3, Ergebnisse geowissenschaftlicher Umfelduntersuchungen, Elektromagnetische Tiefensondierung, S. 173 ff

ZULAUF, G., 1990. Spät- bis postvariszische Deformationen und Spannungsfelder in der nördlichen Oberpfalz (Bayern) unter besonderer Berücksichtigung der KTB-Vorbohrung. Frankfurter Geowissenschaftliche Arbeiten, Serie A Geologie-Paläontologie, Band 8

DETERMINATION OF ELEMENTS THROUGH GEOCHEMICAL LOGGING IN CRYSTALLINE ROCKS OF THE KTB-OBERPFALZ HB

H. Gatto

Abstract

Measurements of elemental concentrations contribute significantly to enhance interpretation of quantitative estimation of minerals which make up the complexity of crystalline rocks. Through recent developments, the most abundant and a few rare elements in the earth's crust can be determined in counting natural activity, delayed activation and prompt neutron-induced capture gamma rays. Whereas K and Al are obtained directly in weight percent through proper algorithms, a geochemical "closure model" is normally used to derive experimentally Si, Ca, Fe, Ti, S and Gd. This procedure is based on the fact that the rock elemental oxides, measured in weight %, sum up to 100%. Major unmeasured elements like O, C, Mg and Na are compensated in assuming that each element is present as one single oxide or carbonate and in using optimized oxide factors for those measured. The validity of this model, developed originally for sedimentary rocks, has been tested by comparison with data from an X-ray fluorescence analysis (XRF) on cuttings.

On the other hand, the densely spaced XRF data, sampled every 2m on average, made it possible to calculate the amount of oxides which can be measured with this tool string. Although lithology dependent, the sums of these oxides show little variation within each rock, so that their averaged values have been used in conjunction with the true oxide factors in the "KTB model". The agreement between the two models on one side and the XRF data on the other can be considered as very good.

Introduction

In the superdeep well of the German Continental Deep Drilling Project (KTB), the open hole section from 6018 to 3000m was recorded with the Geochemical Logging Tool (GLT) of Schlumberger in two sections. The first run took place on October 14, 1991, from 4450m to 3000m, the second on March 14, 1992, from 6007m to 4400m. Due to the large borehole diameter of 14 3/4" with increasing breakouts in the deeper part, the interest was focused on how to minimize and eventually correct these effects.

Consultant, KTB Logging Center, P.O.Box 67
D-92667 Windischeschenbach, Germany

The determination of elemental concentrations through logging provides continuous information on geochemistry and ultimately a better knowledge of quantitative mineralogy. It is achieved through an analysis that combines gamma ray intensities from natural activity, prompt thermal neutron capture reactions and delayed activation to obtain elemental concentrations for ten elements. Despite this fact, not all of the elements present in sufficient quantities can be measured when using NaI detectors. In this well, it is the case for such major elements like Na and Mg. Two models are therefore described to relate the concentrations of measured elements to the unmeasured ones.

Spectral processing of capture gamma rays

It is assumed that the downhole capture spectrum can be represented as a linear combination of the spectrum of each individual element, the so called "standards". These standards represent the spectrum of each pure element. The way these coefficients or fractional elemental gamma ray "yields" are determined is through weighted least squares fitting and the results of the total spectral signal shown in Fig. 1.

This total signal is composed of a formation and a borehole signal. In general, information originating from the borehole is difficult to characterize and therefore not used in geochemical analysis. For this reason, yields from hydrogen and background are not used, although the represent roughly 40% of the total spectrum. The capability of eliminating yields which in the case of the KTB borehole do not contribute to the measured gamma ray spectrum and are below the tool's detection limits has been used to exclude chlorine and sulfur. This selective elimination improves the statistical precision of the elements remaining. The renormalized yields are displayed in Fig. 2.

Elemental processing

To perform a comprehensive elemental analysis involves three separate modes of gamma ray spectroscopy. A set of spectrometers has been assembled to measure absolute elemental concentrations in the rocks. This includes a spectrometer for natural activity, one for delayed activation of Al and one for measuring prompt gamma rays following thermal neutron capture. With the present tool string this data is collected through a single run into the hole. At present, NaI-detectors are commonly used, as they can be operated up to 150°C.

Natural Spectroscopy: K, Th and U

The concentrations of these elements are derived from the gamma ray spectrum recorded from naturally occurring radioactive elements and their daughter products. Among those elements only K is relevant for further elemental analysis, since its total is located within the percentage range. The count rates obtained are directly proportional to weight percent of that element in the formation.

Delayed Activation: Al

In Al activation, the natural isotope Al-27 absorbs thermal neutrons and produces the isotope Al-28, which decays with a half-life of 2.24 min, emitting a 1779 keV gamma ray. Interference with other isotopes is reduced to a low level by using a Cf-252 source. During neutron irradiation, the Al radioactivity reaches saturation, at which point the rate of production and decay are in balance. The gamma rays are counted and the Al spectrum is determined by subtracting the natural gamma ray count rate from the detector situated above the source.

The aluminum count rates must be corrected for the complex effects of borehole environments on the neutron and gamma ray physics. Important factors influencing the gamma ray flux are the neutron slowing down length, the formation and borehole absorption cross section, formation density and the borehole size. The environmental correction algorithm taking care of the terms mentioned above, ignores however any varying stand-off between source/detector and borehole wall, which can be observed in break-out zones below 5000m.

Such a zone is depicted in Fig. 3, where the pronounced reduction in Al-measurement is due to stand-off.

Pulsed neutron-induced capture: Si, Ca, Fe, Ti, S and Gd

The detectable gamma ray flux for each element is proportional to the product of its concentration and its thermal neutron capture cross section. Therefore an element which does not produce enough gamma rays or has a very low neutron capture cross section cannot be detected. For the two dominant rocks in this well, their respective sensitivity products (s.p.) of typical elemental concentrations (wt%) and thermal neutron capture cross sections [barns] divided by its atomic weight (A) are shown for certain elements in Table 1.

Table 1

Elem.	Capture Cross Section	A	Paragneiss		Metabasite	
			wt%	s.p.	wt%	s.p.
Si	0.16	28	30	0.17	24	0.14
Fe	2.56	56	4	0.18	7	0.31
Ca	0.43	40	1	*0.01	6	0.06
Ti	6.40	48	.5	0.06	1	0.13
S	0.52	32	.2	*0.003	.1	*0.001
Gd	49000	157	.0008	0.25	.0008	0.25
K	2.10	39	2	0.10	.7	0.04
Al	0.23	27	8	0.07	8	0.07
Na	0.53	23	2	0.05	3	0.06
Mg	0.06	24	2	*0.005	4	*0.01

Elements in this well which are below the present tool's threshold level of 0.025 for the sensitivity product are marked with an asterisk. Their determination will be difficult, as is the case for S and Mg in both dominant rocks and for Ca particularly in the paragneiss. Another point is the similarity between gamma ray spectra as is the case for Al and Fe. Their principal capture gamma ray energies fall within the resolution of the NaI-detector and can therefore not be separated. However, as discussed, Al is most efficiently detected through delayed activation. The same applies for Na, but its detection is not implemented.

The determination of absolute elemental weight fractions by gamma ray detection is very difficult in the borehole environment. However, relative concentration values can be obtained by dividing each elemental yield Y_i, by a relative spectral sensitivity factor S_i, which is a tool constant determined in the laboratory. These relative concentrations are then related to absolute ones, expressed as weight fractions W_i, by a depth dependent normalization factor F, such that $W_i=FY_i/S_i$. This normalization factor is a complex function of numerous parameters and cannot be calculated directly due to an unknown and variable neutron source output. Therefore

other approaches are needed to obtain F.

Geochemical closure model

This method developed by Grau et al, 1989, is based on the fact that the sum of all elemental weight fraction is unity. It is intended for a broad applicability in all types of rocks, although originally conceived for clastic sediments. However assumptions must be made, as important elements like C, O, Mg and Na, which can contribute substantially to the total weight fraction, cannot be measured with this tool. The closure model takes care of the unmeasured C and O, in assuming that each of the measured element is present as one single oxide or carbonate, which is not true for Ca, Fe and S. The sum of these oxides/carbonates is then made equal to 100, in solving for the calibration factor F at each depth level. This method gives adequate results, except in cases, where Mg and Na is present.

Mathematically it can be expressed as:

$$F(\Sigma X_i Y_i / S_i) + X_K W_K + X_{Al} W_{Al} = 100$$

where:

F	is the normalization factor
Y_i	the yield attributable to element i
S_i	the relative sensitivity for element i
X_i	associated oxide/carbonate factor of element i
W_{Al}	the aluminum weight fraction
W_K	the potassium weight fraction

To account for other important unmeasured elements, such as Mg and Na, some oxide factors were optimized on core samples as listed in Table 2. By this method errors are minimized and dispersion from the ideal 100% fall within 5% on either side, comparable to the statistical precision of the downhole measurements. Fig. 4 depicts XRF data and log-derived weight fractions.

This condition satisfies all but one major mineral found in this well, with the exception being Ca feldspar. When using above stated equation, its closure sum amounts to 129%, therefore introducing an error of 6% from an estimated concentration of 20% Ca feldspar. The situation is worse for Pyrite with a closure sum of 156.7%, but since its concentration is small, the error it causes is negligible.

Table 2

Element	Oxide	Closure Model Oxide Factor	KTB Model Oxide Factor
Si	SiO2	2.139	2.139
Fe	Fe2O3	2.075	1.429
Ca	CaO	2.497	1.399
Ti	TiO2	1.668	1.668
K	K2O	0.615	1.204
Al	Al2O3	2.741	1.889

KTB model

A somewhat different approach has been adopted for this well. Its application is however limited to cases, where two preconditions are fulfilled, namely the availability of XRF data and a lithological profile containing only a few rock types. Being the case, the XRF oxides fractions were summed up for all measurable elements detectable through downhole spectroscopy. The histograms in Fig. 5 show that very little variation can be observed in the two main rocks. So for instance totals the mean in the paragneiss 90.7% with a standard deviation (sd) of 1.2 and in the metabasite 85.3% with a sd of 1.0. The sum of 100% in the above formula was therefore changed to these means and triggered according to the prevailing lithology. Using the true oxide factors eliminated also the uncertainty in the calculation with optimized factors for sediments in crystalline rocks.

One further improvement, although not limited to this model, is the possibility of applying a cut-off on unrealistic low values for Al concentrations in breakout zones. This allows a better fractional distribution for the other elements. The log-derived and XRF data are displayed in Fig. 6.

Discussion of results

The results of elemental processing from 3000 to 6010m are compared with XRF data analysed by the KTB field laboratory on cuttings. In general the agreement is good,

as can be seen in the annex in Plots 1a,b,c. Major discrepancies are observed for the elements Th and U. Especially for Th, the differences seem to worsen with increasing depth with XRF data propably too high in the metabasites. A comparison for the element Al reveals good agreement in the top section. Differences are limited to intervals where the borehole is severly ovalized, as below 5000m. Despite trials to orient the tool towards the short axis, which is more or less in gauge, occasional tool rotations into the long axis are responsible for this reduction in quality. For the other elements, the agreement is better for the first logging run than for the second.

Conclusions

The availability of XRF data, although not compulsory, is useful to compare with the geochemical data from in-situ spectroscopy. Whenever differences occur, they might be attributed to cavings which contaminate the cuttings.

The differences between the two models are minor, and within the range of the differences of two consecutive runs using either model. This implies that the optimized oxidation factors of the geochemical closure model, developed for sediments, are also valid for the crystalline rocks encountered in the KTB well.

The results of elemental determination by both geochemical models are in good agreement with XRF data.

Nomenclature

K ..potassium
Si ..silicon
Al ..aluminum
Ca ..calcium
Fe ..iron
Ti ..titanium
Gd ..gadolinium
Cf ..californium

References

Grau J. A. and Schweitzer J. S. (1987) Prompt gamma ray spectral analysis of well data obtained with NaI(Tl) and 14 MeV neutrons. Nucl. Geophys. 1 157-165.

Grau J. A. and Schweitzer J. S. (1989) Elemental concentration from thermal neutron capture gamma ray spectra in geological formations. Nucl. Geophys. 3 1-9.

Grau J. A. and Schweitzer J. S. and Herzog R. C.(1990) Statistical uncertainties of elemental concentrations extracted from neutron-induced gamma ray measurements. IEEE Trnas.Nucl.Sci. 37 2175-2178.

Herron M. M. (1987) Future applications of elemental concentrations from geophysical well logging. Nucl. Geophys. 3 87-96.

Hertzog R. et al. (1987) Geochemical Logging with Spectrometry Tools. SPE 16792.

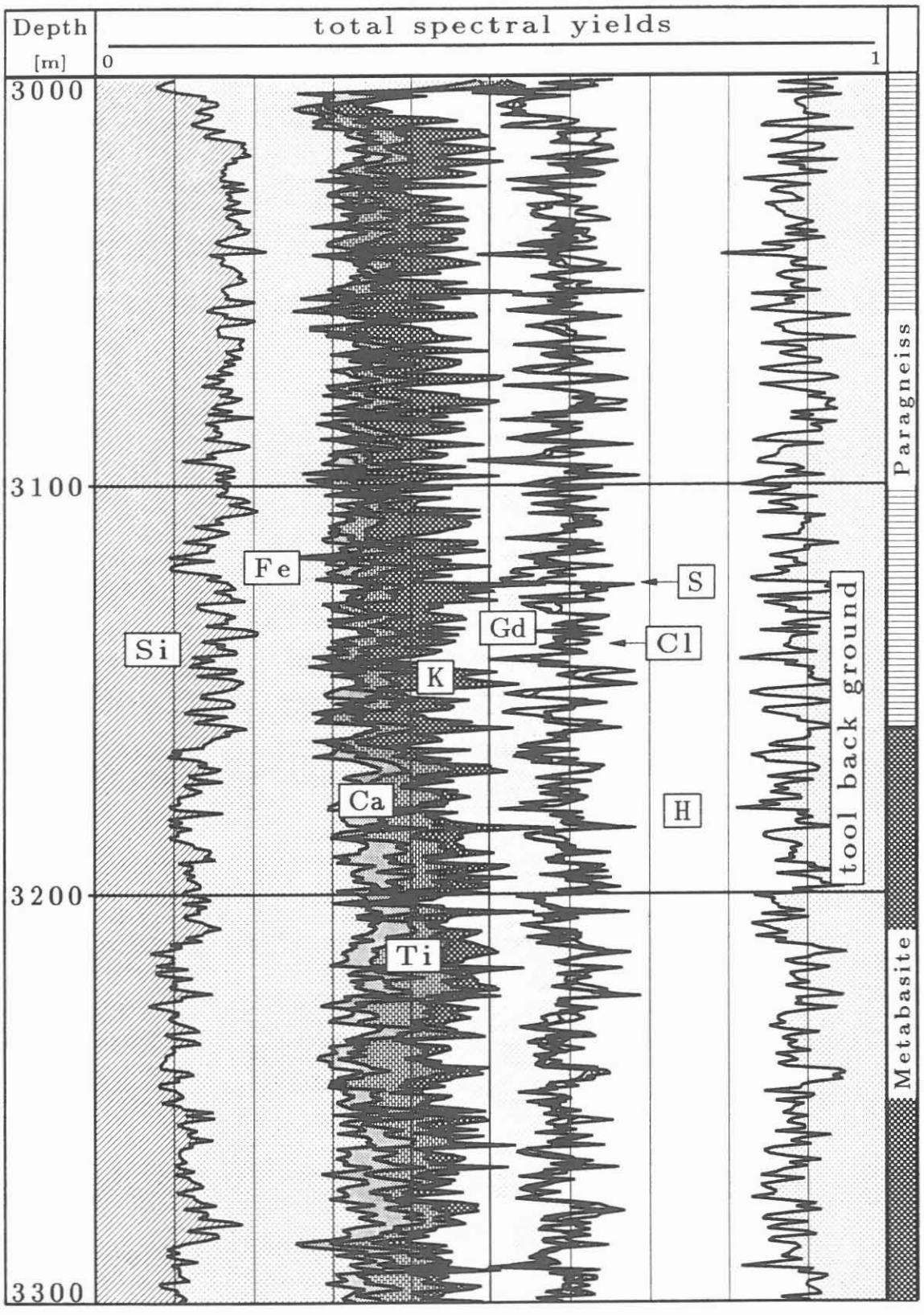

Fig.#1: Total spectral yields

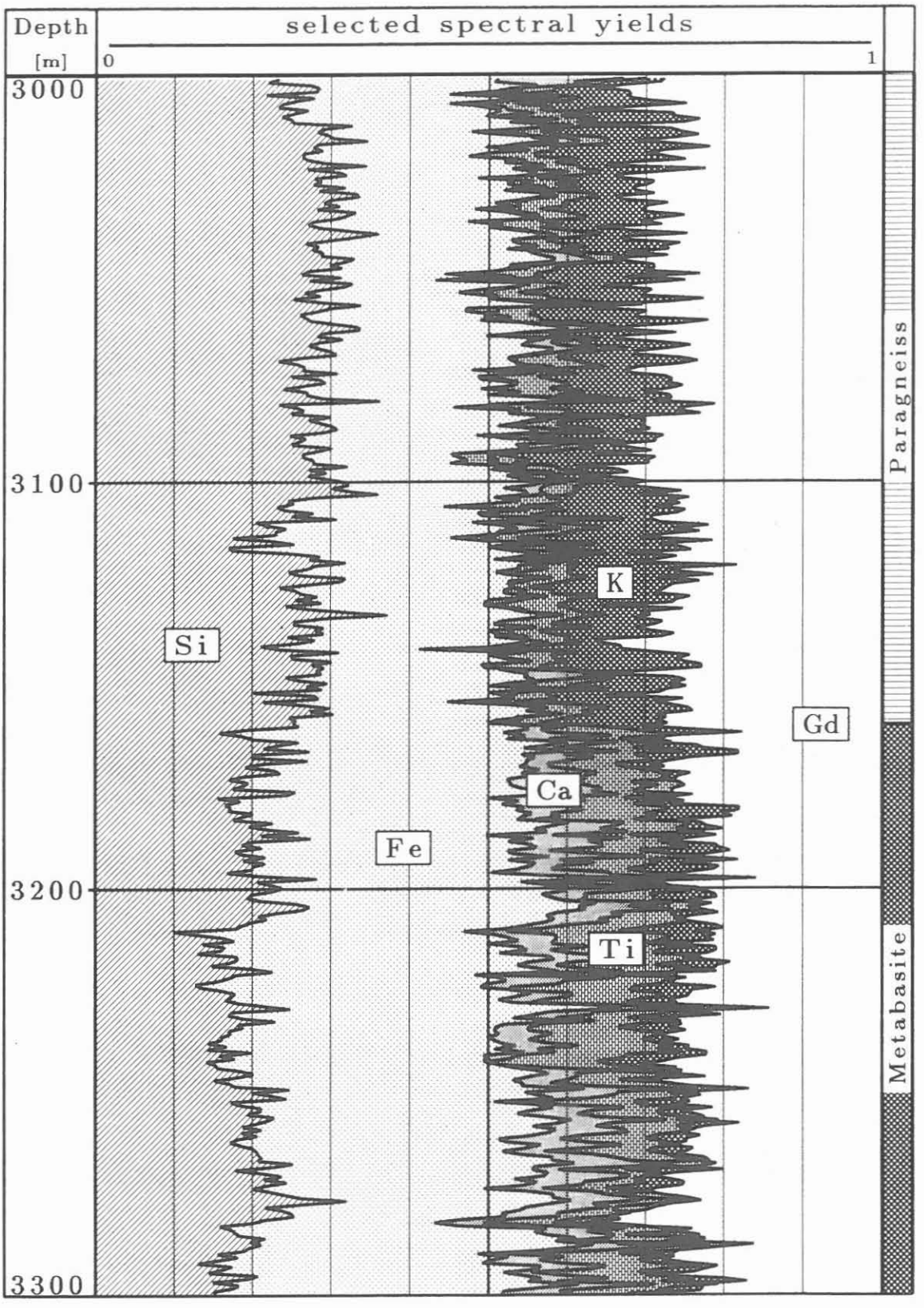

Fig.#2: Selected spectral yields (normalized)

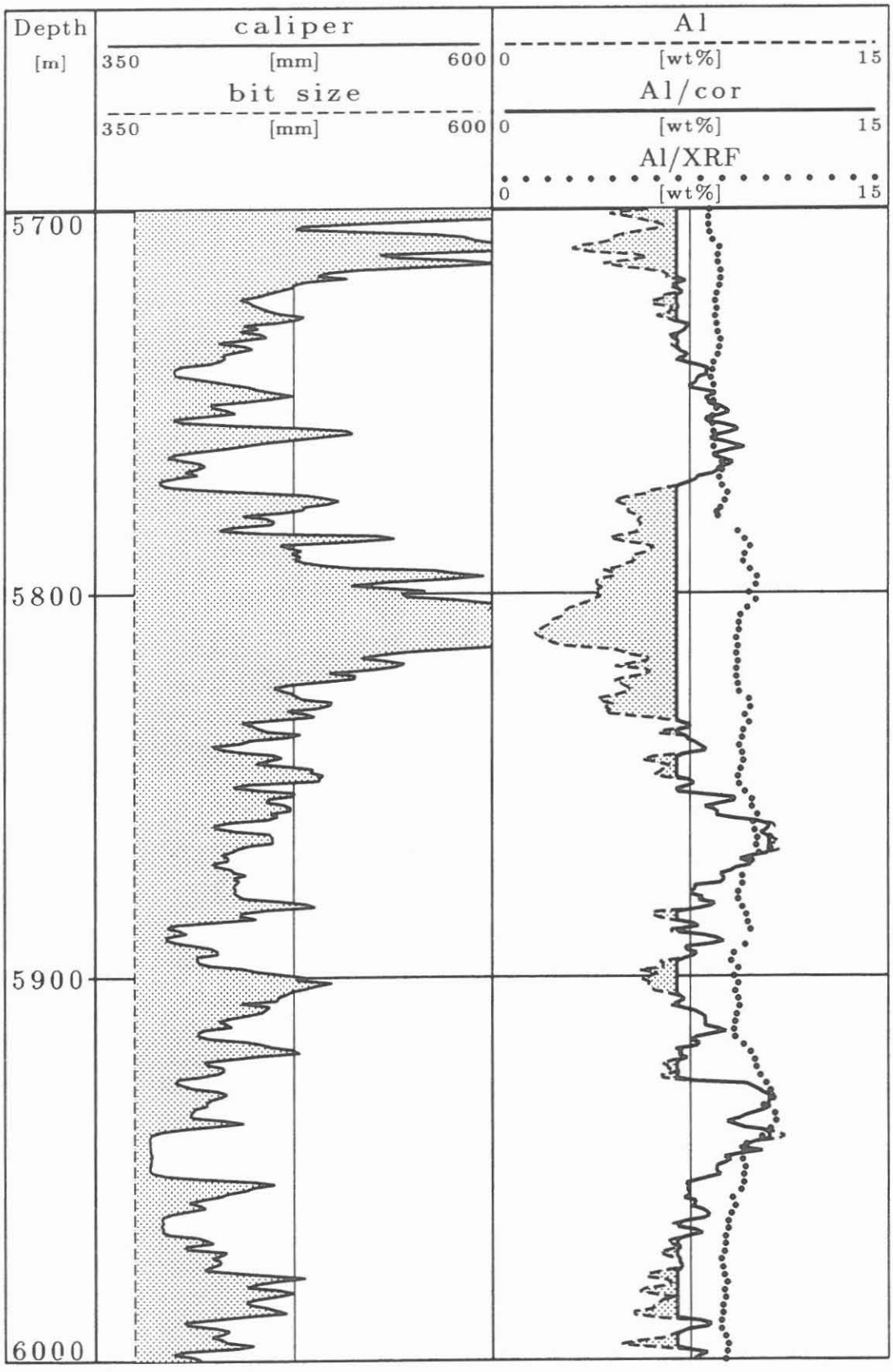

Fig.#3: Cut-off for unrealistic low Al values in break-outs

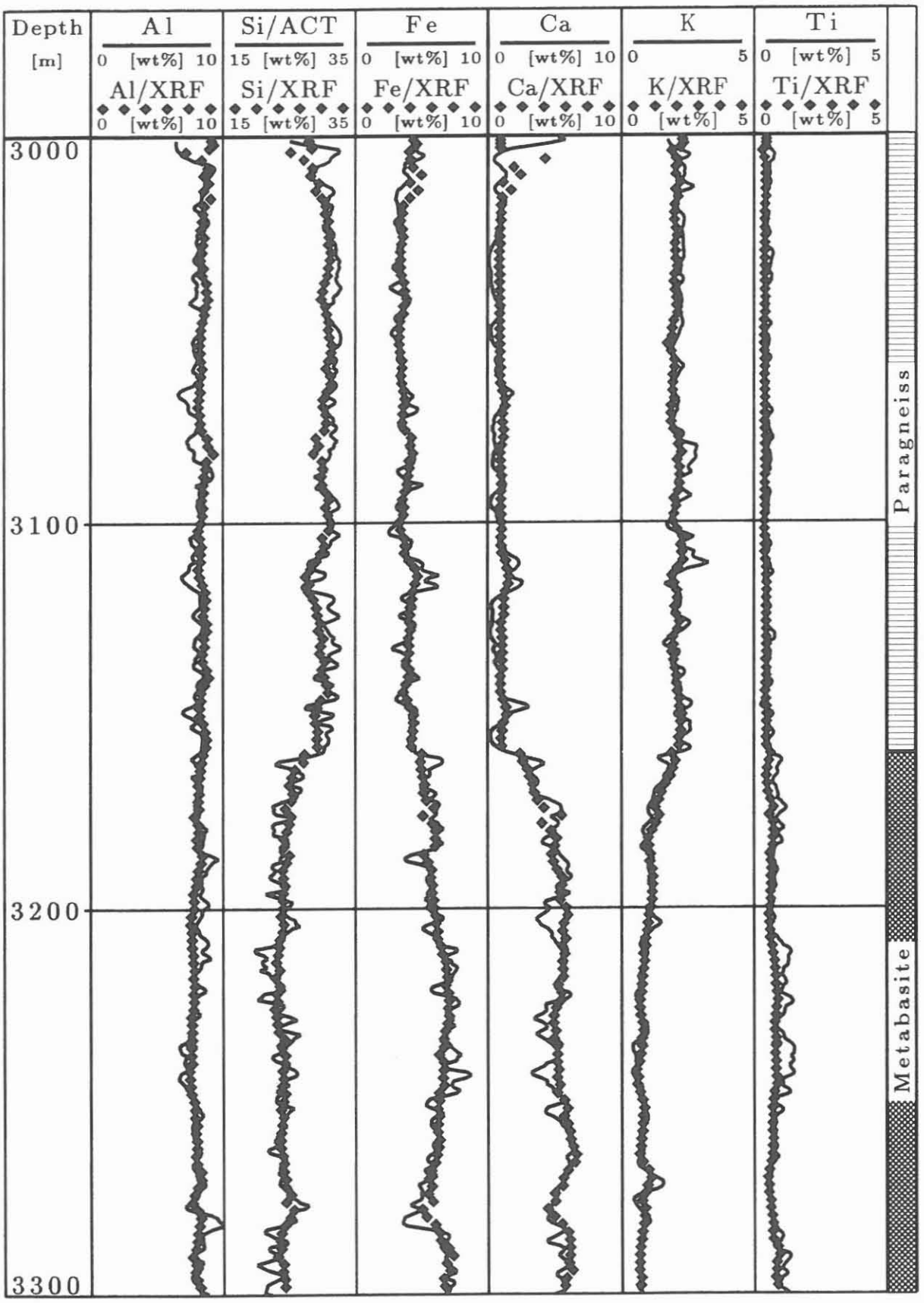

Fig.#4: Log-derived elements (closure model) and XRF

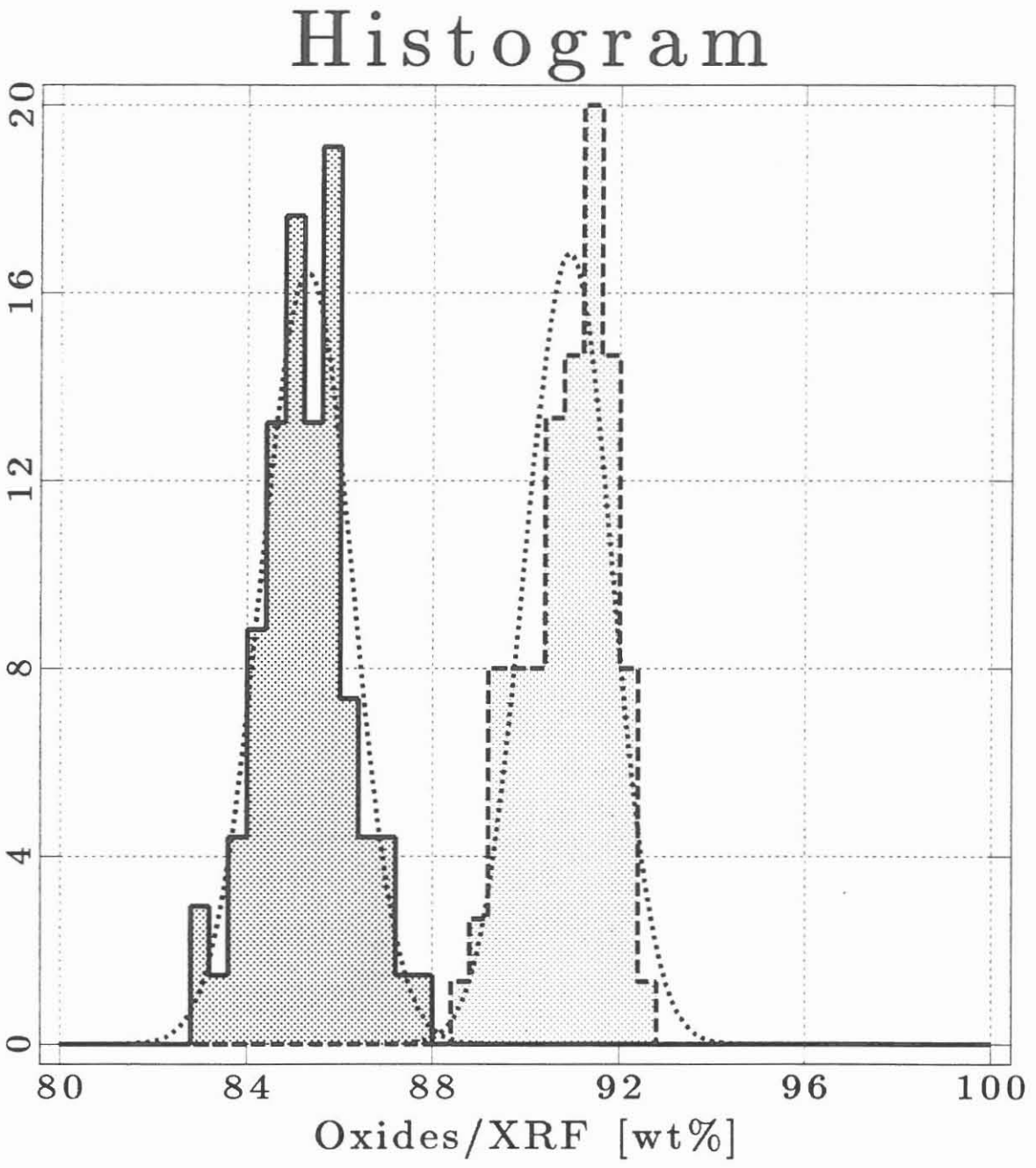

Fig.#5: Oxides/XRF sum of Al+Si+Fe+Ca+Ti+K
in metabasite/ mean= 85.3, stand.dev.= 1.0
in paragneiss/ mean= 90.7, stand.dev.= 1.2

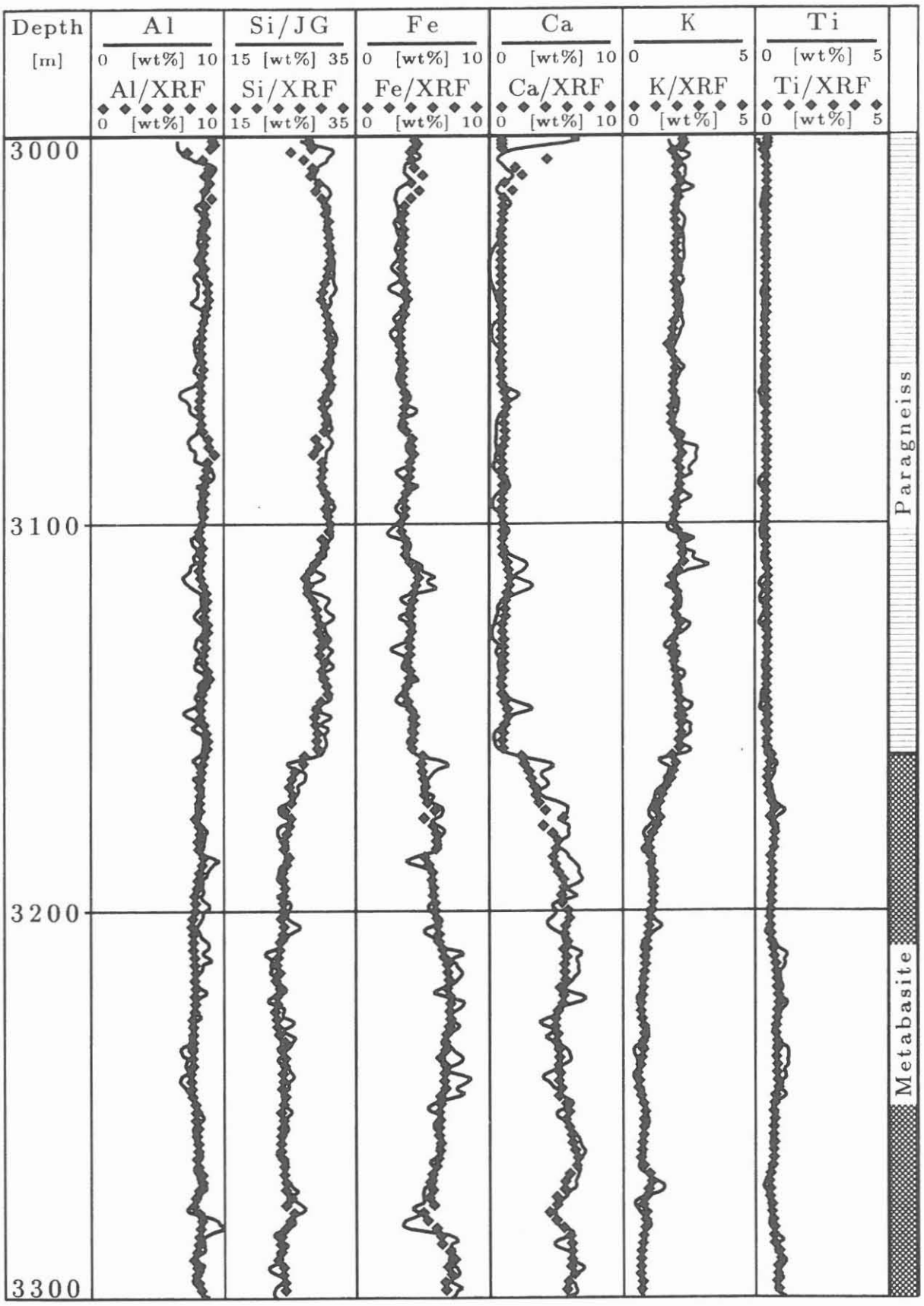

Fig.#6: Log-derived elements (KTB model) and XRF

EFA-LOG - The upper 3 km of the KTB-Hauptbohrung

R. PECHNIG & J. WOHLENBERG
RWTH Aachen, Lehrgebiet für Angewandte Geophysik, Lochnerstr. 4-20, 52064 Aachen

Summary

The main target of the research project EFA-LOG is the reconstruction of the lithology of the drilled through rocks in the scope of the Continental Deep Drilling Project (KTB), by using borehole-geophysical measurements. HAVERKAMP & WOHLENBERG (1991) developed a log interpretation technique enabling a transformation of logging responses to lithological characteristics also for crystalline rocks. Based on this method, succesfully tested in the KTB-VB, also for the uncored section from 280 m to 3000 m of the KTB-HB an unbroken synthetic lithological profile, the EFA-LOG, could be reconstructed. In contrast to the extensively measured KTB-VB only the logs of NGS, DLL and SDT were available for the interpretation of the first 3 km of the KTB-HB. Nevertheless 16 of 37 electrofacies calibrated at the lithology of the KTB-VB could be transferred to the logs of the KTB-HB in so far, that besides various gneiss- and amphibolitevarieties, also meta-gabbros and cataclastic or faulted zones could be reliably differentiated in the resulting EFA-LOG. Even for hitherto unobserved lithotypes, like the plagioclas-rich gneisses, a clear identification was possible. To established an EFA-LOG from only a few geophysical data sets will be important to reconstruct deeper sections of the KTB-HB when high temperatures will limit data acquisition.

Introduction

To understand the lithological conditions of the crystalline basement drilled through is one of the major objectives of the KTB-project. To reach this target the application of borehole-measurements is of fundamental importance, especially when cores are taken only rarely and geophysical logs are, besides the cuttings, the most important information available, as is the case for the *KTB-Hauptbohrung* (KTB-HB). Geophysical logs, as a continuous in situ vertical data set reflect crystalline lithologies very well. This was shown by HAVERKAMP & WOHLENBERG (1991) when they applied a newly developed method to reconstruct the lithology of the KTB-Vorbohrung (KTB-VB). To calibrate geophysical data with the well-known lithology of the almost completely cored pilot hole an extensive database was built up characterizing all differentiated lithotyps by specific electrofacies patterns. The result was a synthetic lithological profile called EFA-LOG. Now the objective is to use the EFA-LOG to reconstruct the lithology of the KTB-HB assuming a similar lithology at both drill sites. In the following the results of the upper 3 km of the KTB-HB will be presented.

Method and Quality Control

The method is based on a calibration of the borehole measurements with the drilled lithology correlating the logs with all available petrographical, geochemical and petrophysical data for the rocks. So each differentiated lithological unit, normally characterized by a specific mineralogical composition, will be classified by an individual set of log responses. This resulting electrofacies stores the definite minimum and maximum values

of all logs used for each lithotype distinguishing one lithotype from all the others. The application of the calibrated electrofacies to the logs results in a continuous lithological profile, the EFA-LOG (HAVERKAMP & WOHLENBERG 1991).

With this approach 37 different electrofacies were defined in the KTB-VB, each one classified by 18 geophysical logs. Due to the reduced measuring program only six of these parameters (SGR, POTA, THOR, URAN, LLD and DT) are available for the EFA-LOG to reconstruct the section 280 - 3000 m of the KTB-HB (for the first 280 m no data are available). According to experiences gained in the pilot hole LLD and DT mainly reflect structural properties like cataclastics, faults and fissure zones. Being strongly affected by the anisotropy of the drilled rocks electric and sonic data are less suitable for detailed lithology determination. In contrast NGS data reflect lithological variations very well thus most of the calibrated electrofacies are discriminated by these logs.

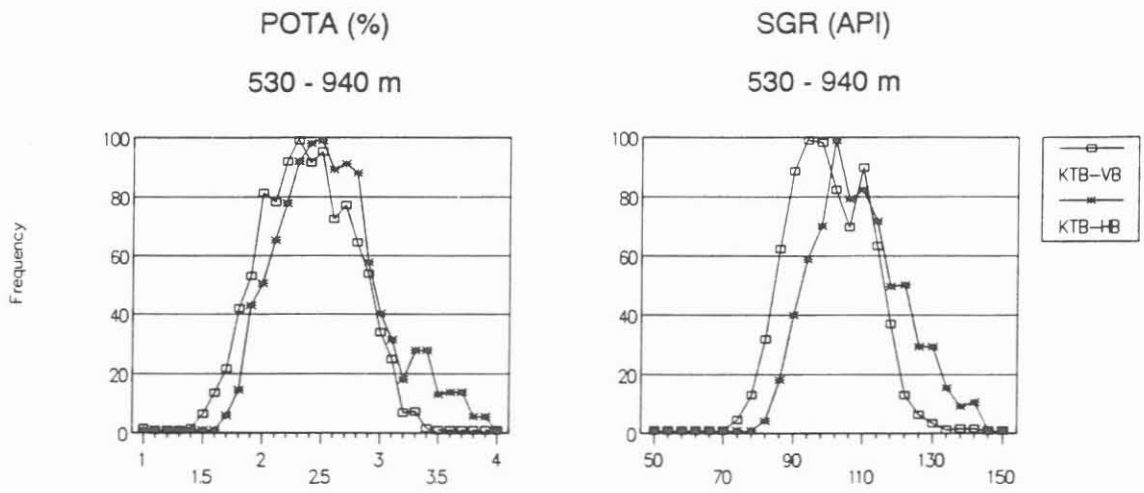

Fig. 1: Frequency distributions of the logs POTA and SGR in similar lithologies of the KTB-HB and KTB-VB.

	SGR (API)	POTASSIUM (%)	THORIUM (ppm)	URANIUM (ppm)
GNEISSES	+ 7	+ 0,15	+ 0,5	+ 0,8
METABASITES	+ 5	+ 0,20	+ 0,1	+ 0,4

Table 1: Average destinations of the KTB-HB NGS data in relation to the KTB-VB.

Transferring the electrofacies to the KTB-HB requires an extensive quality control including a comparison of the NGS logging data with laboratory measurements on cuttings as well as with KTB-VB logging data. Generally the correlation between laboratory and borehole measurements for the gamma ray and the evaluated contents of potassium,

thorium and uranium is obvious. In order to check the logs also for slight differences between KTB-HB and KTB-VB a comparision of the data obtained from similar lithological sections was carried through. The NGS data of the KTB-HB are systematically shifted to higher values (*Fig. 1*). These slight deviations, different in gneiss and massive metabasite units (*Table 1*), were taken into account by transferring the electrofacies to the logs of the KTB-HB.

Results

Similar to the pilot hole the drilling interval down to 3 km of the KTB-HB revealed a succession of gneisses alternating with metabasites and some minor intercalations of calc-silicates all crosscutted by younger lamprophyric and aplitic dykes. After different stages of metamorphism with major overprint under amphibolite facies conditions a deformation in the brittle field resulted in the formation of abundant, often graphite-bearing cataclasites (LICH 1992). Considering all relations between the rocks penetrated and the tool responses known from the KTB-VB, a detailed EFA-LOG was established for the upper 3 km of the KTB-HB (*Fig. 3-12*). Although much less logging data were available it was possible to transfer 16 of 37 calibrated electrofacies as well as to identify hitherto unobserved lithotypes. The typical lithological characteristics of the applied electrofacies defined for gneisses and amphibolites are summarized in *Table 2*.

GNEISSES:

IIb biotite potassium feldspar gneiss
+ graphite, ore minerals and radioactive accessories

IIIa hornblende garnet biotite gneiss
IIIb (hornblende) biotite gneiss with higher proportions of potassium feldspar

IVa-h alumino-silicate-bearing paragneisses
IVa phyllosilicate-rich
IVb quartz-rich
IVc very quartz-rich

modified by cataclastic overprint
IVd + graphite / ore minerals
IVe + graphite / ore minerals + potassium feldspar
IVg + graphite / ore minerals + radioactive accessories
IVh faulted or fissured without graphite

VIIa-b plagioclase-rich gneiss (calc-silicate-bearing)
VIIa + radioactive accessoires

AMPHIBOLITES:

3a,d,e garnet-bearing massive amphibolites
3b calc-silicate-bearing amphibolite
3f amphibolite which leads to hornblende gneisses

Table 2: Lithological characteristics of all applied electrofacies for gneissic and amphibolitic rocks establishing the EFA-LOG *in the upper 3000 m of the KTB-HB.*

In accordance with the cuttings profile the EFA-LOG is divided into six larger lithostratigraphic sequences. Down to 520 m the logs reflect a heterogenic, partly strong cataclastic overprinted gneiss/metabasite alternation (*Fig. 3*). In this section the maximum values of the upper 3 km KTB-HB were recorded by the NGS. Besides the main rock types of massive amphibolites (3a,d,e), paragneisses (IVa-c) and hornblende gneisses (IIIa) also varieties like calc-silicate amphibolites (3b) and (hornblende) gneisses (IIIb) with high contents of potassium feldspar are separated in the EFA-LOG. Various cataclastic rock types all characterized by low measured resistivities could also be distinguished.

Between 520 - 1180 m, 1410 - 2375 m and 2700 to 3000 m more or less homogeneous successions of alumino-silicate-bearing paragneisses were drilled trough. In the paragneiss units the recorded gamma ray, as well as density and neutron porosity, is clearly dependent on the quartz/phyllosilicate ratio of the rocks. This was shown by HAVERKAMP & WOHLENBERG (1991) for paragneisses of the KTB-VB. Based on this experience also the paragneiss successions of the KTB-HB could be divided into alternations of quartz- and phyllosilicate rich varieties by using the logs. The observed mineralogical and physical differences of the gneisses may be related to their sedimentary educts in so far that quartz-rich lithotypes (IVb/IVc) are products of greywackes whereas the phyllosilicate-rich type (IV) with higher gamma activity and density is formed from more clayey sediments. Plagioclase-rich gneisses, unknown in the KTB-VB, were identified by their characteristic low potassium contents. For this rocktype, drilled through between 950 and 980 m (*Fig. 5*), two electrofacies were distinguished by the logs; lithotype VIIa is characterized by higher thorium contents than the lithotype VIIb.

Most of the metabasic rocks are related to two larger lithostratigraphic units, different in origin and material composition. The massive metabasite sequence (1180 to 1410 m, *Fig. 6*), sharply separated from the paragneisses by significant low gamma activity, is derived from mafic intrusives (PATZAK et al. 1991). This sequence is mainly composed of amphibolites with intercalated metagabbros which are more abundant in the EFA-LOG than in the cuttings profile. Differentation of the metagabbros, distinguished in the almost completely cored KTB-VB by relict magmatic fabrics, was not always possible by analysing the cuttings samples of the KTB-HB (see GODIZART et al. 1991). Applying the calibrated electrofacies to the KTB-HB it was possible to distinguish the more mafic metagabbros by characteristic low gamma activity as well as the amphibolite variety 3f which leads to gneissic rocks. The second mafic lithostratigraphic unit, a heterogeneous gneiss/amphibolite succession, was drilled through between 2375 - 2700 m (*Fig. 10*). Similar to the unit down to 520 m this sequence is probably derived from volcanic rocks and intercalated sediments (PATZAK et al. 1991). According to the strong variations of the recorded log responses the EFA-LOG shows a detailed alternation of hornblende gneisses, amphibolites and alumino-silicate-bearing paragneisses. Furthermore the lithotype amphibolite gneiss was distinguished by the logs as a linkage between gneissic and amphibolitic rocks.

Besides the discrimant electrofacies also the relations between various logs, often specific for the main lithological units were found suitable for establishing an EFA-LOG even when less data were available. Especially the TH/U as well as the SGR/POTA-ratios are important. *Figure 2* shows the typical pattern of the main lithological groups in the cross-plot SGR versus POTA. Despite overlapping NGS-logging responses the three distinguished gneiss groups (alumino-silicate-bearing paragneisses, plagioclase-rich gneisses and hornblende gneisess) can clearly be separated by different SGR/POTA ratios. In general, the following trends can be derived from the calculated average ratios of the main lithological units: The SGR/POTA ratio decreases from acid to mafic rocks whereas the THOR/URAN ratios are significant higher in the massive amphibolites and metagabbros than in the gneissic rocks (*Table 3*).

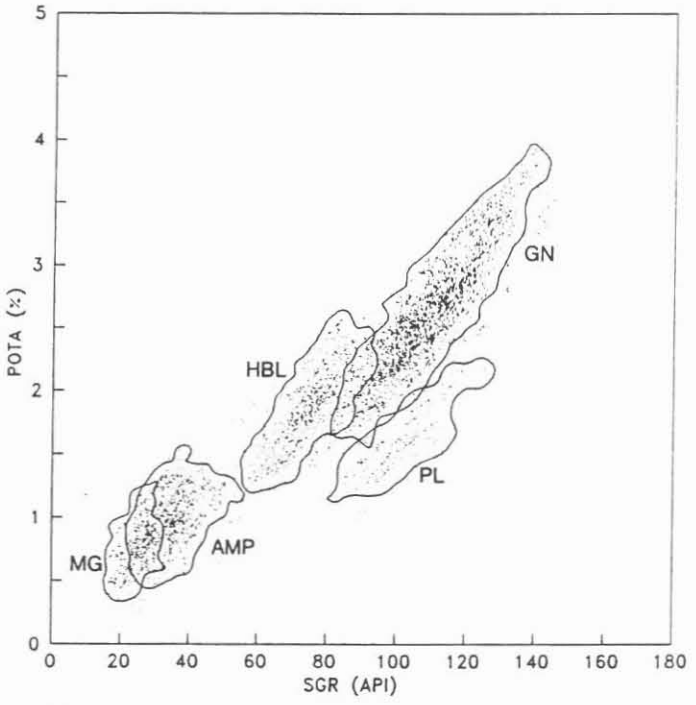

Fig. 2: Cross-plot SGR versus POTA with the typical distribution of the main lithological units which are distinguished in the EFA-LOG.- *GN: alumino-silicate-bearing paragneisses, HBL: hornblende gneisses, PL: plagioclase-rich gneisses, AMP: amphibolites, MG: metagabbros.*

	plagioclase rich gneiss	alumo silicate paragneiss	hornblende gneiss	amphibolite	metagabbro
THOR/URAN	3.40	2.81	2.56	5.49	4.39
SGR/POTA	64.35	43.73	40.48	36.66	33.64

Table 3: Average values of the SGR/POTA and THOR/URAN ratios for the main lithological units calculated from the first 3000 m of the KTB-HB.

Considering the results presented the following can be concluded:
Based on a careful quality control, the application of calibrated electrofacies from one well to another is possible also in crystalline rocks, assuming more or less similar lithologies. Even in the case of meagre available logging data, a detailed synthetic profile of the drilled lithology can be established with this applied method. The high sampling rate of borehole measurements provides not only better depth resolution than analysis of cuttings but also better differentiation of the lithological units. To this extent the EFA-LOG should be used as an additional tool for special geological objectives, such as questions related to lithostratigraphy and tectonic features or for detailed correlation of the KTB-VB with the KTB-HB.

Following pages:
Fig. 3-11: Comparision of EFA-LOG *and cuttings profile for the depth interval 280 - 3000 m KTB-HB. In the* EFA-LOG *the main lithological groups are marked in the left column; their varieties in the right column.*
The depth of the cuttings profile is related to lag time.

References

GODIZART, G., GLEIß, N., HANSMANN, J., HÄUSSINGER, H., KEYSSNER, S., KOHL, J. & LAPP, M. (1991): Tiefbohrung KTB-Oberpfalz HB, Ergebnisse der geowissenschaftlichen Bohrungsbearbeitung im KTB-Feldlabor (Windischeschenbach), Teufenbereich von 0 bis 1720 m: B. Geologie.- In: Emmermann, R., Dietrich, H.-G., Lauterjung, J. & Wöhrl, Th. (Hrsg.): KTB-Report **91.3**: Hannover.

HAVERKAMP, S. & WOHLENBERG, J. (1991): EFA-LOG - Rekonstruktion kristalliner Lithologie anhand von bohrlochgeophysikalischen Messungen für die Bohrungen Urach 3 und KTB-Oberpfalz VB.- KTB-Report **91-4**: Stuttgart (Schweizerbart'sche Verlagsbuchhandlung).

LICH, S., DUYSTER, J., GODIZART, G., KEYSSNER, S. & WALL, H., de (1992): German Continental Deep Drilling Program (KTB) - geological survey of the Hauptbohrung 0-6000 m: B. Geologie.- In: Emmermann, R., Dietrich, H.-G., Lauterjung, J. & Wöhrl, Th. (Hrsg.): KTB-Report **92.2**: Hannover.

PATZAK, M., OKRUSCH, M. & RÖHR, C. (1991): Die Metabasite der KTB-Vorbohrung: Petrographie, Geochemie, Mineralchemie und Metamorphoseentwicklung. - In: Emmermann, R. & Lauterjung, J. (eds.): Forschungsergebnisse im Rahmen des DFG-Schwerpunktprogrammes "KTB", 1986 - 1990. - KTB Report **91-1**, 63-82, Hannover.

We would like to express our thanks to the well logging group of the KTB-Project and to the field laboratory, for providing the digitized cuttings profile, geochemical, petrograpical, and petrophysical data.

LEGEND

CUTTINGS-PROFILE		EFA-LOG	
paragneiss: gnt-sil-bio-gneiss mus-bio-gneiss	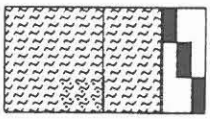	IVa IVb IVc	paragneiss (alumo silicate bearing)
plagioclase rich gneiss	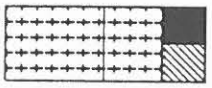	IIVa IIVb	plagioclase rich gneiss
hornblende gneiss		IIIa IIIb	hornblende gneiss
amphibolite	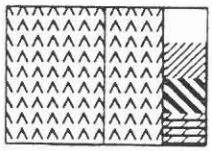	3a,d,e 3b 3f	amphibolite amphibolite gneiss
metagabbro			metagabbro
lamprophyre	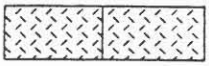		lamprophyre
cataclastic gneiss	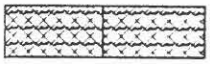	IVd-h	cataclastic gneiss
cataclasite			cataclasite
cataclastic amphibolite			cataclastic amphibolite
alternation gneiss/amphibolite			
calcsilicate rock	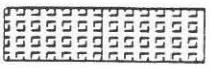		

ccc: graphite
◆: pyrrhotine
x: quartz-vein
*: pyrite

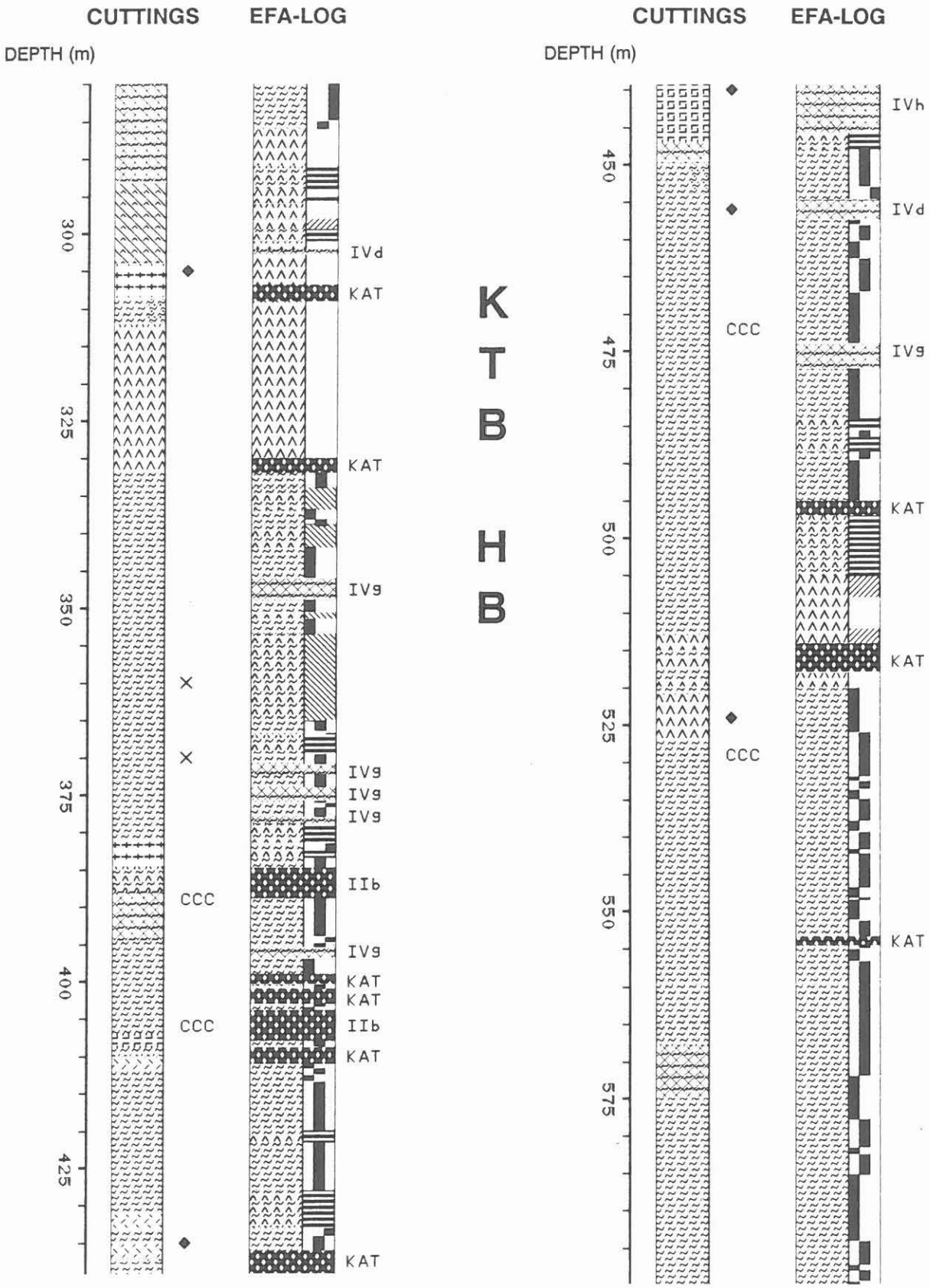
CUTTINGS
EFA-LOG
DEPTH (m)
300
325
350
375
400
425
IVd
KAT
KAT
IVg
IVg
IVg
IVg
IIb
IVg
KAT
KAT
IIb
KAT
KAT
CCC
CCC
KTB HB
CUTTINGS
EFA-LOG
DEPTH (m)
450
475
500
525
550
575
CCC
CCC
IVh
IVd
IVg
KAT
KAT
KAT

fig. 3

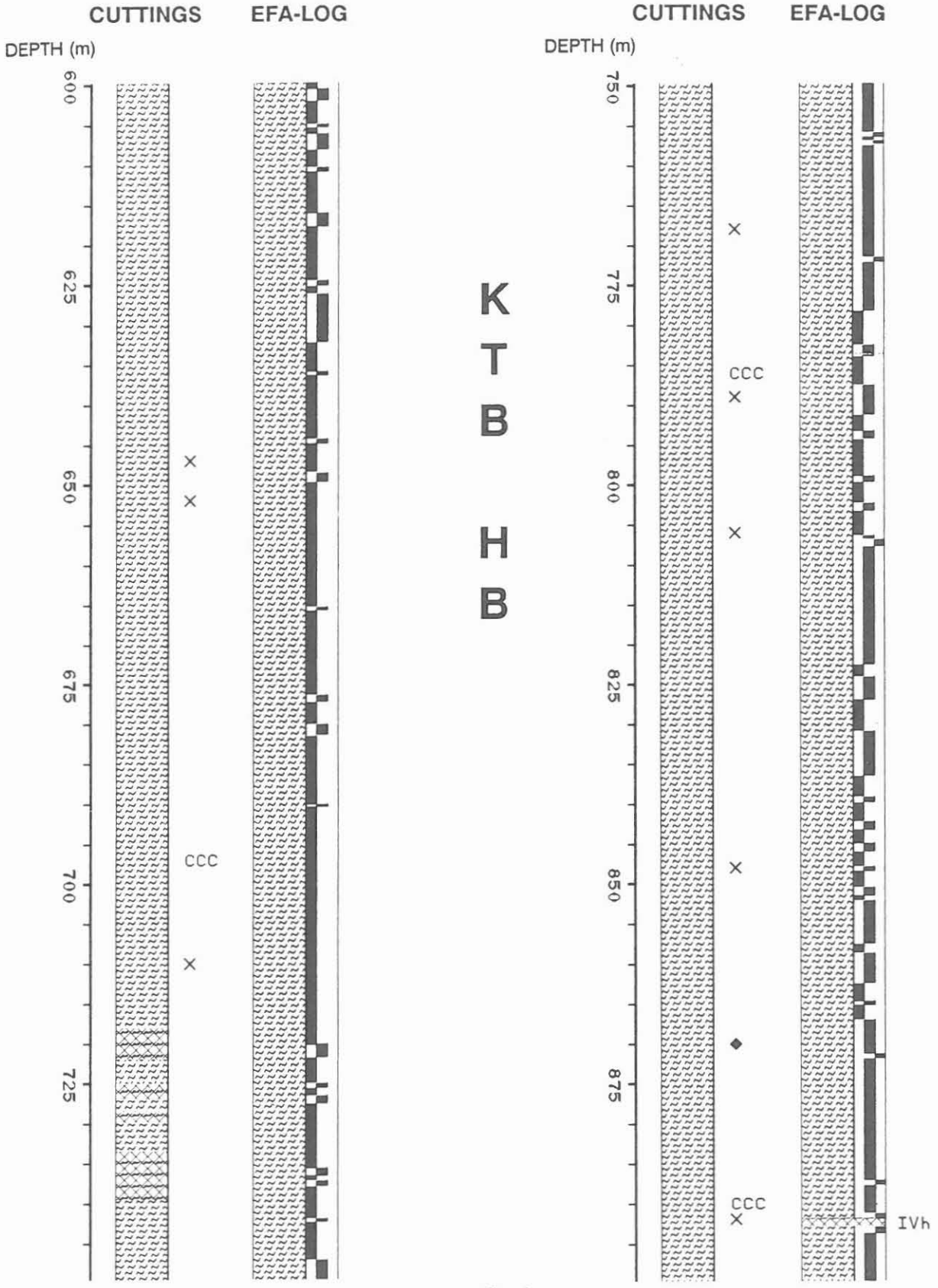
CUTTINGS
EFA-LOG
DEPTH (m)
600
625
650
675
700
725
CCC
K
T
B
H
B
CUTTINGS
EFA-LOG
DEPTH (m)
750
775
800
825
850
875
CCC
CCC
IVh

fig. 4

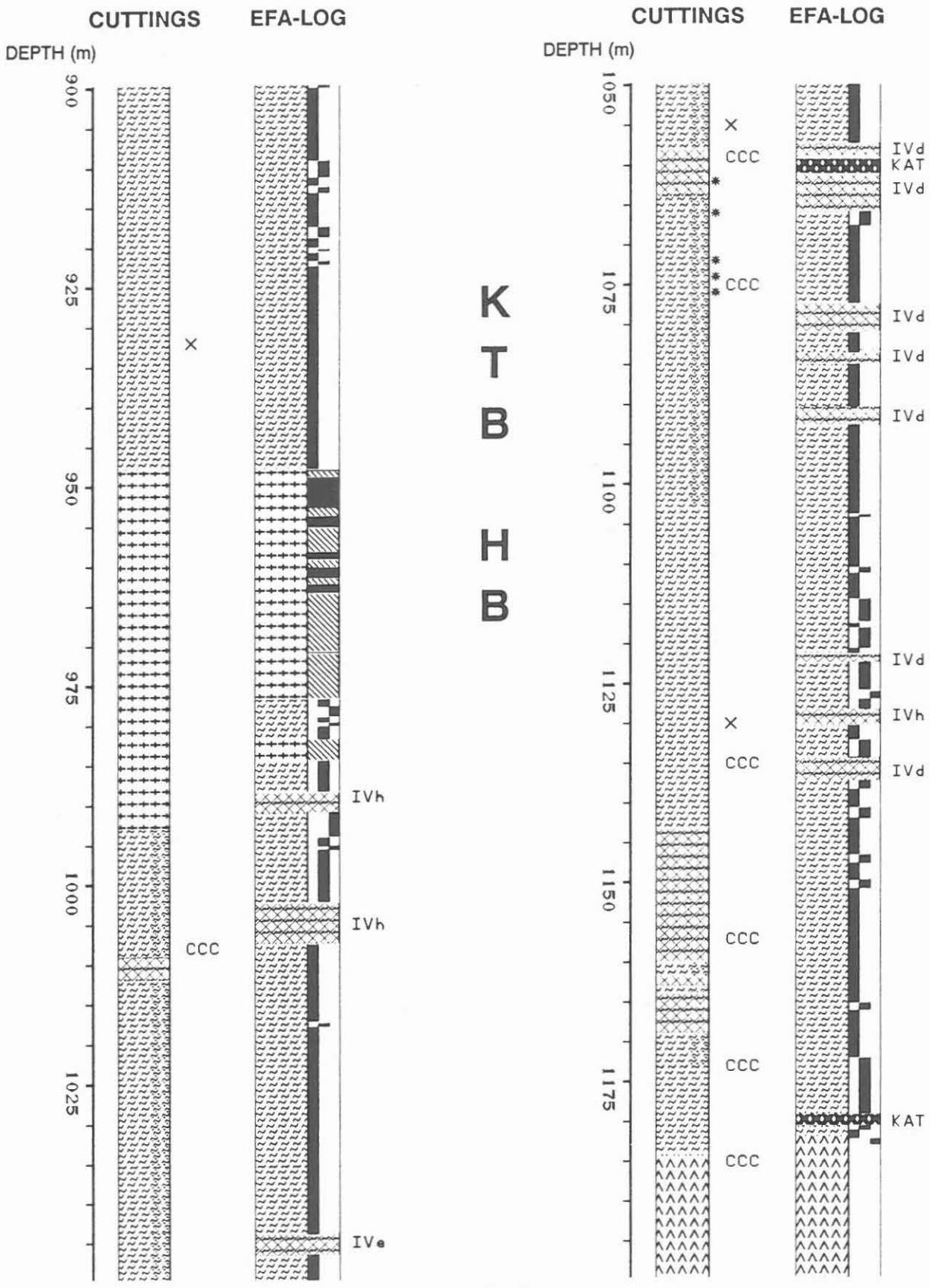
CUTTINGS
EFA-LOG
DEPTH (m)
900
925
950
975
1000
1025
CCC
IVh
IVh
IVe
KTB HB
CUTTINGS
EFA-LOG
DEPTH (m)
1050
1075
1100
1125
1150
1175
CCC
CCC
CCC
CCC
CCC
IVd
KAT
IVd
IVd
IVd
IVd
IVh
IVd
KAT

fig. 5

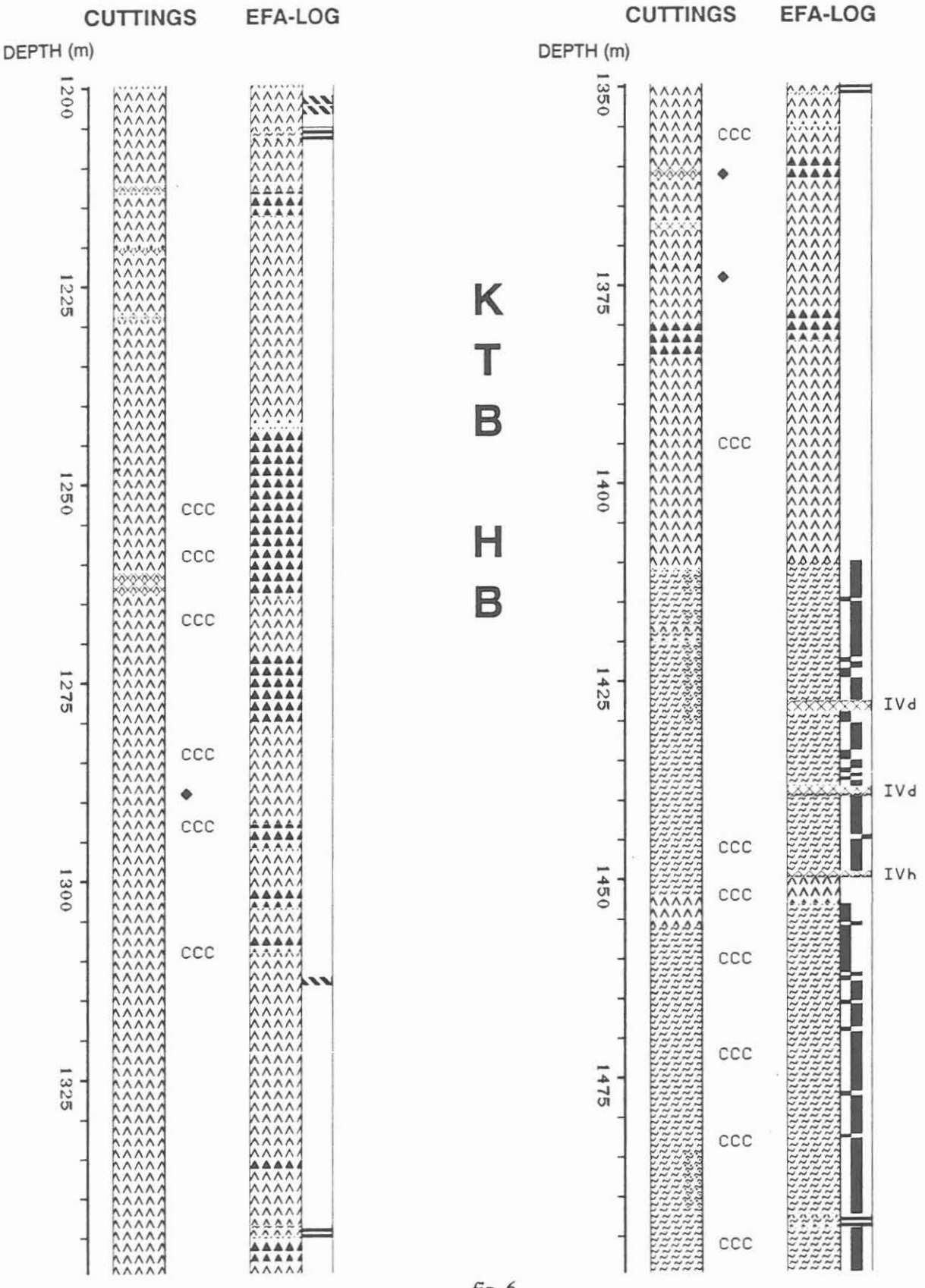
CUTTINGS
EFA-LOG
DEPTH (m)
1200
1225
1250
1275
1300
1325
CCC
CCC
CCC
CCC
CCC
CCC
KTB HB
CUTTINGS
EFA-LOG
DEPTH (m)
1350
1375
1400
1425
1450
1475
CCC
CCC
CCC
CCC
CCC
CCC
CCC
IVd
IVd
IVh

fig. 6

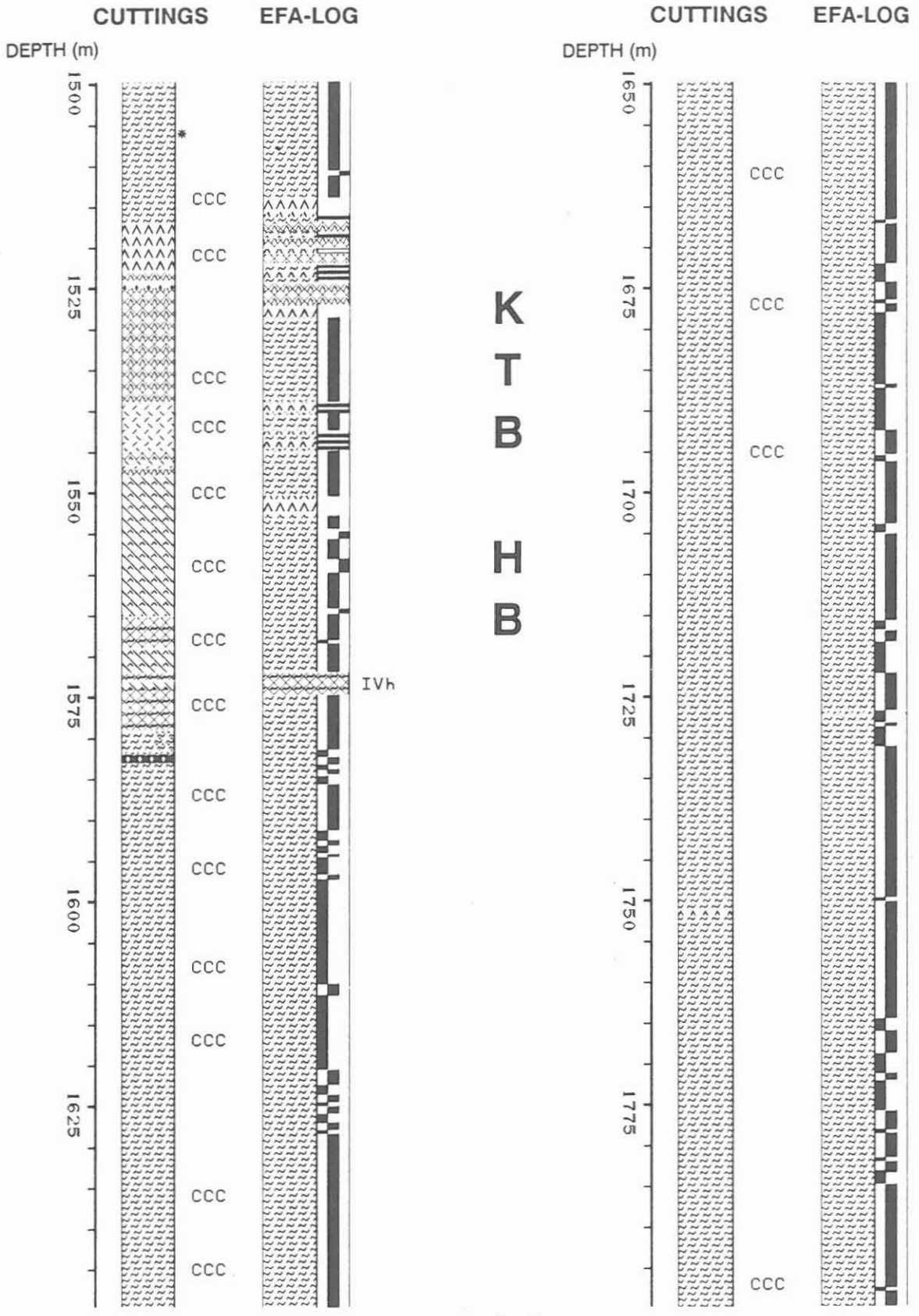
CUTTINGS
EFA-LOG
DEPTH (m)
1500
1525
1550
1575
1600
1625
CCC
IVh
K
T
B
H
B
CUTTINGS
EFA-LOG
DEPTH (m)
1650
1675
1700
1725
1750
1775
CCC

fig. 7

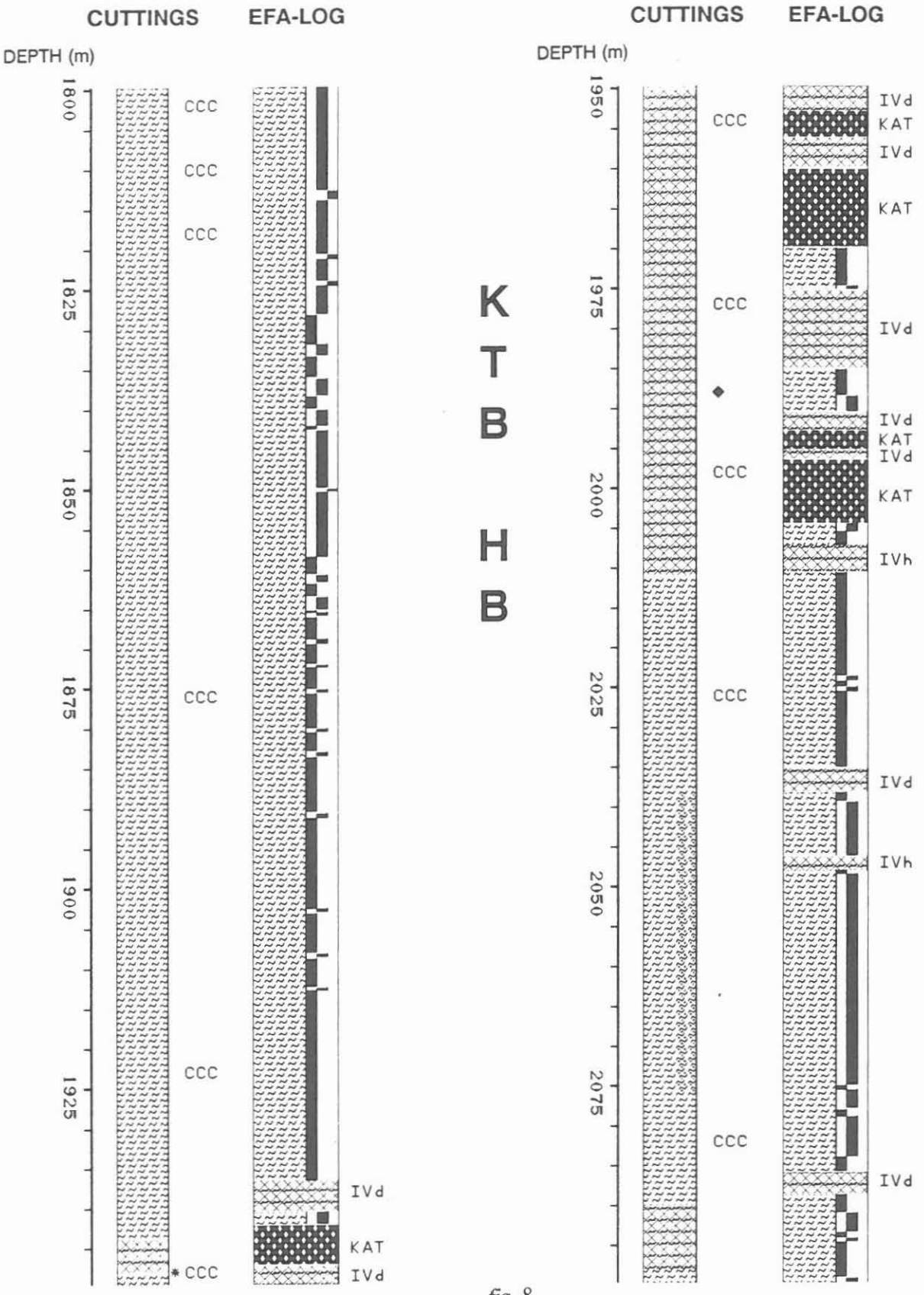
CUTTINGS
EFA-LOG
DEPTH (m)
1800
1825
1850
1875
1900
1925
CCC
CCC
CCC
CCC
CCC
* CCC
IVd
KAT
IVd
K
T
B
H
B
CUTTINGS
EFA-LOG
DEPTH (m)
1950
1975
2000
2025
2050
2075
CCC
CCC
CCC
CCC
IVd
KAT
IVd
KAT
IVd
KAT
IVd
KAT
IVd
KAT
IVh
IVd
IVh
IVd

fig. 8

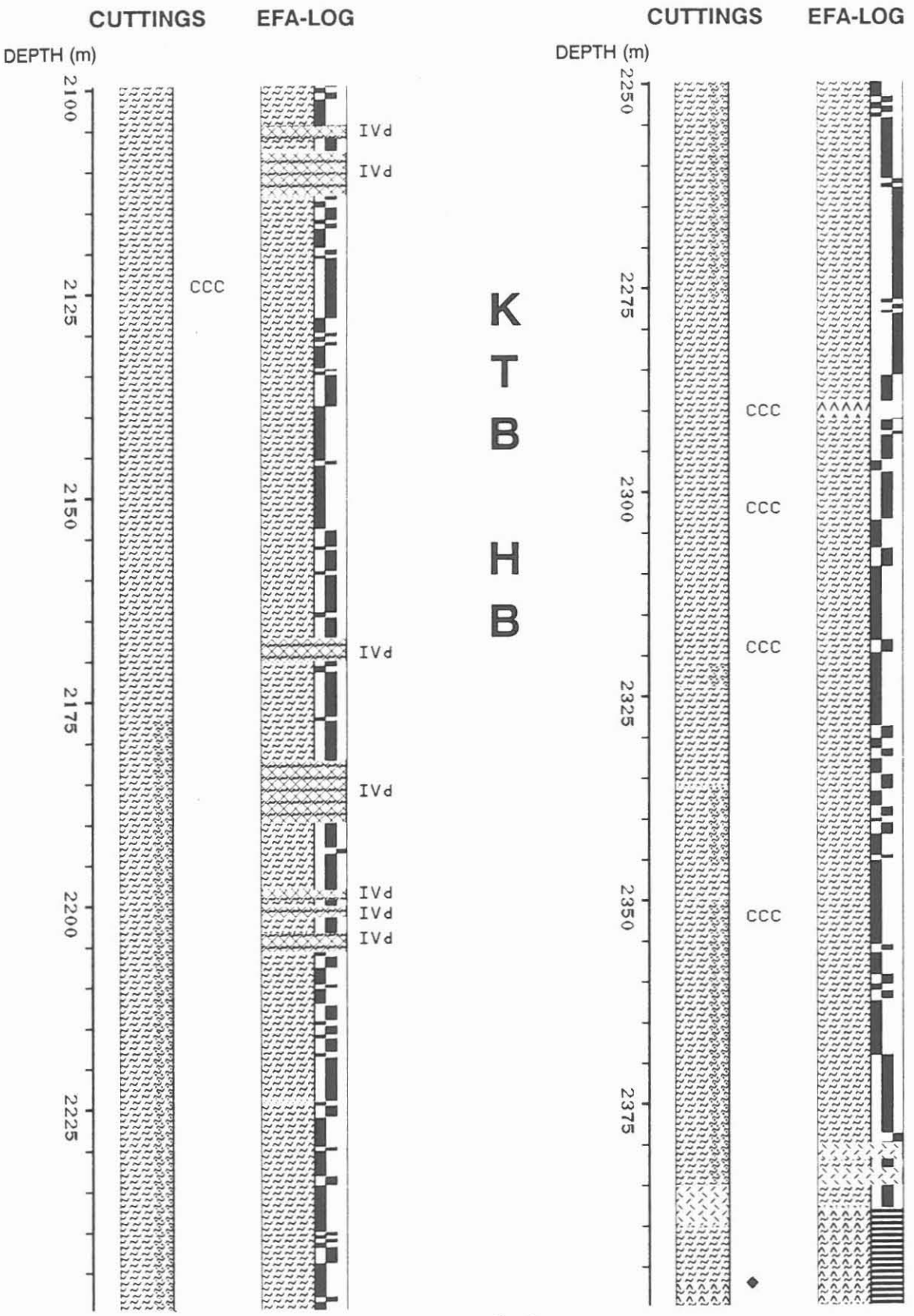
CUTTINGS
EFA-LOG
DEPTH (m)
2100
2125
2150
2175
2200
2225
CCC
IVd
IVd
IVd
IVd
IVd
IVd
K
T
B
H
B
CUTTINGS
EFA-LOG
DEPTH (m)
2250
2275
2300
2325
2350
2375
CCC
CCC
CCC
CCC

fig. 9

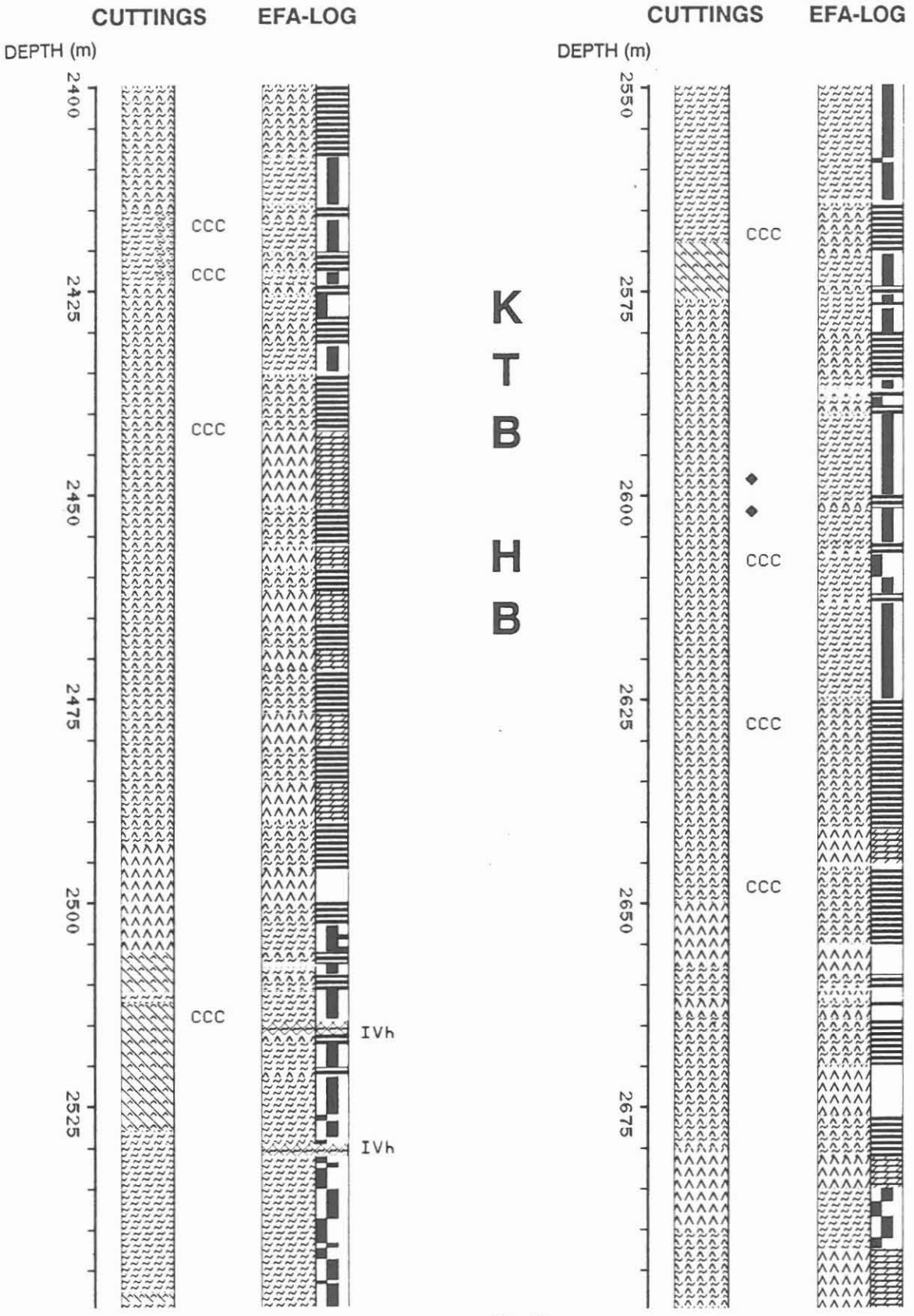
CUTTINGS
EFA-LOG
DEPTH (m)
2400
2425
2450
2475
2500
2525
CCC
CCC
CCC
CCC
IVh
IVh
K
T
B
H
B
CUTTINGS
EFA-LOG
DEPTH (m)
2550
2575
2600
2625
2650
2675
CCC
CCC
CCC

fig. 10

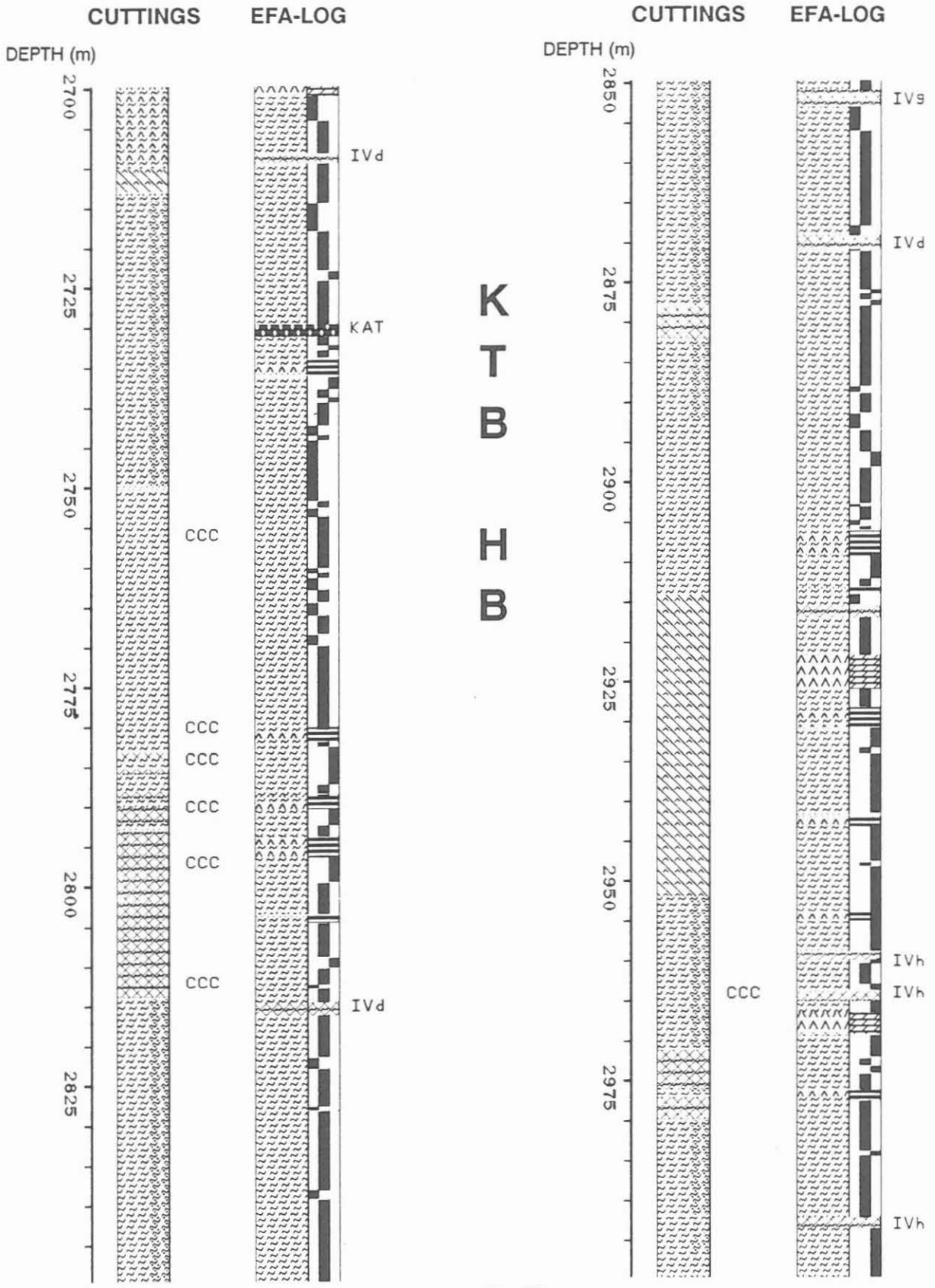
CUTTINGS
EFA-LOG
DEPTH (m)
2700
2725
2750
2775
2800
2825
IVd
KAT
IVd
CCC
CCC
CCC
CCC
CCC
CCC
KTB HB
CUTTINGS
EFA-LOG
DEPTH (m)
2850
2875
2900
2925
2950
2975
IVg
IVd
IVh
IVh
IVh
CCC

fig. 11

Stress Orientation Profile to 6 km Depth in the KTB Main Borehole

M. Brudy, K. Fuchs*, M.D. Zoback***

Introduction

The determination of the orientation of the in-situ stress tensor is a basic part of the "Integrated Stress Measurement Strategy" as it is suggested by Fuchs, Zoback and Rummel (1992, subm.). At the great depths of the main borehole the only confident and continuously applicable method to determine the orientation of the horizontal principal stresses is the analysis of stress-induced failure of the borehole wall. Two types of failure occur: Compressive failure of the wellbore wall (breakouts) which form at an azimuth orthogonal to the orientation of the maximum horizontal principal stress S_{Hmax} and drilling-induced tensile failures which are near-vertical fractures in the wellbore wall in the direction of S_{Hmax}. These failure modes are examined by three different logging tools, the Borehole Geometry Tool (BGT), the BoreHole TeleViewer (BHTV) and the Formation MicroImager (FMI). We used all of the information available from these tools to determine a stress orientation profile to a depth of 6000 m in the KTB main hole.

The resulting S_{Hmax} orientations from the analysis of the three data sets in the main borehole are consistent with each other, with the results in the pilot well and the regional stress orientation. The mean orientation of S_{Hmax} in the KTB main well between 3000 m and 6000 m determined from the analysis of BHTV images is N149°E ± 18°. This is the most accurate of the applied methods, as it has full coverage of the wellbore wall. The analysis of drilling induced vertical fractures from FMI logs between 3000 m and 6000m reveals an orientation of S_{Hmax} (N166°E ± 17°) which is somewhat more northerly. The breakout analysis of BGT logs in the same depth interval shows an orientation of N159°E±23° which is also slightly more northerly than the result from the BHTV analysis. These shifts in the orientations are method immanent in the Caliper and the FMI method as is shown in the discussion.

An interesting phenomena is seen in the breakout orientation. There are obviously variations of the breakout orientation over various depth scales that means with different wave lengths. The variations in the breakout orientation seem to be caused by structural heterogeneities like faults or changes in fabric and composition. Therefore the ±18° error in the determination of

---

Authors' addresses

*) Geophysical Institute, University of Karlsruhe, Hertzstr. 16, 76187 Karlsruhe, Germany

**) Dep. of Geophysics, Stanford University, Stanford, CA94305, U.S.A.

the breakout orientation is not due to random noise, but is instead caused by stress changes due to the structural heterogeneities of the rock mass. The same phenomena is already described for the breakouts recorded in the Cajon Pass scientific borehole in California by Shamir and Zoback, 1992.

Determination of the orientation of the horizontal principal stress from stress-induced borehole failures

Stress-induced borehole breakouts are diametrically opposed zones of compressive failure of the borehole wall in the direction of the least horizontal principal stress S_{hmin}. (Bell and Gough, 1983, Zoback et al., 1985). A number of case studies have shown that breakouts are a reliable tool for the determination of tectonic stress orientation consistent with other stress field indicators. This is shown in case studies e.g. for North America by Zoback and Zoback (1980), Plumb and Cox (1987), for Europe by Klein and Barr (1986), Müller et al. (1992) and throughout the world by Zoback et al. (1989) and Zoback (1992).

The analysis of stress induced borehole breakouts was also successfully applied to the pilot well (Mastin et al., 1991). Below 3000 m depth breakouts occur in moderately-dipping gneiss and in massive to weakly-foliated amphibolite. As their orientations agree between massive and foliated intervals and the derived stress orientation coincides with results from other measurement techniques, they are considered to be reliable stress indicators. The orientation of S_{Hmax} is determined to N161°E±14° in the depth interval between 3000 m and 4000 m. This value is close to the average stress orientation in Central Europe of N146°E as it is determined by Müller et al. (1992). Other stress measurement techniques reveal about the same stress orientation also in the depth interval above 3000 m in the pilot hole.

Vertical drilling-induced fractures are symmetrical features which develop due to tensile stresses in the wellbore wall which overcome the tensile strength of the rock. As shown by Apel et al. (subm.,1992) for the case of the KTB borehole, the tensile stress causing failure results from both the tectonically induced tensile stress and additional tensile stress caused by the cooling of the rock due to the circulation of relatively cold drilling mud and by increased pumping pressure during drilling operations. As the last two stress components affect the wellbore wall isotropically the initiation of the vertical fractures is helped by them but the orientation is solely determined by the tectonic stress component. The good agreement between the stress orientations determined from the analysis of vertical drilling induced fractures in the KTB pilot hole (Apel et al.,1992, subm.) and determined from breakout analysis proofed the possibility of an independent determination of the stress orientation from vertical fractures.

An a priori assumption of both the analysis of breakouts and of drilling-induced fractures is that the vertical stress is a principal stress and that the borehole axis is parallel to it. Brudy and Zoback (subm., 1993) show that for nearly all tectonic states of stress, deviations of one principal stress from vertical of as much as 30° introduces little error into the determination of principal horizontal stress directions from borehole failure.
As breakouts and drilling-induced fractures are found to be the only two methods which will give reliable information on the stress orientation in the great depths of the main borehole their analysis is of great importance for the determination of a stress profile to the final depth in the main borehole (Fuchs et al., 1992, subm.).

Measurements used for the Analysis

To determine the orientation of breakouts and vertical fractures data from three different tools were analyzed. The BoreholeGeometryTool (KTB) records mechanically two orthogonal hole diameters, the BoreHole TeleViewer (Deutsche Montan Technologie) scans the wellbore wall with an acoustic impulse and the FormationMicroImager (Schlumberger) provides an image of the electrical conductivity of the wellbore wall. In the following paragraphs the principles of the tools and the evaluation procedures are briefly explained.

BGT: The BGT is a Four-Arm Caliper Tool which records the borehole orientation (Hole azimuth and deviation), the corresponding tool orientation with respect to magnetic north and two orthogonal diameters of the borehole. As this tool is very important for the drilling engineers to control the borehole orientation and cross section, it is run frequently and often in overlapping sections. For this investigation a total of 50 logging runs, with a total length of about 45 km between 290 m and 6000 m, was analyzed.
For the interpretation of the data the oriented diameters measured in a depth interval of 100 m are projected on a common crossection and plotted as a so-called contour-plot (Blümling, 1986). In the contour-difference plot the differences between the larger and smaller caliper are plotted in the same way. From these two kinds of plots the breakout orientation is determined manually and ranked in four quality categories. High quality is given to data if the entire circumference of the borehole wall is sampled in the depth interval and if the shape of the breakout is clearly visible. A further necessary criterion for high quality data is that the tool rotates below and above the breakout depth interval and it is locked in the breakout direction while it is in the breakout interval. The less these criteria are fulfilled the less quality is assigned to the data.

BHTV: This tool scans the borehole wall acoustically with ultrasonic pulses emitted and received by a piezo-electrical transducer (Zemanek & Caldwell,1967; Zemanek et al.,1970). Breakouts, natural faults and fractures can be detected from the resulting traveltime and amplitude images. Breakouts show up in the traveltime images as zones of increased traveltime, which is due to an increase in borehole diameter by the breakout formation. In the amplitude images they are marked as zones of low amplitude. This decrease in the received amplitude is due to two effects. The longer traveltime leads to a geometrical attenuation of the beam and the rough surface in the breakout zone to an increased scattering.
Interactive analysis of the data is done using a system described by Barton et al., 1992. To determine the orientation of maximum principal horizontal stress S_{Hmax} the orientation of breakouts and vertical drilling induced fractures is determined. The breakout orientation is picked in a cross sectional view of the BHTV-data. Depth, orientation and opening angle of the breakouts are stored automatically in a file for further analysis. Drilling-induced vertical fractures are picked from the amplitude image of the borehole wall, although the detectability of such features with the BHTV is much less than with the FMI.

FMI: The FMI tool creates a microresistivity image of sections of the borehole wall (Ekstrom et al.,1987). Each of the four arms consists of a pad and an expandable flap each with two rows of small electrodes (diameter 4 mm). These electrodes are held at a constant voltage and the emitted current is measured. The resulting image displays the electrode contact resistivity of the borehole wall at extremely fine scale. Due to the conductivity contrast associated with faults, drilling induced fractures and foliation such features are recognized very clearly in the images. A drawback of this tool is the incomplete coverage of the borehole wall, which can lead to errors in the determination of the stress orientation if the tool is not rotating freely, that means if the tool is preferably recording the same azimuths of the borehole wall.
Measurements from three different logging dates are used in this investigation (16.10.91, 4.1.92, 17.3.92). These measurements cover the entire depth section between 3001m to 6023m with three short intervals where the measurements overlap each other (3925m-3958m, 4269m-4513m, 5419m-5504m)

Orientation of breakouts and drilling induced fractures

We divide this analysis into two parts corresponding to two depth sections from 1000 m to 3000 m and from 3000 m to 6000 m. Due to the large hole diameter (17.5") it was not possible to run the BHTV tool above 3000 m and therefore the only information on the hole geometry above 3000 m is collected by the BGT. FMI logs are available from 1800 m to 6000 m but we excluded the FMI logs between 1800 m and 3000 m from the determination of

the stress orientation because of the following reason. The analysis of the FMI logs in this depth interval reveals two populations of vertical fractures, one in the direction of the breakouts and the other perpendicular to it with almost the same frequency of occurrence. We think that the fractures perpendicular to the breakout orientation are drilling induced and reflect the stress orientation and that the second population of fractures is caused by the steep foliation striking in this direction. As we can not proof this hypothesis, we decided not to use the FMI data in this depth interval and to rely only on the analysis of breakouts from BGT logs.
In the deeper section (3000 m to 6000 m) the hole diameter is decreased to 14.75" which allowed the BHTV to be used. Therefore information from all three tools is used in this depth interval.

Depth interval 1000 m to 3000 m:

The lithology in this depth section is determined by various types of gneisses (exception between 1180 m and 1410 m Amphibolite). Frequently the borehole diameter is enlarged severely. In some sections it even reaches values of two times bitsize. The enlargements are significantly smaller in the Amphibolite section and below 2500 m depth.
An overview on all determinations of the breakout orientation from BGT measurements is given in Fig.1. The borehole enlargements in shallow depths between 290 m and 1000 m are not used to determine a stress orientation, because they seem to be strongly influenced by structural heterogeneities like foliation, fractures and faults. That means their orientation is not only stress controlled as it is true for an isotropic homogeneous rock. In the depth section between 1000 m and 3000 m a fairly constant breakout orientation of N50°E is found with a standard deviation of only ±14°. A histogram of the azimuthal distribution of the breakout orientations which also includes the quality ranking is given in Fig. 2a.

Depth interval 3000 m to 6000 m:

Information from all three tools is available for the depth section 3000 m to 6000 m. Therefore the orientation of breakouts derived from BGT and BHTV measurements and the orientation of vertical drilling induced fractures derived from FMI and BHTV measurements is used to determine the orientation of the principal horizontal stresses independently from different measurements and from different failure modes.
Fig. 1 displays the orientations of the breakouts determined from the analysis of BGT data. As in the depth section between 1000 m and 3000 m the orientation is fairly constant over the entire depth section. The increased scatter of the results between 3000 m and 5000 m is due to the fact that the breakouts are less deep than in the sections above and below. The histogram

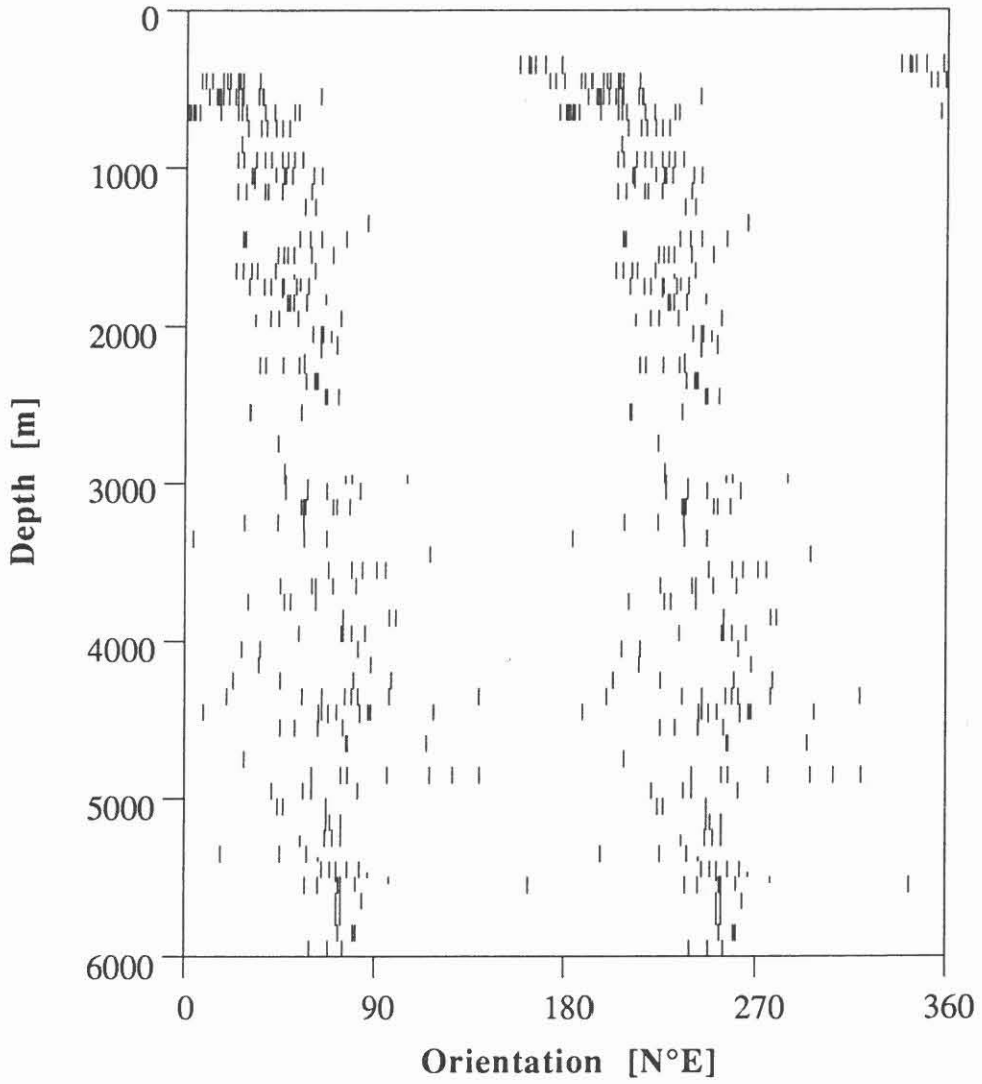

Fig. 1: Orientation of breakouts versus depth derived from the analysis of breakouts recorded by the BoreholeGeometryTool in the entire depth interval from 290 m to 6000 m. The enlargements between 290 m and 1000 m are not used for the determination of the stress orientation, because they are supposed to be influenced by structural heterogeneities. Therefore their orientation is not solely determined by the stress field. Between 1000 m and 6000 m the orientation of the breakouts is fairly constant about N50°E with a standard deviation of only ±14°. In the depth section between 3000m and 5000m the variance of the orientations is significantly increased what is due to the smaller depth of the breakouts. Below this section where the breakouts are larger again accordingly the scatter is less.

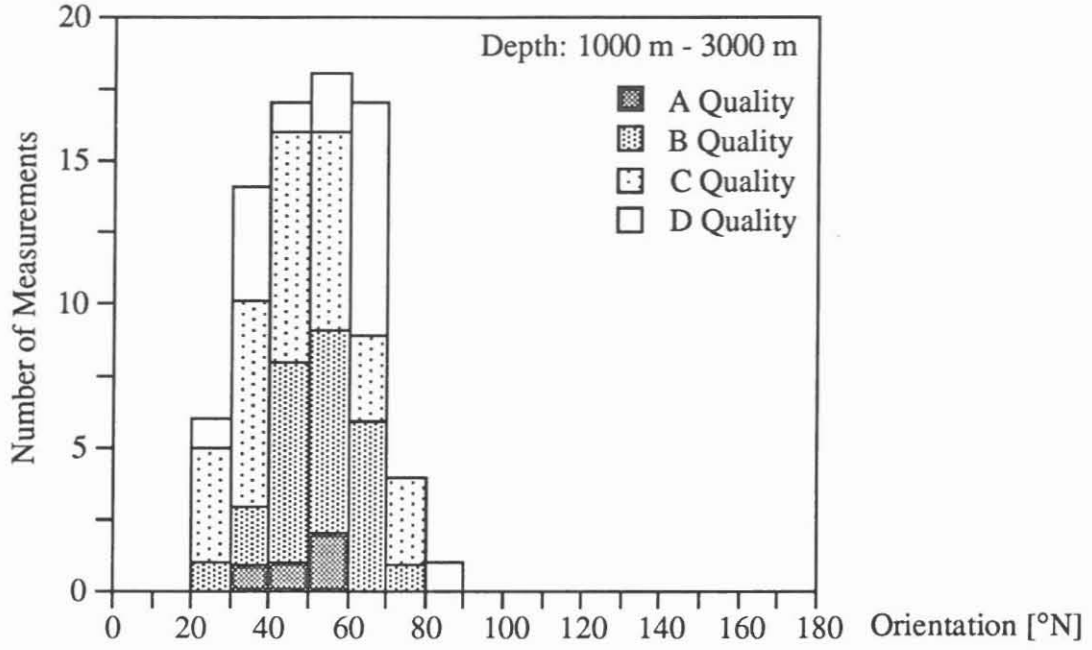

Fig. 2a: Histogram of the orientation of breakouts inferred from BGT measurements in the depth interval 1000 m to 3000 m. The columns include the ranking of the observations in different quality categories (A,B,C,D). The resulting mean value for the orientation of the breakouts for all qualities is N50°E ± 14° which leads to an orientation of S_{Hmax} N140°E ±14°.

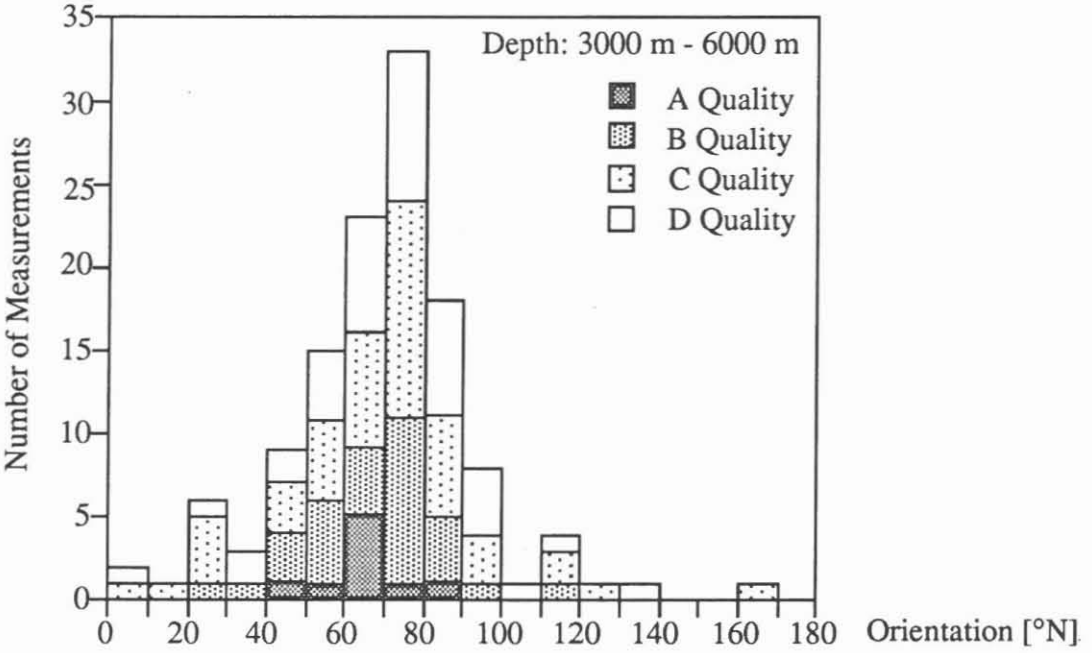

Fig. 2b: Histogram of the orientation of breakouts inferred from BGT measurements in the depth interval 3000 m to 6000 m. The columns include the ranking of the observations in different quality categories (A,B,C,D). The resulting mean value for the orientation of the breakouts is N69°E ± 23° which leads to an orientation of S_{Hmax} of N159°E ± 23°.

of the orientation of the breakouts in the entire interval (Fig.2b) gives a mean value of N69°E ± 23° and thus an orientation of S_{Hmax} of N159°E ± 23°. (It is of interest to note that this mean value could also be derived from the C - and D-quality breakouts which is not possible in the depth section 1000 m to 3000 m. There the low quality breakouts do not have a distribution similar to the distribution of the complete dataset of breakout orientations.)

The borehole geometry was studied in detail using the BHTV over the entire 3000 - 6000 m depth interval. These measurements are analyzed for both the occurrence and orientation of breakouts and of vertical drilling induced fractures. About 17000 picked breakout orientations are shown in Fig. 3.

Obviously the breakouts do not occur continuously. There are several long sections of the borehole without breakouts, for instance around 4700 m, 5000 m and 5600 m. The orientation of the breakouts is fairly constant over the entire logging interval. The observed variations in the breakout orientation are due to local stress heterogeneities, which can be caused by either material heterogeneities or drilling induced dislocations along faults, which are intersected by the borehole. As the depth interval over which breakouts occur is quite large, the regional stress orientation can be determined accurately by the average orientation of the observations. The histogram of the orientations of the breakouts (Fig.4) shows a distribution with a mean value of N59°E ± 18° which leads to an orientation of S_{Hmax} of N149°E ± 18°.

Another source of information which is used to determine the orientation of S_{Hmax} is the orientation of vertical drilling induced fractures. The orientation versus depth for these fractures is shown in Fig. 5 (determined from BHTV) and Fig. 6 (determined from FMI). Like the breakouts, the vertical fractures do not occur continuously. They become significantly less abundant below 5500 m, what is probably due to the fact that the rock in this section experienced relatively little cooling to initiate fractures. The orientation of the fractures is fairly constant over the entire logged section, but shows local perturbations of the same extent as the breakout orientations. The fact that the perturbations in the fracture orientation are parallel to the perturbations in the breakout orientation, is evidence for the fact that both features are stress controlled. The only structural heterogeneity which could cause both changes in the orientation of compressive and tensile failure is foliation. But it is very unlikely that the observed congruence of the perturbations is caused by foliation because the amphibolites in this depth interval are only weakly foliated and there is no systematical correlation between dip direction of the foliation and the orientation of breakouts and vertical fractures, respectively. A histogram of the orientation of the fractures picked in the FMI images (Fig. 7) shows a mean value of N166°E ±17°. This value is identical to the orientation of S_{Hmax} as the fractures develop in the direction of S_{Hmax}. The histogram of the vertical fractures picked in the BHTV images (Fig.8) reveals a mean orientation of N148°E ±19°. The discrepancy between the orientations of the vertical fractures in the BHTV and FMI images is discussed below.

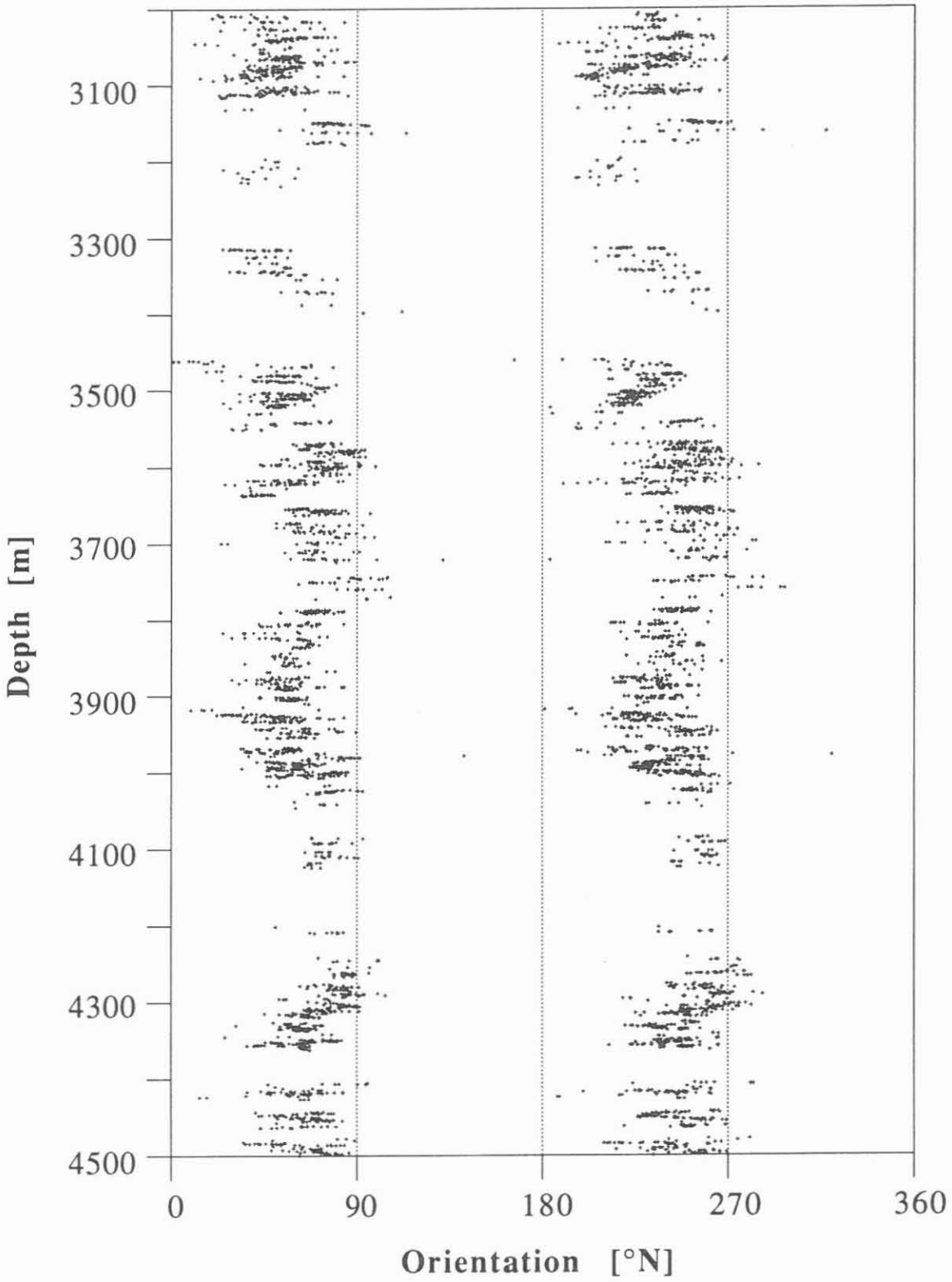

Fig. 3a: Explanation see next page

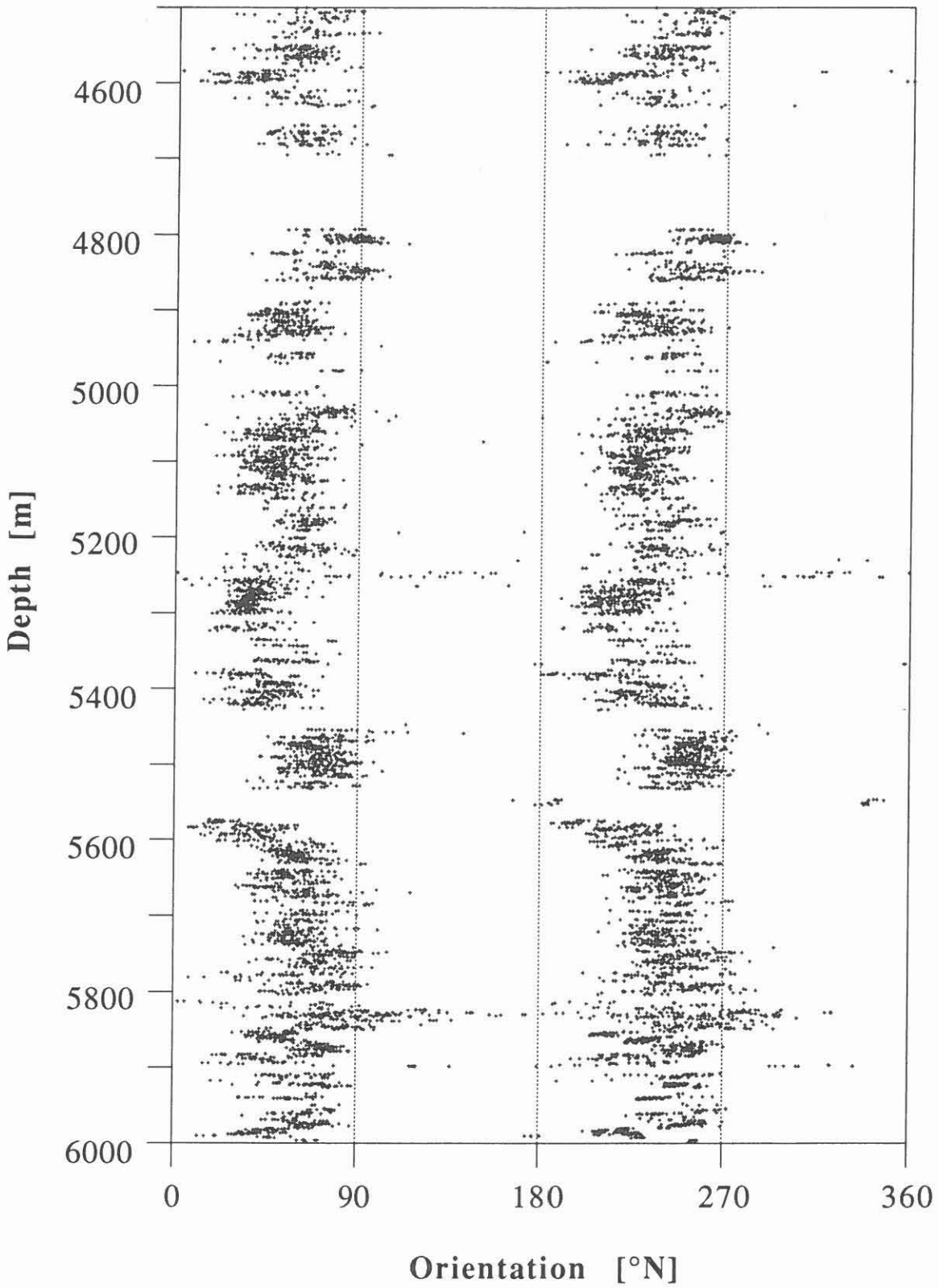

Fig. 3: Breakout orientations picked in the BHTV images are shown versus depth. [a) 3000 m to 4500 m and b) 4500 m to 6000 m]. The breakouts exhibit a fairly constant orientation but they also show minor local perturbations which are caused by sructural inhomogeneities.

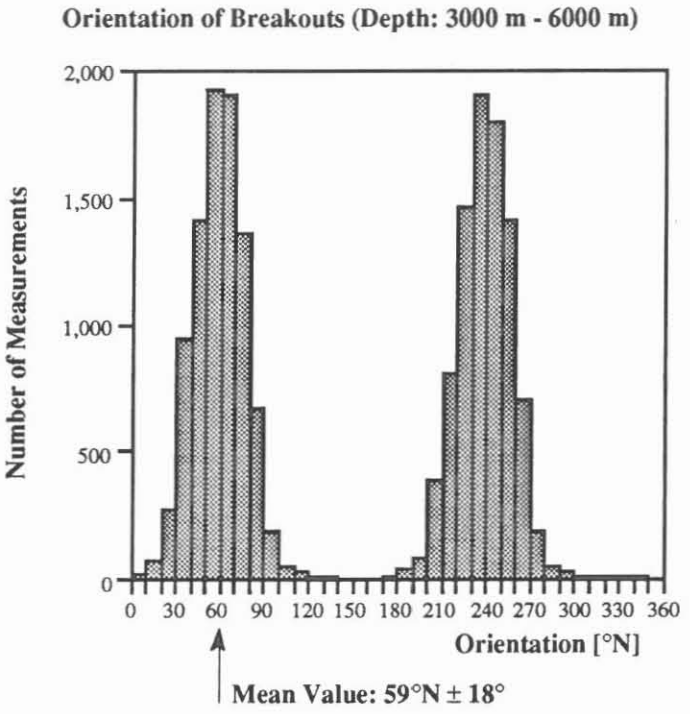

Fig. 4: Histogram of the breakout orientation picked from the BHTV measurements in the depth interval 3000 m to 6000 m. The mean value for the breakout orientation is N59°E ± 18° which leads to an orientation of S_{Hmax} of N149°E ± 18°.

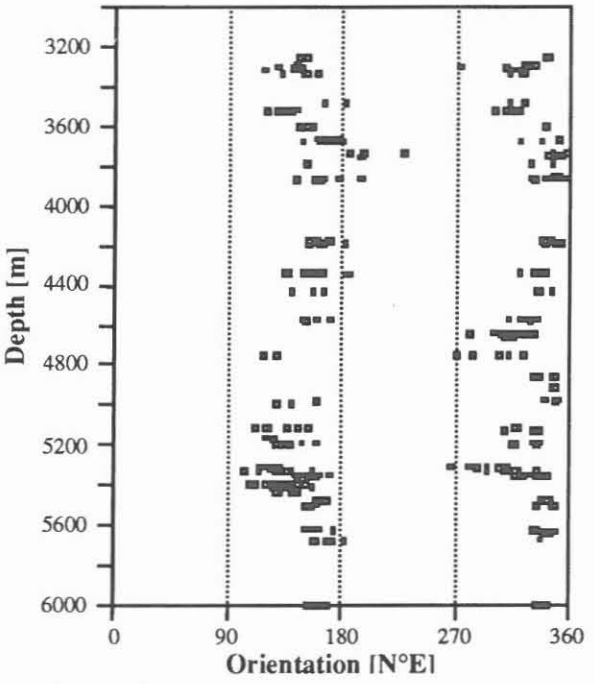

Fig. 5: Orientation of vertical drilling-induced fractures determined from BHTV images in the depth section 3000 m to 6000m. The total number of fractures which are seen in the BHTV images is much less than in the FMI images (Fig. 6) because only very prominent fractures can be recognized by the BHTV.

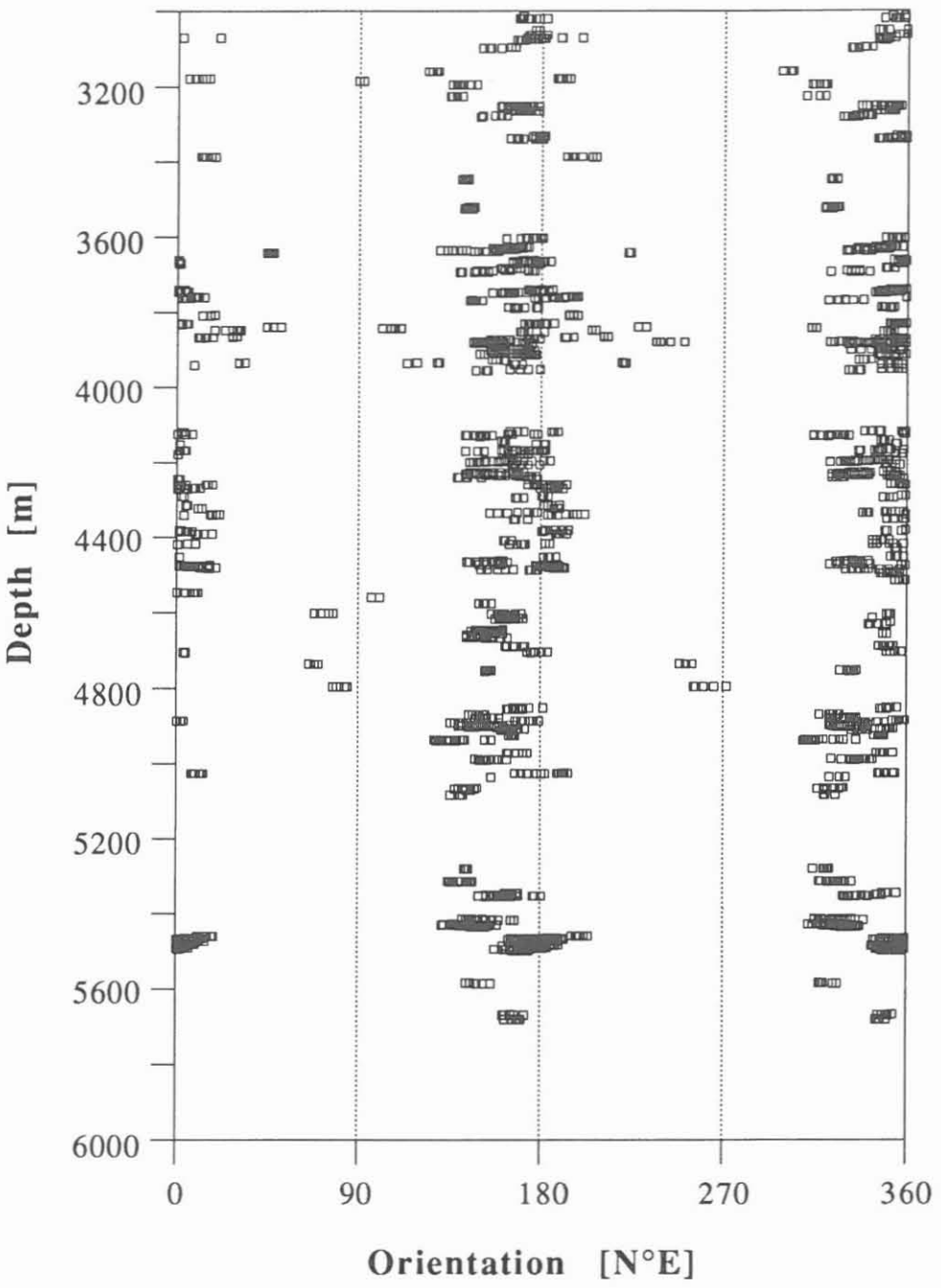

Fig. 6: Orientation of vertical drilling-induced fractures derived from FMI measurements in the depth section 3000 m to 6000m. The vertical fractures occur intermittent throughout the entire depth interval. Below 5500 m significantly less fractures are discovered than above. Also the vertical fractures show a quite constant orientation in the entire depth interval with only minor local perturbations.

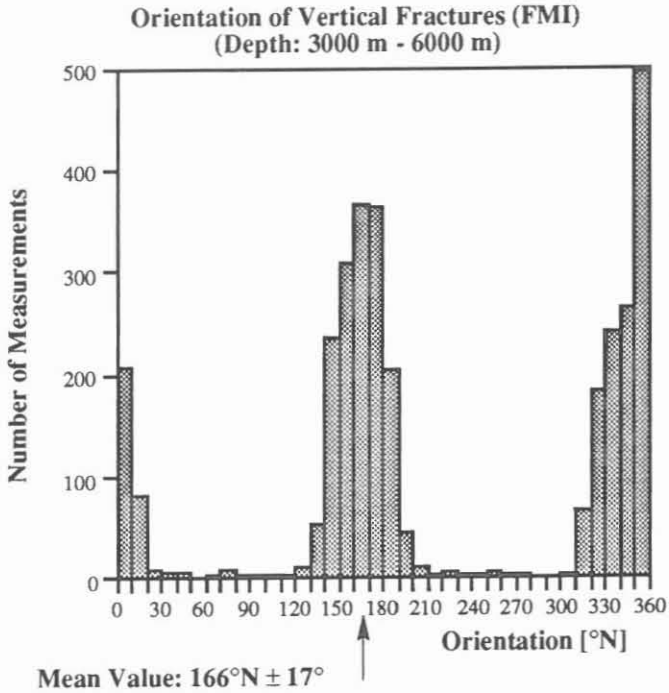

Fig. 7: Histogram of the orientation of vertical fractures inferred from FMI measurements between 3000 m and 6000m. The mean value for the orientation of the fractures is N166°E ± 17° which is identical to the orientation of S_{Hmax} .

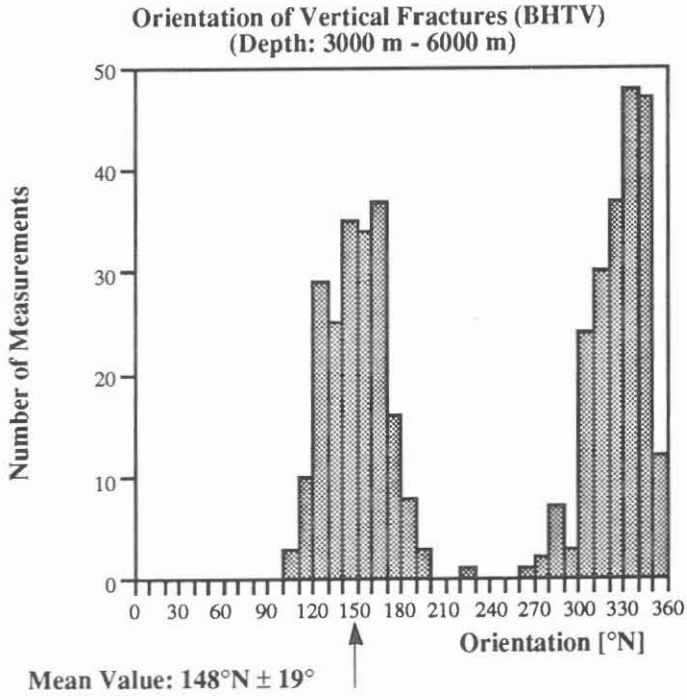

Fig. 8: Histogram of the orientation of vertical fractures inferred from BHTV measurements between 3000 m and 6000 m. The mean value for the orientation of the fractures is N148°E ± 19° which is identical to the orientation of S_{Hmax} .

Discussion

A comparison of the breakout orientations determined from the BGT measurements between 3000 m and 6000 m and from the BHTV measurements in the same depth interval shows a discrepancy of about 10° (N69°E compared to N59°E). As the BHTV records a complete image (360°) of the borehole wall we think the breakout orientation determined from the BHTV logs is the true orientation. The offset in the breakout orientation inferred from the BGT logs is probably due to the cable torque which causes the BGT to preferably record slightly higher angles as the true centers of the breakouts. The breakout orientation determined in the depth interval 1000 m to 3000 m by the analysis of BGT measurements is N50°E. If we use the difference of 10° between the results from BHTV and BGT found in the deeper section for correction of the BGT analysis, the mean breakout orientation becomes about N40°E. This coincides quite accurate with the dip direction of the foliation of the gneisses in this section. Thus we think that the breakouts in this section are influenced by steeply dipping foliation and do not reflect the appropriate stress orientation.

The comparison of the orientation of the near-vertical fractures picked from BHTV and FMI images shows a disturbingly large offset of about 18°, whereas the orientation of the fractures and the breakouts both picked from BHTV images correspond very well. The mean orientations of these two structures are almost perpendicular to each other (91°) as demanded by the elastic theory. While the FMI is much better at detecting fine scale fractures than the BHTV, an advantage of the BHTV is the 100% coverage of the borehole wall. Therefore we think the population of the prominent fractures detected in the BHTV images is a correct representation of the true fracture population at the borehole wall.

In the following discussion of the discrepancy between the mean orientation of the drilling-induced fractures determined from the BHTV and the FMI logs we assume that the true fracture population has the same standard deviation (±19°) as the one seen in the BHTV images. One arm of the FMI tool scans an angular range of about 36° of the borehole wall in a 14.75" bit size hole. Thus the FMI tool should record almost the entire fracture population, if it is centered in the breakout. As the cable torque tends to preferably orient the tool a few degrees off the center of the breakouts, it therefore records only a part of the fracture population and causes a too high mean value (Fig. 9). An analysis of the FMI logs revealed that about 70% of the recorded fractures were on the more northerly half of the measuring interval of one arm of the tool. If the fractures are distributed symmetrically around the mean value with a standard deviation of ±19° this means that the FMI tool sees only about half of the population of the fractures (as half the width of the measurement interval of one arm is 18°). Therefore this effect can maximally cause a misorientation which is equal to the half of the standard deviation of the true fracture population (about 8° to 10°). Thus the proposed effect can not explain the entire difference in the mean orientations of the population of the

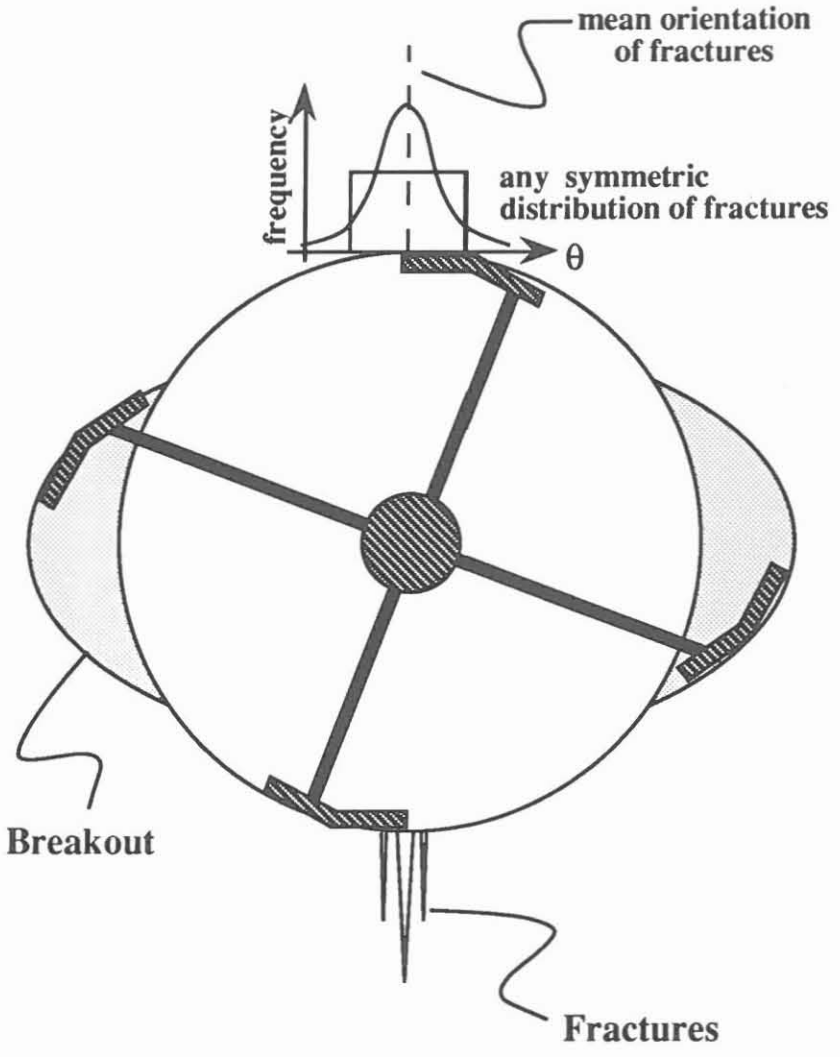

Fig. 9: Schematical explanation for the uncomplete record of the population of drilling-induced fractures by the FMI tool. Due to the cable torque the tool is preferably oriented a few degrees off the center of the breakouts. The arbitrary but symmetrical fracture population indicated 90° to the breakouts is therefore only partly recorded by the FMI tool.

near-vertical fractures determined from BHTV and FMI measurements[1].

The stress orientation exhibits small scale variations (within tens of meters) and large scale variations (within several hundreds of meters). From 3000 m to 4900 m the S_{Hmax} orientation is fairly constant, then it decreases slowly by about 20° to 5300 m and increases again to the orientation in the upper section at 5500 m. Also the small scale variations are not greater than

[1] As the discrepancy can not be fully explained by the concept proposed above, the authors investigate this difference in the orientations in close collaboration with the service companies and the project managment of KTB. This investigation is still under progress and has not yet led to a final conclusion.

about 30°. The same pattern of variations in the breakout and stress orientation, respectively, is seen in the Cajon Pass scientific drill hole in California (Shamir and Zoback, 1992).
Breakouts and drilling induced fractures are observed in the same depth intervals and are not inversely correlated. Nevertheless a trend in the likelihood for the occurrence with depth can be seen. Breakouts become more frequent with depth, whereas the near vertical fractures become less frequent.
It is also of importance to relate the stress orientation determined in this investigation to the stress orientations determined by various methods in the KTB pilot well (Mastin et al., 1991, Wolter, 1990; Zang, 1989,1990). As the boreholes are very close to each other (about 200 m at the surface) and they penetrate the same lithology the stress orientations determined in the two wells should be identical. Table 1 gives a compilation of the S_{Hmax} orientations derived by various methods in the pilot and in the main hole.

Method (Wellname)	Depth Interval [km]	Stress Orientation [N°E]
BGT (HB)	3 - 6	159°±23°
BHTV-BO (HB)	3 - 6	149°±18°
BHTV-VF (HB)	3 - 6	148°±19°
FMI (HB)	3 - 6	166°±17°
BHTV-BO (VB)	3 - 4	161°±14°
FMS (VB)	3 - 4	154°±17°
HF (VB)	0.5 - 3 *	149°±15°
CoDi (VB)	3.2 - 3.6 *	163°±22°
Strain (VB)	2 - 3.6 *	168°±25°

* Discontinuous measurements

Table 1: Compilation of SHmax orientations determined by various methods and tools in the main hole (HB) and in the pilot hole (VB).
Abbreviations: Methods: BO: Breakouts, VF: Drilling induced fractures, HF: Hydraulic-Fracturing, CoDi: Core discing, Strain: Strain retardation
Tools: BGT: Borehole Geometry Tool, BHTV: Borehole TeleViewer, FMS: Formation Microscanner , FMI: Formation MicroImager
The references for the stress orientations in the pilot well are: FMS: Apel et al. (1992, subm.), HF: Baumgärtner et al. (1990), BHTV-BO: Mastin et al. (1991), CoDi: Wolter et al. (1990), Strain: Zang et al. (1990).

There is generally a good agreement between the results from the various methods. Motivated by the reasons explained above we think the most reliable values for the stress orientation in

the main well between 3000 m and 6000 m depth are given by the analysis of the BHTV images (N149°±18° for the breakout analysis and N148°E±19° for the fracture analysis). These orientations are also in perfect agreement with the mean S_{Hmax} orientation derived from hydraulic fracturing experiments in the pilot well (N149°E ± 15°) (Baumgärtner et al., 1990) and from the analysis of near vertical fractures in FMS images in the pilot well (N154°E ±17°) (Apel et al., 1992). From the BHTV measurements in the main and in the pilot hole and from the FMS measurements in the pilot hole we constructed a rose diagram (Fig.10). For this purpose the resulting stress orientations from these measurements are weighted by their length. We did not include the discontinuous measurements (Hydraulic fracturing, core disking and strain recovery). All these results fit to the mean S_{Hmax} orientation in Central Europe of N146°E determined by Müller et al. (1992) (Fig.11). Only the results from the analysis of core discing structures, from strain retardation experiments and from the breakout analysis (all in the pilot well) show slightly higher values for the orientation of S_{Hmax}, but are still inside the range of the standard deviation.

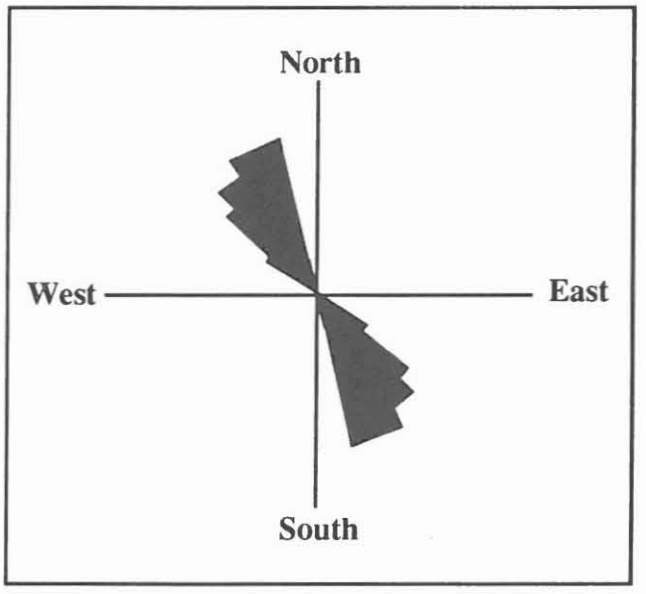

Fig. 10: The rose diagram shows the statistical distribution of the S_{Hmax} orientation as it is determined from breakout analysis (BHTV) in the main and pilot hole and from the analysis of drilling-induced fractures from BHTV logs (in the main hole) and from FMS logs (in the pilot hole). The results from these analysis are weighted by the length of the studied interval. Results from hydraulic fracturing, the analysis of core disking structures and strain recovery experiments are excluded because they are discontinuous measurements at only a few depths. The orientations and depth ranges for all methods are presented in table 1.

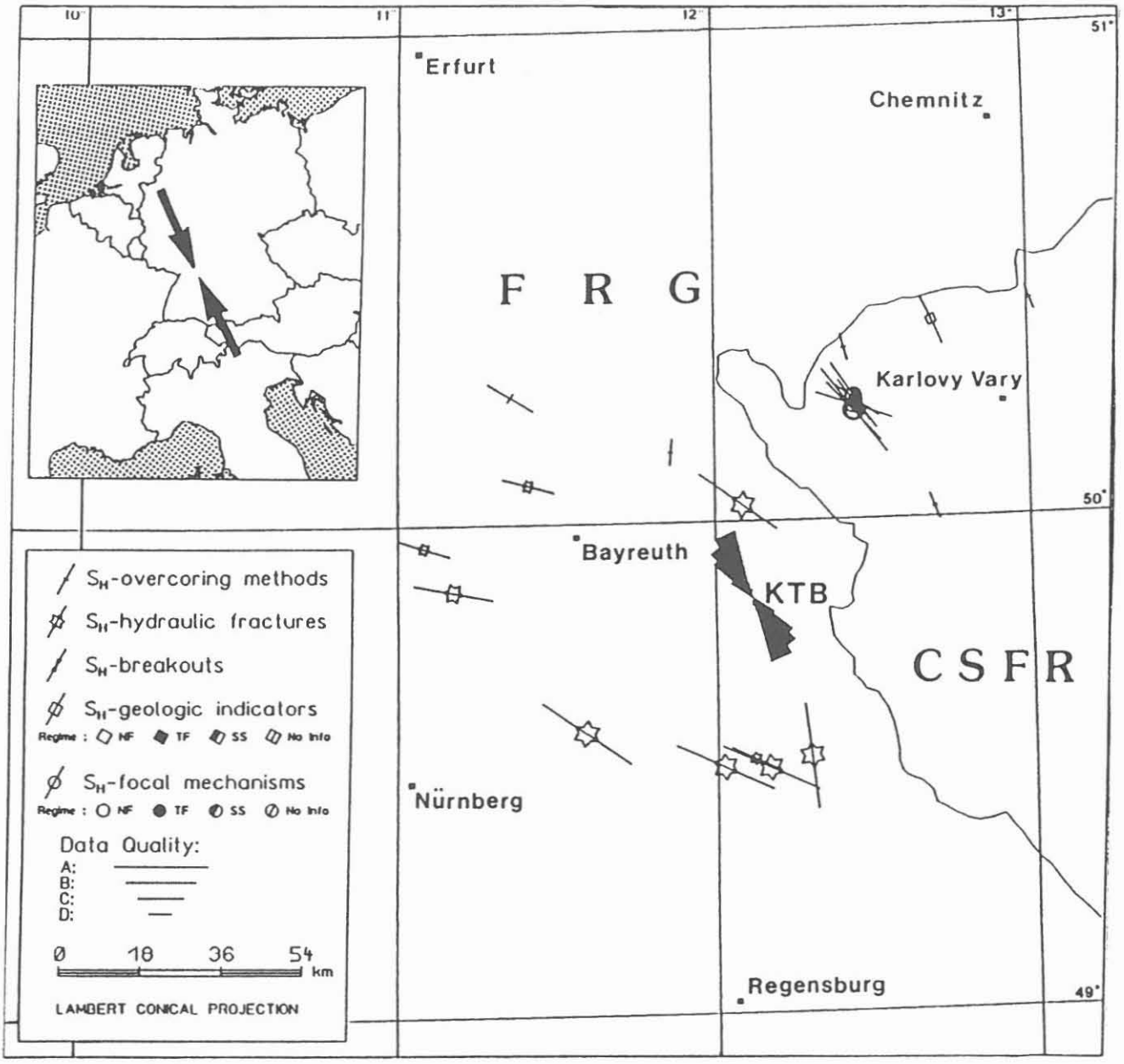

Fig. 11: The rose diagram shown in Fig. 10 is displayed in the context of the regional and the Central European stress field (Müller et al., 1992). The stress orientation determined for the KTB site consists very well with other stress orientations in the area and in central Europe.

Acknowledgments

We thank Th. Finkbeiner and O. Hengst for the time-consuming data processing and picking of the breakouts and fractures. A. Krammer adjusted the BHTV conversion software to the DMT data format. We thank him for his commitment. We also owe thanks to Dr. R. Apel for his help in processing the BGT data. This research is financially supported by the Deutsche Forschungs Gemeinschaft under grant FU55/31-4.

References

Apel, R., M.D. Zoback, and K. Fuchs, Drilling-induced tensile fractures in the KTB pilot hole, subm. to Log Analyst, 1992.

Barton, C.A., L.G. Tesler, and M.D. Zoback, Interactive image analysis of borehole televiewer data, In Automated pattern analysis in petroleum exploration, ed. Palaz, I. and S.K. Sengupta. 223-248. Springer Verlag, 1992.

Baumgärtner, J., F. Rummel, and M.D. Zoback, Hydraulic Fracturing in situ Stress Measurements to 3km Depth in the KTB Pilot Hole VB, In KTB Report90-6a, ed. KTB, P. 1990.

Bell, J.S. and D.I. Gough, The use of borehole breakouts in the study of crustal stress, In Hydraulic fracturing stress measurements, ed. Zoback, M.D. and B.C. Haimson. 201-209. Washington, D.C.: National Academy Press, 1983.

Blümling, P., In-situ Spannungsmessungen in Tiefbohrungen mit Hilfe von Bohrlochrandausbrüchen und die Spannungsverteilung in der Kruste Mitteleuropas und Australiens, PhD, Karlsruhe, 1986.

Brudy, M. and M.D. Zoback, Stability of boreholes inclined with respect to the principal stresses, in prep., 1993.

Ekstrom, M.P., C.A. Dahan, M.Y. Chen, P.M. Lloyd, and D.J. Rossi, Formation imaging with microelectrical scanning arrays, The Log Analyst, 28, 1987.

Fuchs, K., M.D. Zoback, and F. Rummel, An integrated strategy to obtain a stress profile to the midcrust in the KTB Hauptbohrung, subm. to Scientific Drilling, 1992.

Klein, R.J. and M.V. Barr, Regional state of stress in western Europe, In International Symposium on Rock Stress and Rock Stress Measurements in Stockholm, edited by Stephansson, O., Centek, 33-45, 1986.

Mastin, L.G., B. Heinemann, A. Krammer, K. Fuchs, and M.D. Zoback, Stress orientation in the KTB pilot hole determined from wellbore breakouts, Sci. Drill., 2, 1-12, 1991.

Müller, B., M.L. Zoback, K. Fuchs, L. Mastin, S. Gregersen, N. Pavoni, O. Stephansson, and C. Ljunggren, Regional patterns of tectonic stress in Europe, J. Geophys. Res., 97, 11783-11803, 1992.

Plumb, R.A. and J.W. Cox, Stress directions in eastern North America determined to 4.5 km from borehole elongation measurements, J. Geophys. Res., 92, 4805-4816, 1987.

Shamir, G. and M.D. Zoback, Stress orientation profile to 3.5 km depth near the San Andreas Fault at Cajon Pass, California, J. Geophys. Res., 97, 5059-5080, 1992.

Wolter, K., T. Röckel, C. Bücker, H. Dietrich, and H. Berckhemer, Core disking in the KTB drill cores and the determination of the in situ stress orientation, In KTB-Report 90-8, ed. Emmermann, R. and P. Giese. G1-G12. Hannover: 1990.

Zang, A., H. Berckhemer, and K. Wolter, Inferring the in-situ state of stress from stress relief microcracking in drill cores, In KTB-Report 90-8, ed. Emmermann, R. and P. Giese. F1-F20. Hannover: 1990.

Zang, A. and H. Berkhemer, Residual stress features in drill cores, Geophys. J. Int., 99, 621-626, 1989.

Zemanek, J. and R.L. Caldwell, The borehole televiewer - a new logging concept for fracture location and other types of borehole inspection, J. Petr. Techn., 25, 762-774, 1967.

Zemanek, J., E.E. Glenn, L.J. Norton, and R.L. Caldwell, Formation evaluation by inspection with the borehole televiewer, Geophysics, 35, 254-269, 1970.

Zoback, M.D., D. Moos, and L. Mastin, Well bore breakouts and in situ stress, J. Geophys. Res., 90, 5523-5530, 1985.

Zoback, M.L., First and second order patterns of tectonic stress: World Stress Map Project, J. Geophys. Res., 1992.

Zoback, M.L. and M.D. Zoback, State of stress in the conterminous United States, J. Geophys. Res., 85, 6113-6156, 1980.

Zoback, M.L., M.D. Zoback, J. Adams, M. Asssumpcao, S. Bell, E.A. Bergman, P. Blümling, N.R. Brereton, D. Denham, J. Ding, K. Fuchs, N. Gay, S. Gregersen, H.K. Gupta, A. Gvishiani, K. Jacob, R. Klein, P. Knoll, M. Magee, J.L. Mercier, B. Müller, C. Paquin, K. Rajendran, O. Stephansson, G. Suarez, M. Suter, A. Udias, Z.H. Xu, and M. Zhizhin, Global patterns of tectonic stress, Nature, 341, 1989.

The 6000 m hydrofrac test in the KTB main borehole design, implementation and preliminary results

B. Engeser[1], E. Huenges[1], W. Kessels[1], J. Kück[2] & L. Wohlgemuth[2]

[1]NLfB KTB-Projektgruppe Stilleweg 2, D-30665 Hannover

[2] NLfB KTB-Projektgruppe, Mailbox 67, D-92667 Windischeschenbach

1. Background and objectives

Gaining knowledge and understanding of the stress state in the upper levels of the earth's crust by means of a deep borehole is of fundamental importance for understanding the structure and dynamics of continental lithosphere. The determination of the magnitude and direction of crustal stresses is therefore considered to be a key experiment within the geoscience objectives of the KTB.

Of particular importance in this regard is the determination of the magnitude of the minimum horizontal principle stress, S_{hmin}, from the results of hydrofrac experiments, and the determination of their orientation via FMST or BHTV measurements.

In the KTB pilot borehole, these techniques allowed the successful measurement of the magnitude of the minimum horizontal principle stress to a depth of 3 km (Baumgärtner et al. 1990).

Included in the integrated stress measurement strategy were plans for carrying out hydrofrac experiments in the 3000 - 6000 m depth zone of the KTB main borehole; the tests were planned to be carried out within 6 m long and 96 mm diameter pilot core holes cut at the base of the 14 3/4" borehole (374.65 mm). In the higher levels the pilot core holes were to be cut using coiled tubing technology, whilst at deeper levels, they were to be cut using a drill string operated newly developed special pilot coring system. The hydrofrac experiments were actually to be carried out using wireline equipment from Mesy with specially manufactured aluminium packer elements. However, because the cutting of pilot core holes at the base of the 14 3/4" borehole had to be abandoned because of technical problems, the plans had to be changed to concentrate solely on carrying out the hydrofrac experiment after setting and cementation of the planned 13 3/8" / 13 5/8" casing at a depth of 6000 m.

In addition to the determination of the magnitude and orientation of S_{hmin}, the experiment also had the objective of collecting information on the hydraulic rock parameters. The planning and implementation of the experiment took place in close cooperation with the KTB project management and the scientists participating in the Stress Measurement Research Group.

2. Planning

2.1 Ambient conditions

- Temperature:

On the basis of the results of the 6000 m logging programme and model calculations, the undisturbed static formation temperature at 6 km depth was estimated to be as follows:

$$T_{6km} = 175\ ^{\circ}C +/- 3\ ^{\circ}C$$

- *Pressure:*

The pressure required to create hydraulic fractures at the bottom of the hole was estimated to be approx. 97 MPa taking into consideration the hydrofrac results from the pilot hole and frac simulation calculations (BAUMGÄRTNER et al. 1990, RUMMEL, pers. communication 1992). Taking into consideration the hydrostatic column (mud density 1.04 kg/dm^3) this therefore meant that the injection pressure required at the surface had to be at least 36 MPa (excluding friction pressure). On the basis of results from drawdown tests, a maximum leakoff-rate at the assumed injection pressures was estimated to be approx. 100 l/min.

2.2 Borehole situation

The evaluation of the different technical possibilities, taking into consideration the ambient conditions and the planned borehole and casing design, led to the decision being made that the hydrofrac experiment should be carried out as a casing packer test from out of the 13 3/8" casing using conventional drillstem testing equipment on the KTB drillstring.

The borehole situation immediately prior to carrying out the hydrofrac experiment is shown in Fig. 1. A total of 17.5 m of open borehole was available for the frac interval. This included 13 m (6018 m - 6031 m) of new borehole at a nominal diameter of 12 1/4 " (311.15 mm). Table 1 shows the relevant volumetric data for the test and its evaluation.

Tab. 1: KTB-HB/hydrofrac experiment. Borehole volumetrics.

Section description	contents m^3	explanation OH: open hole
Drill string + test interval		CS : casing shoe
OH (bottom 6031 m to CS 6013.5 m)	2.3	BP: bottom of packer
CS to BP packer (6005 m)	0.65	TP: top of packer
String cont. pack. to TV (5887 m)	0.54	TV: test valve
String contents TV to TH	56.2	TH: test head
Total	59.69	DP: drill pipe
Annulus DP/13 3/8" casing		BOP: Blowout preventer
TP packer to BOP	387.9	TC: Top of cement
Annulus 13 5/8" / 16 casing		WHF: Wellhead Flange
TC (4350 m) to 16" CS (3000.5 m)	47.3	
CS to WHF	60	
Total	107.3	

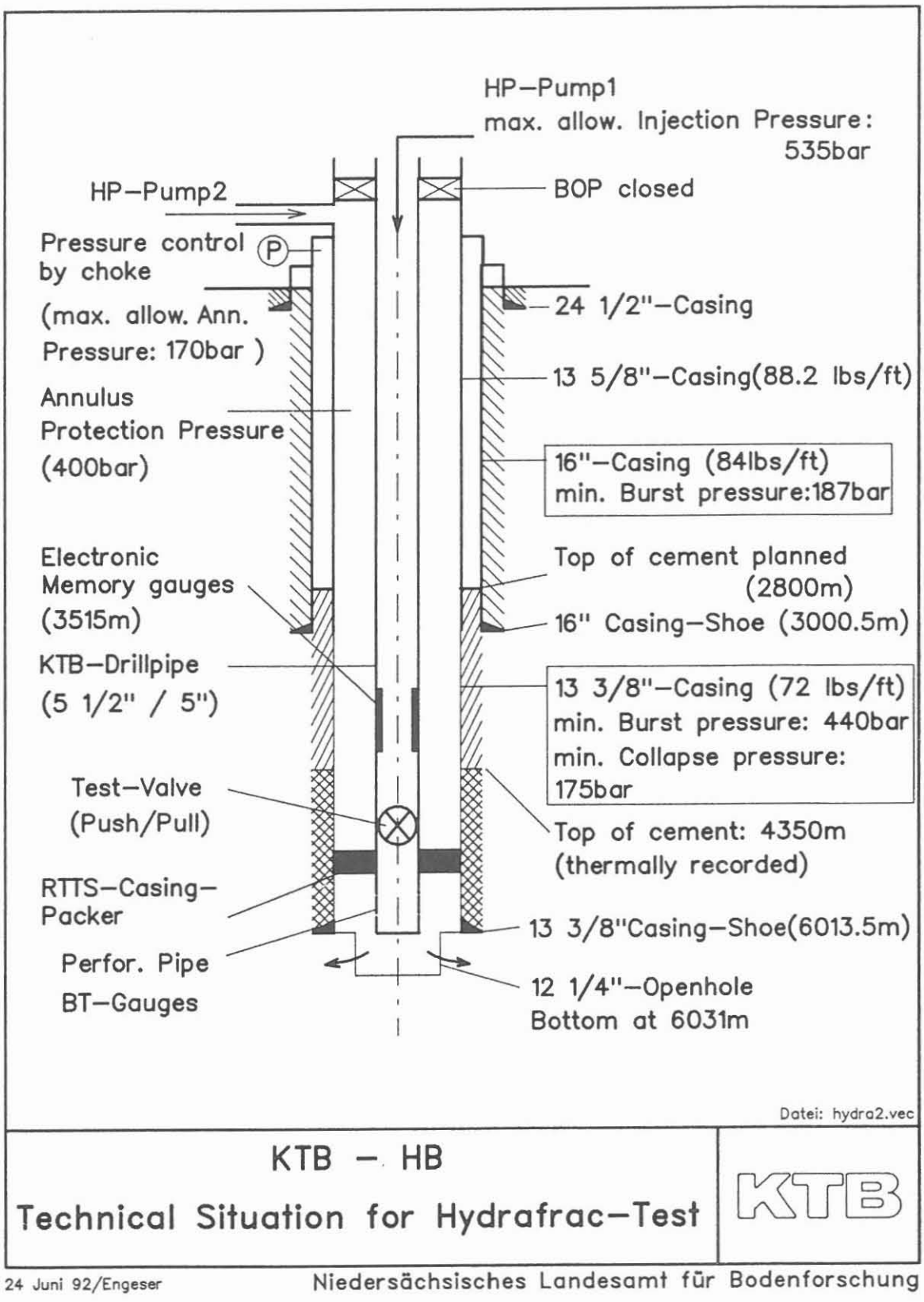

Fig. 1: Technical situation for the hydrofrac test KTB-HB 6000 m. Units: 10 bar = 1 MPa. See text for abbreviations

The maximum permissible injection pressure or bottom hole pressure was primarily determined from the minimum internal and external burst pressure of the 13 3/8" and 16" casing according to Fig. 1. Taking into consideration the minimum internal burst pressure of the 13 3/8" casing of 44.0 MPa, the maximum protection pressure in the annulus between the drill pipe and 13 3/8" casing was determined to be 40.0 MPa. Taking into consideration the minimum external burst pressure of the 13 3/8" casing of 17.5 MPa, and the fact that hydraulic communication in the cemented area behind the casing could not be ruled out, the maximum permissible injection pressure was limited to 53.5 MPa (40.0 MPa + 17.5 MPa - 4.0 MPa safety margin) in order to safely rule out the collapse of the lower part of the casing.

Moreover, a possible hydraulic communication between the frac interval via the cemented region of the 13 3/8" casing with the non-cemented annulus between the 13 5/8" casing and the 16" casing could also not be ruled out, mainly because the required quality of the cementation could not be guaranteed because of the very restricted annulus. The chances of there being possible communication were considered to have been increased because of the losses which occurred during the cementation (total 30 m3) and the associated deeper lying position of the cement head (plan: 2800 m, thermal 4350 m). The potential danger of exceeding the internal burst pressure of the 16" casing (minimum 18.7 MPa) which could result if there was communication, was avoided by taking the appropriate pressure monitoring steps and maintaining control over the 13 3/8" / 16" annulus via the choke manifold, as well as laying down a maximum permissible pressure of 17.0 MPa. In addition, an hydraulic tightness test of the cementation was planned before carrying out the hydrofrac experiment.

2.3 Technical Set-up

The planning and selection of the equipment required for carrying out the hydrofrac experiment was largely based on the following criteria:

- The utilization of conventional - and taking into consideration the specific test conditions to be encountered here - field proven and reliable drillstem testing equipment.
- The use of suitable high pressure pump equipment with sufficient flexibility to cope with a pump rate range from 1 - 150 l/min.
- Data aquisition and storage equipment appropriate to the needs of the scientific objectives.

2.3.1 Downhole test equipment

The configuration of the downhole test equipment is shown in Fig. 2. The following were of particular importance for the planning:

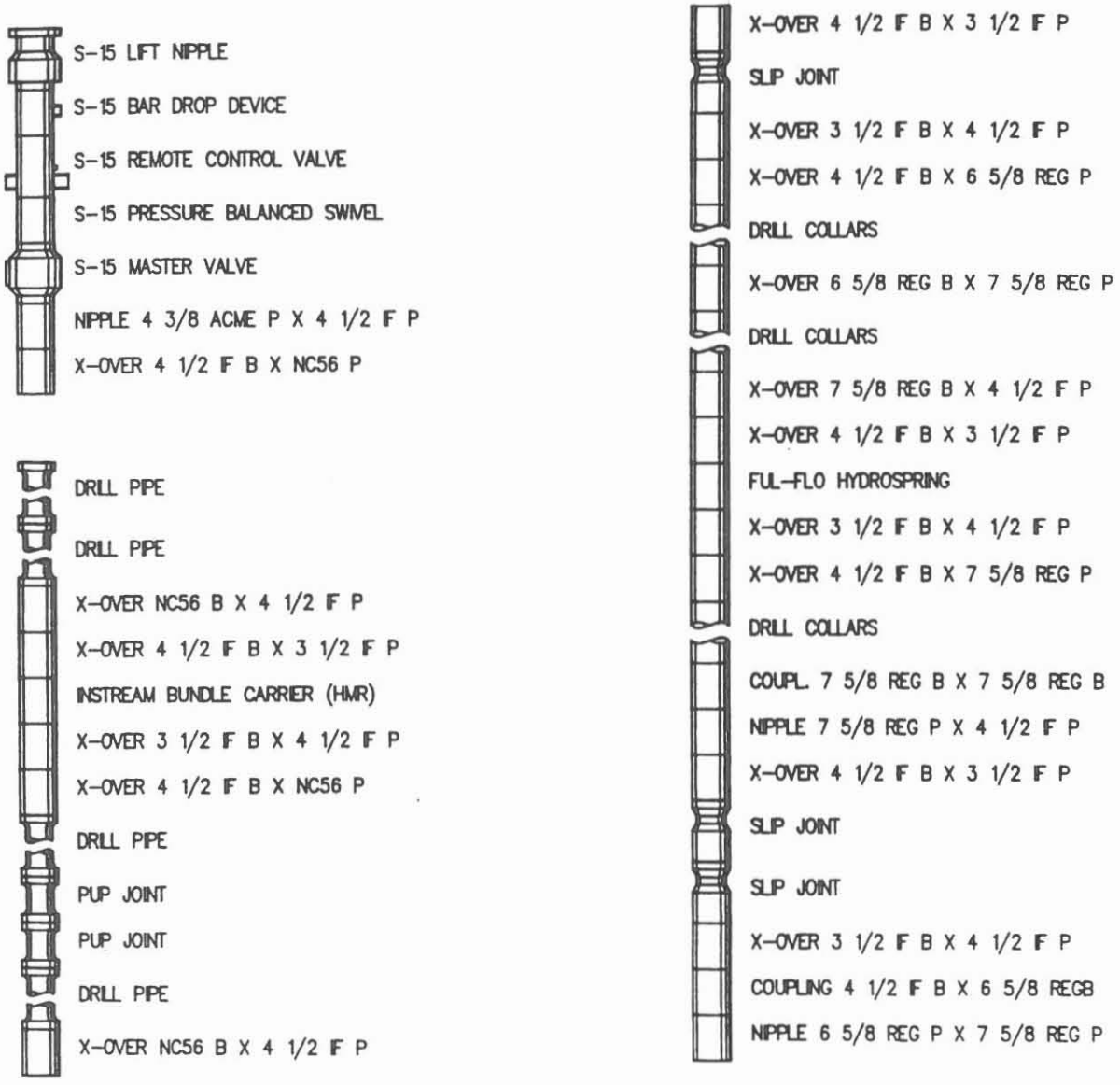

Fig. 2: Downhole test equipment. Test string configuration for hydrofrac test.

- Packer

To isolate the test interval, a weight loaded, casing wall anchored, mechanical packer of RTTS type was used (Fig. 3). The packer which has a J-slot, is set by turning right and loading with the weight of the drill collars (15-20 t) located above the packer. Hydraulically activated slips prevent the tool from beeing pumped up the hole due to the axial stress resulting from the high injection pressures are carried upwards.

The size of packer that can be used in a 13 3/8" casing is suitable for differential pressures up to 51.7 MPa (7,500 PSi) at temperatures up to 230 ØC (450 ØF).

- Test valve

A test valve of "Ful/Flo Hydrospring" type was used for the downhole closing and opening of the test interval. There is no limit to the number of times this type of valve can be opened and closed - and it can be opened and closed by unloading/loading (down/up movement) respectively. Moreover, it's internal diameter is not restricted, end to end. Slip joints between the packer and the test valve ensure that the load on the packer is not released while the test valve is being manipulated.

Tab. 2: Details on the mech. and elect. measuring equipment

	mechanical (Bourdon-tube)	electronic (quartz)
Pressure		
Range	up to 170 MPa	up to 110 MPa
Accuracy	0.2 % of range	6.9 KPa + 0.01% of measured value
Resolution	0.05 % of range	0.07 KPa
Temperature		
Range	up to 340Ø C	up to 180Ø C
Accuracy	(+/-) 2Ø C	(+/-) 0.1Ø C
Resolution	0.05 % of range	0.06Ø C
Time		
Accuracy	poor	1 s

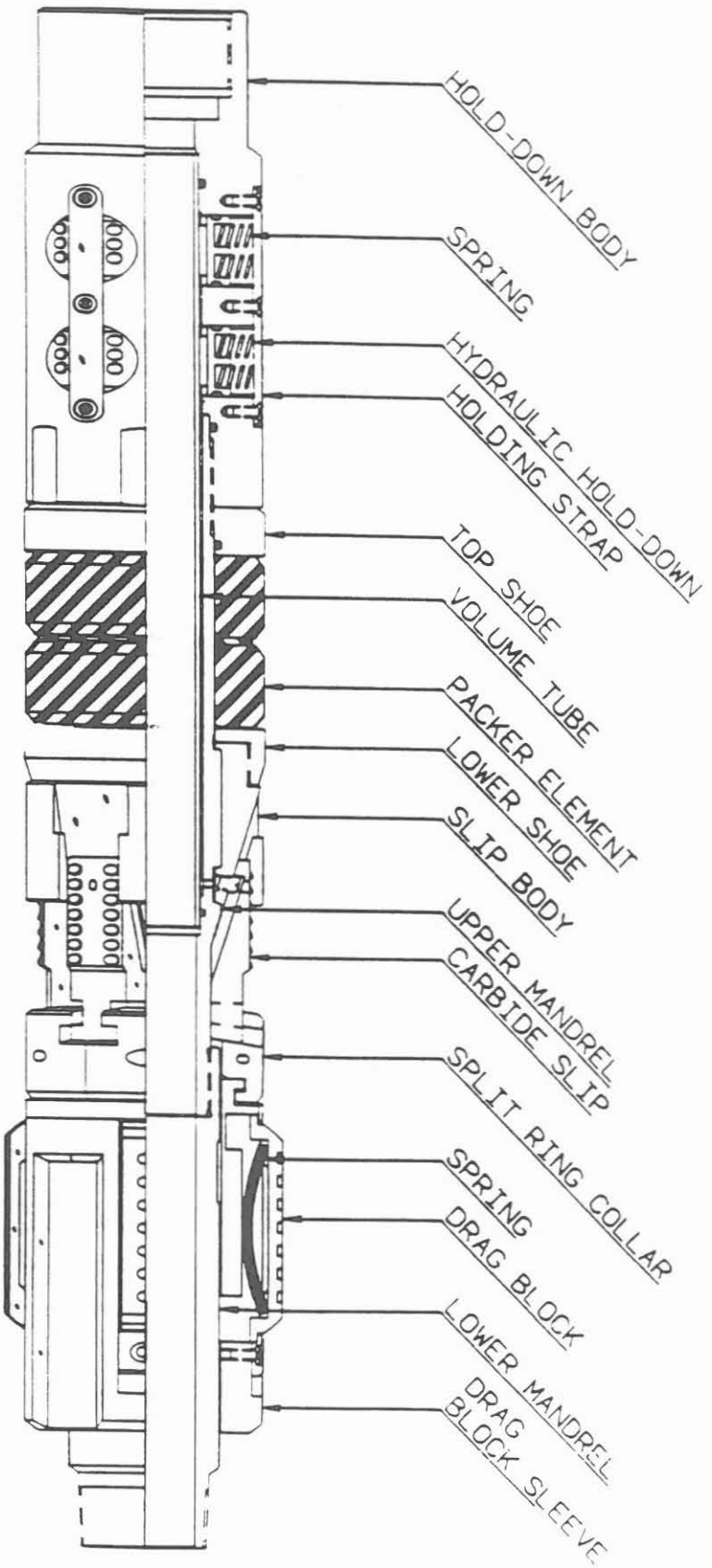

Fig. 3: Mechanical packer type RTTS

- Logging equipment

The downhole pressure and temperature recording was done both mechanically and electronically. Three mechanical probes (Bourdon tube measuring principle) were located below the packer, immediately adjacent to the test interval, for recording the pressure (2 probes) and temperature (1 probe).

The electronic measuring equipment with quartz probes - which have considerably greater resolution and accuracy (see Tab. 2) than the mechanical probes - could not be installed in the test interval zone because the ambient pressure and temperature conditions were too extreme. Two memory recording tools (type HMR) were, therefore, set at a depth of 3518 m - within their permissible rating conditions.

- Test string

The KTB drillstring was used as the test string. Data relevant to the test is shown in Table 3.

Tab. 3: KTB-HB-hydrofrac-experiment. Drill string details.

Nominal diameter (inch)	grade	nominal weight (lbs/ft)	displacement open (l/m)	displacement closed (l/m)	capacity (l/m)	yield pressure burst (bar)	yield pressure collapse (bar)	section length (m)
5	G-105	19.5	4	13.2	9.1	863	603	2079.8
5	S-135	19.5	4.1	13.2	9.1	1110	690	2009.4
5 1/2	S-135	24.7	5.2	16	10.7	1159	770	1762

2.3.2 Surface equipment

- Test equipment

The surface test equipment consisted of a conventional test head (Fig. 2). Wireline equipment was not used for running in the pressure recorders or for taking fluid samples during the test because of the absence of crossovers and other necessary supplementary equipment.

- High pressure pump equipment

The main criteria for selecting the high pressure pump equipment were as follows:

. Variable pump rate range between 1 - 150 l/min at 53.5 MPa to create the frac.

. Constant availability of pump equipment for maintaining the protection pressure of 40.0 MPa in the drill string/ 13 5/8" casing annulus.

. Guarantee of sufficient pump rate capacity in the event of their being communication to the 16" / 13 5/8 " annulus - by adding extra pumps to the injection string.

The high pressure pump equipment was integrated into the surface line system in such a way that the planned pump situations could quickly be covered by setting gate valves (Fig. 4). The following pump equipment was on hand:

1 HT 400 with HP1 = 150 l/min at 53.0 MPa (HP1 = Halliburton pump 1)
HP2 = 100 l/min at 45.0 MPa (HP2 = Halliburton pump 2)
1 HT 150 with HP3 = 90 l/min at 53.0 MPa (HP3 = Halliburton pump 3)
1 Mesy-compressed air pump = 9 l/min at 60.0 MPa

- Data acquisition:

The objective of the surface data acquisition was the continuous digital measurement and storage of the injection rates and pressures at the highest possible accuracy, resolution and sampling rate. For data security reasons, redundant and independent data acquisition was integrated into the system. The following parameters were digitally aquired and stored as shown in the diagram in Fig. 4:

- Injection rates:

. stroke counter at the Halliburton pump equipment.

. turbine - flowmeter for measuring in the range 1 - 10 l/min (Mesy)

- Pressures

* DP injection pressure (P1): Halliburton
Mesy pressure recorders.

* Protection pressure in the annulus
DP / 13 5/8" casing (P2): Halliburton Mesy - pressure recorder.

* Pressure in the annulus
13 5/8 "/16" casing (P3): Halliburton pressure recorder.

In the event of communication to the 13 5/8" / 16" annulus, a Halliburton turbine-flowmeter was installed for the control of the leakoff rate.

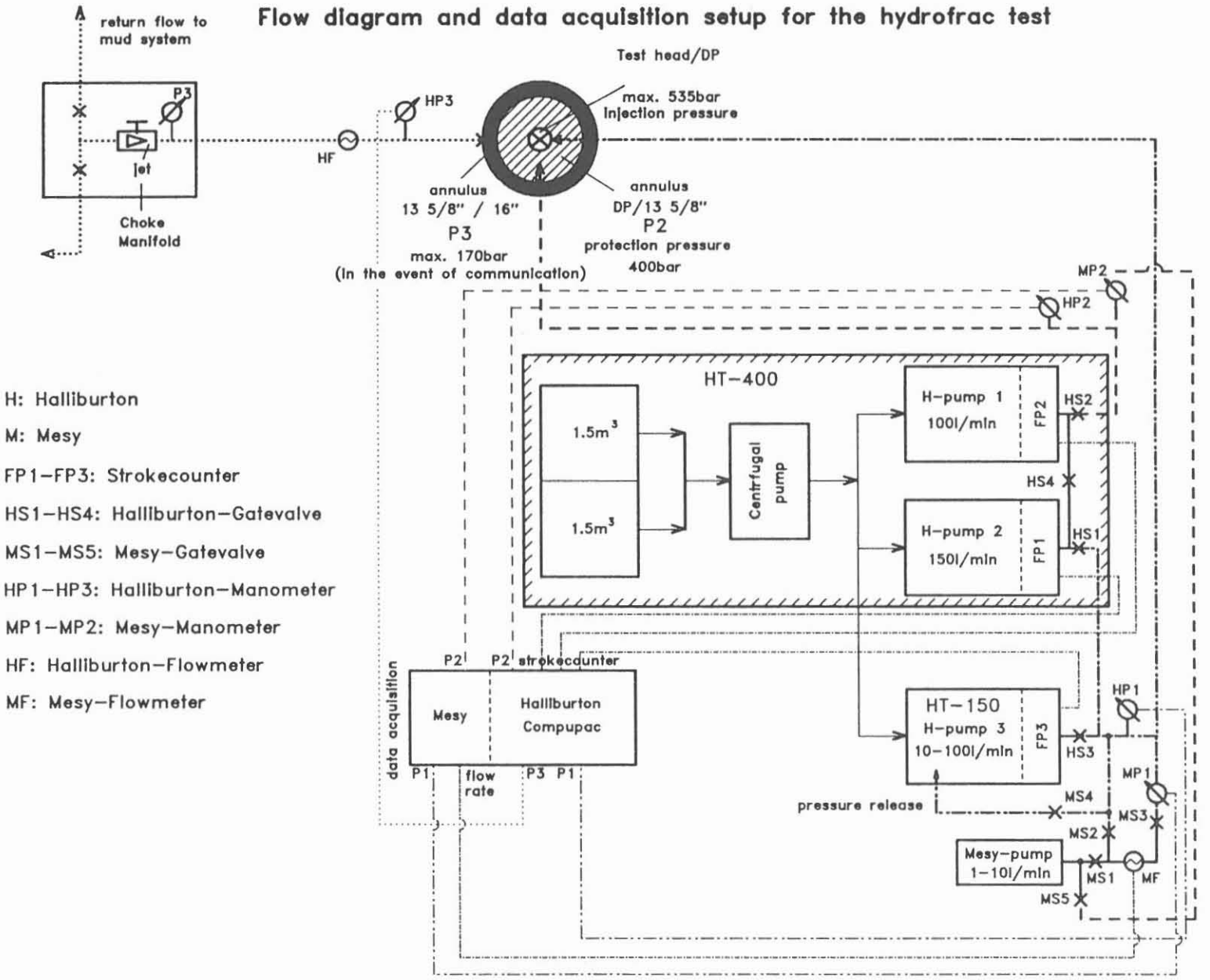

Fig. 4: Flow diagram and data acquisition setup for the hydrofrac test.

2.4 Program

The program of the main steps planned for the hydrofrac experiment after the running and cementation of the 13 3/8" / 13 5/8" casing, including the technical preparation work, was as follows:

1. Drilling out the casing collar and shoe with subsequent deepening of the hole by approx. 50 m at 12 1/4" diameter.
2. Scraper run with GR and CCL logs (to ensure that the packer can be run safely).
3. Multifinger caliper log (not in relation with the hydrofrac experiment).
4. BHTV and/or FMI log as the initial measurement for subsequent determination of the frac orientation following the hydrofrac test.
5. Pressuring the drill string and ther surface equipment.
6. Running in the test equipment: In order to carry out the flow test for determining the hydraulic parameters - which was to be carried out prior to the hydrofrac test - it was planned to run in the test equipment closed. The maximum differential pressure for the flow test was to be 7.0 MPa, and the test string was accordingly filled with mud to a depth of 700 m.
7. Setting the packers above the casing shoe and opening the test valve.
8. Flow period for the flow test.
9. Closing the test valve and shut-in period for the flow test with pressure build up.
10. Filling the test string prior to the injection tests.
11. Carrying out a step injection test for determining the pressure dependency of the permeability prior to the frac test.
12. Frac test with increasing the pressure up to the frac pressure and pressure monitoring.
13. Re-frac test with the lowest possible pump rate.
14. Step injection test for determining the permeability after the frac test.
15. Running out the test equipment and lowering the mud level to 700 m (by partial refilling of the mud volume displaced whilst running out the sealed test equipment).
16. BHTV and/or FMI logging to determine the frac orientation.
17. Fluid sampler run.

The planning included making the precise program, particularly for the frac and re-frac tests, dependent on the progress of operations.

3. Implementation

3.1 General program

The preparatory work for the hydrofrac experiment began on 22.04.1992 with the tightness test of the 13 3/8" cementation, after (in connection with drilling out of the casing collar and casing shoe) confirming the tightness of the casing by increasing the pressure to 30.0 MPa. The hydrofrac experiment was concluded on 02.05.1992 with fluid level measurements and a fluid sampler run.

The chronological sequence of events and the time involved for the most important steps of the hydrofrac experiment are shown in Table 4 below. Figure 5 shows the time brakdown for the hydrofrac-experiment.

Tab. 4: Chronological sequence of events of the hydrofrac test.

Date/time from	date/time to	steps carried out	duration (h)	to hydrofrac (h)
22.4.92 0900	22.4.92 1345	Cementation tightness test	4.75	4.75
22.4.92 1345	24.4.91 0130	Scraperrun/GR-CCL log	35.75	23
24.4.91 0130	24.4.92 1830	Multifinger-caliper	17	
24.4.92 1830	27.4.92 1730	Drilling from 6022 m-6031 m	71	
27.4.92 1730	27.4.92 2245	Positioning mud pill for BHTV Pressuring drillstring	5.25	5.25
27.4.92 2245	28.4.92 1000	Running out and laying down PHA	11.25	
28.4.92 1000	28.4.92 1630	BHTV logging	6.5	6.5
28.4.92 1630	29.4.92 1900	Assembly testing equipment running and pressurizing	26	26
29.4.92 1830	29.4.92 1900	Set packer	0.5	0.5
29.4.92 1900	29.4.92 2000	Open test valve/flow period	1	1
29.4.92 2000	30.4.92 1045	Close test valve/shut-in period	14.75	14.75
30.4.92 1045	01.5.92 0115	Injecting/frac test	14.5	14.5
01.5.92 0115	01.5.92 0245	Pulling free packer	1.5	1.5
01.5.92 0245	02.5.92 0100	Running out and laying down test eq.	22.25	22.25
02.5.92 0100	02.5.92 1900	AMS-SP/BHTV/Mud level measing fluid sampler run	18	18
			total:	138

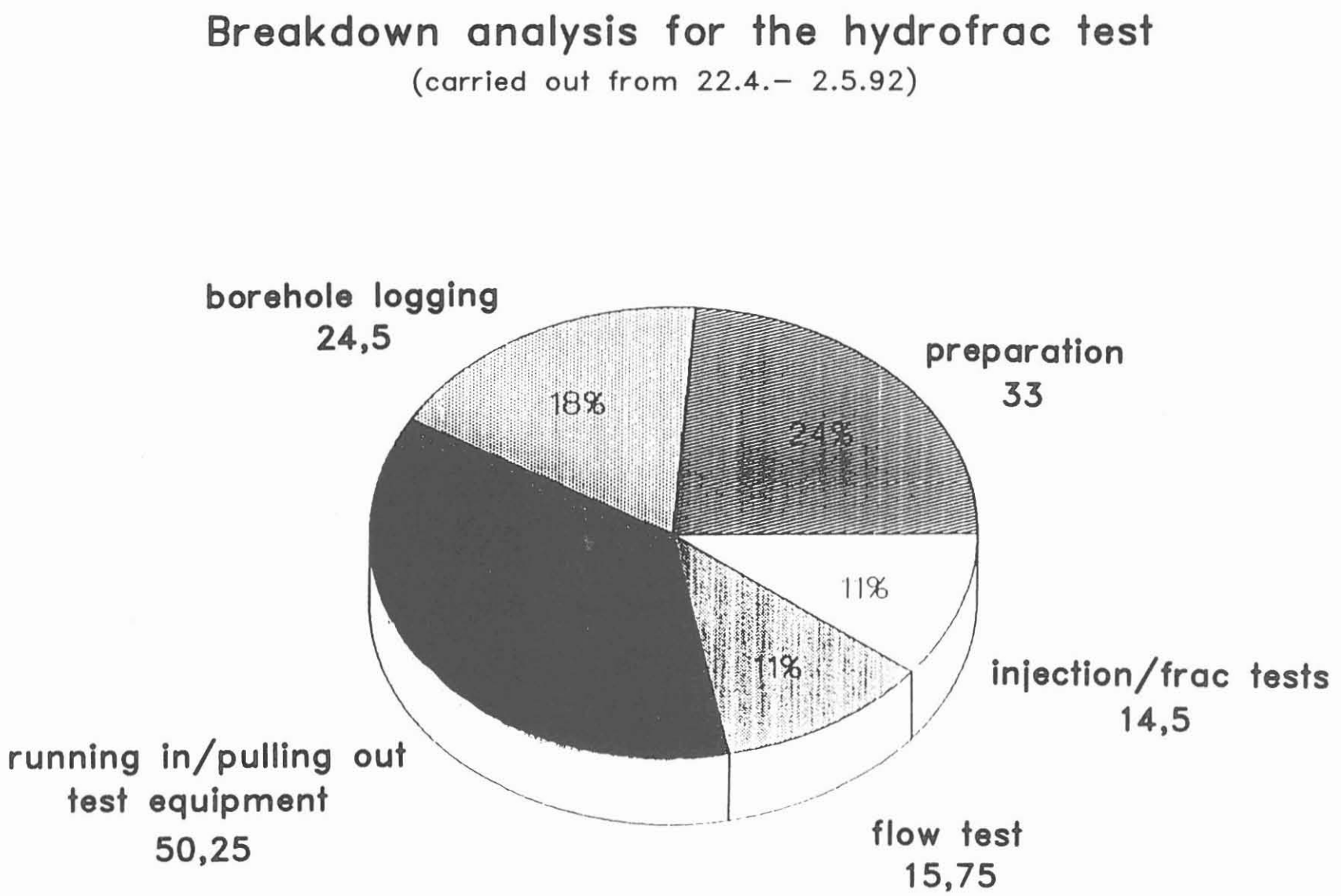

Fig. 5: Time analysis for the hydrofrac test.

3.2 Cementation tightness test

As discussed in section 2.2, prior to carrying out the actual hydrofrac test, a hydraulic tightness test of the 13 3/8" casing cementation was carried out because there was the possibility of communication to the non-cemented 16"/13 5/8" annulus - in the event of which it would not have been possible to carry out the hydrofrac test.

Thus, on 22.04.1992, after deepening the well to 6022 m and running out the drill string up to the BHA (bottom hole assembly) the borehole pressure was raised to a head pressure of 23.0 MPa with closed preventer, with subsequent monitoring of the pressure development. The following pressures were measured and recorded:

injection pressure:	P1
annulus pressure: drill string / 13 3/8" casing:	P2
annulus pressure: 16" / 13 3/8" casing:	P3

The pressure log results are shown in Fig. 6. The four columns in the diagram from left to right show the following as a function of time:

1. P1 and P3
2. P3 high resolution
3. P1 high resolution
4. difference between P1 - P3

Up to 2500 sec, the P3 pressure in the 13 3/8"/16" annulus corresponded with the increase within the casing to approx. 5.2 MPa. This increase in pressure is considered to arise from the ballooning effect of the casing and the associated volume compression in the annulus. The pressure reduction in P3 from 2500 sec to the end of the logging period is probably caused by the permeability in the non-cemented annulus of the 13 3/8" casing between 3000 and 6000 m. With the decrease in P3, the ballooning effect also decreases and accordingly so does P1. Apart from this, there were no significant pressure changes so that the cementation can be considered to be tight from a technical point of view. An assessment of the permeability in the openhole area from 6013 to 6022 m is not possible because of the above mentioned effects and because of the large wellbore-storage-coefficient of the borehole. The upper limit of the permeability probably lies around 1 μD.

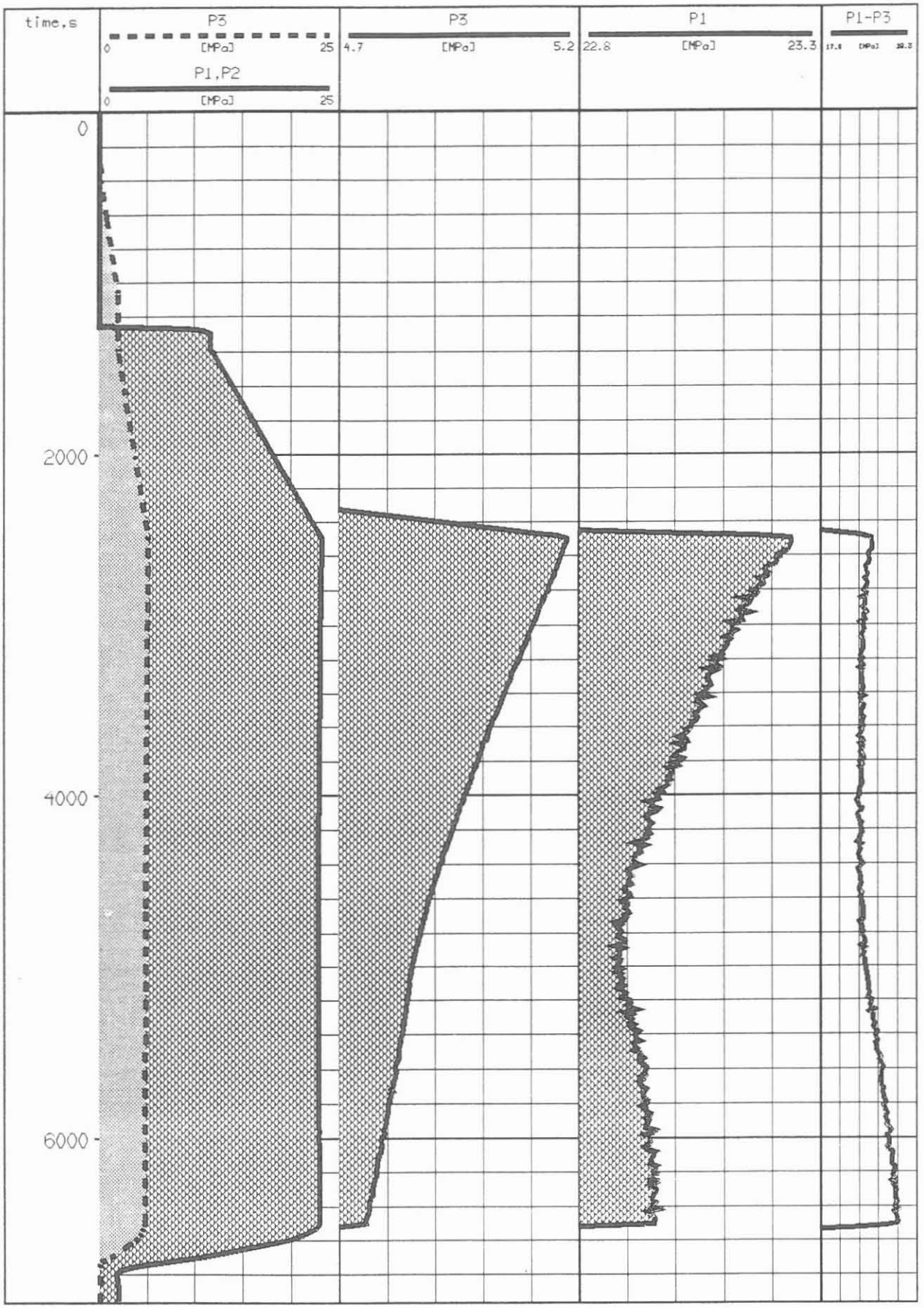

Fig. 6: Pressure measurements during the cementation tightness tests on 22.04.1992. Tracks: 1. P1 and P3, 2. P3 high resolution, 3. P1 high resolution, 4. difference P1-P3

3.3 Packer test

In a deviation from the plans, see section 2.4, the borehole was deepened to 6031 m. On 28.04.1992, the test equipment was run in to 6009 m and the packer set at 6005 m with 230 KN (Fig. 2). The progress of the test can be followed on the basis of the recorded pressure, pump rate and volume data - that are shown in the following figures as a function of time. The time is calculated in seconds from 28.04.1992, 21.00 hours. Figure 7 gives an overview of the sequence of events during the test. Important points are marked in capital letters.

3.3.1 Running in the test equipment and setting the packer

Figure 8 shows the change in pressure over the section A - F, that marks the technical operation up to the opening of the test valve for carrying out the first slug test. This section can be differentiated as follows according to the pressure curves.

A-B: Running in the test equipment up to the rigging up of the memory tools.
B-C: Continue running in the test equipment.
C-D: Continuing the run in whilst filling the string with mud.
D-E: Running in the test equipment without filling the string with mud.
E-F: Setting the packer and compliance phase of the packer.

The pressure difference in the pressure diagram (based on the data recorded by the mechanical pressure recorder (BT) at a depth of 6005 m) between points E and F of approx. 7.0 MPa represents the initial pressure drop with respect to the ground level for carrying out the first slug tests - caused by the upper 700 m of drill string not being filled with mud.

3.3.2 Inflow test (Drawdown test)

The total flow test is shown in Figure 9 between letters F to I and is divided up as follows:

F: Opening the test valve
F-G: Flow phase
G: Closing the test valve
G-I: Shut-down phase (pressure build-up with small wellbore storage).
H1-H2: Filling the string with a closed test valve.

No significant pressure changes were recorded during the pressure build-up, which can be explained by the very large wellbore storage (for a small change in pressure a large volume of fluid must flow in) and the relatively low permeability.

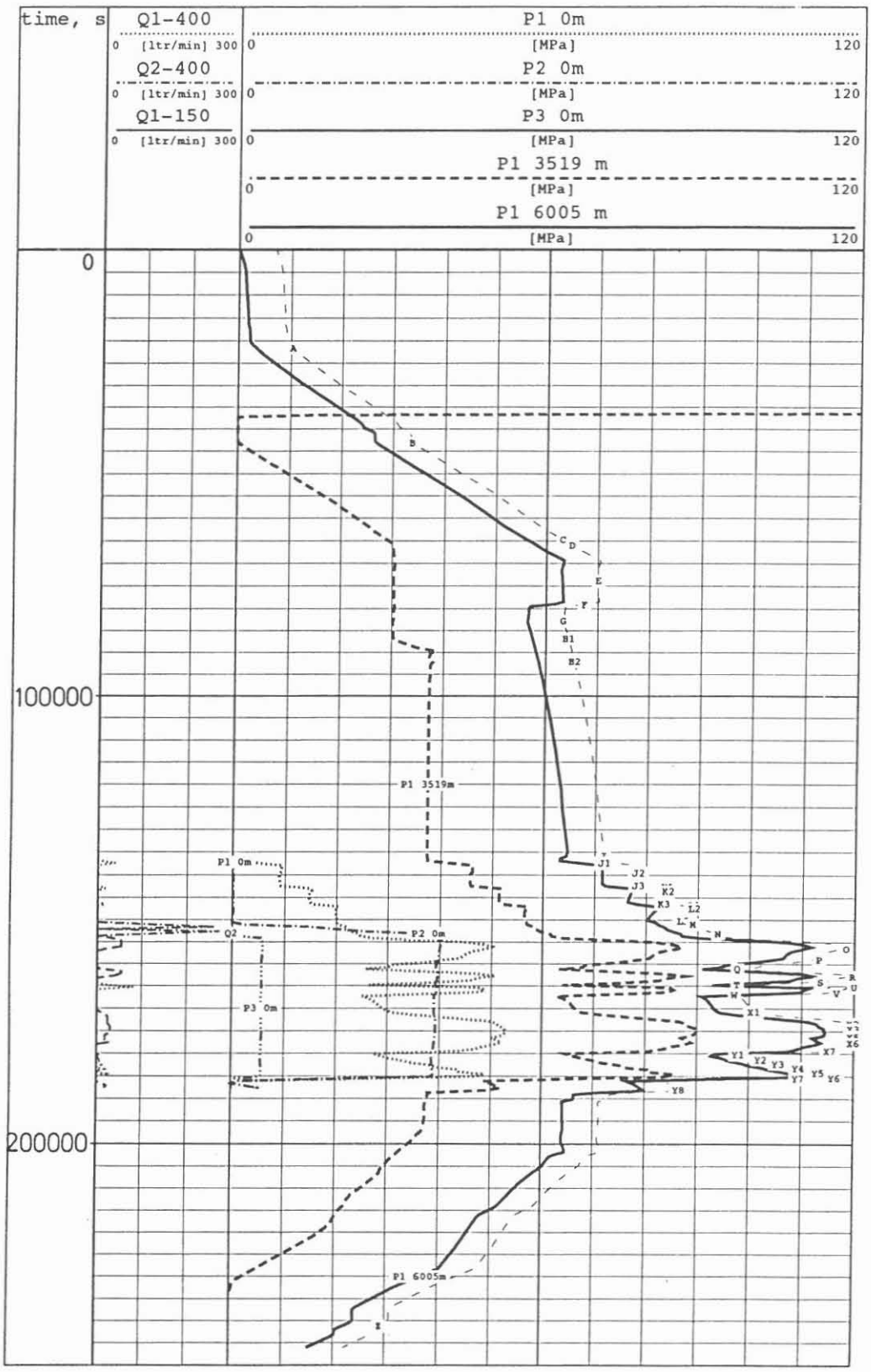

Fig. 7: Pump rate, volumes and pressures during the hydrofrac tests. Time zero is 28.04.1992, 21.00 hours. Tracks: 1. pump rates with pump system HT-150 and HT-400 into drill pipe (1) and annulus. DP/13 5/8" = (2), 2. volumes in (1) and (2), 3. pressure recorded in the annulus 13 5/8"/16" = (3), (2) and in the three depth intervals in (1) at 0 m, 3519 m and 6005 m.

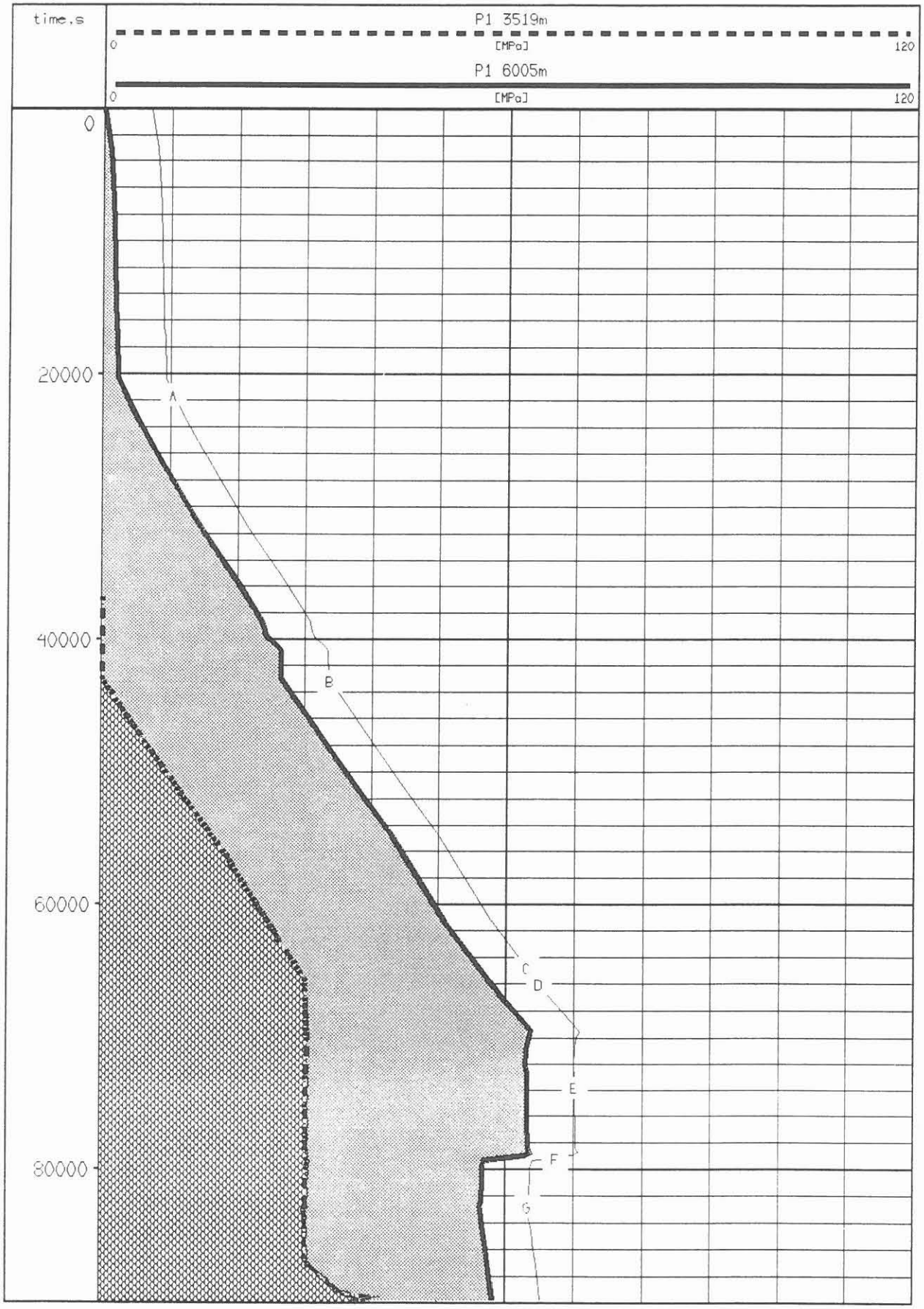

Fig. 8: Pressures while running in the test equipment and during the setting of the packer.

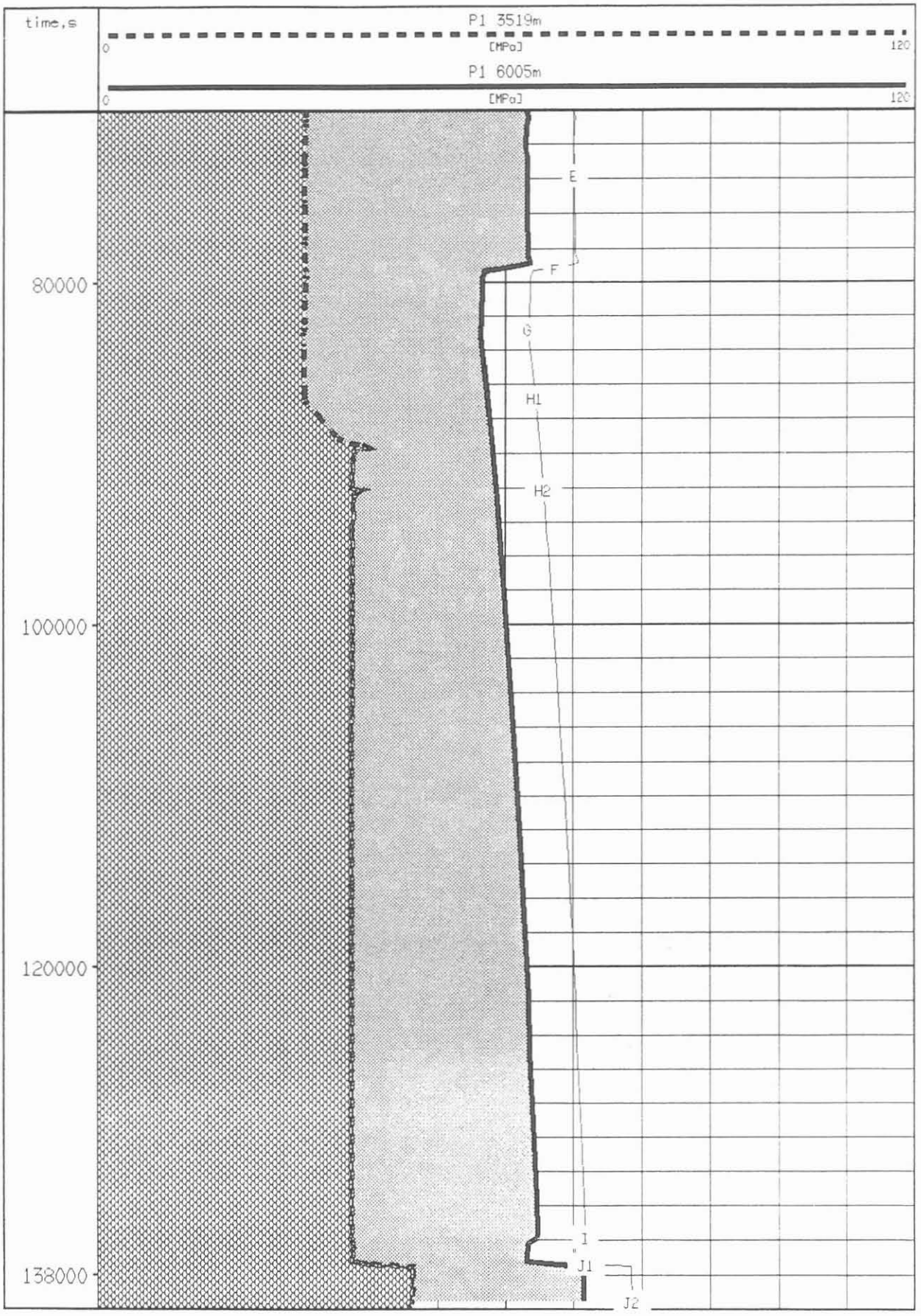

Fig. 9: Pressures during the flow test.

By closing the test valve (G) the storage ability of the borehole was reduced by a factor of 0.06, giving a slow but clearly recordable build-up of pressure. An initial estimate gave an average permeability of 0.5 µD. This test showed, in the interval to be tested by the frac test, that no well developed, naturally occurring, hydraulically conducting fracs existed. During the test, an increase of the temperature of $4^{\circ} \pm 0.5^{\circ}$ C was registered in the test interval. Furthermore, the pressures recorded in the test interval do not indicate any effects caused by the filling up of the test string, which makes it clear that the test valve is tight.

3.3.3 The pressure step test prior to the frac test

The pressure step test (J1-M in Fig. 10) was intended to determine the pressure dependence of the permeability and to establish the formation pressure. To this end, the pressure in the test interval was increased in three steps of approx. 6.5 MPa. The final pressure measurement was then carried out after the third step for a period of approx. 10 min. with an open test valve, so that the relatively large shut-in liquid volume had a relatively high wellbore-storage-coefficient.

Subsequently, the test valve was closed, in order to reduce this storage capacity via the small shut-in volume of mud, in order to achieve a more rapid build-up or decline in pressure.

The test steps are marked in Figure 10 as follows:

J1: Raising the pressure with the pumps
J1-J2: Monitoring the pressure with surface shut-in test interval.
J2: Closing the downhole test valve
J2-J3: Monitoring with downhole closed-in test interval.
J3-K1: Opening the downhole test valve and increasing the pressure with the pumps.
K1-K2: Monitoring the pressure with surface shut-in test interval.
K2: Closing the downhole test valve.
K2-K3: Monitoring the pressure with downhole shut-in test interval:
K3-L1: Opening the surface test valve and increasing the pressure with the pumps.
L1-L2: Monitoring the pressure with surface shut-in test interval.
L2: Closing the downhole test valve.
L2-L3: Monitoring the downhole shut-in test interval.

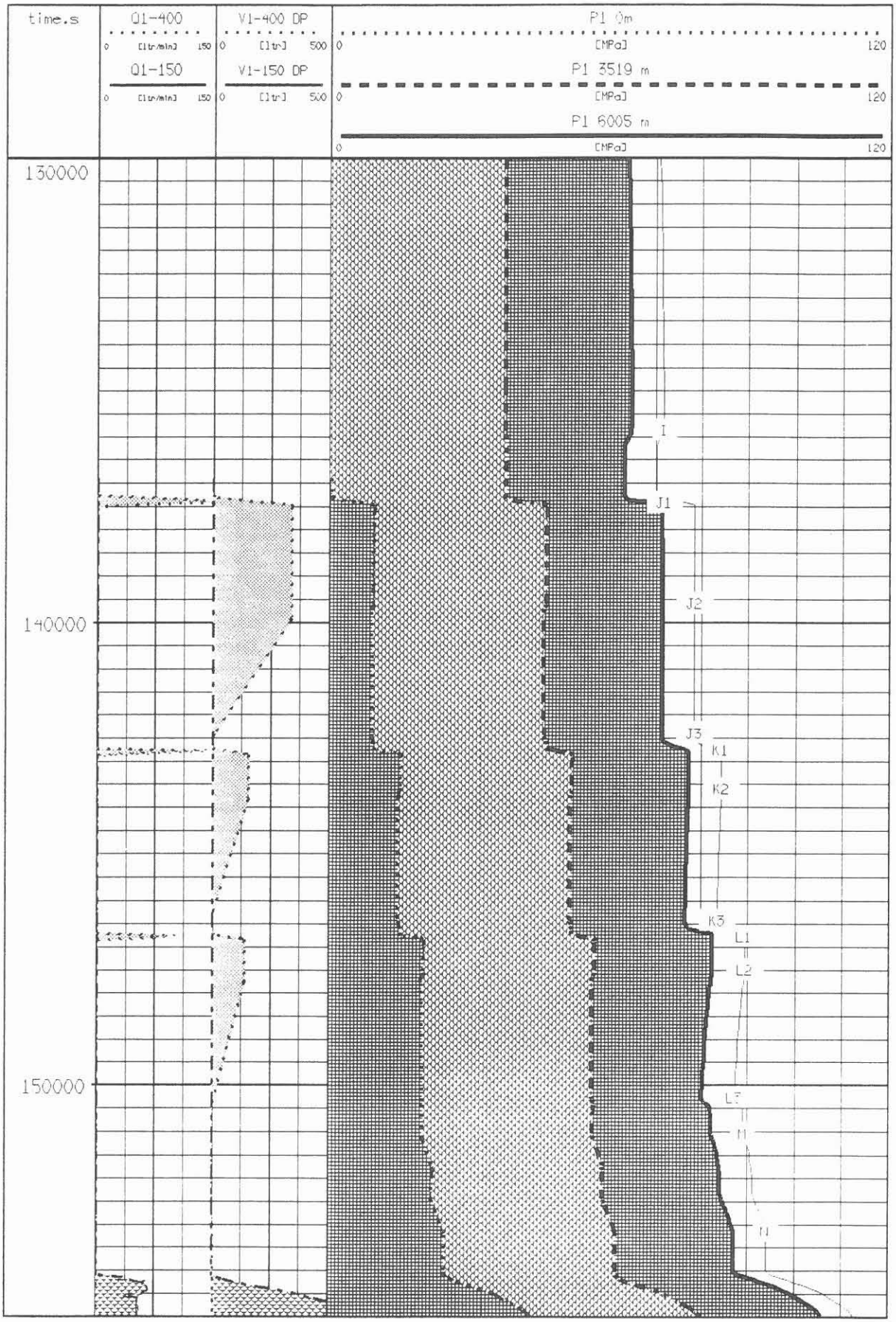

Fig. 10: Pump rates, volumes and pressures during the pressure step tests before the frac test.

From the log it is clear that significant pressure changes only occur when the surface test valve is closed. During the first shut-in phase (J2-J3) only a very slight pressure reduction was recorded, which indicates that the original formation pressure lies slightly below the pressure of 71.5 MPa raised in the first pressure step. It must in any case be at least larger than the pressure of 64.7 MPa measured at the end of the shut-in test (I). The last pressure decline curve (L2-L3) at a pressure level of 82.3 MPa already shows a clear pressure decline. To what extent this more rapid pressure decline can also be attributed to an increase in permeability can only be determined with the results of the hydraulic evaluations.

3.3.4 Frac test

The region in Figure 11 marked with the letters M to Y1 represents the actual frac test. The equipment layout is shown in Figure 4. The HT-400 system with the HP1 and HP2 pumps supplies both the annulus (P2) as well as the drill pipe (P1). The pump rate of the HT-400 system and the HT-150 system are shown separately in Figure 11. This test can be divided into the following steps:

M-N: Building up the protection pressure (P2) in the annulus (see Fig. 4).

N-O: Injecting with a constant pump rate of approx. 60 l/min. with the objective of reaching the frac pressure.

O: Stopping the pumps.

O-P: Monitoring the pressure with surface shut-in.

P-Q: Stepwise pressure reduction.

Q-R: Renewed pressure build-up by pumping at 60 l/min. to achieve the frac pressure.

R: Turning off the pumps.

R-S: Pressure decline curve with downhole shut-in.

S-T: Releasing the pressure.

T-U: Increasing the pressure with 150 l/min. up to the maximum allowable pressure.

U-V: Pressure decline curve with surface shut-in.

V-W: Releasing the pressure.

W-X1: Pressure buildup curve to determine the existing reservoir pressure

X1-X2: Pumping at a constant pump rate of 30 l/min. Figure 11, and at a higher resolution, Figure 12, show that despite continued pumping (see tracks 1 and 2) that the pressure, P1, at the three depths did not increase after X2. This shows that a frac opened at 114 ± 5 MPa. This value - that equates with the minimum principle stress - is higher than was predicted by extrapolating the hydrofrac data between 1 and 3 km.

X2-X6: Different pump phases to observe the opening and closing of the frac.

X6-X7: Pressure decrease after surface shut-in.

X7-Y1: Releasing the pressure.

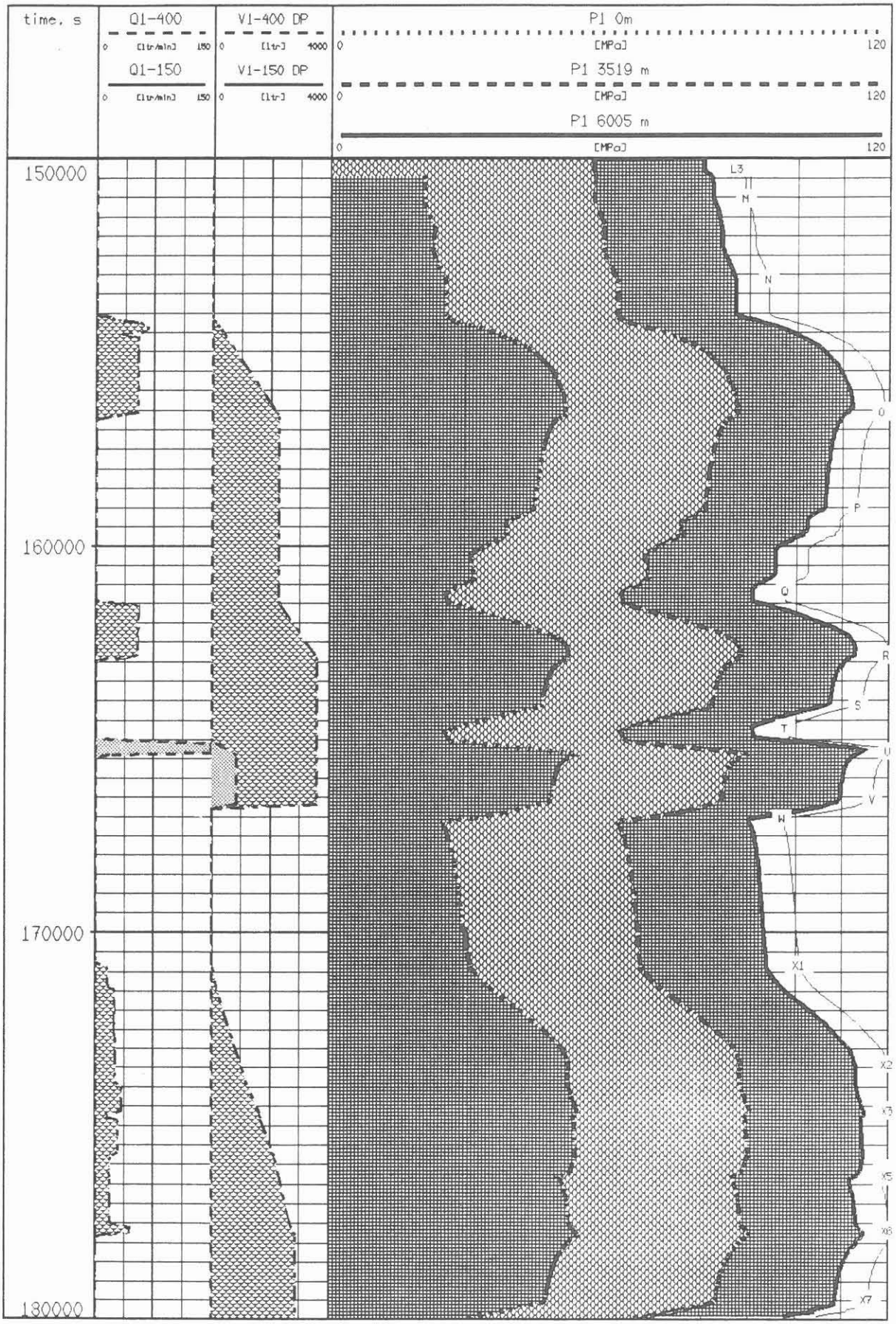

Fig. 11: Pump rates, volumes and pressures during the frac test.

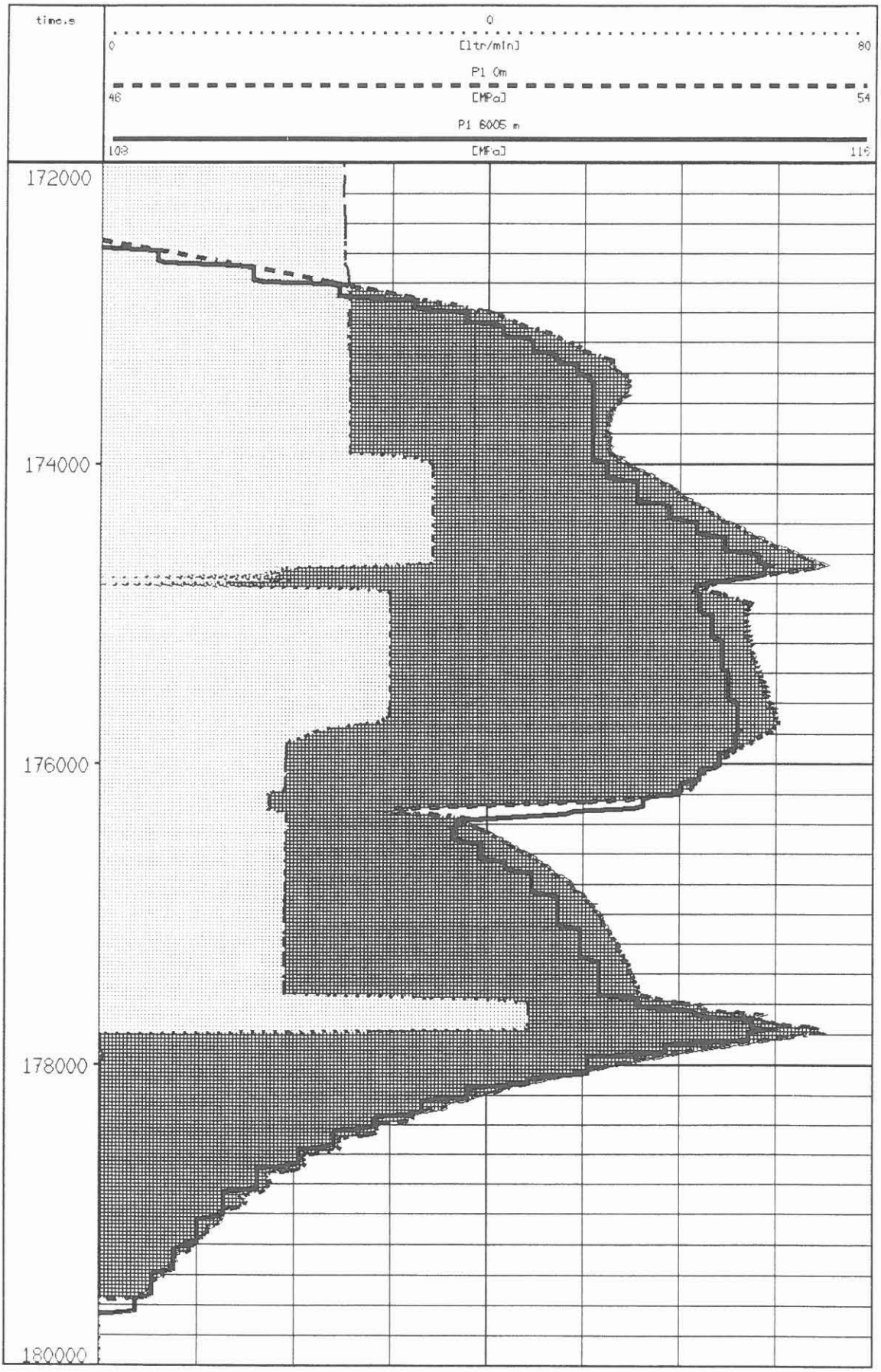

Fig. 12: Pump rates and pressures during the frac test. At 173500 sec the pressure P1 at 0 m falls while the pressure P1 at 6005 m remains constant even though pumping continued.

The pressure increase in section W-X1 already shows that the reservoir pressure in the region of the borehole has been significantly increased as a result of the pumped-in liquid. The pressure at X1 was already 94 MPa.

3.3.5 The pressure step test following the frac test

The last part of the test involved carrying out another pressure step test with two objectives:

1. the determination of the formation pressure in the region adjacent to the borehole and,
2. the determination of the pressure dependence of the permeability.

As shown in Figure 13, the pressure was increased stepwise and surface shut-in was carried out (Y1-Y7). Even without detailed hydraulic evaluations, one can see here, that at the various test levels there is a relatively rapid pressure change. The pressure in the frac system when the step tests were carried out lay between the Y4 and Y5 pressure steps shown. This is indicated by the increase in pressure, at the Y4 pressure step and by the pressure decrease at the Y3 pressure step. Thus, the pressure in the frac system at the time that the pressure step tests were carried out lay between 99.3 MPa and 102.7 MPa. This very slow decline in pressure also becomes immediately apparent when one compares the pressure increase from Y7-Y8 with the pressure increase from L2-N.

3.3.6 Running out of the hole

At the end of the pressure step test, the packer was released with 450 KN overpull and the test equipment pulled out of the hole. The last section from Y9-Z marks the removal from the hole of the test equipment.

3.4 Drawdown test and fluid sampling

A drop in the mud level of approx. 700 m was achieved by only partially replacing the mud displaced by the test equipment. By running in the fluid sample taker, the rise in mud level was measured with the AMS (see Fig. 14). This revealed an inflow of approx. 0.1 m^3. Subsequently, fluid samples were taken at depths of 6021.5 m and 6030 m. The fluid samples showed a strong contamination of the mud with a highly saline formation fluid, and also revealed a significant proportion of gas. The gas consisted predominantly of nitrogen, with approx. 85 %, and methane, with approx. 8.5 % (field laboratory report). One can therefore assume, that as a result of the frac, a connection was made to an hydraulic reservoir lying some distance from the borehole.

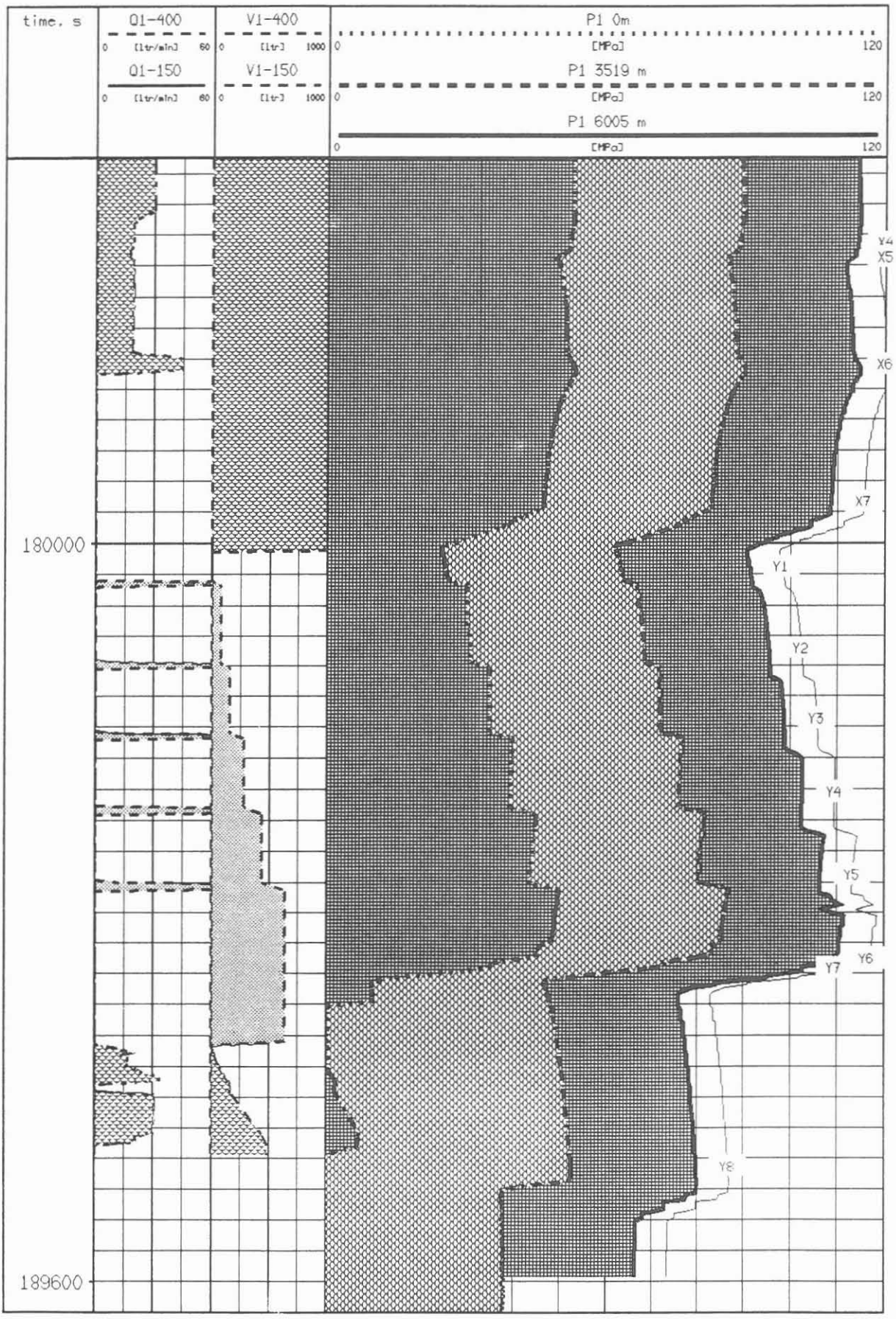

Fig. 13: Pump rates, volumes and pressures during the pressure step test after the frac test.

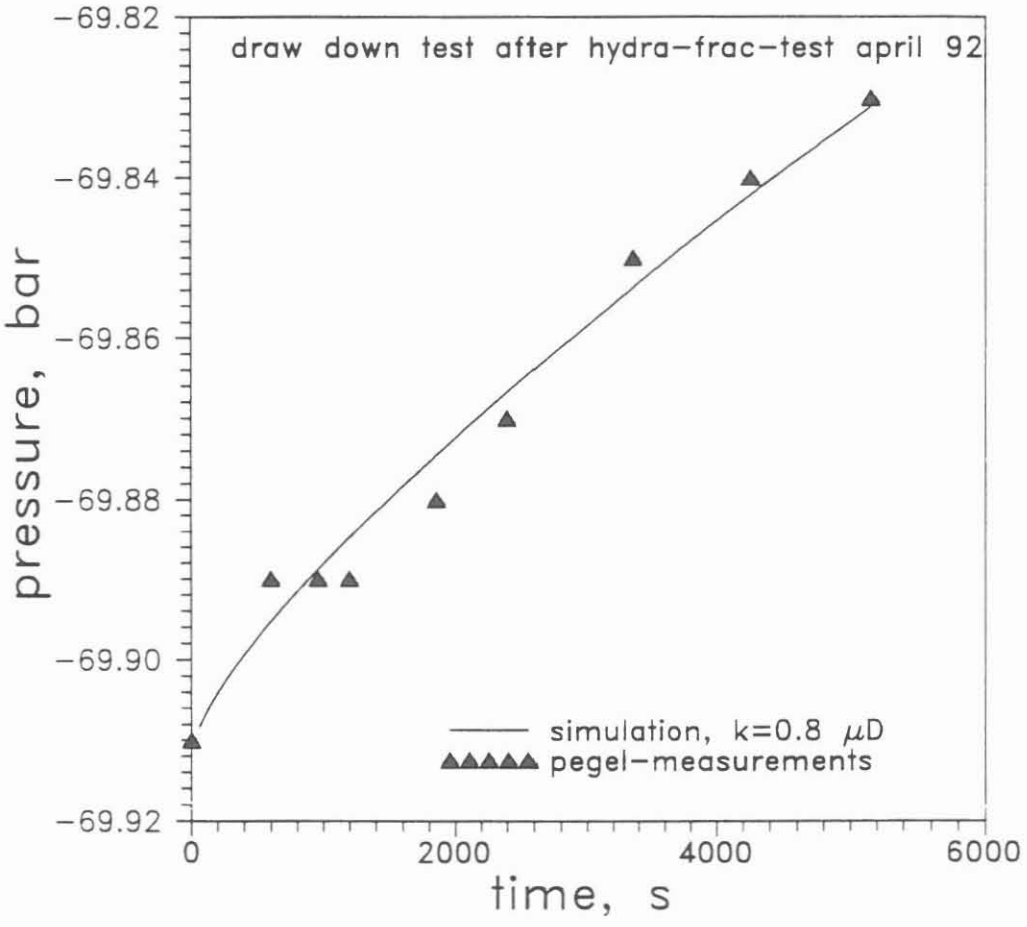

Fig. 14: After the mud level had dropped to 700 m while pulling the packer equipment out of the hole: pressures calculated from the level increase.

3.5 Borehole televiewer log

In order to determine the frac orientation, a borehole televiewer log was planned to be run before and after the frac test. The additional use, as originally planned, of an FMI log, was subsequently abandoned on economic grounds. This was in the knowledge that the BHTV log would identify fewer structures than would have been possible with the FMI log. However, fractures in borehole walls are among the most easily identifiable structures, so that there was some justification for the hope that the logging objective, namely the orientation of the fractures, could still be achieved using the significantly cheaper log.

The televiewer log run was to be carried out by DMT. However, on running in the televiewer log and carrying out a test measurement, a malfunction in the data transmission electronics of the logging tool was revealed that could not be repaired on site. Thus, the measurement prior to the frac test had to be abandoned in order to keep the overall test within budget and on time. Although the televiewer log after the frac test produced technically perfect data, it did not produce an interpretable amplitude image suitable for frac orientation. Discussions on site established the following reasons to explain the failure to determine frac orientation:

1. The relatively high amount of borehole caving within the test interval.

2. A multiple reflection in the acoustic window of the borehole televiewer that at the given diameter of the test interval had approximately the same travel time as the signal reflected from the borehole wall.

One can only hope that the latter problem in particular can be solved when it comes to running the next televiewer log, so that frac orientation will be possible during the 7000 m log run which includes FMI logging.

3.6 Seismic monitoring (see Appendix)

4. Discussion of the results

4.1 Quality of the log data

The allowable deployment range of downhole logging tools meant that only mechanical pressure recorders (Bourdon tube) could be used beneath the packer. However, because electronic probes can be used at a max. depth of 3519 m, the possibility arose of comparing the data, taking into consideration the height and density of the mud column. Figure 15 shows the comparison curves, determined with three different mud densities (1.06; 1.04 and 1.02 g/cm^3). The difference curves, set

out from -2.0 to +2.0 MPa, show systematic discrepancies over comparable time periods, i.e. with no separation of the measuring equipment after downhole shut-in. These are obviously independent of the mud density and the injected volumes. Thus, the Bourdon tube values at low pressure levels, e.g. F-G, Q, T and W-X1, are lower than those measured with the electronic measuring equipment. On the other hand, they are higher at the higher pressure levels, e.g. O, R, U, X2 to X7. The records after X7 are influenced by a discrepancy in the time, as has already been shown in Table 2. The accuracy of the pressure recorders on the basis of these results, and in contrast to the values given in Table 2, must be given as higher than 1.0 MPa for one or the other of the tools.

4.2 Preliminary evaluation

4.2.1 Hydraulic parameters

A preliminary hydraulic evaluation of the pressure data was carried out with the simulation program "HYDRANT" (KESSELS & ZINNER 1990). After interactive establishment of the starting values it was eventually possible to almost fully match the fluid pressure in the formation to a permeability without a skin factor. The geometrical parameters are given in Table 1 and Fig. 1. Material values such as the compressibility and viscosity of water were used

$$(4.4\ 10^{-10}\ Pa^{-1} \text{ and } 8\ 10^{-4}\ Pas).$$

HYDRANT is a finite differentiation program which makes it possible, with a preset number of grid points and reservoir expansions, to carry out a time-dependent pressure simulation for a horizontal, homogenous and hydraulic conductor. In order to fit the calculated pressures to the measured pressures it is possible to carry out multidimensional iterative parameter adaptions (permeability, skin, formation pressure etc.). Figure 16 shows in addition to the already displayed curves, the pump rate, volumes and pressures, the pressures measured at 6005 m, the permeability classified according to each test phase, and the fluid pressure in the near formation - all as a function of time. As time progresses, one can see that the fluid pressure within the formation at a given time lies above or below the fluid pressure in the borehole. There is no doubt that during the first drawdown tests, it lay above the hydrostatic pressure that was calculated with a density of 1.04 g/cm^3, and is shown in Figure 15 as the lower edge of the hatchured area in the "pressure rock" track. As the fluid pressure in the formation increases, i.e. with decreasing effective stress (stress minus fluid pressure considered tensorially) the permeability increases by several orders of magnitude. After releasing the fluid pressure, the permeability returns to a µD level, as indicated by the evaluation of the drawdown test after the removal of the test equipment. The change in the permeability with pressure is at any rate higher than that measured in the laboratory on intact rock samples. This already provides evidence that a fracture system was responsible for the hydraulic transport.

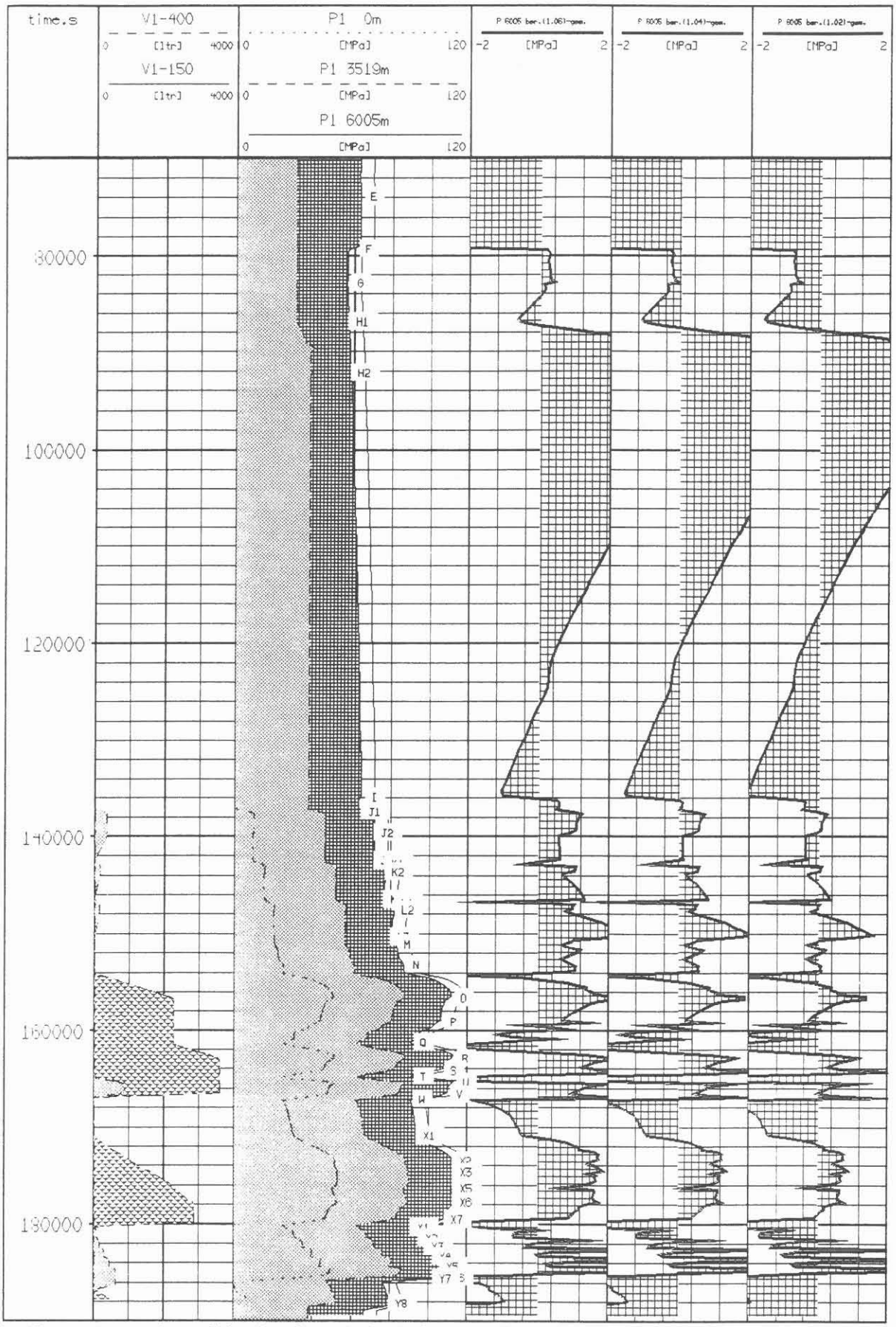

Fig. 15: Comparison of the data from the hydrofrac test. Track: 1. volumes, 2. pressures, 4. to 6.: difference between the pressures converted to 6005 m derived from the 3519 m data with different mud densities (1.06; 1.04 and 1.02 g/cm^3) minus the pressures measured at 6005 m.

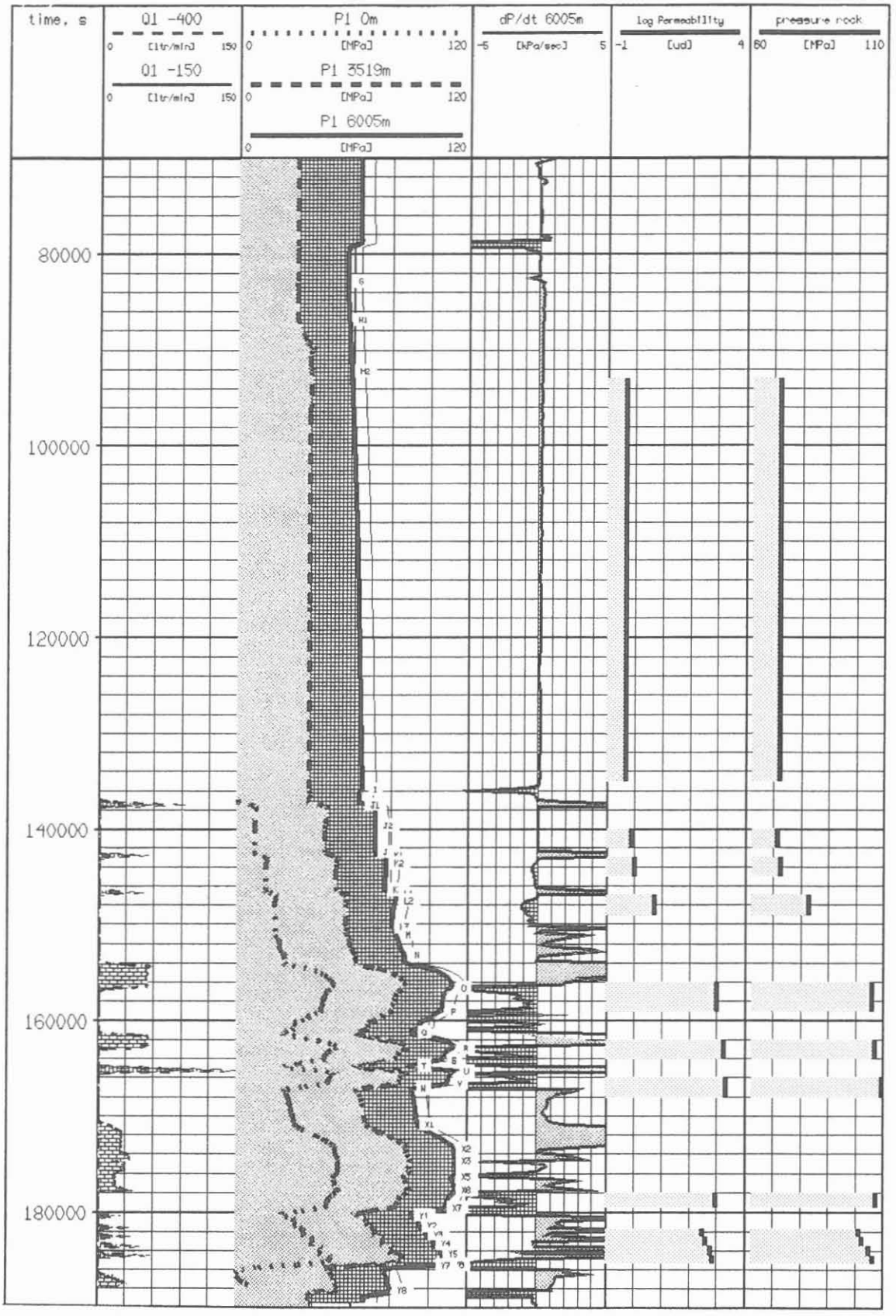

Fig. 16: Preliminary evaluation of the hydraulic parameters. Permeability and fluid pressure related to the separate test phases. Tracks: 1. pump rates, 2. pressures, 3. time derivative of the pressures measured at 6005 m, 4. permeability, 5. fluid pressures (lower edge of the hachured area = hydrostatic pressure calculated using a density of 1.04 g/cm3).

Communication between the pilot borehole and the main borehole

The mud level monitoring tests carried out in the pilot hole, in contrast to the drawdown test carried out prior to running in the casing and the cementation of the casing, showed no indication of the existance of any hydraulic communication between the deepest part of the pilot borehole and the fractured region.

4.2.2 Minimum principle stress

As already shown in section 3.3.4, no increase in the pressure above 114.5 MPa could be achieved despite continuous pumping. Figure 17 shows this value together with the data from the pilot hole. It can be seen that the extrapolation of all hydrofrac data from the first 3 km of the borehole, points to a lower value than that actually measured at 6 km. It is interesting to note that the value at 6 km lies almost on the same line as the values from 2 km and 3 km.

Thus, the hydrofrac experiments in the KTB pilot borehole and the main borehole confirmed an increase with depth in the gradient of the minimum principle stress.

4.3 Optimisation for future hydrofrac experiments

The following notes summarise the main points to be considered for optimising the hydrofrac experiment:

- *Directional information*: this requires more work in order for the BHTV to be used successfully.
- *Volume flow measurements*: it is essential to measure the outflow volume.
- Making it possible to *shut-in downhole:* an optimisation of the evaluation could be achieved if it was possible to shut in downhole. This was not possible here because of the required protection pressure in the annulus and because the drill string could not be moved to manipulate the test valve - because of the closed preventer.
- *Downhole log data:* in future planning it is necessary to take into consideration the fact that certain recording instruments malfunction at a higher rate than reported by the manufacturer.
- *Differential pressure and shut-in times:* for the drawdown test as well as for the pressure step tests, higher differential pressures and longer shut-in times would result in a great improvement in the determination of the hydraulic parameters.

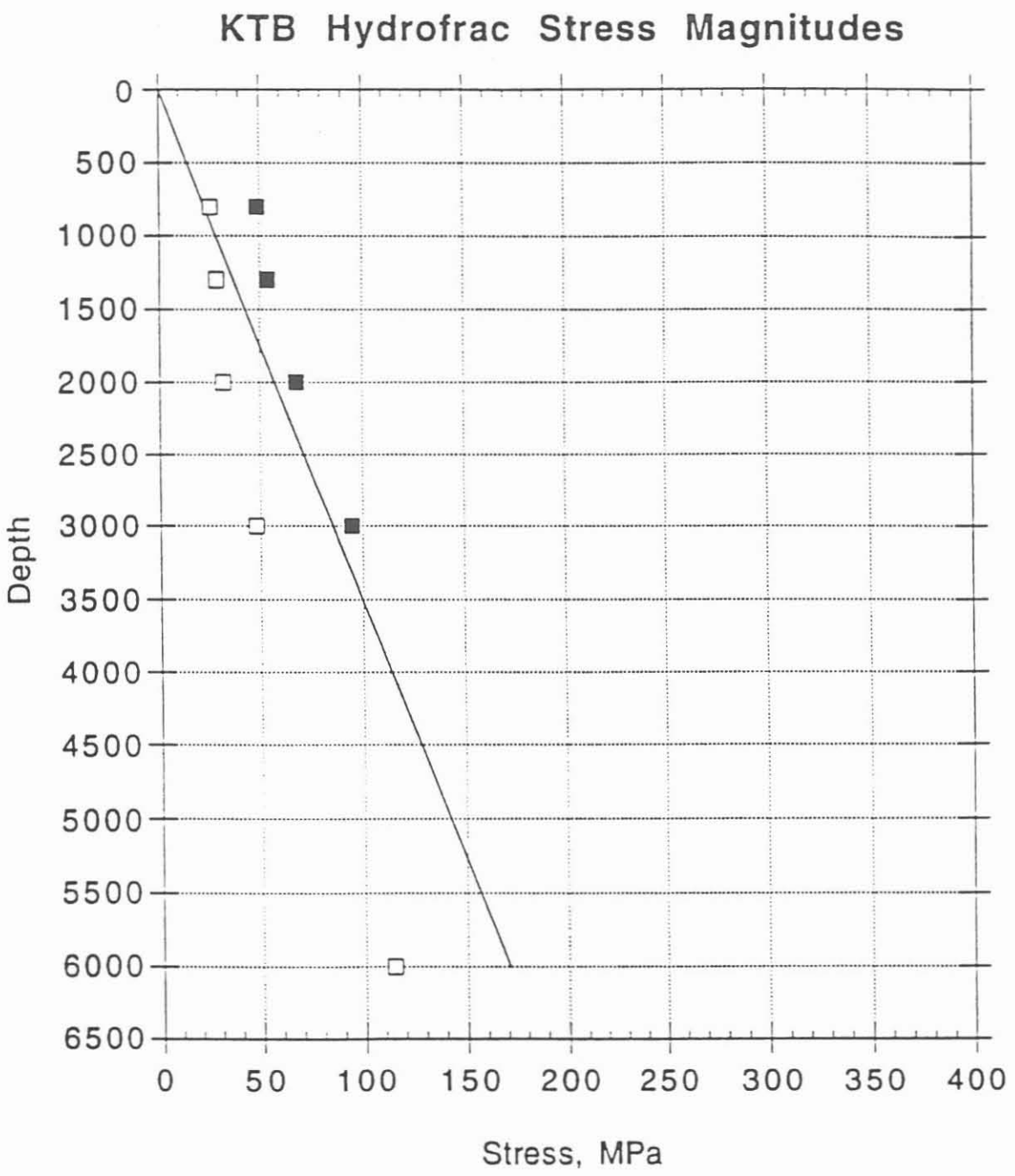

Fig. 17: Compilation of the stress magnitudes (ZOBACK et al., 1992) from the KTB pilot borehole down to 3000 m and from the value at 6 km from the KTB main borehole. Black squares for maximum, and open squares for minimum principle stress. The line represents the change in the vertical principle stress with depth.

5. Summary

The hydrofrac experiment at 6000 m carried out in April 1992, made a significant contribution to the determination of the stress state in the upper part of the earth's crust. Thus, the minimum principle stress was measured for the first time at a depth of 6 km and determined to be 114 ± 5 MPa. In connection with the results from the hydrofrac experiments in the pilot borehole, an increase in the gradient of the minimum principle stress with depth was proven.

Permeabilities between 0.4 and 2500 μD were determined dependent on the effective formation pressure. The initial formation pressure was higher than the hydrostatic pressure of the mud column.

Fluid samples contained highly saline formation fluids, which contained gas predominantly made up of approx. 85 % nitrogen and 8.5 % methane.

References:

BAUMGÄRTNER, J., RUMMEL, F. & M.D. ZOBACK (1990): Hydraulic Fracturing in situ Stress Measurements to 3 km Depth in the KTB Pilot Hole VB. A summary of a prelimary data evaluation.-in: K.Bram, J.Draxler, W. Kessels & G. Zoth KTB-Report 90-6a, NLfB, Hannover.

KESSELS W. & ZINNER, G. (1991): Abschätzung drer beim Pumptest in der KTB-Oberpfalz VB zu erwartenden Zuflußmengen anhand der Ergebnisse des Absenktestes. -in: Kessels, W. KTB-Report 90-5, NLfB, Hannover.

ZOBACK M.D., APEL R., BAUMGÄRTNER J., BRUDY M., EMMERMANN R., ENGESER B., KESSELS W:, FUCHS K., RISCHMÜLLER H., RUMMEL F. & VERNIK L. (1992) Strength of Continental Crust and the Transmission of Plate-Driving Forces: Implications of In Situ Stress Measurements in the KTB Scientific Borehole, Germany.- submitted to Nature.

Appendix

Project: Seismic recording Hydrofrac - KTB-HB 6000 m

Objectives: Seismic verification of formation stress reduction during frac testing.

Scientific supervision: **Prof. Dr. H. Gebrande, H.-A. Dahlheim**

Institut für Allgemeine und Angewandte Geophysik (IfAAG), University of Munich

Financing: a) Budget IfAAG Uni. of Munich approx. DM 3.000

b) DFG So 72/41-3,4 approx. DM 500

Recording Design

Number of recording stations: 3 3-comp. stations
Station 1: seismological station NOTT (650 m south of KTB-HB)
Station 2: borehole geophon VSP-6000 in 70 m depth
Station 3: geophon on drillstring

Recording period: app. 6 h continuous from 11:00 UTC - 23:00 UTC, April 30, 1992

Station	Sensor	Period	3 comp. rate	Sample. width	Band-system	Data Acq.
1	STS-2	120 sec	V,NS,EW	125 Hz	50 Hz	MARS-88 MC 21 bit
2	SM-6	4.5 Hz	V,H1,H2	250 Hz	100 Hz	MARS-88 FD 16 bit
3	SM-6	4.5 Hz	V,H1,H2	250Hz	100 Hz	MARS-88 FD 16 bit

Data:

Data volume: approx. 250 MB

Data storage: all data are archived in a UNIX data base on the Sun workstation of the KTB seismic network

Data Processing and Interpretation

Seismic station 2 and 3 received so much interference from activities by the experiment (pumping, etc.), that the preliminary evaluation has been limited to the seismic record collected at the NOTTersdorf station (1).

In the first step the data have been visually evaluated on the screen. Single seismic events have not been identified so far, escpecially at the time just before and during the frac. To analyse for a change in the seismic noise level, we applied a bandpass filter (width of 5 Hz) to selected time windows. The filter was applied in steps of 5 Hz in the frequency range 1 - 60 Hz. An increase in high frequency seismic noise of sofar unknown origin was observed at different times.

A detailed digital processing and evalution of the seismic noise and possible seismic activity is in progress. Preliminary results show no evidence for a correlation with frac related activities such as pump rates and pressure changes.

Hydraulic communication in crystalline rocks between the two boreholes of the Continental Deep Drilling Programme in Germany

KESSELS, W. & KüCK, J.

Abstract

Hydraulic communication was established at a depth of 4000 m between the two boreholes of the Continental Deep Drilling Programme in the Federal Republic of Germany (KTB). The distance between the two boreholes at this depth is approximately 250 m. The proven communication was stimulated by a draw down test and by casing cementation in the KTB super-deep borehole. The very rapid pressure transmission that was established points to a fracture system connecting both boreholes.

A "fracture evaluation" can be carried out by the determination of the hydraulic diffusion constant. The determination of the mechanical deformability (frac compressibility) of the fracture system is critical for the evaluation of mean apparent frac widths and mean apparent frac numbers. We show here how this determination is possible via the pressure dependence of the transmissibility.

The result shows that mean frac widths are around 5 to 7 μm and form a hydraulic connection.

1. Introduction

One of the main objektives of the KTB Projekt is to investigate the fluid system at great depth (ALTHAUS, E. et al., 1984; KESSELS, W., 1991). Hydraulic experiments in the KTB borehole were intended to determine the hydraulic parameters of the fractured zones and to recover formation fluids as uncontaminated as possible (BAUMGÄRTNER, J. et al., 1990; ENGESER, B. et al., 1990; ENACESCU, C. et al., 1990; KESSELS, W. et al., 1990; LODEMANN, M. et al., 1990).

The 4000 m deep pilot borehole, in the following the Vorbohrung of the Continental Deep Drilling Programme already penetrated an extensive fracture system with good hydraulic conductivity in the deepest part of the borehole (KESSELS et al. 1990).

Ion contents (PEKDEGER, A. et al., 1990; KESSELS, W. et al., 1990; HEINSCHILD, H.-J., OSTROWSKI, L., 1990) measured from in situ samples (ZOTH, G., 1990) and surface samples taken during two pump tests showed that the formation water was a calcium rich deep ground water with a relatively high gas content (0.8 m^3 gas at normal conditions per m^3 water). The most important gas components were nitrogen and methane. Isotope analysis of the methane showed that it was probably of sedimentary origin and possibly had migrated out of the

sedimentary zone to the west of the Franconian Line (fault zone between crystalline and sedimentary rock) which runs at a distance of approx. 7 km from the borehole (FABER, 1990).

A pump test carried out at the end of 1990 for a period of 4 months produced 480 m^3 of formation water (LODEMANN, 1992). No measurable limit to the boundary of the fractured reservoir was apparent.

Drilling of the KTB main borehole, in the following the Hauptbohrung, was started on October 1990 approx. 200 m distance from the pilot hole. Upon reaching a depth of 6000 m a draw down test established four significant inflow horizons between 3000 and 6000 m. The inflow horizons are quantified in KüCK and KESSELS (1993) based on fluid logging carried out during the draw down test.

Fig. 1 shows the most important inflow zones of the Vorbohrung and Hauptbohrung down to a depth of 6000 m. The inflow zones are determined from electric logs during the draw down test on the basis of a high NaCl equivalent concentration. The NaCl equivalent concentration was calculated from the electrical resistivity of the mud (KÜCK, J. & KESSELS, W., 1993; KÜCK, W. et al., 1993).

The spatial location of

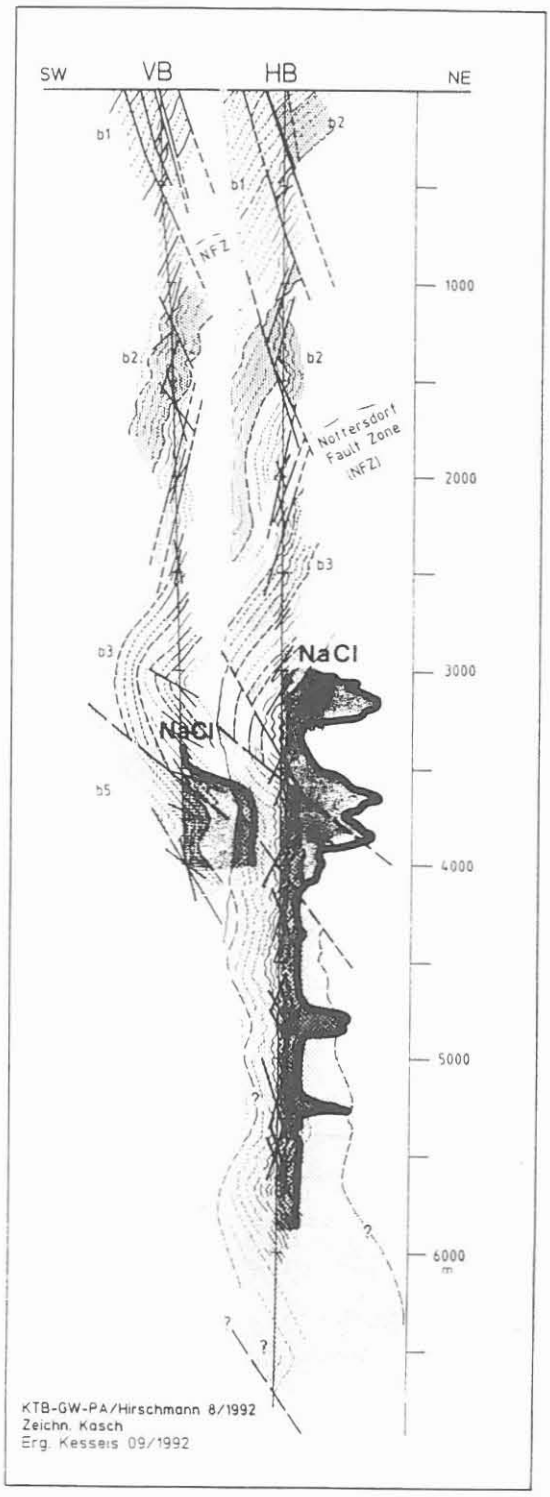

Fig. 1:
Inflow zones of highly saline fluids into both KTB boreholes indicated on the basis of NaCl equivalent concentrations calculated from the electrical resistivity of the mud (Geology after HIRSCHMANN, 1992).

the fluid producing fracture system is shown i the horizontal borehole path diagram in Fig. 2.

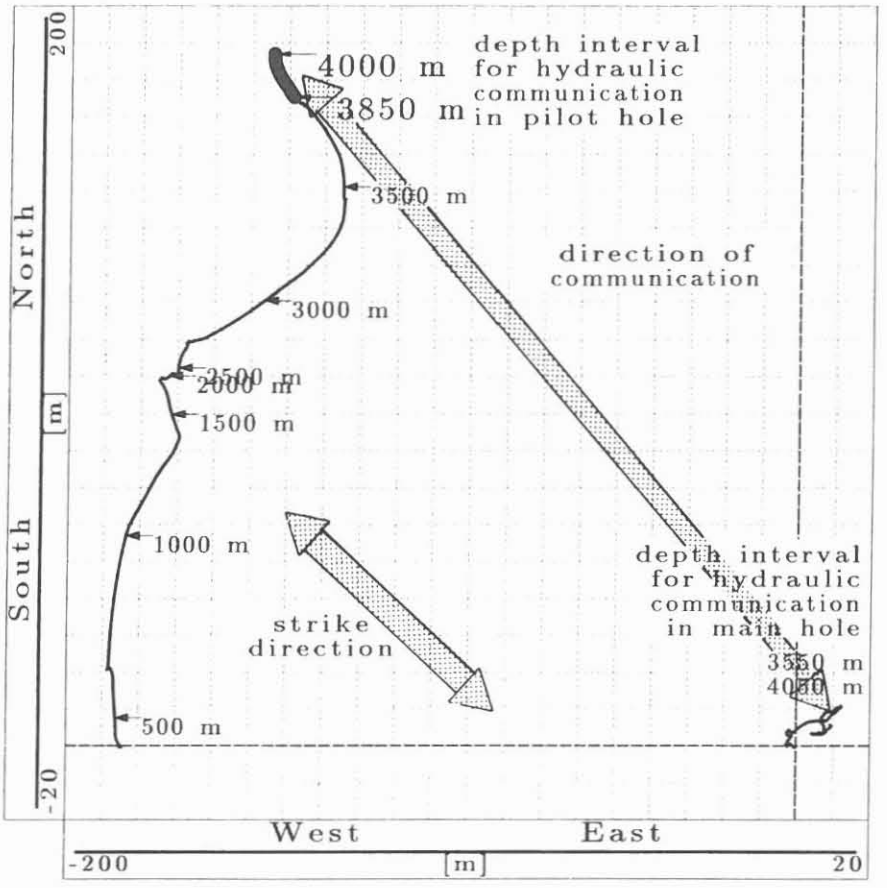

Fig. 2: Horizontal projection of the borehole paths for both KTB boreholes showing the significant inflow zones (strike direction after KESSELS & KÜCK, 1992)

Changes in the mud level in the Vorbohrung have been monitored since drilling began in the Hauptbohrung. During the draw down test that was carried out in the Hauptbohrung at a drill depth of 6018 m, the Vorbohrung incurred a rapid drop in mud level (Fig. 3). One week later during the cementation of the 6000 m casing in the Hauptbohrung an increase in mud level was recorded - again confirming the presence of communication between the two boreholes (Fig. 3). The cement head determination following cementation revealed a cement loss of approximately 30 m^3. This volume of losses matches the volume that entered the fracture system during the 6000 m draw down test in the Hauptbohrung. The pressure changes recorded in the Vorbohrung on both occasions reflected similar volumes. The very rapid pressure transmission over a distance of approx. 250 m points to the existence of a frac or a fracture

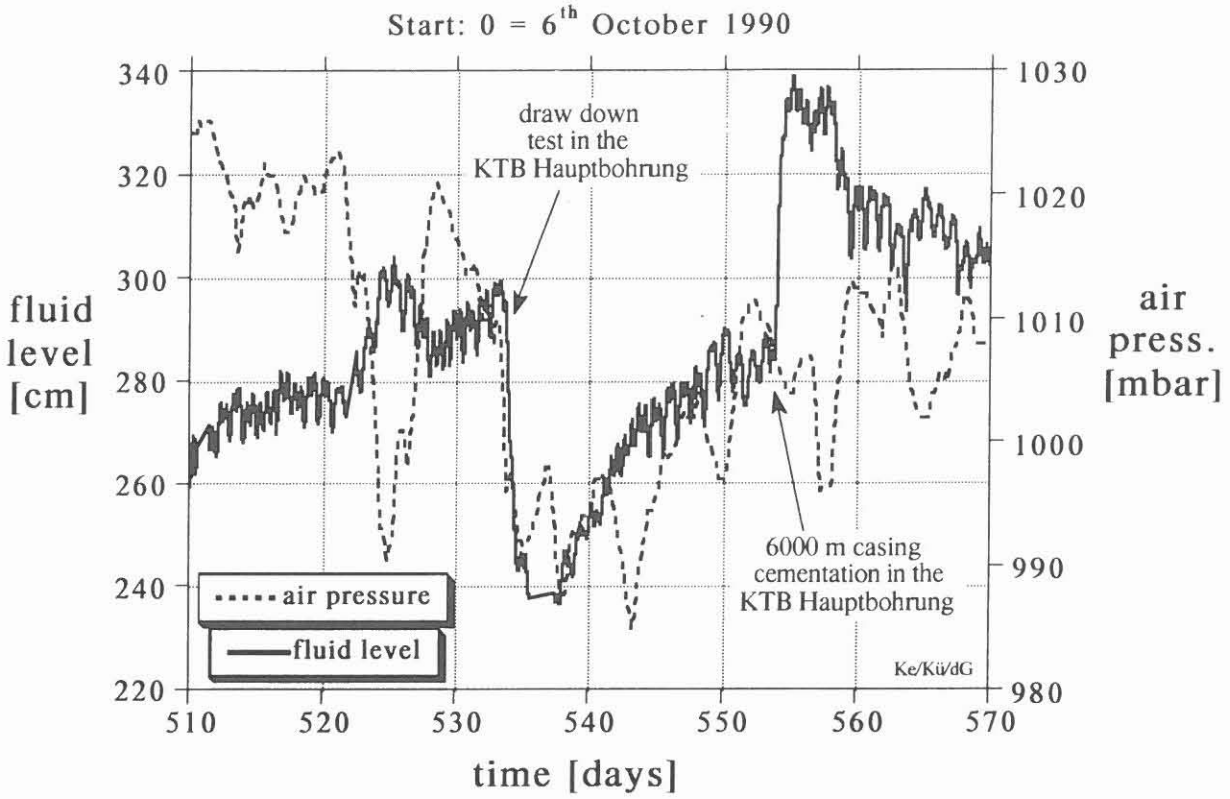

Fig. 3: Mud level fluctuations in the KTB Vorbohrung during the draw down test and the cementation of the 6000 m casing without air pressure and tidal correction.

In the following the evaluation assumes the presence of horizontal parallel fractures with identical fracture widths representing the simplest model of a fracture system. This has the advantage that the storage coefficient and the transmissibility - that are required to explain such rapid communication - bear a relationship to the actual hydraulic system and are not merely operands.

The storage capacity of the Vorbohrung that gives rise to a reduction in the pressure pulse radiating out from the Hauptbohrung was ignored.

2. Communication during the draw down test and cementation of the 6000 m casing

After the completion of drilling and logging in the Haupt-bohrung a pressure sensor was suspended approximately. 2 m below the top surface of the mud in the Vorbohrung. The objective was to record periodic changes in the mud level. In particular, tidal and air pressure variations (HSIEH et al., 1987; NARASIMHAN, 1984; BREDEHOEFT, 1967) and possible communication with the Hauptbohrung were to be investigated.

The Vorbohrung is cased to a depth of 3850 m, and the lower section of the casing is cemented. Therefore the fracture zone which is responsible for communication must lie in the deepest part of the Vorbohrung (KESSELS et al., 1990; OSTROWSKI, 1990).

Fig. 3 shows the mud level fluctuations recorded during the draw down test and cementation work carried out in the Hauptbohrung. It is clearly shown that the mud level fluctuations cannot be attributed to tidal variations or changes in air pressure.

Fig. 4 shows in more detail the mud level fluctuations in the Vorbohrung the draw down test was being carried out, and shows the very rapid change of the mud level in the Vorbohrung after the draw down test had begun in the Hauptbohrung. The drop in mud level in the Hauptbohrung is caused by the non-replacement of mud in the borehole as the drill string is run out of the hole. The total drop in mud level in the Hauptbohrung was 540 m. Equilibrium between mud (ρ = 1.05 g/cm^3) and the formation fluid is reached when the mud level drops to approx. 180 m below ground level - in other words the hydraulically effective drop in mud level below a depth of 180 m was not achieved until the latter stages of pulling the drill string out of the hole.

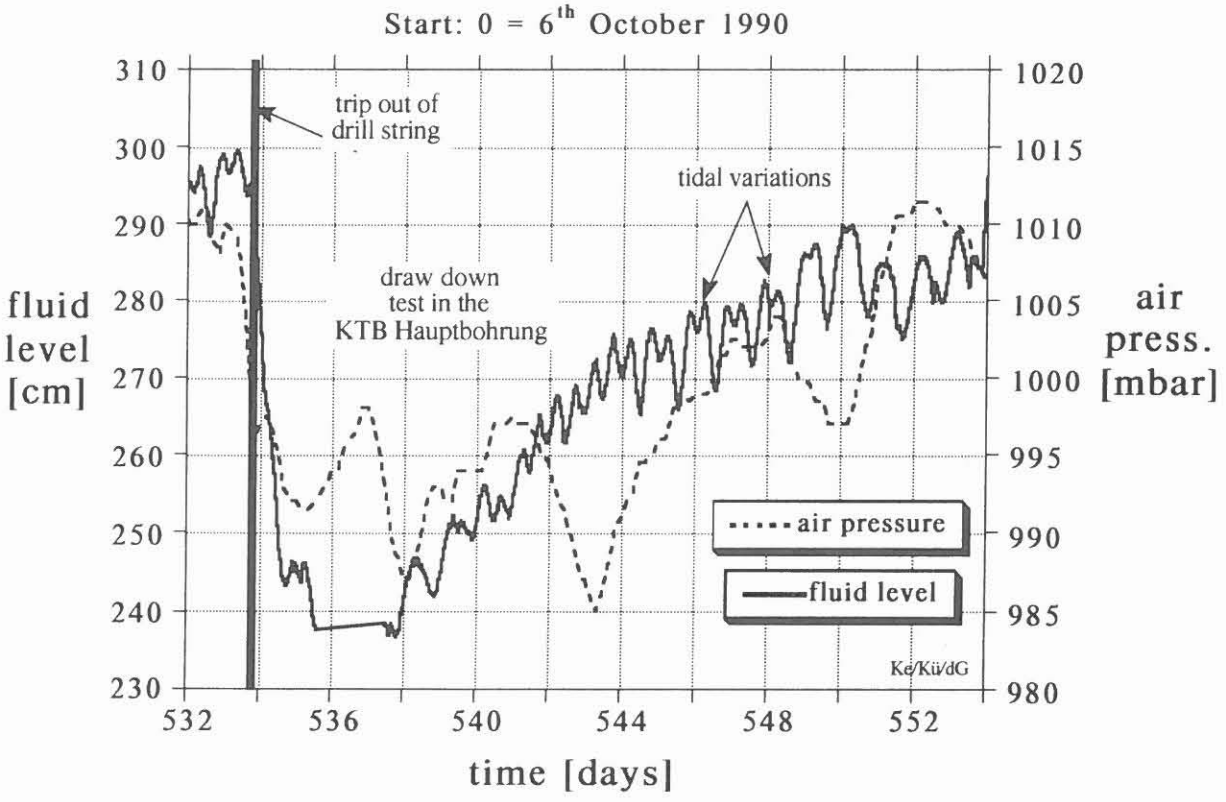

Fig. 4: Mud level plot of the KTB Vorbohrung during the 6000 m draw down test.

Fig. 5 in the pressure Variation in the Vorbohrung after the cementation of the 6000 m casing is shown. The tidal effect in particular can be seen very clearly here.

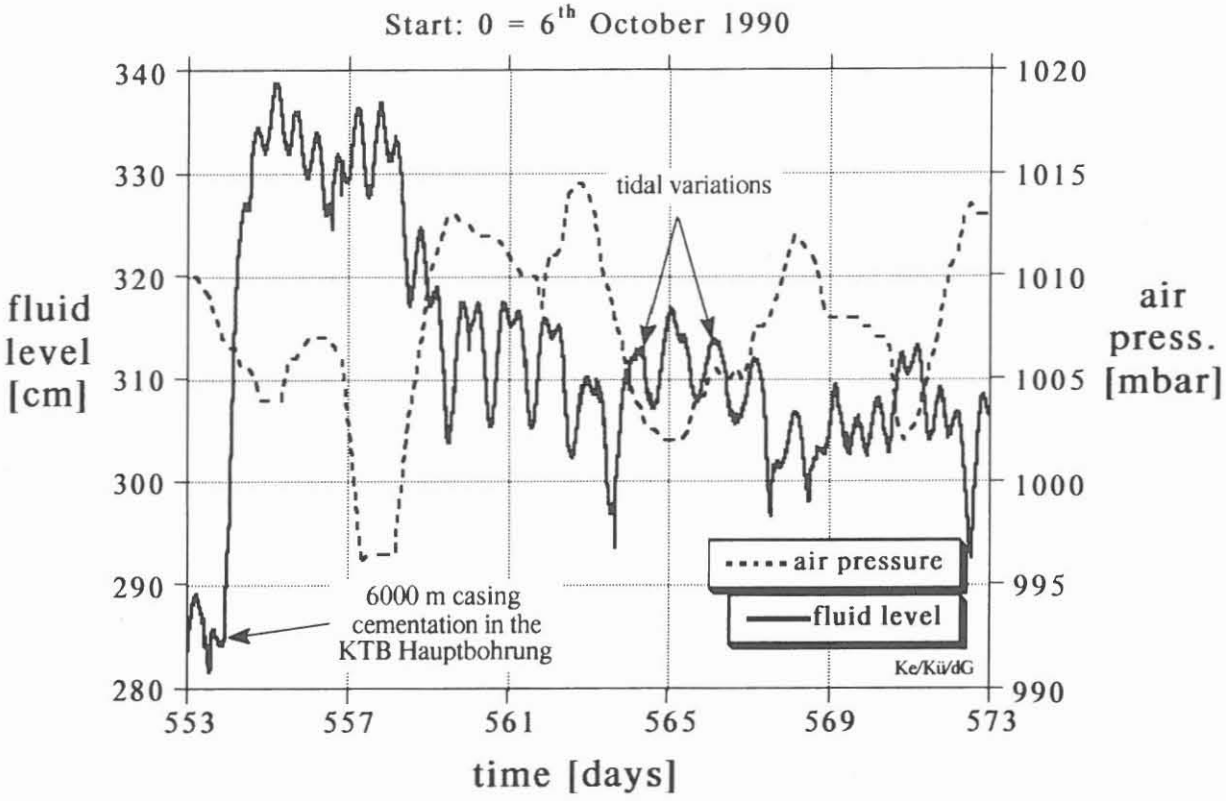

Fig. 5: Mud level plot of the KTB Hauptbohrung during cementation of the 6000 m casing.

The air pressure fluctuations show a clear anti correlation with the mud level variations, because the borehole does not have a gas tight seal. In Fig. 3 one can see that the air pressure fell very strongly during the draw down test and that a weaker air pressure increase followed during the cementation, in other words, an air pressure correction produces a slightly stronger drop in the mud level in the Vorbohrung during the draw down test, and a slightly weaker mud level rise during the cementation.

The draw down test and the cementation, however, differ slightly in the way the pressure in the Hauptbohrung is stimulated.

In the case of the draw down test one is actually dealing with a slug test in which the under pressure (mud level drop) is preserved over a longer period of time.

The cementation works more like a pulse test (a short period of cement injection being responsible for the pressure propagation).

Fig. 1 clearly shows that because of the geometric relationship of the fluid bearing horizons, the Hauptbohrung zone between 3550 to 4100 m is probably responsible for communication.

A more precise discussion of the fracture system connecting the two boreholes must take into account the fact that the Vorbohrung in particular is not vertical (Fig. 2).

It can be assumed from the fluid logging evaluation (KÜCK & KESSELS, 1993) that of the total of 30 m^3 of formation fluid that flowed in, 14 m^3 can be attributed to this zone. In the following evaluation - that is based in particular on the cementation - a cement injection of 14 m^3 is therefore assumed. Dimension figures used in the following analytical evaluation are the occurrence of a mud level maximum after a period of 1.5 days and the maximum mud level rise of 0.5 m.

3. Determination of transmissibility, storage coefficient and hydraulic diffusion constants, by an analytical line source calculation

The starting point for each hydraulic evaluation of time dependent pressure curves is the hydraulic diffusion equation

$$\Delta p = \frac{1}{D}\frac{\partial p}{\partial t} \qquad 1$$

Δ = Laplace operator
p = pressure
t = time
D = hydraulic diffusivity

based on the mass conservation of the pore space fluid and Darcy's law.

The hydraulic diffusion constant D is therefore

$$D = \frac{h*k}{\eta*h*S} = \frac{T}{\eta*h*S} \qquad 2$$

where
T = transmissibility
η = viscosity
h = thickness
s = storage coefficient
k = permeability.

This assumes the existence of a horizontal hydraulic conductor with a thickness h. Particularly in crystalline

rocks this immediately raises the question of what is the proper geometric model to be used for the hydraulic conductors being calculated. The complicated geological bedding conditions (HIRSCHMANN, 1992) suggest that in the crystalline rocks penetrated by the KTB boreholes the hydraulic conductors are neither:

1. of cylindrical symmetry around the borehole,

2. homogeneous,

3. of constant thickness, transmissibility or storage capacity,

4. or arranged horizontally.

Notwithstanding the above, it still makes sense - for the reasons given below - to carry out a hydraulic evaluation of the communication between the Vorbohrung and the Hauptbohrung using a model with horizontal plane hydraulic conductors. The reasons for such an evaluation are as follows:

1. A hydraulic model should if possible be one dimensional (in other words, plane, cylindrically symmetrical, or spherically symmetrical (a more complicated model requires the availability of more information).

2. The cylindrically symmetrical borehole is the reason for using a cylindrically symmetrical calculation.

3. Inclined, plane hydraulic conductors (e.g. fractures) can be calculated sufficiently accurately for long periods of time with a one dimensional cylindrically symmetrical model.

4. Practically all hydraulic test evaluation methods are based on cylindrically symmetrical calculations with horizontal plane hydraulic conductors thus guaranteeing comparability.

5. The hydraulic parameters determined make it possible to carry out pretest calculations of the way the pressure will change or of a given test layout.

The hydraulic parameters determined for a test evaluation, in particular in fractured crystalline rocks, must only be seen as parameters analogous to a simple electrical substitute wiring diagram for a complicated electronic circuit.

For the first approximation of the evaluation of the hydraulic communication between the Vorbohrung and the Hauptbohrung, the Hauptbohrung can be considered as a linear source into which a volume V is injected for a short period

of time. The following equation after CARSLAW and JAEGER (1976) is valid:

$$P(r,t) = \frac{V}{S*h*D*t*4\pi} e^{-\frac{r^2}{4D*t}} \qquad 3$$

D = hydraulic diffusivity
V = injection volume
S = specific storage capacity
h = thickness of the hydraulic conductor (considered as a homogeneous unit)
r = radius
t = time

The conditions for a short term injection are best filled by the cementation of the 6000 m casing. The injection time for the cement loss of approx. 30 m^3 that occurred during cementation is taken here as approx. 3 - 4 hours. In the first approximation this time period can be considered as small compared with tmax = 1.5 days - the build up time for the maximum pressure peak recorded in the pilot hole. 13.1 m^3 of the total cement losses were attributed to the communicating fracture zone. This time period, tmax = 1.5 days, and the recorded pressure amplitude of approx. pmax = 0,005 MPa, are used in the following evaluation (rmax = 250 m).

Differentiation of equation 3 gives the relationship between rmax and tmax shown in equation 4:

$$\frac{\partial P}{\partial t} = 0 \Longrightarrow \frac{r^2}{4D*t_{max}^3} - \frac{1}{t_{max}^2} = 0 \qquad 4$$

After conversion this gives the diffusion constant D as

$$D = \frac{r^2}{4t_{max}} \qquad 5$$

For the values rmax = 250 m and tmax = 1.5 d this then gives a hydraulic diffusion constant of approx.

$$D = 0.12 \frac{m^2}{sec}$$

Equation 5 demonstrates that the determination of the hydraulic diffusion constant between two communicating boreholes can be achieved with a relatively high degree of reliability. In the first approximation only the length of the hydraulic connection between both boreholes (the

distance r) and the point in time of the maximum pressure peak are used to calculate the hydraulic diffusion constant.

In equation 5 the storage capacity of the Vorbohrung is ignored. This storage capacity results in a minor shift in the maximum pressure to longer times and larger values, so that the hydraulic diffusion constant calculated here can be considered as a minimum value.

Furthermore, the horizontal distance rmax = 250 m at a depth of 4000 m was used for the length of the fracture system between both boreholes. Fig. 1 shows that the possible fracture zone accounting for the communication in the Hauptbohrung could be considerably longer than this. This also shows that the given value for the hydraulic diffusion constant must be considered as a minimum. For the calculation of transmissibility and the storage capacity of the plane horizontal hydraulic conductors assumed in the model, the measured pmax value is used and equation 3 converted to S . h whereby - when taking into consideration equation 5 - the storage capacity is given as shown in equation 6.

$$S*h = \frac{V}{P_{max}*D*t_{max}*e*4\pi} \qquad 6$$

The most uncertain part of this consideration is the determination of the injection volume V that has entered the fracture zone responsible for communication in the Hauptbohrung. This is especially true for the cementation. In the calculations undertaken here a volume of 13.1 m^3 is used which reflects that part of the overall transmissibility of the borehole section from 3000 to 6000 m that can be attributed to the fracture zone (KÜCK & KESSELS, 1993). This gives a storage coefficient of

$$S*h = 5E\text{-}9 \text{ m/Pa} \qquad 7$$

The transmissibility can now be calculated from equation 2 if one converts to T according to equation 7.

$$T = D*S*h*\eta \qquad 8$$

The viscosity value used ($0.27 \cdot 10^{-3}$/sec.) reflects the formation temperature of 120 °C at 4000 m depth (HUENGES & ZOTH, 1991). This gives a transmissibility of

$$T = 1.62 - 10^{-13} \text{ m}^3.$$

With these values it is now possible to calculate the pressure changes over time in the pilot hole according to equation 3. In Fig. 6 the change in pressure over time (calculated using these parameters) is shown together with the measured mud level fluctuations. It can be seen that the calculated and the measured pressure change over time show a good correlation with respect to size and pressure variation when one takes into consideration that the evaluation is based on relatively imprecise assumptions concerning the injection volume and the injection time.

The latter gives rise to the fact that the subsequent pressure increase after the draw down test is lower than that expected from the calculations.

A better fit was possible using the finite difference program "Hydrant" (KESSELS et al., 1990).

A separate matching for the pressure versus time dependency in the Vorbohrung and Hauptbohrung gave the results down in table 1. It was necessary to introduce a skin area of 24 m with a lower permeability.

Table 1: Results from curve-fit calculations on data from the draw down test (DD) ion the KTB Hauptbohrung and from a cross-hole communication experiment (X-hole) between Vorbohrung and Hauptbohrung. The mean permeability and storage coefficient was calculated for the 300 m long open hole section; the skin radius was 24 m. (1 μD = 10^{-18} m^2).

test type	shell	transmissibility [m^3]	mean permeability [μD]	storage [1/Pa]
DD	skin	$0.174\ 10^{-13}$	5.8	$3.7\ 10^{-10}$
DD	rock	$5.580\ 10^{-13}$	186	$3.7\ 10^{-10}$
X-hole	skin	$0.174\ 10^{-13}$	5.8	$3.7\ 10^{-10}$
X-hole	rock	$5.400\ 10^{-13}$	180	$2.2\ 10^{-10}$

The calculated and measured datas show an excellent agreement for the pressure in the Hauptbohrung as well as in the Vorbohrung (Fig. 6 and 7).

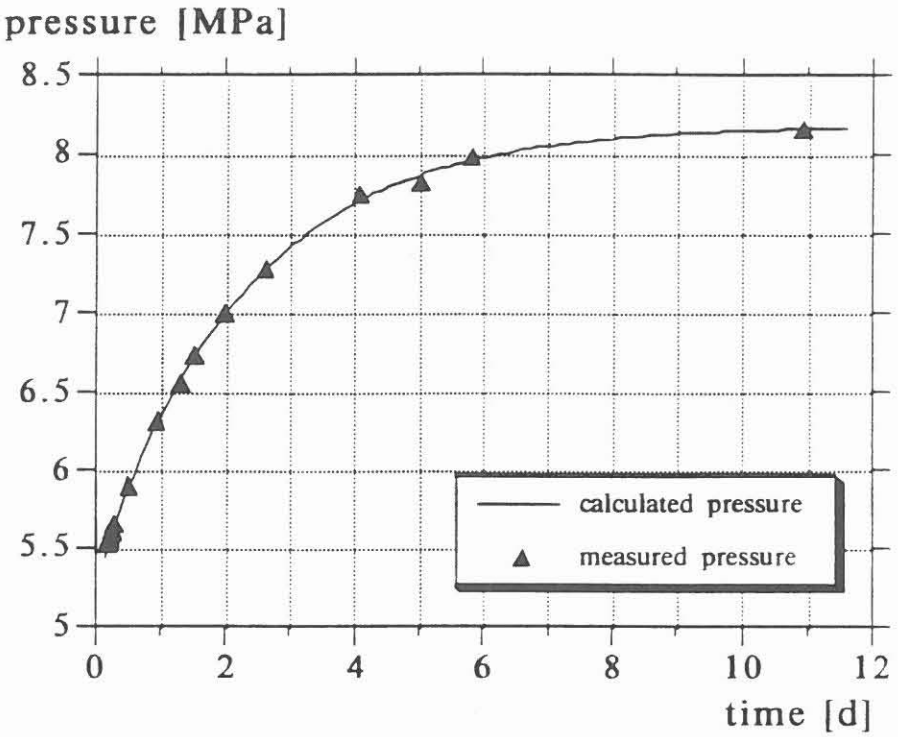

Fig. 6: Pressure recovery after draw down in the KTB Hauptbohrung. The pressure is calculated for a theoretical sensor depth of 1000 m. Triangles present measured data, the line is the fitted curve from 'HYDRANT' evaluations.

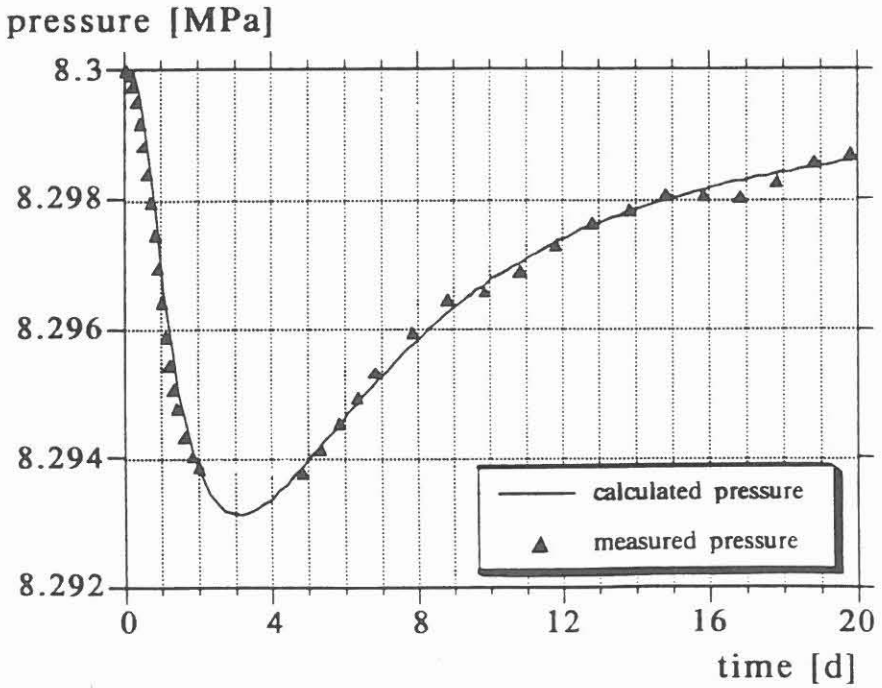

Fig. 7: Affection of fluid level in the KTB Vorbohrung after draw down in the KTB Hauptbohrung. The pressure is calculated for a theoretical sensor depth of 1000 m. Triangles present measured data, the line is the fitted curve from 'HYDRANT' evaluations. The mud level fluctuations have been corrected for tidal and air pressure effects.

As part of the hydraulic interpretation it is now necessary to test what type of hydraulic conductors were responsible for the communication. In the first step an assessment for an assumed homogeneous conductor is carried out, in the second step, a model of plane-parallel fractures is considered. In the pilot borehole, the only fractures that come into consideration for hydraulic communication are those drilled in the last few meters (KESSELS, W. et al., 1990).

In the Hauptbohrung the possible fracture zone responsible for hydraulic communication lies between 3550 and 4100 m. If one assumes that hydraulic communication is via a homogeneous hydraulic conductor with a thickness of 550 m, then, from the average transmissibility of

$T = 1.6 \cdot 10^{-13} m^3$, an average permeability of

$2.91 - 10\text{-}16 m^2 = 0.291$ mD can be calculated.

For the storage coefficient of the plane hydraulic conductors a value of

$$s \cdot h = 5 \cdot 10^{-9} m/Pa$$

was calculated, giving a specific storage coefficient at the given thickness of

$$s = 9.1 \cdot 10^{-12} 1/Pa.$$

The following is now valid for the storage coefficient:

$$s = \Phi \cdot (Cp + Cw)$$

where Ø = compressibility, Cw = water compressibility, and Cp = pore space compressibility (EARLOUGHER, 1977). The pore space compressibility describes the deformability of the hydraulic conductors as a result of formation pressure changes. NEWMANN (1973) shows that very high pore space compressibilities up to values of $Cp = 140 \cdot 10^{-4}$ 1/Pa are possible particularly in low porosity rock formations.

This means that the storage capacity of low porosity rocks is determined by the formation of relatively soft, easily deformable fractures, rather than the compressibility of water.

KESSELS (1989) used compressibility measurements derived from the Westerly granite from BRACE et al. (1965) to calculate the pore space compressibility. For small effective stresses this also gave a rock storage capacity mainly attributed to the pore space compressibility.

If, in the first approximation, one uses a pore space geometry with no pore space compressibility (Cp = 0) then,

for a water compressibility of Cw = $4.4 \cdot 10^{-4}$ l/Pa, after conversion of equation 8, this gives

$$\Phi = \frac{S}{Cw} \qquad 9$$

and thus a value of

$$\Phi = 0207.$$

If one assumes that mechanically this is a very soft system of hydraulic conductors reflecting a Cp value of $140 \cdot 10^{-4}$ l/Pa, then this gives a porosity of $\emptyset = 6.5\ 10^{-4}$.

The porosity calculated in this way is significantly smaller than the mean porosity derived from core analysis (SOFFEL et al., 1991; ZIMMERMANN et al., 1990) where the values lay around 0.5 %. Furthermore, if one compares the mean permeability of the cores that is approx. three orders of magnitude smaller than that determined for the 550 m long borehole section (Fig. 8), then it becomes clear that the significant hydraulic conductors are not associated with matrix porosity but rather with a fracture system.

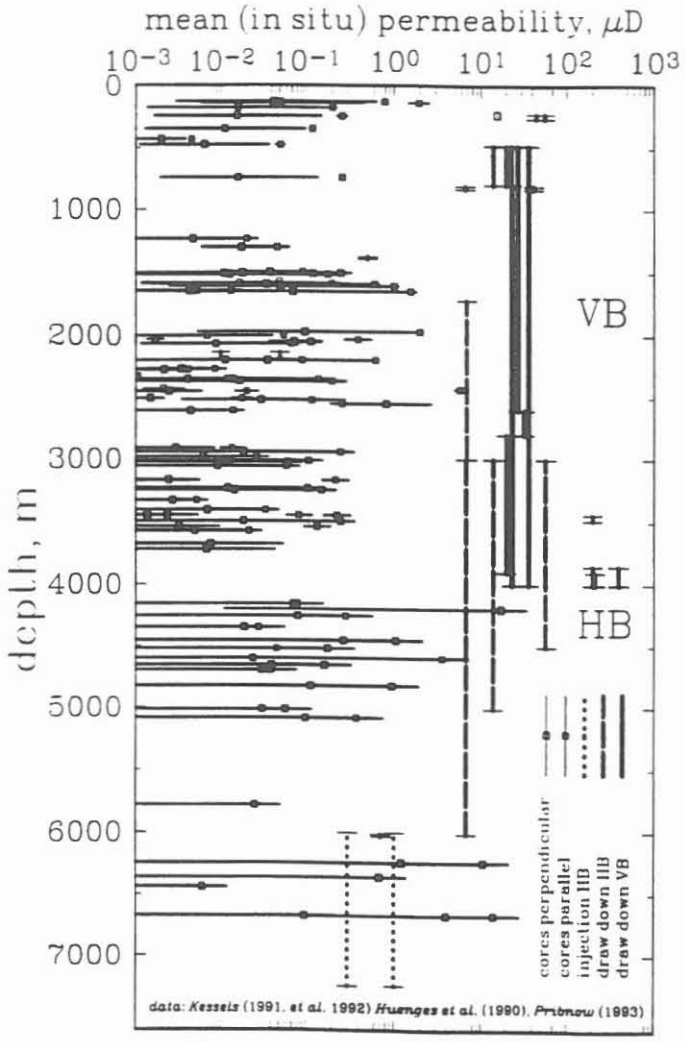

Fig. 8:

Comparison of mean permeabilities in the KTB Vorbohrung and the KTB Hauptbohrung determined from cores and in situ tests (HUENGES, et al., 1993).

4. Evaluation of mean fracture parameters

In order to gain a picture of the type and number of hydraulic conductors, an evaluation is carried out in the following of the model with horizontal, plane-parallel, fractures having the same fracture width (Fig. 9). Superficially, this model does not appear any less idealised than the model with homogeneous isotropic hydraulic conductors. However, the advantage of the former fracture evaluation lies in the fact that the mean hydraulically effective fracture width is determinable. The result of the evaluation is therefore the determination of a "hydraulic fracture system" that can be used as a hydraulic "substitute system" to describe the transport processes in the crystalline rocks. However, one must be aware of the fact that in reality a much more complicated hydraulic system with much more complicated microscopic and macroscopic fracture geometries is present (BROWN & SCHOLZ, 1985; GALE, 1982; BANDIS et al., 1983; BERNABE, 1986, WALSH & GROSENBAUGH, 1979). Critical for the evaluation is that the time dependent pressure propagation in the fractures can only be determined from its compressibility and their mean fracture width.

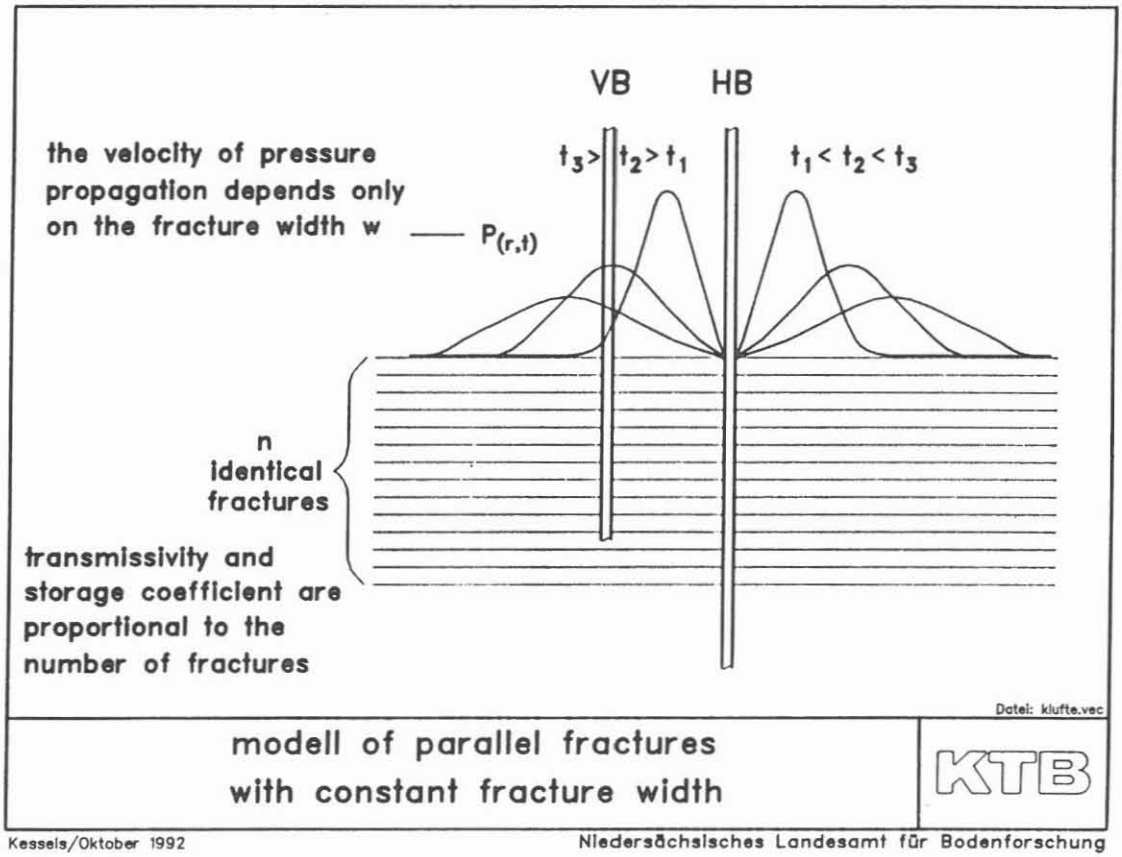

Fig. 9: Model of parallel individual fractures with constant fracture width.

In the hydraulic diffusion equation, the speed of the pressure propagation is determined via the hydraulic diffusion constant, that - as already shown in equation 2 - is independent of the thickness of the hydraulic conductor, but rather only from its specific hydraulic characteristics.

A similar interpretation can be carried out when considering fractures using a model with hydraulic resistances arranged in parallel. The total transmissibility of the borehole proportional to the number of fractures 'n', and also the storage capacity of the fracture system, is n-times the storage capacity of a single fracture. This makes clear that the hydraulic diffusion constant is particularly suited to calculating average fracture widths.

$$T = n*T_k \qquad 10$$

$$S = n*S_k \qquad 11$$

If this relationship is included in equation 2 then this gives:

$$D = \frac{n*T_k}{\eta*n*S_k} = \frac{T_k}{\eta*S_k} \qquad 12$$

When considering a homogeneous hydraulic conductor, the hydraulic properties of the rock are described by the material specific parameters: permeability K, specific storage capacity S, and porosity Ø.

Another material specific parameter for determination of the storage capacity of a porous rock is the pore space compressibility Cp.

When considering a model with plane parallel fracs, the calculation includes the frac transmissibility Tk, the frac storage capacity Sk and the number of fracs. Naturally, this assumes that all fracs have the same hydraulic characteristics. With this assumption it is possible to define frac porosity using equation 13. This gives the size of the pore volume (frac volume) that is largely responsible for the observed hydraulic pressure equalisation.

$$\Phi_{frac} = \frac{n*W}{h} \qquad 13$$

Naturally, this also gives rise to problems when the pressure equalisation is split into short and long time periods. In the latter, other communication paths than are the case for short time periods could be critical for pressure equalisation.

In the next step, the relationships between transmissibility and storage coefficient and the fracture width and the apparent number of fracs n must be given. For laminar flow (WITHERSPOON et al., 1980) the transmissibility is given as

$$T = n*T_k = n*\frac{W^3}{12} \qquad 14$$

and the storage coefficient as (JUNG, 1989)

$$S = n*S_k = n*\left(\frac{dW}{dP} + W*Cw\right) \qquad 15$$

whereby it is still prudent to include the frac compressibility with

$$Cf = \frac{dW}{WdP} \qquad 16$$

and

$$S = n*W*(Cf + Cw) \qquad 17$$

For purely linear elastic behaviour of the rock matrix, Cf is then only dependent on the elastic property of the rock matrix and the shape of the fracs. This means that two fracs whose frac geometries and matrix properties only differ in scale, have the same Cf value even if their frac widths differ considerably.

According to equation 12 the diffusion constant D can be described from the quotient of individual frac transmissibility Tk and individual frac storage capacity Sk. Thus, a calculated hydraulic diffusion constant can be described by either a mechanically rigid fracture system and a small individual frac transmissibility, or a mechanically soft fracture system with a large transmissibility (large frac widths). In Fig. 10 the changes in the hydraulic frac parameters are carried out by changing the storage coefficients Sk. All dependencies were carried out for the hydraulic diffusion constant of

$$D = 0.12\ m^2/sec,$$

derived from the communication between the Vorbohrung and the Hauptbohrung.

Bearing in mind equations 12 and 14, the fracture width W was calculated from

$$W = (12*\eta*S_k*D)^{1/3}$$

and the apparent frac number n from

$$n = \frac{W^3/12}{T}$$

using the transmissibility determined in chapter 3. The frac porosity was then determined using equation 13.

The S values given here are from BANDIS et al. (1983) which were determined from artificial fractures (laboratory tests) as well as values from JUNG (1989) derived from in situ measurements. JUNG's values were derived from fractures with very large widths at relatively shallow depths so they do not fall on the lines of possible frac widths.

The frac width of the fracture system connecting the two boreholes is limited by the apparent fracture number that cannot be smaller than 1 (marked in Fig. 10). This gives a maximum frac width from 0.1 to 0.2 mm assuming that only one frac is responsible for the communication. If the frac widths are too small, a limitation arises because the storage coefficient cannot be smaller than the compressibility of water. If equation 17 is converted accordingly, then the fracture porosity can be derived from

$$\Phi_{frac} = \frac{n*W}{h} = \frac{S}{(Cf+Cw)*h} \qquad 18$$

and an upper limit for the fracture porosity can be calculated when the fracture compressibility Cf = 0 is used (non-deformable fractures). This consideration gives an upper value for the frac porosity of

$$\Phi f = 0.207 \cdot 10^{-2}$$

Thus, as shown in Fig. 10, the average frac widths are limited and must lie between 1 micrometer and 100 micrometers.

It is now necessary to determine the frac compressibility from a hydraulic test.

This is best achieved by carrying out a pressure step test, which gives a pressure dependent permeability determined by establishing different pressure levels in the formation (KESSELS, 1993).

If the pressure dependence of the transmissibility is already known, then, as shown in equation 19, a relationship can be found for the fracture model with plane fractures as follows:

$$\frac{dT}{dP} = n\frac{d(W^3/12)}{dP} = \frac{n*W^2}{4}\frac{dW}{dP}$$

$$\frac{dT}{dP} = \frac{W^2}{4}(S-n*Cw*W)$$

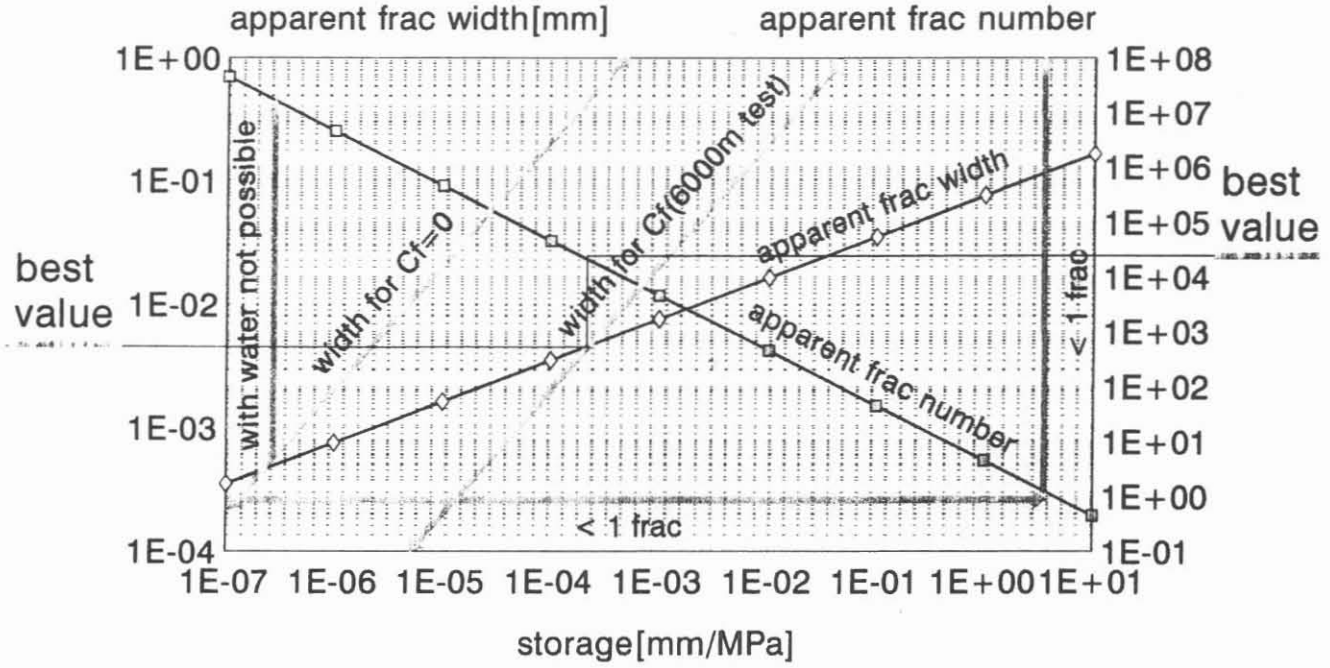

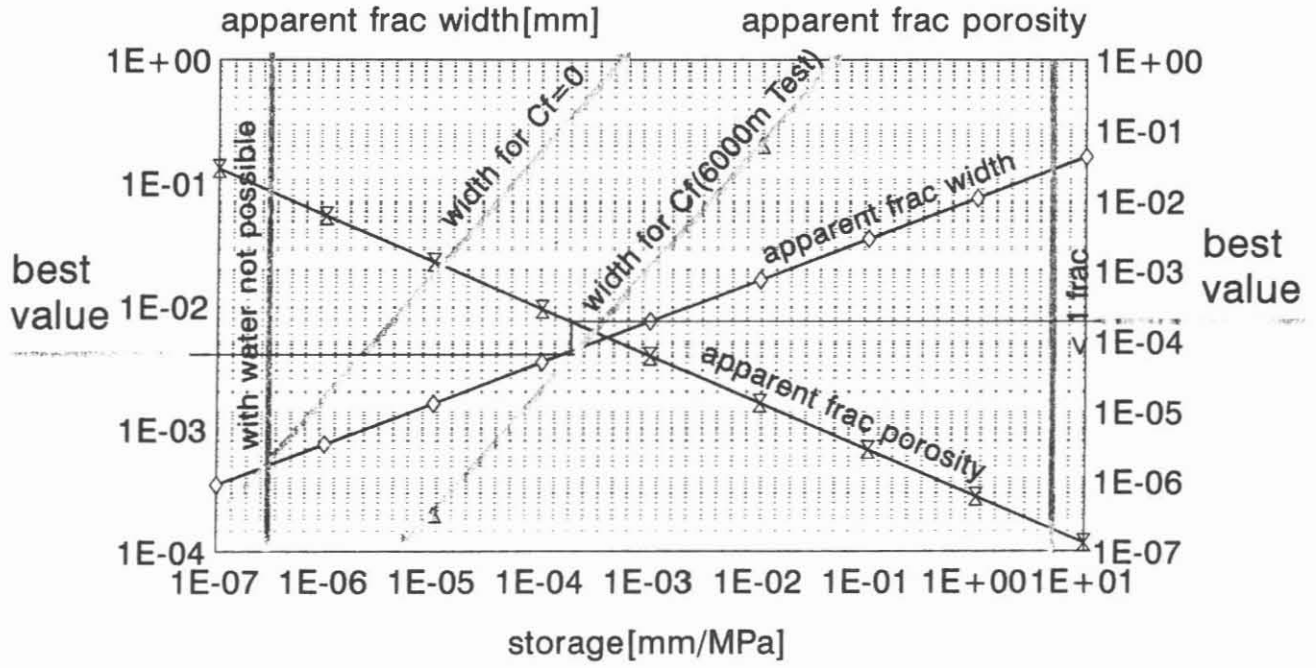

Fig. 10: Frac widths, frac number and frac porosities calculated for the diffusion constant and the transmissibility of the hydraulic communicationbetween the KTB Vorbohrung and the KTB Hauptbohrung. The storage capacity of the individual fracs shown on the abscissa establishes the frac combination that is compatible with the hydraulic results.

where the storage coefficient is established from equation 15.

Together with equation 11

$$\frac{dT}{dP} = n \frac{W^3}{4} \frac{dW}{WdP}$$

this gives the relationship

$$\frac{dT}{TdP} = 3 \frac{dW}{WdP} = 3*Cf \qquad 19$$

This, with equation 12, shows that the diffusion constant D is only dependent on the average frac width.

$$D = \frac{W^3/12}{\eta * W * (Cf+Cw)}$$

If the frac compressibility is known this equation can be converted to W to give equation 20.

$$W = (12*D*(Cf+Cw)*\eta)^{1/2} \qquad 20$$

For known hydraulic diffusion constants the frac width can now be directly calculated from equation 20 if the pressure dependence of the transmissibility is also known. Equation 19 gives the dependence according to equation 21 for constant Cf values assuming that $dP = d\sigma_{eff}$ is valid. A more precise examination must take into consideration the Biot constant α ($0<\alpha<1$) (BERNABE, 1986).

$$\frac{dT}{TdP} = -\frac{dT}{Td\sigma_{eff}} = -3 \frac{dW}{Wd\sigma_{eff}} = 3*Cf \qquad 21$$

After integrating, this gives

$$T = To\, e^{-3cf*\sigma_{eff}} \qquad 22$$

For a single frac, σ_{eff} must be replaced by $\underline{S}_n = (\sigma * \underline{n}) * \underline{n} - P$ if n is the normal vector of the frac.

If one considers permeability measurements from cores and fractures (e.g. MORROW et al., 1986; BERNABE, 1986) than one can see in logarithmic plots of permeability against pressure that the curves show a similar gradient despite the variability of the samples even when the permeabilities differ by several orders of magnitude. This clearly shows that frac compressibilities Cp derived from equation 21 vary much less than the permeabilities.

The permeabilities determined by BERNABE (1986) in the Celmsford granite and Barre granite differ from one another by a factor of 10 (see Fig. 11) but only differ slightly when one compares the frac compressibilities cf determined from equation 21 (see Fig. 12). A direct determination of frac compressibilities is given in BANDIS et al. (1983). From these closure measurements with mismatched roughnesses he discovered the following dependency.

$$\log \alpha_{eff} = q*W+p \qquad 23$$

The frac compressibility can be derived directly from the closure measurement using equation 16. The above mentioned frac compressibilities are summarised in Fig. 12. This shows - not unexpectedly - that the frac compressibilities determined by BANDIS are larger than the values determined from the pressure dependent permeabilities by BERNABE.

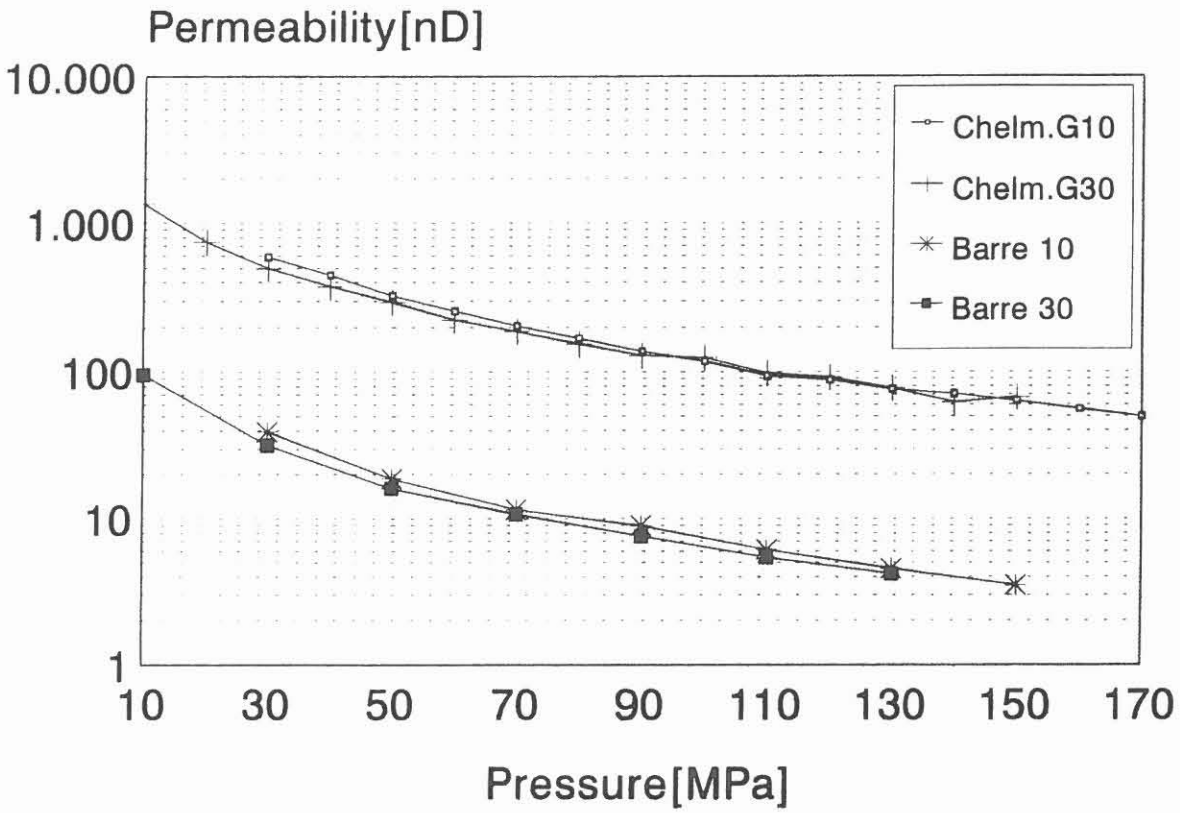

Fig. 11: Permeability measurements from the Celmsford and Barre granites after BERNABE (1986)

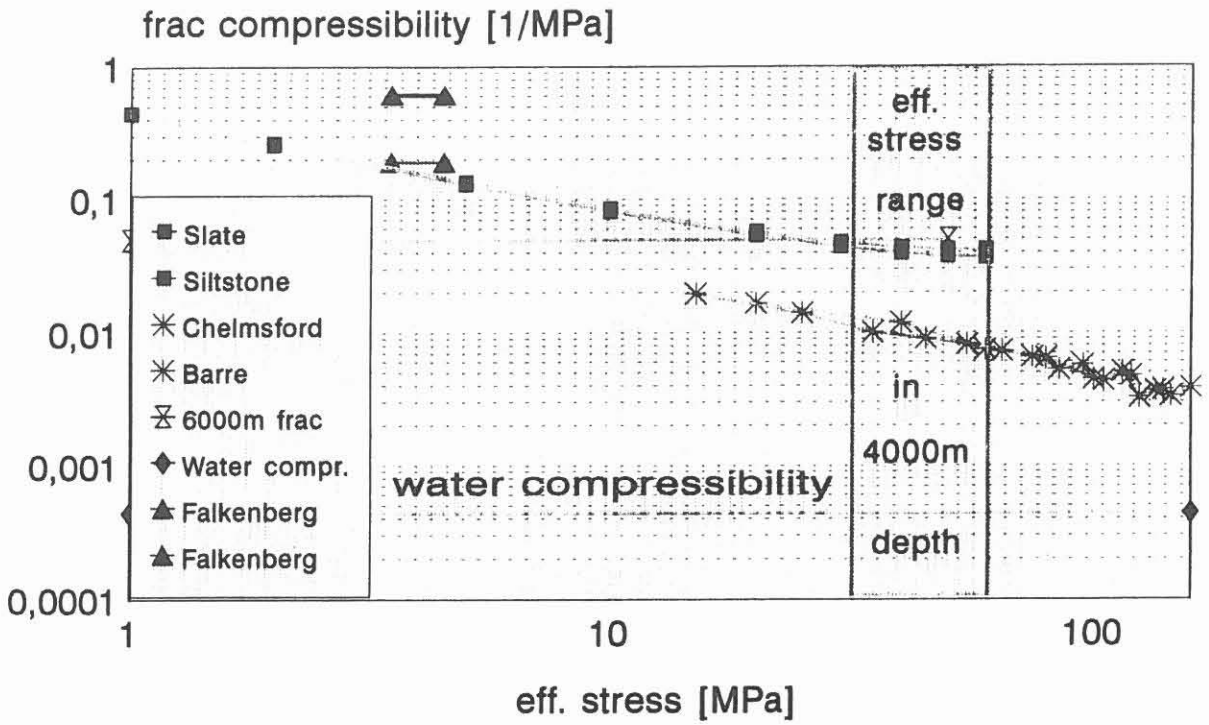

Fig. 12: Selection of frac compressibilities derived from laboratory and in situ measurements.

(1) Closure measurements from BANDIS et al. (1983) from slate and siltstone. (2) In situ measurement from JUNG (1898) from artificial fracs in Altenwerk granite. (3) Evaluation of pressure dependent transmissibility in the 6000 m frac experiment in the KTB Hauptbohrung (HUENGES & KESSELS, 1993). (4) Measurements from BERNABE (1986) on the Celmsford and Barre granites (see Fig. 10).

If one considers the frac compressibilities that are determined from the pressure dependence of transmissibility in a 6000 m hydrofrac experiment (ZOBACK et al., 1993; HUENGES & KESSELS, 1993), then we see good agreement with the values determined by BANDIS in the expected effectiv stress in the depth of 4000 m. Fig. 12 also shows the water compressibility Cw. One can see from this that the water compressibility is around one to two orders of magnitude smaller than the determined frac compressibilities. Assuming that the frac compressibility for the hydraulic communication system between the Vorbohrung and the Hauptbohrung is

$$Cf = 5 \cdot 10^{-8}\ 1/Pa,$$

this gives a frac width, $W = 4.94 \cdot 10^{-6}$ m. In Fig. 13 and 14 the average frac width the frac porosity and the

apparement frac number determined from the hydraulic communication between the boreholes, is shown dependent on the frac compressibility used for the evaluation. This shows that in the region of possible compressibilities, mean frac widths occur that differ by almost an order of magnitude. It is therefore recommended, particularly when carrying out hydraulic tests in fractured zones, that the pressure dependent transmissibility be determined experimentally.

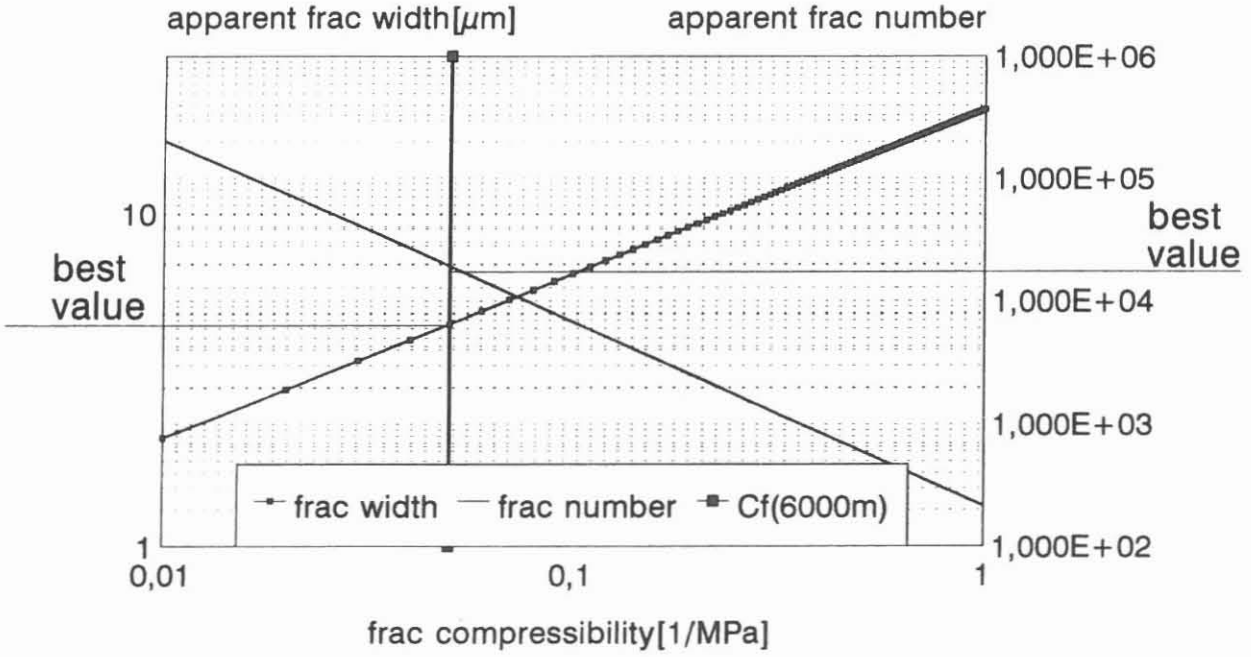

Fig. 13: Mean frac width and apparent frac number dependent on frac compressibility for the communication between the KTB Vorbohrung and the KTB Hauptbohrung.

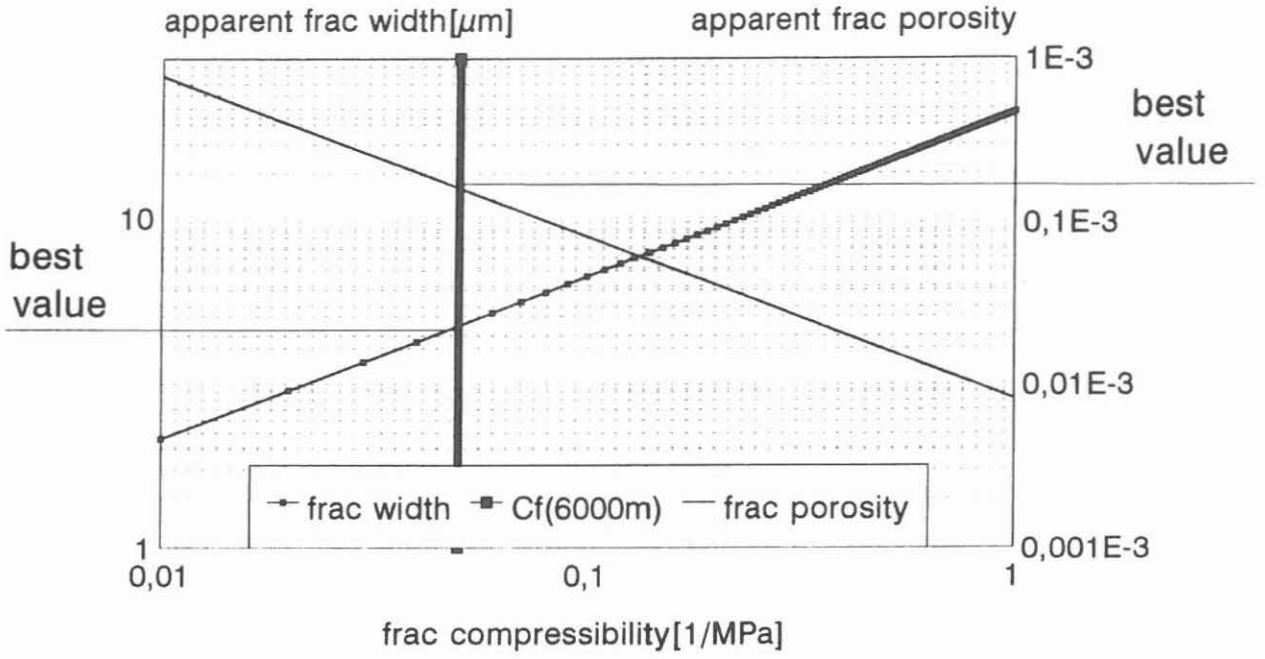

Fig. 14: Mean frac width and apparent frac porosity dependenton frac compressibility for the communication between the KTB Vorbohrung and the KTB-Hauptbohrung.

Summary and conclusion

At a depth of 4000 m, hydraulic communication was established to be present between the two boreholes of the Continental Deep Drilling Programme, from which a hydraulic diffusion constant of D = 0.12 m^2/sec. could be determined. This very extensive hydraulic communication pathway with a highly saline fluid environment shows that at a depth of 4000 m relatively quick material transport in fracture systems is possible.

By using the concept of mean fracture parameters it is also possible to restrict the number of hydraulic interpretations especially when one also lays down the condition that frac compressibility can only have values that can be explained by the mechanical rock conditions and frac conditions (elastic matrix parameters, surface properties of the fracture system). An evaluation using a model with horizontal, plane-parallel fracs gives average frac widths of approximately 5-7 micrometers. This shows that with this model it is possible to include the pressure dependence of the transmissibility in an evaluation.

Information on the frac compressibility can be derived using

this model from determinations of pressure dependent compressibility. The model with a plane, plane-parallel frac system differs from geometrical reality in particular in the complexly folded crystalline rocks penetrated by the Continental Deep Drilling Programme boreholes. The parameters derived for the "hydraulic substitute system" of plan-parallel, plane fracs do however allow the determination of characteristic parameters of frac systems that are relatively closely related to rock specific conditions. In particular, the frac porosity specified here shows that the porosity share of the hydraulically "dominant" fractures (porosity $\emptyset = 10^{-4}$ to 10^{-6}) is significantly smaller than the porosities measured in cores (porosity $\emptyset = 10^{-2}$).

References

ALTHAUS, E., BEHR, H., EDER, W., GOERLICH, F., MARONDE, D. & ZIEGLER, W.: 1984. Kontinentales Tiefbohrprogramm (KTB) der Bundesrepuplik Deutschland - Fortschritte und Stand 1984, Mitteilung XIX der Kommission für Geowissenschaftliche Gemeinschaftsforschung, DFG, VCH Verlagsgesellschaft, Weinheim.

BANDIS, S.C., LUMSDEN, A.C. & BARTON, N.R.: 1983. Fundaments of rock joint deformation. Int. J. Rock Mech. Min. Sci. & Geomech. Abstr. Vol. 20, 249-268.

BAUMGÄRTNER, J. & RUMMEL, F.: 1990. In Situ Permeability Measurements in the KTB Pilot Hole VB. Using a Wireline-Operated, Hydraulic Fracturing Straddle Packer Assembly, KTB Report 90-5, 333-340, Hannover.

BERNABE, Y.: 1986. The Effective Pressure Law for Permeability in Chelmsford Granite and Barre Granite. Int. J. Rock Mech. Min. Sci. & Geomech. Abstr. Vol. 23, No. 3, 267-275.

BRACE, W.F., ORANGE, A.S. & MADDEN, T.R.: 1965. The Effect of Pressure on the Electrical Resistivity of Water-Saturated Crystalline Rocks. J. Geophys. Res., 60 (22).

BREDEHOEFT, J.D.: 1967: Response of well-aquifer systems to earth tides. J. Geophys. Res. 72 (12) 3075-3087.

BROWN, S.R. & SCHOLZ, CH.H.: 1985. Broad Bandwidth Study of the Topography of Natural Rock Surfaces. Journal of Geophysical Research. Vol. 90, No. B14. 12575-12582.

CARSLAW, H.S. & JAEGER, J.C.: 1959. Conduction of Heat in Solids, 2nd ed. Oxford University Press, New York.

EARLOUGHER, R.C.Jr.: 1977. Advances in Well Test Analysis. American Institute of Mining, Metallurgical and Petroleum Engineers, Inc. Monograph Vol. 5, Henry L. Doherty Series, 2. Auflage, New York/Dallas.

ENACESCU, C., MIEHE, R. & PUSCH, G.: 1990. Auswertung geohydraulischer Teste in der Bohrphase der KTB-Vorbohrung. KTB Report 90-5, 173-232, Hannover.

ENGESER, B. & KESSELS, W.: 1990. Technische Durchführung hydraulischer Teste in der KTB-Oberpfalz VB. KTB Report 90-5, 21-81, Hannover.

FABER, E.: 1990. C- und H- Isotopenverhältnisse in leichtflüchtigen Kohlenwasserstoffen, Kohlendioxid und Wasserstoff aus Testuntersuchungen der KTB-Vorbohrung. KTB Report 90-5, 541-547, Hannover.

GALE, J.E.: 1982. Fundamental Hydraulic Characteristics of Fractures from Field and Laboratory Investigations. Australian Water Resources Council, Conf. Series No. 5.

HEINSCHILD, J.:1990. Ergebnisse der geochemischen Bearbeitung gewonnener Fluidproben. KTB Report 90-5, 439-470, Hannover.

HIRSCHMANN, G.: 1992. On the geological Interpretation of the 3-D Seismic Data with Special Regard to the Information from the KTB Boreholes. KTB Report 92-5, DEKORP Report, 351-373, Hannover.

HUENGES, E. & ZOTH, G.: 1991. KTB-Oberpfalz VB: temperature, thermal conductivity and heat flow density. Scientific Drilling, 2:81-89.

HUENGES, E. & KESSELS, W.: 1993. Effective stress dependency of permeability and transmissibility of rocks during the 6 km hydrofrac-experiment in the KTB main hole. - Meeting of the European Geophysical Society 1993 in Wiesbaden.

HSIEH, P.A., BREDEHOEFT, J.D. & FARR, J.M.: 1987. Determination of aquifer transmissivity from Earth tide analysis. Wat. Resour. Res. 23, 1824-1832.

JUNG, R.: 1989. Hydraulic In Situ Investigations of an Artificial Fracture in the Falkenberg Granite. Int. J. Rock Mech. Min. Sci. & Geomech. Abstr. Vol. 26, No. 3/4, 301-308.

KESSELS, W.: 1989. The Storage Coefficient with Regard to Matrix Compressibility. KTB Report 89-1, 229-260, Hannover.

KESSELS, W., & PUSCH, G.: 1990. Auswahl hydraulischer Testzonen an der KTB-Oberpfalz VB anhand von Bohrlochmessungen, KTB Report 90-5, 139-169, Hannover.

KESSELS, W., ZOTH, G. & KÜCK, J.: 1990. Absenk- und Injektionstest in der KTB-Oberpflaz VB, KTB Report 90-4, 474, Hannover.

KESSELS, W., ZOTH, G. & KÜCK, J.: 1990. Erste Ergebnisse eines Absenkungs- und Injektionstestes in der KTB-Oberpfalz VB. KTB Report 90-5, 235-283, Hannover.

KESSELS, W. & ZINNER, G.: 1990. Abschätzung der beim Pumptest in der KTB-Oberpfalz VB zu erwartenden Zuflußmengen anhand der Ergebnisse des Absenktestes. KTB Report 90-5, 343-358, Hannover.

KESSELS, W.: 1991. Objectives and execution of hydraulic experiments in the KTB-Oberpfalz borehole within the longterm measurement and test programme in the Continental Deep Drilling pilot borehole. Scientific Drilling 2. 287-298.

KESSELS, W. & KÜCK, J.: 1992. Computer-aided Matching of Plan Core Structures with Borehole Measurements for Core Orientation. Scientific Drilling 3. 225-238.

KESSELS, W.: 1993. Formationsdruckverhältnisse in der KTB-Hauptbohrung unter Berücksichtigung des Druckstufentestes vom 08. und 09.02.1993. KTB-interne Notiz vom 11.02.1993 (unpublished).

KÜCK, J. & KESSELS, W.: 1993. Investigation of open fracture systems in the crystalline rock of the borehole KTB-Oberpfalz HB by fluid logging (in preparation).

LODEMANN, M. & FRITZ, P.: 1990. Isotopenhydrologische Untersuchungen im Rahmen der Hydraulik-Fluidteste in der KTB-Vorbohrung. Erste Ergebnisse. KTB Report 90-5, 497-517, Hannover.

LODEMANN, M.: 1992 (personal communication).

MORROW, C.A., ZHANG BO-CHONG & BYERLEE, J.D. 1986. Effective Pressure Law for Permeability of Westerly Granite Under Cyclic Loading. Journal of Geophysical Research, Vol. 91, No. B3, 3870-3876.

NARASIMHAN, T.N., KANEHIRO, B.Y. & WITHERSPOON, P.A.: 1984. Interpretation of earth tide response of three deep, confined aquifers. J. Geophys. Res. 89 (B3), 1913-1924.

NEWMANN, G.H.: 1973. Pore-Volume Compressibility of Consolidated. Friable and Unconsolidated Reservoir Rocks Under Hydrostatic Loading. J. Pet. Tech. 129-134.

OSTROWSKI, L.: 1990. Hydraulisches Testprogramm KTB-VB. Ergebnisse der Feldauswertungen. KTB Report 90-5, 359-435, Hannover.

PEKDEGER, A., SOMMER- VON JARMERSTED, C. & WOITH, H.: 1990. Zwischenbericht über erste Ergebnisse der Hydrochemie (Pumpversuch vom 07.04.90 - 11.04.90) in der KTB-VB. KTB Report 90-5, 473-481, Hannover.

SOFFEL, H.C., BÜCKER, C., GEBRANDE, H., HUENGES, E., LIPPMANN, E., POHL, J., RAUEN, A., SCHULT, A., STREIT, M. & WIENAND J.: 1991. Physical properties measured on cores and cuttings from the pilot well (0-400.1 m) of the German Continental Deep Drilling Program (KTB) in the Oberpfalz area, Bavaria, Federal Republic of Germany. - Surveys in Geophysics, 13, 1-34.

WALSH, J.B. & GROSENBAUGH, M.A.: 1979. A New Model for Analyzing the Effect of Fractures on Compressibility. Journal of Geophysical Research, Vol. 84, No. B7.

WITHERSPOON, P.A., WANG, J.S.Y., IWAI, K. & GALE, J.E.: 1980. Validity of Cubic Law for Fluid Flow in a Deformable Rock Fracture. Water Resources Research, Vol. 16, No. 6, 1016-1024.

WITHERSPOON, P.A., AMICK, C.H., GALE, J.E. & IWAI, K.: 1979. Observations of a Potential Size Effect in Experimental Determination of the Hydraulic Properties of Fractures. Water Resources Research. Vol. 15. No. 5.

ZIMMERMANN, G., BURKHARDT, H. & MELCHERT, M.: 1990. Abschätzung der Porosität kristalliner Gesteine aus Bohrlochmessungen mit Hilfe multivariabler Verfahren. KTB Report 90-4, 159-170, Hannover.

ZOTH, G.: 1990. Untertage-Probenahmesystem zur Gewinnung von in situ-Fluidproben. KTB Report 90-5,85-120, Hannover.

ZOBAK, M.D., APEL, R., BAUMGÄRTNER, J., BRUDY. M., EMMERMANN, R., ENGESER, B., KESSELS, W., FUCHS, K., RISCHMÜLLER, H., RUMMEL, F. & VERNIK, L.: 1993. Strength of Continental Crust and the Transmission of Plate-Driving Forces: Implications of In Situ Stress Measurements in KTB Scientific Borehole, Germany. Submitted to Nature.

10. Annexe

K T B R E P O R T S related to Borehole Measurements already published:

KTB Report 87-2 (1987)
Grundlagenforschung und Bohrlochgeophysik. Beiträge zur Tagung der Deutschen Geophysikalischen Gesellschaft in Clausthal-Zellerfeld (31.03.-04.04.1987). Hsg.: R. Hänel und R. Schopper

KTB Report 87-3 (1987)
Grundlagenforschung und Bohrlochgeophysik (Bericht 2). Arbeitsprogramm KTB-Bohrlochgeophysik sowie Bohrlochmeßprogramm KTB-Oberpfalz VB (01.09.1987). Hsg.: R. Hänel

KTB Report 87-4 (1987)
Grundlagenforschung und Bohrlochgeophysik (Bericht 3). Bohrlochmessungen in der KTB-Oberpfalz VB - Intervall 0-478,5 m -. Hsg.: J.K. Draxler und R. Hänel

KTB Report 88-4 (1988)
Grundlagenforschung und Bohrlochgeophysik (Bericht 4). Bohrlochmessungen in der KTB-Oberpfalz VB - Intervall 478,5-1529,4 m. Hsg.: J. K. Draxler und R. Hänel

KTB Report 88-7 (1988)
Grundlagenforschung und Bohrlochgeophysik (Bericht 5). Bohrlochmessungen in der KTB-Oberpfalz VB Intervall 1529,4-3009,7 m. Hsg.: J. Draxler und R. Hänel

KTB Report 88-11 (1988)
Grundlagenforschung und Bohrlochgeophysik (Bericht 6). Forschung und Entwicklung - Berichte laufender und abgeschlossener Vorhaben. Hsg.: P. Kehrer und W. Kessels.

KTB Report 89-1 (1989)
Grundlagenforschung und Bohrlochgeophysik (Bericht 7). Auswertung von Bohrlochmessungen der KTB-Oberpfalz VB. Hsg.: R. Hänel

KTB Report 90-1 (1990)
Grundlagenforschung und Bohrlochgeophysik (Bericht 8). Auswertung von Bohrlochmessungen der KTB-Oberpfalz VB. Hsg.: J.K. Draxler

KTB Report 90-5 (1990)
Grundlagenforschung und Bohrlochgeophysik (Bericht 9). Hydraulische Untersuchungen in der Bohrung KTB-Oberpfalz VB. Hsg.: W. Kessels

KTB Report 90-6a (1990)
Grundlagenforschung und Bohrlochgeophysik (Bericht 10). Langzeitmeß- und Testprogramm in der KTB-Oberpfalz VB. Hsg.: K. Bram, J.K. Draxler, W. Kessels und G. Zoth

KTB Report 90-6b (1990)
DEKORP REPORT. Integrated Seismics Oberpfalz 1989. Longterm Logging and Testing Programme of the KTB-Oberpfalz VB. Eds.: H.-J. Dürbaum, Ch. Reichert, K. Bram

KTB Report 91-2 (1991)
Grundlagenforschung und Bohrlochgeophysik (Bericht 11). Bohrlochmessungen in der KTB-Oberpfalz HB - Intervall 0-1720,0 m Hsg.: K. Bram, J.K. Draxler, G. Zoth

KTB Report 91-4 (1991)
Grundlagenforschung und Bohrlochgeophysik (Bericht 12). Forschung und Entwicklung. EFA-LOG - Rekonstruktion kristalliner Lithologie anhand von bohrlochgeophysikalischen Messungen für die Bohrungen URACH 3 und KTB-Oberpfalz VB

KTB Report 92-1 (1992)
Grundlagenforschung und Bohrlochgeophysik (Bericht 13). Bohrlochmessungen in der KTB-Oberpfalz HB - Intervall 1720,0 - 4512,0 m -. Hsg.: K. Bram, J. Draxler

KTB Report 93-1 (1993)
Basic Research and Borehole Geophysics (Report 14). Borehole logging in the KTB-Oberpflalz HB - Interval 4512.0-6018.0 m. Eds.: K. Bram, J.K. Draxler

Niedersächsisches Landesamt für Bodenforschung
KTB-Project Management
att. M. Sowa
P.O.Box 67
D-92667 Windischeschenbach

Phone: (49) 9681-40062
Fax: (49) 9681-40067

Subj.: Request of KTB logging data

For my/our research project .... the following logging data is kindly requested:

Measurement Evaluation Test KTB list n°	date of acquisition	interval		data on floppy, film, tape etc	remarks
		from (m)	to (m)		
Further remarks:					

Data on tapes or floppies is provided in LIS format. Only exceptionally data can be made available in ASCII format after consultation.
Scientists must then report regularily on the progress of their studies either to the Project Management or to the Chief-Coordinator of the DFG priority programme KTB. Results should first be published in the "KTB Report" series.

Status of data request (KTB internal)

Please, send the data to:

Make sure that your address is complete and correct, including phone and fax number!

Date and place

Signature

Niedersächsisches Landesamt für Bodenforschung
KTB-Project Management
att. M. Sowa
P.O.Box 67
D-92667 Windischeschenbach

Phone: (49) 9681-40062
Fax: (49) 9681-40067

Subj.: Request of KTB logging data

For my/our research project .... the following logging data is kindly requested:

Measurement Evaluation Test KTB list n°	date of acquisition	interval		data on floppy, film, tape etc	remarks
		from (m)	to (m)		
Further remarks:					

Data on tapes or floppies is provided in LIS format. Only exceptionally data can be made available in ASCII format after consultation.
Scientists must then report regularily on the progress of their studies either to the Project Management or to the Chief-Coordinator of the DFG priority programme KTB. Results should first be published in the "KTB Report" series.

Status of data request (KTB internal)

Please, send the data to:

Make sure that your address is complete and correct, including phone and fax number!

Date and place

Signature

Niedersächsisches Landesamt für Bodenforschung
KTB-Project Management
att. M. Sowa
P.O.Box 67
D-92667 Windischeschenbach

Phone: (49) 9681-40062
Fax: (49) 9681-40067

Subj.: Request of KTB logging data

For my/our research project .... the following logging data is kindly requested:

Measurement Evaluation Test KTB list n°	date of acquisition	interval		data on floppy, film, tape etc	remarks
		from (m)	to (m)		
Further remarks:					

Data on tapes or floppies is provided in LIS format. Only exceptionally data can be made available in ASCII format after consultation.
Scientists must then report regularily on the progress of their studies either to the Project Management or to the Chief-Coordinator of the DFG priority programme KTB. Results should first be published in the "KTB Report" series.

Status of data request (KTB internal)

Please, send the data to:

Make sure that your address is complete and correct, including phone and fax number!

Date and place

Signature

Niedersächsisches Landesamt für Bodenforschung
KTB-Project Management
att. M. Sowa
P.O.Box 67
D-92667 Windischeschenbach

Phone: (49) 9681-40062
Fax: (49) 9681-40067

Subj.: Request of KTB logging data

For my/our research project .... the following logging data is kindly requested:

Measurement Evaluation Test KTB list n°	date of acquisition	interval		data on floppy, film, tape etc	remarks
		from (m)	to (m)		

Further remarks:

Data on tapes or floppies is provided in LIS format. Only exceptionally data can be made available in ASCII format after consultation.
Scientists must then report regularily on the progress of their studies either to the Project Management or to the Chief-Coordinator of the DFG priority programme KTB. Results should first be published in the "KTB Report" series.

Status of data request (KTB internal)

Please, send the data to:

Make sure that your address is complete and correct, including phone and fax number!

Date and place

Signature

ISSN 0939-8732
ISBN 3-928559-09-5